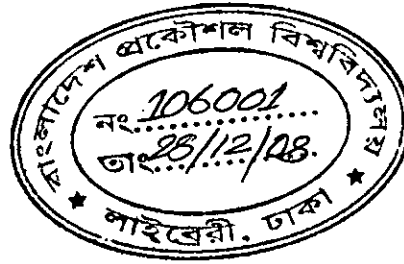


**EXPERIMENTAL STUDY ON LOCAL SCOUR AROUND PIER  
LIKE STRUCTURE AT FLOODPLAIN OF COMPOUND CHANNEL**



**A Thesis**

**Submitted by**

**Debjit Roy**

**Roll: 100516001 F**

In partial fulfillment of the requirement for the degree of  
**Master of Science in Engineering (Water Resources)**

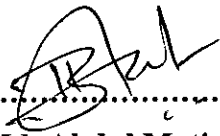


**DEPARTMENT OF WATER RESOURCES ENGINEERING  
BANGLADESH UNIVERSITY OF ENGINEERING AND TECHNOLOGY  
DHAKA**

**OCTOBER 2008**

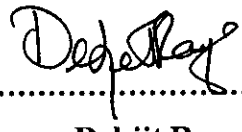
## CERTIFICATE OF RESEARCH

This is to certify that this thesis work has been done by me and neither this thesis nor any part of thereof has been submitted elsewhere for the award of any degree or diploma.



.....  
**Dr. Md. Abdul Matin**

Countersigned by the Supervisor



.....  
**Debjit Roy**

Signature of the candidate

DEPARTMENT OF WATER RESOURCES ENGINEERING  
BANGLADESH UNIVERSITY OF ENGINEERING AND TECHNOLOGY  
DHAKA

We here by recommend that the thesis work by

**Debjit Roy**

entitled

**“EXPERIMENTAL STUDY ON LOCAL SCOUR AROUND PIER LIKE  
STRUCTURE AT FLOODPLAIN OF COMPOUND CHANNEL”**

has been accepted as satisfactory in partial fulfillment for the degree of

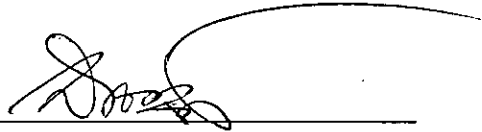
**Master of Science in Engineering (Water Resources)**



**Dr. Md. Abdul Matin**

Professor, Department of Water Resources Engineering  
BUET, Dhaka-1000, Bangladesh

**Chairman**



**Dr. Md. Mirjahan**

Professor and Head, Department of Water Resources Engineering  
BUET, Dhaka-1000, Bangladesh

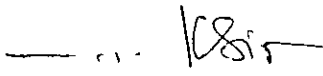
**Member**



**Dr. Md. Monowar Hossain**

Professor, Department of Water Resources Engineering  
BUET, Dhaka-1000, Bangladesh

**Member**



**Dr. M.R. Kabir**

Professor and Pro-Vice Chancellor, University of Asia Pacific  
Dhaka, Bangladesh

**Member  
(External)**

**29 OCTOBER 2008**

## ACKNOWLEDGEMENT

The author feels deep pleasure to express his gratification on the occasion of this thesis paper to the following personalities whose cordial and valuable advice and help contributes to complete the work.

The author feels proud in expressing his deep sense of gratitude and obligation to his respected teacher and supervisor Professor Dr. Md. Abdul Matin, Department of Water Resources Engineering, Bangladesh University of Engineering and Technology, Dhaka for his worthy guidance, valuable suggestion, constructive criticism and helpful comments throughout the whole course of study. His best leveled specialized knowledge and experience helped the author for better understanding and successful completion of this study.

The author also sincerely expresses his heartiest gratitude and indebtedness to Professor Dr. Md. Mirjahan, Head, Department of Water Resources Engineering, BUET; Professor Dr. Md. Monowar Hossain, Department of Water Resources Engineering, BUET and Professor Dr. M.R. Kabir, Pro-Vice Chancellor, University of Asia Pacific for being the honorable members of Examination board and for sparing valuable time to evaluate the thesis paper and putting precious comment and suggestion.

The author feels pleasure to express special thanks to all the teachers of the Department of Water Resources Engineering, Bangladesh University of Engineering and Technology, Dhaka for their helpful advice, support and co-operation through out the work.

Sincere thank is due to Mr. Md. Jahangir Alam for his helpful technical support and heartiest co-operation during the experimental work in Physical Model Laboratory. Thanks are also for other staffs of River Engineering Laboratory and Department of Water Resources Engineering whose respect and kindness made it relaxing and enjoyable throughout the period of study.

Special acknowledgement is due to the author's parent and family members for their well wishes, prayers, encouragement and inspiration during the period of work.

And above all, the author feels the great almighty God, grateful to Him to complete his work successfully.

**Debjit Roy**

**OCTOBER 2008**

## ABSTRACT

Scour around structure is a well known problem for engineers around the world. It has been studied extensively for a long time as a serious threat to human life safety and sever structural damage due to scour results huge economical loss. Most of rivers in Bangladesh are compound in nature and alluvial. Pier like structures are often constructed at floodplain of compound channel which are also subjected to local scour and may cause failure of structure. This current experimental research has been carried out to investigate general behavior of local scour around pier like structure at floodplain of compound channel. Also effect of river bed material on local scour and comparison with main channel local scour characteristics was studied in present work.

A compound channel of 22 m long and 20 cm deep having one adjacent floodplain of 80 cm wide with 165 cm wide main channel has been constructed to conduct present experiment. Flow depth was kept 7 cm on floodplain and 27 cm in main channel considering relative depth ratio ( $Y_r$ ) 0.26. Uniform flow and live bed scour condition has been maintained throughout experiment. General behavior of local scour at floodplain has been investigated for three locally available bed materials having sediment size ( $d_{50}$ ) of 0.75 mm, 0.18 mm and 0.12 mm respectively. Commonly used circular and round nose shaped structures were used in this study. In total 36 experimental runs has been conducted for three discharges (200 l/s, 175 l/s, 150 l/s) and for four length-width ratio ( $l/b=1$  for circular pier and  $l/b=2,3,4$  for round nose pier). To evaluate comparison between floodplain and main channel scour, one structure was placed on floodplain when another one in main channel at a time. Scour map, bed profile, velocity profile,  $V/V_c$  contour map and 3D perspective plot were analyzed for both floodplain and main channel.

Generally maximum scour depth was found for finer bed material at higher discharge. Scour depth significantly decreases with increasing length-width ratio and increases from coarse sediment to finer. Finer bed material resulted more steeper, uniform and deeper scour comparing with coarse sediment. Circular pier scour depth was highest than any other structure shapes. Scour depth varied with velocity variation of flow and an increasing tendency of scour depth has been observed with increasing flow intensity. Flow velocity and scour was always higher in main channel than floodplain. Floodplain velocity distribution is associated with vortex generation as mid of channel. Maximum scour depth has been varied almost linearly with Froude number irrespective of pier shape. An empirical relationship was developed using experimental data to predict floodplain scour depth. Proposed equation has been compared with available scour equations.

# TABLE OF CONTENT

	Page
<i>Acknowledgement</i>	i
<i>Abstract</i>	ii
<i>Table of Content</i>	iii
<i>List of Tables</i>	vii
<i>List of Figures</i>	viii
<i>List of Photographs</i>	xiii
<i>List of Notations</i>	xiv
<b>Chapter 1 INTRODUCTION</b>	
1.1 Background	1
1.2 Objectives with specific aims	4
<b>Chapter 2 LITERATURE REVIEW</b>	
2.1 Introduction	5
2.2 Scour process in river	5
2.3 Aggradation and Degradation	6
2.4 Types of scour	7
2.5 Local scour	8
2.6 Clear water and live bed scour	8
2.6.1 Clear water scour	8
2.6.2 Live bed scour	8
2.7 Threshold condition for sediment motion	10
2.8 Flow and morphology around structure	12
2.9 Relative depth ratio	12
2.10 Local scour mechanism	13
2.11 Variables affecting local scour	16
2.11.1 Fluid property	17
2.11.2 Flow parameters	17
2.11.3 Sediment parameters	17
2.11.4 Pier geometry	18
2.11.5 Time	18
2.11.6 Approach flow velocity	19

	2.11.7	Depth of flow	21
	2.11.8	Temporal development of local scour	22
	2.11.9	Sediment size	25
	2.11.10	Angle of attack	26
	2.11.11	Sediment gradation	27
	2.11.12	Froude number	28
	2.12	Scour formulae	29
	2.13	Assumptions of equations	35
	2.14	Practices of local scour depth prediction in Bangladesh	35
	2.15	Remarks	36
<b>Chapter</b>	<b>3</b>	<b>EXPERIMENTAL FACILITY</b>	
	3.1	Introduction	37
	3.2	Physical model components	37
	3.2.1	Straight flume	37
	3.2.2	Storage pool	39
	3.2.3	Upstream reservoir	39
	3.2.4	Pump	40
	3.2.5	Flow modifying devices at inlet	40
	3.2.6	Tail gate	41
	3.2.7	Sediment trap and downstream reservoir	42
	3.2.8	Re-circulating canal	42
	3.3	Measuring methods and devices	43
	3.3.1	Discharge measurement	43
	3.3.2	Measuring bridge	44
	3.3.3	Velocity meter	45
	3.3.4	Point gauge	46
	3.3.5	Bed Level Measuring Instrument (BLMI)	47
	3.4	Modification of Physical model facility	48
<b>Chapter</b>	<b>4</b>	<b>TEST PROCEDURE AND DATA COLLECTION</b>	
	4.1	Introduction	49
	4.2	Experimental design	49
	4.2.1	Bed material	49

4.2.2	Structure geometry	52
4.2.3	Hydraulic parameters	53
4.2.4	Test duration	54
4.2.5	Test program	56
4.3	Measurement	58
4.3.1	Discharge	58
4.3.2	Water level	58
4.4	Data collection	59
4.4.1	Velocity	59
4.4.2	Maximum scour development	59
4.4.3	Scour depth	60
4.5	Test procedure of experiment	60

## **Chapter 5 EXPERIMENTAL RESULTS AND DISCUSSIONS**

5.1	Introduction	63
5.2	Live bed condition	64
5.3	Maximum scour depth comparison	65
5.4	Equilibrium scour depth and equilibrium time	67
5.5	Analysis of scour and bed profile	71
5.5.1	Scour contour map	71
5.5.1.1	Circular pier (length-width ratio, $l/b=1$ )	72
5.5.1.2	Round nose pier (length-width ratio, $l/b=2$ )	73
5.5.1.3	Round nose pier (length-width ratio, $l/b=3$ )	74
5.5.1.4	Round nose pier (length-width ratio, $l/b=4$ )	75
5.5.2	Bed profile	76
5.5.2.1	Longitudinal cross section bed profile	77
5.5.2.2	Lateral cross section bed profile	78
5.5.2.3	X-Y-Z perspective plot of bed profile	78
5.6	Analysis of velocity	97
5.6.1	Velocity variation in longitudinal direction	98
5.6.2	Velocity variation in lateral direction	98
5.6.3	Velocity variation in vertical direction	99
5.6.4	Velocity vector diagram	118
5.6.5	$V/V_C$ contour map	119



5.7	Analysis of floodplain maximum scour depth	120
5.7.1	Variation of floodplain scour ( $d_s/b$ ) with floodplain flow intensity ( $V_f/V_a$ )	120
5.7.2	Variation of floodplain local scour ( $d_s/b$ ) with flow Froude number ( $F_r$ )	120
5.7.3	Variation of floodplain scour ( $d_s/b$ ) with length-width ratio ( $l/b$ )	122
5.7.4	Variation of floodplain scour ( $d_s/b$ ) with sediment size ( $b/d_{50}$ )	122
5.8	Proposed empirical relationship for floodplain scour prediction	124
<b>Chapter</b>	<b>6 CONCLUSIONS AND RECOMMENDATIONS</b>	
6.1	Introduction	129
6.2	Conclusions	129
6.3	Recommendations for further study	131
	<i>Reference</i>	132
	<i>Appendix A Armour velocity, <math>V_a</math></i>	136
	<i>Appendix B Scour map and photograph</i>	137
	<i>Appendix C Velocity vector</i>	209
	<i>Appendix D <math>V/V_C</math> contour map</i>	245
	<i>Appendix E Sample bed level and velocity data</i>	281

## LIST OF TABLES

	Page
Table 2.1 Pier scour equations	31
Table 3.1 Elevation of the Reference plates	46
Table 4.1 Properties of bed materials used in experiment	51
Table 4.2 Properties of structures used in experiment	53
Table 4.3 Hydraulic parameters of experimental study	54
Table 4.4 Summary of Test program	57
Table 5.1 Experimental values of relative flow velocity with respect to critical flow velocity	64
Table 5.2 Comparison between floodplain scour depths of experimental runs and calculated from developed relationship	125
Table 5.3 Comparison of floodplain scour depth calculated from different equations with experimental values	127

## LIST OF FIGURES

	Page	
Figure 2.1	Types of scour	7
Figure 2.2	Local scour depth variation with time and flow velocity	9
Figure 2.3	Shield's diagram	10
Figure 2.4	Scour and deposition for (a) pier and (b) abutment	13
Figure 2.5	Local scour mechanism around a circular pier	14
Figure 2.6	Scour depth for a pier in a sand bed stream as a function of time	18
Figure 2.7	Local scour depth variation with relative flow velocity for coarse and ripple forming sediment	19
Figure 2.8	Local scour depth variation with flow intensity	20
Figure 2.9	Local scour depth variation with relative flow depth	22
Figure 2.10	Temporal development of local scour depth at piers for clear water	23
Figure 2.11	Equilibrium time scale variation with flow depth, flow velocity and sediment size	24
Figure 2.12	Local scour depth variation with sediment coarseness	25
Figure 2.13	Local scour depth variation with angle of attack	27
Figure 2.14	Local scour depth variation with sediment	28
Figure 3.1	Plan of Physical model facility	38
Figure 3.2	Schematic cross-section of straight flume after modification	48
Figure 4.1	Grain size distribution curves for bed material 1 ( $d_{50}=0.75$ mm), 2 ( $d_{50}=0.18$ mm) and 3 ( $d_{50}=0.12$ mm)	50
Figure 4.2	Comparison between 12 hrs and 8 hrs runs for bed material 1 ( $d_{50}=0.75$ mm), 2 ( $d_{50}=0.18$ mm) and 3 ( $d_{50}=0.12$ mm)	55
Figure 5.1	Comparison between floodplain maximum scour and main channel maximum scour for each run	66
Figure 5.2	Temporal development of scour as a function of time at floodplain for bed material 1 ( $d_{50} = 0.75$ mm)	68
Figure 5.3	Temporal development of scour as a function of time at main channel for bed material 1 ( $d_{50} = 0.75$ mm)	68

Figure 5.4	Temporal development of scour as a function of time at floodplain for bed material 2 ( $d_{50} = 0.18$ mm)	69
Figure 5.5	Temporal development of scour as a function of time at main channel for bed material 2 ( $d_{50} = 0.18$ mm)	69
Figure 5.6	Temporal development of scour as a function of time at floodplain for bed material 3 ( $d_{50} = 0.12$ mm)	70
Figure 5.7	Temporal development of scour as a function of time at main channel for bed material 3 ( $d_{50} = 0.12$ mm)	70
Figure 5.8	Bed profile variation in longitudinal direction for 200 l/s discharge (Floodplain)	79
Figure 5.9	Bed profile variation in longitudinal direction for 200 l/s discharge (Main channel)	80
Figure 5.10	Bed profile variation in longitudinal direction for 175 l/s discharge (Floodplain)	81
Figure 5.11	Bed profile variation in longitudinal direction for 175 l/s discharge (Main channel)	82
Figure 5.12	Bed profile variation in longitudinal direction for 150 l/s discharge (Floodplain)	83
Figure 5.13	Bed profile variation in longitudinal direction for 150 l/s discharge (Main channel)	84
Figure 5.14	Bed profile variation in lateral direction for 200 l/s discharge (Floodplain)	85
Figure 5.15	Bed profile variation in lateral direction for 200 l/s discharge (Main channel)	86
Figure 5.16	Bed profile variation in lateral direction for 175 l/s discharge (Floodplain)	87
Figure 5.17	Bed profile variation in lateral direction for 175 l/s discharge (Main channel)	88
Figure 5.18	Bed profile variation in lateral direction for 150 l/s discharge (Floodplain)	89
Figure 5.19	Bed profile variation in lateral direction for 150 l/s discharge (Main channel)	90

Figure 5.20	X-Y-Z perspective plot for Run 1-Circular Pier ( $l/b=1$ ) Bed material 1 ( $d_{50} = 0.75$ mm)	91
Figure 5.21	X-Y-Z perspective plot for Run 4-Round nose pier ( $l/b=2$ ) Bed material 1 ( $d_{50} = 0.75$ mm)	91
Figure 5.22	X-Y-Z perspective plot for Run 7-Round nose pier ( $l/b=3$ ) Bed material 1 ( $d_{50} = 0.75$ mm)	92
Figure 5.23	X-Y-Z perspective plot for Run 10-Round nose pier ( $l/b=4$ ) Bed material 1 ( $d_{50} = 0.75$ mm)	92
Figure 5.24	X-Y-Z perspective plot for Run 13-Circular Pier ( $l/b=1$ ) Bed material 2 ( $d_{50} = 0.18$ mm)	93
Figure 5.25	X-Y-Z perspective plot for Run 17-Round nose pier ( $l/b=2$ ) Bed material 2 ( $d_{50} = 0.18$ mm)	93
Figure 5.26	X-Y-Z perspective plot for Run 19-Round nose pier ( $l/b=3$ ) Bed material 2 ( $d_{50} = 0.18$ mm)	94
Figure 5.27	X-Y-Z perspective plot for Run 22-Round nose pier ( $l/b=4$ ) Bed material 2 ( $d_{50} = 0.18$ mm)	94
Figure 5.28	X-Y-Z perspective plot for Run 25-Circular Pier ( $l/b=1$ ) Bed material 3 ( $d_{50} = 0.12$ mm)	95
Figure 5.29	X-Y-Z perspective plot for Run 28-Round nose pier ( $l/b=2$ ) Bed material 3 ( $d_{50} = 0.12$ mm)	95
Figure 5.30	X-Y-Z perspective plot for Run 31-Round nose pier ( $l/b=3$ ) Bed material 3 ( $d_{50} = 0.12$ mm)	96
Figure 5.31	X-Y-Z perspective plot for Run 34-Round nose pier ( $l/b=4$ ) Bed material 3 ( $d_{50} = 0.12$ mm)	96
Figure 5.32	Velocity variation in longitudinal direction at Floodplain for Bed material 1 ( $d_{50} = 0.75$ mm)	100
Figure 5.33	Velocity variation in longitudinal direction at Main channel for Bed material 1 ( $d_{50} = 0.75$ mm)	101
Figure 5.34	Velocity variation in longitudinal direction at Floodplain for Bed material 2 ( $d_{50} = 0.18$ mm)	102
Figure 5.35	Velocity variation in longitudinal direction at Main channel for Bed material 2 ( $d_{50} = 0.18$ mm)	103

Figure 5.36	Velocity variation in longitudinal direction at Floodplain for Bed material 3 ( $d_{50} = 0.12$ mm)	104
Figure 5.37	Velocity variation in longitudinal direction at Main channel for Bed material 3 ( $d_{50} = 0.12$ mm)	105
Figure 5.38	Velocity variation in lateral direction at Floodplain for Bed material 1 ( $d_{50} = 0.75$ mm)	106
Figure 5.39	Velocity variation in lateral direction at Main channel for Bed material 1 ( $d_{50} = 0.75$ mm)	107
Figure 5.40	Velocity variation in lateral direction at Floodplain for Bed material 2 ( $d_{50} = 0.18$ mm)	108
Figure 5.41	Velocity variation in lateral direction at Main channel for Bed material 2 ( $d_{50} = 0.18$ mm)	109
Figure 5.42	Velocity variation in lateral direction at Floodplain for Bed material 3 ( $d_{50} = 0.12$ mm)	110
Figure 5.43	Velocity variation in lateral direction at Main channel for Bed material 3 ( $d_{50} = 0.12$ mm)	111
Figure 5.44	Velocity variation in vertical direction at Floodplain for Bed material 1 ( $d_{50} = 0.75$ mm)	112
Figure 5.45	Velocity variation in vertical direction at Main channel for Bed material 1 ( $d_{50} = 0.75$ mm)	113
Figure 5.46	Velocity variation in vertical direction at Floodplain for Bed material 2 ( $d_{50} = 0.18$ mm)	114
Figure 5.47	Velocity variation in vertical direction at Main channel for Bed material 2 ( $d_{50} = 0.18$ mm)	115
Figure 5.48	Velocity variation in vertical direction at Floodplain for Bed material 3 ( $d_{50} = 0.12$ mm)	116
Figure 5.49	Velocity variation in vertical direction at Main channel for Bed material 3 ( $d_{50} = 0.12$ mm)	117
Figure 5.50	Variation of maximum scour with floodplain flow velocity	121
Figure 5.51	Variation of maximum scour depth with Froude number for circular pier	121
Figure 5.52	Variation of maximum scour depth with Froude number for round nose pier	122

Figure 5.53	Variation of maximum scour depth with different length-width ratio of structure for different discharges	123
Figure 5.54	Variation of maximum scour with sediment size for different discharges	123
Figure 5.55	Graphical comparison of floodplain scours depths between experiment and calculated from developed equation	126

## LIST OF PHOTOGRAPHS

		Page
Photograph 3.1	Physical Model Facility	37
Photograph 3.2	Entrance of Physical Model Facility	37
Photograph 3.3	Storage pool and upstream reservoir	39
Photograph 3.4	Pumps	40
Photograph 3.5	Flow divider	41
Photograph 3.6	Baffle wall	41
Photograph 3.7	Tail gates	41
Photograph 3.8	Re-circulating channel, sediment trap and downstream reservoir	42
Photograph 3.9	Rehbok weir and stilling basin with point gauge	43
Photograph 3.10	Measuring bridge with velocity meter fixed on bridge trolley	44
Photograph 3.11	Various components of P-EMS velocity meter	45
Photograph 3.12	Velocity measurement using velocity meter	45
Photograph 3.13	Water level measurement using Point gauge	46
Photograph 3.14	Discharge measuring using Point gauge	46
Photograph 3.15	Bed Level Measuring Instrument (BLMI)	47
Photograph 3.16	Bed level measurement using BLMI	47
Photograph 3.17	During modification	48
Photograph 3.18	After modification	48
Photograph 4.1	Types of structure used in present study	53
Photograph 5.1	Flow around circular pier and round nose pier	97



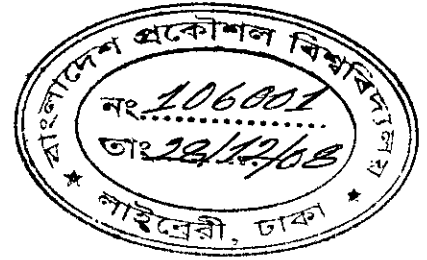
## LIST OF NOTATIONS

$A_l$	parameters describing alignment of pier or abutment
$a$	pier width
$a'$	projected pier width with respect to direction of flow or angle of attack
$B$	foundation width
$b$	pier width
$b_a$	abutment length
$b_p$	pier diameter
$C$	cohesiveness of sediment
$C_d$	coefficient of discharge
$d$	particle diameter
$d_{15.9}$	particle size for which 15.9% are finer by weight
$d_{50}$	median size of sediment particle size distribution
$d_{50}/b$	sediment size
$d_{50a}$	median particle size of armour layer
$d_{84.1}$	particle size for which 84.1% are finer by weight
$d_s$	depth of local scour around pier or abutment
$d_{se}$	equilibrium depth of scour
$Fr$	Froude number
$Fr_c$	Froude number at critical velocity
$f$	"a function of"
$G$	parameter describing effects of lateral distribution of flow in approach channel and cross-sectional shape of approach channel
$g$	acceleration due to gravity
$h$	depth of flow
$K_d$	sediment size factor
$K_G$	channel geometry factor
$K_l$	flow intensity factors
$K_s$	pier or abutment shape factor
$K_t$	time factor
$K_{yB}$	flow depth-foundation size factor
$K_{yb}$	flow depth-foundation size factor for piers

$K_{yL}$	flow depth-foundation size factor for abutments
$K_0$	pier or abutment alignment factor
$K_1$	correction factor for pier nose shape
$K_2$	correction factor for angle of attack
$K_3$	correction factor for bed condition
$K_4$	correction factor for armoring by bed material size
$L$	projected abutment length
$L_{weir}$	length of weir crest
$l$	pier length
$l/b$	pier length to pier width ratio
$l/s$	liter per second
$M$	Constant for a specific river
$n$	Manning's roughness coefficient
$Q$	discharge
$R$	channel hydraulic radius
$Re_s$	grain Reynolds number
$S$	energy level slope
$S_0$	channel slope
$Sh$	parameters describing shape of pier or abutment
$S_s$	specific gravity of sediment particles
$t$	time
$t_e$	time to develop equilibrium depth of scour
$t^*$	dimensionless time scale for local scour
$u_s$	approach bed shear velocity
$u_{*c}$	critical shear velocity
$V$	mean approach flow velocity
$V/V_C$	flow intensity
$V_a$	mean velocity of flow at the "armour peak" for non uniform sediment which is equivalent to $V_C$ for uniform sediment
$V_C$	critical mean approach flow velocity for entrainment of bed sediment
$V_{ca}$	limiting mean velocity of flow for bed sediment armoring for non uniform sediments
$V_f$	floodplain flow velocity

$V_x$	streamwise velocity
$V_y$	transverse velocity
X,Y,Z	Cartesian coordinate system
$Y_r$	relative depth ratio
y	flow depth
$y_f$	floodplain flow depth
$y_1$	flow depth directly upstream of pier
$\gamma$	unit weight of water
$\Delta H$	head above weir crest
$\theta$	alignment to flow or angle of attack
$\theta_c$	critical Shield value
$\nu$	kinematic viscosity
$\sigma_g$	geometric standard deviation of sediment particle size distribution
$\Delta$	relative submerged sediment density
$\rho$	water density
$\rho_s$	sediment density
$\tau$	bed shear stress
$\tau_c$	critical shear stress of bed material
$\tau_o$	minimum shear stress required to move a particular exposed grain on surface of bed

Chapter 1  
INTRODUCTION



1.1 Background

Scour process is complex and subjected to many factors. Relationships for estimating scour depths are inevitably approximate and some aspects of scour processes remain in adequately understood despite many years of scour research. Scant situations of hydraulic engineering are more complex than those associated with scour in vicinity of a pier like structure, especially one located in a compound channel.

Scour is the problem that costs millions of dollars of damage. It leaves infrastructure such as bridge piers and bridge abutments in unsafe conditions requiring maintenance and occasionally results in loss of life. During serious scour events, foundation material below pier footing may be eroded, leaving structure unsupported and in jeopardy of collapse. Scour is a dynamic process. During a single high-flow event, scour may occur during rising stages and near peak. Deposition of sediments into scoured area may occur during falling stages and during low flow. These uncompacted materials are quickly removed during next scour event and foundation material continues to be removed. In effect, scour process progressively deteriorates structural integrity of bridge foundation.

Damage of hydraulic structure is a world wide concern which is mainly caused by local scouring. Problems of local scour and many empirical equations and models have been studied extensively for several decades by many investigators like temporal and equilibrium scour (Melville and Chiew, 1999; Kothari et al, 1992a), clear water and live bed scour (Vittal et al, 1994; Jain, 1981; Kothari et al, 1992b; Laursen, 1962), scour in uniform and non uniform bed materials (Radukivi and Ettema, 1977), scale effect in pier scour (Ettema et al, 1998; Kabir, 1984; Shen et al, 1969) and so on. Again many empirical equations (Kandasamy and Melville, 1998; Laursen, 1998; Melville and Sutherland, 1988; Chang, 1988; Garde and Raju, 1985) and Mathematical models (Laursen, 1996; Dey et al, 1995) are available for predicting pier scour depth, which are usually intended to estimate ultimate scour depth.

Scouring can progressively undermine foundation of a structure. Because, complete protection against scouring, is usually prohibitively expensive. Designer must seek ways to guide and control process to minimize risk of failure. Guidance comes both from controlled studies in laboratories and from field experiences. Despite much study, principles of analysis of scouring are not well established and results of various investigations often show different trends.

Based on experiment, Laursen (1963) developed a formula for prediction of scour for various shapes of bridge pier. But its application is limited because numbers of empirical constants that used in formula are difficult to estimate. Melville (1997) proposed an empirical formula for prediction of maximum scour depth around circular piers. He also applied his formulae for different shaped pier by introducing a shape correction factor,  $K_s$ . Formula for scour prediction methods which are currently practiced in Bangladesh, are mostly developed using experimental results in a single rectangular channel. Khatun (2001) conducted an experiment on local scour around bridge pier in a single rectangular channel using cohesive and non cohesive bed materials and established an empirical relationship to estimate local scour.

Major damages to bridges at flood plain and river crossing occur during floods. Damages are caused for various reasons; main reason is being flood plain scour and riverbed scour at bridge foundations, namely piers and abutments. Bridge scour can lead also to environmental damage, for example excessive bed scour and bank erosion, which may damage downstream spawning beds (Melville and Coleman, 2000)

A compound channel refers to a two-stage channel composed of both main channel and side channel in floodplain. Relative depth ( $Y_r$ ) of compound channel is expressed as ratio of flow depth in side channel (floodplain) to flow depth in main channel. Lyness and Myers (1994) showed that Manning's  $n$  reaches a minimum value at a relative depth of 0.25 for over bank flow. Also Sturm (2004) investigated that relative depth ratio varied from 0.13 to 0.32 for compound channel having one floodplain and a main channel.

Cordoso and Bettess (1999) investigated local scour at bridge abutments that extended different distances onto floodplain in a two-stage channel. They measured time evolution of local scour and ultimate scour depth. Hasan (2003) also conducted similar work on protrusion scour at toe of abutment. Haque and Rahaman (2003) investigated scour around rectangular bridge pier both in rectangular and compound channel for fixed and mobile bed condition. In clear water condition, flat region scour was observed around rectangular pier.

Piers and abutments are integral part of bridge structures that obstruct natural river flow resulting from scouring around them. One of main causes of bridge failure is extensive local scouring around piers and abutments during floods. Also, failure of groins, spur-dikes and guide banks frequently occurs during flood season due to scouring. Structures extended from river banks towards lateral direction are called abutment-like structures. It is very important to estimate maximum scour depth precisely around these structures for safety. Piers are subjected to scour especially at high flood conditions. Scour at bridge piers and abutments are a problem of great importance for bridge designers.

In Bangladesh, most of natural channels are compound in nature, consisting of a main channel and adjoining floodplains. Main channel normally always carries flow and floodplain carries flow only at above bank full stage. Abutment, bridge piers and river crossing towers are often constructed on floodplains which are also subjected to local scour. But no mentionable studies have been conducted to observe behavior of local scour and effect of different bed materials on local scour for flow condition at floodplain. Therefore, in this present study, an attempt has been made to carry out an experiment at a channel with associated floodplain to investigate shape, extent and depth of local scour, effect of different bed materials on local scour. Development of an empirical relationship for estimation of scour depth is also attempted. This relationship has been compared with available methods to assess difference between actual and predicted scour at flood plain flow condition.

The present study will be beneficial for engineers to estimate maximum local scour, provide necessary data and information on scour type and extent in floodplains and will help designer to design pier like structures such as bridge pier, foundation of river crossing towers etc. at floodplain.

## **1.2 Objectives with specific aims:**

Following objectives have been setup for present study:

1. To investigate effect of different bed materials on local scour for different shapes of pier like structure at floodplains of compound channel.
2. To compare local scour around pier like structures placed in main channel as well as at floodplains of compound channel.
3. To develop an empirical relationship to predict local scour around pier like structures at flood plains of compound channel.

## Chapter 2

### LITERATURE REVIEW

#### 2.1 Introduction

Natural channels are compound in nature consisting of a main channel and adjoining floodplains. Main characteristics of this complex flow situation is strong transverse transfer of longitudinal momentum from fast moving flow in main channel to slow moving flow in floodplain. This phenomenon is more pronounced in interface region between main channel and floodplain, where there exists a strong transverse gradient of longitudinal velocity. Because of velocity gradient and anisotropy of turbulence, there are vortices rotating about vertical and horizontal axes along main channel-floodplain interface. These vortices are responsible for transfer of water mass, momentum and species concentration from main channel flow in to floodplain flow. Flow distribution in compound channel and its alteration by bridge pier is an important determinant of equilibrium scour depth. Bridge piers and river crossing towers at flood plain often obstruct flow of floodwater, causing an increase in velocity and development of vortices. Increased velocity and vortices often cause scour near bridge foundations. Damage and failure of bridge and towers caused by scour are problems of national concerns. In this chapter scour around structures are discussed in brief. Purpose of this chapter is to present an overview of relevant theory, scouring process in river, flow and morphological behavior around structures, mechanism, influencing factors etc. on local scour as derived from previous studies.

#### 2.2 Scour process in river

Scour is process of lowering of level of riverbed by water erosion. Amount of this reduction below an assumed natural level (generally riverbed prior to commencement of scour) is termed as depth of scour or scour depth (Melville and Coleman 2000). This scouring process is result of interaction between secondary currents and vortices that occur in conjunction with river features like bends, abrupt flow direction, obstruction, constrictions, confluences, control structures etc. Depth and dimensional extent of scour is dependent upon strength of secondary currents developed at concerned river features.



### 2.3 Aggradation and Degradation

Aggradation, involving building up of bed levels, influences level of scour at a bridge site. Short-term and long-term aggradations are differentiated herein by the terms fill and progressive (or general) aggradation respectively. Progressive aggradation can proceed upstream and/or downstream (Melville and Coleman, 2000).

Degradation is lowering of bed levels over a region generally larger than bridge near-field control volume, where this degradation can proceed in upstream and/or downstream directions. Long-term degradation is described herein as progressive or general degradation (Melville and Coleman, 2000).

Aggradation and Degradation are result of change in a geomorphic control within watershed, which in turn causes a long term change in streambed elevation. Reference surface for aggradation and degradation must be established at some discrete time in river's history.

Determining long term changes at a bridge site is very difficult if historical stream flow data are not available. In such situations, a paleogeomorphologist can evaluate sediment stratigraphy and vegetation to estimate stability and magnitude of past and future geomorphic changes for a particular river. If stream flow data are available, then development of specific gauge, and plots, analysis of rating shifts and analysis of historical changes in streambed elevation are the best means of estimating stability and magnitude of geomorphic changes. Selecting one or more discharges and then analyzes using only measured stage and discharge at each discharge and then plotting a graph of stage-versus-time for each of selected discharges develops specific gage plots. General slope of line will indicate long term change in bed elevation, and irregularity of line indicates changes in roughness or short term changes in bed elevation. Comparing pre flood and flood cross sections will not yield magnitude of long term streambed elevation change. It does yield a combination of long term and short term streambed elevation change, but then only if uncontracted sections (such as approach section) are used, difference between pre-flood and flood cross-sections will also include contraction scour.

## 2.4 Types of Scour

According to Richardson and Davis (1995), total scour at a bridge pier is comprised of three components:

1. General scour at bridge:
2. Contraction scour
3. Local scour at piers and abutments

These three scour components are added to obtain total scour at a pier or abutment. This assumes that each component occurred is independent of other. Considering these components additive adds some conservatism to design. In addition, lateral migration of stream must be assessed when evaluating total scour at bridge piers and abutments.

At any particular bridge site, scouring can be either one or a combination of following types of scour processes, which are shown in flow diagram (Figure 2.1).

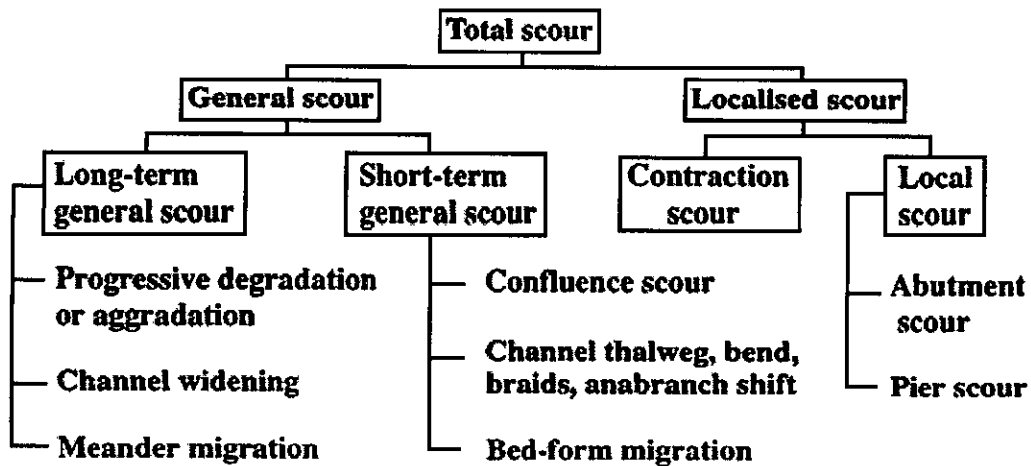


Figure 2.1: Types of scour  
(Source: Melville and Coleman, 2000)

## **2.5 Local scour**

Local scour near an obstruction is caused by vortices and flow acceleration resulting from flow striking obstruction and moving past it. Depth of local scour is difference between where bed would be if obstruction were not present and where bed is with obstruction in place. Concurrent ambient bed surface is preferred reference for local scour determinations. Concurrent ambient bed surface is determined from data collected at time scour hole was measured (concurrent with scour data). This reference surface is typically taken as average of several points measured in vicinity of obstruction but beyond limits of local scour hole (Mueller and Wagner, 2005). Local scour will occur where erodible material is present on streambed. Flow approaches pier or abutment and is deflected down towards channel bed. At bed surface strong vortices form, eroding sediment and forming a local scour hole. Eroded material is transported downstream. Scour hole will continue to deepen until an equilibrium condition is reached.

## **2.6 Clear water and live bed scour**

There are two conditions for contraction and localised scour:

- a. Clear water scour
- b. Live bed scour

### **2.6.1 Clear water scour**

Clear water scour occurs when there is no movement of bed material in flow upstream of crossing or bed material being transported in upstream reach is transported in suspension through scour hole at pier or abutment at less than capacity of flow. At pier or abutment acceleration of flow and vortices created by these obstructions cause bed material around them to move.

### **2.6.2 Live bed scour**

Live bed scour occurs when there is transport of bed material from upstream reach into crossing. Live bed local scour is cyclic in nature; that is, scour hole that develops during rising stage of a flood refills during falling stage.

Clear water scour reaches its maximum over a longer period of time than live bed scour. This is because clear water scour occurs mainly in coarse bed material streams. In fact, local clear water scour may not reach a maximum until after several floods. Maximum local clear water pier scour about 10 percent greater than the equilibrium local live-bed pier scour (Richardson and Davis, 2001)

Clear water scour conditions exist for both uniform and non uniform sediments when flow intensity,  $V/V_c < 1$  or  $[V - (V_a - V_c)]/V_c < 1$ , respectively. Live bed scour occurs for uniform sediment ( $\sigma_g < 1.3$  to 1.5) when  $V/V_c > 1$ . For non uniform sediment ( $\sigma_g > 1.5$ ), armouring occurs on channel bed and in scour hole. Armour layer formation within scour hole reduces local scour depth. The ratio  $V/V_a$  is a measure of flow intensity for scour with non uniform sediments.  $V_a$  which marks transition from clear water to live bed conditions for non uniform sediments is equivalent to  $V_c$  for uniform sediments. Thus, for non uniform sediments, live bed conditions pertain when  $V/V_a > 1$ . Method to determine  $V_a$  for non uniform sediment is described in Melville and Coleman (2000). Variation of local scour depth at piers and abutments with flow velocity and time for both clear water and live bed conditions as evident from laboratory data is shown in Figure 2.2.

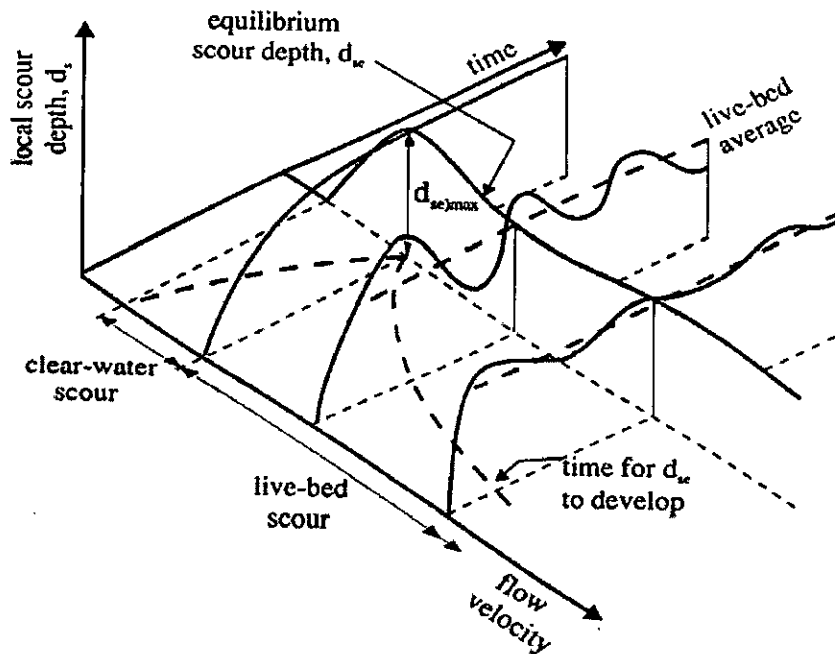


Figure 2.2: Local scour depth variation with time and flow velocity  
(Source: Melville and Coleman, 2000)

## 2.7 Threshold condition for sediment motion

A particle on a river bed will be set in motion when disturbing forces (i.e. drag and lift forces due to over crossing flow) overcome resisting forces (gravity and cohesion). Scour criteria are involved with physical conditions pertaining to threshold of motion for material. Incipient motion analysis based on Shield's diagram (Figure 2.3) can be used to evaluate threshold flow conditions for motion of given sediment.

Shield diagram indicates that for flows less than threshold conditions for boundary material, a channel is stable with no motion of sediment. For flows exceeding these conditions, boundary sediment will be entrained in flow. Depending on continuity of sediment supply along channel, transport of sediment may not necessarily result in erosion of channel boundary.

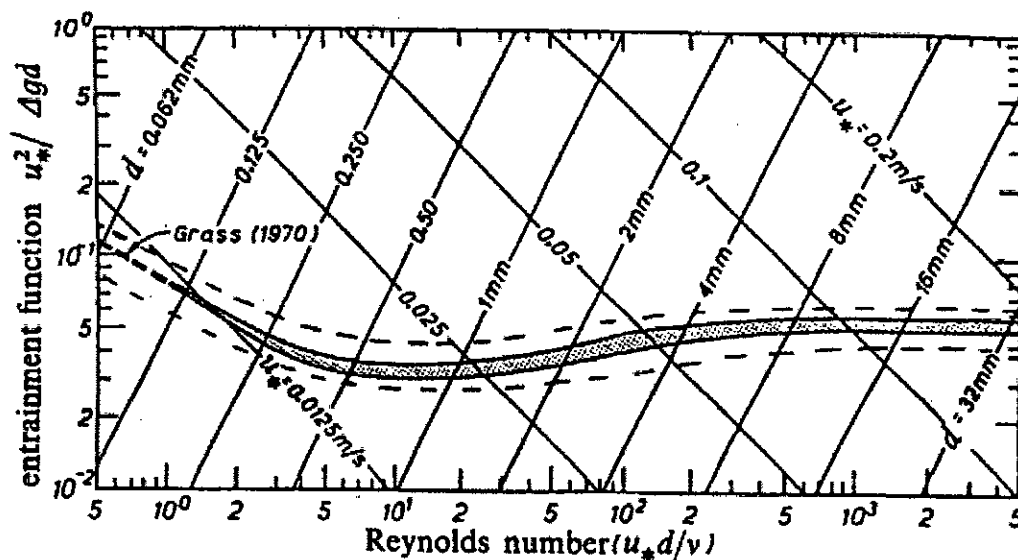


Figure 2.3: Shield's diagram

(Source: Breusers and Raudkivi, 1991)

Shield's diagram depicts relation between grain Reynolds number ( $Re_*$ ) and critical Shield value ( $\theta_c$ ) defined as below:

$$Re_* = \frac{u_* d}{\nu} \quad (2.1)$$

$$\theta_c = \frac{u_*^2}{g\Delta d} = \frac{\tau}{[(S_s - 1)\rho g d]} \quad (2.2)$$

Where,

$$u_* = \text{shear velocity} = \sqrt{ghS}$$

$$\Delta = \frac{\rho_s - \rho}{\rho} = \text{relative submerged sediment density}$$

$\rho_s$  = sediment density

$\rho$  = water density

d = particle diameter

Thus, Shield's diagram describes incipient flow conditions in terms of a critical shear stress,  $\tau_c = \rho U_{*c}^2$ , associated with incipient entrainment of bed sediment.

However, a critical mean channel velocity of flow ( $V_c$ ) that will transport bed material of size  $d_{50}$  and smaller is also preferred to describe incipient sediment motion. It can be determined from critical shear velocity using:

$$\frac{V_c}{u_{*c}} = \left( \frac{R^{\frac{1}{3}}}{gn^2} \right)^{\frac{1}{3}} \quad (2.3)$$

$$\text{or, } \frac{V_c}{u_{*c}} = 5.75 \log \left[ 5.53 \frac{y}{d_{50}} \right] \quad (2.4)$$

Critical shear velocity  $u_{*c}$  for a particular  $d_{50}$  size can be determined from Shield's diagram or using following formulae:

$$u_{*c} = 0.0115 + 0.0125d_{50}^{1.4} \quad \text{for } 0.1 \text{ mm} < d_{50} < 1 \text{ mm} \quad (2.5)$$

$$u_{*c} = 0.0305d_{50}^{0.5} - 0.0065d_{50}^{-1} \quad \text{for } 1 \text{ mm} < d_{50} < 100 \text{ mm} \quad (2.6)$$

Alternatively, various empirical relations exist for critical mean velocity of flow at threshold condition for sediment movement. Following equation is given by Neill (1968):

$$V_c = 1.41[(S_s - 1)gd_{50}]^{0.5} \left( \frac{y}{d_{50}} \right)^{\frac{1}{6}} \quad (2.7)$$

With  $S_s=2.65$  for quartz sediment, above equation can be simplified to:

$$V_c = 5.67y^{\frac{1}{6}}d_{50}^{\frac{1}{3}} \quad (2.8)$$

## 2.8 Flow and morphology around structure

Structures like bridge pier and abutment obstruct and change incoming flow field that also cause changes in initial bed configuration. With passage of time an equilibrium stage is reached with sufficient scour depth around those structures. If such scour extends below foundation level structure will collapse. So study of flow field and resultant morphological effect around piers and abutments is important to protect any foundation. Such study will ultimately lead to choose necessary protection measures against such phenomenon.

## 2.9 Relative depth ratio

A compound channel refers to a two-stage channel composed of both main channel and side channel in floodplain. According to Lyness and Myers (1994), Relative depth ( $Y_r$ ) of compound channel is expressed as the ratio of flow depth in side channel (floodplain) to the flow depth in main channel.

$$\text{i.e. } Y_r = \frac{\text{Flow Depth on Floodplain}}{\text{Total Flow Depth}} \quad (2.9)$$

They also showed that Manning's  $n$  reaches a minimum value at a relative depth of 0.25 for overbank flow. Also Sturm (2004) investigated that the relative depth ratio varied from 0.13 to 0.32 for compound channel having one floodplain and a main channel.

## 2.10 Local scour mechanism

Basic mechanism causing local scour at piers or abutments is formation of vortices (known as horseshoe vortex) at their base. Horseshoe vortex results from pileup of water on upstream surface of obstruction and subsequent acceleration of flow around nose of pier or abutment. Action of vortex removes bed material from around base of obstruction (Figure 2.4a and 2.4b). Transport rate of sediment away from base region is greater than transport rate into region and consequently a scour hole develops. As depth of scour increases, strength of horseshoe vortex is reduced, thereby reducing transport rate from basin region. Eventually for live bed local scour, equilibrium is reestablished between bed material inflow and outflow and scouring ceases. For clear water scour, scouring ceases when shear stress caused by the horseshoe vortex equals critical shear stress of sediment particles at bottom of scour hole.

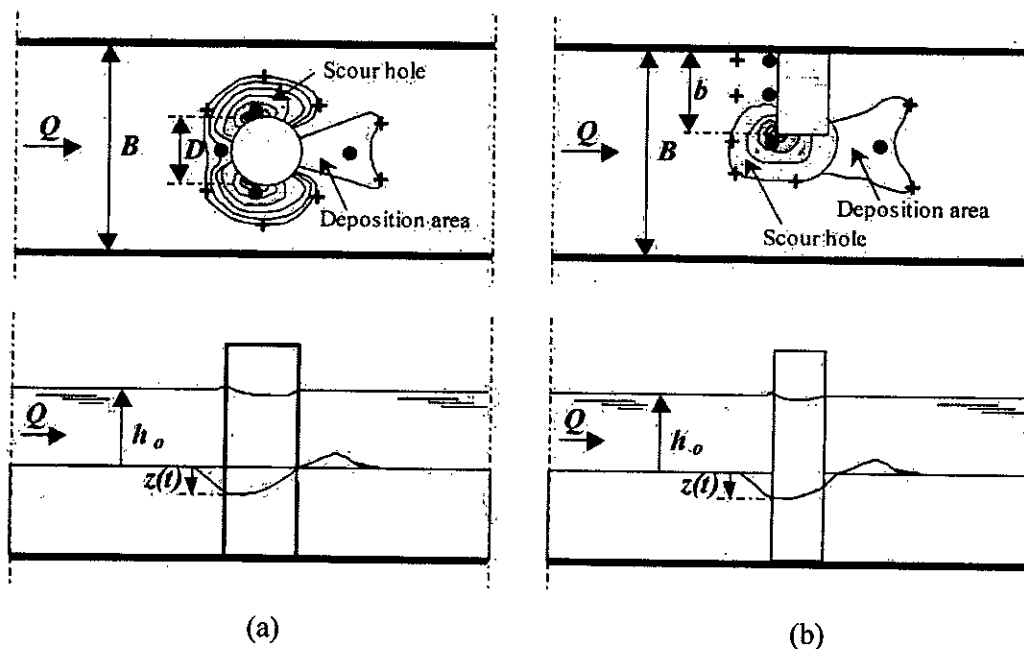


Figure 2.4: Scour and deposition for (a) pier and (b) abutment

(Source: Oliveto and Hager, 2002)

In addition to horseshoe vortex around base of a pier, there are vertical vortices downstream of pier called wake vortex. Both horseshoe and wake vortices remove material from pier base region. However, intensity of wake vortices diminishes rapidly as downstream of pier increases. Therefore, immediately downstream of a long pier there is often deposition of material.



Following four mechanisms associated with local scour at piers are illustrated in Figure 2.5a, 2.5b and 2.5c:

- Down flow in front of pier
- Wake and cutoff vortices
- Horseshoe vortex and
- Surface roller

Local shear stresses and initial scour holes propagate upstream around perimeter of pier to meet centerline (Melville, 1975).

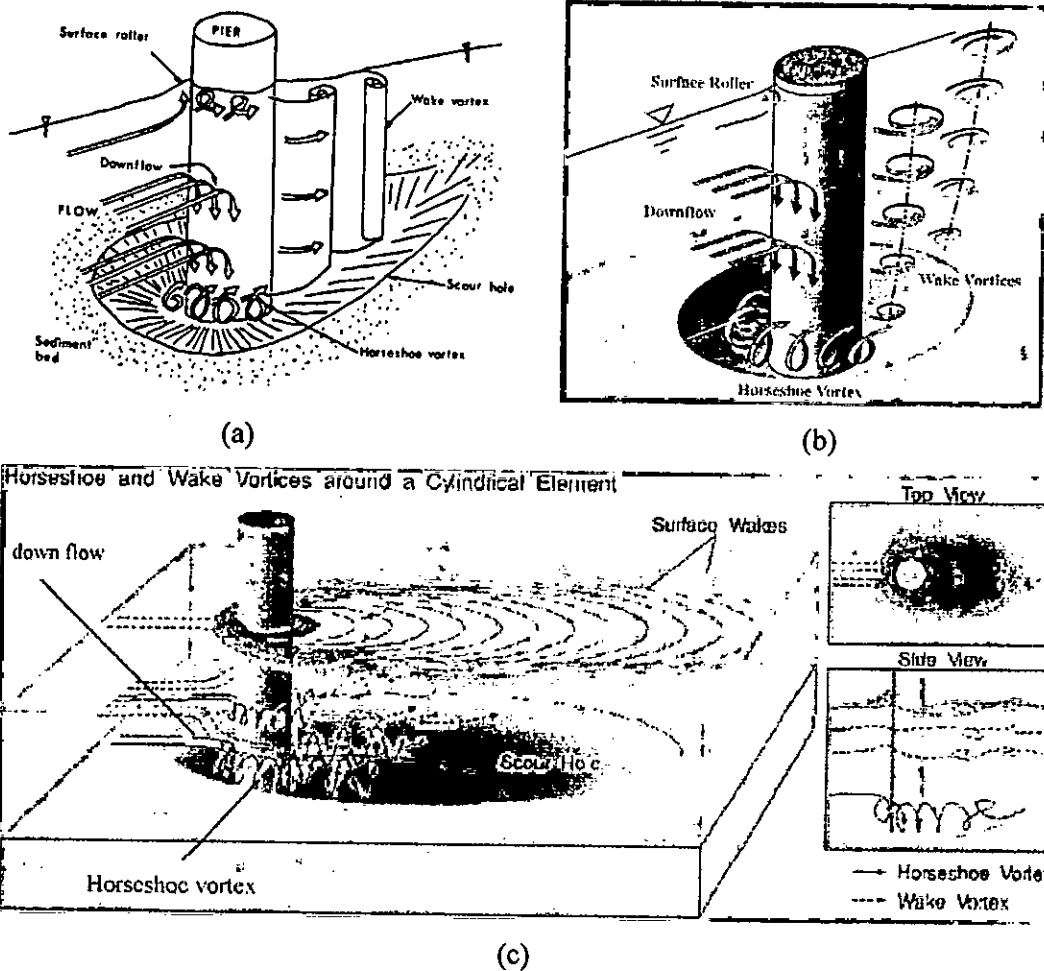


Figure 2.5: Local scour mechanism around a circular pier  
 (Source: (a) Breusers and Raudkivi, 1991, (b) Melville and Coleman, 2000 and  
 (c) Internet)

Subsequent development of scour hole is due to strong down-flow in front of cylinder. At upstream of pier, approach flow velocity goes to zero and stagnation pressure decreases. This caused a downward pressure gradient that drives down-flow at upstream face of pier. Maximum velocity of down-flow reaches 0.8 times mean approach flow velocity and occurs in scour hole at about one pier diameter below bed level. Down-flow acts like a vertical jet and removes sediment at face of pier (Breusers and Raudkivi, 1991).

Horseshoe vortex forms due to separation of flow at upstream rim of scour hole. This extends downstream, past sides of pier before becoming part of general turbulence. Horseshoe vortex is a consequence of scour, not cause of it, and its spiral motion acts to carry away material eroded by down-flow. In describing development of horseshoe vortex and scour hole, Melville (1975) made following observation:

- Horseshoe vortex is initially small and roughly circular in cross section and comparatively weak
- With formation of scour hole, vortex rapidly grows in size and strength as additional fluid attains a downward component and strength of down-flow increases.
- Horseshoe vortex moves down into developing scour hole and expands as hole enlarges.
- When scour hole enlarges further, circulation associated with horseshoe vortex increases, due to expanding cross-sectional area, but at a decreasing rate.

In contrast to observations made by Melville (1975), Baker (1980) stated that initial circulation is equal to circulation within equilibrium scour hole. This implies that circulation associated with horseshoe vortex remains constant throughout development of scour hole (Chiew, 1984).

Wake and cutoff vortices occur where flow separates at sides of pier, that is, at interfaces to main flow. Velocity of vortices increases until it regains free stream velocity about eight times cylinder diameter downstream of pier (Melville, 1975).

Surface roller develops at surface of flow with rotation in opposite direction to that in horseshoe vortex. It is important in relatively shallow flows as it interferes with approach flow and reduces strength of down-flow.

### 2.11 Variables affecting local scour

There are many inter-related parameters on which local scour around bridge pier is dependent. The functional relationship between local scour depth and its dependent parameters can be written as:

$$d_s = f[\text{Flood flow } (\rho, \nu, V, y, G, g), \text{ Bed sediment } (d_{50}, \sigma_g, \rho_s, V_c), \text{ Bridge geometry } (B, Sh, Al), \text{ Time } (t)] \quad (2.10)$$

Where  $\rho$  and  $\nu$  = fluid density and kinematic viscosity, respectively;  $V$  = mean approach flow velocity;  $y$  = flow depth;  $G$  = parameter describing effects of lateral distribution of flow in approach channel and cross-sectional shape of approach channel;  $g$  = acceleration of gravity;  $d_{50}$  and  $\sigma_g$  = median size and geometric standard deviation of sediment particle size distribution;  $\rho_s$  = sediment density;  $V_c$  = critical mean approach flow velocity for entrainment of bed sediment;  $B$  = foundation width, where  $B \equiv b$ , pier width for piers and  $B \equiv L$ , projected abutment length, including approach embankment (measured perpendicular to flow), for abutment;  $Sh$  and  $Al$  = parameters describing shape and alignment of pier or abutment;  $t$  = time; and  $f$  denotes "a function of".

Assuming constant relative density of sediment and absence of viscous effect, i.e. neglecting  $\rho$ ,  $\rho_s$  and  $\nu$ , equation 2.11 can be written as:

$$\frac{d_s}{B} = f\left(\frac{V}{V_c}, \frac{y}{B}, \frac{B}{d_{50}}, \rho_g, Sh, Al, G, \frac{Vt}{B}, \frac{V}{\sqrt{gB}}\right) \quad (2.11)$$

First three parameters on right hand side of equation represent, respectively: Stage of sediment transport on approach flow bed, termed *flow intensity*; depth of flow relative to size of foundation, termed as *flow shallowness*; and foundation size relative to sediment median size, termed as *sediment coarseness*. Last two terms are a time scale for development of scour ( $Vt/B$ ) and a Froude number,  $Fr_B$  based on foundation size. A similar relation is obtained if  $d_s$  and  $d_{50}$  are normalized using  $y$  rather than  $B$ .

### 2.11.1 Fluid property

In fluid mechanics, a fluid can be defined in terms of its density ( $\rho$ ) and kinematic viscosity ( $\nu$ ), both of which are dependent on temperature. Under laboratory conditions, temperature can be controlled and data usually relate to constant temperature. Nevertheless, in field, temperature could have a bearing on scour depth through its influence on fluid properties. No data are available, however, to ascertain extent of influence of temperature on scour depth.

### 2.11.2 Flow parameters

Flow of a fluid is empirically analyzed by its mean depth ( $y$ ), channel slope ( $S_o$ ) and gravitational acceleration ( $g$ ). In uniform flow, shear stress ( $\tau_o$ ) associated with a certain channel slope and flow depth can be expressed as follows:

$$\tau_o = \gamma y S_o \quad (2.12)$$

or more conveniently as shear velocity ( $u_*$ )

$$u_* = \sqrt{g y S_o} \quad (2.13)$$

When flow over an initially plane bed of granular material exceeds critical velocity associated with entrainment of bed material, bed features are formed. With formation of these bed features resistance of bed will increase. Einstein and Barbarossa (1952) suggested a resistance relationship by considering total resistance of a bed with bed features to be sum of surface (or grain) resistance and form resistance due to bed features (Chiew, 1984).

### 2.11.3 Sediment parameters

Sediment can be defined in terms of its specific gravity and sieve diameter of its particles. Uniformity of particle size distribution can be defined by its geometric standard deviation ( $\sigma_g$ ). Other factors, which come into consideration, are cohesiveness of sediment ( $C$ ), shape factor ( $Sh$ ), angle of repose, fall velocity etc.

#### 2.11.4 Pier geometry

Effect of pier are mainly determined by its size although there are other effects, which may be significant, such as shape of pier, angle of attack of flow with respect to pier axis, ratio of channel width to pier width, aspect ratio, surface condition of pier, orientation of pile group (in case of a piled foundation), blockage of flow channel by debris collecting at pier.

#### 2.11.5 Time

Scouring is a process in which scour geometry of sediment bed approaches its new equilibrium shape gradually. Consequently, it takes time for such equilibrium to be established. This is especially significant in case of flood. Duration of flood determines if flood peak lasts long enough to establish maximum scour depth. Particularly duration of early stages of flood recession may be important. This is because maximum scour depth can occur during early stages of receding flood at which stage, elevation of bed level is at its lowest level due to general scour and with decreasing flow and general sediment transport is reduced to such an extent that clear water scour condition can prevail. At this time, rate of scour development can have an important role on maximum scour depth. Figure 2.6 represents scour depth of a pier for both clear water and live bed scour as a function of time.

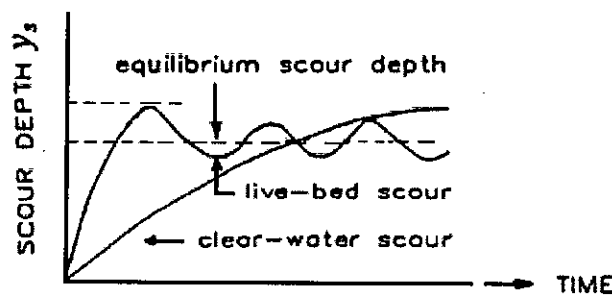


Figure 2.6: Scour depth for a pier in a sand bed stream as a function of time  
(Source: Breusers and Raudkivi, 1991)

### 2.11.6 Approach flow velocity

No local scour was observed at low flow velocities,  $u_* / u_{*c} < 0.5$ , by Hancu (1971), Nicollet (1971) and Verstappen (1978), where  $u_* / u_{*c}$  is relative shear velocity in which  $u_*$  is bed shear velocity and  $u_{*c}$  is critical shear velocity for particle entrainment (Chiew, 1984). Chabert and Engeldinger (1956), Maza Alvarez and Sanchez Bribiesca (1966, 1967, 1968), Hancu (1971), Nicollet (1971) and Ettema (1980) found, from their clear water experiments that local scour depth increases almost linearly with increasing values of shear velocity from  $u_* / u_{*c} = 0.5$  to  $u_* / u_{*c} = 1.0$  (Chiew, 1984).

Local scour depth under live bed condition was found to remain constant at about 90% of maximum scour depth at critical velocity by Chabert and Engeldinger (1956) and Laursen (1958, 1962). Chee (1982) carried out a series of experiments and recognized that trend of increasing scour depth with flow velocity was only true for a certain range of velocities. He discovered that second peak of scour is less than first peak for non-ripple forming sediments and reverse is true for ripple forming sediments (Figure 2.7).

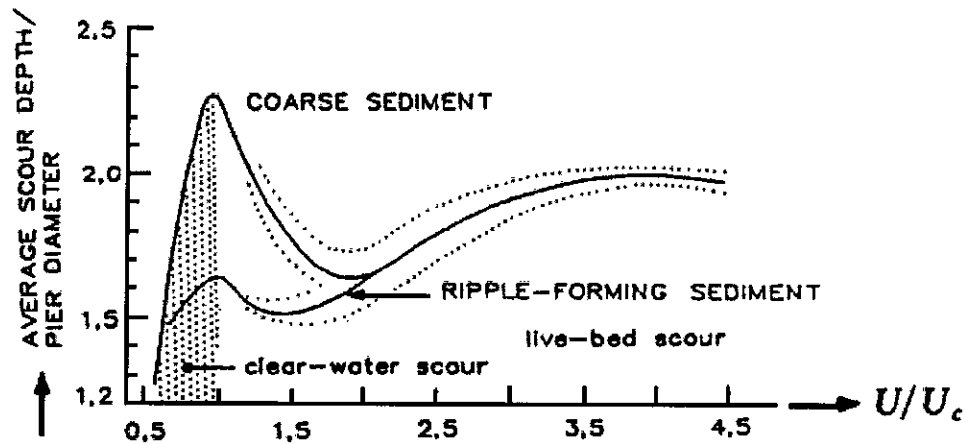


Figure 2.7: Local scour depth variation with relative flow velocity for coarse and ripple forming sediment

(Source: Breusers and Raudkivi, 1991)

Raudkivi (1986), Melville and Sutherland (1988) found that clear water condition exists for both uniform and non-uniform sediments when flow intensity,  $V/V_c < 1$  or  $[V - (V_a - V_c)]/V_c < 1$ , respectively. Live bed scour occurs for uniform sediment ( $\sigma_g < 1.3$  to 1.5) when  $V/V_c > 1$  and for non-uniform sediment when  $V/V_a > 1$ . If  $V/V_a < 1$ , for non-uniform sediment, armoring of bed occurs as scour proceeds and clear water conditions are considered to exist. Variation of local scour depth at pier with flow intensity as evident from laboratory data is shown in Figure 2.8. Under clear water conditions, local scour depth in uniform sediment increases almost linearly with velocity to a maximum at threshold peak. Maximum scour depth is called threshold peak. As velocity exceeds threshold velocity, local scour depth in uniform sediment first decreases and then increases again to a second peak, change being relatively small, but threshold peak is not exceeded providing sediment is uniform. Second peak occurs at about transition flat bed stage of sediment transport on channel bed and is termed as live bed peak. As velocity exceeds threshold velocity, local scour depth in uniform sediment first decreases and then increases again to a second peak, change being relatively small, but threshold peak is not exceeded providing sediment is uniform. Second peak occurs at about transition flat bed stage of sediment transport on channel bed and is termed as live bed peak.

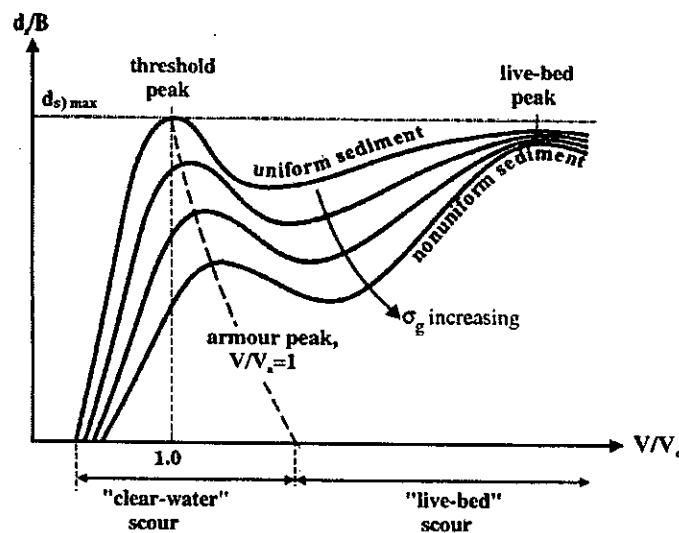


Figure 2.8: Local scour depth variation with flow intensity  
(Source: Melville and Coleman, 2000)

These trends have been observed by others, including Chabert and Engeldinger (1956), Grade et al (1961), Shen et al (1966), Maza Alvarez (1968), Gill (1972), Ettema (1980), Raudkivi and Ettema (1983), Chiew (1984), Baker and Dongol (1994) (after Melville and Coleman, 2000). Thus in laboratory, maximum local depth in uniform sediments occurs at threshold condition and live bed scour depth is largely

independent of flow velocity. This fact is acknowledged in many other studies, including Laursen and Toch (1956), Shen et al (1969), Shen (1971) and Breusers et al (1977) (after Melville and Coleman, 2000). Under live bed conditions, scour depth variation are a consequence of size and steepness of bed features occurring at particular flow velocities (Chiew (1982), Chiew (1984), Melville (1984), Raudkivi (1986), Melville and Sutherland (1988), Dongol (1994) [after Melville and Coleman, 2000]). The steeper and higher the bed forms, the lesser the observed scour depth, because of sediment supplied with passage of a given bed form is not fully removed from scour hole prior to arrival of next bed form. Live bed peak occurs at about transition flat bed condition when bed forms are very long and of negligible height. Antidunes dissipate some energy at higher velocities and local scour depth appears to decrease again. Magnitude of scour depth fluctuations due to bed form migration is approximately equal to half amplitude of bed forms, indicating that scour depth due to bed forms is about one half the bed form height (Shen et al (1966), Chee (1982), Chiew (1984), and Dongol (1994) [after Melville and Coleman, 2000]).

#### **2.11.7 Depth of flow**

Relatively wide pier compared to shallow flows or shallow flows compared to pier, scour depth increases proportionately with  $y$  and is independent of  $B$ , because of with decreasing flow depth, surface roller becomes more dominant and renders base vortices less capable of entraining sediment. Again for deep flows compared to pier or for narrow piers, scour depth increases proportionately with foundation size and is independent of  $y$  as strength of horseshoe vortex and associated down flow is related to transverse size of pier. While for intermediate depth of flows,  $d_s$  depends on both  $y$  and  $B$  due to reason that flow depth influences local scour depth when horseshoe vortex or principal vortex are affected by formation of surface roller. These trends are shown schematically in Figure 2.9 and also supported by laboratory data of many researchers including Chabert and Engeldinger (1956), Laursen and Toch (1956), Laursen (1963), Hancu (1971), Bonasoundas (1973), Basak (1975), Breusers et al (1977), Jain and Fischer (1979), Ettema (1980), Chee (1982), Chiew (1984) and Raudkivi (1986) for piers (after Melville and Coleman, 2000).



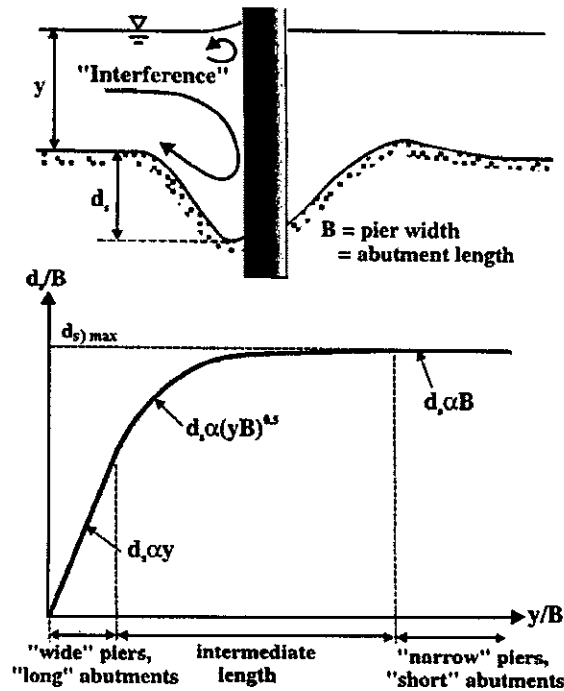


Figure 2.9: Local scour depth variation with relative flow depth  
(Source: Melville and Coleman, 2000)

### 2.11.8 Temporal development of local scour

Under clear water scour conditions, scour depth develops asymptotically towards equilibrium depth of scour. In order to achieve equilibrium conditions in small scale laboratory experiments of clear water condition, it is necessary to run experiments for several days. Data obtained for lesser times say 10 to 12 hours can exhibit scour depths less than 50% of equilibrium scour depth. Most equations for depth of local scour give equilibrium depth and are, therefore, conservative regarding temporal effects. Under live bed conditions, equilibrium is reached more quickly and thereafter scour depth oscillates due to passage of bed features past pier (Figure 2.2). Chiew and Melville (1996, 1999) presented many laboratory data that describes temporal development of local scour at circular bridge piers (of diameter  $D$ ) under clear water conditions. Figure 2.10 shows that local scour depths at same stage of development ( $t/t_e$ , where  $t_e$  is time to develop equilibrium depth of scour) are reduced at lower values of  $V/V_c$ .

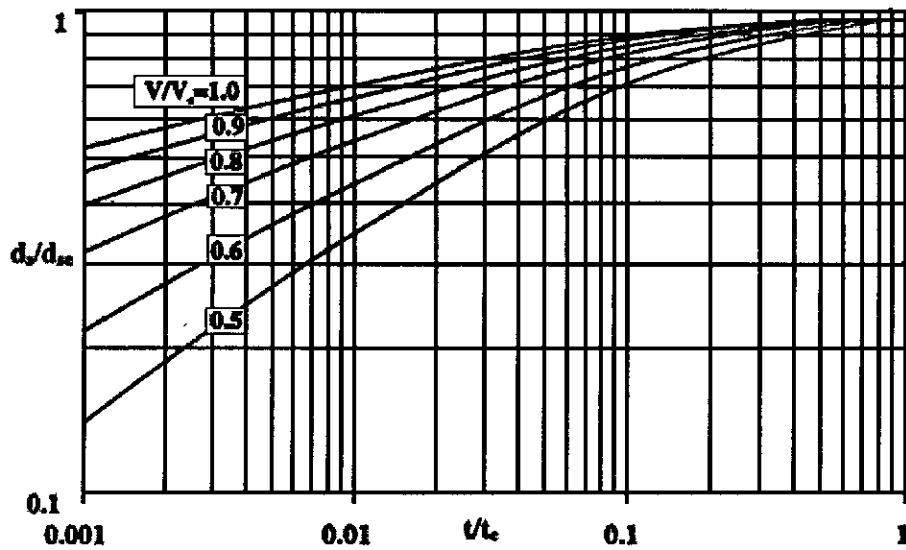


Figure 2.10: Temporal development of local scour depth at piers for clear water  
(Source: Melville and Chiew, 1999)

Melville and Chiew (1999) show also that both  $t_e$  and  $d_{se}$  are subjected to similar influences of flow and sediment properties, as might be expected because they are inherently interdependent. Figure 2.11 shows dependence of a dimensionless equilibrium time scale  $t^*(Vt_e/b)$  on flow shallowness ( $y/b$ ), flow intensity ( $V/V_c$ ) and sediment coarseness ( $b/d_{50}$ ). Equilibrium time scale increases with  $y/b$  for shallow flows and becomes independent of  $y/b$  for deep flows. Equilibrium time scale increases rapidly with flow intensity for clear water scour conditions, attaining a maximum value at threshold condition and at higher live bed flows,  $t^*$  is expected to rapidly decrease again. Also  $t^*$  increases asymptotically with  $b/d_{50}$ .

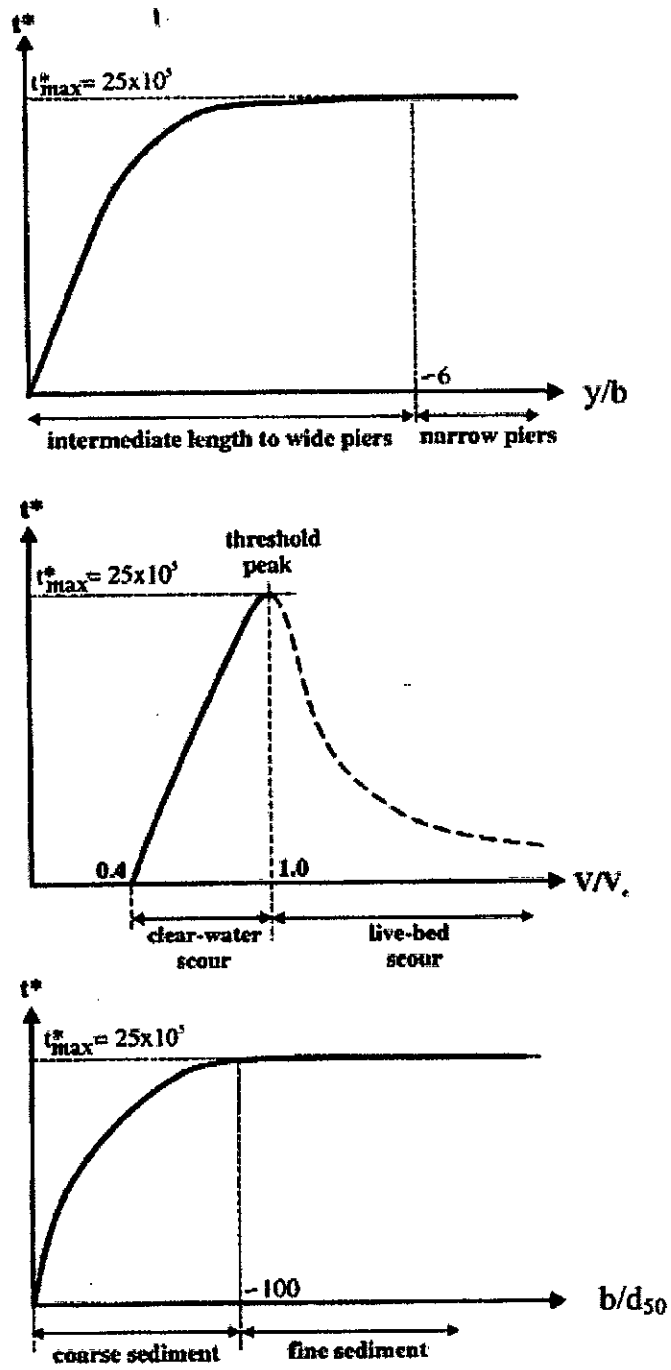


Figure 2.11: Equilibrium time scale variation with flow depth, flow velocity and sediment size

(Source: Melville and Colleman, 2000)

### 2.11.9 Sediment size

For uniform sediments, local scour depths are unaffected by sediment coarseness ( $b/d_{50}$ ) unless sediment is relatively large (Figure 2.12). Ettema (1980) explained that for smaller values of sediment coarseness ratio, individual grains are large relative to groove excavated by down flow. When  $b/d_{50} < 8$ , individual grains are so large relative to pier that scour is mainly due to erosion at sides of pier and scour is further reduced. Experiments satisfy same for sediment size influence on local clear water scour at piers (Ettema, 1980) and for live bed scour at piers (Chiew, 1984).

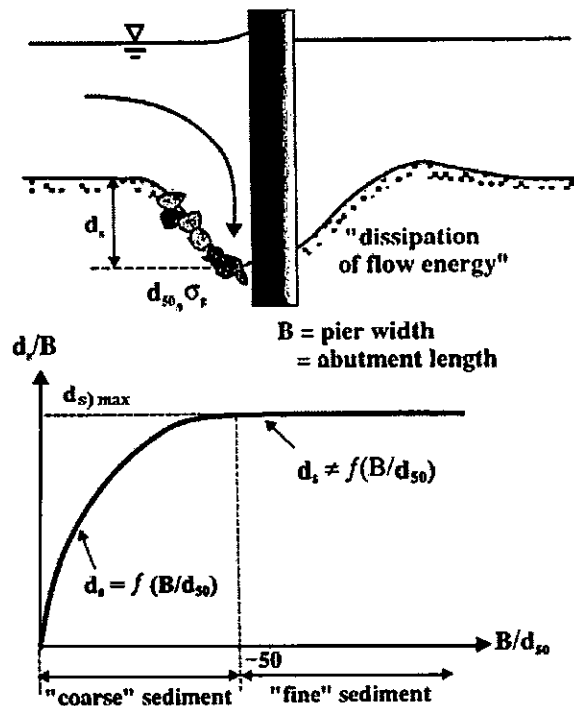


Figure 2.12: Local scour depth variation with sediment coarseness

(Source: Melville and Coleman, 2000)

According to Ettema (1998), sediment size limit for cohesion less sediments exists because there is a natural size range in which accumulations of alluvial particles behave cohesionlessly. Range extends from fine silts of about 0.66 mm up to boulders. Numerous river sides have sediments with average particle size of about 0.1 to 10 mm. therefore, a laboratory experiment to replicate scour in, say, a sand bed

river must use a flume fitted with sand and have nominally same particle size as sand in river. Cohesive behavior of sediment much finer than about 0.1 mm precludes their use to simulate a bed of cohesion less sediment finer than about 0.6 mm. such sediment has a propensity to form ripples, because particles are small relative to viscous layer formed by flow over a bed of such particles. Sediments coarser than about 0.6 mm do not form ripple and difficulties may ensue when one simulate sediment that does not form ripple using one that does. Formation of ripples with fine sands ( $d_{50} < 0.7$  mm) limits scour depth observed in laboratory experiments under clear water conditions with relatively coarse sand because ripples can form at sub-threshold conditions with associated sediment transport.

#### 2.11.10 Angle of attack

Depth of local scour for all shapes of pier, except circular, is strongly dependent on alignment to flow,  $\theta$ . As angle increases scour depth increases because effective frontal width of pier is increased. Laursen and Toch's (1956) chart of multiplying factor  $K_\theta$  given in Figure 2.19 is recommended to be used with most existing pier scour equations.  $K_\theta$  values are obtained by normalizing measured scour depth with value at  $\theta = 0^\circ$ . The chart was derived for rectangular piers but can be used for other shapes with care. Data on which the chart is based have never been published. Ettema et al (1998) show that Figure 2.13 is reasonably consistent with new laboratory data (Mostofa, 1994) and also reflect that maximum scour depths at skewed piers of low aspect ratio (small  $l/b$ ) occurs at skew angles slightly less than  $90^\circ$ . Figure 2.17 demonstrates that local scour depth at a rectangular pier with  $l/b = 8$  is nearly tripled at an angle of attack of  $30^\circ$ .

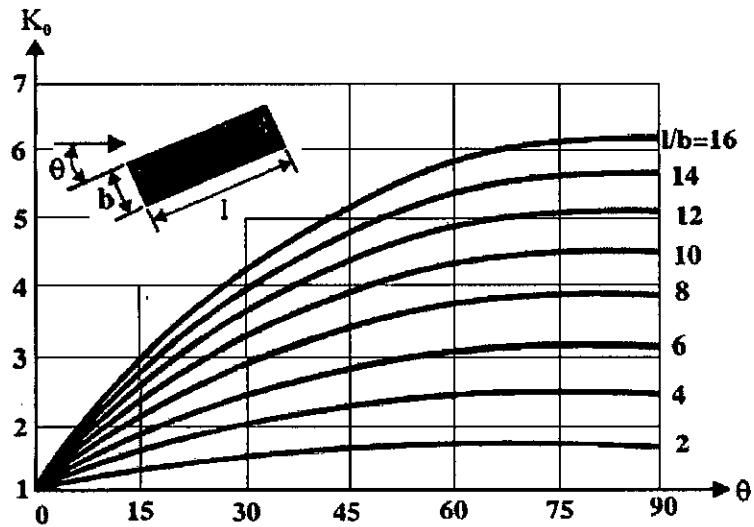


Figure 2.13: Local scour depth variation with angle of attack

(after Laursen and Toch, 1956)

(Source: Melville and Coleman, 2000)

#### 2.11.11 Sediment gradation

Ettema (1976, 1980) carried out systematic laboratory studies of effects of sediment non-uniformity on local scour depth under clear water conditions at piers. Chiew (1984) and Baker (1986) conducted similar experiments under live bed conditions for pier scour. Figure 2.14 summarizes trends evident from those studies.

Around threshold condition  $V/V_c \approx 1$  armouring occurs on approach flow bed and at base of scour hole. Armoured bed in erosion zone at bed of scour hole significantly reduces local scour depth. Conversely, at high values of  $V/V_c$ , when flow is capable of entraining most grain sizes within non-uniform sediment, sediment non-uniformity has only a minor effect on scour depth. Conversely, at high value of  $V/V_c$ , effect of non-uniformity reduces progressively with increasing flow velocity between these two limits, as more or more of grains are transported by flow.

**Zone I: Armour Layer Formation**  
**Zone II: Progressive Break-up of Armour**  
**Zone III: All Particle Sizes in Motion**

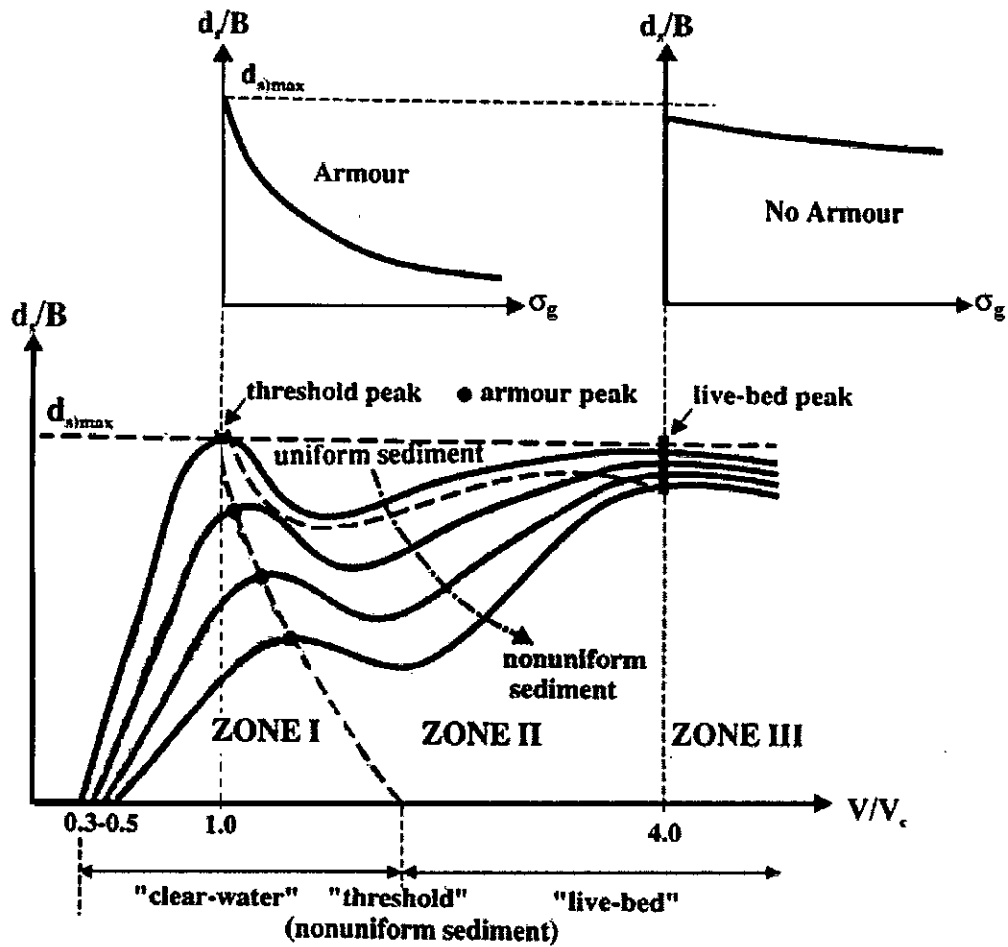


Figure 2.14: Local scour depth variation with sediment  
 (Source: Melville and Coleman, 2000)

### 2.11.12 Froude number

An investigation by Jain and Fischer (1979) concluded that scour depth under live bed conditions is influenced by flow velocity and results of experiments were presented by plotting scour depth versus Froude number,  $Fr$ . They conducted that for  $Fr > Fr_c$  (Froude number at critical velocity), scour depth first slightly decreases and then increases with an increase in Froude number. Scour depths at high Froude numbers were found to be higher than maximum clear water scour depth. Since Froude number is a linear function of approach velocity, it can be said that for a given approach

depth, scour depth is directly proportional to approach velocity. Positive relationship between scour depth and Froude number has been used in various empirical equations as suggested by Shen et al, Chitale and Bata (Kabir, 1984 and Kabir et al, 2000).

Scour depth at piers does not scale linearly with pier width unless there is more or less complete geometric similitude of pier, flow and bed sediment particles (Ettema et al, 1998). Many laboratory experiments have been undertaken to model sand bed river but model bed material relative to pier size is larger than its scaled counterpart in field. To ensure similitude of state of bed mobility requires that value of  $V/V_c$  be maintained same in laboratory and field, implying that flow velocity used in laboratory experiments may be larger than that for corresponding field conditions. Ettema et al (1998) shows that scour depth relative to pier width may increase with pier Froude number,  $V/(gb)^{0.5}$ . Flow field similitude requires preservation of flow patterns such that pressure head along flow path scale directly proportional with geometric scale relating a model pier in laboratory to a pier in field. For same stagnation head  $V^2/2g$ , steeper gradients occur at narrower piers and induce a smaller value of  $d_s/b$  than a wider pier.

## 2.12 Scour formulae

Local pier scour has been a popular topic of study for many laboratory researchers. A literature review by McIntosh (1989) found that more than 35 equations had been proposed for predicting depth of scour at a bridge pier. But there is found no specific equation to predict local scour on flood plain. Indeed local scour of piers on flood plain are calculated by equation of bridge piers. Most local scour equations are based on research in laboratory flumes with non cohesive, uniform bed material and limited verification of results with field data. For estimation of depth of local scour at bridge piers, numerous equations have been proposed and are arranged in Table 2.1.

Extended solutions for rectangular contraction to local scour at piers by Laursen (1958, 1960, 1962 and 1963) is based on observation that depth of local scour does not depend on contraction ratio until scour holes form neighboring piers to overlap. For sand, width of scour hole normal to flow was observed to be about  $2.75d_s$ . Laursen assumed scour in contraction defined by width to be a fraction of scour depth at pier or abutment, leading to several other equations. Laursen's equation can be



simplified to the following form, which is consistent with a basic equation in the method proposed by Melville (1997):

$$d_s \propto \sqrt{By} \quad (2.14)$$

Equation of Gao et al (1993) was developed from Chinese data of local scour at bridge piers and has been used in China for more than 20 years by highway and railway engineers. This equation has been tested using field data given by Froehlich (1989) and 184 field data from the U.S.S.R. (Melville and Coleman, 2000).

Ansiri and Qadar (1994) fitted envelop to more than 100 field measurements of pier scour depth, derives from 12 different sources and several countries and presented a comparison of field data with estimates of scour depth obtained using equations by Laursen (1963), by Breusers (1965), by Neill (1973), by Breusers and Raudkivi (1991) and by Melville and Sutherland (1988) [Melville and Coleman, 2000].

Haque and Rahaman (2003) investigated scour around rectangular bridge pier both in rectangular and compound channel for fixed and mobile bed condition. In clear water condition, flat region scour was observed around rectangular pier. Rahaman and Haque (2003) also modified Lacey formula for predicting local scour for abutments and piers as follows:

$$\text{For abutments: } \frac{d_s}{h} = 0.47M^{1/3} \left( 1 + 1.5 \frac{b_a}{h} \right)^{1/3} - 1 \quad (2.15)$$

$$\text{For piers: } \frac{d_s}{b_p} = \left[ 0.47M^{1/3} \left( 1 + 4.5 \frac{b_p}{h} \right)^{1/3} - 1 \right] \times \left( \frac{h}{b_p} \right) \quad (2.16)$$

They observed that Modified Lacey formula is applicable for abutment-like-structure within  $b_a/h < 10$  and for pier-like-structure within  $h/b_p < 1.50$ . However, results obtained by this method would be difficult to use when variation of side slope of structure is significant.

Table 2.1: Pier scour equations (Source: Melville and Coleman, 2000)

Reference	Equation	Standard format (for comparison)	Notes
Laursen (1958)	$\frac{b}{y} = 5.5 \frac{d_s}{y} \left[ \left( \frac{d_s}{11.5y} + 1 \right)^{1.7} - 1 \right]$	$\frac{d_s}{b} \approx 1.11 \left( \frac{y}{b} \right)^{0.5}$	applies to live-bed scour
Laursen (1963)	$\frac{b}{y} = 5.5 \frac{d_s}{y} \left[ \frac{\left( \frac{d_s}{11.5y} + 1 \right)^{7/6}}{\left( \frac{\tau_1}{\tau_c} \right)^{0.5}} - 1 \right]$	At the threshold condition, $\frac{d_s}{b} \approx 1.34 \left( \frac{y}{b} \right)^{0.5}$	applies to clear water scour $\tau_1$ = grain roughness $\tau_c$ = critical shear stress at threshold of motion
Larras (1963)	$d_s = 1.05 K_s K_\theta b^{0.75}$	$\frac{d_s}{b} = 1.05 K_s K_\theta b^{-0.25}$	
Breusers (1965)	$d_s = 1.4b$	$\frac{d_s}{b} = 1.4$	derived from data for tidal flows
Blench (1969)	$\frac{d_s + y}{y_r} = 1.8 \left( \frac{b}{y_r} \right)^{0.25}$	$\frac{d_s}{b} = 1.8 \left( \frac{y_r}{b} \right)^{0.75} - \frac{y}{b}$	$y_r$ = regime depth = $1.48(q^2/F_B)^{1/3}$ where $F_B = 1.9(d)^{0.5}$ , $d$ in mm and $q$ in $m^2/s$
Shen et al. (1969)	$d_s = 0.000223 \left( \frac{Vb}{\nu} \right)^{0.619}$	$\frac{d_s}{b} = 2.34 \left( \frac{y}{b} \right)^{0.381} F_r^{0.619} y^{-0.06}$	Standard equation is given for kinematic viscosity of water, $\nu = 1 \times 10^{-6} m^2/s$
Coleman (1971)	$\frac{V}{\sqrt{2gd_s}} = 0.6 \left( \frac{V}{b} \right)^{0.9}$	$\frac{d_s}{b} = 0.54 \left( \frac{y}{b} \right)^{0.19} F_r^{1.19} y^{0.41}$	
Hancu (1971)	$\frac{d_s}{b} = 2.42 \left( \frac{2V}{V_c} - 1 \right) \left( \frac{V_c^2}{gb} \right)^{1/3}$	$\frac{d_s}{b} = 2.42 \left( \frac{y}{b} \right)^{1/3} F_r^{2/3}$	$(2V/V_c - 1) = 1$ for live bed scour Standard equation given at threshold condition
Neill (1973)	$d_s = K_s b$	$\frac{d_s}{b} = K_s$	$K_s = 1.5$ for round nosed and circular piers; $K_s = 2.0$ for rectangular piers
Breusers et al. (1977)	$\frac{d_s}{b} = f \left( \frac{V}{V_c} \right) \left[ 2.0 \tanh \left( \frac{y}{b} \right) \right] K_s K_\theta$	$\frac{d_s}{b} = 2.0 \tanh \left( \frac{y}{b} \right) K_s K_\theta$	$f(V/V_c)$ = 0 $V/V_c \leq 0$ = $(2V/V_c - 1)$ $0.5 < V/V_c < 1$ = 1 $V/V_c > 1$ Standard equation is given at the threshold condition
Jain and Fischer (1980)	$\frac{d_s}{b} = 1.86 \left( \frac{y}{b} \right)^{0.5} (Fr - Fr_c)^{0.25}$	$\frac{d_s}{b} = 1.86 \left( \frac{y}{b} \right)^{0.5}$	$Fr = V/(gy)^{0.5}$ $Fr_c = V_c/(gy)^{0.5}$ Standard equation is given at the threshold condition

Table 2.1 (continued): Pier scour equations (Source: Melville and Coleman, 2000)

Reference	Equation	Standard format (for comparison)	Notes
Jain (1981)	$\frac{d_s}{b} = 1.84 \left(\frac{y}{b}\right)^{0.3} Fr_c^{0.25}$	$\frac{d_s}{b} = 1.84 \left(\frac{y}{b}\right)^{0.3}$	Standard equation given at the threshold condition
Chitale (1988)	$d_s = 2.5b$	$\frac{d_s}{b} = 2.5$	
Melville and Sutherland (1988)	$\frac{d_s}{b} = K_l K_y K_d K_s K_\theta$	$\frac{d_s}{b} = 2.4 K_y K_d K_s K_\theta$	For an aligned pier, $d_{s,max} = 2.4 K_s K_d b$ Standard equation given at the threshold condition
Breusers and Raudkivi (1991)	$\frac{d_s}{b} = 2.3 K_y K_s K_d K_\sigma K_\theta$	$\frac{d_s}{b} = 2.3 K_y K_s K_d K_\sigma K_\theta$	For an aligned pier, $d_{s,max} = 2.3 K_s K_d K_\sigma b$
Richardson and Davis (1995)	$\frac{d_s}{b} = 2 K_s K_\theta K_3 K_4 \left(\frac{y}{b}\right)^{0.35} Fr_c^{0.43}$	$\frac{d_s}{b} = 2 K_s K_\theta K_3 K_4 \left(\frac{y}{b}\right)^{0.35} Fr_c^{0.43}$	$K_3$ = factor for mode of sediment transport $K_4$ = factor for armouring by bed material $d_{s,max} = 2.4b$ $Fr_c \leq 0.8$ $d_{s,max} = 3b$ $Fr_c > 0.8$
Gao et al. (1993)	$d_s = 0.46 K_\zeta b^{0.60} y^{0.15} d^{-0.07} \left(\frac{V - V'_c}{V_c - V'_c}\right)$ $V_c = \left(\frac{y}{d}\right)^{0.14} \left[17.6 \left(\frac{\rho_s - \rho}{\rho}\right) d + 6.05 \times 10^{-7} \left(\frac{10 + y}{d^{0.72}}\right)\right]^{0.5}$ $V'_c = 0.645 \left(\frac{d}{b}\right)^{0.053} V_c$ where $d_s, b, y, d, V, V_c, V'_c$ are in S.I. units.	$\frac{d_s}{b} = 0.46 K_\zeta \left(\frac{y}{b}\right)^{0.4} \left(\frac{y}{d}\right)^{0.07} y^{-0.32}$	$V'_c$ = incipient velocity for local scour at a pier $K_\zeta$ = shape and alignment factor $\eta = 1$ for clear water scour $< 1$ for live bed scour i.e. $\eta = \left(\frac{V_c}{V}\right)^{0.35 + 2.23 \log d}$ where $d$ is in S.I. units Standard equation is valid for the threshold condition
Ansari and Qadar (1994)	$d_s = 0.86 b_p^{3.0}$ $b_p < 2.2$ m $d_s = 3.60 b_p^{0.4}$ $b_p > 2.2$ m	$\frac{d_s}{b_p} = 0.86 b_p^2$ $b_p < 2.2$ m $\frac{d_s}{b_p} = 3.60 b_p^{-0.6}$ $b_p > 2.2$ m	$b_p$ = projected width of pier
Melville (1997)	$d_s = K_{yb} K_l K_d K_s K_\theta$	$d_s = K_{yb} K_d K_s K_\theta$	$K_{yb} = 2.4b$ $b/y < 0.7$ $K_{yb} = 2(yb)^{0.5}$ $0.7 < b/y < 5$ $K_{yb} = 4.5y$ $b/y > 5$ Standard equation given at the threshold condition

Mohammed et al (2005) used four commonly cited formulae, namely Colorado State University (CSU), Melville and Sutherland, Jain and Fisher, Laursen and Toch formula, for estimating depth of local scour at bridge pier and validated using both experimental and field data. The study shows that Laursen and Toch and CSU formulae appear to give a reasonable estimate of local scour depth. While Melville and Sutherland and Jain and Fisher formulae appear to over predict scour depth. Compared with other formulae, it appears that Melville and Sutherland formula tend to give a greater over prediction, especially when compared with recorded scour at pier site of studied bridges. Above observation was supported by statistical tests, i.e., when Theil's coefficient, U, Mean Absolute Error (MAE), Root Mean Square Error (RMSE) of each of above formulae are compared.

Design approach proposed by Melville and Coleman (2000) consider bridge piers and abutments together and they develop a design method that can be applied in both cases. Design method rests on following relation for depth of local scour (Melville and Coleman, 2000):

$$d_s = K_{yB} K_I K_d K_s K_\theta K_G K_t \quad (2.17)$$

Where

$K_{yB}$  = flow depth-foundation size factor

=  $K_{yb}$  for piers

=  $K_{yL}$  for abutments;

$K_I$  = flow intensity factors;

$K_d$  = sediment size factor;

$K_s$  = pier or abutment shape factor;

$K_\theta$  = pier or abutment alignment factor;

$K_G$  = channel geometry factor and

$K_t$  = time factor

Khatun (2001) developed a flow diagram for design of bridge pier considering both clear water and live bed condition. She also introduced normalized standard deviation factor,  $K_\sigma$  and proposed a relationship to predict scour depth. The equation is:

$$d_s = K_{yb} K_f K_d K_t K_\sigma K_s K_\theta \quad (2.18)$$

Where

$$K_\sigma = 1.0194(\sigma/d_{50})^{-0.0853} \quad \text{for Live bed scour } (d_{50} < 0.7 \text{ mm})$$

$$= 1.0 \quad \text{for Clear water scour } (d_{50} > 0.7 \text{ mm})$$

Richardson and Davis equation (1995), more commonly known as CSU (Colorado State University) equation, is recommended in HEC-18 and extensively used in U.S.A. The equation was determined from a plot of laboratory data for circular piers. Both CSU and Shen et al (1969) used data of Chabert and Engeldinger (1956). The equation predicts maximum scour depth and it is as follows:

$$\frac{y_s}{y_1} = 2.0 K_1 K_2 K_3 K_4 \left( \frac{a}{y_1} \right)^{0.65} F_r^{0.43} \quad (2.19)$$

Where

$y_s$  = Scour depth, m

$y_1$  = Flow depth directly upstream of pier, m

$K_1$  = Correction factor for pier nose shape  
= 1.0 for Round nose and Circular cylinder

$K_2$  = Correction factor for angle of attack

$K_3$  = Correction factor for bed condition  
= 1.1 for clear bed scour, plane bed and antidune flow

$K_4$  = Correction factor for armoring by bed material size  
= 1.0 for  $D_{50} < 2 \text{ mm}$  or  $D_{95} < 20 \text{ mm}$

$a$  = Pier width, m

$F_r$  = Flow Froude number

Froehlich's equation is another available scour equation which is developed using linear regression analysis of many field observations (Froehlich, 1991). The developed equation is:

$$y_s = 0.32K_1(a')^{0.62} y_1^{0.47} F_r^{0.22} D_{50}^{-0.09} + a \quad (2.20)$$

Where

$K_1$  = Correction factor for pier nose shape

= 1.3 for Square nose, 1.0 for Round nose and 0.7 for sharp nose

$a'$  = Projected pier width with respect to direction of flow or angle of attack

Other symbols represent usual meaning in m.

### 2.13 Assumptions of equations

Laboratory experiments are designed to isolate specific scour process. Thus, resulting equations may not account for complex and dynamic field conditions. Some field conditions that effect scour undefined in selected equations and assumptions are required to apply equations. Flow in field is assumed to be steady state and uniform to allow application of laboratory based equations to predict scour at bridges. Laboratory research has been primary tool for defining relations among variables affecting depth of pier scour. Validity of these relations has not been proven in field. Landers et al (1999) evaluated many relations developed in laboratory by use of transformed data (to obtain a more normal distribution) and smoothing techniques to assess general trends in data. They found only minimal agreement between field data and laboratory based relations. Unlike data set used by Landers et al (1999), all data at skewed piers were removed to prevent bias by these data.

### 2.14 Practices of local scour depth prediction in Bangladesh

Scour predicting methods which are used for design purpose and which are currently practiced in Bangladesh, are mostly developed using field data or experimental results in a simple rectangular channel and are empirical in nature. Use of Lacey formula is common practice for estimation of design local scour depth. It is important to note that in Lacey's formula, dimensions of structure are not incorporated. Flow discharge and sediment characteristics are contributing parameters in determining maximum

local scour depth. This means that in a river reach, same scour depths are predicted around bridge piers, whatever size of structure is. This is quite unrealistic. As the method is developed on the basis of observed field data considering extreme values of scour, it over-predicts scour depths around structures having smaller size and under predicts for structure having larger sizes.

To overcome constrains explained above, Laursen's (1963) formula, which is developed using experimental results, is also used in some structures where dimensions of structures are taken in to account. But its application is limited because of number of empirical constants that are used in formula that are difficult to estimate. Therefore, it is necessary to select appropriate formulae or to develop a new method with different approach for estimation of design scour depth around bridge piers. Also, approach of considering a simple rectangular channel may or may not be applicable when channel section is compound by nature (Haque and Rahaman, 2003).

### **2.15 Remarks**

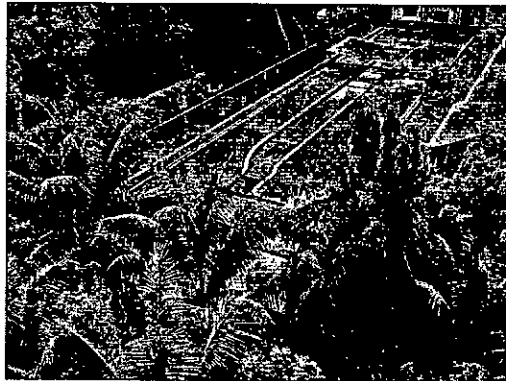
Scour has been investigated for long time to determine its behavior, characteristics and prediction method. For compound channel, pier like structures situated at floodplain that associated with main channel are also subjected to local scour. This may cause serious damage to bridge piers, foundation of river crossing towers etc. Result of huge damage would be reason for human life threats and financial hazards. But unfortunately, studies on floodplain local scour are not mentionable compare to main channel i.e. rectangular channel local scour studies as floodplain does not achieve more importance from researchers like main channel. A good designer must have in depth knowledge on local scour behaviour, flow characteristics and scour formation mechanism both in main channel and floodplain to complete a successful design of river structures. Beside this, estimation of maximum scour depth at bridge pier or river crossing tower site is necessary for safety and economy of river structures. But available most of scour prediction formulas are developed from main channel data set and designed to predict main channel scour. These formulas can not predict floodplain scour accurately. However, more attention and research for floodplain local scour is required for compound channel like rivers in Bangladesh.

## Chapter 3

### EXPERIMENTAL FACILITY

#### 3.1 Introduction

The experiment has been conducted in physical model facility of Department of Water Resources Engineering, built in a large open air space behind institute building of BUET. A brief description of its various components and modification of existing physical model facilities is described below:



Photograph 3.1: Physical Model Facility



Photograph 3.2: Entrance of Physical Model Facility

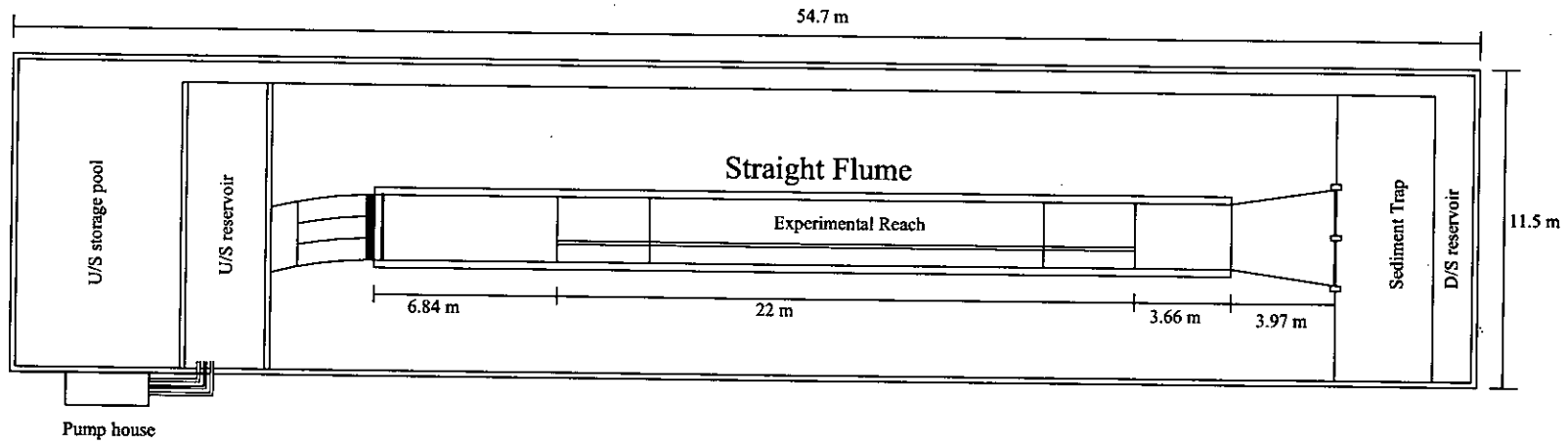
#### 3.2 Physical model components

Physical model facility comprises of a straight flume, water supply system, a recirculating canal, measuring devices, a measuring bridge, point gauge, tail gates etc. In following paragraphs, schematic diagram and overview of physical model components of physical model facility are described in brief.

##### 3.2.1 Straight flume

Rectangular straight flume is of 28 m long, 2.45 m wide and 1.095 m deep. Channel is bounded by 0.28 m wide brick walls. Starting and ending part of channel bed (3 m length on either side) are fixed, while 22 m channel bed in between these two extreme fixed bed ends has been prepared with sand.



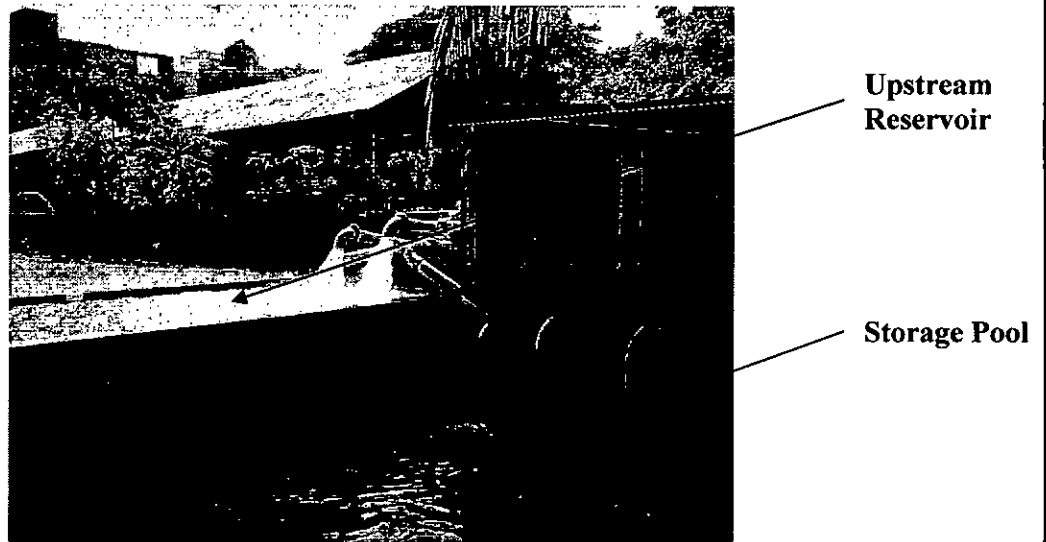


PLAN OF PHYSICAL MODEL FACILITY

Figure 3.1: Plan of Physical model facility

### 3.2.2 Storage pool

To ensure uninterrupted water supply to flume one storage pool having size of 10.67 m length, 6.09 m width and 3.2 m deep is situated in northernmost part of model. Capacity of pool is almost 210 cubic meter. Three intake pipes of pumps are installed inside pool to pump water to upstream reservoir. A direct water supply line is connected to this pool to fill it up to desired capacity before running experiments.



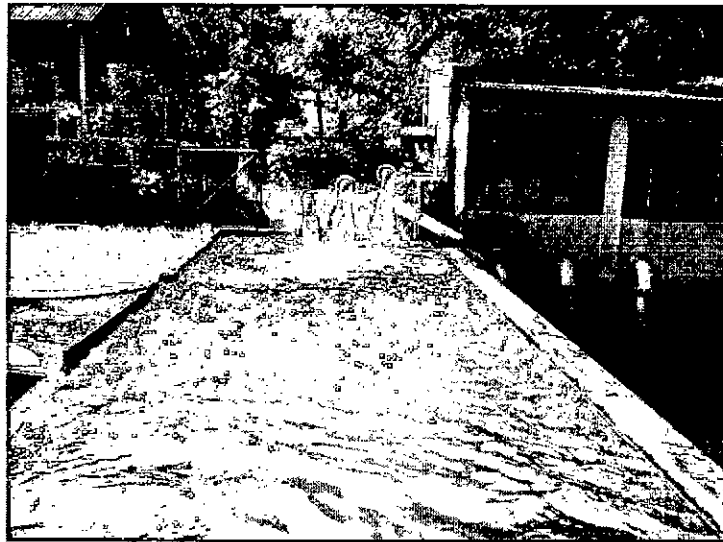
Photograph 3.3: Storage pool and upstream reservoir

### 3.2.3 Upstream reservoir

Water is pumped directly from storage pool to upstream reservoir which is located at southern side adjacent to storage pool. Purpose of this reservoir is to store water and bring it to a steady state before delivering to straight flume. Size of reservoir is 10.67 m x 3.04m x 1.37m. Storage capacity is 44.16 cubic meter.

### 3.2.4 Pump

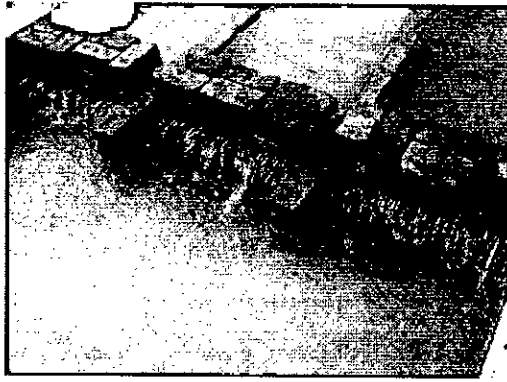
Three centrifugal electric water pumps are installed inside pump house located at western side of storage pool. Total discharge capacity of all three pumps together is 220 l/s. Two pumps (northern and middle) are of same capacity (80 l/s). Capacity of southern pump is 60 l/s. A loss line is connected to outlet of middle pumps to control supply of water to upstream reservoir by redirecting excess water to the storage pool.



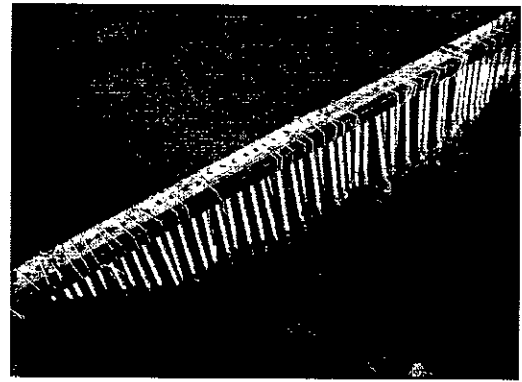
Photograph 3.4: Pumps

### 3.2.5 Flow modifying devices at inlet

To improve flow conditions in straight flume so that uniformity in flow is achieved and also to minimize water level oscillation, water from upstream reservoir to straight flume is led past through a series of devices. Water is first flowed through a flow divider placed just downstream of reservoir, then guided by curved guide vanes, followed by another flow divider and finally obstructed by baffle wall placed just at beginning of straight flume. Flow dividers consist of number of PVC pipes to force flow to divide into number of channels. Guide vanes are provided by constructing two brick walls inside channel parallel to channel sidewalls, thereby allowing water to flow through two curved channel to next flow divider. Baffle wall consists of a perforated wooden beam resting on sidewalls through which PVC pipes are lowered at a desired level.



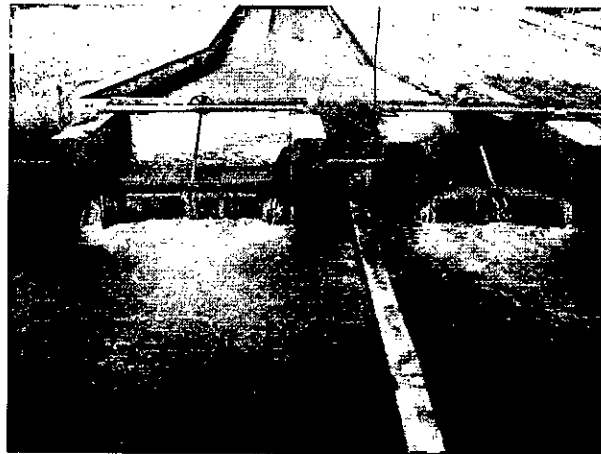
Photograph 3.5: Flow divider



Photograph 3.6: Baffle wall

### 3.2.6 Tail gate

Just at downstream of straight flume there are two tail gates and associated protection works. With the help of these tail gates water level in straight flume is maintained at desired level. Each gate is made up of 1 mm thick MS plate, rubber sheets, cross bars and adjusting rod. About 0.45 m height of water can be manipulated by operating the tailgates.

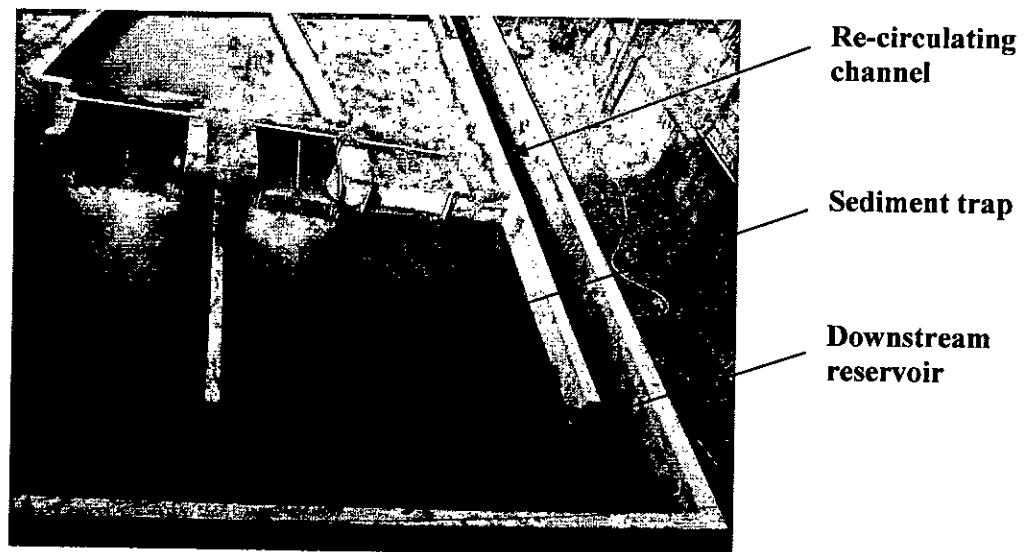


Photograph 3.7: Tail gates

### 3.2.7 Sediment trap and downstream reservoir

Sediment trap tank is located between straight flume and downstream reservoir. It is provided to trap sediments before it can reach downstream reservoir and thereby ensure sediment free water to re-circulate system. Trap is designed based on factors, such as, sediment size, weight, shape, velocity and water depth. Its size is 10.67 m x 3.66 m with a depth of 1.40 m.

Downstream reservoir is southernmost element of physical model facility. It is connected with sediment trap on north and with re-circulating channel on east. Its size is 10.67 m x 1.52 m with a depth of 0.61 m. Capacity of reservoir is 9.75 m<sup>3</sup>.



Photograph 3.8: Re-circulating channel, sediment trap and downstream reservoir

### 3.2.8 Re-circulating channel

Re-circulating channel flows along with eastern periphery of physical model area connecting downstream reservoir and storage pool. Flow of water from downstream reservoir to storage pool through this canal ensures recirculation of water within whole system. Channel is 52.44 m long, 0.76 m wide and 1.28 m deep. A 0.76 long weir is installed across this canal for measuring discharge through straight flume.

### 3.3 Measuring methods and devices

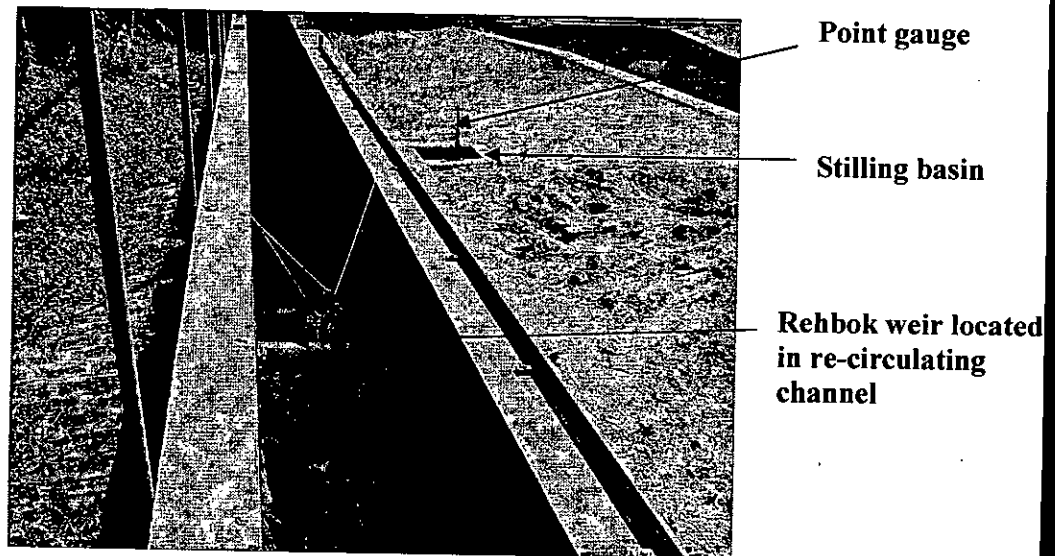
To measure and monitor various experimental parameters and to collect necessary data necessary for subsequent analysis various types of methods and devices are utilized during experiment. Following paragraphs describe such methods and devices used in this experiment.

#### 3.3.1 Discharge measurement

Two sharp crested Rehbok weirs are installed in this model facility; one is located between upstream reservoir and straight flume and other is installed in re-circulating canal. In this experiment only weir located in re-circulating canal is used to measure discharge through flume. Discharge can be calculated from reading point gauge in adjacent stilling basin using following formula:

$$Q = \frac{2}{3} C_d L_{weir} \sqrt{2g} (\Delta H)^{\frac{3}{2}} \quad (3.1)$$

Free flow has been ensured at weir located in re-circulating canal and coefficient of discharge ( $C_d$ ) has been calculated to be 0.6.

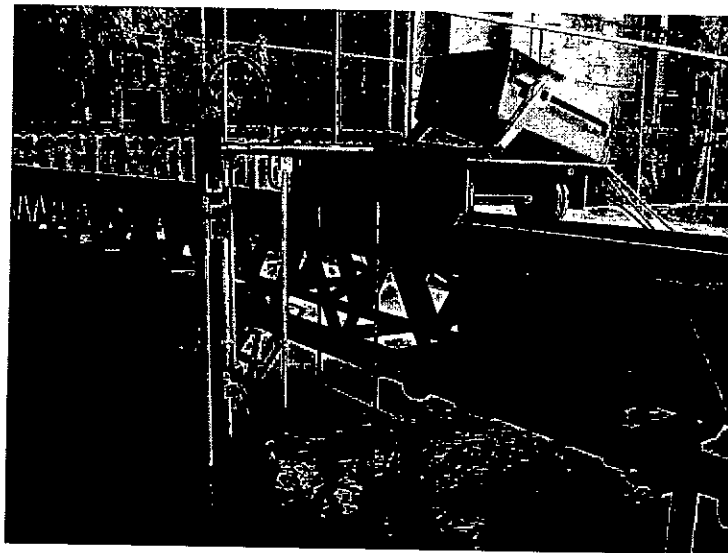


Photograph 3.9: Rehbok weir and stilling basin with point gauge

### 3.3.2 Measuring bridge

Velocities at selected grids are measured using a P-EMS velocity installed at a trolley fitted with measuring bridge.

11 m long measuring bridge made of steel truss structure has been installed stretching entire width of model area with provision of motorized locomotives along length of bed. Bridge can run over rail on two sidewalls. A manually operated trolley is fitted on bridge which can move laterally on rails fitted to the bridge. P-EMS velocity meter is fitted over a base plate of trolley. As such, by moving bridge and trolley across longitudinal and lateral direction respectively, velocity meter can be pointed at any desired direction. Tapes placed over flume side walls and over trolley rail provide necessary measuring facility for this operation.

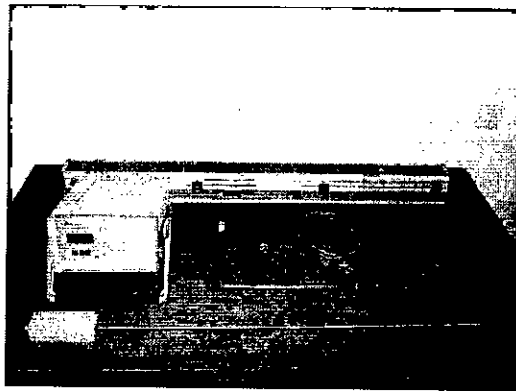


Photograph 3.10: Measuring bridge with velocity meter fixed on bridge trolley

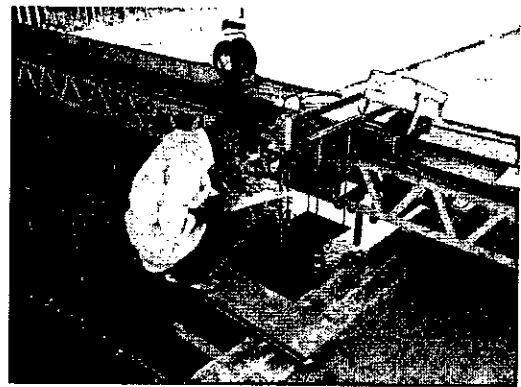
### 3.3.3 Velocity meter

Programmable electromagnetic velocity meter (P-EMS) employs Faraday's induction law for velocity measurement of conductive liquid moving through a magnetic field. This magnetic field is induced by a pulsed current through a coil inside body of sensor. Diametrically opposed platinum electrodes sense Faraday-induced voltage produced by flow past sensor. By means of advanced electronics low level output signals are converted to high level output signals from which magnitude and direction of velocity can be derived.

In general, instrument consists of three basic parts: probe with built-in pre-amplifier, control unit with display screen and connection cables. It is capable of measuring velocity components in a 2D plane. In this experiment, P-EMS equipped with a probe has been used to measure flow velocity components in horizontal plane (in X and Y direction)



Photograph 3.11: Various components of P-EMS velocity meter



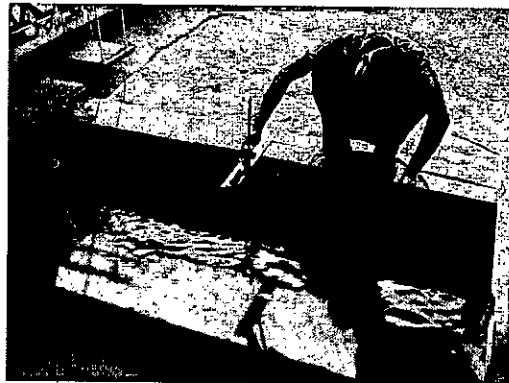
Photograph 3.12: Velocity measurement using velocity meter



### 3.3.4 Point gauges

Water level in straight flume is measured using three point gauges attached on right wall of straight flume. They are named as PG1 at  $X=-1000$  cm, PG2 at  $X=-50$  cm and PG3 at  $X=1000$  cm. Another point gauge,  $PG_{bf}$  has been installed on edge of stilling basin connected to re-circulating canal. This point used for measuring discharge.

Each point gauge is accompanied by a reference plates located at a vertical distance just beneath individual point gauge needle. Elevations of reference plates have been measured with water level instrument in relation to reference level (assumed zero level). Table 3.1 shows elevation of reference plates accompanying point gauges.



Photograph 3.13: Water level measurement using Point gauge



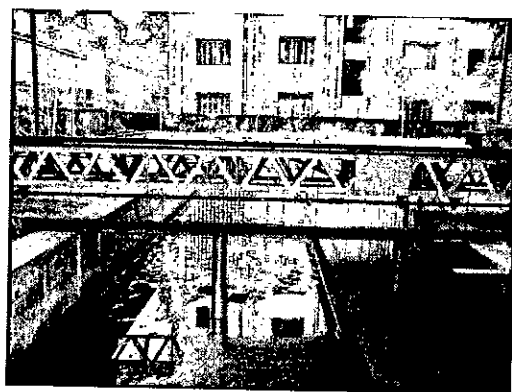
Photograph 3.14: Discharge measuring using Point gauge

Table 3.1: Elevation of the Reference plates

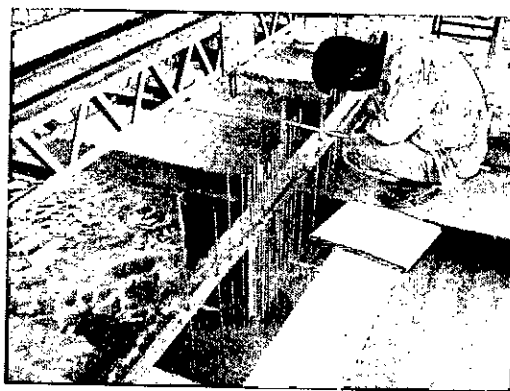
Name of the Point Gauges	Location	Elevation with respect to Zero Level in cm
PG1	Along the length of the flume	55.2
PG2		54.6
PG3		53.2
$PG_{bf}$	Stilling basin connected with re-circulating canal	36.2

### 3.3.5 Bed Level Measuring Instrument (BLMI)

Bed level measuring instrument is made out of an IPE 100 beam which is designed to conduct bed level and scour depth measurement. For this, one side of beam flanges has been perforated at an interval of 2.5 cm. Sharp ended steel rods are lowered through those perforated holes until tip of rod touches bed surface. Length of rods equals to 80 cm. Local bed levels can be determined from readings of portion of rod above beam level. In order to prevent sliding of rods, rubber cascades in between flanges are used through which rod is allowed to lower.



Photograph 3.15: Bed Level Measuring Instrument (BLMI)

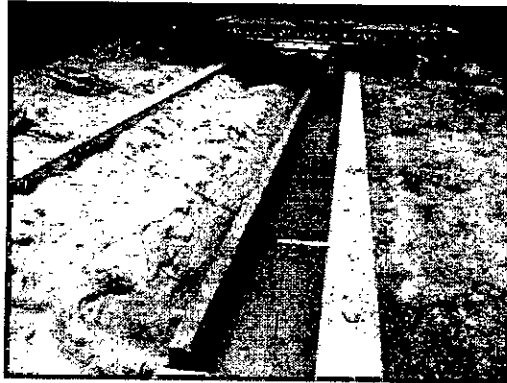


Photograph 3.16: Bed level measurement using BLMI

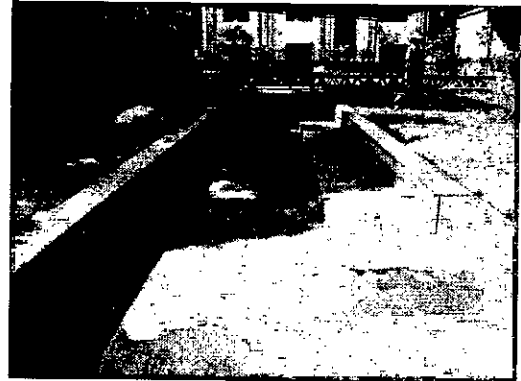
There were other uses of this BLMI as well. This instrument was used to monitor the development of maximum scour hole. While installing structures on main channel and flood plain, BLMI was used for centering of them.

### 3.4 Modification of experimental channel

In order to conduct experiment, some modification had been done in existing straight flume channel. A compound channel was constructed which was 22 m long, 20 cm deep and had 165 cm wide main channel and one adjacent floodplain of 80 cm wide. Existing physical model facility was remodeled and reconstructed as per design scheme to conduct experimental runs for study. It was completed by demolishing and modifying previous experimental flume used for previous research. Total duration to complete modification and repair procedure e.g. digging up sand, cleaning, construction of artificial flood plain with brick and mortar, lying brick layer, filling up channel with bed material over brick layer, cleaning of storage pools, upstream reservoir, sediment trap, downstream reservoir and re-circulating canal, flume leakage repair, flume renovation, tail gate repair; was three and half weeks.



Photograph 3.17: During modification



Photograph 3.18: After modification

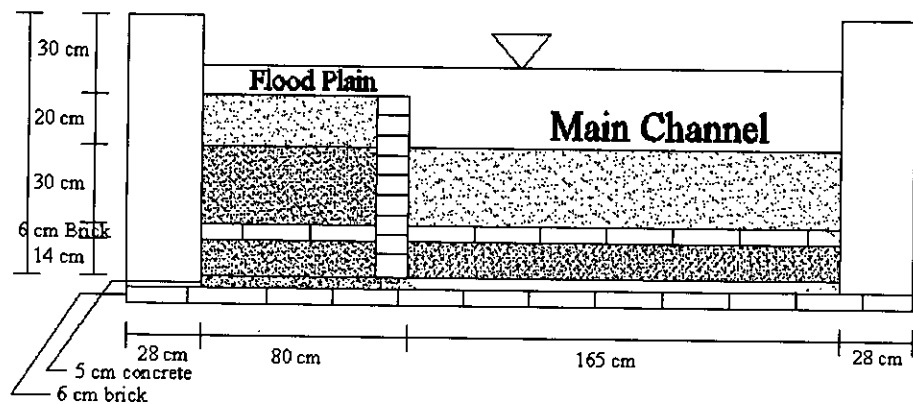


Figure 3.2: Schematic cross-section of straight flume after modification

## Chapter 4

### TEST PROCEDURE AND DATA COLLECTION

#### 4.1 Introduction

Most of natural channels are compound in nature, consisting of a main channel and adjoining floodplains. Main channel normally always carries flow and floodplain carries flow only at above bank full stage. Abutment, bridge piers and river crossing towers are often constructed on floodplains which are also subjected to local scour. But no mentionable studies have been conducted to observe behavior of local scour and effect of different bed materials on local scour for flow condition at floodplain.

In this present study, an attempt has been made to carry out an experiment at a channel with associated floodplain to investigate shape, extent and depth of local scour, effect of different bed materials on local scour. This chapter contains experimental design and methodology for conducting test runs. Here a detailed discussion has been given about bed materials and structure geometry used for present experiment, hydraulic parameters, test duration, test procedure of experiment, measurement procedure, data collection method and test program.

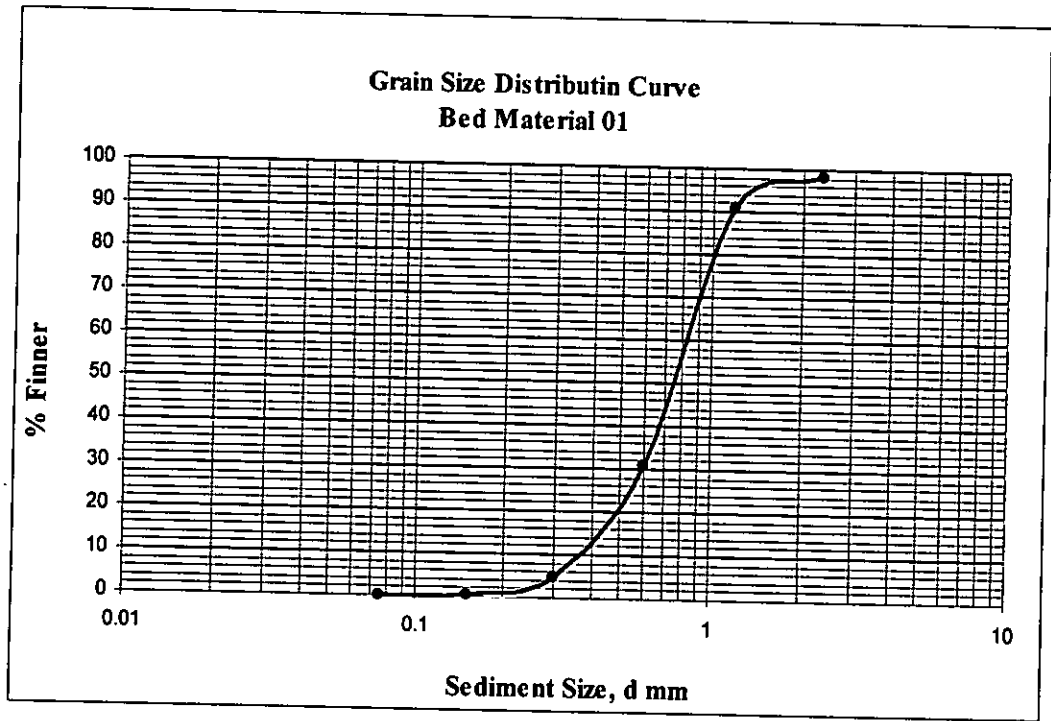
#### 4.2 Experimental design

In following articles, experimental setup of present study is discussed in details.

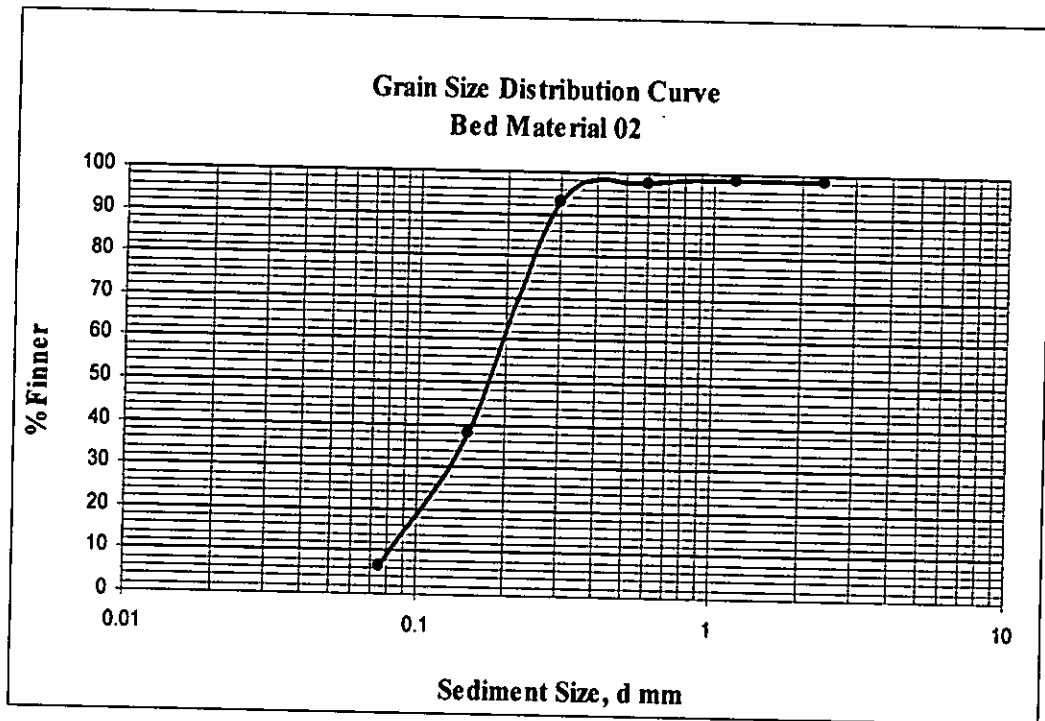
##### 4.2.1 Bed material

In this study, general behavior of local scour at flood plain has been investigated for locally available three different bed materials having sediment size ( $d_{50}$ ) 0.75 mm, 0.18 mm and 0.12 mm respectively. Bed material formed ripple, as sediment size is less than 0.7 mm. Grain size distribution curves are given for each bed material in Figure 4.1.

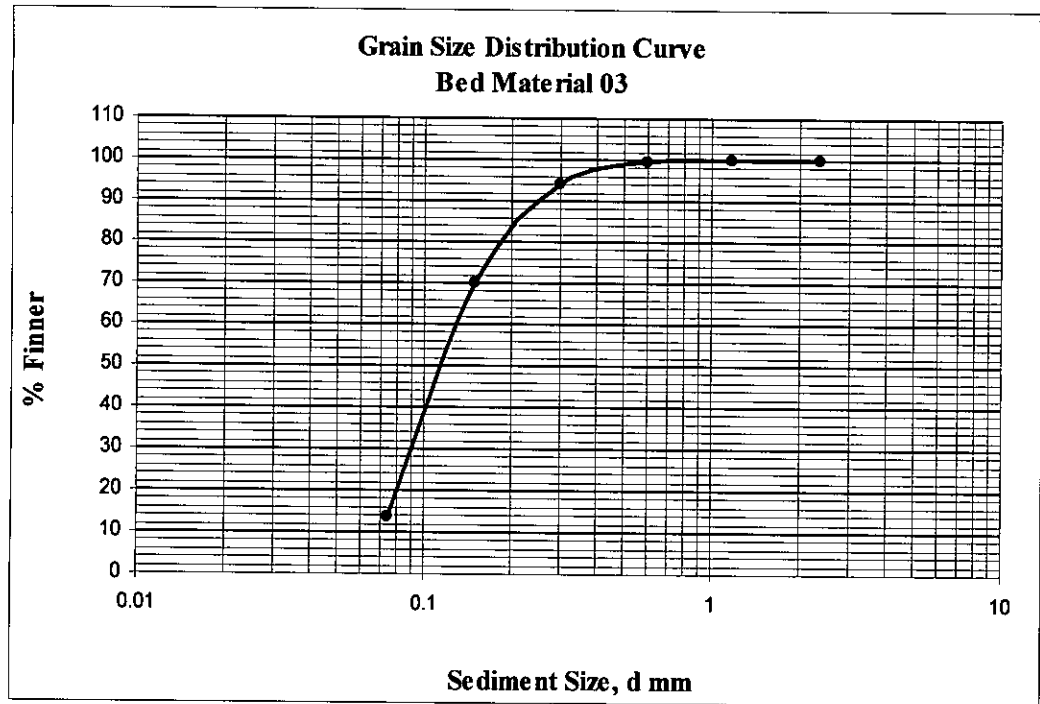
Median particle size ( $d_{50}$ ) for bed material is taken as characteristic particle size for all experiments. Geometric standard deviation ( $\sigma_g$ ) of bed material is calculated from grading curves and considered to be uniform if  $\sigma_g < 1.3-1.5$  and non uniform if  $\sigma_g > 1.5$ .



(a)



(b)



(c)

Figure 4.1: Grain size distribution curves for bed material 1 ( $d_{50} = 0.75$  mm), 2 ( $d_{50} = 0.18$  mm) and 3 ( $d_{50} = 0.12$  mm)

Properties of sediments of bed materials found from grain size distribution curve are listed in Table 4.1 below:

Table 4.1: Properties of bed materials used in experiment

Bed material	$d_{50}$ (mm)	$d_{84.1}$ (mm)	$d_{15.9}$ (mm)	$\sigma_g = \sqrt{\frac{d_{84.1}}{d_{15.9}}}$	Comment
1	0.75	1.2	0.45	1.63	Non uniform Non ripple forming
2	0.18	0.26	0.094	1.66	Non uniform Ripple forming
3	0.12	0.20	0.068	1.72	Non uniform Ripple forming

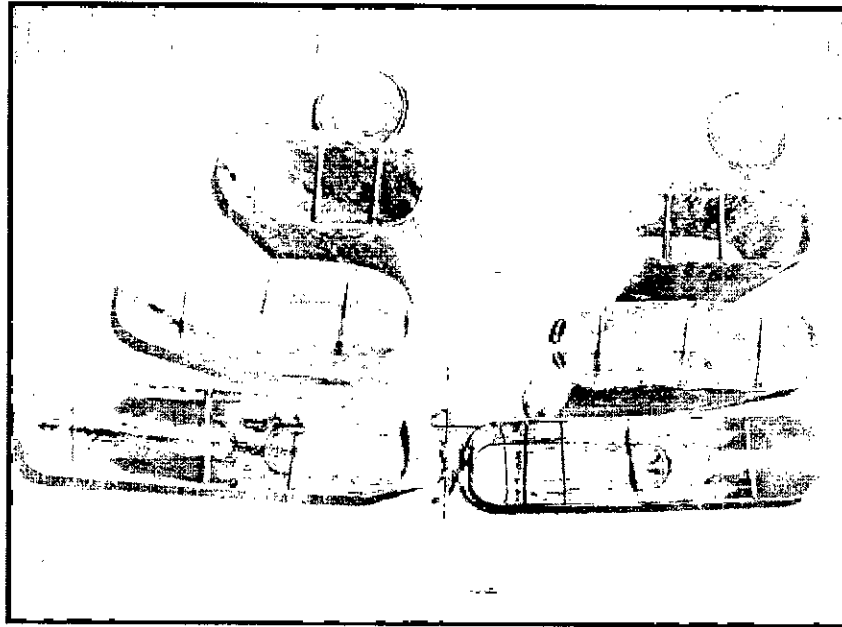
Both main channel and flood plain bed materials are same in compound channel. Initial thickness of sediment bed is 20 cm for flood plain and 30 cm for main channel. Compaction provided in bed preparation is more or less uniform. As sediment is not replaced by sediment feeder, effect of small amount of sediment transportation and consolidation is encountered by taking average depth of mobile bed for measurement of local scour depth.

#### **4.2.2 Structure Geometry**

Circular and Round nose pier shaped structures are used for this experiment, because these are most common shapes in Bangladesh context.

To evaluate effect of shape of structure in general responses of local scour, this study is conducted for four pier length to pier width ratio ( $l/b$ ) in which  $l/b=1$  for Circular pier structure and  $l/b=2$ ,  $l/b=3$ ,  $l/b=4$  for Round nose pier structure. For this reason, a constant pier width has been maintained.

One pier is placed in flood plain when another one having same shape and same pier length to pier width ratio ( $l/b$ ) is placed in main channel. While choosing pier width, ratio of pier to flood plain width is checked so that effect of sidewall can be ignored. Again, this ratio is constant for every pier shapes to allow relative comparison. All structures are protruded above water surface at all conditions. Again, structures are always kept align with flow so that effect of angle of attack is negligible. PVC pipe and Metallic sheet is used for fabrication of structures. Photograph 4.1 shows different types of structure used for present study. Structures are located at 11 meter from upstream end of channel to allow full development of flow. Detail information of structures is presented in Table 4.2.



Photograph 4.1: Types of structure used in present study

Table 4.2: Properties of structures used in experiment

Shape of pier	Length-Width ratio of pier (l/b)	Width of pier (cm)	Pier to Floodplain width ratio	Material
Circular	1	8	0.1	PVC Pipe
Round nose	2			Metallic Sheet
	3			
	4			

### 4.2.3 Hydraulic Parameters

Total practical discharge of all three pumps together is between 200-220 l/s in this flume. Discharge can be varied from 60 l/s to 200 l/s. Considering different hydraulic parameters like velocity, bed shear stress, freeboard, water depth etc. a maximum discharge of 200 l/s is selected. Three discharges are taken into account to evaluate general behavior of local scour for three different bed materials.



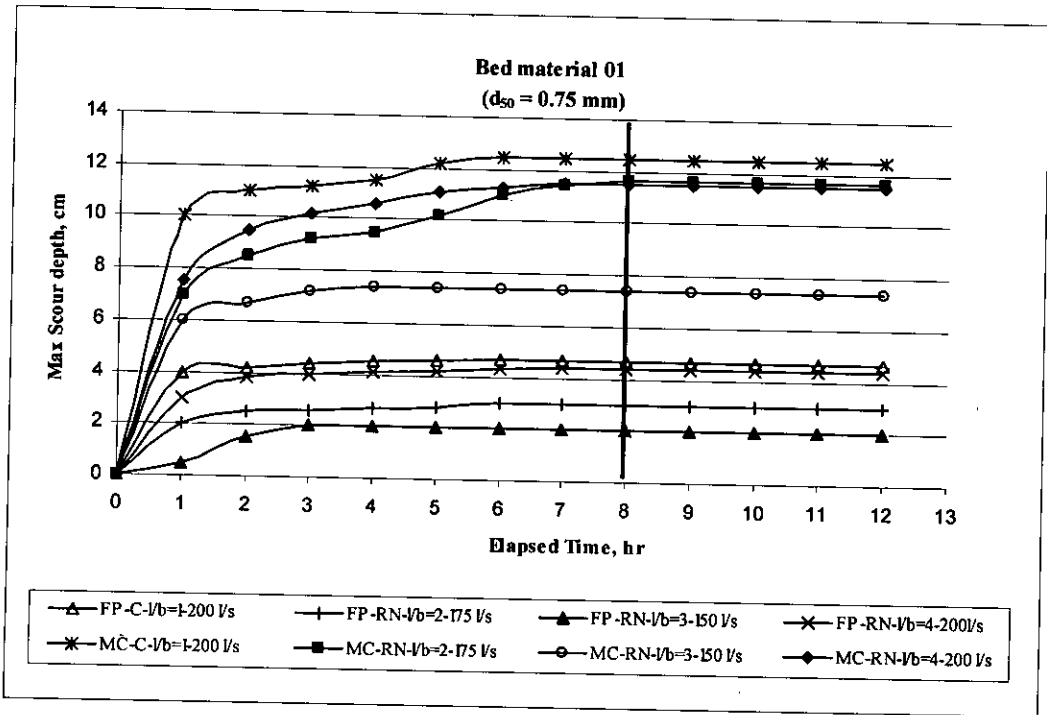
Uniform flow and live bed scour condition is maintained in all cases. For the present study a relative depth ratio ( $Y_r$ ) of 0.26 is considered to maintain experimental condition in constructed compound channel. Total depth of flow and depth of flow on floodplain has been kept 27 cm and 7 cm respectively. Various hydraulic parameters are presented in Table 4.3.

Table 4.3: Hydraulic parameters of experimental study

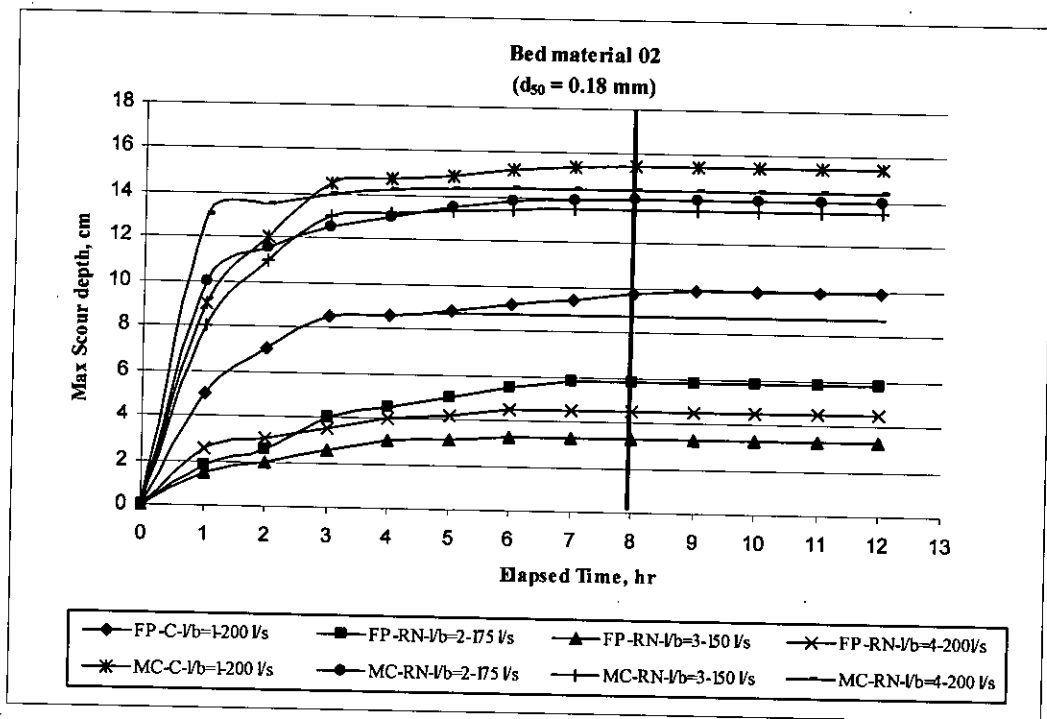
Discharge $Q$ ( $m^3/s$ )	Flow depth in floodplain $y_f$ (cm)	Flow depth in main channel $y$ (cm)	Flow velocity in floodplain $V_f$ (m/s)	Flow velocity in main channel $V$ (m/s)
0.200	7	27	0.224	0.425
0.175			0.196	0.372
0.150			0.179	0.339

#### 4.2.4 Test duration

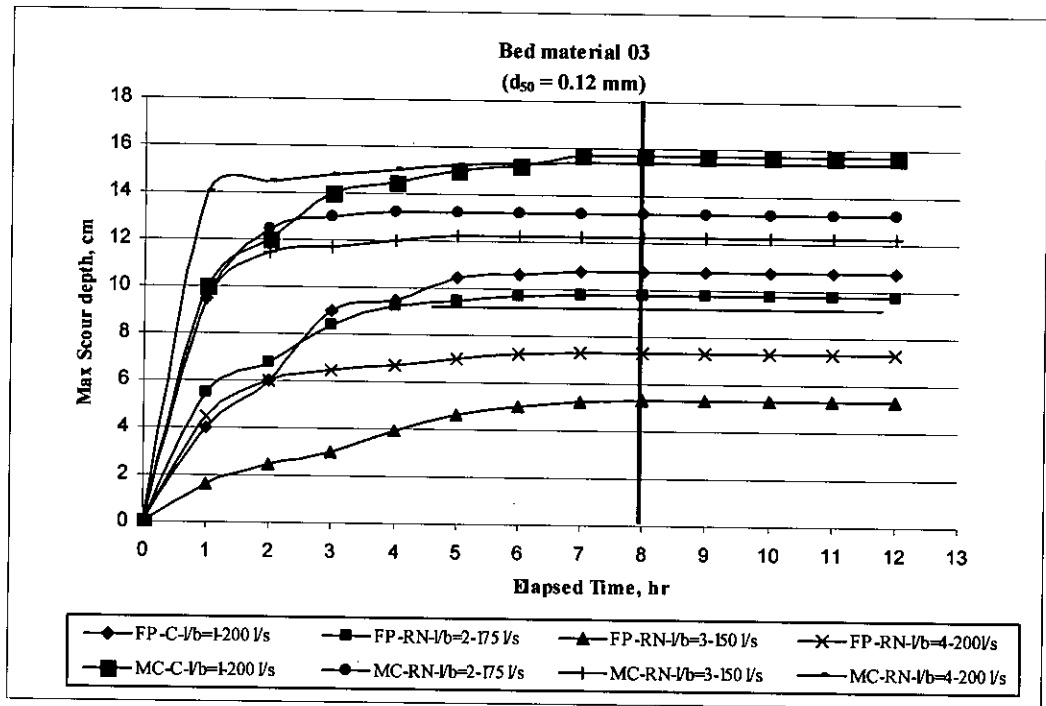
Duration of each run depends on recommended maximum running time of pumps at a stretch, time required for reaching a quasi-equilibrium condition and time required for completing velocity measurement in intended grid sections. A quasi-equilibrium condition after which rate of scour development is negligible can be taken as an ideal condition to compare results of various tests than to run test up to actual equilibrium condition. Some tests are conducted to find out suitable test duration to attain quasi-equilibrium condition at flood plain and main channel for different bed materials and different discharges. Results of such few tests are shown in Figure 4.2 (a), (b) and (c).



(a)



(b)



(c)

Figure 4.2: Comparison between 12 hrs and 8 hrs runs for bed material 1 ( $d_{50} = 0.75 \text{ mm}$ ), 2 ( $d_{50} = 0.18 \text{ mm}$ ) and 3 ( $d_{50} = 0.12 \text{ mm}$ )

In Figure 4.2a, 4.2b and 4.2c, it has been observed that for all three bed materials, maximum scour development is achieved after 4 hours in almost all cases. Scour development in next four hours is considerably less than first four hours and remains constant after 8 hours duration. Considering negligible rate of development of scour which becomes almost constant after 8 hours run and recommended maximum running time of pumps at a stretch which is also 8 hours, duration of each test run is selected as 8 hours. It has also been observed that within these 8 hours, velocity measurement at intended sections can be completed. This 8 hours duration of test run ensures completion of one complete test run including scour depth measurements and preparation of bed for next test run by 2 working days.

#### 4.2.5 Test program

Test program includes experimental runs conducted for investigating general behavior of local scour around pier like structure at flood plain of compound channel. A total of 36 runs have been carried out for this purpose. In total three sets of tests have been designed for three different bed materials. Test program contents information with

respect to run no, bed material, pier shape, pier length to pier width ratio (l/b) and discharge in which experiment is done. A summary of experimental runs conducted in present study is summarized in Table 4.4.

Table 4.4: Summary of Test program

Run no	Bed material	Sediment Size $d_{50}$ (mm)	Pier shape	Pier length to Pier width ratio (l/b)	Discharge (l/s)	
1	1	0.75	Circular	1	200	
2					175	
3					150	
4					200	
5			Round nose	2	3	175
6						150
7						200
8						175
9			Round nose	4	3	150
10						200
11						175
12						150
13	2	0.18	Circular	1	200	
14					175	
15					150	
16					200	
17			Round nose	2	3	175
18						150
19						200
20						175
21			Round nose	4	3	150
22						200
23						175
24						150
25	3	0.12	Circular	1	200	
26					175	
27					150	
28					200	
29			Round nose	2	3	175
30						150
31						200
32						175
33			Round nose	4	3	150
34						200
35						175
36						150

### **4.3 Measurement**

In this study, following measurements are undertaken and measurement methods are described below:

#### **4.3.1 Discharge**

Rehboke weir in re-circulating canal and accompanying point gauge in stilling basin in front of weir is used to measure discharge. Discharges have been controlled by gate valve of each pump and by adjusting loss line to middle pump so that stilling basin point gauge reading adjusted with corresponding levels of discharges. During course of experimental run, it is difficult to maintain a constant discharge for all time. This uncertainty has occurred mainly due to power fluctuations, reduction of pump capacity due to aging, accumulation of moss around pipe mouth in flow divider. Therefore, discharge readings are taken after every 1 hour and necessary adjustment in loss line flow is carried out accordingly.

#### **4.3.2 Water Level**

In this study, constant water depths of 7 cm above floodplain bed level and 27 cm above main channel bed level are kept respectively throughout experiment. Desired water levels are maintained by adjusting tail gates after discharge reaching stable condition. Water level above flood plain is monitored by point gauge reading, located in experimental reach. Readings of two point gauges attached along flume right wall are taken regularly to observe water surface slope. Beside point gauges, BLMI with sharp ended steel rods fixed at  $X=0$  is used for continuous checking of water level above flood plain and main channel.

#### **4.4 Data collection**

In the subsequent paragraphs, various data collection procedure used in this study is discussed in brief:

##### **4.4.1 Velocity**

Velocity measurements are taken three to four hours later to allow most of scour holes development around pier shaped structure. In live bed condition, this scour development is drastic. Velocities are measured with a programmable electromagnetic velocity meter (P-EMS). Total velocity measurement procedure required three to four hours. Each velocity reading has been taken as average velocity of 60 seconds duration. Two velocity components, i.e.  $V_x$  and  $V_y$ , with standard deviations are read from display screen of control unit at a time. P-EMS probe is placed at a constant 0.6 depth from top of water level surface to obtain velocity data which is used as average velocity for all of experimental runs. 0.2, 0.4, 0.6 and 0.8 depths velocity data are also collected always from particular grid point (-0.5 m from upstream end of structure in longitudinal direction and 0 m in lateral direction) for both floodplain and main channel and these data are used to develop velocity profile. Areas selected for velocity measurement are 0.20 m upstream and 0.20 m downstream from centre of pier (both floodplain and main channel) in longitudinal direction and +0.20 m to -0.20 m (i.e. both sides of each pier) in lateral direction. These areas are divided into grid system at an interval of 0.05 m to 0.20 m. Measurements are taken at each grid point.

##### **4.4.2 Maximum Scour development**

To observe scour development rate around different shaped pier structures, maximum scour depth is measured at variable time intervals. Maximum scour development and its location are quite visible and maximum scour depth is measured by BLMI. In order to measure maximum scour depth, beam with one sharp ended steel rod is placed at appropriate position. Rod has been lowered and sharp tip of rod is allowed to touch bed surface inside of maximum scour hole. Measurement of rod portion above beam level is used to determine maximum scour depth.

#### **4.4.3 Scour depth**

Scour depth measurements for local scour are made with bed level measurement instrument. After each experimental run, water has been drained away by lowering tail gates before starting measurement. An area is selected and measurements are taken at various sections by placing BLMI using measuring tapes placed over flume side walls. Extents of measured areas are selected depending upon extents of scour holes. Numbers of sharp edged rods are fixed with beam, each spaced at a distance of 2.5 cm laterally, are lowered to touch deformed bed. Gap between two longitudinal sections varies between 2.5 cm to 20 cm depending on severity of bed deformation. Average mobile bed level is used as reference for maximum scour depth measurement. Any data found to be below this reference point is taken as negative value and indicates scour. Similarly, any data found to be above same reference point is taken as positive value and indicates deposition. These scour data are processed to generate grid data to plot scour contour map and are used to study scour pattern, scour extent, maximum scour depth and its location.

#### **4.5 Test procedure of experimental run**

A specific sequence of test procedure has been followed for every experimental run. these includes major works like flume channel cleaning, bed preparation, structure installation, pump operation and conducting test run, different data collection during and after experimental run and preparation for next run. Methodology has been discussed briefly here:

- Generally straight flume, upstream and downstream reservoirs and recirculating canal are cleaned to make free from debris, moss and floating dirt before starting each experimental run. Special concern has been given to inlet pipes at flow divider where moss accumulation would reduce discharge to straight flume. Upstream and downstream reservoirs water are drained out fully, cleaned thoroughly and refilled with fresh water in a regular period of completing 6 to 8 experimental runs. Cleaning has been done with bleaching powder to prevent moss and fungi infestation.

- Both floodplain and main channel structures are placed at central location of straight flume channel at a distance of 11 m downstream from upstream so that flow can be developed fully. Flood plain structure and main channel structure are installed at midpoint of floodplain and main channel width respectively. In case of round nose pier, extra attention is needed for aligning pier with flow to avoid effect of angle of attack. In all cases, structures are protruded above water level.
- After installing structures, necessary filling and leveling operations have been done to level floodplain and main channel bed.
- Leveled beds have been kept under water for at least 10-12 hours duration. It must be done to avoid initial excessive scouring taking place if pumps are started without any water over bed. A portable pump is used for backfilling water from downstream reservoir to keep leveled beds under water.
- When sufficient water is being backfilled, pumps are switched on one by one after priming with certain time gap.
- Specific discharge is checked by corresponding water level in stilling basin of weir after full development of flow. Discharge is adjusted by pump gate valve and loss line of middle pump.
- In straight flume channel, constant water depths are maintained above floodplain and main channel beds respectively. It has been done by adjusting tailgate after settling stable discharge and it has been monitored continuously with a regular time interval throughout experiment.
- Maximum scour development data is monitored and collected with time intervals.
- Velocity measurements are started and continued after most of scour holes development completed. Total measurement procedure would take three to four hour duration.



- After 8 hours experimental run duration, pumps are stopped gradually one after another and water is completely drained away from straight channel by lowering tailgates.
- Scour data are measured and recorded by BLMI with sharp ended steel rods.
- Photographs of scour formation around both floodplain and main channel structures are obtained.
- After finishing a complete cycle, test procedure is repeated for next run.

EXPERIMENTAL RESULTS AND DISCUSSIONS

5.1 Introduction

In scouring process, both flow and structure interact to create a complex flow field and remove bed material from, around and beneath the structure. Sufficient knowledge on scouring process is mandatory to design a structure placed in river.

Most of rivers in Bangladesh are compound in nature. A compound channel is a two stage channel consists of both main channel and side channel in floodplain. In such a compound channel, scouring in floodplain is an important issue as river crossing towers, pier like structures, abutments etc are often constructed on floodplain and they are also subjected to local scour. Beside this, rivers of Bangladesh are naturally alluvial. So bed material of these rivers is also a considerable matter for local scour study on floodplain.

Mentionable research on floodplain scour is limited because; researches are mostly done to study main channel scouring. Practically, study of local scour in river system like Bangladesh rivers, which are compound and alluvial and where live bed scour is normal condition, are not available.

In this present study, an experimental investigation has been carried out and floodplain local scour behavior and characteristics around pier like structures in three different locally available river bed materials were examined. For this purpose, 36 experimental runs have been conducted with variable discharges, structure shapes and length-width ratio. Uniform flow condition is maintained for all experimental runs. In all cases, live bed scour condition is kept as like rivers of Bangladesh.

106001

## 5.2 Live bed condition

Live bed scour occurs for uniform sediment ( $\sigma_g < 1.3$  to 1.5) when  $V/V_c > 1$ . For non uniform sediment ( $\sigma_g > 1.5$ ), armouring occurs on the channel bed and in the scour hole. Armour layer formation within the scour hole reduces the local scour depth. The ratio  $V/V_a$  is a measure of flow intensity for scour with non uniform sediments.  $V_a$  which marks the transition from clear water to live bed conditions for non uniform sediments is equivalent to  $V_c$  for uniform sediments. Thus, for non uniform sediments, live bed conditions pertain when  $V/V_a > 1$  (Melville and Coleman, 2000). In this study, values of geometric standard deviation ( $\sigma_g$ ) for three bed materials are 1.63, 1.66 and 1.72 respectively. So, all these bed materials are non uniform and for this reason,  $V_a$  is considered as critical flow velocity ( $V_c$ ). It has been observed that both in floodplain and main channel,  $V/V_a$  is always greater than unity. So, it is well proved that live bed condition ( $V/V_a > 1$ ) is maintained in almost all experimental runs. In Table 5.1, experimental values of relative flow velocity with respect to critical flow velocity both in floodplain and main channel are shown.

Table 5.1: Experimental values of relative flow velocity with respect to critical flow velocity

Bed material	Sediment size $d_{50}$ (mm)	Discharge ( $m^3/s$ )	$V/V_a$	
			Floodplain	Main channel
1	0.75	0.200	1.12	1.50
		0.175	0.98	1.31
		0.150	0.90	1.20
2	0.18	0.200	1.32	1.90
		0.175	1.15	1.64
		0.150	1.10	1.50
3	0.12	0.200	1.30	1.86
		0.175	1.14	1.63
		0.150	1.04	1.48

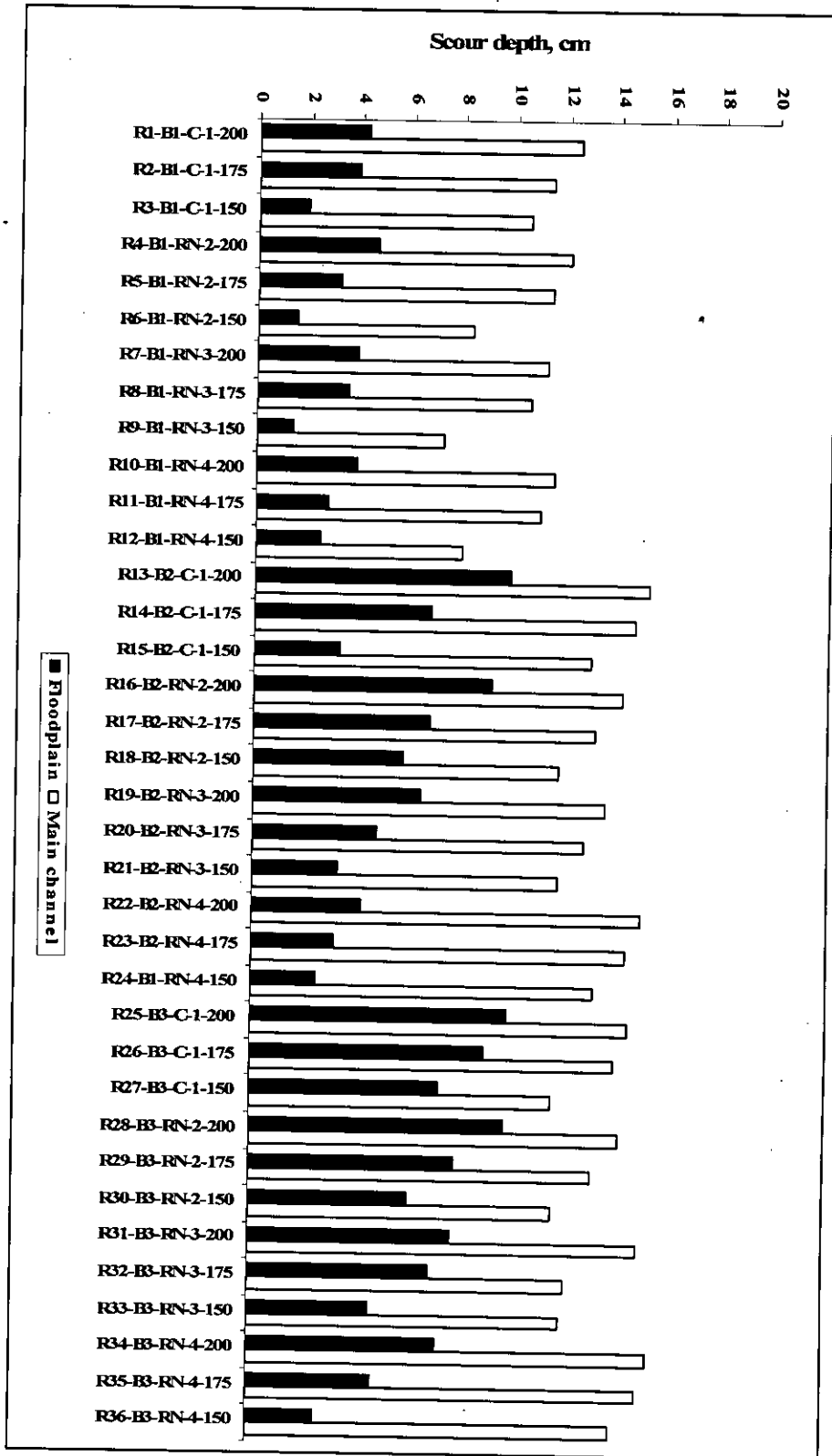


Figure 5.1: Comparison between floodplain maximum scour and main channel maximum scour for each run

### 5.3 Maximum scour depth comparison

For every run conducted in three different bed materials, maximum scour depth in floodplain and maximum scour depth in main channel are shown in Figure 5.1. Generally it has been observed that higher discharge causes higher scour in both main and floodplain and scour depth has a downward tendency to decrease with decreasing discharge. Scour depth in all runs for bed material 1 ( $d_{50} = 0.75$  mm) shows less than that of other two bed materials as their sediment size is finer than bed material 1 ( $d_{50} = 0.75$  mm). Between bed material 2 ( $d_{50} = 0.18$  mm) and 3 ( $d_{50} = 0.12$  mm), scour depth is comparatively higher for bed material 3 ( $d_{50} = 0.12$  mm) than that for bed material 2 ( $d_{50} = 0.18$  mm) in case of same discharge. The reason may be that sediment size of bed material 3 ( $d_{50} = 0.12$  mm) is smaller in compare with bed material 2 ( $d_{50} = 0.18$  mm).

In general, scour in main channel is much deeper than that in floodplain. Increasing or decreasing tendency of scour depth in main channel for same discharges in different bed materials is nearly same as floodplain scour trend. It is notified that scour depth is more for circular pier than that of round nose pier in floodplain and shows a lowering trend with higher  $l/b$  ratio for round nose pier.

#### 5.4 Equilibrium scour depth and equilibrium time

Scour depth in clear water regime increases logarithmically with time upto limiting depth at equilibrium (Melville and Chiew, 1997). But in live bed regime, equilibrium depth is reached relatively quickly. At higher velocities, equilibrium can be attained very rapidly (Chee, 1982). Temporal development of relative scour depth at floodplain as a function of time are represented in Figure 5.2, Figure 5.4 and Figure 5.6 for bed material 1 ( $d_{50} = 0.75$  mm), bed material 2 ( $d_{50} = 0.18$  mm) and bed material 3 ( $d_{50} = 0.12$  mm) respectively. Similar graphical presentation of temporal relative scour depth development at main channel is also shown in Figure 5.3, Figure 5.5 and Figure 5.7 for bed material 1 ( $d_{50} = 0.75$  mm), 2 ( $d_{50} = 0.18$  mm) and 3 ( $d_{50} = 0.12$  mm) respectively. These curves clearly show similar characteristics for live bed scour as Figure 2.2 (Melville and Coleman, 2000) and Figure 2.6 (Breusers and Raudkivi, 1991). Time required for reaching equilibrium scour depth in live bed scour condition is dependent on velocity of flow, sediment property and structure size. At equilibrium state, it has been observed that scour depth oscillates with time. After a certain time, scour development rate becomes negligible and scour depth remains near about fixed.

Figure 5.2 to Figure 5.7 show equilibrium time requirement for developing equilibrium scour depth both in floodplain and main channel for all three bed materials. . Equilibrium time for attaining equilibrium scour depth can be understood from following description. A live bed scour is formed when amount of sediment leaving scour hole is greater than amount of sediment entering scour hole. After increasing of scour depth with time, size of vortex also increases and shear stress beneath vortex system decreases at same time until equilibrium scour depth is obtained. At equilibrium scour depth, shear stress is no longer able to keep sediment particle in suspension. At this state, amount of sediment entering scour hole equals to amount of sediment leaving scour hole and this state is named as equilibrium state.

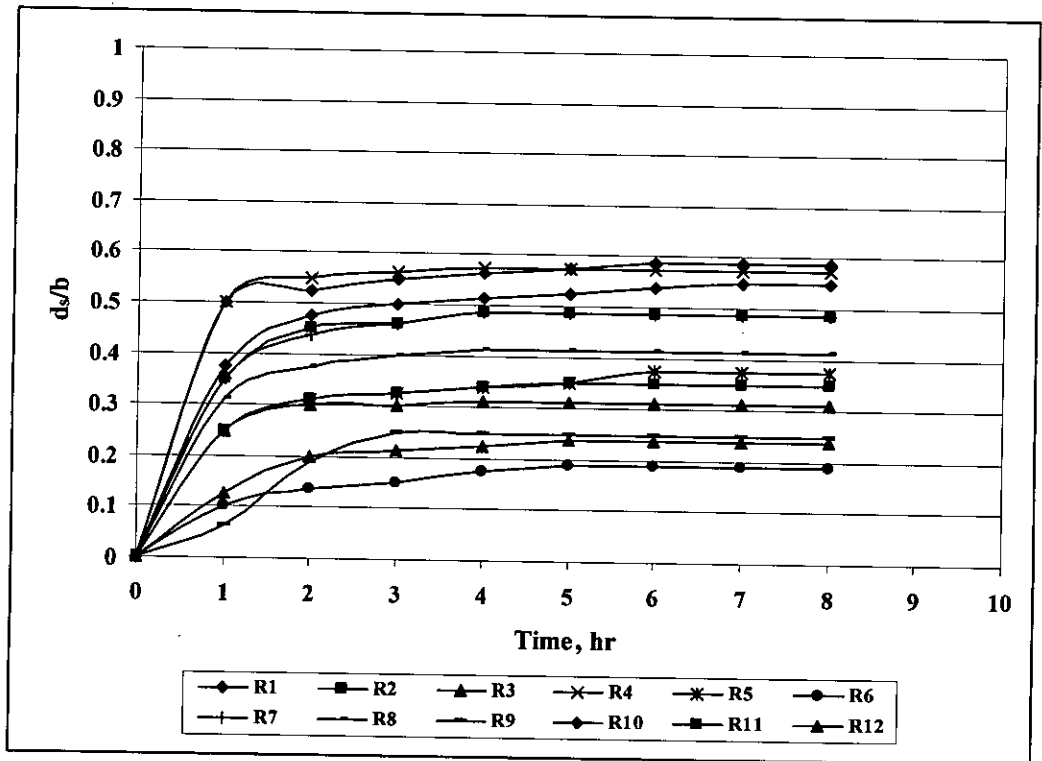


Figure 5.2: Temporal development of scour as a function of time at floodplain for bed material 1 ( $d_{50} = 0.75$  mm)

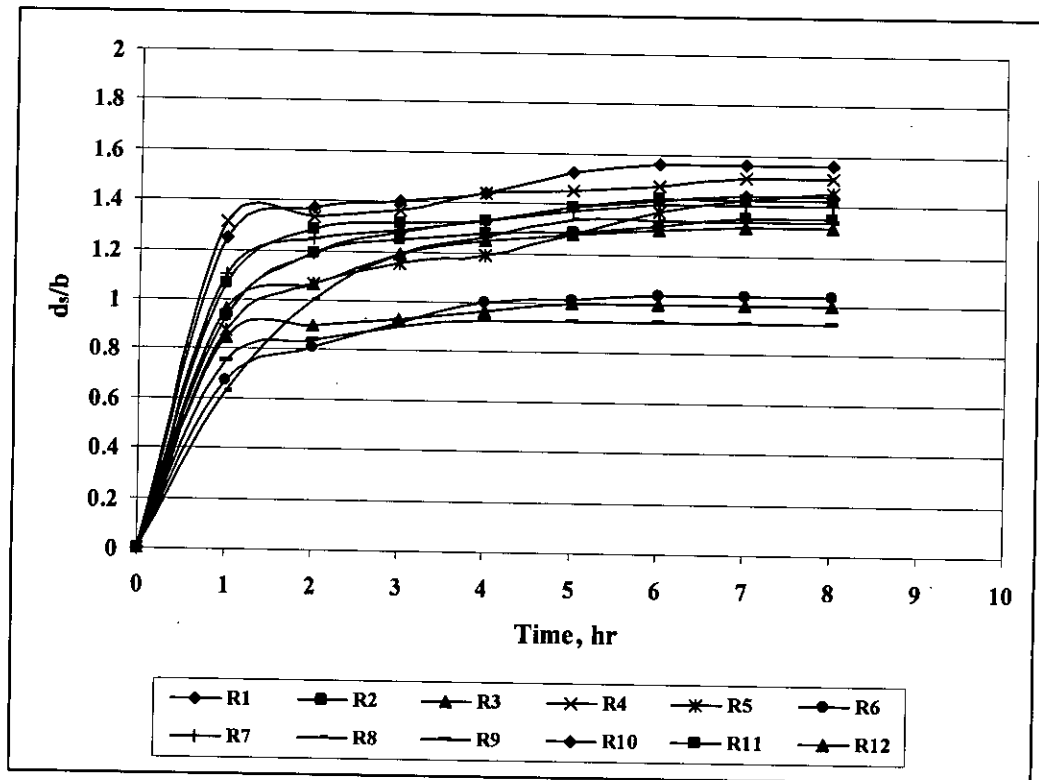


Figure 5.3: Temporal development of scour as a function of time at main channel for bed material 1 ( $d_{50} = 0.75$  mm)

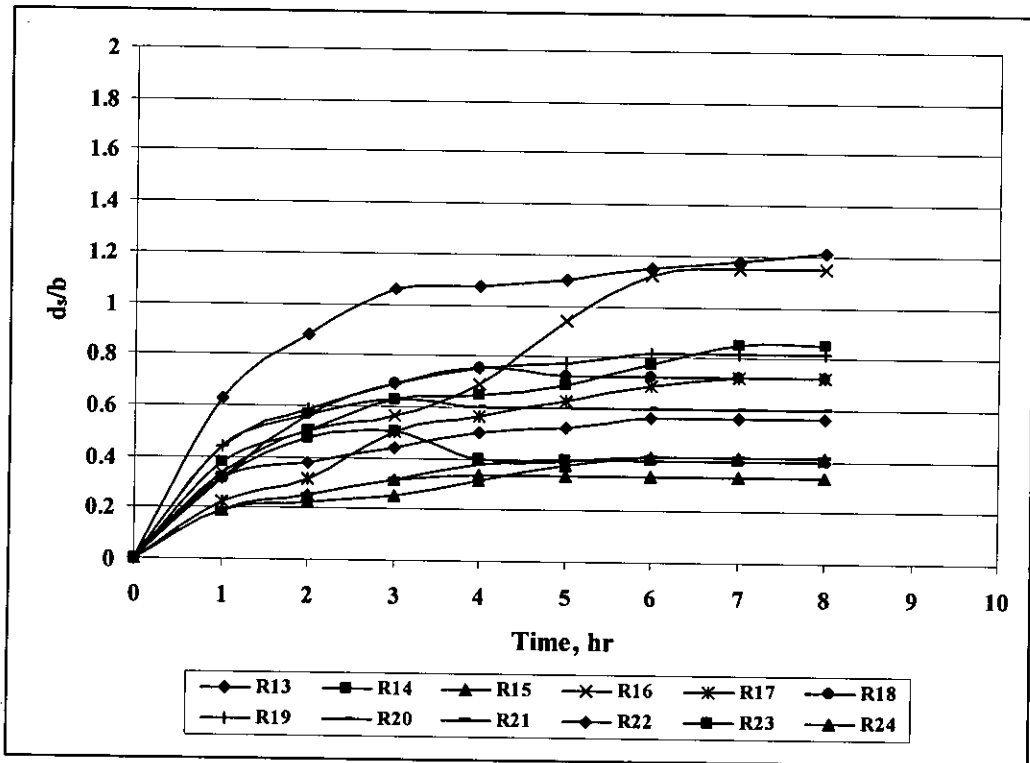


Figure 5.4: Temporal development of scour as a function of time at floodplain for bed material 2 ( $d_{50} = 0.18$  mm)

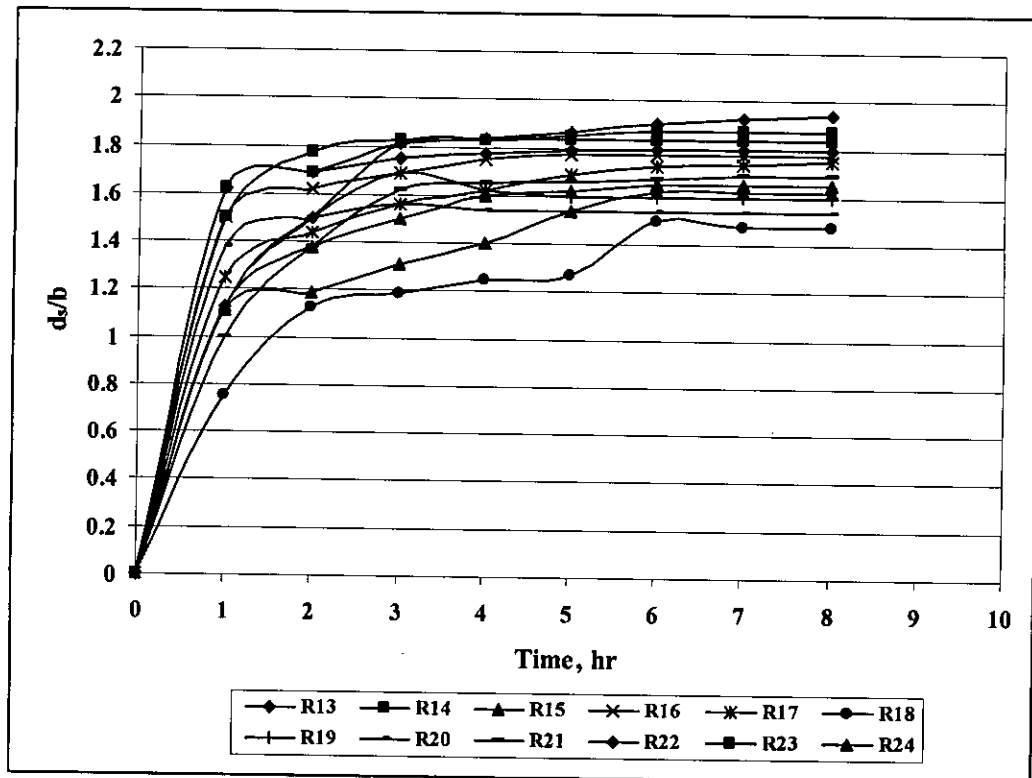


Figure 5.5: Temporal development of scour as a function of time at main channel for bed material 2 ( $d_{50} = 0.18$  mm)



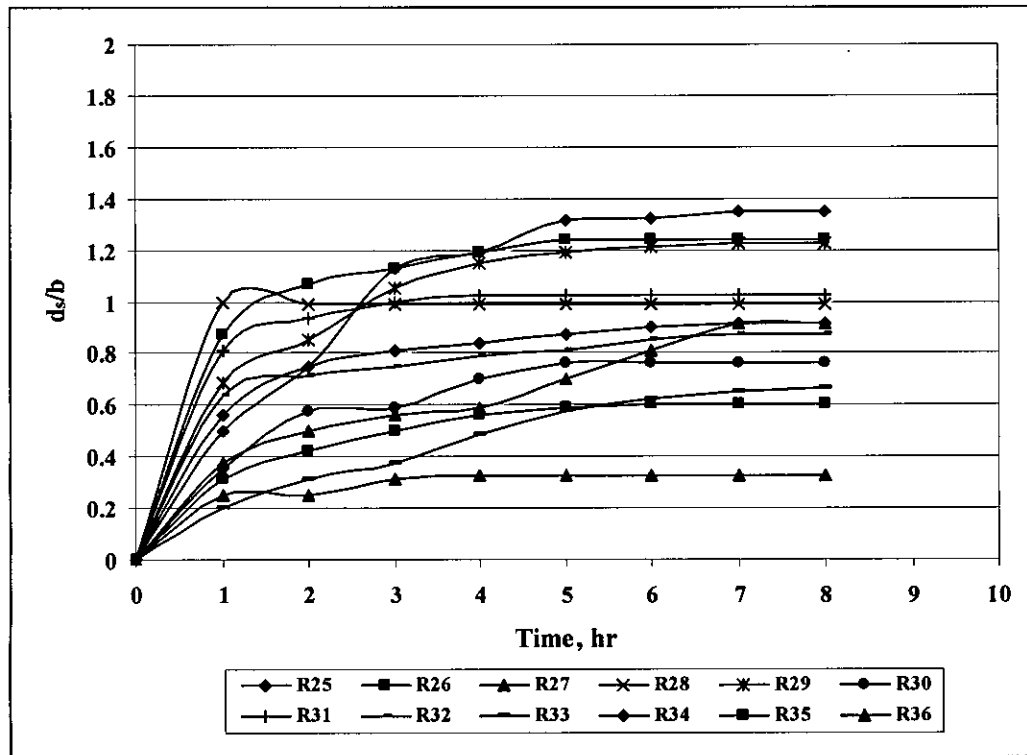


Figure 5.6: Temporal development of scour as a function of time at floodplain for bed material 3 ( $d_{50} = 0.12$  mm)

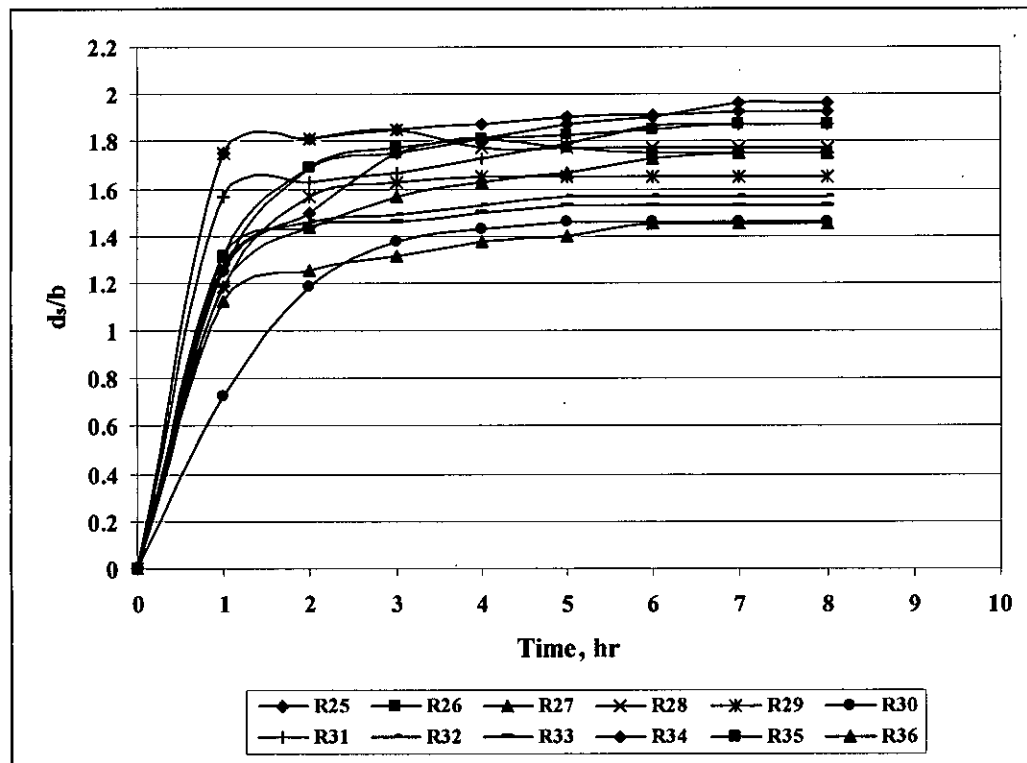


Figure 5.7: Temporal development of scour as a function of time at main channel for bed material 3 ( $d_{50} = 0.12$  mm)

## 5.5 Analysis of scour and bed profile

Bed level data collected after every run have been plotted using Surfer software and examined critically to analyze shape, extent and depth of scour around structure with respect to variable discharge, structure shapes and length-width ratio for 3 different bed materials. This is done for both floodplain and main channel. Comparison is made between floodplain and main channel scour maps. For this purpose, 2D contour maps of scour around structures have been plotted for all 36 runs for both floodplain and main channel. In each plot, location of maximum scour has been marked. Photographs of all 36 experimental runs both for floodplain and main channel are provided for necessary evidence of actual situation. Difference in levels is indicated with the help of threads around structure. Longitudinal cross section bed profile and lateral cross section bed profile are also developed to show differences between different runs. In addition of these, X-Y-Z perspective plots of bed profile are created by using HEC-RAS software to get a clear idea about scour around structures.

### 5.5.1 Scour contour map

2-D scour contour maps and corresponding photographs, indicating local scour around structure for variable discharges, structure shapes and length-width ratio for both floodplain and main channel, are presented in Appendix B. Figure B.1 to B.24, Figure B.25 to B.48, Figure B.49 to B.72 represent both floodplain scour maps and main channel scour maps for bed material 1 ( $d_{50} = 0.75$  mm), bed material 2 ( $d_{50} = 0.18$  mm) and bed material 3 ( $d_{50} = 0.12$  mm), respectively. Photograph B.1 to B.24, Photograph B.25 to B.48, Photograph B.49 to B.72 represent corresponding photographs of floodplain scour and main channel scour for bed material 1 ( $d_{50} = 0.75$  mm), bed material 2 ( $d_{50} = 0.18$  mm) and bed material 3 ( $d_{50} = 0.12$  mm), respectively. Maximum scour depth location is shown in all runs. Variable location of maximum scour indicates effect of bed form which passes through structure. Lateral extent of local scour around structure is not symmetric as local scour of clear water conditions. Longitudinal extent of local scour around structure mostly depends on length-width ( $l/b$ ) ratio of structure and discharge. In subsequent paragraphs individual and comparative observation for each type structure and comparison between floodplain and main channel scour are discussed.

### 5.5.1.1 Circular pier (length-width ratio, $l/b=1$ )

From floodplain scour maps, generally maximum scour location is observed closer to upstream face of circular pier for variable discharge in all three bed materials except for 150 l/s discharge for bed material 1 ( $d_{50} = 0.75$  mm) and 3 ( $d_{50} = 0.12$  mm).

With higher discharge, scour hole slope is found steeper. Scour line intensity decreases with decreasing discharges and becomes flatter for lower discharge. In general, scour hole slope is steepest at front side of structure and gradually decreases side wise. Slope of scour hole at front side of pier is more uniform for higher discharge than that of lower discharge.

Mostly it is observed that scour hole has maximum extent around structure for higher discharges and decreases gradually with decreasing discharges. Total lateral extent is found 3 b, 2.75 b, 2 b for bed material 1 ( $d_{50} = 0.75$  mm); 4.5 b, 4 b, 2.6 b for bed material 2 ( $d_{50} = 0.18$  mm) and 4.3 b, 3.75 b, 3.6 b for bed material 3 ( $d_{50} = 0.12$  mm) in case of 200 l/s, 175 l/s and 150 l/s discharge respectively. Scour extent at upstream front of structure is 1.4 b, 1.75 b, 3 b for 200 l/s discharge; 1.3 b, 1.4 b, 2 b for 175 l/s discharge and 0.6 b, 0.75 b, 2.4 b for 150 l/s discharge for bed material 1 ( $d_{50} = 0.75$  mm), bed material 2 ( $d_{50} = 0.18$  mm) and bed material 3 ( $d_{50} = 0.12$  mm) respectively.

In bed material 1 ( $d_{50} = 0.75$  mm), less or no extent of scour hole is found at rear side of structure in comparison with bed material 2 ( $d_{50} = 0.18$  mm) and 3 ( $d_{50} = 0.12$  mm). Scour extent at rear face is observed 2 b and 1.8 b in case of 200 l/s discharge; 1.9 b and 1.75 in case of 175 l/s discharge; 0.6 b and 1.75 b in case of 150 l/s discharge for bed material 2 ( $d_{50} = 0.18$  mm) and bed material 3 ( $d_{50} = 0.12$  mm) respectively. Sediment deposition is found nearer to rear face of structure for lower discharge whereas sediment is deposited slightly downstream for higher discharge.

Comparing with main channel scour maps, it has been found that maximum scour point is located near front face of structure same as floodplain in all cases except in bed material 3 ( $d_{50} = 0.12$  mm) for 200 l/s discharge. As like floodplain scour, scour hole slope is found steeper and uniform for higher discharge and comparatively flatter and less uniform for lower discharge in main channel. Scour shape is more or less

same as floodplain scour shape but extent of scour is much larger than floodplain. Sediment deposited comparatively far downstream than floodplain in main channel.

#### 5.5.1.2 Round nose pier (length-width ratio, $l/b=2$ )

In floodplain, maximum scour location is observed just at front face for all discharges in three bed materials. But for 200 l/s discharge in bed material 1 ( $d_{50} = 0.75$  mm), it is produced at side, closer to upstream face of structure.

Generally, scour hole slope is found steeper at upstream face and both sides of structure, but it is observed flatter at rear face for all experimental runs. Scour hole slope is steeper for higher discharge and it decreases with lower discharges. Uniformity of scour slopes is observed more or less equal at upstream side and lateral sides of structure.

A decreasing trend of scour extent is observed from higher discharge to lower discharge. Total lateral extent of scour hole is 2.9 b, 2.5 b, 2.3 b for bed material 1 ( $d_{50} = 0.75$  mm); 4.3 b, 3.5 b, 3.3 b for bed material 2 ( $d_{50} = 0.18$  mm) and 3.9 b, 3.75 b, 3 b for bed material 3 ( $d_{50} = 0.12$  mm) in case of 200 l/s, 175 l/s and 150 l/s respectively. Upstream face scour extents are found 1.5 b, 1 b, 0.5 b for 200 l/s, 175 l/s and 150 l/s respectively for bed material 1 ( $d_{50} = 0.75$  mm); 1.9 b, 1.5 b, 1 b for 200 l/s, 175 l/s and 150 l/s respectively for bed material 2 ( $d_{50} = 0.18$  mm); 1.9 b, 1.75 b, 1.5 b for 200 l/s, 175 l/s and 150 l/s respectively for bed material 3 ( $d_{50} = 0.12$  mm). Scour extent at rear face is observed only for 200 l/s discharge in bed material 2 ( $d_{50} = 0.18$  mm), for 200 l/s and 175 l/s discharges in bed material 3 ( $d_{50} = 0.12$  mm). These are 1.75 b, 1.8 b and 1.6 b.

Sediment deposition is observed around and closer to downstream face of structure. For 150 l/s discharge in bed material 1 ( $d_{50} = 0.75$  mm), deposition is found side of structure near to rear front. Deposition of sediment shifted adjacent to rear side of structure with decreasing discharge.

In main channel, maximum scour location is marked at front face of structure in every experimental run. A secondary scour hole is observed at the end of rear face scour extent for bed material 2 ( $d_{50} = 0.18$  mm) and bed material 3 ( $d_{50} = 0.12$  mm). In

comparison with floodplain scour, longer extent of scour hole is found downstream from rear face of structure in main channel. Lateral and front face scour extent is also found larger than floodplain scour. Shifting of sediment deposition is observed becoming nearer to rear side same as floodplain scour with decreasing discharge. Steepness and uniformity of scour hole show same trend as floodplain scour.

### 5.5.1.3 Round nose pier (length-width ratio, $l/b=3$ )

Location of maximum scour is observed adjacent to upstream face or just in front of upstream face of structure in floodplain scour.

Slope of scour hole is steeper at front face and becomes flatter gradually to downstream direction. In case of bed material 1 ( $d_{50} = 0.75$  mm), mostly bed forms have been observed for all three discharges in downstream side of structure. Slope and uniformity of scour hole show decreasing tendency for lower discharge.

Extent of scour hole has been found increasing with finer sediment size for same discharges. Again scour extent is observed decreasing from higher discharge to lower discharge for same bed material. Total lateral extent has been found 3 b, 2.5 b, 2 b for 200 l/s, 175 l/s, 150 l/s discharges respectively in bed material 1 ( $d_{50} = 0.75$  mm); 4 b, 3 b, 2 b for 200 l/s, 175 l/s, 150 l/s discharges respectively in bed material 2 ( $d_{50} = 0.18$  mm) and 3.9 b, 3.7 b, 2.8 b for 200 l/s, 175 l/s, 150 l/s discharges respectively in bed material 3 ( $d_{50} = 0.12$  mm). In case of front side, scour extents are found 1.3 b, 1.75 b, 2.4 b for 200 l/s discharge; 0.9 b, 1.4 b, 1.5 b for 175 l/s discharge and 0.6 b, 0.9 b, 1 b for 150 l/s discharge in bed material 1 ( $d_{50} = 0.75$  mm), bed material 2 ( $d_{50} = 0.18$  mm) and bed material 3 ( $d_{50} = 0.12$  mm) respectively.

At rear face of structure, scour extent has not been found for lowest discharge, 150 l/s in all three bed materials. Scour extents at this face are 0 b, 0.25 b, 1 b in case of 200 l/s discharge and 0 b, 0 b, 0.5 b in case of 175 l/s discharge for bed material 1 ( $d_{50} = 0.75$  mm), bed material 2 ( $d_{50} = 0.18$  mm) and bed material 3 ( $d_{50} = 0.12$  mm) respectively. Closer to rear side sediment deposition is observed for lower discharge when sediment deposits a little downstream for higher discharge.

Maximum scour is located in front of and around upstream face and in few runs along the length of structure in case of main channel scour. It has been observed that main

channel scour follows same trend for slope, shape and uniformity as floodplain scour. Downstream scour extent is found longer in bed material 2 ( $d_{50} = 0.18$  mm) and bed material 3 ( $d_{50} = 0.12$  mm) than that of bed material 1 ( $d_{50} = 0.75$  mm). Development of secondary scour hole at far end of downstream is also observed. Sediment deposition shifting with discharge variation is found same as floodplain deposition but distance of deposition from rear face of structure is longer than floodplain.

#### 5.5.1.4 Round nose pier (length-width ratio, $l/b=4$ )

From floodplain scour maps, maximum scour location is found just in front of upstream face of structure for all discharges in case of all three bed materials.

Scour hole slope is observed steepest for highest discharge and decreases with lower discharges. Slope is found steeper at front face of structure and gradually becomes flatter to downstream. At downstream side, scour maps show bed forms rather than scour. Uniform slope has been observed for higher discharge and it decreases with decreasing discharges.

Scour extent towards downstream has been found limited to half length of structure in all cases. Generally it is observed that this structure has comparatively smaller scour extent than others. It is important to notify that among all structures, scour depth is found minimum for this structure in all three bed materials with respect to same discharge. Total scour extent for floodplain has been found  $2.3 b$ ,  $2 b$ ,  $1.8 b$  for bed material 1 ( $d_{50} = 0.75$  mm);  $2.5 b$ ,  $2.3 b$ ,  $1.75 b$  for bed material 2 ( $d_{50} = 0.18$  mm) and  $3.75 b$ ,  $3 b$ ,  $1.75 b$  for bed material 3 ( $d_{50} = 0.12$  mm) in case of 200 l/s, 175 l/s and 150 l/s discharges respectively. Scour extents at front face are  $1.5 b$ ,  $1.8 b$ ,  $2 b$  for 200 l/s discharge;  $1 b$ ,  $1.2 b$ ,  $1.4 b$  for 175 l/s discharge and  $0.9 b$ ,  $0.9 b$ ,  $0.75 b$  for 150 l/s discharge in bed material 1 ( $d_{50} = 0.75$  mm), bed material 2 ( $d_{50} = 0.18$  mm) and bed material 3 ( $d_{50} = 0.12$  mm) respectively.

It is observed that no scour extent has been found at rear face of structure for all discharges in three bed materials at floodplain. For higher discharges, sediment deposition is located closer to rear end of structure and deposition shifts towards upstream side with lower discharges.

From main channel scour maps, maximum scour locations are marked in front of upstream face of structure. In bed material 1 ( $d_{50} = 0.75$  mm), secondary scour hole has been disappeared and sediment deposition is located. In bed material 2 ( $d_{50} = 0.18$  mm), secondary scour hole is also removed and extent of scour at rear face of structure lengthens so far to downstream. It is even so long than that shown in scour map. As like floodplain scour, same trend for steepness and uniformity is observed for main channel scour but extent of scour hole at all sides of structure is much larger than floodplain scour.

### 5.5.2 Bed profile

Longitudinal cross section and lateral cross section bed profiles both for floodplain and main channel for variable discharges, shapes and length-width ratio for three bed materials are organized from Figure 5.8 to Figure 5.19. For floodplain longitudinal cross section, bed level data at  $Y/b = 5$  (40 cm away from left bank) and for main channel longitudinal cross section, bed level data at  $Y/b = 20.3$  (162.5 cm away from left bank) are considered. Bed level data at 2.5 cm upstream of front face of structure are used to develop both floodplain and main channel lateral cross section bed profiles.

Figure 5.8 represents longitudinal cross section bed profile of three bed materials for 200 l/s discharge in floodplain while Figure 5.9 stands for same discharge in main channel. Similarly floodplain longitudinal bed profiles are shown in Figure 5.10 and Figure 5.12 for 175 l/s and 150 l/s discharges respectively. Figure 5.11 and Figure 5.13 provide main channel longitudinal bed profiles for 175 l/s and 150 l/s discharges respectively.

Lateral cross section bed profiles are arranged in between Figure 5.14 and Figure 5.19. Among these, Figure 5.14, Figure 5.16, Figure 5.18 present floodplain lateral bed profiles and Figure 5.15, Figure 5.17, Figure 5.19 present main channel lateral bed profiles for 200 l/s, 175 l/s and 150 l/s discharges respectively.

X-Y-Z perspective plots of bed profile for some experimental runs are produced from bed level data and presented in between Figure 5.20 and Figure 5.31 for three different bed materials. These perspective plots represent scour and bed forms around structure both for floodplain and main channel.

#### 5.5.2.1 Longitudinal cross section bed profile

Longitudinal cross section bed profiles for floodplains indicate variation of scour depth, extent and deposition of sediment in three bed materials namely, B1 ( $d_{50} = 0.75$  mm), B2 ( $d_{50} = 0.18$  mm) and B3 ( $d_{50} = 0.12$  mm) for different discharges. It has been observed that higher discharge causes higher scour depth and scour depth decreases with lower discharges. It is also found that maximum scour depth is obtained for  $l/b=1$  and scour depth reduces with increasing of length-width ratio for same discharge. Comparing three bed materials, it is observed that scour occurs less in bed material 1 ( $d_{50} = 0.75$  mm) than other two. Scour between bed material 2 ( $d_{50} = 0.18$  mm) and bed material 3 ( $d_{50} = 0.12$  mm) is close to each other. However, in most cases, scour in bed material 3 ( $d_{50} = 0.12$  mm) is found higher than that of bed material 2 ( $d_{50} = 0.18$  mm). Sediment size may be the reason for this situation as scour is less in coarse bed material than finer one. Scour follows an increasing trend from coarser bed material to finer bed material.

Generally, a scour hole at rear face of structure has been observed in case of bed material 2 ( $d_{50} = 0.18$  mm) and bed material 3 ( $d_{50} = 0.12$  mm). Depth of this scour hole decreases gradually from smaller length-width ratio to greater length-width ratio in case of same discharge. It is also found that this scour depth has a varying tendency from higher to lower with variation of higher discharge to lower discharge in case of same length-width ratio. Sediment deposition is observed comparatively lower and nearer to rear front of structure in bed material 1 ( $d_{50} = 0.75$  mm) and deposition depth and distance is increased for finer bed materials. It has also been observed that deposition comes lower in height and closer to rear face of structure with lower discharge and greater length-width ratio.

From main channel longitudinal cross section bed profile, all scour depth is found so higher than that of floodplain. Extent of scour hole is found greater in all cases. Generally, no sediment deposition is observed in main channel within same floodplain



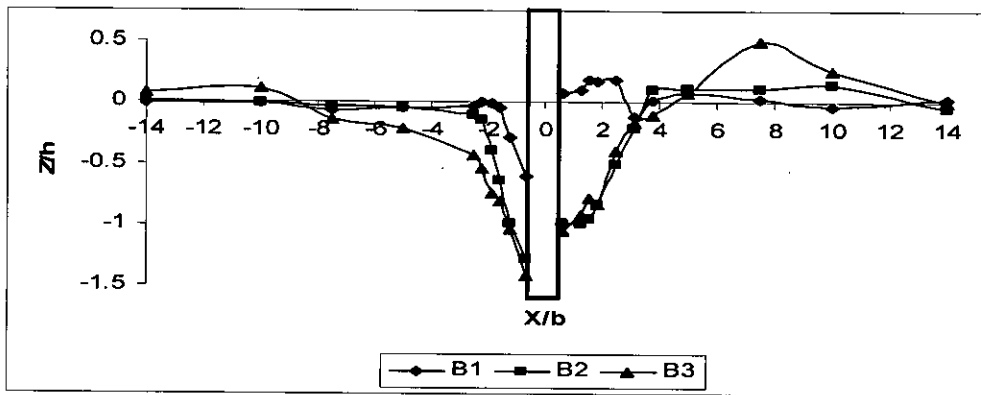
longitudinal distance. Higher velocity of main channel in comparison with floodplain velocity may be responsible for this occurrence as it carries sediment scoured around structure to a far downstream distance of main channel.

#### **5.5.2.2 Lateral cross section bed profile**

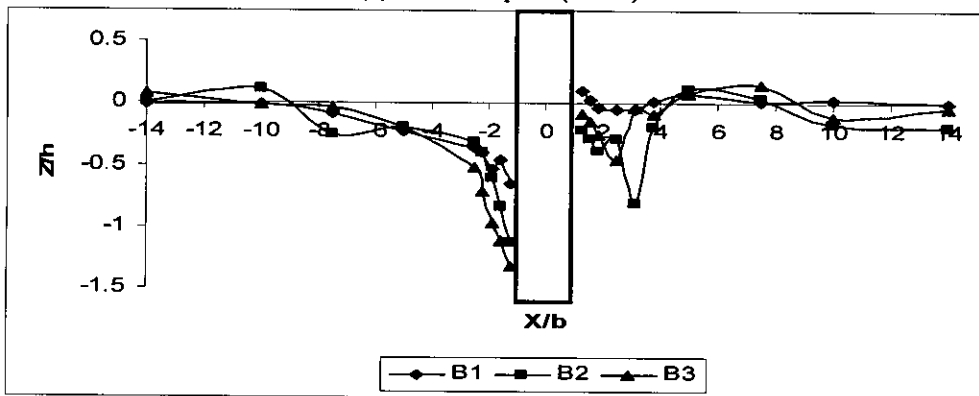
In general, uniform extent and slope of scour hole has been observed from floodplain lateral cross section bed profiles in all three bed materials for variable discharges, shapes and length-width ratio. Scour depth in lateral direction is found comparatively less for coarse bed material and increases with finer bed materials. A decreasing trend of scour depth from smaller length-width ratio to greater length-width ratio and from higher discharge to lower discharge is also marked. Scour depth extent and slope are found uniform from main channel lateral cross section bed profiles same as floodplain except depth is found greater as usual. But scour depth decreasing trend, for length-width ratio and discharge, is not as prominent as observed in floodplain lateral cross section bed profiles.

#### **5.5.2.3 X-Y-Z perspective plot of bed profile**

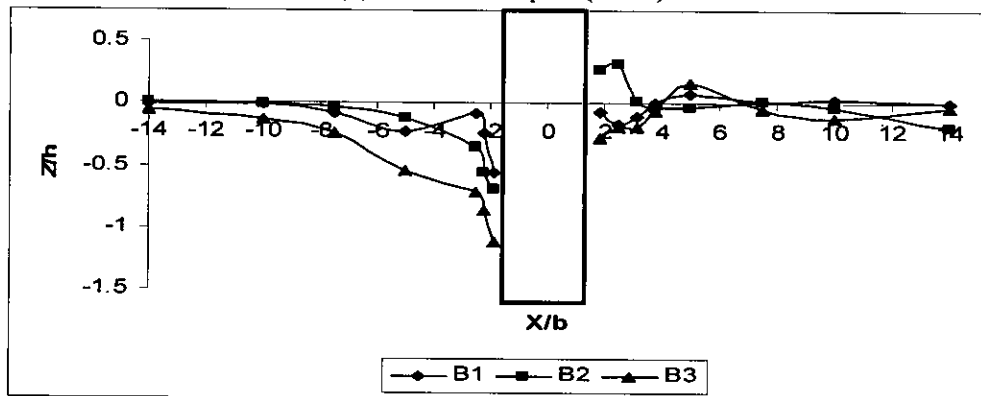
A significant and clear view of scour and bed profile around structure can be obtained from X-Y-Z perspective plots (3D plots) of bed profile. These perspective plots of bed profiles can be able to give a better understanding about shape, extent, slope, deposition etc of scour around different shapes of structure with variable length-width ratio. Comparative idea about difference between floodplain and main channel scour can also be achieved at a glance as these 3 dimensional figures present both floodplain and main channel scouring situation at a time. From these 3D plots, it is very easy to notify that shape of scour hole is symmetrical with shape of structure. They are also evident figures about observations made earlier both for floodplain and main channel scour.



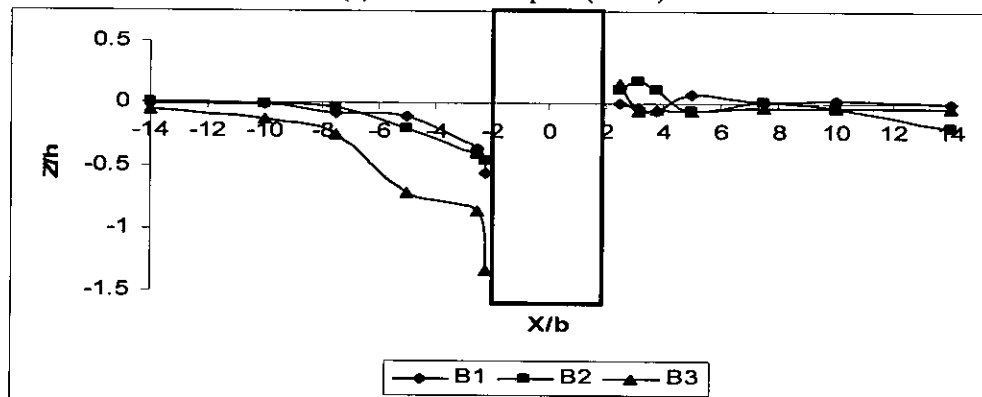
(a) Circular pier ( $l/b=1$ )



(b) Round nose pier ( $l/b=2$ )

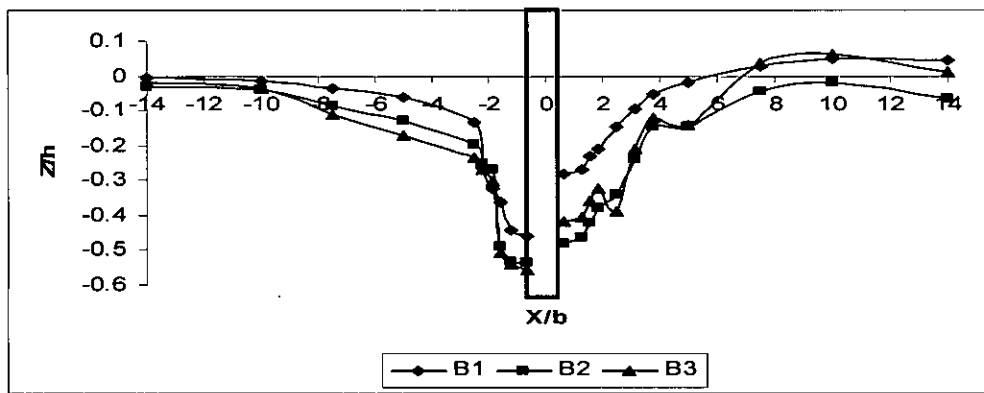


(c) Round nose pier ( $l/b=3$ )

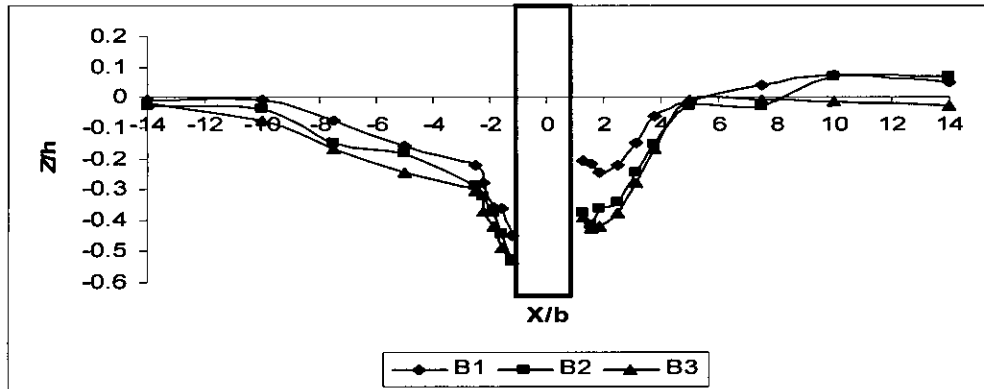


(d) Round nose pier ( $l/b=4$ )

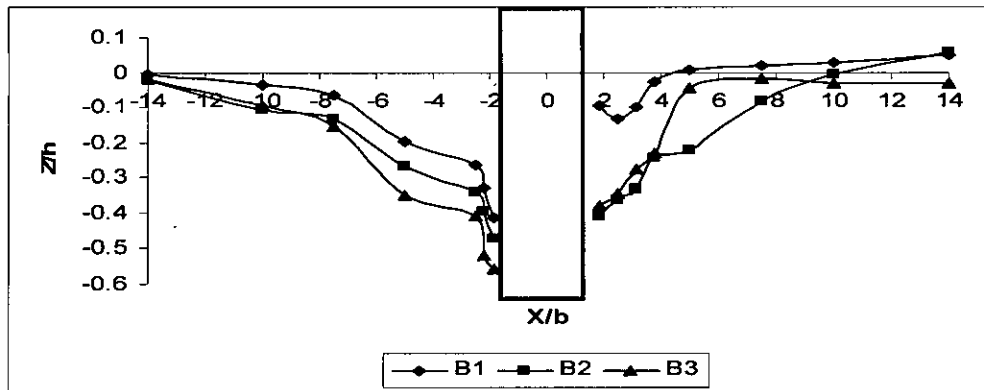
Figure 5.8: Bed profile variation in longitudinal direction for 200 l/s discharge (Floodplain)



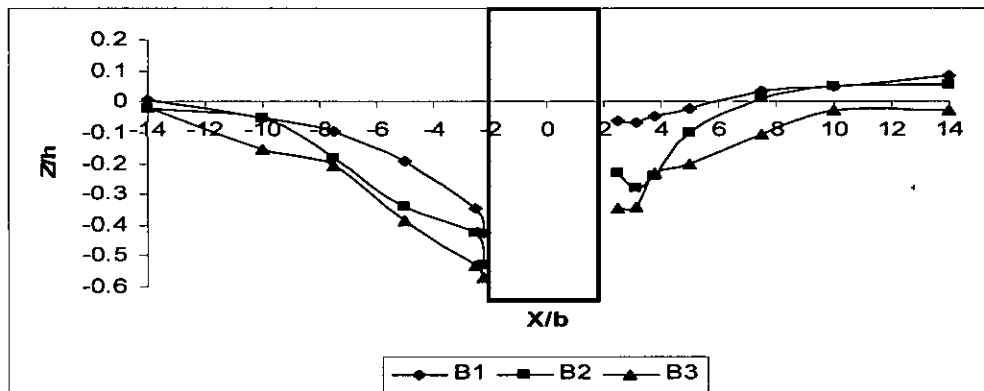
(a) Circular pier ( $l/b=1$ )



(b) Round nose pier ( $l/b=2$ )

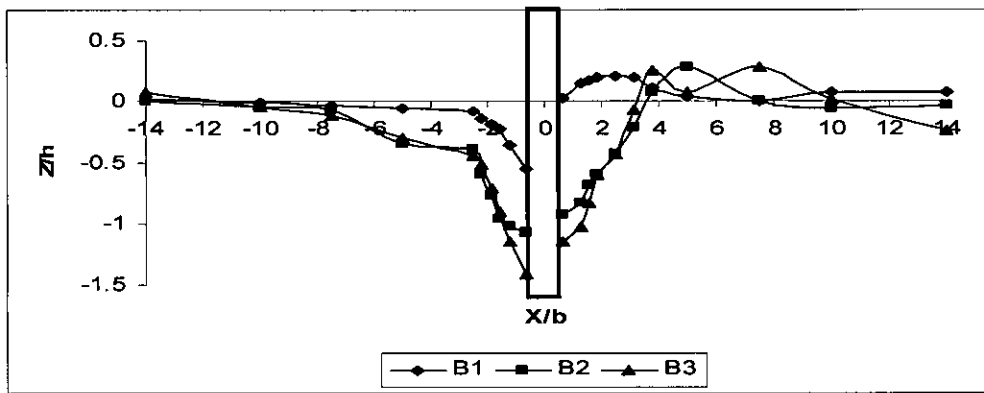


(c) Round nose pier ( $l/b=3$ )

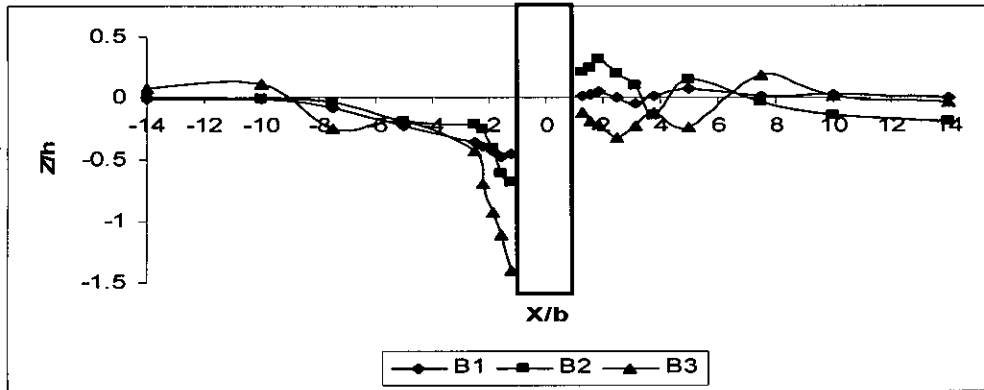


(d) Round nose pier ( $l/b=4$ )

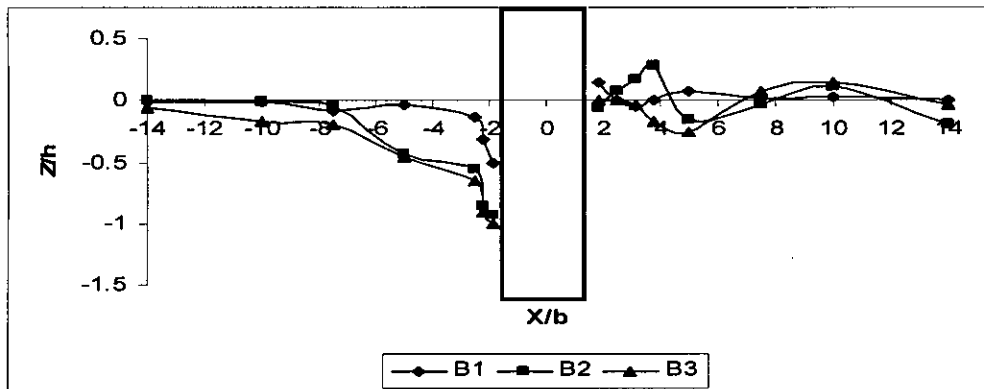
Figure 5.9: Bed profile variation in longitudinal direction for 200 l/s discharge (Main channel)



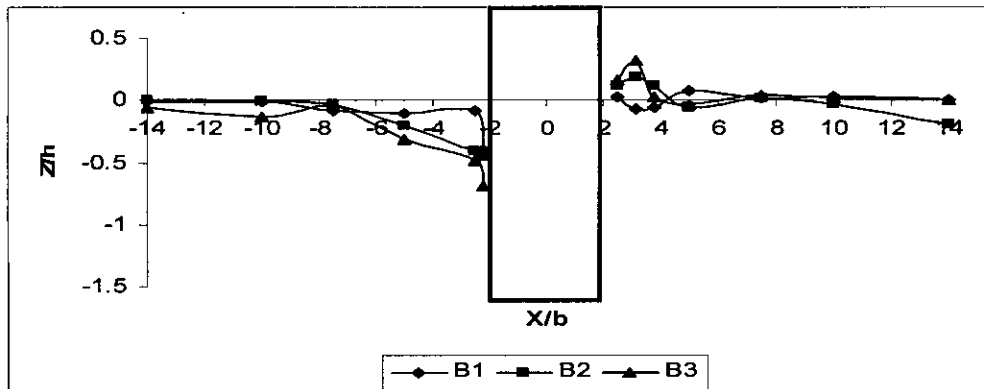
(a) Circular pier ( $l/b=1$ )



(b) Round nose pier ( $l/b=2$ )

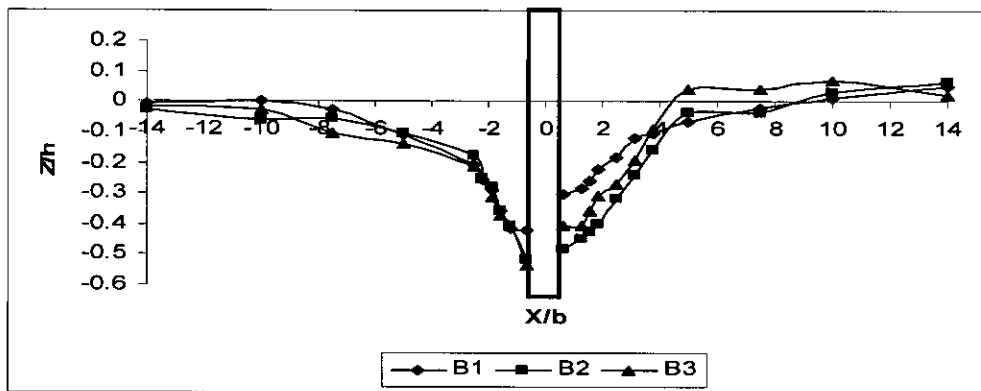


(c) Round nose pier ( $l/b=3$ )

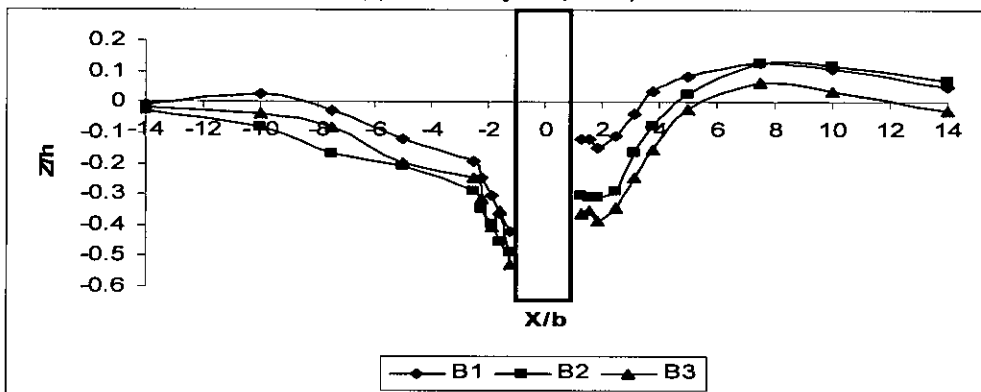


(d) Round nose pier ( $l/b=4$ )

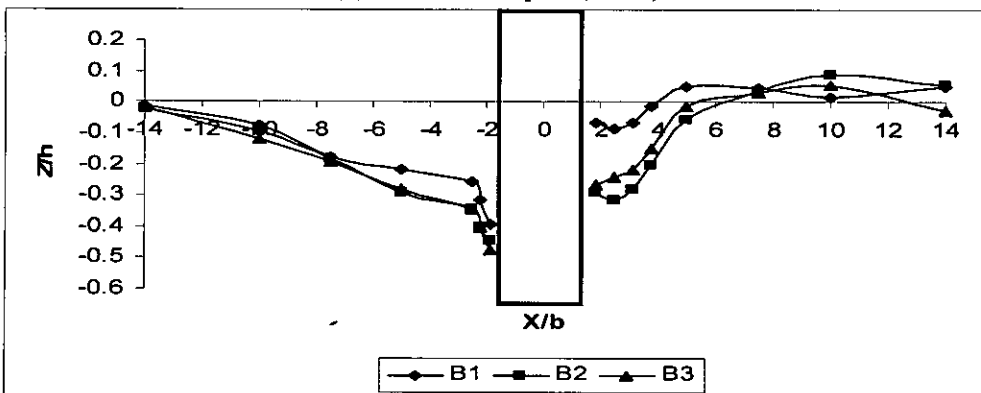
Figure 5.10: Bed profile variation in longitudinal direction for 175 l/s discharge (Floodplain)



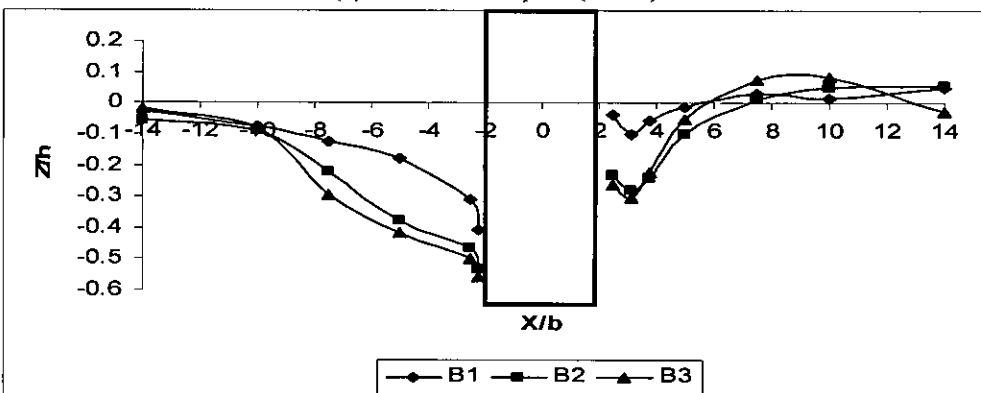
(a) Circular pier ( $l/b=1$ )



(b) Round nose pier ( $l/b=2$ )

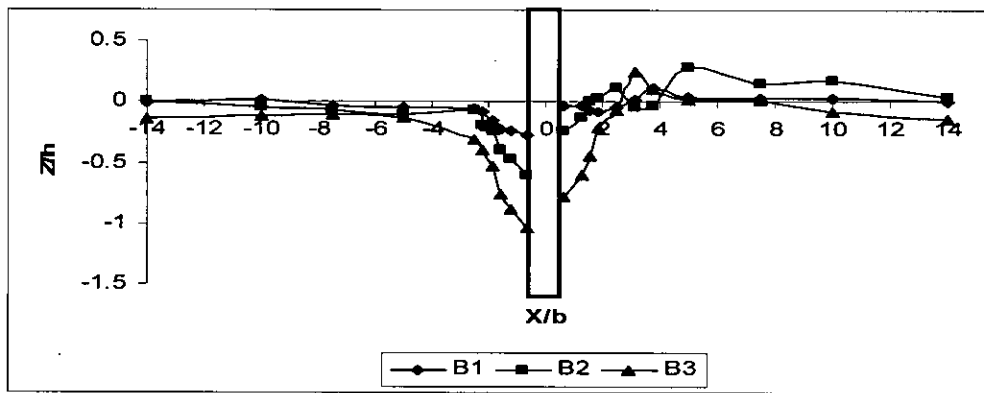


(c) Round nose pier ( $l/b=3$ )

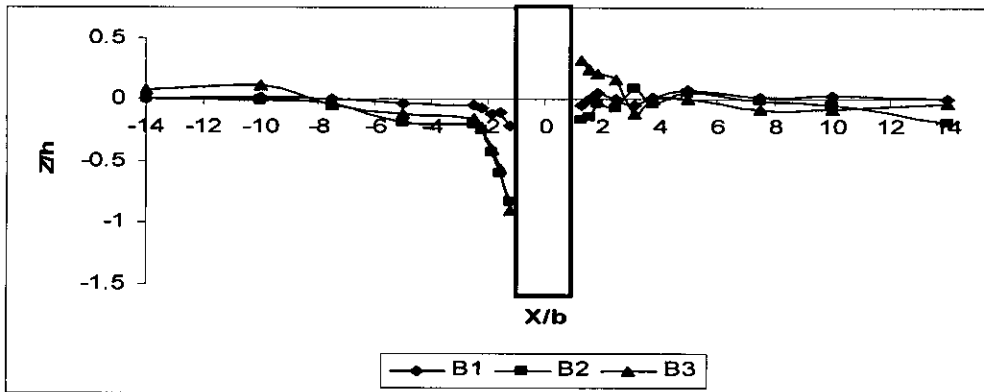


(d) Round nose pier ( $l/b=4$ )

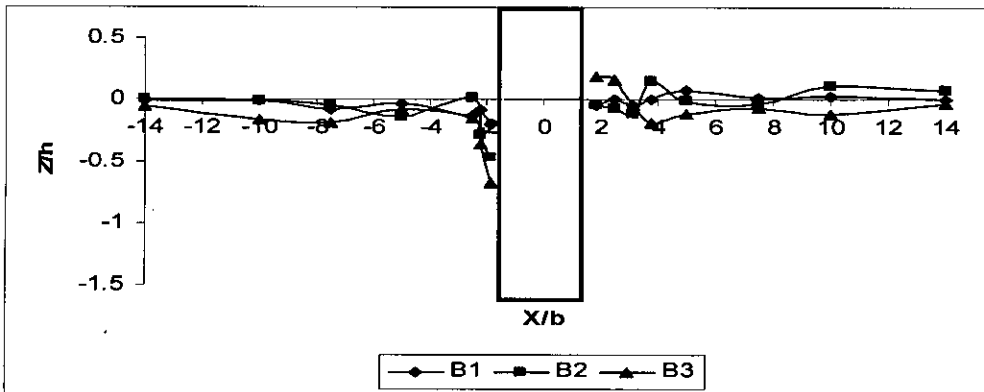
Figure 5.11: Bed profile variation in longitudinal direction for 175 l/s discharge (Main channel)



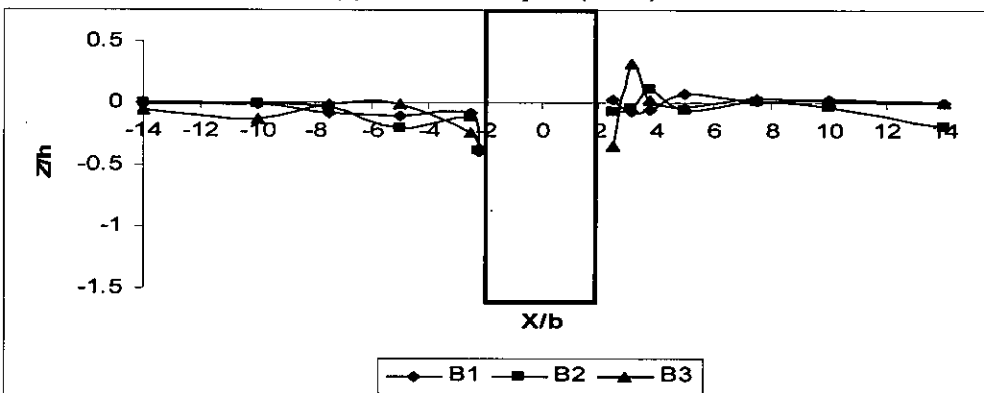
(a) Circular pier ( $l/b=1$ )



(b) Round nose pier ( $l/b=2$ )

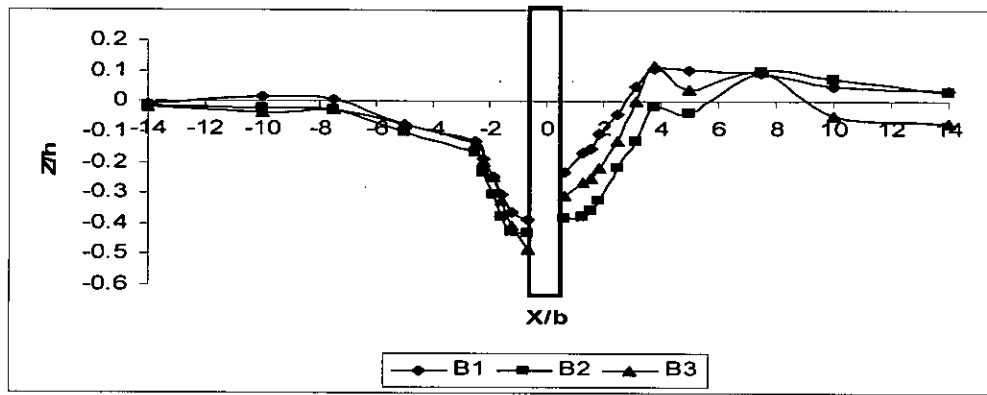


(c) Round nose pier ( $l/b=3$ )

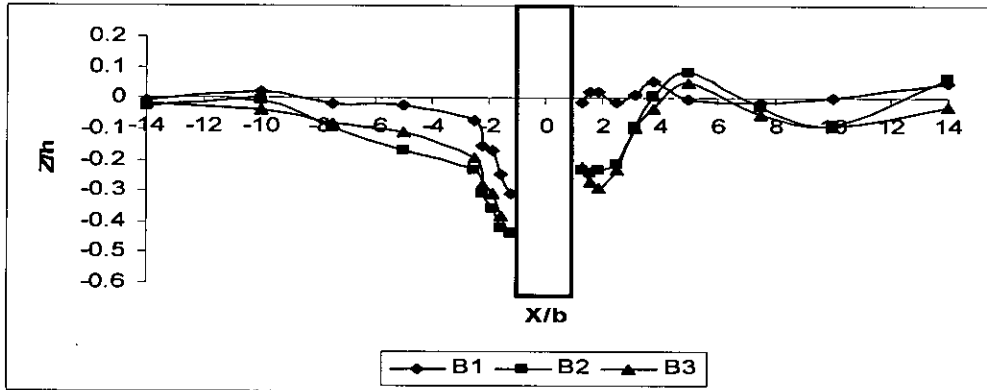


(d) Round nose pier ( $l/b=4$ )

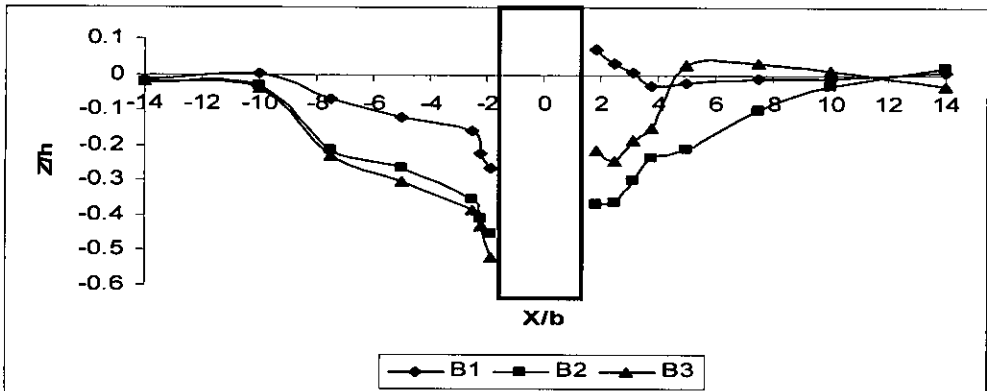
Figure 5.12: Bed profile variation in longitudinal direction for 150 l/s discharge (Floodplain)



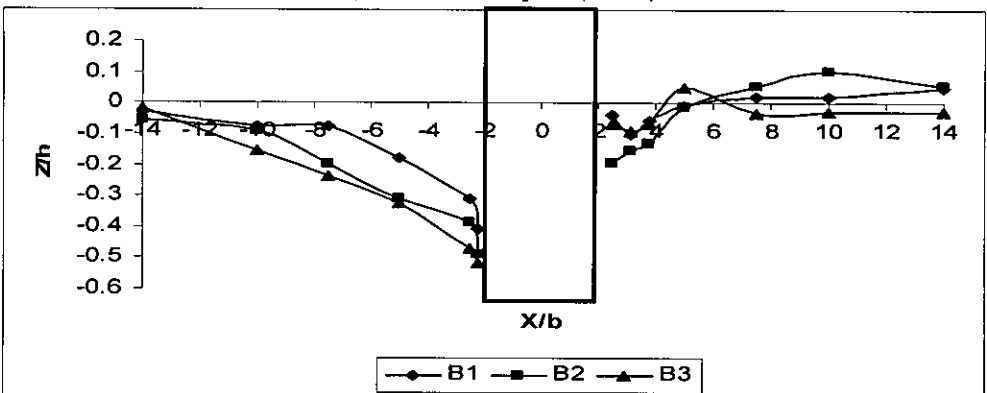
(a) Circular pier ( $l/b=1$ )



(b) Round nose pier ( $l/b=2$ )

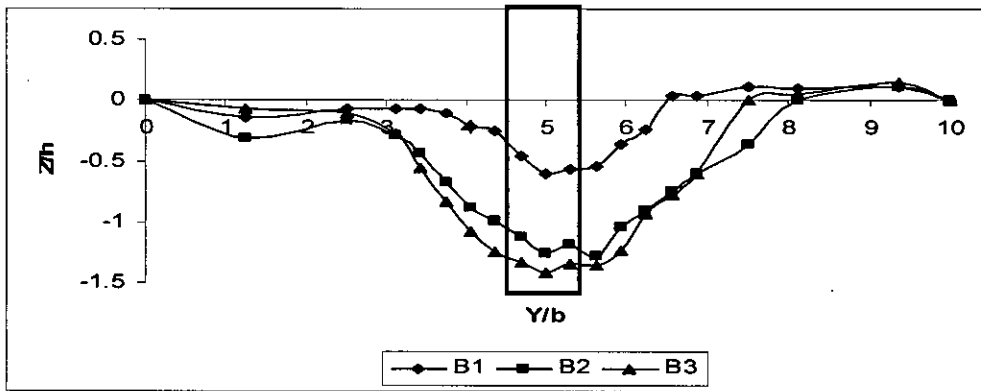


(c) Round nose pier ( $l/b=3$ )

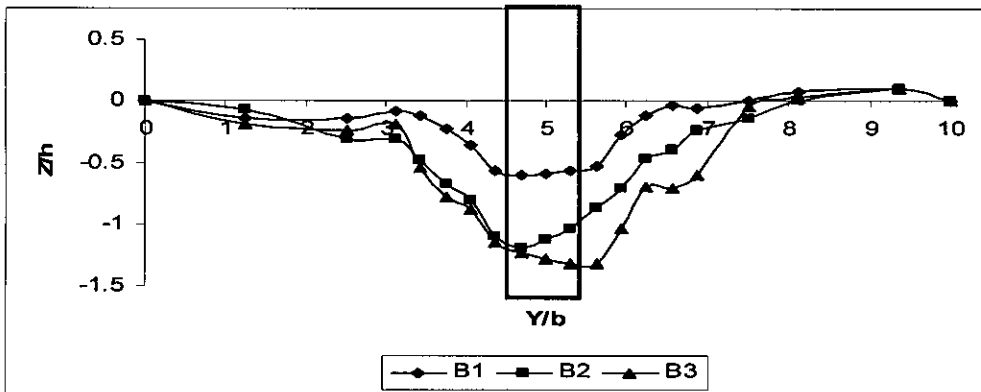


(d) Round nose pier ( $l/b=4$ )

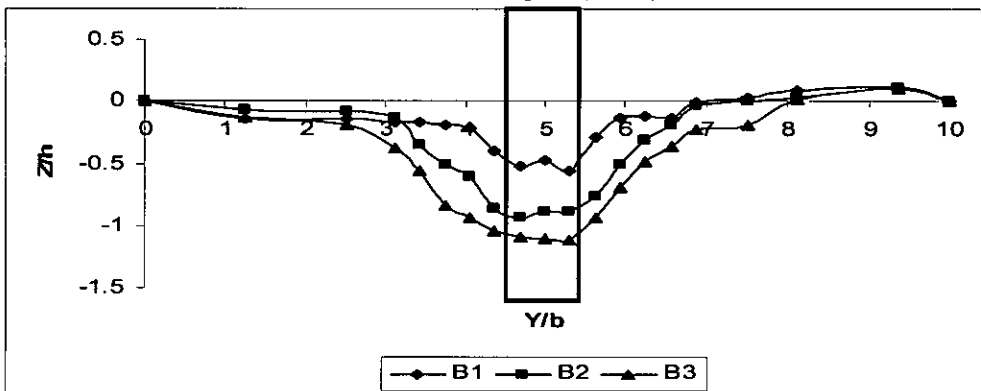
Figure 5.13: Bed profile variation in longitudinal direction for 150 l/s discharge (Main channel)



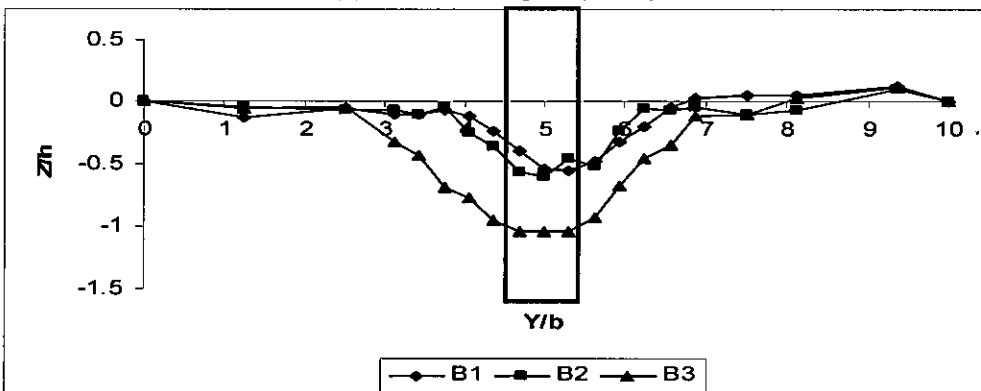
(a) Circular pier ( $l/b=1$ )



(b) Round nose pier ( $l/b=2$ )



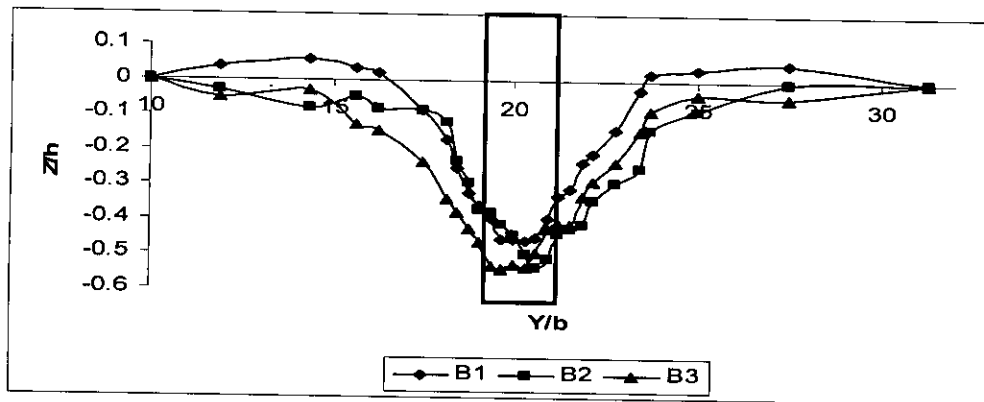
(c) Round nose pier ( $l/b=3$ )



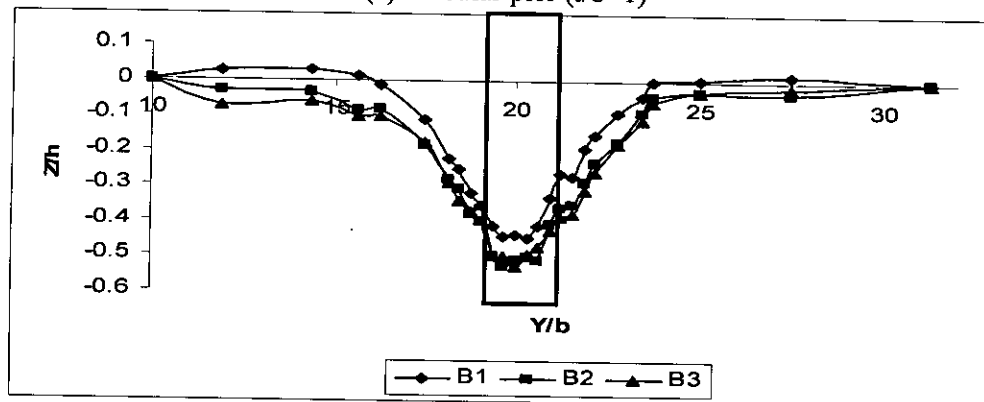
(d) Round nose pier ( $l/b=4$ )

Figure 5.14: Bed profile variation in lateral direction for 200 l/s discharge (Floodplain)

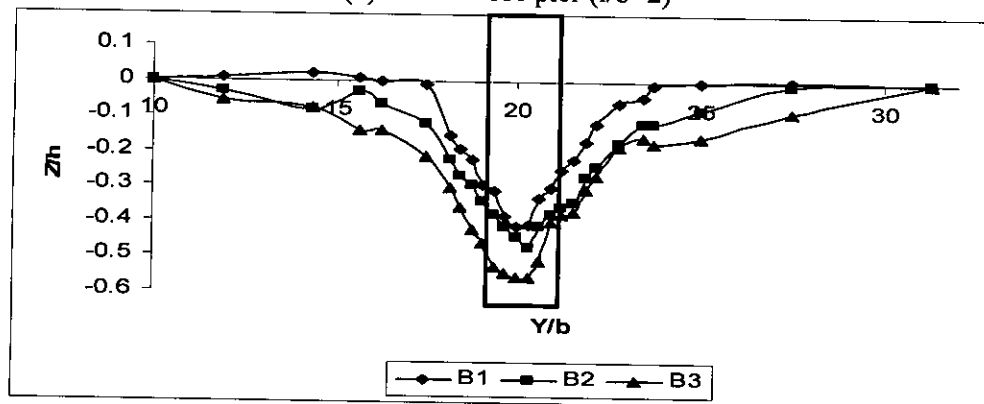




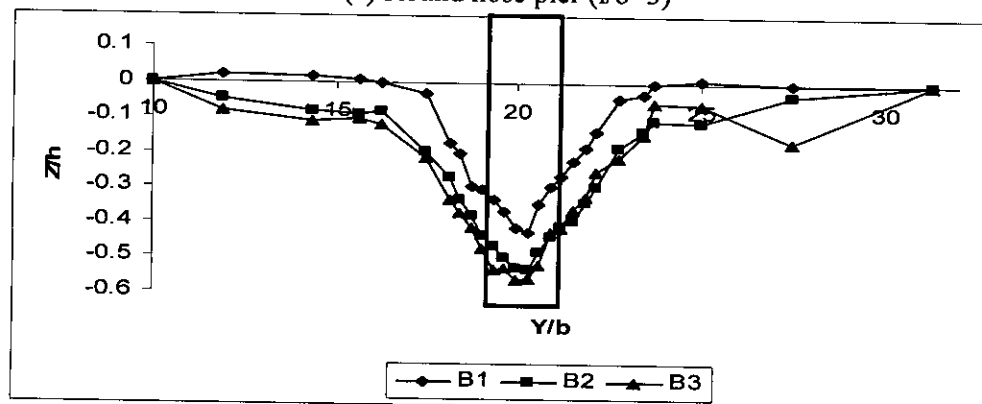
(a) Circular pier ( $l/b=1$ )



(b) Round nose pier ( $l/b=2$ )

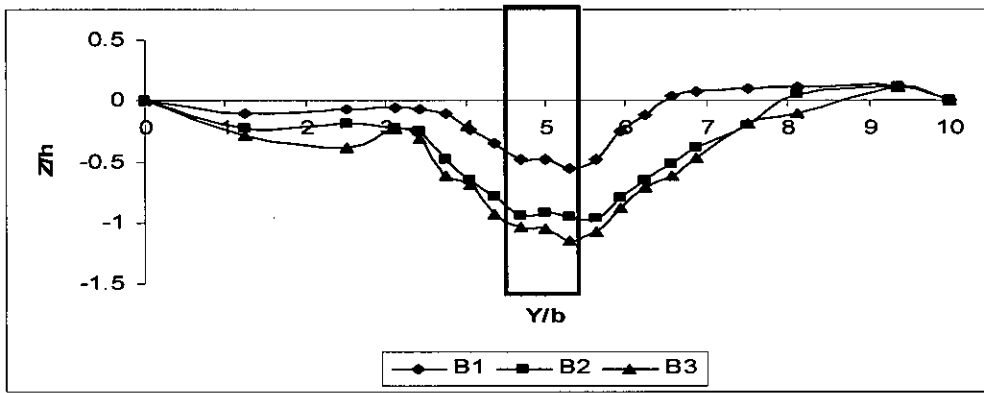


(c) Round nose pier ( $l/b=3$ )

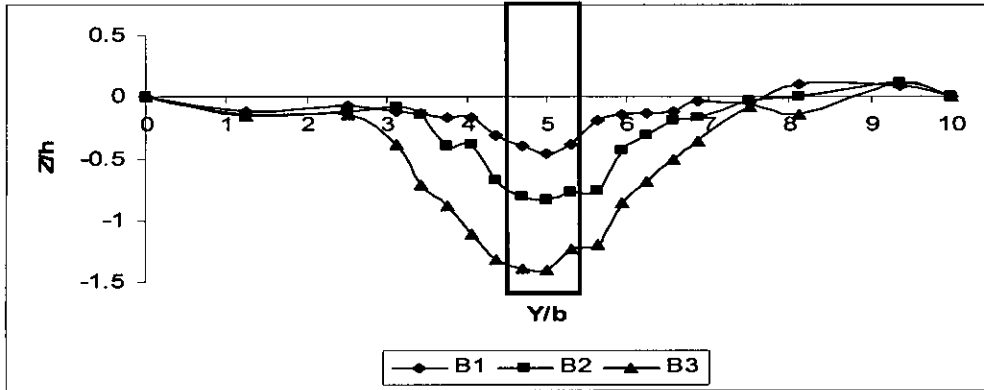


(d) Round nose pier ( $l/b=4$ )

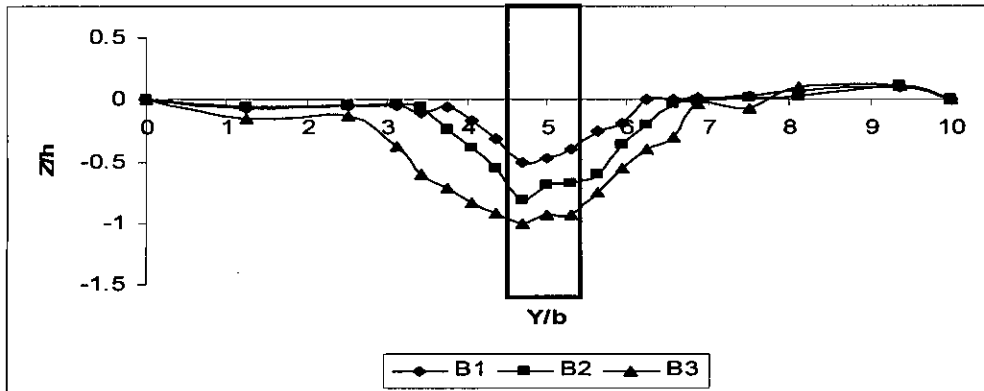
Figure 5.15: Bed profile variation in lateral direction for 200 l/s discharge (Main channel)



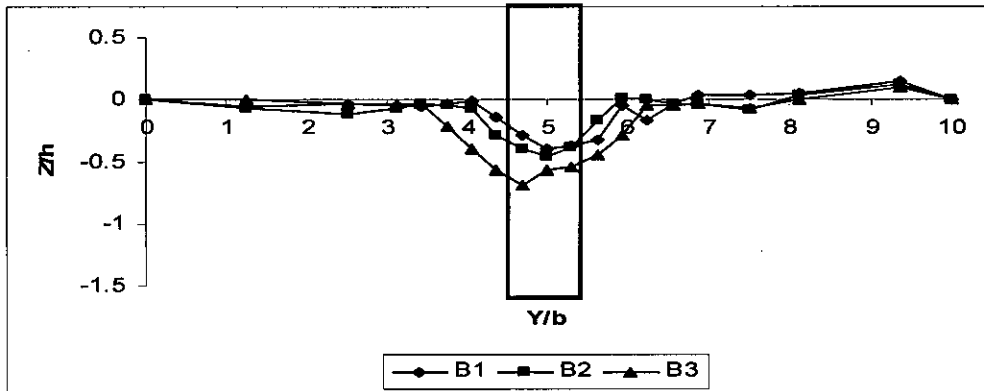
(a) Circular pier ( $l/b=1$ )



(b) Round nose pier ( $l/b=2$ )

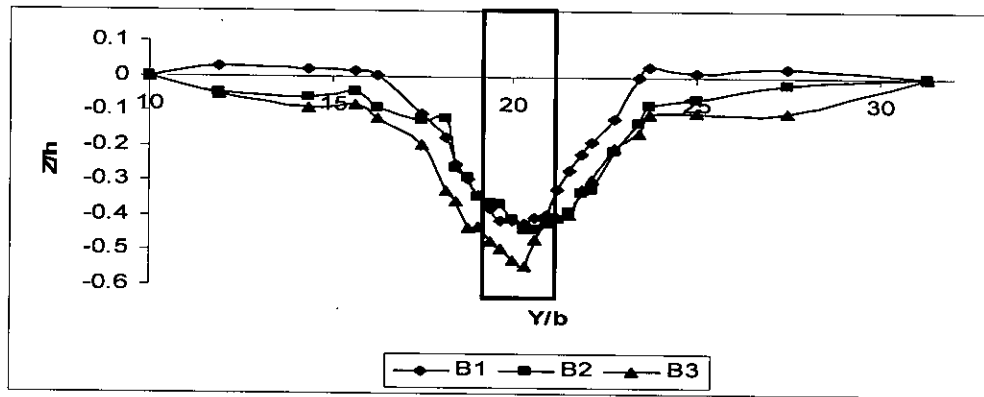


(c) Round nose pier ( $l/b=3$ )

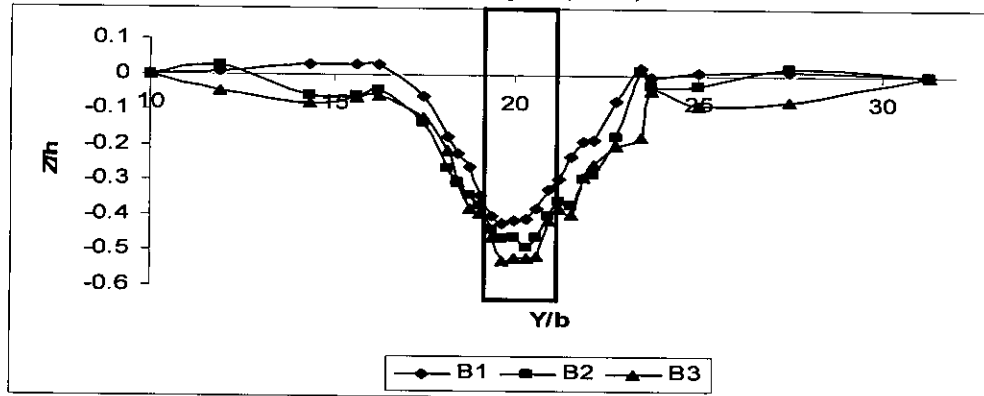


(d) Round nose pier ( $l/b=4$ )

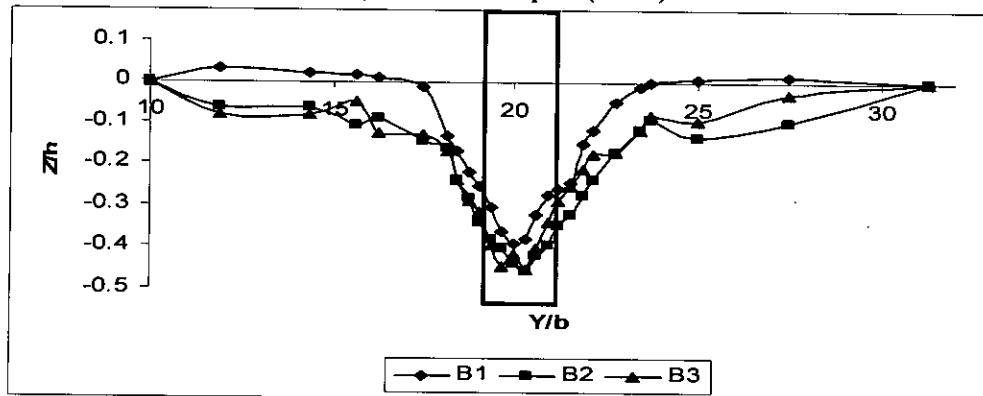
Figure 5.16: Bed profile variation in lateral direction for 175 l/s discharge (Floodplain)



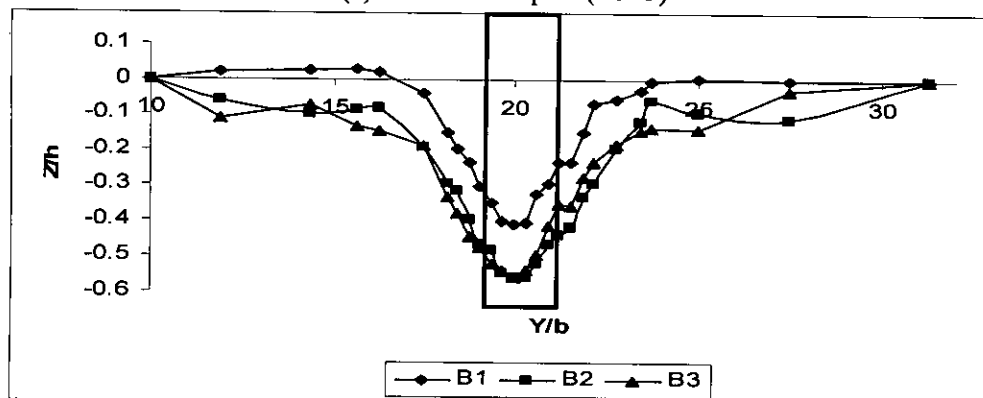
(a) Circular pier ( $l/b=1$ )



(b) Round nose pier ( $l/b=2$ )

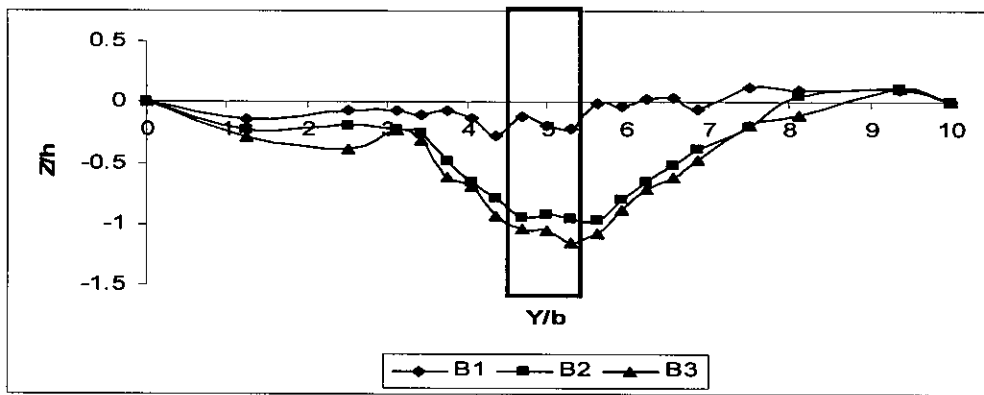


(c) Round nose pier ( $l/b=3$ )

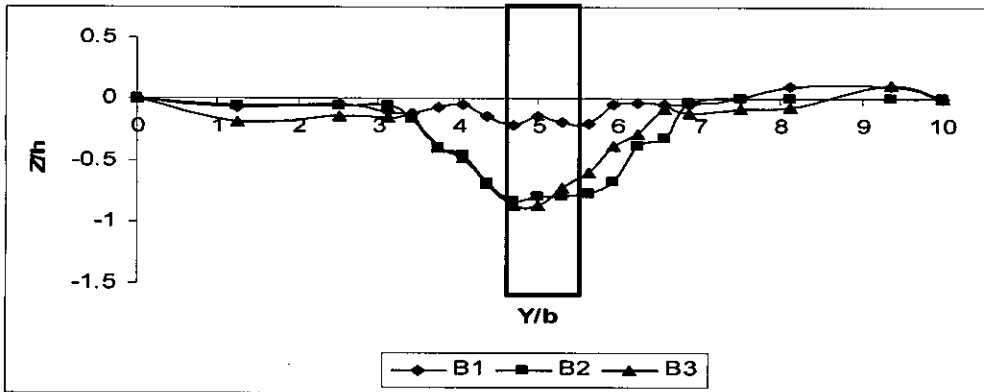


(d) Round nose pier ( $l/b=4$ )

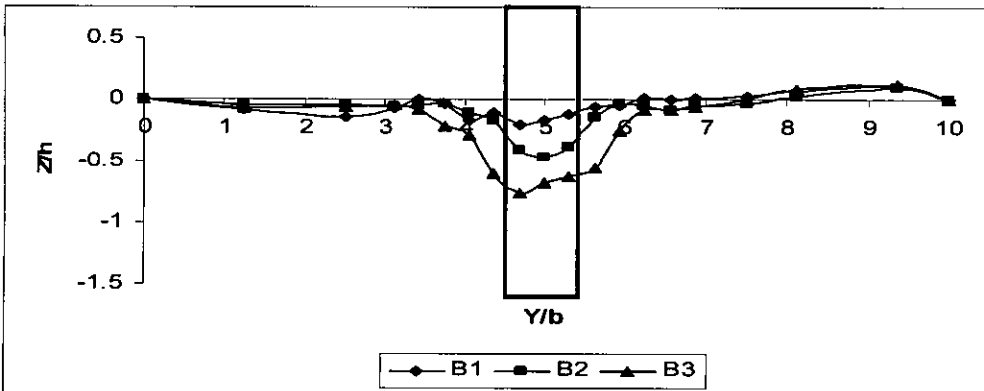
Figure 5.17: Bed profile variation in lateral direction for 175 l/s discharge (Main channel)



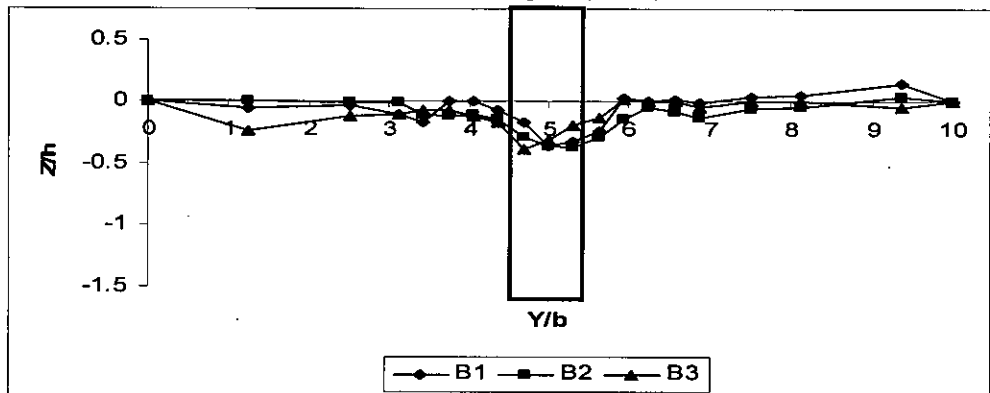
(a) Circular pier ( $l/b=1$ )



(b) Round nose pier ( $l/b=2$ )

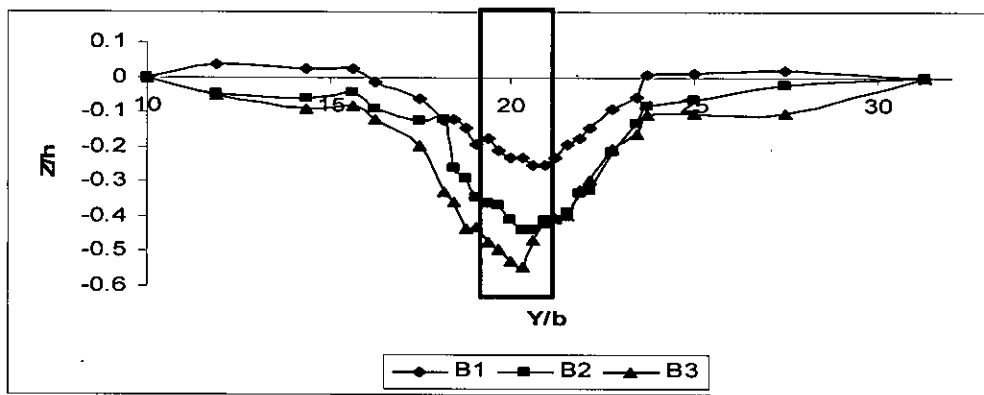


(c) Round nose pier ( $l/b=3$ )

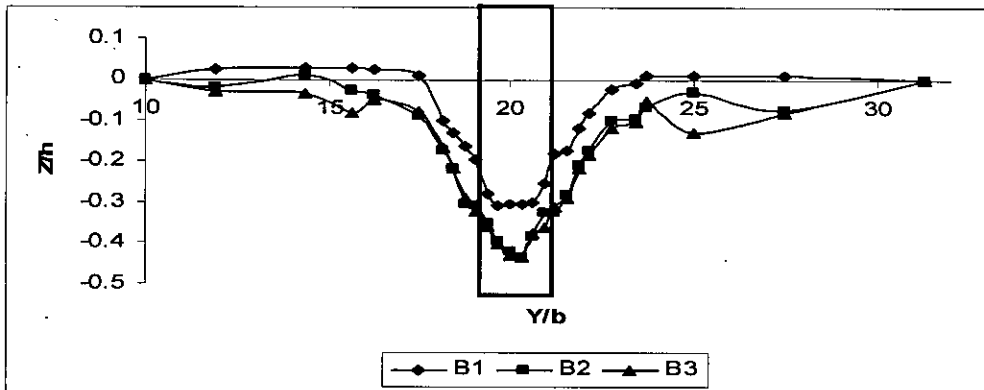


(d) Round nose pier ( $l/b=4$ )

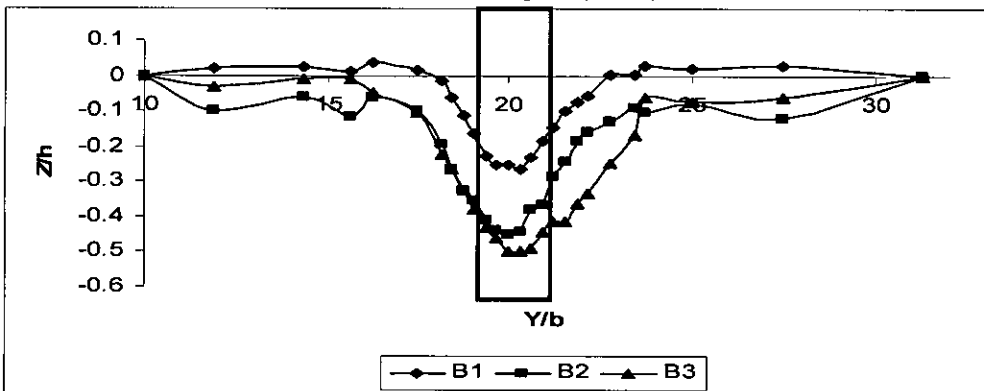
Figure 5.18: Bed profile variation in lateral direction for 150 l/s discharge (Floodplain)



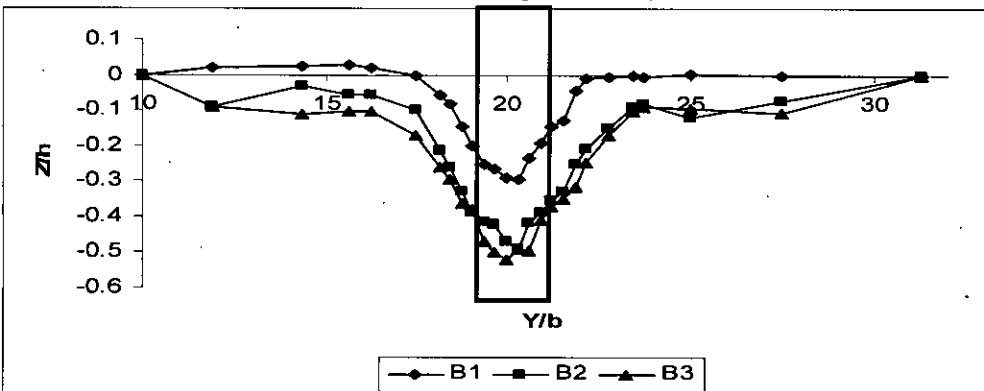
(a) Circular pier ( $l/b=1$ )



(b) Round nose pier ( $l/b=2$ )



(c) Round nose pier ( $l/b=3$ )



(d) Round nose pier ( $l/b=4$ )

Figure 5.19: Bed profile variation in lateral direction for 150 l/s discharge (Main channel)

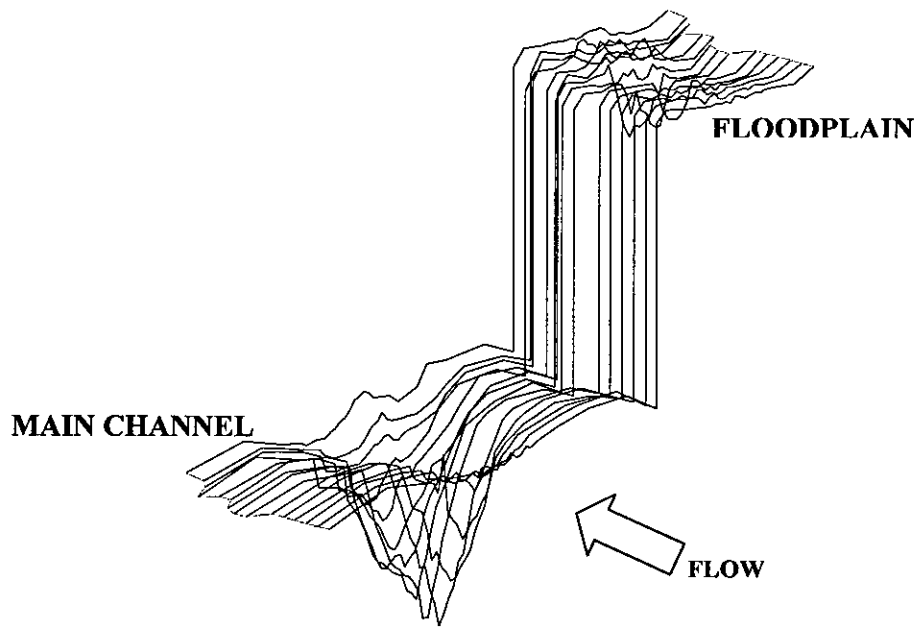


Figure 5.20: X-Y-Z perspective plot for Run 1-Circular Pier ( $l/b=1$ )  
Bed material 1 ( $d_{50} = 0.75$  mm)

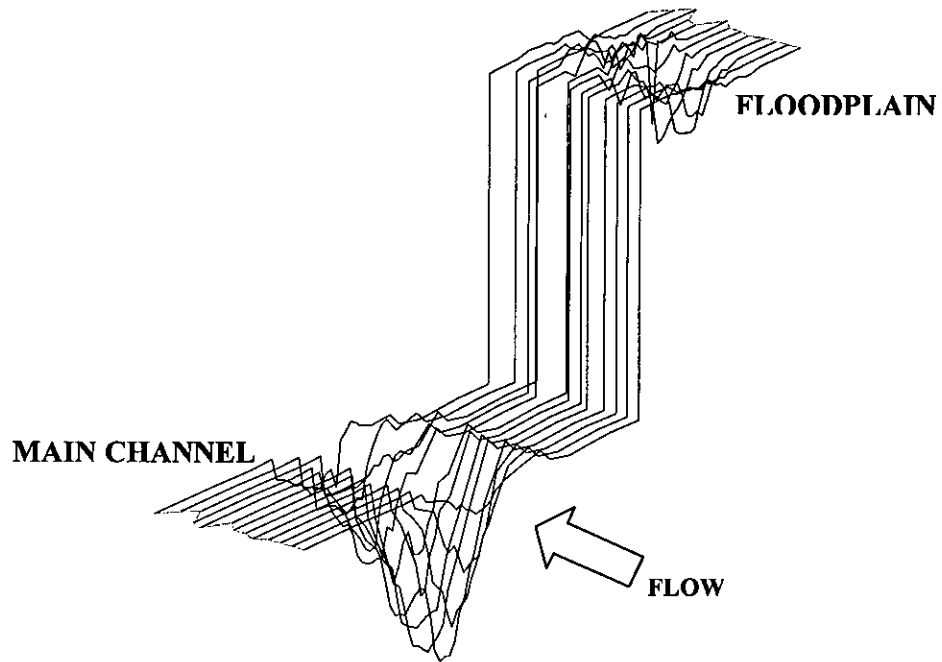


Figure 5.21: X-Y-Z perspective plot for Run 4-Round nose pier ( $l/b=2$ )  
Bed material 1 ( $d_{50} = 0.75$  mm)

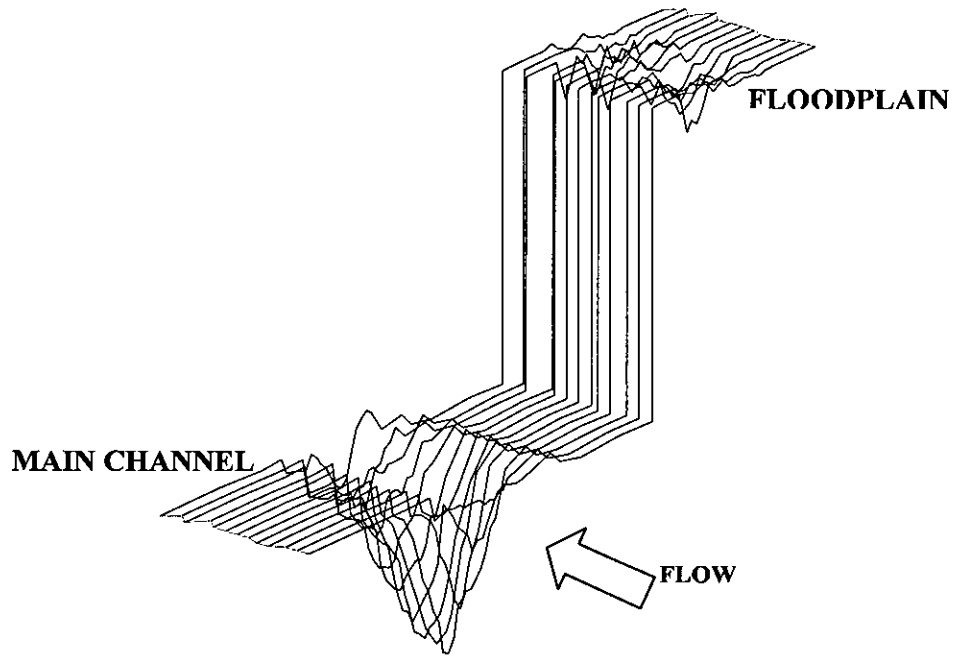


Figure 5.22: X-Y-Z perspective plot for Run 7-Round nose pier ( $l/b=3$ )  
Bed material 1 ( $d_{50} = 0.75$  mm)

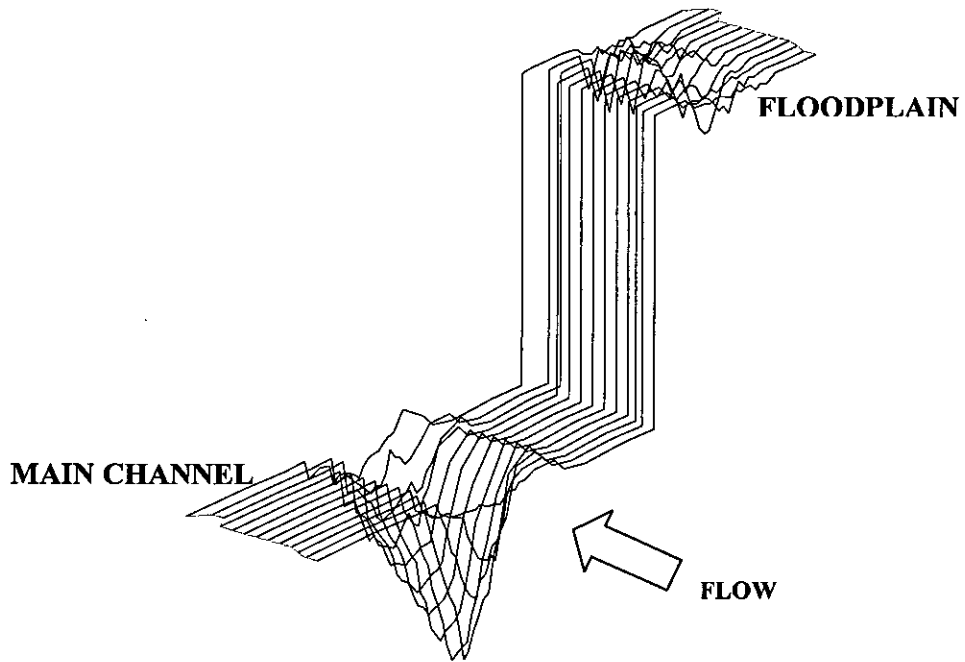


Figure 5.23: X-Y-Z perspective plot for Run 10-Round nose pier ( $l/b=4$ )  
Bed material 1 ( $d_{50} = 0.75$  mm)

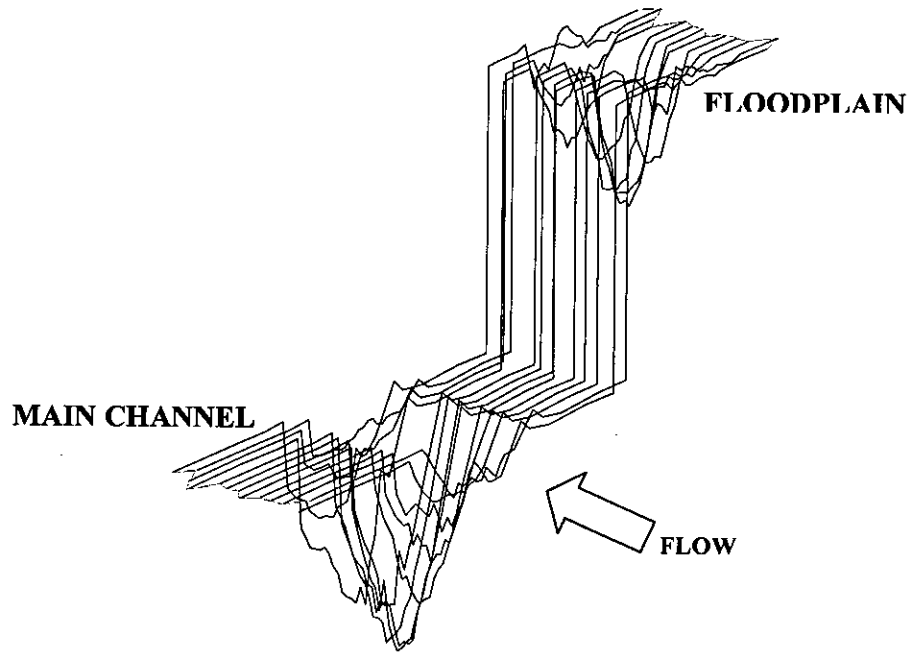


Figure 5.24: X-Y-Z perspective plot for Run 13-Circular Pier ( $l/b=1$ )  
Bed material 2 ( $d_{50} = 0.18$  mm)

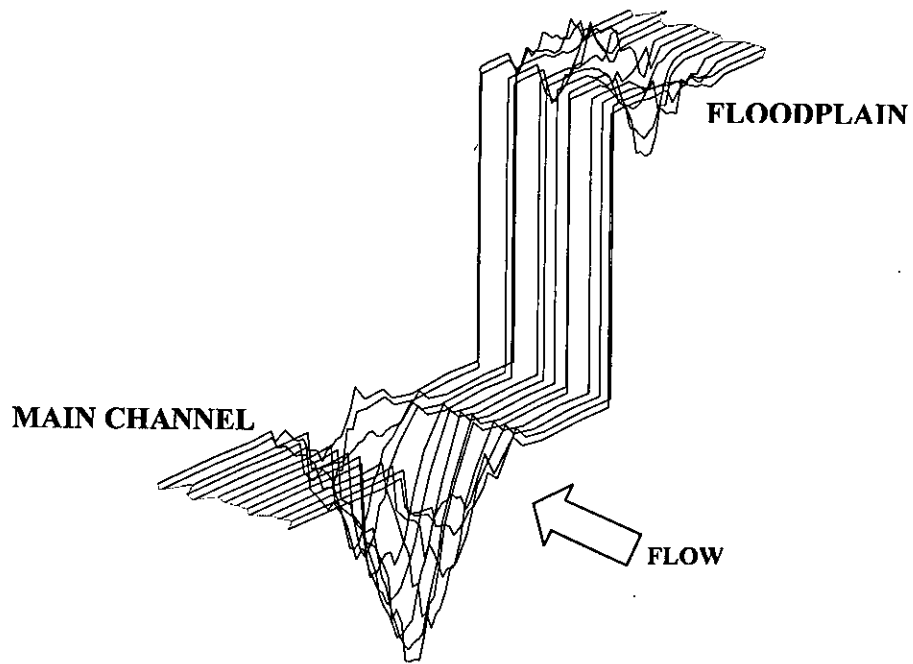


Figure 5.25: X-Y-Z perspective plot for Run 17-Round nose pier ( $l/b=2$ )  
Bed material 2 ( $d_{50} = 0.18$  mm)



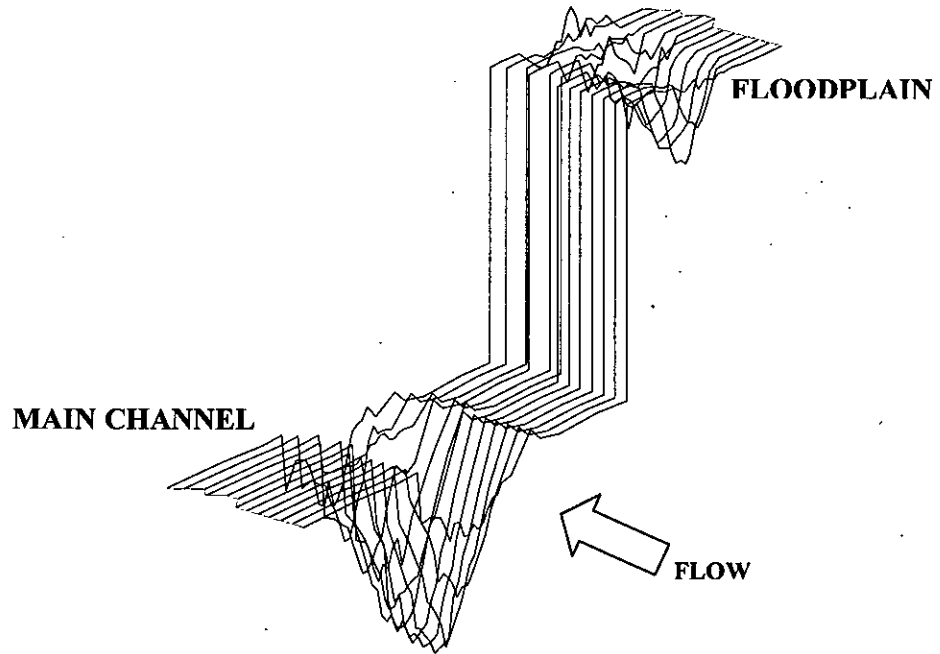


Figure 5.26: X-Y-Z perspective plot for Run 19-Round nose pier ( $l/b=3$ )  
Bed material 2 ( $d_{50} = 0.18$  mm)

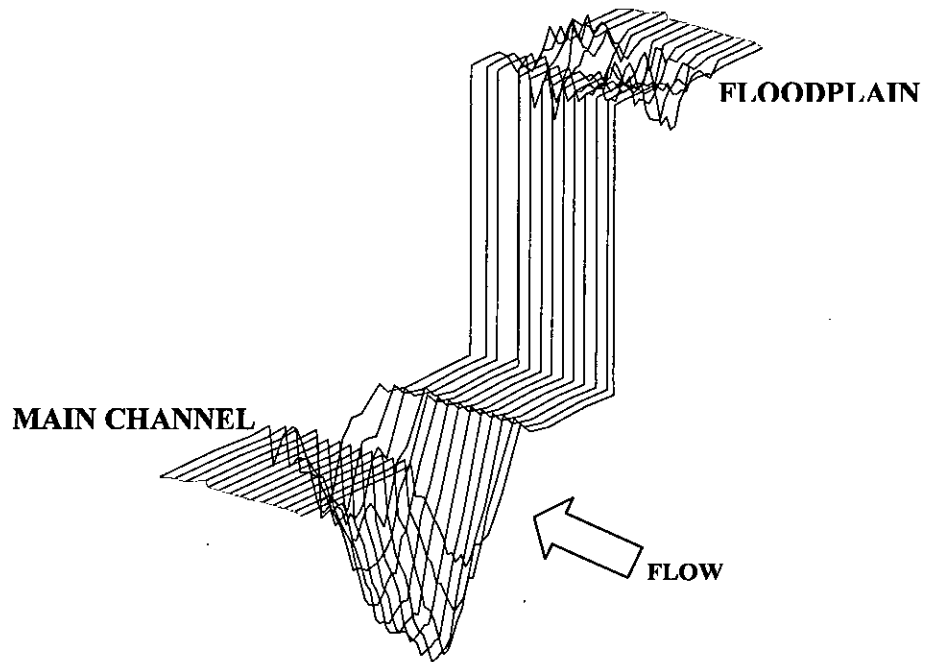


Figure 5.27: X-Y-Z perspective plot for Run 22-Round nose pier ( $l/b=4$ )  
Bed material 2 ( $d_{50} = 0.18$  mm)

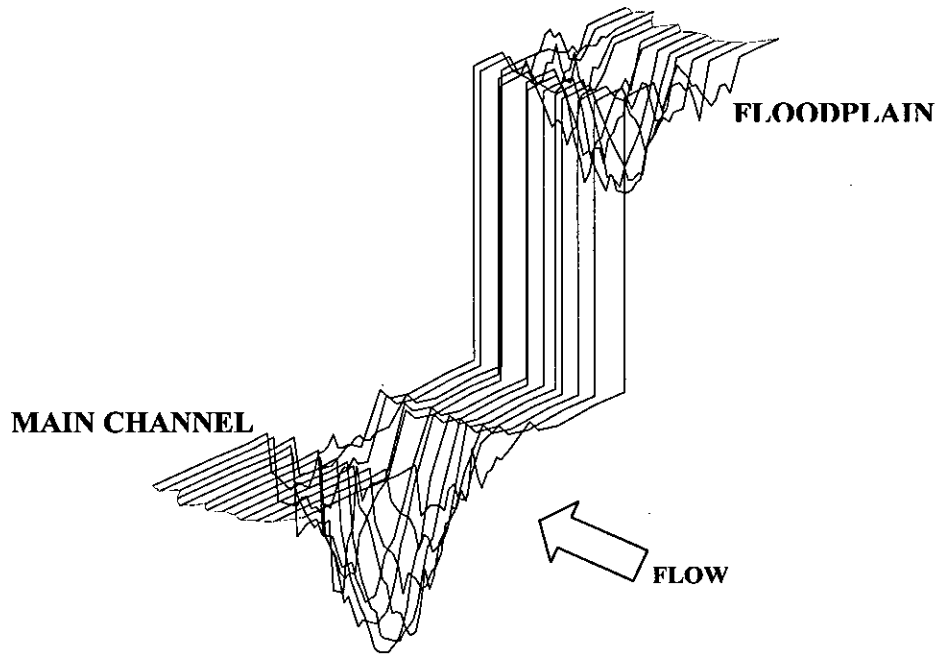


Figure 5.28: X-Y-Z perspective plot for Run 25-Circular Pier ( $l/b=1$ )  
Bed material 3 ( $d_{50} = 0.12$  mm)

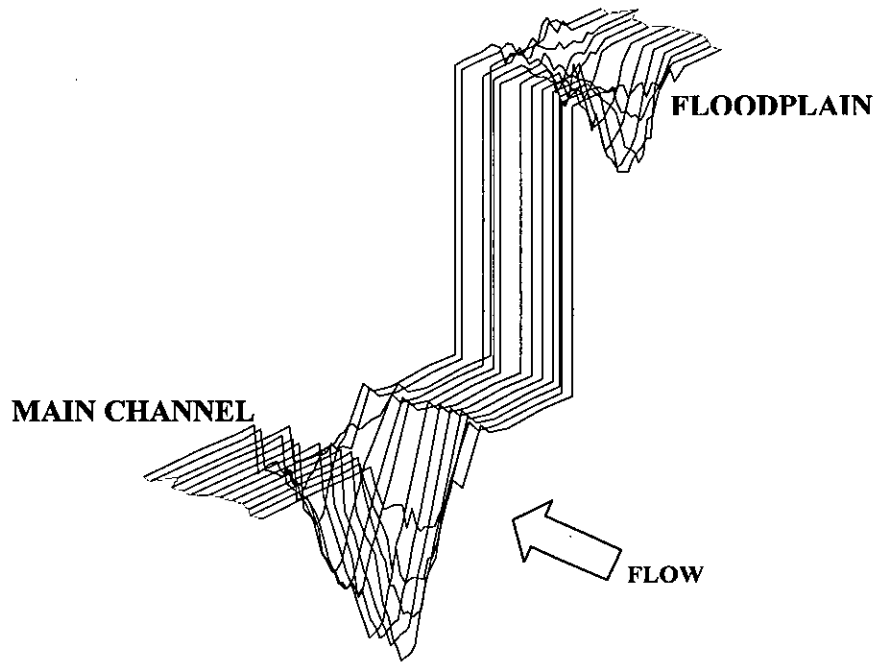


Figure 5.29: X-Y-Z perspective plot for Run 28-Round nose pier ( $l/b=2$ )  
Bed material 3 ( $d_{50} = 0.12$  mm)

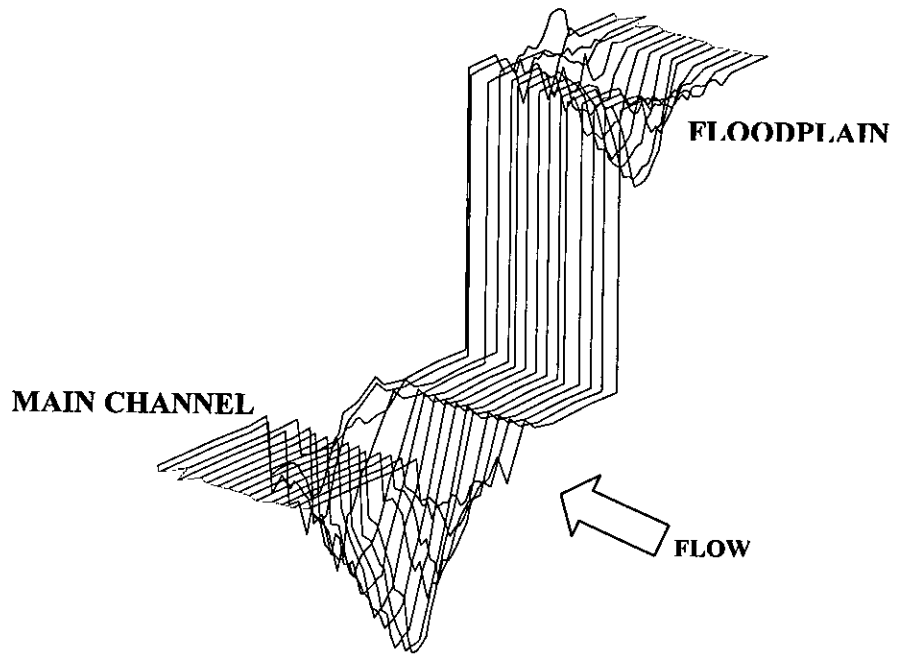


Figure 5.30: X-Y-Z perspective plot for Run 31-Round nose pier ( $l/b=3$ )  
Bed material 3 ( $d_{50} = 0.12$  mm)

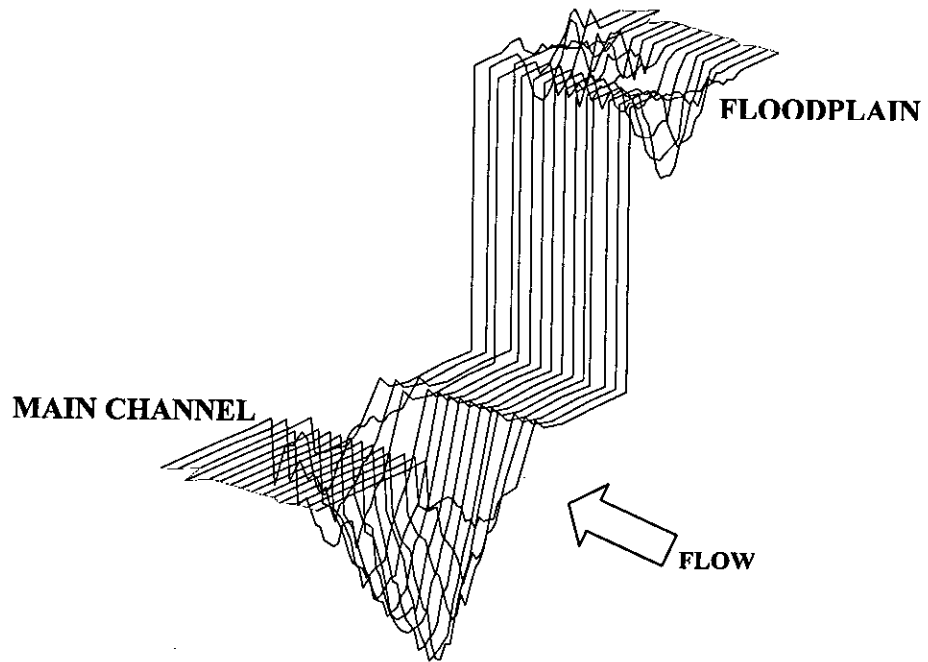


Figure 5.31: X-Y-Z perspective plot for Run 34-Round nose pier ( $l/b=4$ )  
Bed material 3 ( $d_{50} = 0.12$  mm)

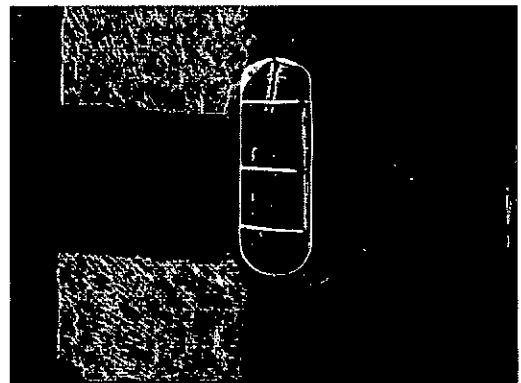
## 5.6 Analysis of velocity

Two velocity components, namely streamwise velocity ( $V_x$ ) and transverse velocity ( $V_y$ ) have been measured at pre-defined grid points and selected depths with a programmable electromagnetic velocity meter (P-EMS) around structure both in main channel and floodplain. To evaluate changes in flow field for variable discharges, structure shapes and length-width ratio in three different bed materials, comparison has been shown in longitudinal, lateral and vertical directions respectively. For floodplain longitudinal direction, velocity data at  $Y/b$  (floodplain width/structure width) = 0 (40 cm away from left bank) and for main channel longitudinal direction, velocity data at  $Y/b$  (main channel width/structure width) = 0 (162.5 cm away from left bank) are considered. Velocity data at 5 cm upstream of front face of structure are used to show velocity variation in lateral direction both floodplain and main channel. Graphical presentation of vertical velocity variation has been produced from velocity data of various  $Z/h$  depths measured at  $Y/b = 0$  and  $X = -5$  cm from front face of structure.

Beside these, velocity vector diagrams (produced by Stanford Graphics software) and  $V/V_c$  contour maps (developed by Surfer software) has been presented to examine flow field around structure. Following photographs (Photograph 5.1) show practical flow scenario around circular pier and round nose pier.



(a) Circular pier



(b) Round nose pier

Photograph 5.1: Flow around circular pier and round nose pier

### 5.6.1 Velocity variation in longitudinal direction

Figure 5.32, Figure 5.34 and Figure 5.36 represent longitudinal velocity variation at floodplain for variable discharges namely 200 l/s, 175 l/s, 150 l/s in bed material 1 ( $d_{50} = 0.75$  mm), bed material 2 ( $d_{50} = 0.18$  mm) and bed material 3 ( $d_{50} = 0.12$  mm), respectively while Figure 5.33, Figure 5.35 and Figure 5.37 present same at main channel.

Velocity along longitudinal direction varies from higher to lower with decreasing discharges. In general, reduction in longitudinal velocity has been observed in front of structure. This may be happened due to separation of flow at upstream face of structure. Velocity is found negligible at rear face of structure and gradually regaining its original velocity after traveling downstream distance. Longitudinal velocity also varies from higher to lower with decreasing length-width ratio. Same findings have been observed both in floodplain and main channel cases except velocity is found higher in main channel than that of floodplain.

### 5.6.2 Velocity variation in lateral direction

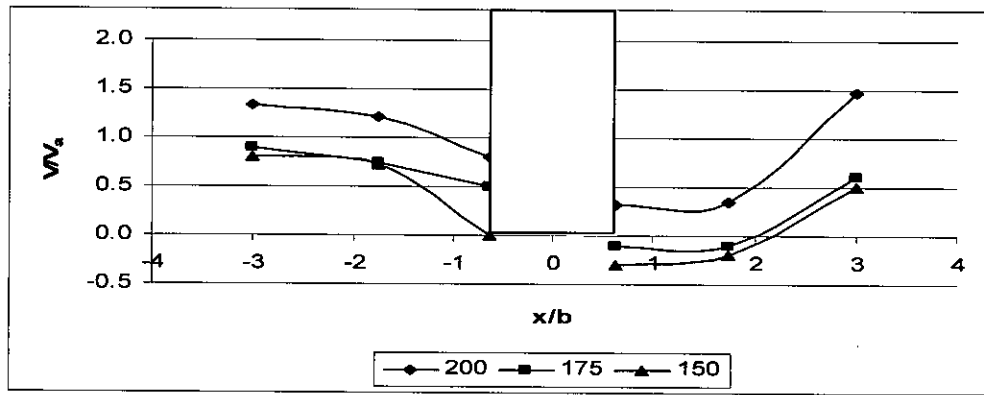
Velocity variation plots in lateral direction have been arranged in Figure 5.38-Figure 5.43. Figure 5.38, Figure 5.40 and Figure 5.42 show velocity variation at floodplain in bed material 1 ( $d_{50} = 0.75$  mm), bed material 2 ( $d_{50} = 0.18$  mm) and bed material 3 ( $d_{50} = 0.12$  mm) respectively for variable discharges. On the other hand, Figure 5.39, Figure 5.41 and Figure 5.43 show velocity variation at main channel for same condition as floodplain.

Velocity variation is found uniform at lateral direction in all experimental runs. Generally it has been observed that velocity starts to decrease steeply at  $Y/b = -1$  and reaches minimum value at  $Y/b = 0$ , i.e. in front of structure. Then it rises sharply till  $Y/b = +1$  and becoming normal after that. Same decreasing trend of velocity has been found for discharge variation and for length-width ratio variation in both floodplain and main channel.

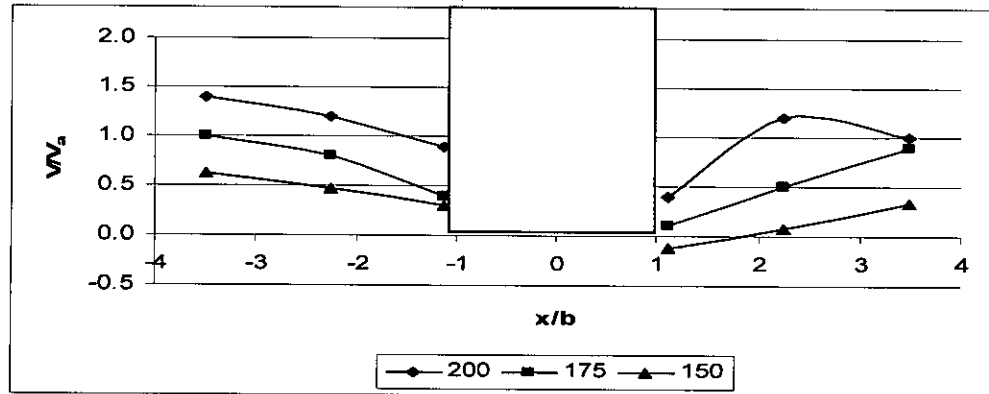
### 5.6.3 Velocity variation in vertical direction

Graphical representation of vertical velocity variation at floodplain has been organized in Figure 5.44 for bed material 1 ( $d_{50} = 0.75$  mm), Figure 5.46 for bed material 2 ( $d_{50} = 0.18$  mm) and Figure 5.48 for bed material 3 ( $d_{50} = 0.12$  mm). Same is performed for main channel in Figure 5.45 for bed material 1 ( $d_{50} = 0.75$  mm), Figure 5.47 for bed material 2 ( $d_{50} = 0.18$  mm) and Figure 5.49 for bed material 3 ( $d_{50} = 0.12$  mm).

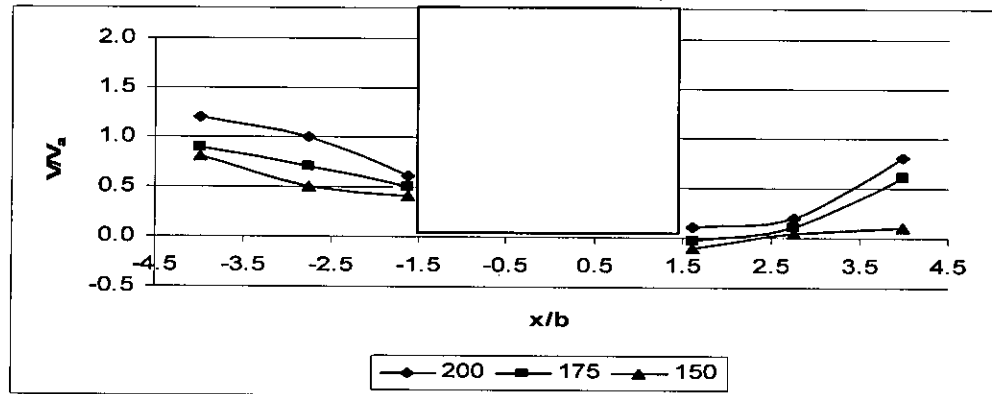
It has been analyzed that vertical velocity profile clearly indicates to downward movement of flow at front face of structure. In most cases, vertical velocity decreases from upper height of profile and shows an increasing trend at lower part of velocity profile. This increasing and decreasing pattern is also clearly associated with vortex generation and may be responsible for scouring around structure. Velocity profile has been found variable with different discharges and does not follow its natural logarithmic pattern. It may be caused due to creation of a complex flow field by interaction between flow and structure. Main channel vertical velocity profiles show same characteristics as floodplain but magnitude is higher in case of main channel velocity.



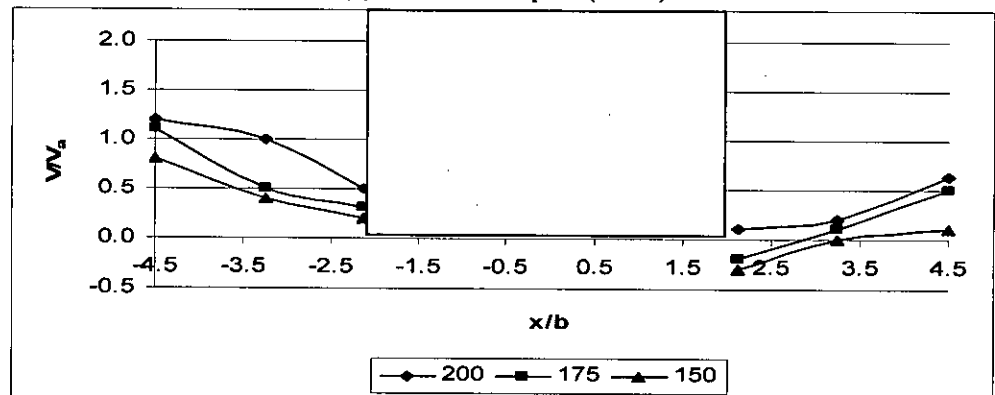
(a) Circular pier ( $l/b=1$ )



(b) Round nose pier ( $l/b=2$ )

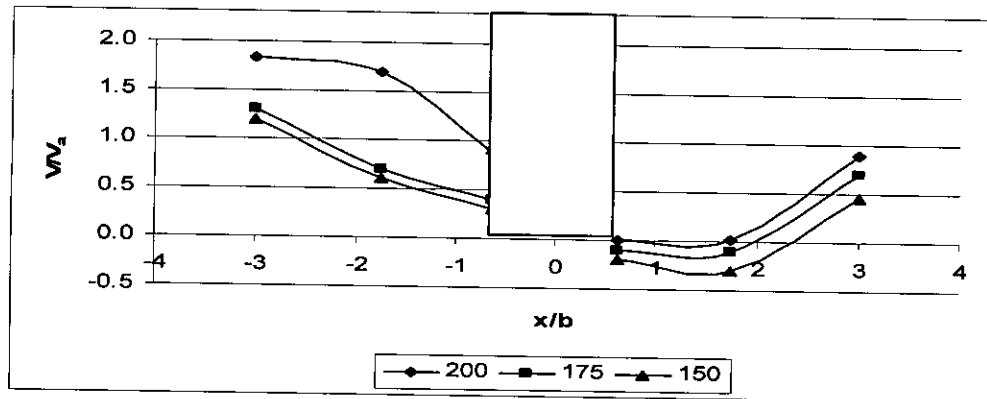


(c) Round nose pier ( $l/b=3$ )

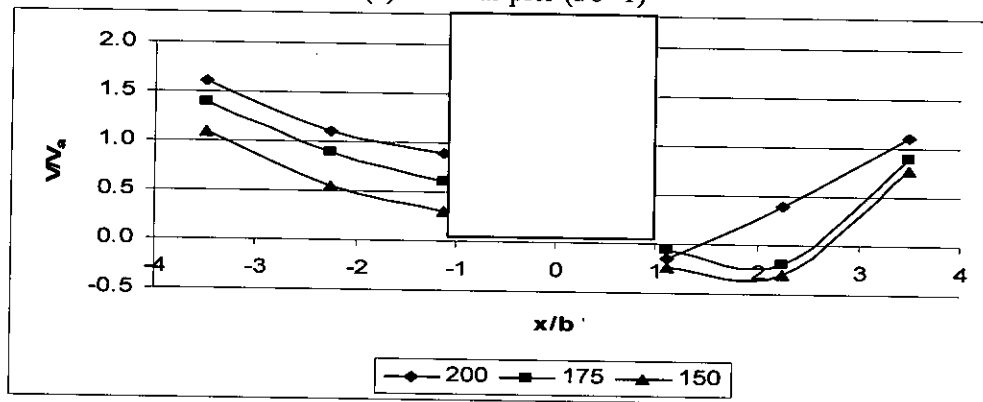


(d) Round nose pier ( $l/b=4$ )

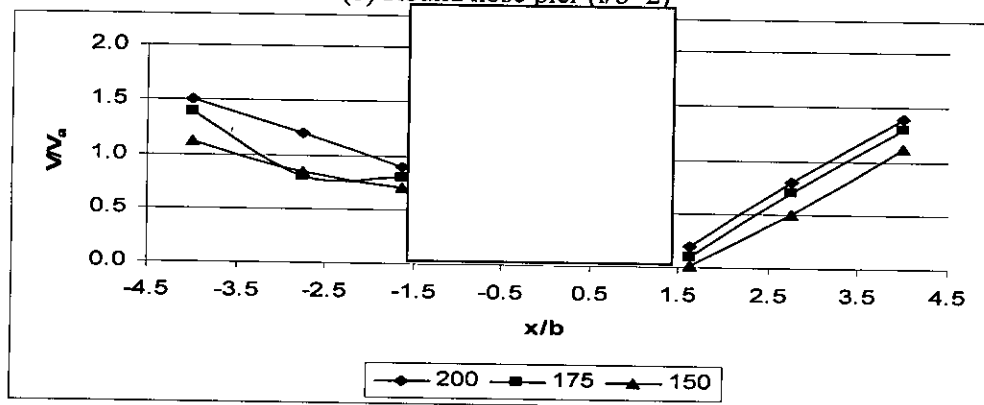
Figure 5.32: Velocity variation in longitudinal direction at Floodplain for Bed material 1 ( $d_{50} = 0.75$  mm)



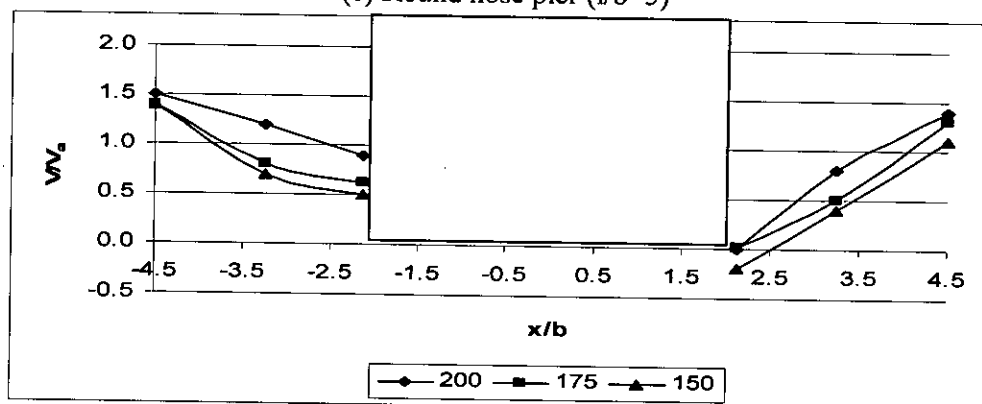
(a) Circular pier ( $l/b=1$ )



(b) Round nose pier ( $l/b=2$ )



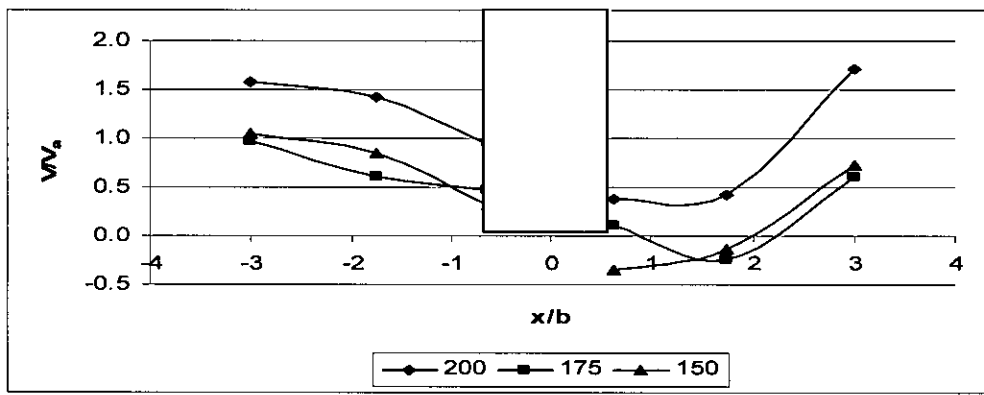
(c) Round nose pier ( $l/b=3$ )



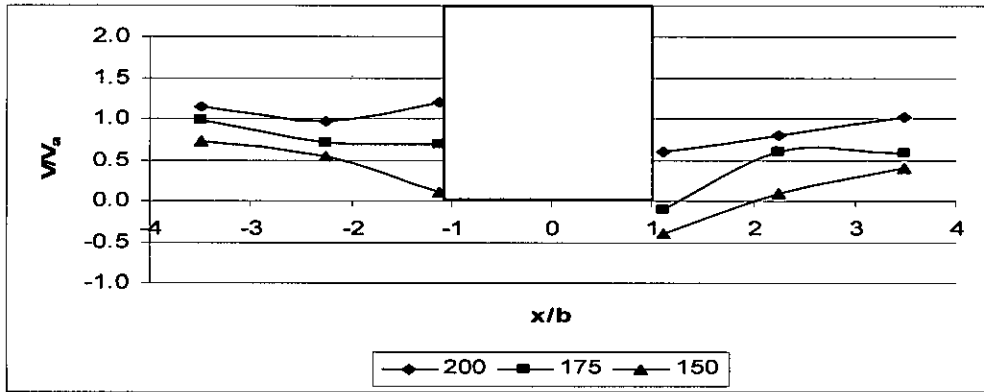
(d) Round nose pier ( $l/b=4$ )

Figure 5.33: Velocity variation in longitudinal direction at Main channel for Bed material 1 ( $d_{50} = 0.75$  mm)

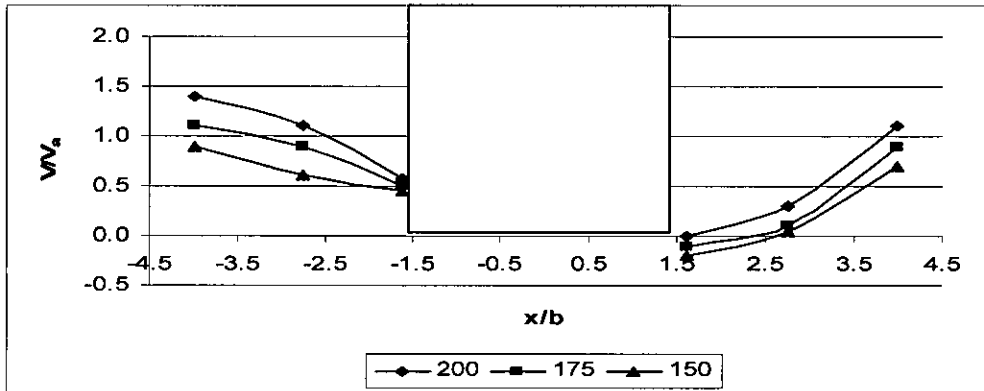




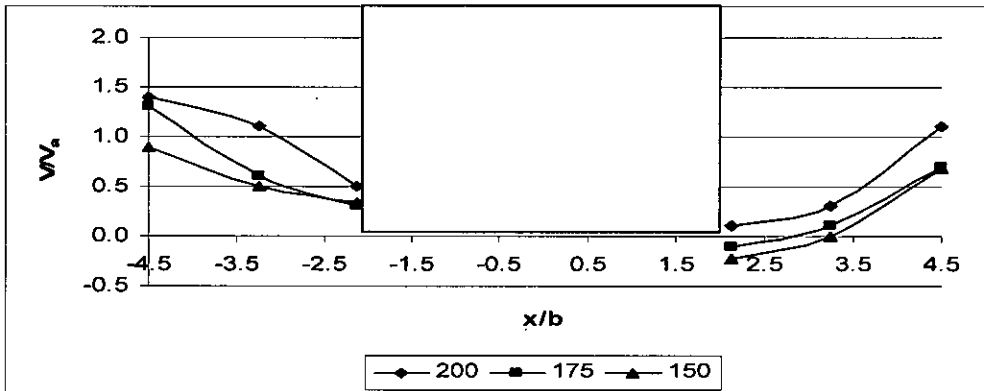
(a) Circular pier ( $l/b=1$ )



(b) Round nose pier ( $l/b=2$ )

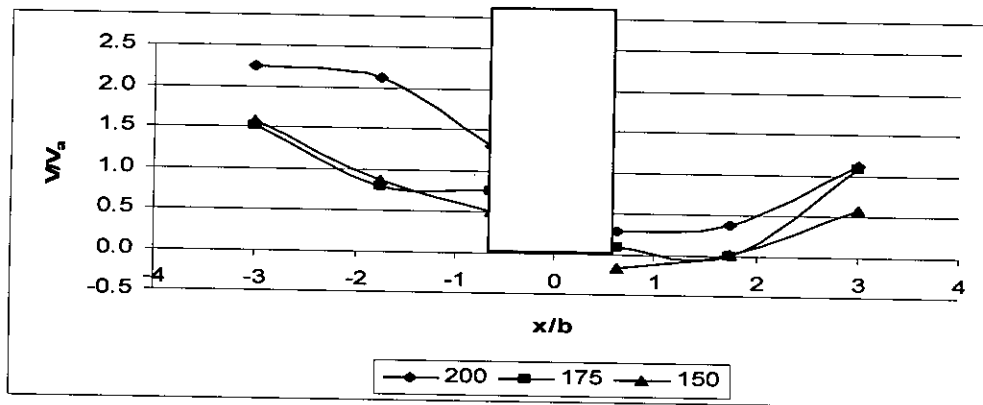


(c) Round nose pier ( $l/b=3$ )

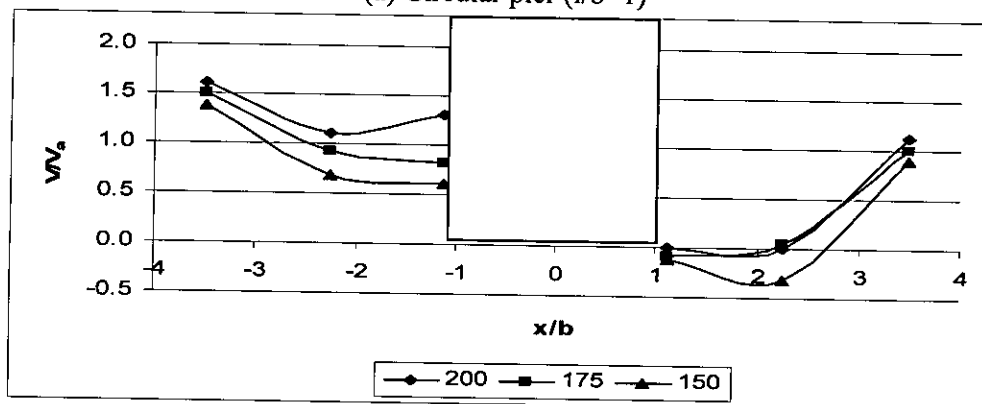


(d) Round nose pier ( $l/b=4$ )

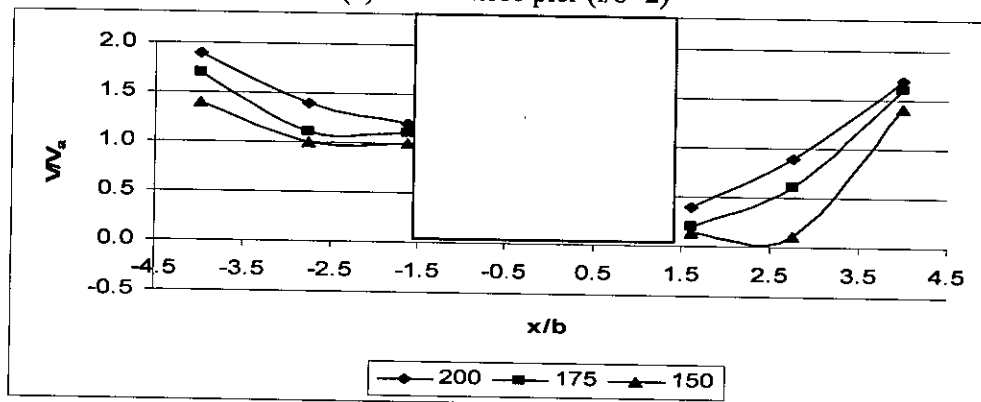
Figure 5.34: Velocity variation in longitudinal direction at Floodplain for Bed material 2 ( $d_{50} = 0.18$  mm)



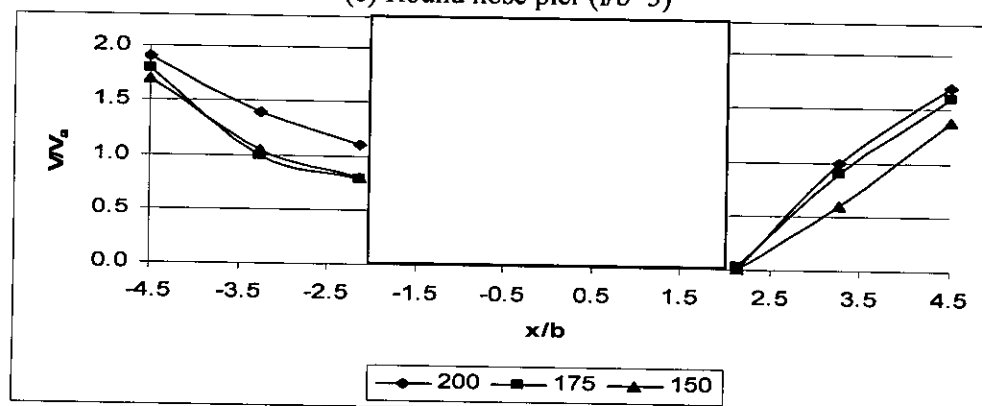
(a) Circular pier ( $l/b=1$ )



(b) Round nose pier ( $l/b=2$ )

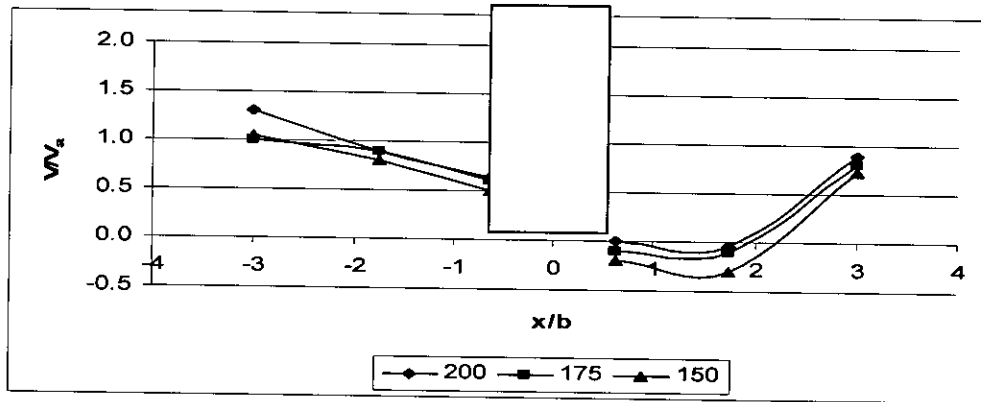


(c) Round nose pier ( $l/b=3$ )

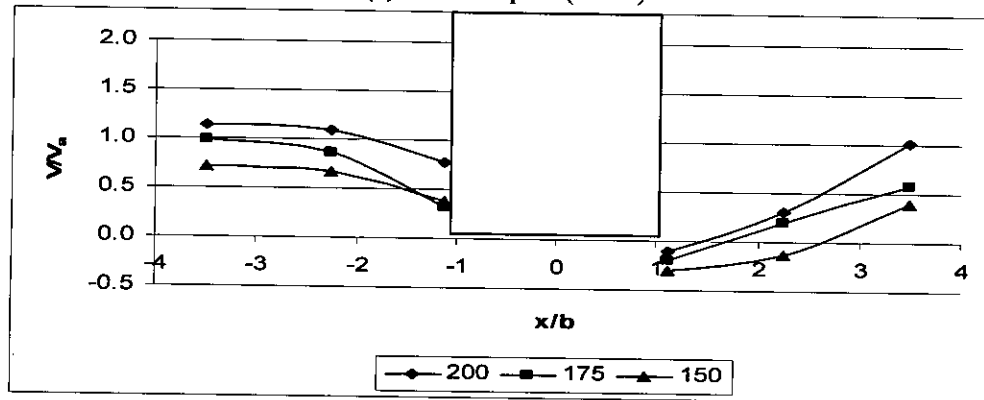


(d) Round nose pier ( $l/b=4$ )

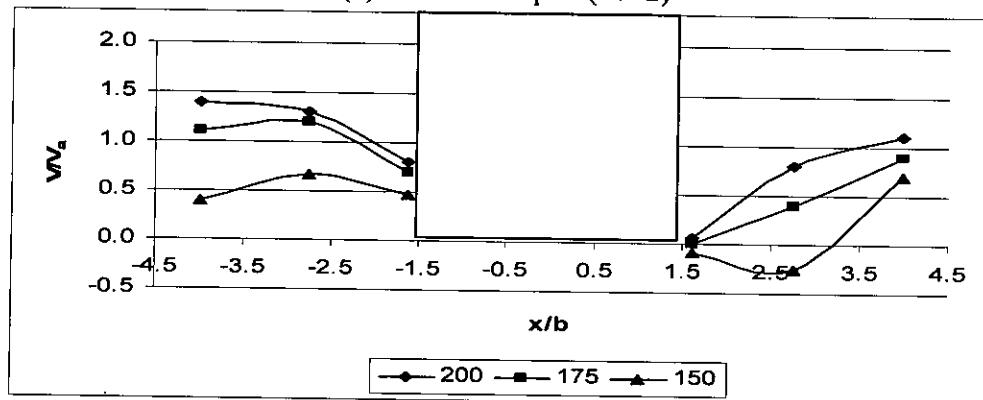
Figure 5.35: Velocity variation in longitudinal direction at Main channel for Bed material 2 ( $d_{50} = 0.18$  mm)



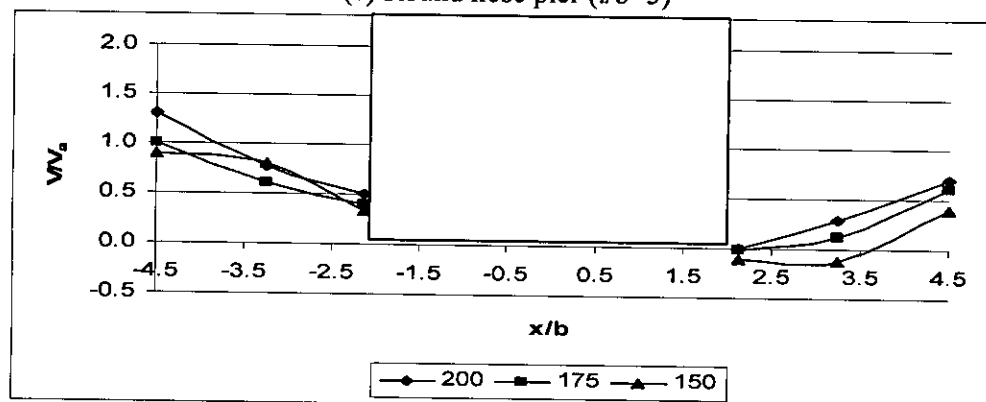
(a) Circular pier ( $l/b=1$ )



(b) Round nose pier ( $l/b=2$ )



(c) Round nose pier ( $l/b=3$ )



(d) Round nose pier ( $l/b=4$ )

Figure 5.36: Velocity variation in longitudinal direction at Floodplain for Bed material 3 ( $d_{50} = 0.12$  mm)

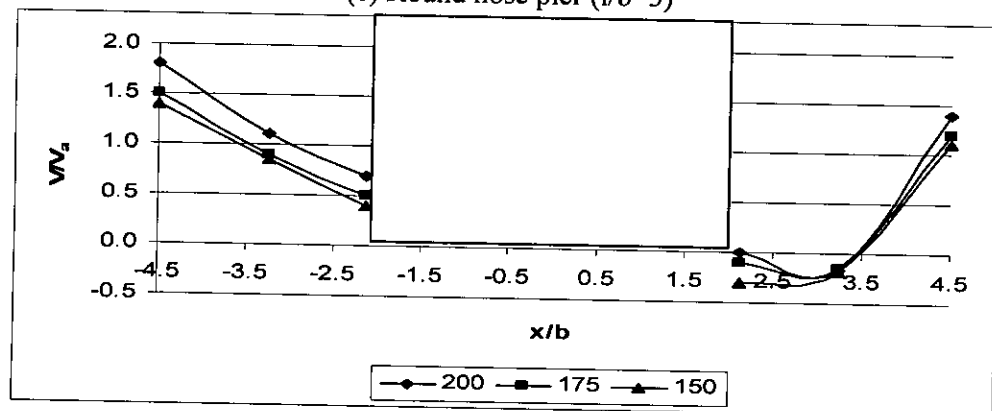
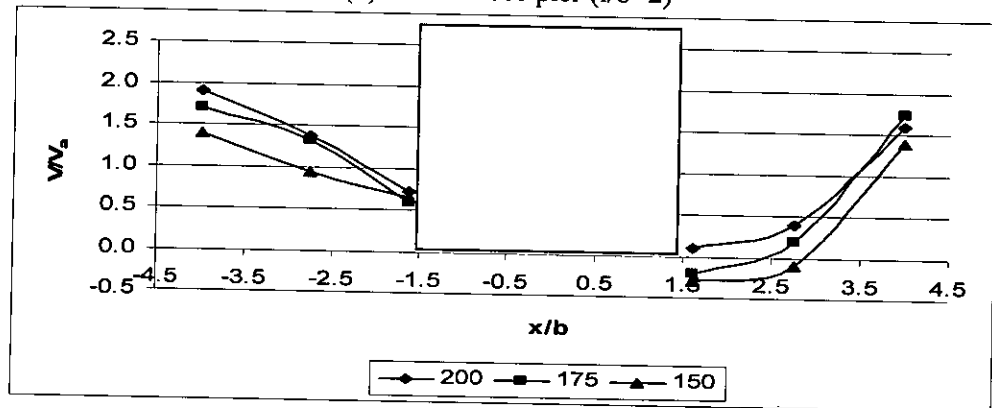
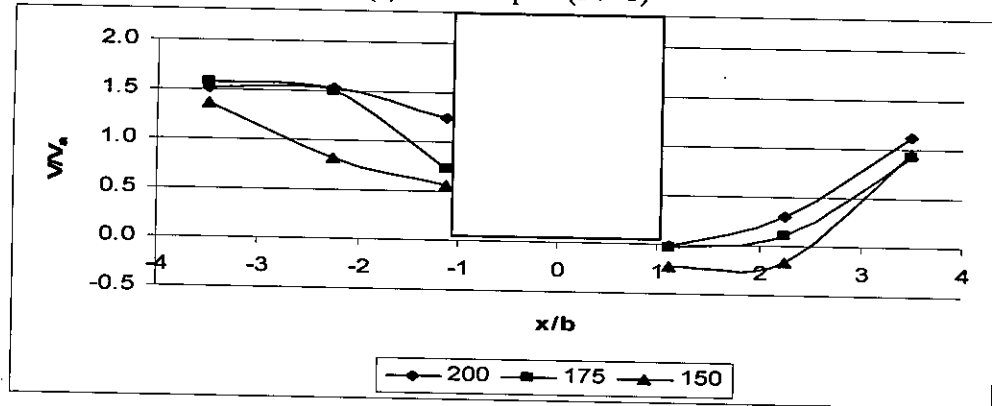
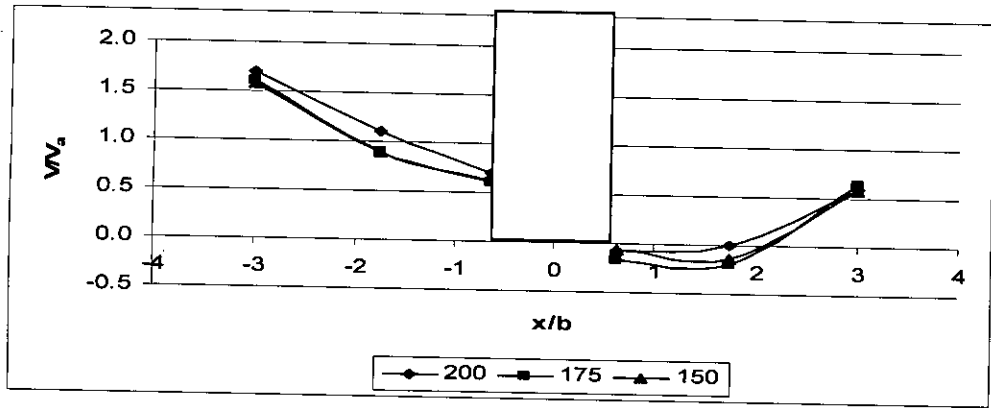


Figure 5.37: Velocity variation in longitudinal direction at Main channel for Bed material 3 ( $d_{50} = 0.12$  mm)

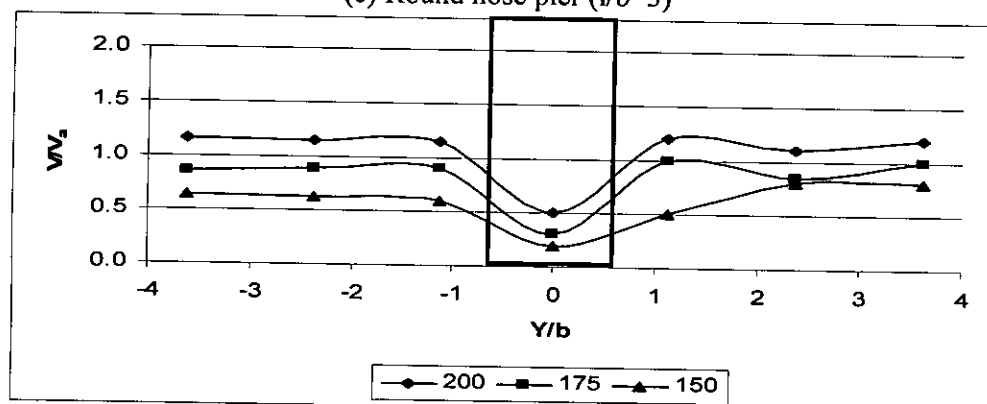
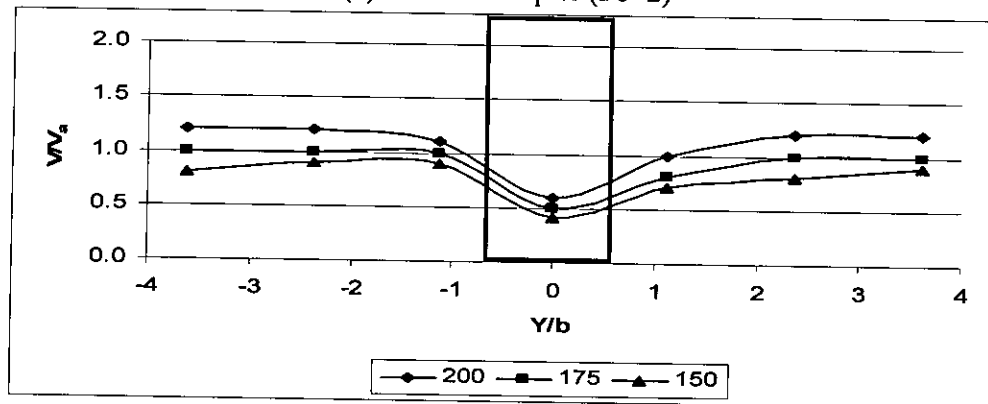
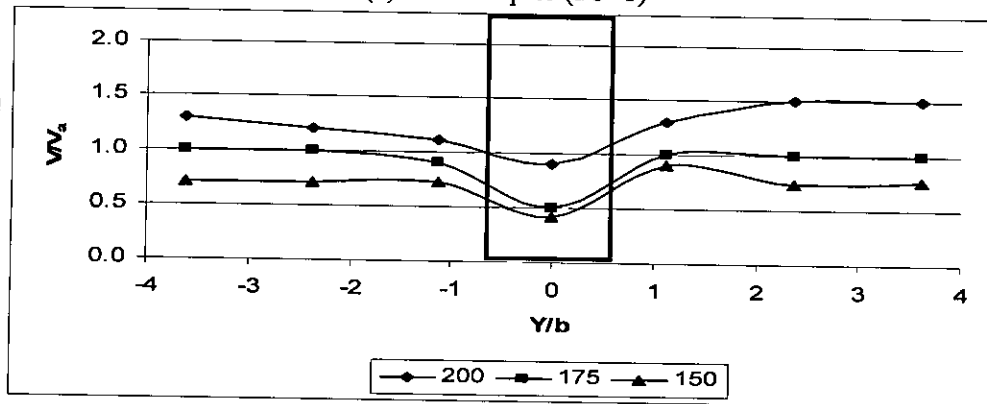
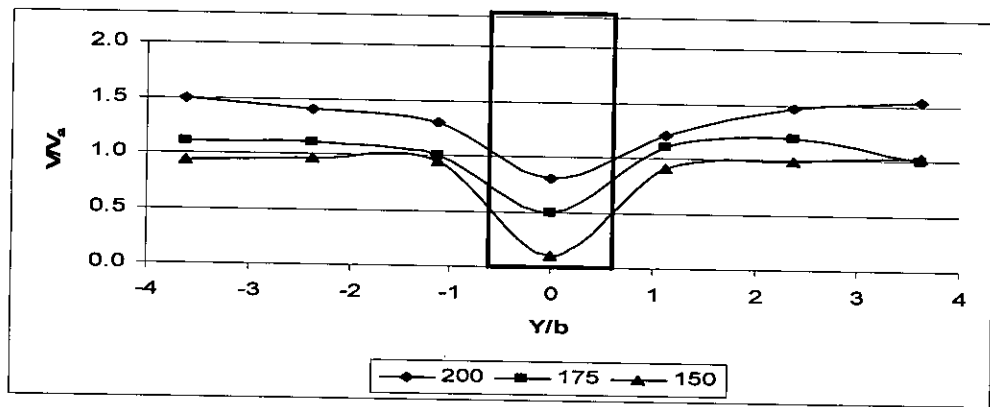
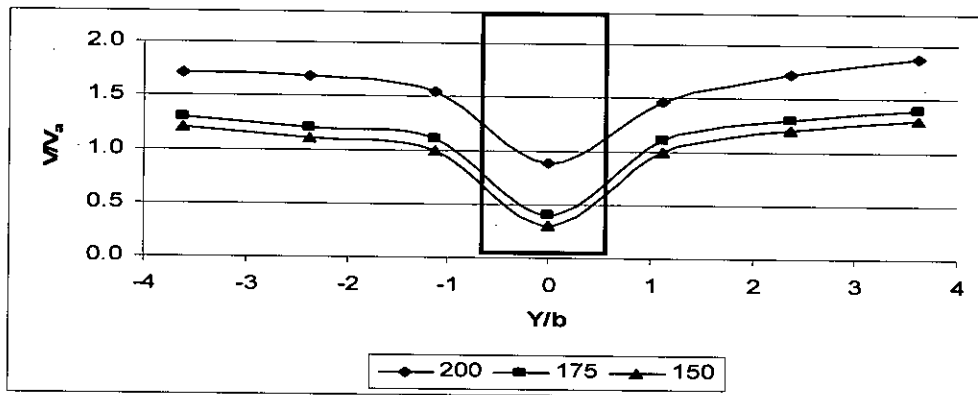
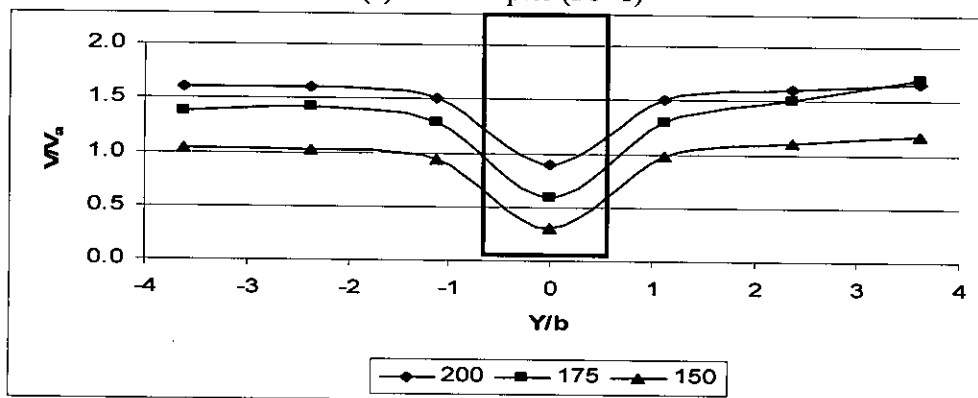


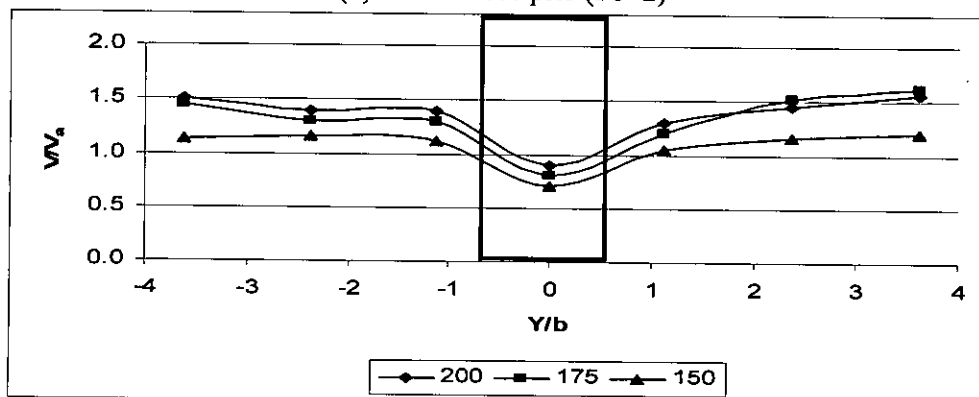
Figure 5.38: Velocity variation in lateral direction at Floodplain for Bed material 1 ( $d_{50} = 0.75$  mm)



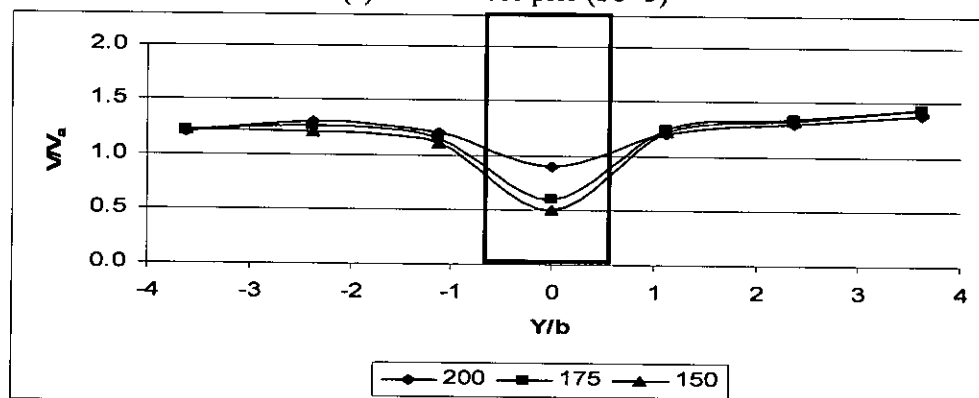
(a) Circular pier ( $l/b=1$ )



(b) Round nose pier ( $l/b=2$ )



(c) Round nose pier ( $l/b=3$ )



(d) Round nose pier ( $l/b=4$ )

Figure 5.39: Velocity variation in lateral direction at Main channel for Bed material 1 ( $d_{50} = 0.75$  mm)

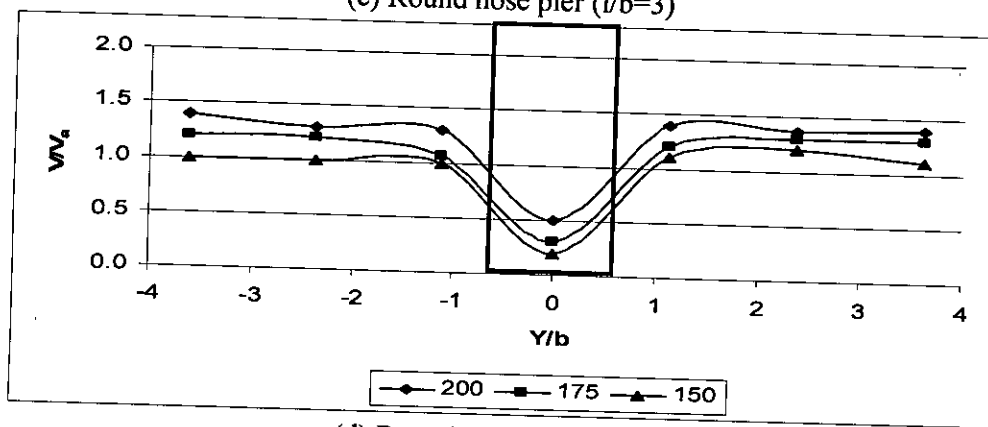
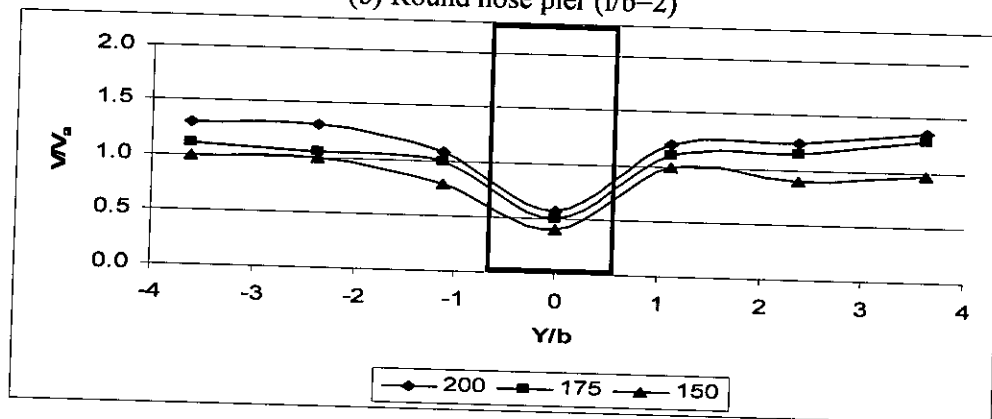
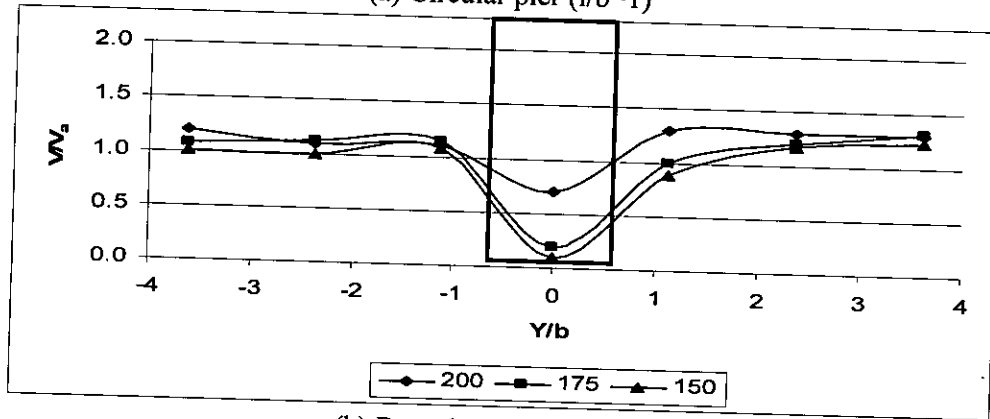
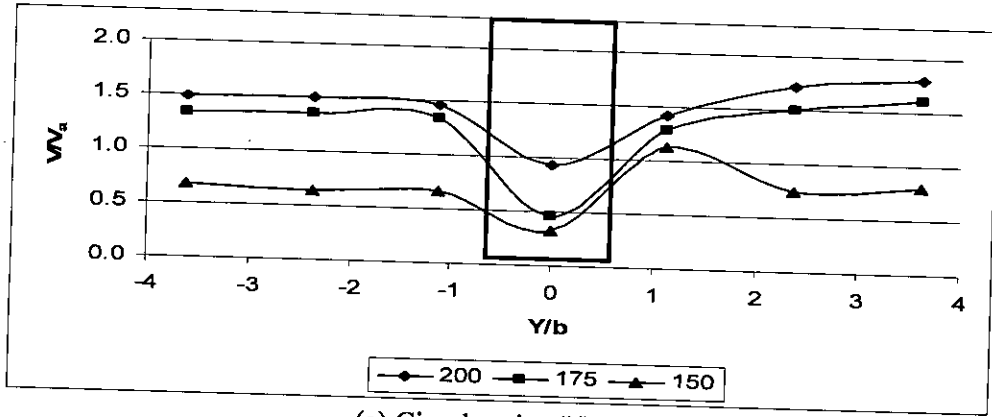


Figure 5.40: Velocity variation in lateral direction at Floodplain for Bed material 2 ( $d_{50} = 0.18$  mm)

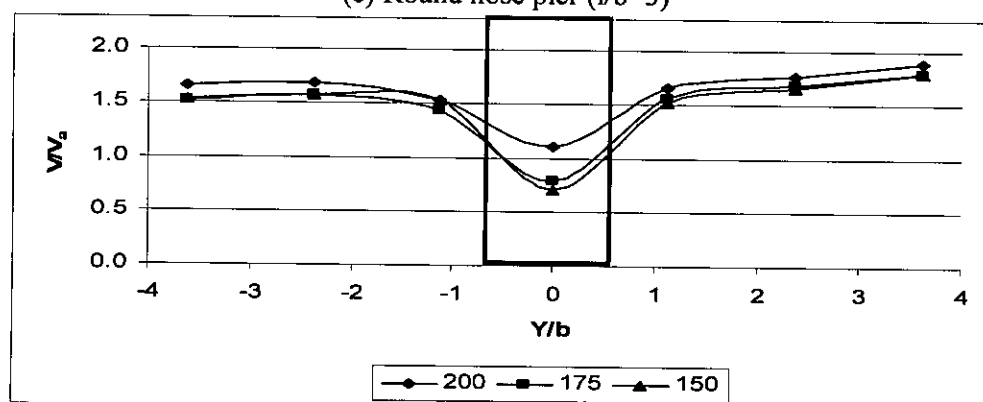
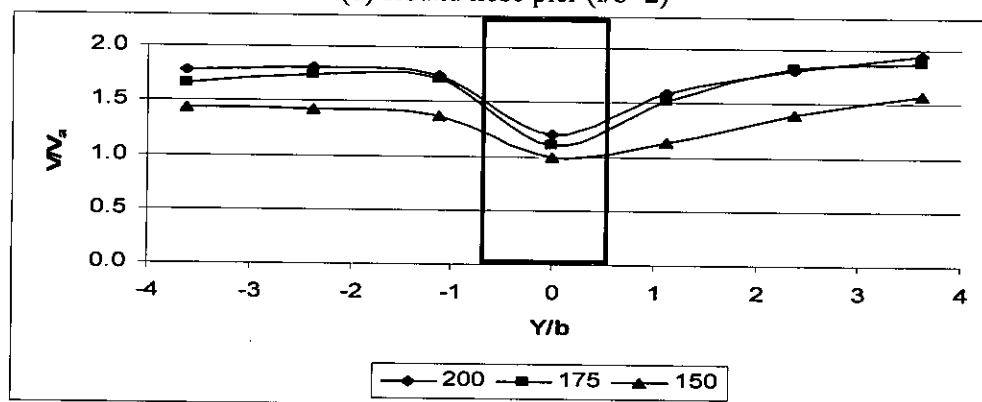
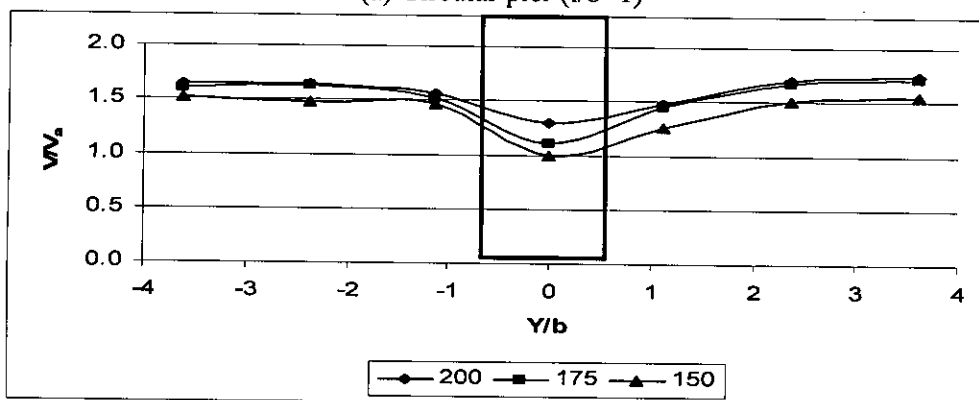
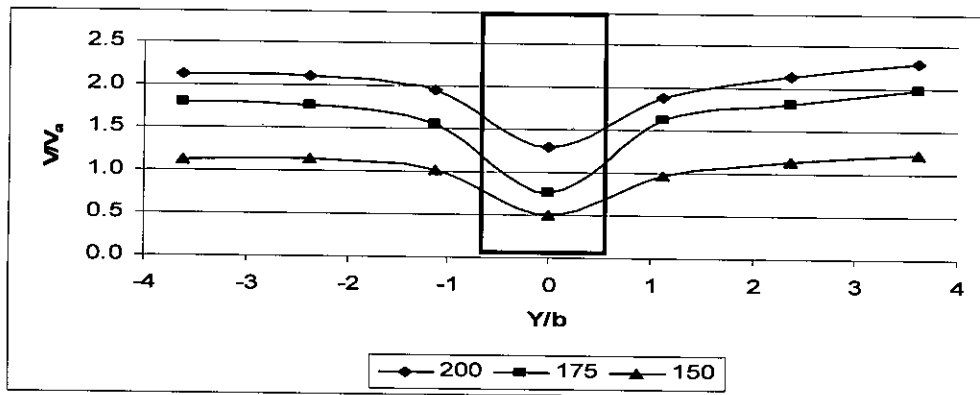
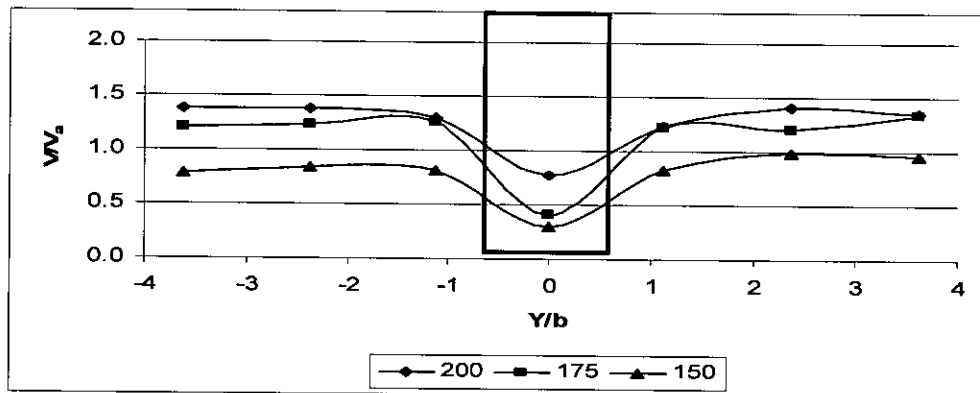
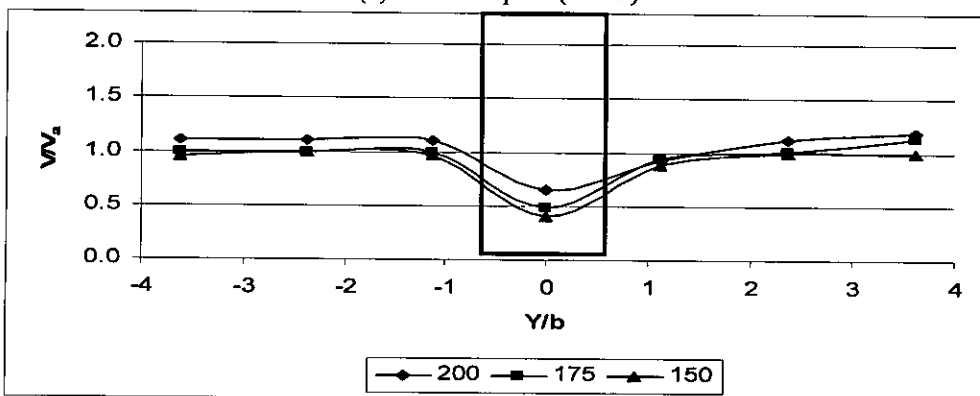


Figure 5.41: Velocity variation in lateral direction at Main channel for Bed material 2 ( $d_{50} = 0.18$  mm)

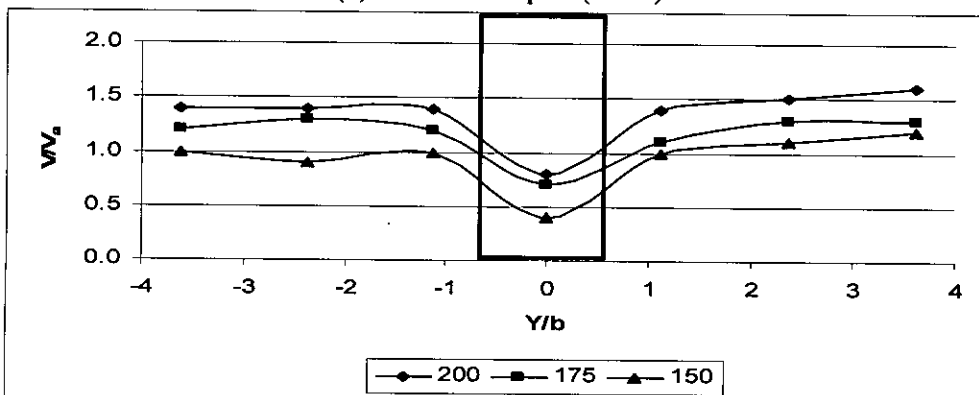




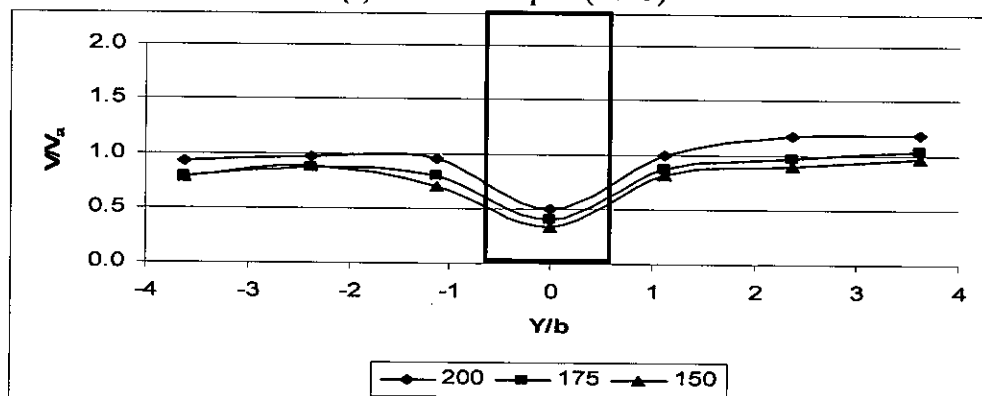
(a) Circular pier ( $l/b=1$ )



(b) Round nose pier ( $l/b=2$ )



(c) Round nose pier ( $l/b=3$ )



(d) Round nose pier ( $l/b=4$ )

Figure 5.42: Velocity variation in lateral direction at Floodplain for Bed material 3 ( $d_{50} = 0.12$  mm)

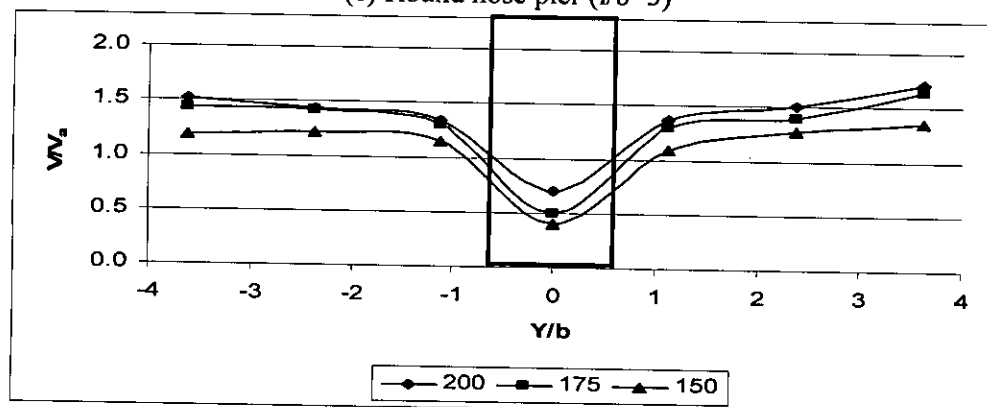
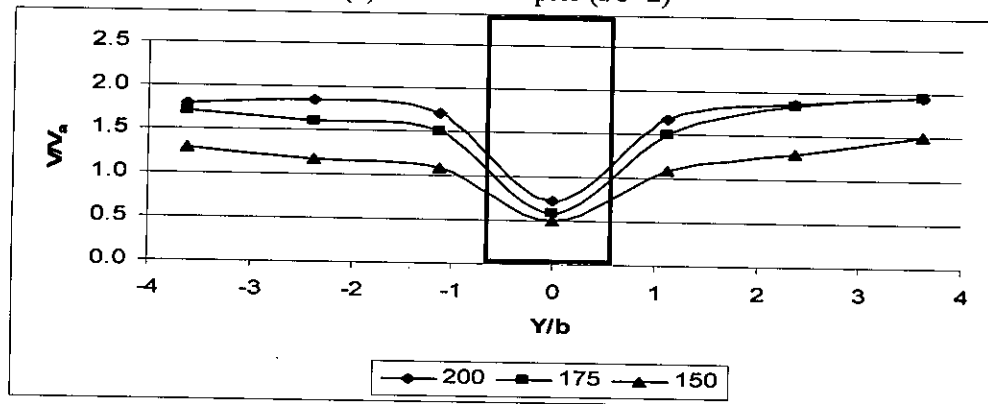
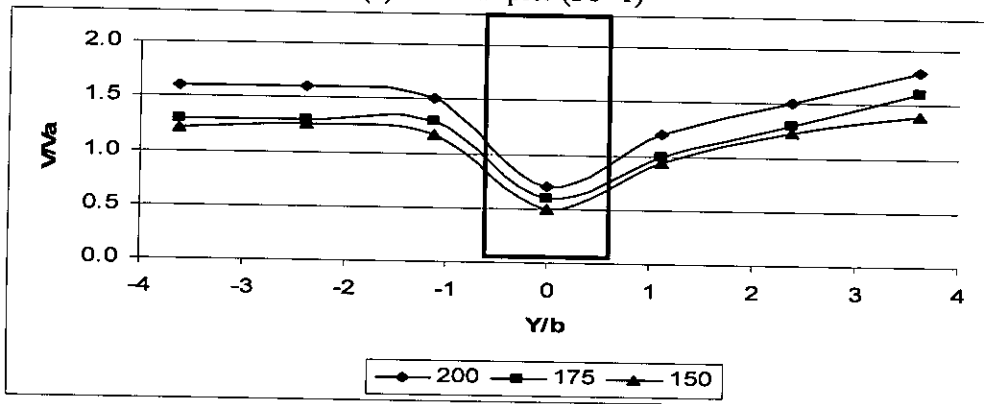
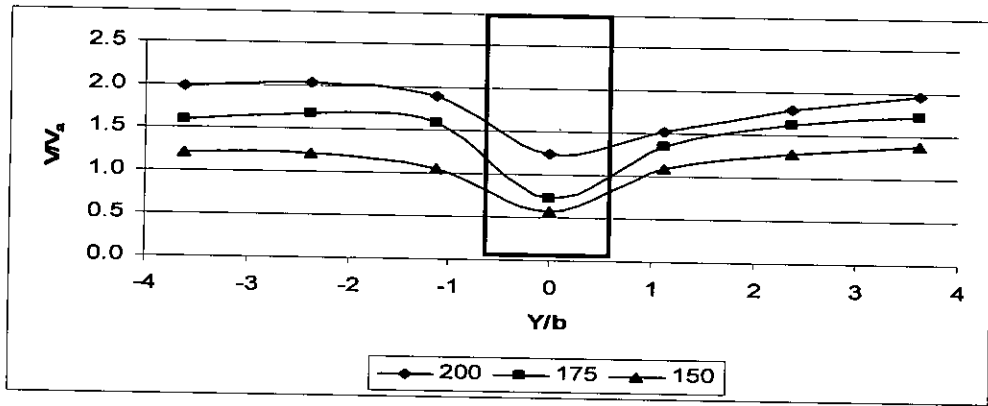
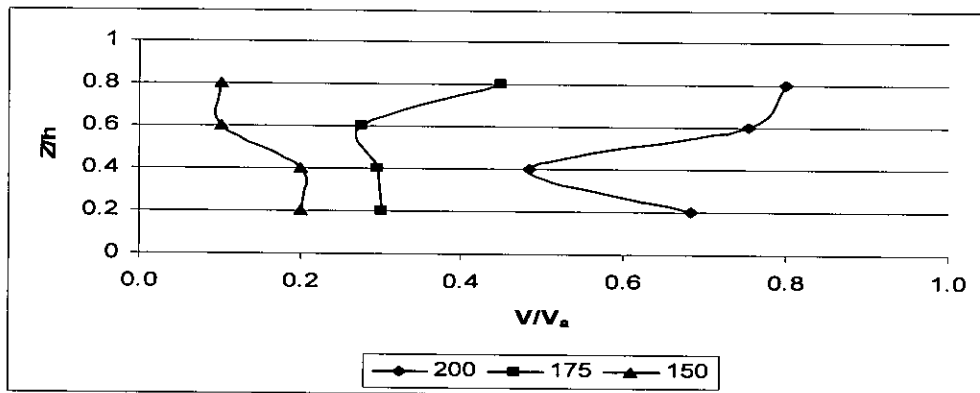
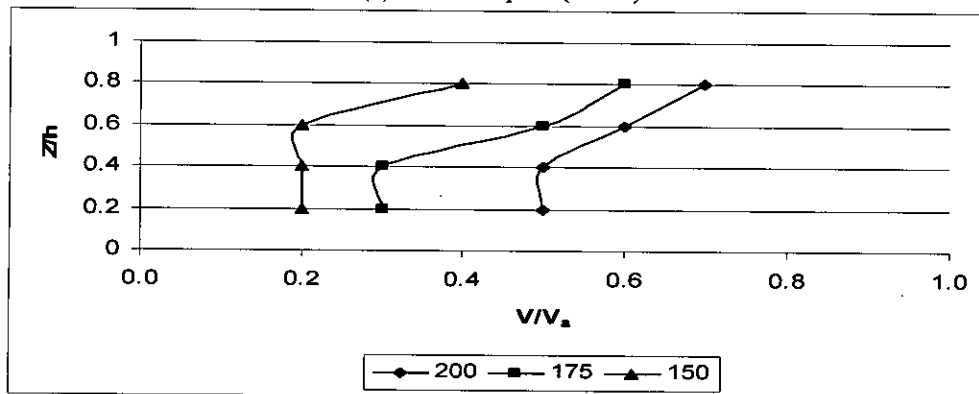


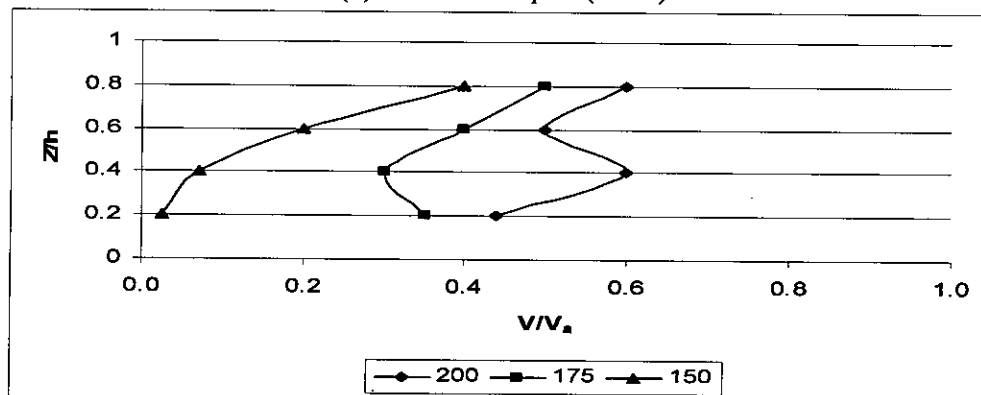
Figure 5.43: Velocity variation in lateral direction at Main channel for Bed material 3 ( $d_{50} = 0.12$  mm)



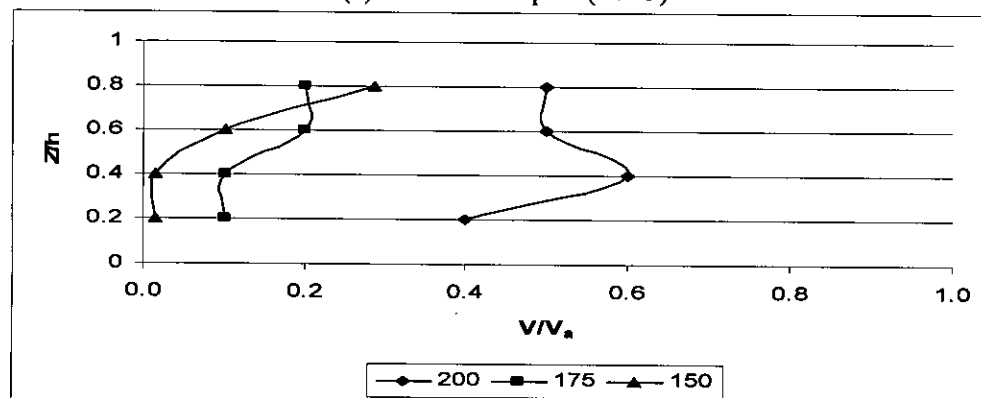
(a) Circular pier ( $l/b=1$ )



(b) Round nose pier ( $l/b=2$ )

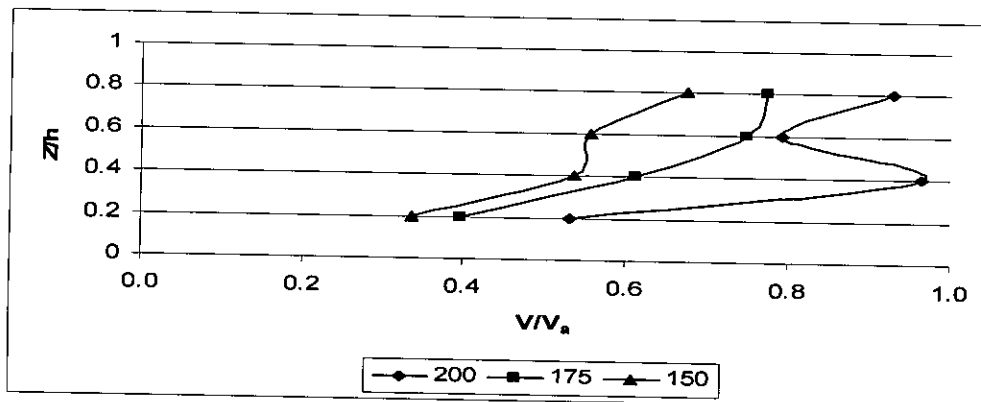


(c) Round nose pier ( $l/b=3$ )

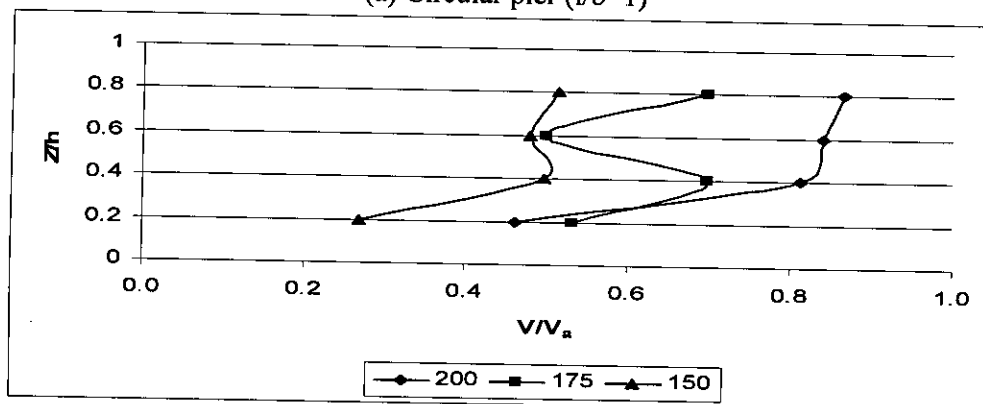


(d) Round nose pier ( $l/b=4$ )

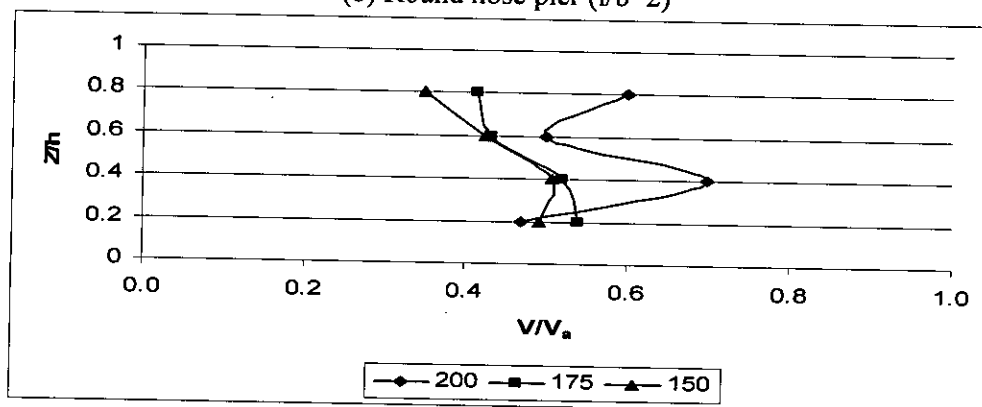
Figure 5.44: Velocity variation in vertical direction at Floodplain for Bed material 1 ( $d_{50} = 0.75$  mm)



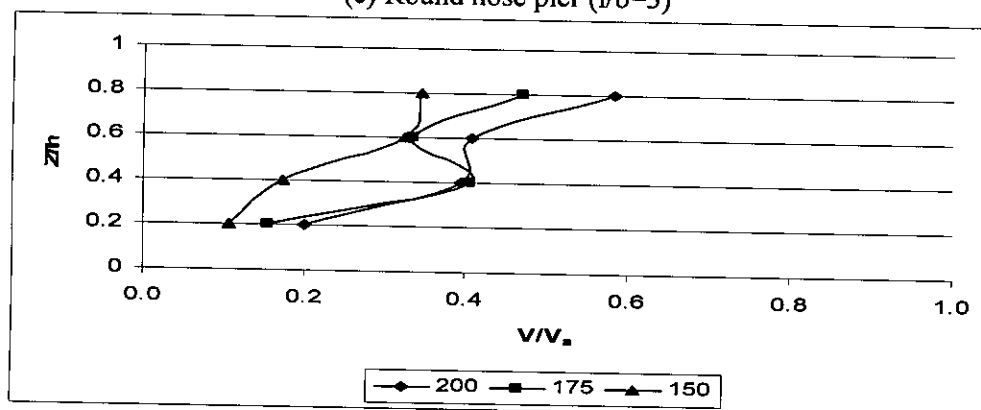
(a) Circular pier ( $l/b=1$ )



(b) Round nose pier ( $l/b=2$ )

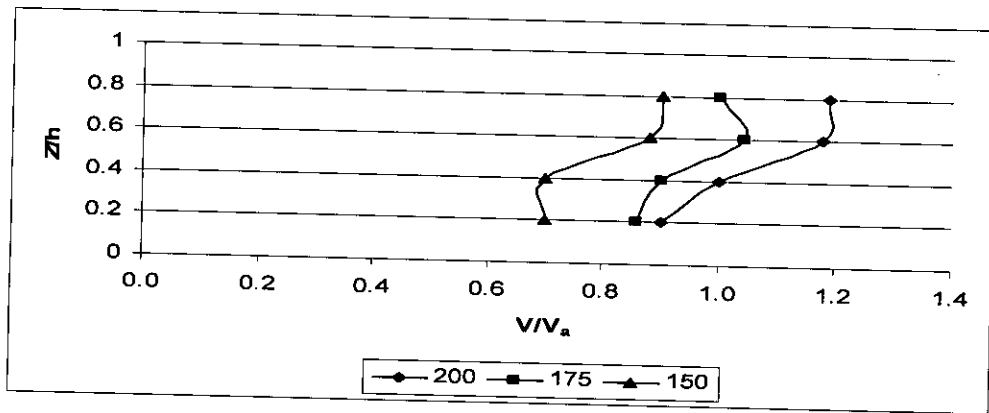


(c) Round nose pier ( $l/b=3$ )

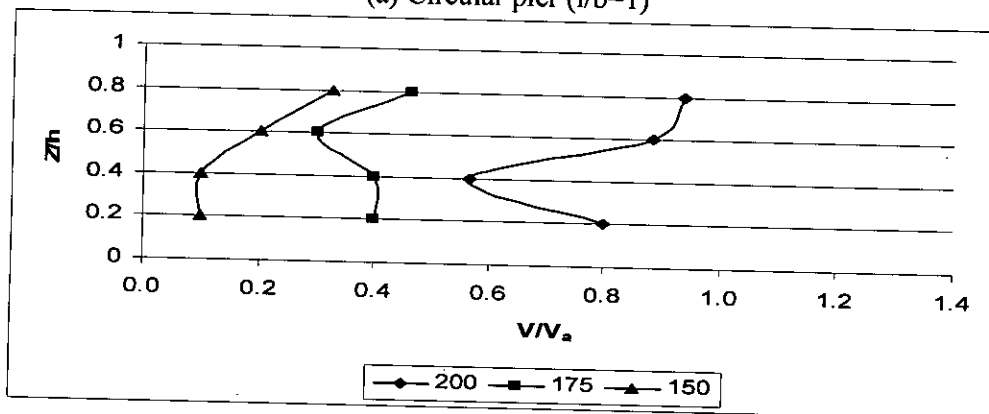


(d) Round nose pier ( $l/b=4$ )

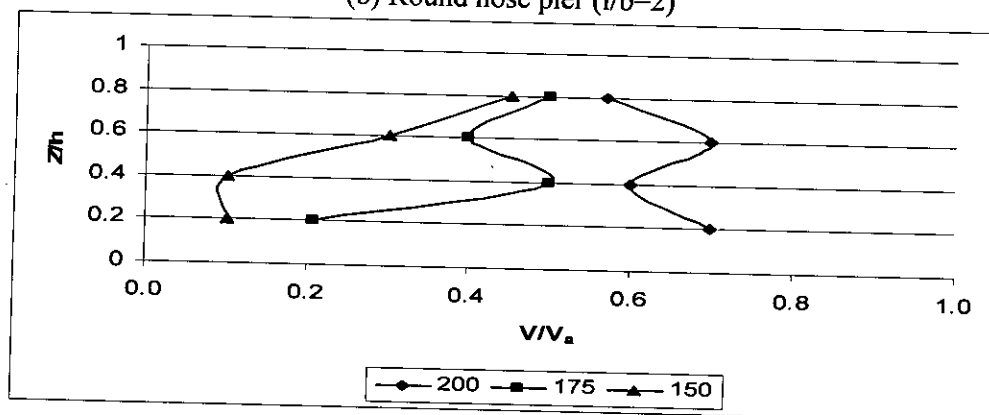
Figure 5.45: Velocity variation in vertical direction at Main channel for Bed material 1 ( $d_{50} = 0.75$  mm)



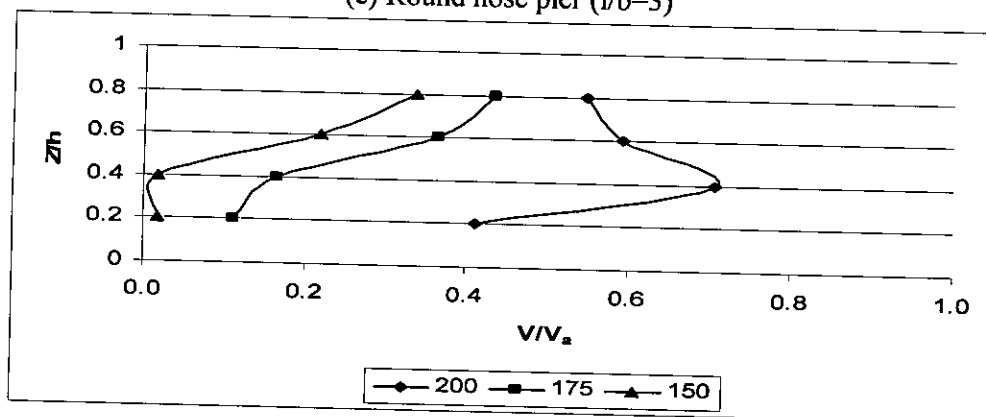
(a) Circular pier ( $l/b=1$ )



(b) Round nose pier ( $l/b=2$ )

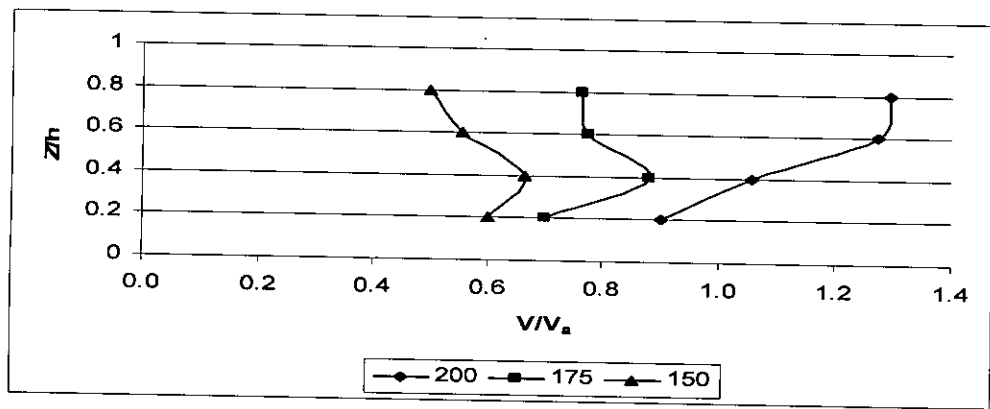


(c) Round nose pier ( $l/b=3$ )

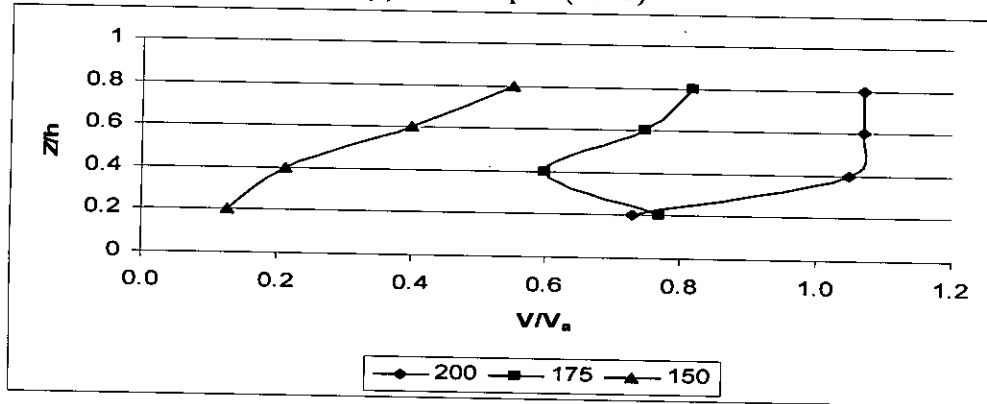


(d) Round nose pier ( $l/b=4$ )

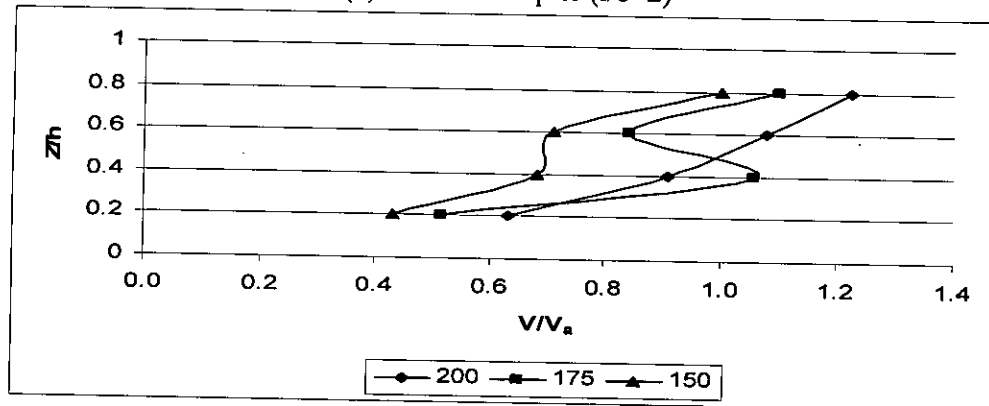
Figure 5.46: Velocity variation in vertical direction at Floodplain for Bed material 2 ( $d_{50} = 0.18$  mm)



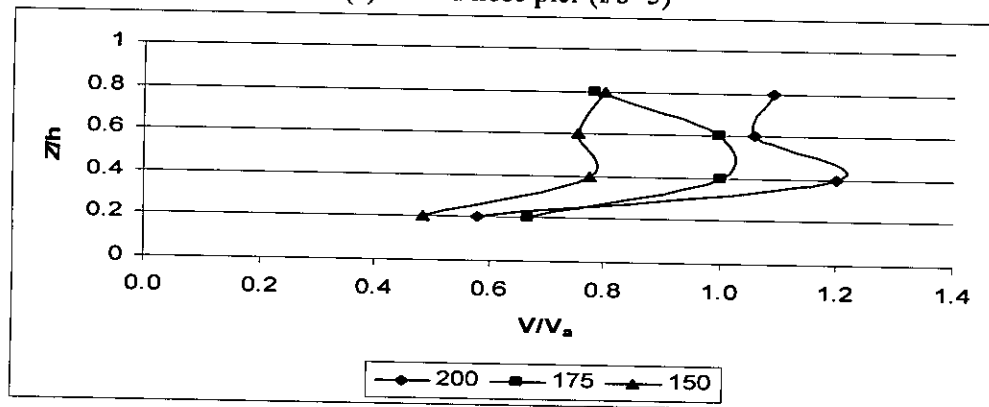
(a) Circular pier ( $l/b=1$ )



(b) Round nose pier ( $l/b=2$ )

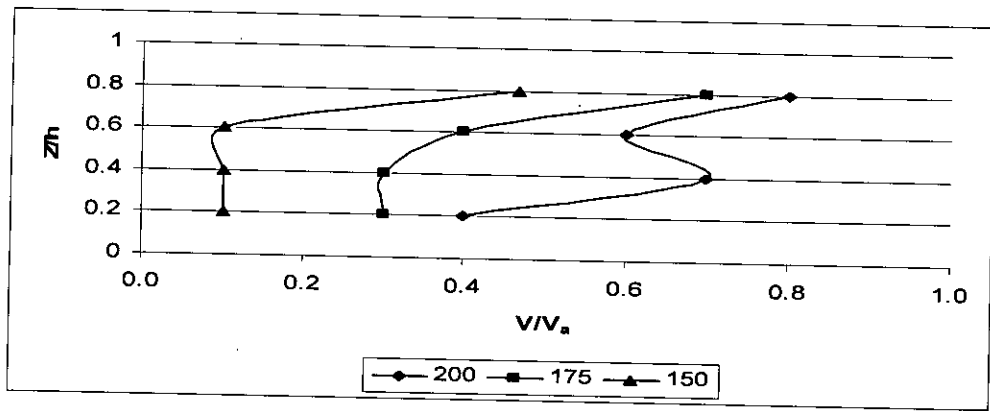


(c) Round nose pier ( $l/b=3$ )

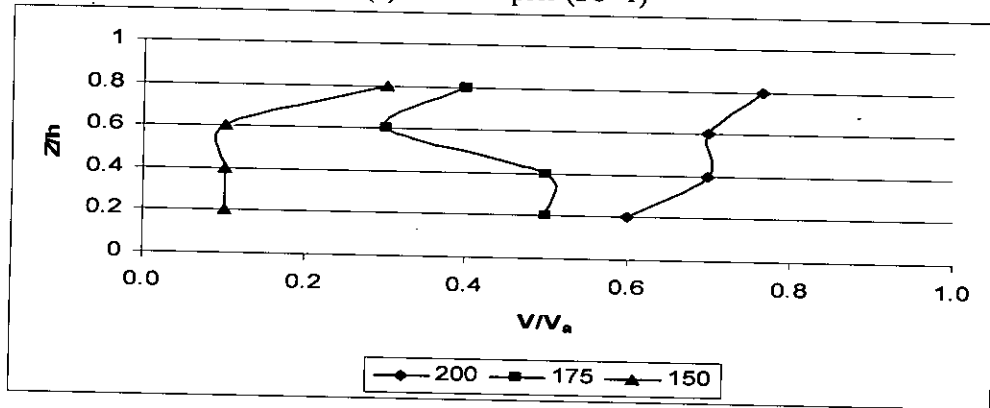


(d) Round nose pier ( $l/b=4$ )

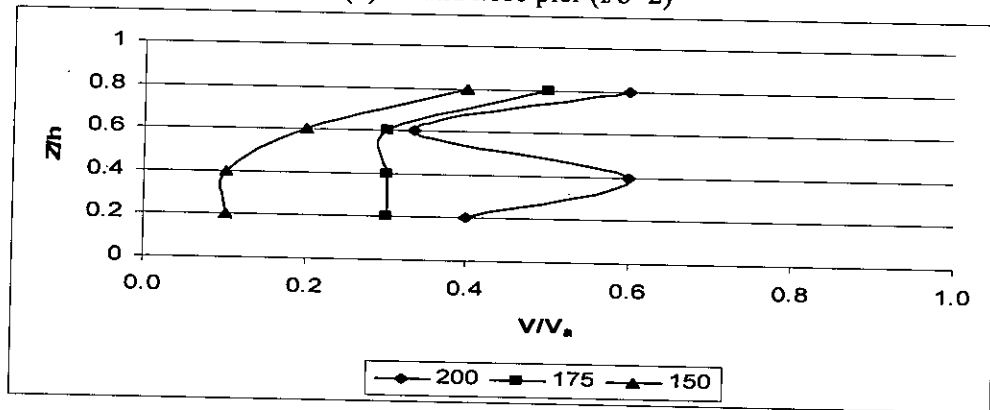
Figure 5.47: Velocity variation in vertical direction at Main channel for Bed material 2 ( $d_{50} = 0.18$  mm)



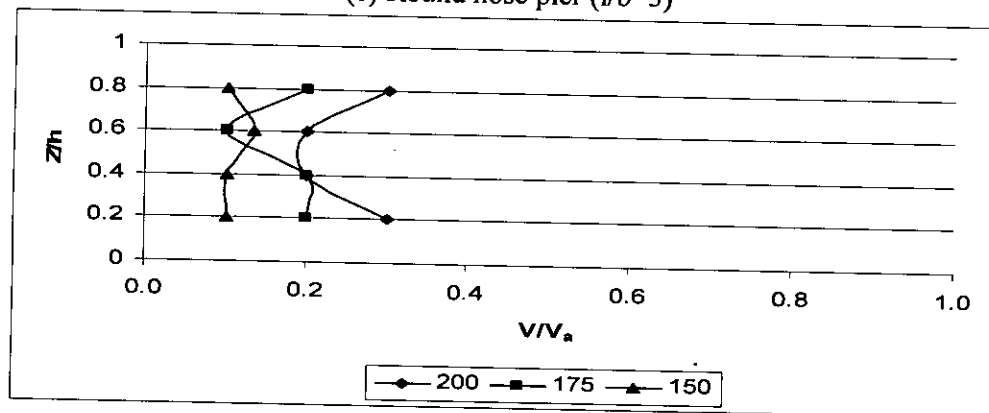
(a) Circular pier ( $l/b=1$ )



(b) Round nose pier ( $l/b=2$ )

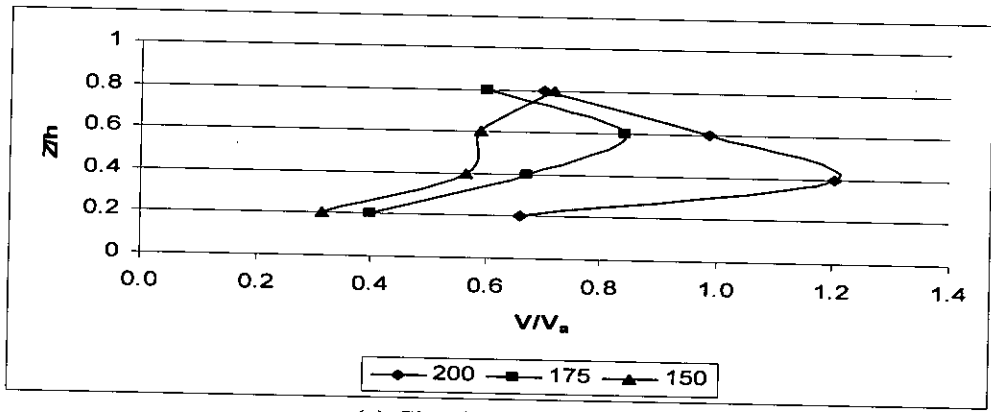


(c) Round nose pier ( $l/b=3$ )

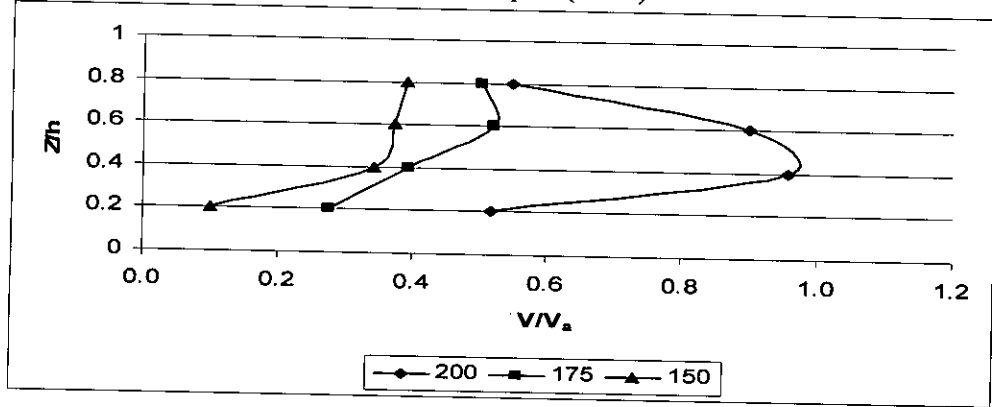


(d) Round nose pier ( $l/b=4$ )

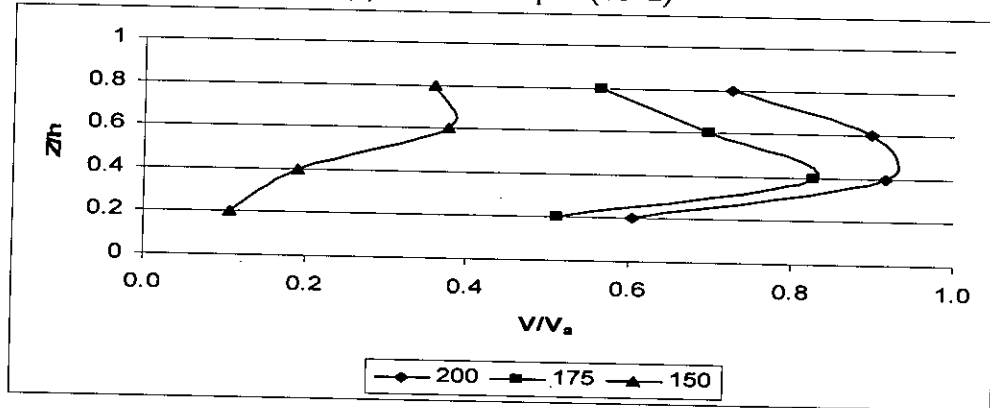
Figure 5.48: Velocity variation in vertical direction at Floodplain for Bed material 3 ( $d_{50} = 0.12$  mm)



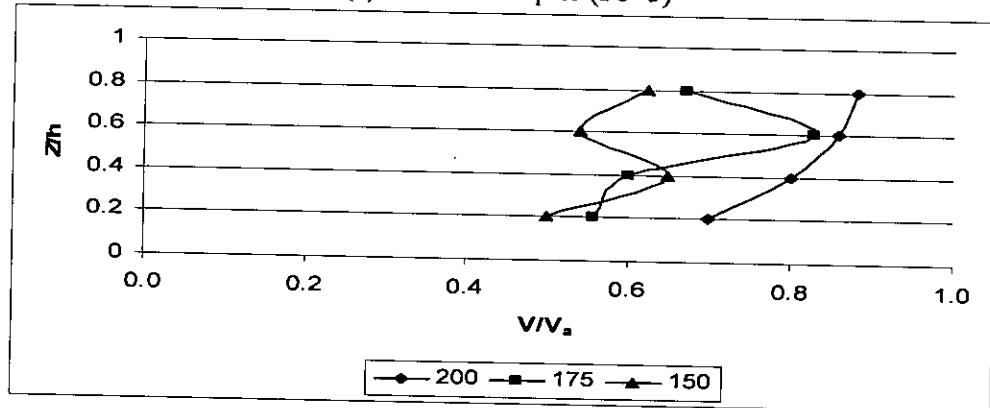
(a) Circular pier ( $l/b=1$ )



(b) Round nose pier ( $l/b=2$ )



(c) Round nose pier ( $l/b=3$ )



(d) Round nose pier ( $l/b=4$ )

Figure 5.49: Velocity variation in vertical direction at Main channel for Bed material 3 ( $d_{50} = 0.12$  mm)



#### 5.6.4 Velocity vector diagram

Resultant vector diagrams of streamwise velocity ( $V_x$ ) and transverse velocity ( $V_y$ ) for variable discharges, structure shapes and length-width ratio for both floodplain and main channel have been represented in Appendix C. Figure C.1 to Figure C.24, Figure C.25 to Figure C.48, Figure C.49 to Figure C.72 show both floodplain velocity vectors and main channel velocity vectors for bed material 1 ( $d_{50} = 0.75$  mm), bed material 2 ( $d_{50} = 0.18$  mm) and bed material 3 ( $d_{50} = 0.12$  mm) respectively.

In case of floodplain velocity vectors, generally it has been found that flow is steady at upstream along longitudinal direction. Then flow is divided just in front of structure and flows through both sides of structure towards downstream. At front face of structure, flow velocity reaches near about zero which may be caused due to a down flow at upstream face of pier. It is same as Breusers and Raudkivi (1991) stated that at upstream of pier, approach flow velocity goes to zero and stagnation pressure decreases. This caused a downward pressure gradient that drives down-flow at upstream face of pier. Down-flow acts like a vertical jet and removes sediment at face of pier.

A circulation of flow has been observed around structure after dividing of flow at structure front face. This may be occurred due to horseshoe vortex. According to Melville (1975), horseshoe vortex forms due to separation of flow at upstream rim of scour hole. This extends downstream, past sides of pier before becoming part of general turbulence.

Immediately after rear front of structure, relatively weak circulation of flow has been found. This may be indication of vertical vortices formation, called wake vortex. Wake vortex is also responsible for downstream scour with horseshoe vortex as these vortices are translated downstream by mean flow and act like vacuum cleaners sucking up sediment from bed and also transporting sediment entrained by down flow and horseshoe vortex (Melville and Coleman, 2000). After leaving rear face of structure, flow is found becoming steady gradually with traveling to far downstream.

Comparing with floodplain, flow field and velocity vector diagrams are observed same in main channel. No significant difference has been found in case of flow separation, flow circulation and horseshoe vortex formation between floodplain and main channel.

#### 5.6.5 $V/V_c$ contour map

In Appendix D, two dimensional (2D)  $V/V_c$  contour maps for variable discharges, structure shapes and length-width ( $l/b$ ) ratio in three different bed materials for both floodplain and main channel have been represented. Floodplain and main channel  $V/V_c$  contour maps are presented in Figure D.1 to D.24, Figure D.25 to D.48 and Figure D.49 to D.72 for bed material 1 ( $d_{50} = 0.75$  mm), bed material 2 ( $d_{50} = 0.18$  mm) and bed material 3 ( $d_{50} = 0.12$  mm) respectively.

Generally it is well known that shear velocity ratio  $u_* / u_{*c}$  is an established parameter to measure flow intensity. It is often used in scour prediction equations. But practically, measurement of shear velocity is difficult. Considering difficulties of measuring shear velocity, velocity ratio  $V/V_c$  has been used in place of shear velocity ratio as a measure of flow intensity. (Raudkivi, 1986; Melville and Sutherland, 1988)

Sufficient insight about flow field around structure in floodplain can be provided by  $V/V_c$  contour maps. It is found that  $V/V_c$  lines are less than unity both in front and rear face of structure in all cases.  $V/V_c$  lines less than unity near to upstream side of structure may indicate that flow intensity reduces in front face of structure. It may be happened due to separation of flow in front of structure and flow moves vertically downward rather than longitudinal direction. At rear face of structure, there is always low flow intensity observed as  $V/V_c$  lines are found much less than unity. The reason may be that flow becomes weak behind structure due to obstruction and only backward movement of flow for circulation is sustained.

In general, it is found that  $V/V_c$  line equals to unity or greater exists around upstream face of structure in case of higher discharge and shifts away with lower discharges. This may be the reason for high scour during higher discharge and also decreasing trend of scouring with lower discharges.

In comparison with main channel  $V/V_c$  contour maps, it is observed that values of  $V/V_c$  lines are greater than that of floodplain. It may be happened due to difference between velocity of floodplain and main channel. Velocity is found higher in main channel than that of floodplain for same discharge as depth of flow is more than that of floodplain. It may also affect scour because, scour depth is found higher in main channel than that of floodplain for same discharge in case of same bed material. Other characteristics are observed generally same as floodplain.

### **5.7 Analysis of floodplain maximum scour depth**

In subsequent articles, variations of floodplain maximum local scour depth with different flow property are analyzed.

#### **5.7.1 Variation of floodplain scour ( $d_s/b$ ) with floodplain flow intensity ( $V_f/V_a$ )**

Figure 5.50 represents variation of dimensionless floodplain scour depth ( $d_s/b$ ) with floodplain flow intensity ( $V_f/V_a$ ). From trend line of this graphical presentation, it has been found that floodplain scour depth increases at an increasing tendency with increasing intensity of flow.

#### **5.7.2 Variation of floodplain local scour ( $d_s/b$ ) with Froude number ( $F_r$ )**

Variation of dimensionless maximum scour depth ( $d_s/b$ ) with Froude number ( $F_r$ ) for circular pier and round nose pier are shown in Figure 5.51 and Figure 5.52, respectively. Trend of scour depth variation for flow Froude number is observed linear in both cases of circular and round nose structure.

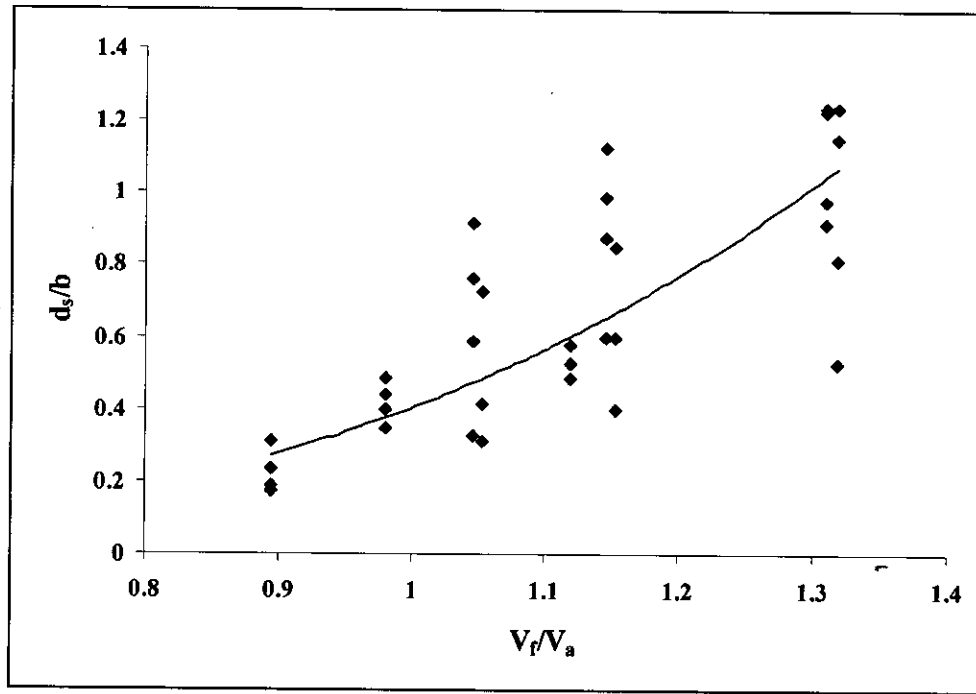


Figure 5.50: Variation of maximum scour with floodplain flow velocity

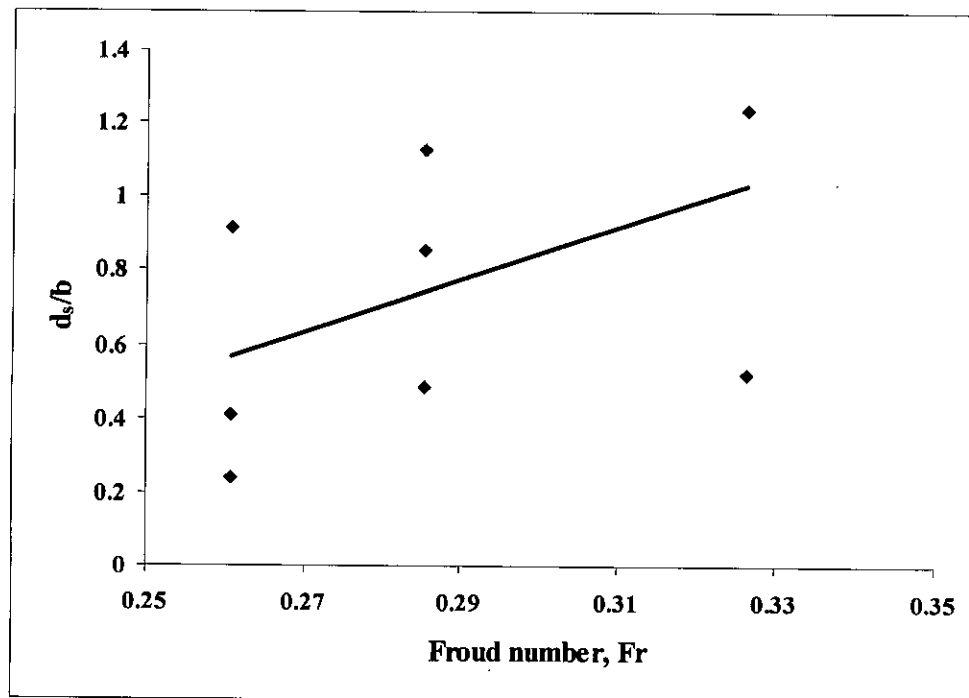


Figure 5.51: Variation of maximum scour depth with Froude number for circular pier

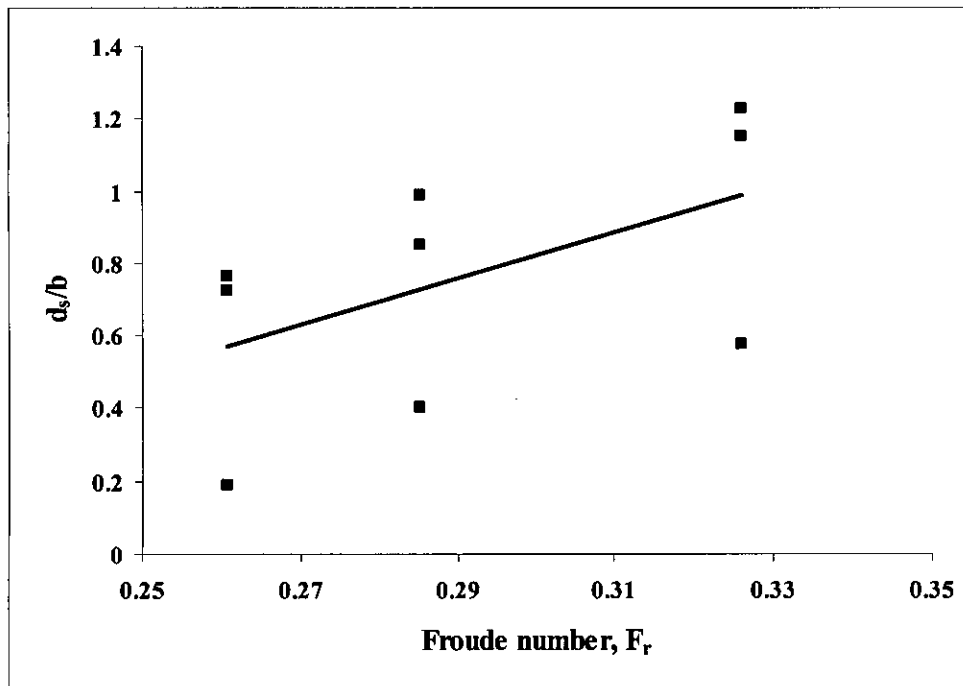


Figure 5.52: Variation of maximum scour depth with Froude number for round nose pier

### 5.7.3 Variation of floodplain scour ( $d_s/b$ ) with length-width ratio ( $l/b$ )

Variation of dimensionless maximum scour depth ( $d_s/b$ ) with different length-width ratio ( $l/b$ ) is represented in Figure 5.53. Scour depth is significantly reduces due to increase in length-width ratio. This is happened as because, when length-width ratio is increased, stream lining of flow occurs that reduces strength of vortex.

### 5.7.4 Variation of floodplain scour ( $d_s/b$ ) with sediment size ( $b/d_{50}$ )

Variation of dimensionless floodplain scour ( $d_s/b$ ) with relative sediment size with respect to width of structure is shown in Figure 5.54 for variable discharges. Scour depth variation follows same trend for different discharges. Scour depth increases with increasing relative sediment size. It indicates that scour depth shows an increasing tendency from coarse to finer bed material.

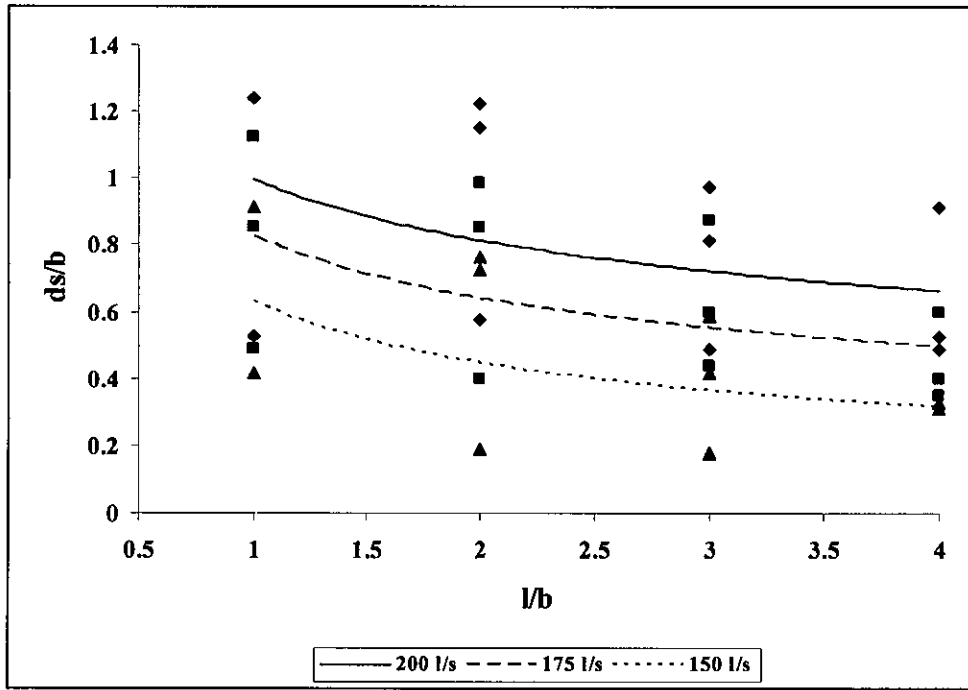


Figure 5.53: Variation of maximum scour depth with different length-width ratio of structure for different discharges

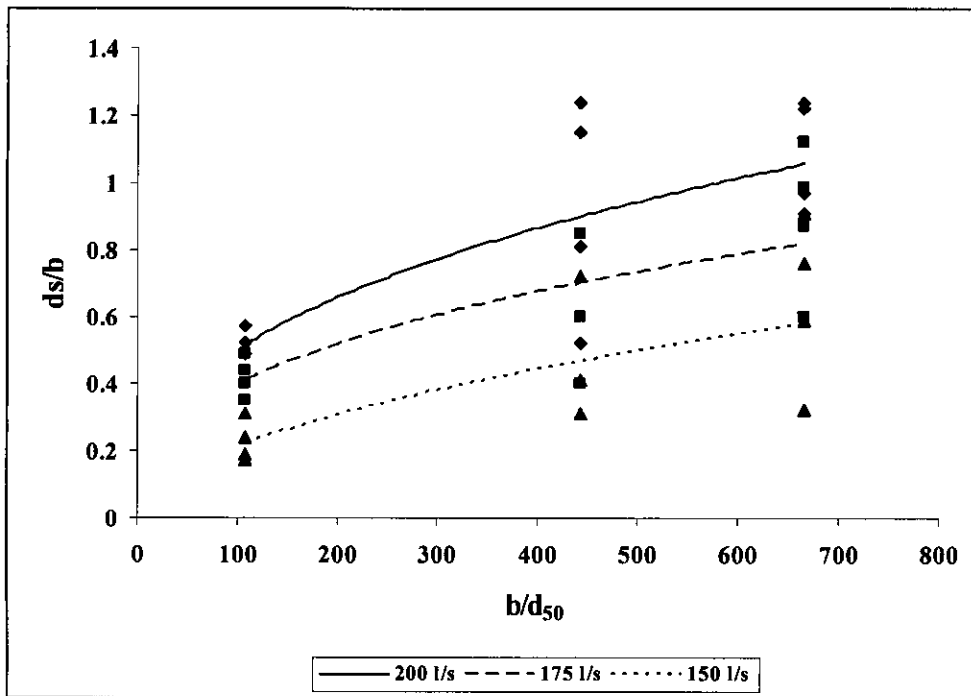


Figure 5.54: Variation of maximum scour with sediment size for different discharges

## 5.8 Proposed empirical relationship for floodplain scour prediction

In this present study, it has been clearly observed that floodplain scour variation shows an increasing trend with increasing floodplain flow intensity ( $V_f/V_a$ ). Beside this, it is also found that floodplain scour depth decreases from smaller length-width ratio ( $l/b$ ) to greater. By considering these significant variations, two relationships have been found from trend analysis of Figure 5.50 and Figure 5.53. They are:

$$\text{From Figure 5.50: } \frac{d_s}{b} = 0.403 \left( \frac{V_f}{V_a} \right)^{3.54} \quad (5.1)$$

$$\text{From Figure 5.53: } \frac{d_s}{b} = 0.87 \left( \frac{l}{b} \right)^{-0.38} \quad (5.2)$$

By combining Equation 5.1 and Equation 5.2, an empirical relationship can be developed for floodplain scour depth prediction as follows:

$$\frac{d_s}{b} = 0.59 \left( \frac{V_f}{V_a} \right)^{1.77} \left( \frac{l}{b} \right)^{-0.19} \quad (5.3)$$

Where

$d_s$  = Floodplain scour depth, cm

$V_f$  = Floodplain flow velocity, m/s

$V_a$  = Floodplain armour velocity, m/s

$l$  = length of structure, cm

$b$  = width of structure, cm

Using this empirical relationship, a comparison has been done between experimental values and values obtained from developed relationship of floodplain scour depth. In Table 5.2, floodplain scour depths from experiment and obtained from empirical relationship have been arranged for all 36 experimental runs.

In addition of this, a graphical comparison between scour depths from experimental runs and scour depths calculated from developed relationship is also produced in Figure 5.55 to get a clear perception about differences among them.

Table 5.2: Comparison between floodplain scour depths of experimental runs and calculated from developed relationship

Experimental Run	$V_f/V_a$	l/b	Floodplain scour depth	
			From experiment	From developed relationship
R1-B1-C-1-200	1.12	1	4.2	5.8
R2-B1-C-1-175	0.98	1	3.9	4.6
R3-B1-C-1-150	0.895	1	1.9	3.9
R4-B1-RN-2-200	1.12	2	4.6	5.1
R5-B1-RN-2-175	0.98	2	3.2	4.0
R6-B1-RN-2-150	0.895	2	1.5	3.4
R7-B1-RN-3-200	1.12	3	3.9	4.7
R8-B1-RN-3-175	0.98	3	3.5	3.7
R9-B1-RN-3-150	0.895	3	1.4	3.1
R10-B1-RN-4-200	1.12	4	3.9	4.4
R11-B1-RN-4-175	0.98	4	2.8	3.5
R12-B1-RN-4-150	0.895	4	2.5	3.0
R13-B2-C-1-200	1.317647	1	9.9	7.7
R14-B2-C-1-175	1.152941	1	6.8	6.1
R15-B2-C-1-150	1.052941	1	3.3	5.2
R16-B2-RN-2-200	1.317647	2	9.2	6.7
R17-B2-RN-2-175	1.152941	2	6.8	5.3
R18-B2-RN-2-150	1.052941	2	5.8	4.5
R19-B2-RN-3-200	1.317647	3	6.5	6.2
R20-B2-RN-3-175	1.152941	3	4.8	4.9
R21-B2-RN-3-150	1.052941	3	3.3	4.2
R22-B2-RN-4-200	1.317647	4	4.2	5.9
R23-B2-RN-4-175	1.152941	4	3.2	4.7
R24-B1-RN-4-150	1.052941	4	2.5	4.0
R25-B3-C-1-200	1.309942	1	9.9	7.6
R26-B3-C-1-175	1.146199	1	9	6.0
R27-B3-C-1-150	1.046784	1	7.3	5.1
R28-B3-RN-2-200	1.309942	2	9.8	6.7
R29-B3-RN-2-175	1.146199	2	7.9	5.3
R30-B3-RN-2-150	1.046784	2	6.1	4.5
R31-B3-RN-3-200	1.309942	3	7.8	6.2
R32-B3-RN-3-175	1.146199	3	7	4.9
R33-B3-RN-3-150	1.046784	3	4.7	4.2
R34-B3-RN-4-200	1.309942	4	7.3	5.8
R35-B3-RN-4-175	1.146199	4	4.8	4.6
R36-B3-RN-4-150	1.046784	4	2.6	3.9



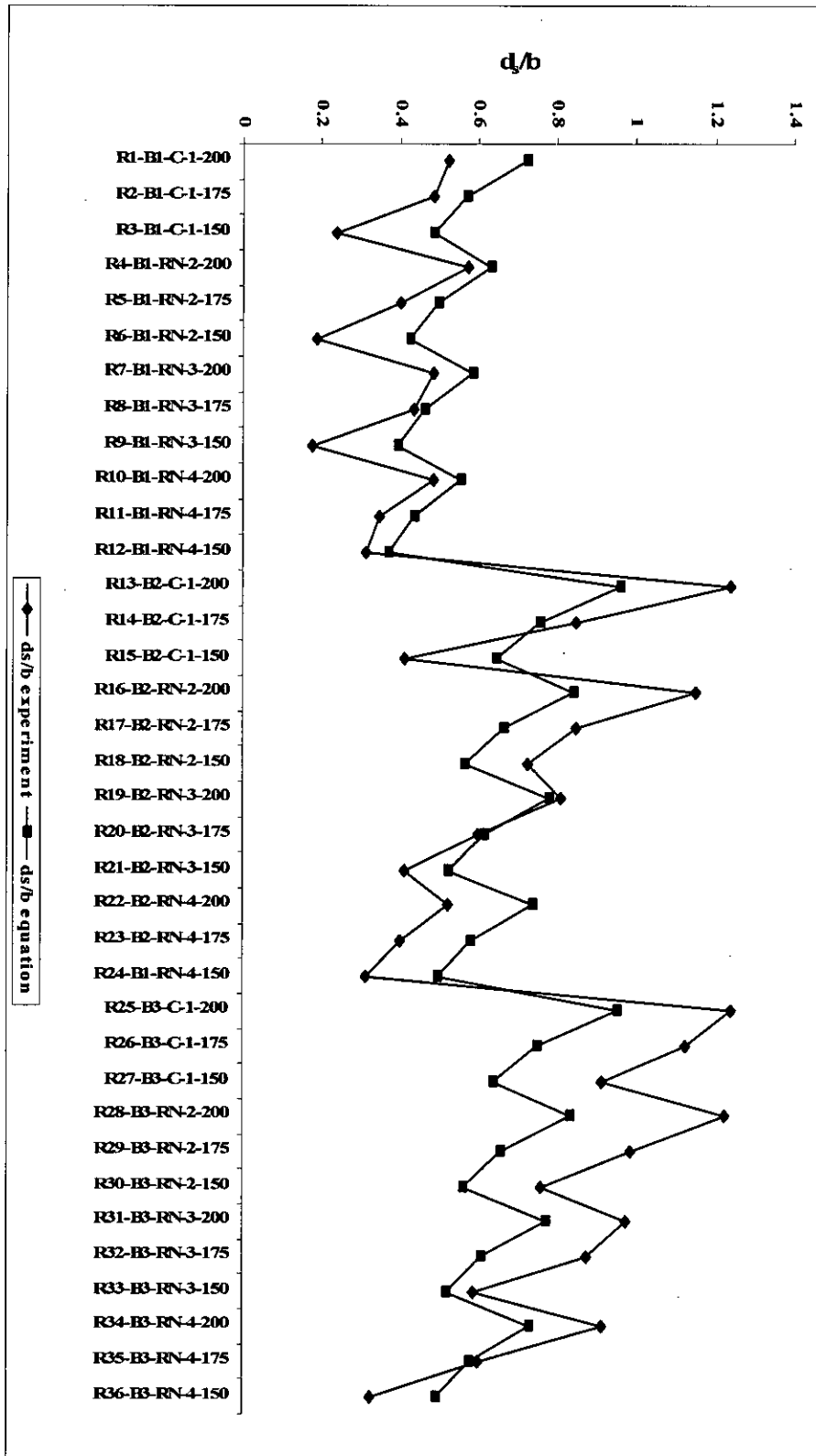


Figure 5.55: Graphical comparison of floodplain scours depths between experiment and calculated from developed equation

In Figure 5.55, it has been observed that calculated floodplain scour depths are close to experimental values for bed material 1 ( $d_{50} = 0.75$  mm) and bed material 2 ( $d_{50} = 0.18$  mm). But slight difference has been found between actual and predicted scour depths in case of bed material 3 ( $d_{50} = 0.12$  mm).

To verify proposed empirical relationship, it is compared with another two scour predicting equations, i.e. Colorado State University (CSU) equation and Froehlich's equation, for some selected experimental runs. All calculated scour depths by these equations are then compared with experimental values and presented in Table 5.3.

Table 5.3: Comparison of floodplain scour depth calculated from different equations with experimental values

Exp. Run	Necessary Data	Floodplain scour depth, cm			
		CSU equation	Froehlich's equation	Developed equation	Experimental value
R7	Round nose pier $F_r = 0.33$ $D_{50} = 0.75$ mm	10.4	10.9	4.7	3.9
R9	Round nose pier $F_r = 0.26$ $D_{50} = 0.75$ mm	9.4	10.7	3.1	1.4
R14	Circular pier $F_r = 0.29$ $D_{50} = 0.18$ mm	9.8	11.2	6.1	6.8
R15	Circular pier $F_r = 0.26$ $D_{50} = 0.18$ mm	9.4	11.1	5.2	3.3
R19	Round nose pier $F_r = 0.33$ $D_{50} = 0.18$ mm	10.4	11.3	6.2	6.5
R25	Circular pier $F_r = 0.33$ $D_{50} = 0.12$ mm	10.4	11.4	7.6	9.9
R35	Round nose pier $F_r = 0.29$ $D_{50} = 0.12$ mm	9.8	11.3	4.6	4.8
R36	Round nose pier $F_r = 0.26$ $D_{50} = 0.12$ mm	9.4	11.2	3.9	2.6

From Table 5.3, it can be identified that calculated floodplain scour depths from CSU equation and Froehlich's equation are much higher in comparison with experimental values. But floodplain scour depth predicted by developed empirical relationship gives much satisfactory and closer result to actual scour depth. Higher difference between actual scour depth and available equation's predicted values may be caused as these equations are mainly developed for main channel or rectangular channel. Earlier observations of this study indicate significant variations between floodplain and main channel scour depth.

## Chapter 6

# CONCLUSIONS AND RECOMMENDATIONS

### 6.1 Introduction

In this present study, local scour around pier like structures at floodplain of compound channel has been investigated for variable discharges, structure shapes, length-width ratio and bed materials. Commonly used Circular and Round nose pier shape with four length-width ratio are used in current research. In total 36 experimental runs have been conducted for three variable discharges and three different locally available bed materials. General behavior of local scour and flow field around structure has been analyzed with respect to discharge, structure shape, length-width ratio and bed material. Effect of available bed materials on local scour is also investigated. Observations and findings made from experimental results are compared between floodplain and main channel situation. An empirical relationship has been developed to predict floodplain scour depth from present experimental data set. This relationship has been compared with other available scour predicting equations.

### 6.2 Conclusions

Based on detailed experimental investigation, analysis and discussion presented in foregoing chapters, following conclusions may be drawn:

1. As critical flow velocity is considered a demarcation line for distinguishing clear water and live bed scour condition, in general live bed scour condition has been maintained both at floodplain and main channel.
2. Circular pier scour depth is highest than any other structure shapes. Main channel scour is always higher than floodplain scour. Scour depth significantly decreases with increasing length-width ratio and increases from coarse sediment to finer. Maximum scour depth varies linearly with Froude number irrespective of pier shape.

3. As present study has been carried out in live bed regime, equilibrium scour depth is reached quickly than that in clear water regime and at higher velocities, equilibrium state is attained very rapidly. Scour depth oscillates with time and becomes more or less steady after a certain time.
4. Maximum scour depth location has been observed around different pier shapes for different discharges, length-width ratio and different bed materials. But generally, maximum scour depth is located just adjacent to structure and close to front face of structure at upstream. Lateral extent of scour hole is not symmetric as local scour in clear water scour condition. Longitudinal extent of scour hole mostly depends on length-width ratio of structure and discharges. Scour hole slope is steepest and uniform for higher discharge and shows a declining trend with lower discharges. A relatively flatter scour hole at rear side of structure is occurred in finer bed materials. Sediment is deposited near rear side of structures and shifts adjacent to rear face for lower discharges and grater length-width ratio. Generally main channel scour shows similar characteristics as floodplain but magnitudes considerably differ.
5. Bed profiles are significantly varies with sediment size. Generally finer bed material results more steeper, uniform and deeper scour comparing with coarse sediment. Structure shapes effect shape of scour hole as both shapes are formed nearly symmetrical.
6. Scour depth varies with velocity variation of flow and an increasing tendency of scour depth has been observed with increasing flow intensity. Flow velocity is higher in main channel than that of floodplain and responsible for deeper scour in main channel than floodplain. Flow velocity reduces at front face of structure due to flow separation and downward movement of flow causes scour. Upward and reverse flow occurs at rear side of structure that causes scour behind structure. At floodplain, velocity distribution is associated with vortex generation as mid of channel.
7. An empirical relationship (Equ. 5.3) has been proposed to predict floodplain scour based on present study data set and compared with available scour equations and actual data.

### 6.3 Recommendations for further study

Based on present research work, some recommendation can be suggested for further study of floodplain scour. They are as follows:

- In current study, two commonly used structure shape in Bangladesh context, i.e. Circular and Round nose have been used. Recommendation can be made to undertake other available structure shapes in consideration.
- Similar type of study can be conducted for widely varied discharges, depth of flow and for different depth ratio.
- Further research can be performed to evaluate effect of sediment on local scour at floodplain by using maximum possible samples of river bed materials available in Bangladesh.
- General behavior of local scour at floodplain of compound channel has been investigated in present study. Floodplain scour reduction measure will be a suitable research area for future investigation.
- Proposed empirical relation to predict floodplain scour is based on present experimental data set only. It can be verified with available practical field data set to evaluate significance of it. This developed relationship will be modified or a new equation can be proposed to predict floodplain scour more accurately.
- Compound channel with one associate floodplain is considered for present experimental work. In future experimental study, compound channel having both floodplains can be suggested as recommendation.

## REFERENCE

- Ansari, S.A. and Qadar, A. (1994) "Ultimate depth of scour around bridge piers." Proceedings, ASCE National Hydraulics Conference, Buffalo, New York, USA, pp. 51-55.
- Baker, C.J. (1980) "The turbulent horseshoe vortex." Journal of Wind Engineering and Industrial Aerodynamics, Vol. 6, No. 1-2, 9-23.
- Baker, R.E. (1986) "Local scour at bridge piers in non-uniform sediment." Report No. 402, Department of Civil Engineering, University of Auckland, New Zealand.
- Breusers, H.N.C. and Raudkivi, A.J. (1991) "Scouring." Hydraulic Structures Design Manual, A.A. Balkema, Rotterdam, The Netherlands.
- Chang, H.H. (1988) "Fluvial processes in river engineering." John Wiley and Sons Inc., USA.
- Chew, Y.M. (1984) "Scour at bridge piers." Report no. 355, Department of Civil Engineering, University of Auckland, New Zealand.
- Cordoso, A.H. and Bettess, R. (1999) "Effect of time and channel geometry on scour at bridge abutments" Journal of Hydraulic Engineering, Volume 125, Issue 4, pp 388-399
- Dey, S., Bose, S.K. and Sastry, G.L.N. (1995) "Clear water scour at circular piers: A model." Journal of Hydraulic Engineering, ASCE, 121(12), 869-876.
- Ettema, R. (1976) "Influence of bed material gradation on local scour." Report No. 124, School of Engineering, The University of Auckland, New Zealand, 226pp.
- Ettema, R. (1980) "Scour at bridge piers." Report No. 216, Department of Civil Engineering, The University of Auckland, New Zealand.
- Ettema, R., Melville, B.W. and Barkdoll, B. (1998) "Scale effect in pier scour experiments." Journal of Hydraulic Engineering, ASCE, 124(7), 756-759.
- Gao, D., Posada, G.L. and Nordin, C.F. (1993) "Pier scour equations used in the Peoples Republic of China-review and summary." Proceedings, ASCE National Hydraulics Conference, San Francisco, California, USA, pp. 1031-1036.
- Grade, R.J. and Raju, K.G.R. (1985) "Mechanics of sediment transportation and alluvial stream problem." 2<sup>nd</sup> edition, Wiley Eastern Ltd, New Delhi, India.
- Haque, A. and Rahaman, M.M. (2003) "Scour around bridge pier in a compound channel" Technical paper-2: Prediction of scour depth, Institute of Water and Flood Management, BUET, Dhaka.

- Hasan, R.M.M. (2003) "Experimental study of local scour at the toe of protected embankment" M.Engg. Thesis, Department of Water Resources Engineering, BUET, Dhaka.
- Jain, S.C. (1981) "Maximum clear water scour around circular piers." *Journal of Hydraulic Engineering, ASCE*, 107(5), 611-626.
- Kabir, M.R. (1984) "An investigation of local scour around bridge piers." M.Sc.Engg. Thesis, Department of Water Resources Engineering, BUET, Dhaka.
- Kabir, M.R., Faisal, I.M. and Khatun, F. (2000) "Laboratory study and field investigation of scour around bridge pier in Bangladesh." *Proceedings, International Symposium on Scour of Foundations, IS-Scour 2000, ISSMGE, TC-33, Melbourne, Australia.*
- Kandasamy, J. K. and Melville, B.W. (1998) "Maximum local scour depth at bridge piers and abutments." *Journal of Hydraulic Research, IAHR*, 36(2), 183-198.
- Khatun, F. (2001) "Experimental study on local scour around bridge piers and its reduction." M.Sc.Engg. Thesis, Department of Water Resources Engineering, BUET, Dhaka.
- Kothiyari, U.C., Grade, R.C.J., and Raju, K.G.R. (1992a) "Temporal variation of scour around circular piers." *Journal of Hydraulic Engineering, ASCE*, 118(8), 1091-1105.
- Kothiyari, U.C., Grade, R.C.J. and Raju, K.G.R. (1992b) "Live bed scour around cylindrical bridge piers." *Journal of Hydraulic Research, IAHR*, 30(5), 701-715.
- Landers, M.N., Mueller, D.S. and Richardson, E.V. (1999) "US geological survey field measurements of pier scour." *ASCE Compendium, Stream Stability and Scour at Bridges, Reston, VA.*
- Laursen, E.M. and Toch, A. (1956) "Scour around bridge piers and abutments." *Bulletin No. 4, Iowa Highways Research Board, Ames, Iowa, USA.*
- Laursen, E.M. (1958) "Scour at bridge crossing." *Bulletin No.8, Iowa Highway Research Board, Ames, Iowa, USA.*
- Laursen, E.M. (1958) "Scour at bridge crossing." *Journal of Hydraulic Engineering, ASCE, Vol. 86, No. HY 2.*
- Laursen, E.M. (1962) "Scour at bridge crossing." *Trans., 127(1), ASCE, Paper 3294.*
- Laursen, E.M. (1963) "An analysis of relief bridge scour." *Journal of Hydraulic Engineering, ASCE, 89(3), 93-118.*
- Laursen, E.M. (1996) "Discussion on modeling uncertainty on prediction of pier scour." *Journal of Hydraulic Engineering, ASCE, 122(2), 822.*



- Laursen, E.M. (1998) "Discussion on pier and abutment scour: integrated approach." *Journal of Hydraulic Engineering, ASCE*, 1, 192-197.
- Lyness, J.F. and Myers, W.R.C. (1994) "Comparison between measured and numerically modeled unsteady flows in a compound channel using different representations of friction slope." 2<sup>nd</sup> International Conference on River Flood Hydraulics, 22-25 March 1994, York, England.
- McIntosh, J.L. (1989) "Use of scour prediction formulae." *Proceedings of the Bridge Scour Symposium, McLean, VA. Federal Highway Administration Research Report FHWA-RD-90-035*, pp.78-100.
- Melville, B.W. (1975) "Local scour at bridge sites." Report No. 117, Department of Civil Engineering, University of Auckland, New Zealand.
- Melville, B.W. (1997) "Pier and abutment scour: integrated approach." *Journal of Hydraulic Engineering, ASCE*, 123(2), 125-136.
- Melville, B.W. and Chiew, Y.M. (1999) "Time scale of local scour around bridge piers." *Journal of Hydraulic Engineering, ASCE*, 125(1), 59-65.
- Melville, B.W. and Sutherland, A.J. (1988) "Design method for local scour at bridge piers." *Journal of Hydraulic Engineering, ASCE*, 114(10), 1210-1227.
- Melville, B.W. and Coleman, S.E. (2000) "Bridge scour." *Water Resources Publications, LLC, USA*.
- Mohamed, T.A., Noor, M.M., Ghazali, A.H. and Huat, B.B.K. (2005) "Validation of some bridge pier scour formulae using field and laboratory data" *American Journal of Environmental Sciences, ISSN 1553-345X*.
- Mostafa, E.A. (1994) "Scour around skewed bridge piers." Ph.D. Thesis, Department of Civil Engineering, Alexandria University, Alexandria, Egypt.
- Mueller, D.S. and Wagner, C.R. (2005) "Field observations and evaluations of streambed scour at bridges." *Federal Highway Administration, Washington D.C., FHWA-RD-03-052*.
- Neill, C.R. (1968) "Notes on initial movement of coarse uniform bed material." *Journal of Hydraulic Research*, 17(2), pp. 247-249.
- Oliveto, G. and Hager, H.H. (2002) "Temporal development of clear water pier and abutment scour." *Journal of Hydraulic Engineering, ASCE*, Vol. 128, No. 9.
- Raudkivi, A.J. and Ettema, R. (1977) "Effects of sediment gradation on clear water scour." *Journal of Hydraulic Engineering, ASCE*, 103(10), 1209-1212.
- Richardson, E.V., Simons, D.B. and Julien, P.Y. (1990) "Highways in the river environment." *National Highway Institute, National Highway Administration, USA*.

Richardson, E.V. and Davis, S.R. (1995) "Evaluating scour at bridges." 3<sup>rd</sup> edition, Federal Highway Administration Hydraulic Engineering, Washington D.C., USA, Circular No. 18, FHWA-IP-90-017, 203p.

Richardson, E.V. and Davis, S.R. (2001) "Evaluating scour at bridges." 4<sup>th</sup> edition, Federal Highway Administration Hydraulic Engineering, Washington D.C., USA, Circular No. 18, FHWA NHI 01-001.

Shen, H.W., Scheider, V.R. and Karaki, S. (1969) "Local scour around bridge piers." Journal of Hydraulic Engineering, ASCE, 95(6), 1919-1940.

Simons, D.B. and Richardson, E.V. (1966) "Resistance to flow in alluvial channels." Geological Survey Professional Paper 422-J, US Department of the interior, United States Government Printing Office, Washington D.C., USA.

Sturm, T.W. (2004) "Enhanced abutment scour studies for compound channels" Federal Highway Administration, US Department of Transportation, Report No.FHWA-RD-99-156.

Vital, N., Kothyari, U.C. and Haghghat, M. (1994) "Clear water scour around bridge pier group." Journal of Hydraulic Engineering, ASCE, 120(11), 1309-1318.

**Appendix A**  
**Amour velocity,  $V_a$**

## Method of determining Armour velocity, $V_a$

### THRESHOLD VELOCITY, $V_c$ :

1. Find  $u_{*c}$  for  $d_{50}$  size from Shields diagram or (for quartz sand in water at 20°C)

$$u_{*c} = 0.0115 + 0.0125d_{50}^{1.4} \quad 0.1\text{mm} < d_{50} < 1\text{mm}$$

$$u_{*c} = 0.0305d_{50}^{0.5} - 0.0065d_{50}^{-1} \quad 1\text{mm} < d_{50} < 100\text{mm}$$

2. Find  $V_c$  from logarithmic velocity distribution (for fully turbulent flow)

$$\frac{V_c}{u_{*c}} = 5.75 \log \left( 5.53 \frac{y}{d_{50}} \right)$$

### ARMOUR PEAK VELOCITY, $V_a$ ( $\sigma_g > 1.3$ only):

3. Find  $d_{50a}$  from

$$d_{50a} = \frac{d_{\max}}{1.8}$$

4. Find  $u_{*ca}$  for  $d_{50a}$  size from Shields diagram or (for quartz sand in water at 20°C)

$$u_{*ca} = 0.0115 + 0.0125d_{50a}^{1.4} \quad 0.1\text{mm} < d_{50a} < 1\text{mm}$$

$$u_{*ca} = 0.0305d_{50a}^{0.5} - 0.0065d_{50a}^{-1} \quad 1\text{mm} < d_{50a} < 100\text{mm}$$

5. Find  $V_{ca}$  from

$$\frac{V_{ca}}{u_{*ca}} = 5.75 \log \left( 5.53 \frac{y}{d_{50a}} \right)$$

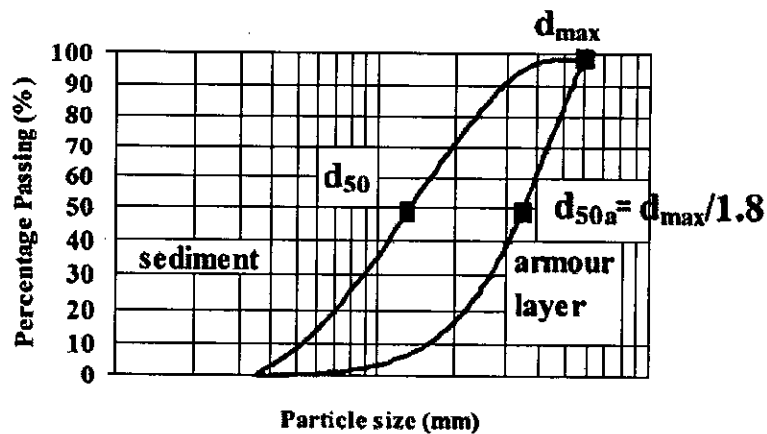
6. Calculate

$$V_a = 0.8V_{ca}$$

### VELOCITY PARAMETER:

7. Evaluate

$$\frac{[V - (V_a - V_c)]}{V_c} \quad \left( \equiv \frac{V}{V_c} \quad \text{for } \sigma_g < 1.3 \right)$$



Source: Bridge Scour; Melville and Coleman (2000); Page: 194

**Appendix B**  
**Scour map and photograph**

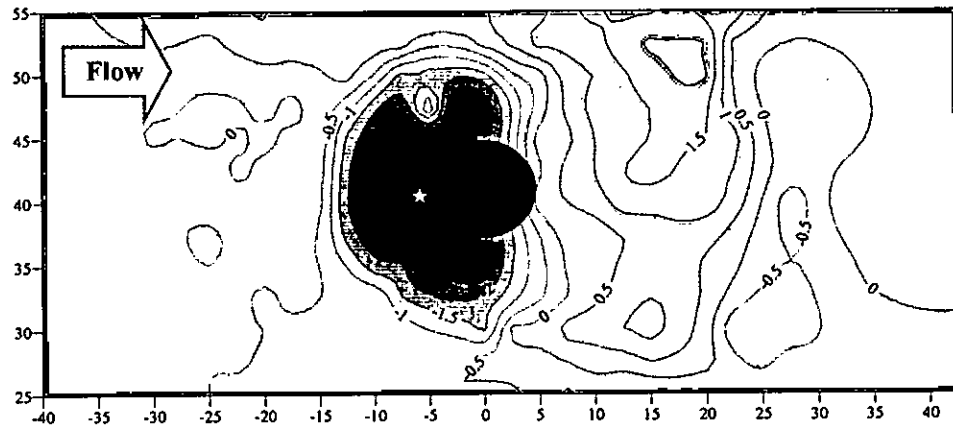


Figure B.1: Run 1-Bed material ( $d_{50} = 0.75$  mm)-Circular pier ( $l/b=1$ )- $Q=200$  l/s  
 ☆ Max.scour location  
 Floodplain

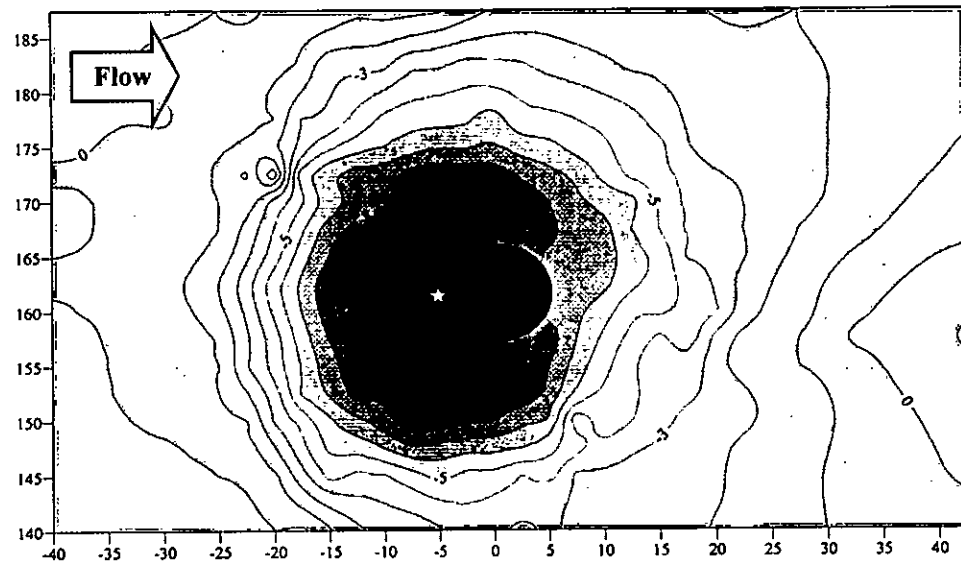
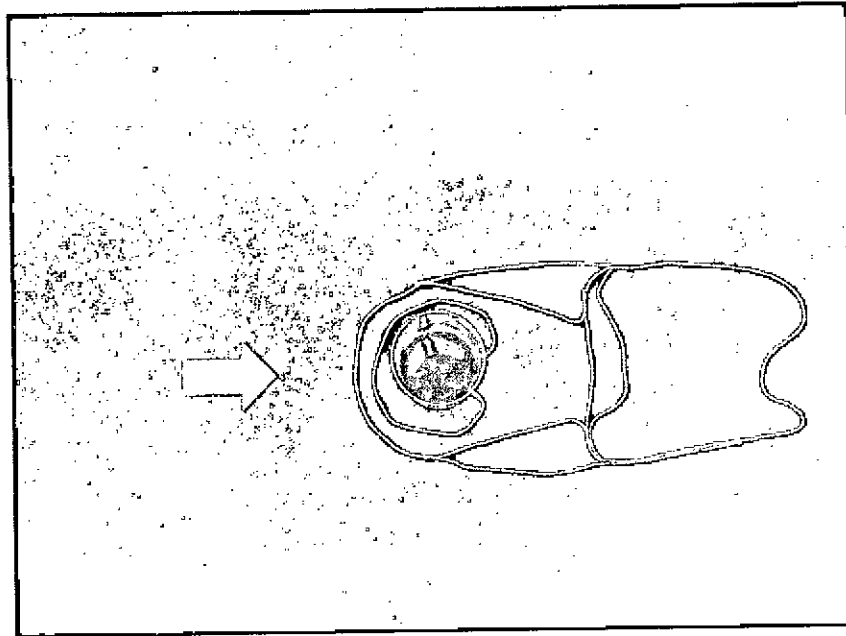
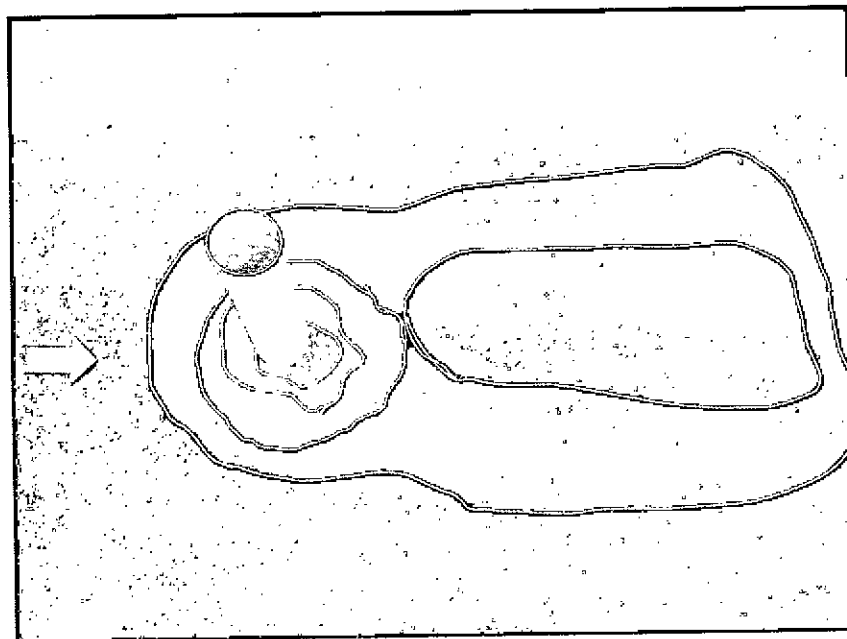


Figure B.2: Run 1-Bed material 1( $d_{50} = 0.75$  mm)-Circular pier ( $l/b=1$ )- $Q=200$  l/s  
 ☆ Max.scour location  
 Main channel



Photograph B.1: Run 1-Bed material 1 ( $d_{50} = 0.75$  mm)-Circular pier ( $l/b=1$ )- $Q=200$  l/s  
Floodplain



Photograph B.2: Run 1-Bed material 1 ( $d_{50} = 0.75$  mm)-Circular pier ( $l/b=1$ )- $Q=200$  l/s  
Main channel

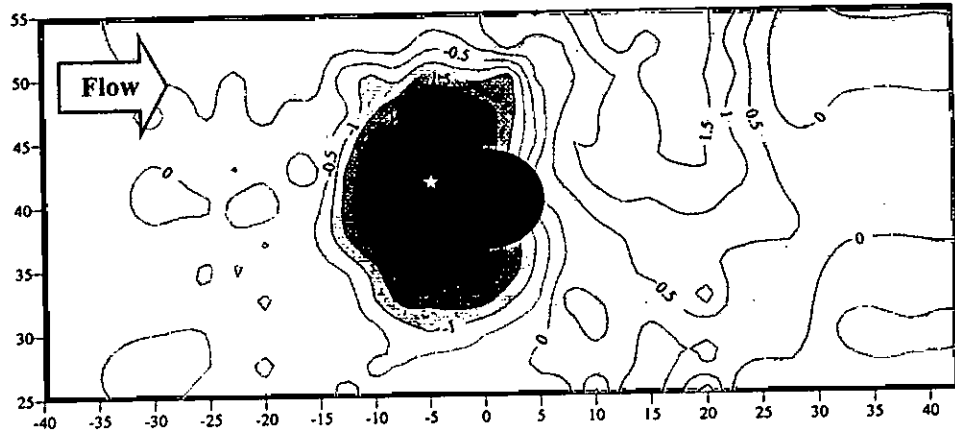


Figure B.3: Run 2-Bed material 1 ( $d_{50} = 0.75$  mm)-Circular pier ( $l/b=1$ )- $Q=175$  l/s  
 ☆ Max.scour location  
 Floodplain

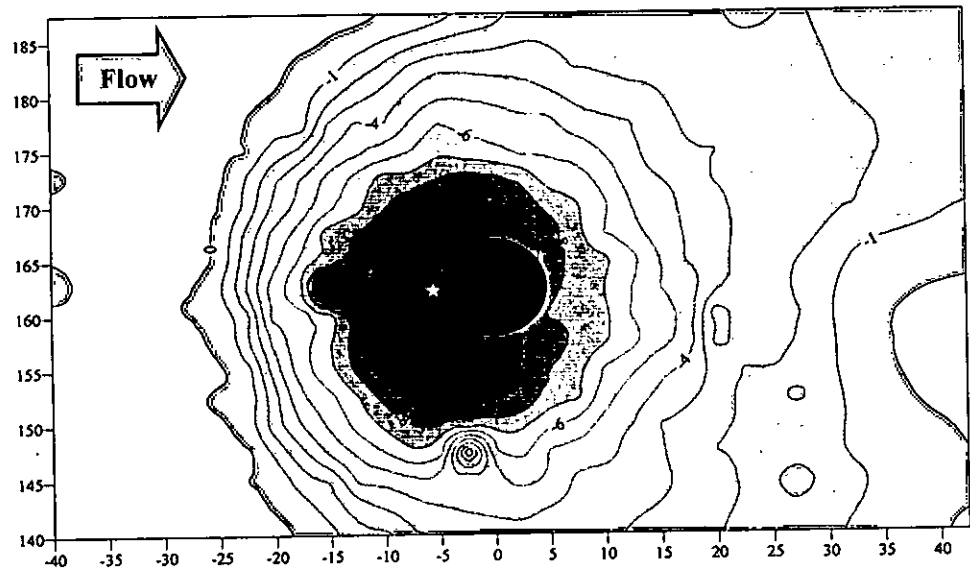
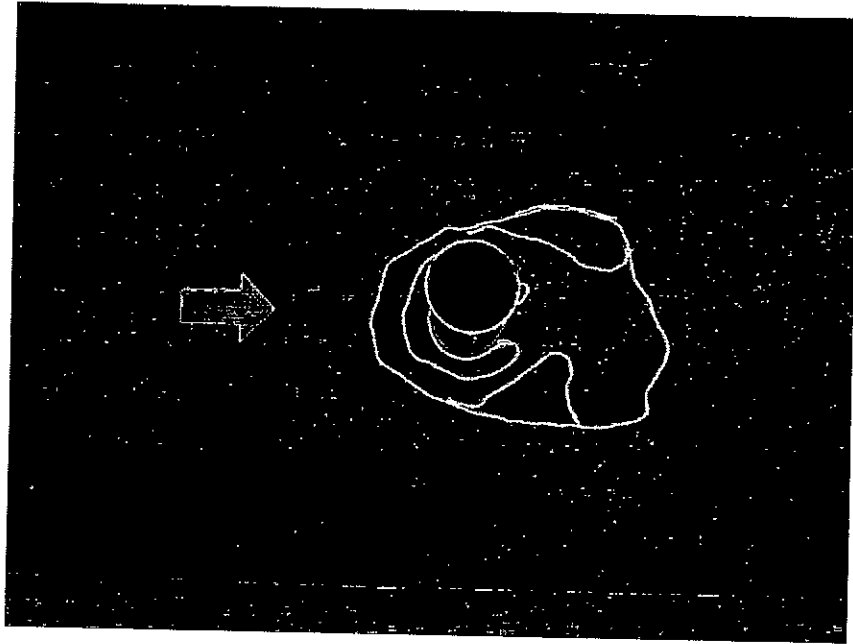
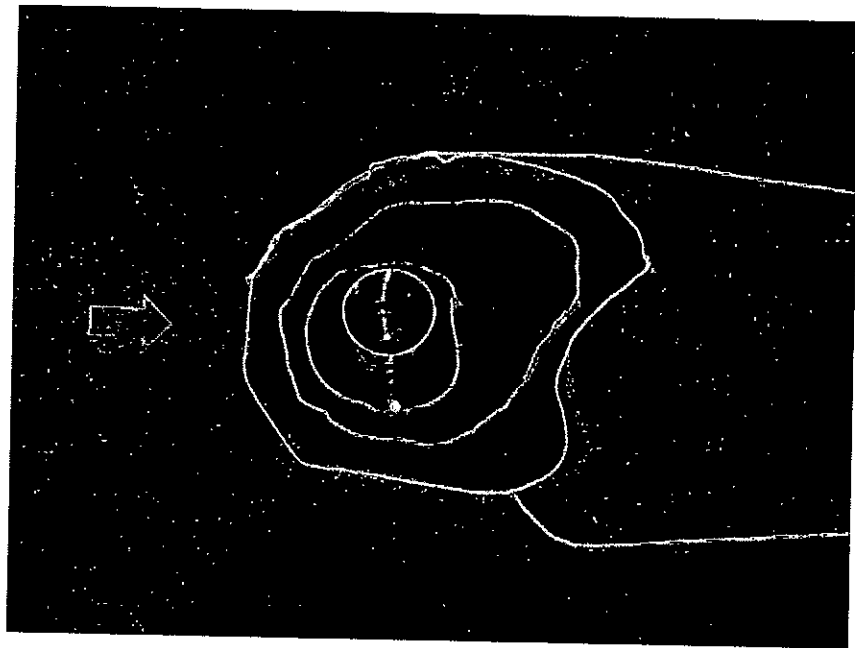


Figure B.4: Run 2-Bed material 1 ( $d_{50} = 0.75$  mm)-Circular pier ( $l/b=1$ )- $Q=175$  l/s  
 ☆ Max.scour location  
 Main channel





Photograph B.3: Run 2-Bed material 1 ( $d_{50} = 0.75$  mm)-Circular pier ( $l/b=1$ )- $Q=175$  l/s  
Floodplain



Photograph B.4: Run 2-Bed material 1 ( $d_{50} = 0.75$  mm)-Circular pier ( $l/b=1$ )- $Q=175$  l/s  
Main channel

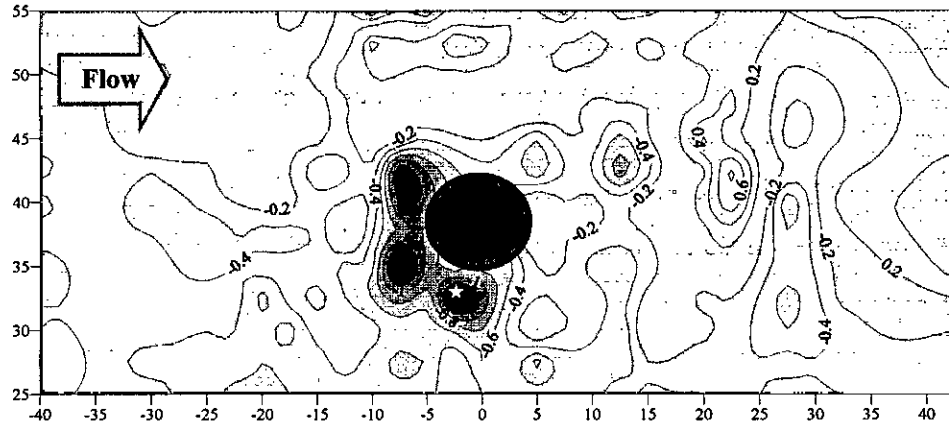


Figure B.5: Run 3-Bed material 1 ( $d_{50} = 0.75$  mm)-Circular pier ( $l/b=1$ )- $Q=150$  l/s  
 ☆ Max.scour location  
 Floodplain

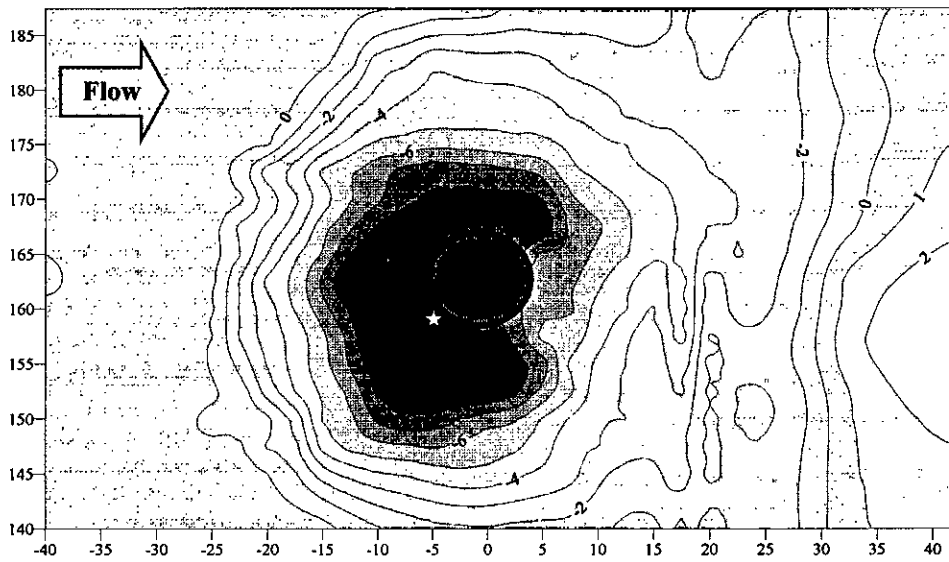
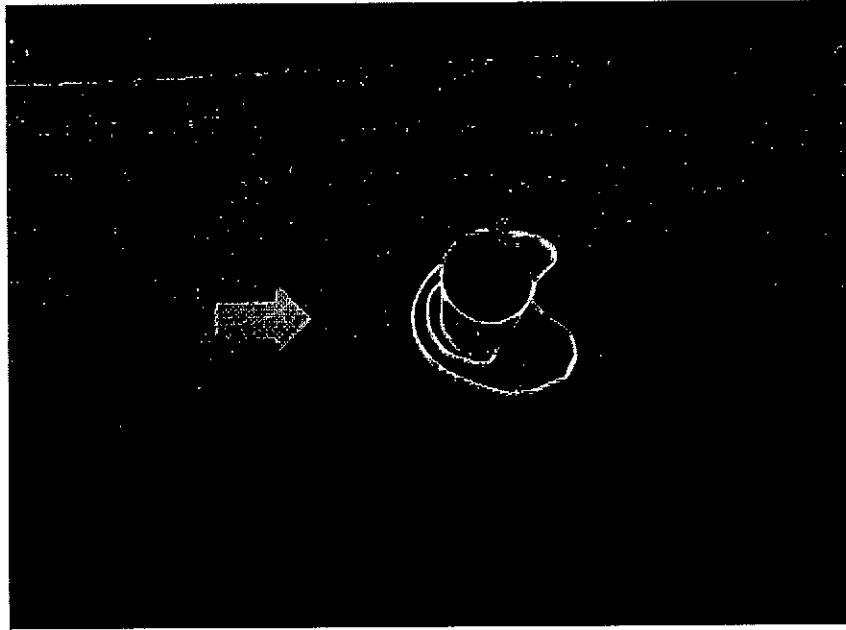
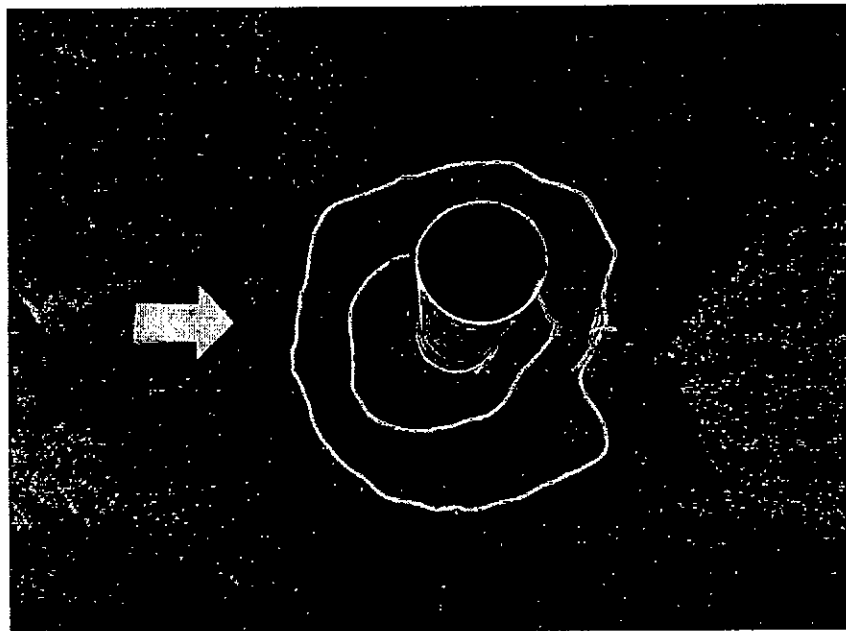


Figure B.6: Run 3-Bed material 1 ( $d_{50} = 0.75$  mm)-Circular pier ( $l/b=1$ )- $Q=175$  l/s  
 ☆ Max.scour location  
 Main channel



Photograph B.5: Run 3-Bed material 1 ( $d_{50} = 0.75$  mm)-Circular pier ( $l/b=1$ )- $Q=150$  l/s  
Floodplain



Photograph B.6: Run 3-Bed material 1 ( $d_{50} = 0.75$  mm)-Circular pier ( $l/b=1$ )- $Q=150$  l/s  
Main channel

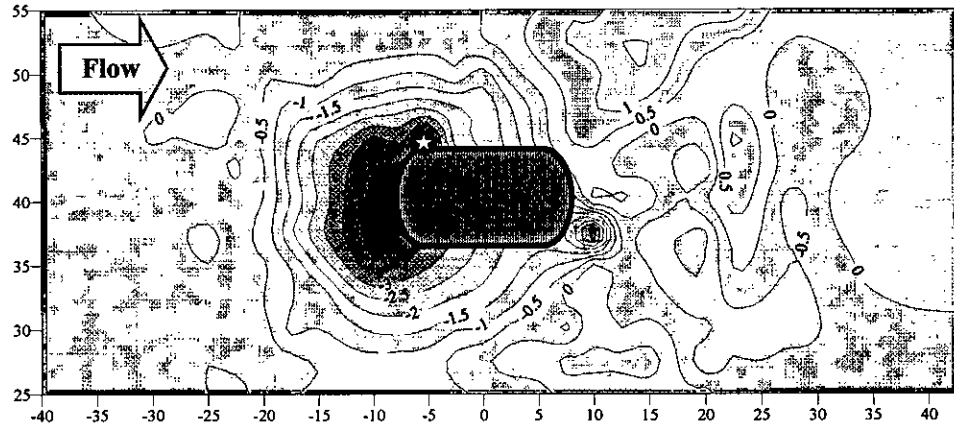


Figure B.7: Run 4-Bed material 1 ( $d_{50} = 0.75$  mm)-Round nose pier ( $l/b=2$ )- $Q=200$  l/s  
 ☆ Max.scour location  
 Floodplain

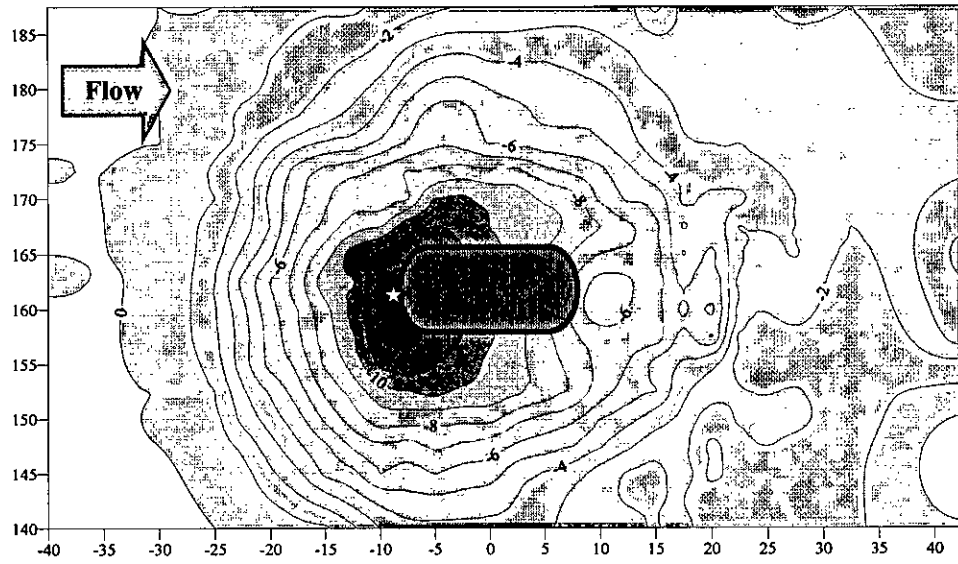
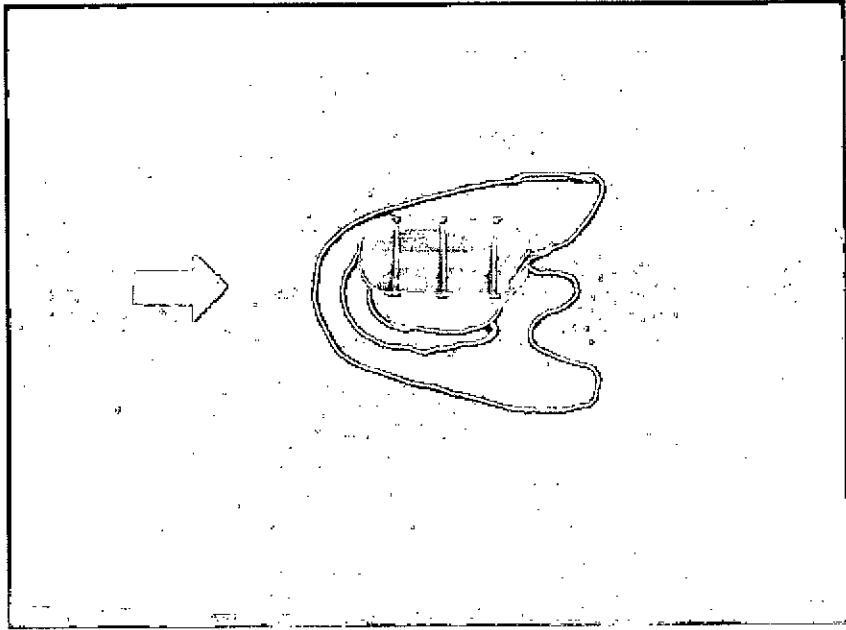
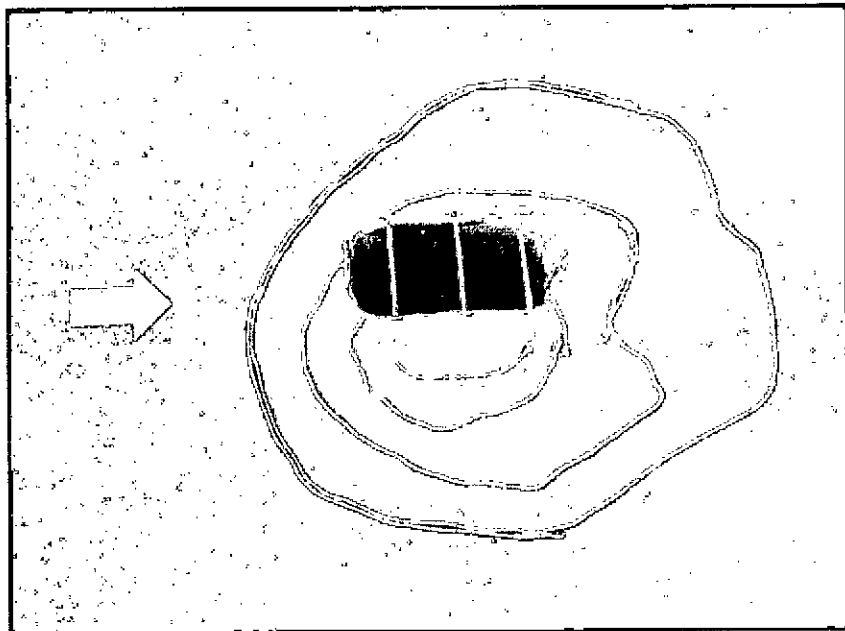


Figure B.8: Run 4-Bed material 1 ( $d_{50} = 0.75$  mm)-Round nose pier ( $l/b=2$ )- $Q=200$  l/s  
 ☆ Max.scour location  
 Main channel



Photograph B.7: Run 4-Bed material 1 ( $d_{50} = 0.75$  mm)-Round nose pier ( $l/b=2$ )- $Q=200$  l/s  
Floodplain



Photograph B.8: Run 4-Bed material 1 ( $d_{50} = 0.75$  mm)-Round nose pier ( $l/b=2$ )- $Q=200$  l/s  
Main channel

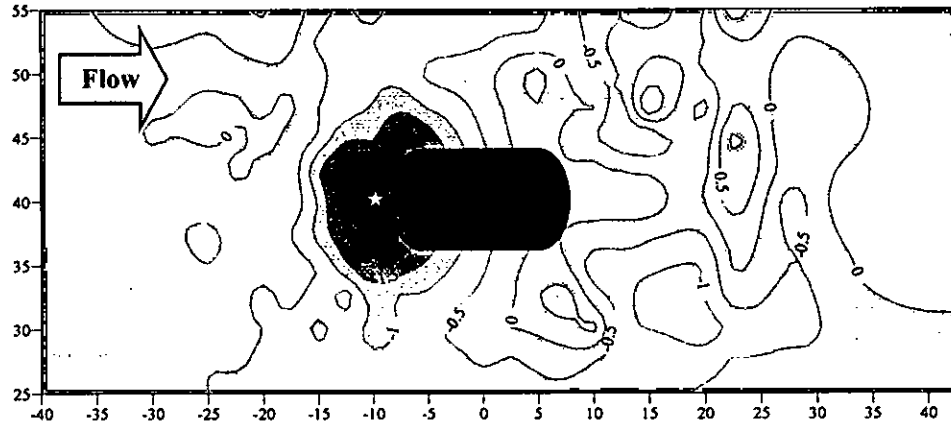


Figure B.9: Run 5-Bed material 1 ( $d_{50} = 0.75$  mm)-Round nose pier ( $l/b=2$ )- $Q=175$  l/s  
 ☆ Max.scour location  
 Floodplain

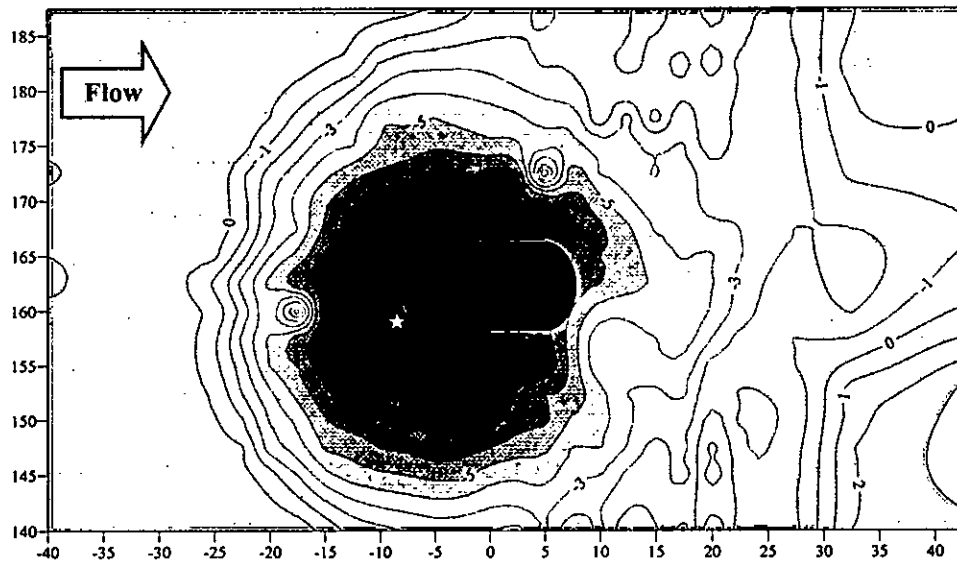
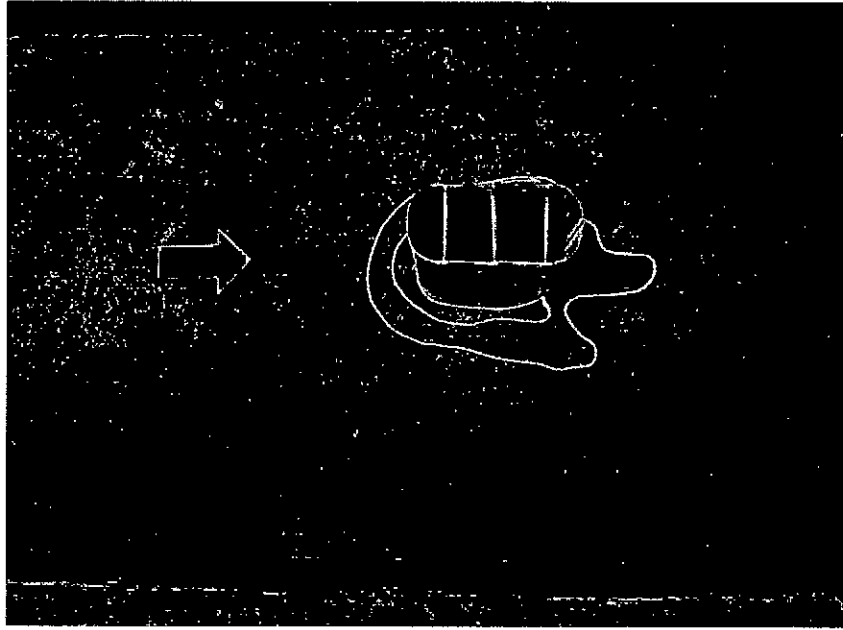
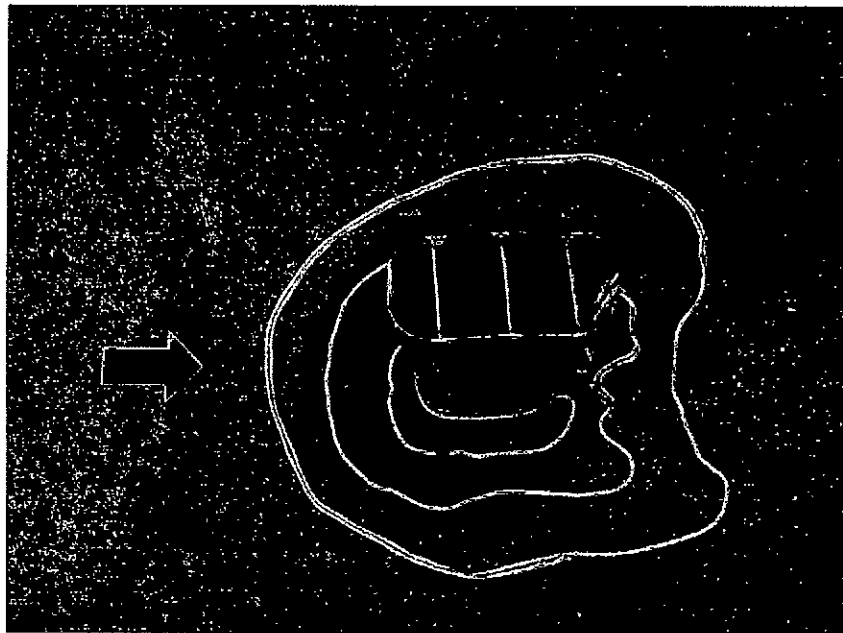


Figure B.10: Run 5-Bed material 1 ( $d_{50} = 0.75$  mm)-Round nose pier ( $l/b=2$ )- $Q=175$  l/s  
 ☆ Max.scour location  
 Main channel



Photograph B.9: Run 5-Bed material 1 ( $d_{50} = 0.75$  mm)-Round nose pier ( $l/b=2$ )- $Q=175$  l/s  
Floodplain



Photograph B.10: Run 5-Bed material 1 ( $d_{50} = 0.75$  mm)-Round nose pier ( $l/b=2$ )- $Q=175$  l/s  
Main channel

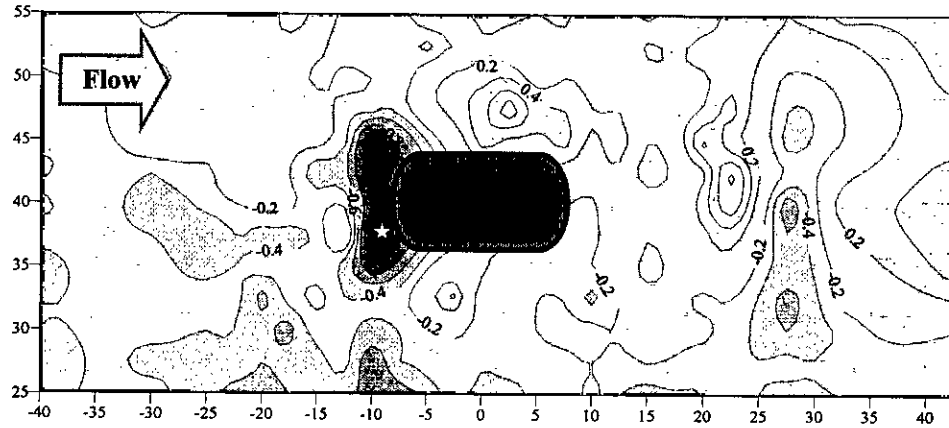


Figure B.11: Run 6-Bed material 1( $d_{50} = 0.75$  mm)-Round nose pier ( $l/b=2$ )- $Q=150$  l/s  
 ☆ Max.scour location  
 Floodplain

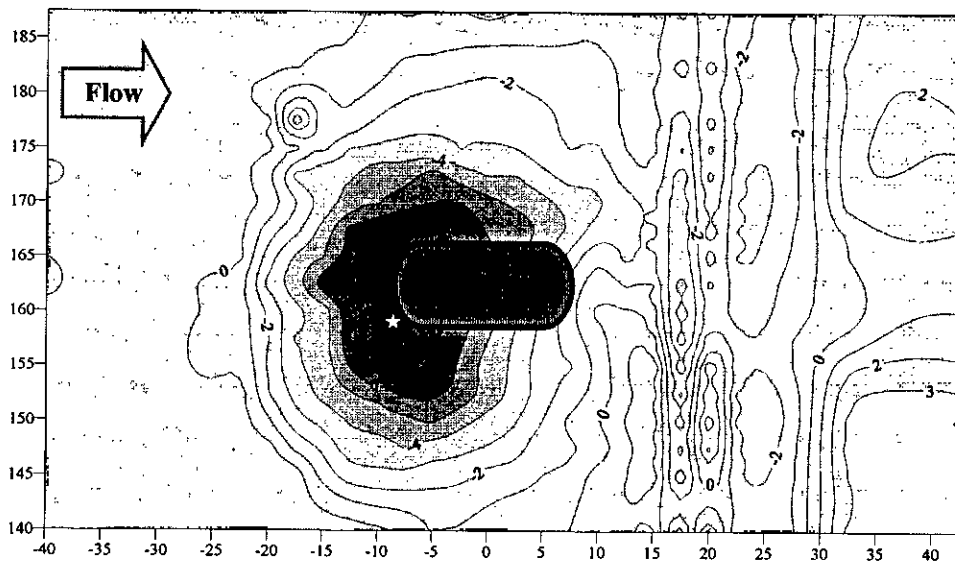
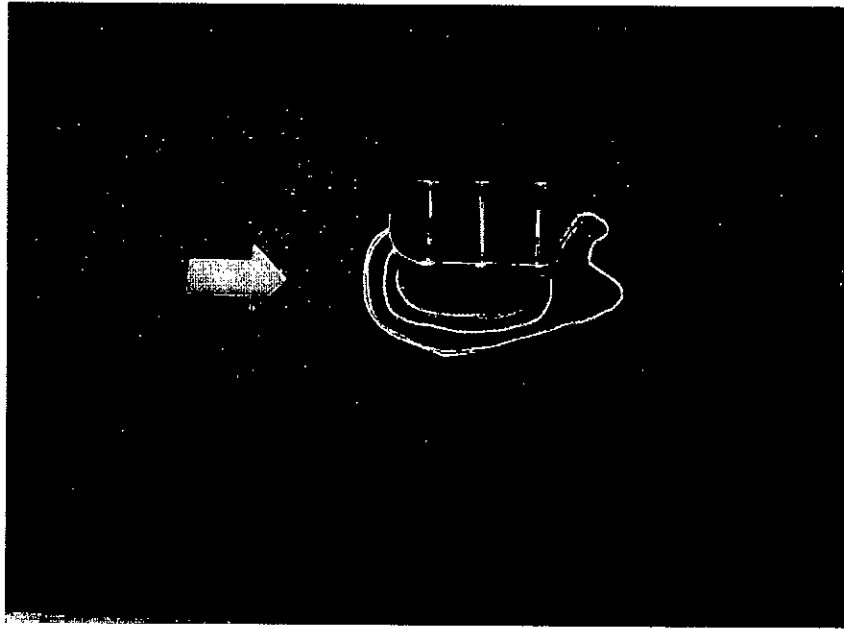
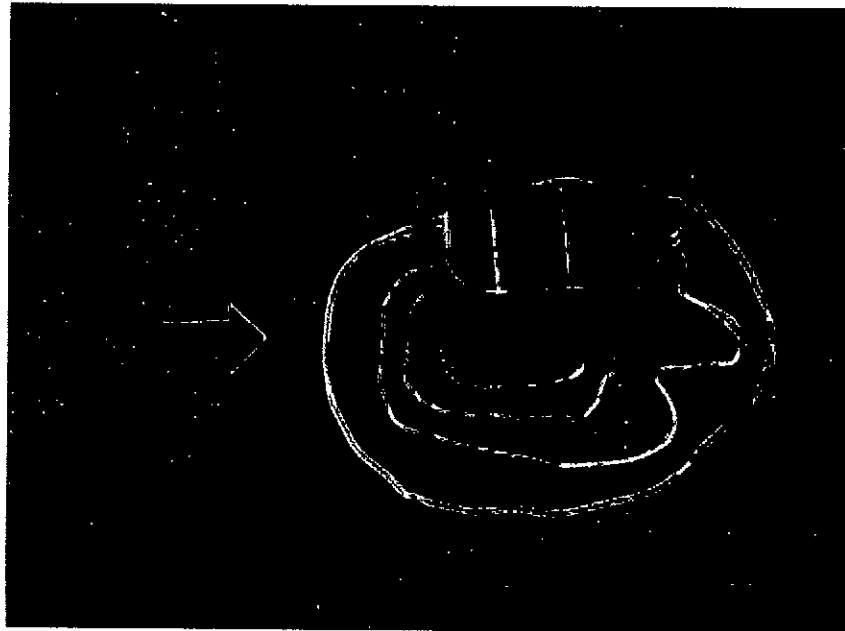


Figure B.12: Run 6-Bed material 1( $d_{50} = 0.75$  mm)-Round nose pier ( $l/b=2$ )- $Q=175$  l/s  
 ☆ Max.scour location  
 Main channel





Photograph B.11: Run 6-Bed material 1 ( $d_{50} = 0.75$  mm)-Round nose pier ( $l/b=2$ )- $Q=150$  l/s  
Floodplain



Photograph B.12: Run 6-Bed material 1 ( $d_{50} = 0.75$  mm)-Round nose pier ( $l/b=2$ )- $Q=150$  l/s  
Main channel

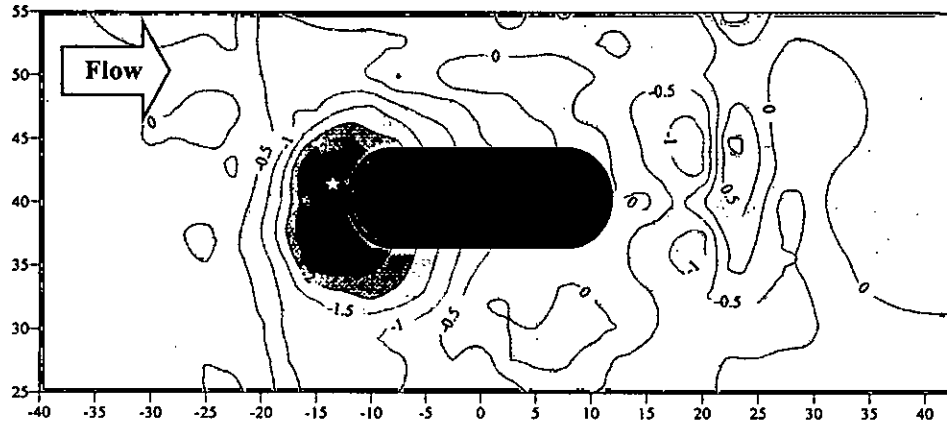


Figure B.13: Run 7-Bed material 1 ( $d_{50} = 0.75$  mm)-Round nose pier ( $l/b=3$ )- $Q=200$  l/s  
 ☆ Max.scour location  
 Floodplain

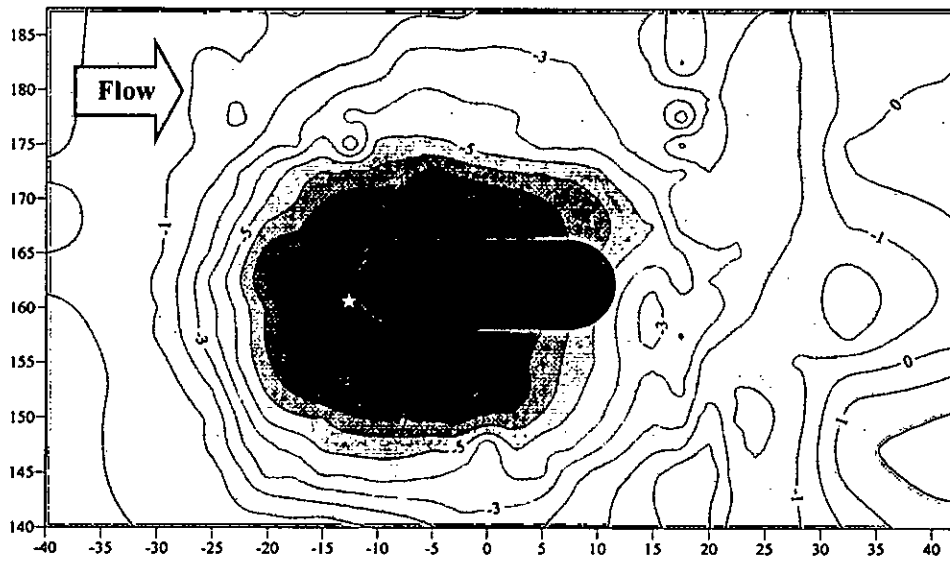
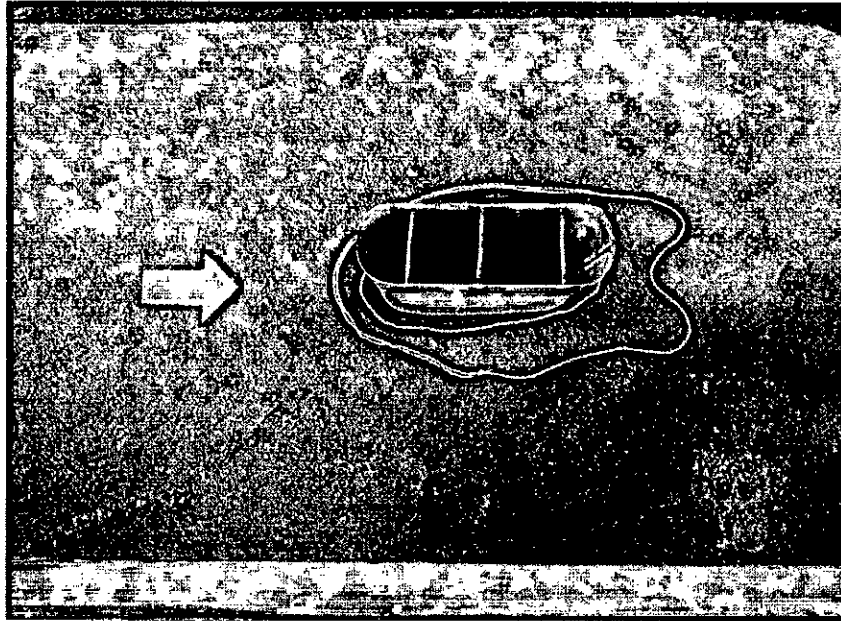
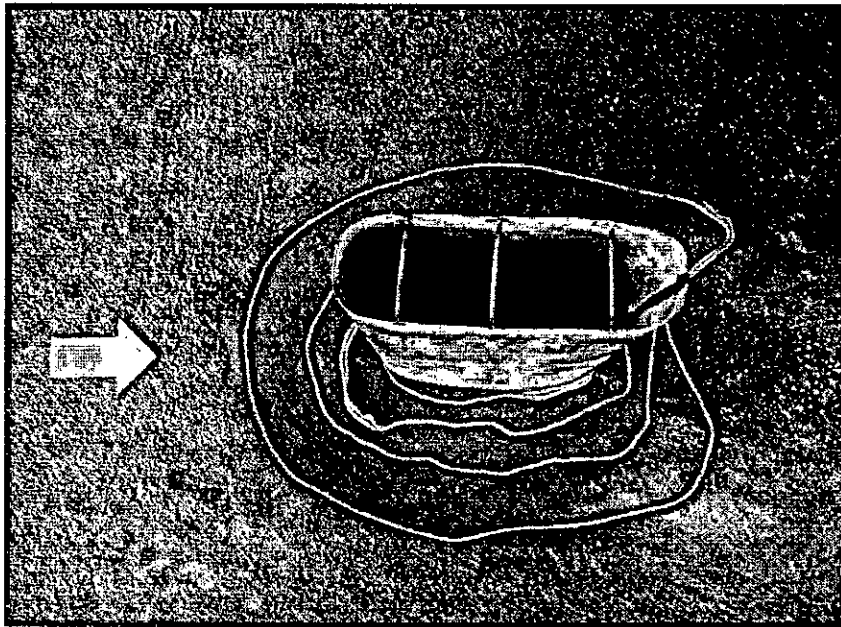


Figure B.14: Run 7-Bed material 1 ( $d_{50} = 0.75$  mm)-Round nose pier ( $l/b=3$ )- $Q=200$  l/s  
 ☆ Max.scour location  
 Main channel



Photograph B.13: Run 7-Bed material 1 ( $d_{50} = 0.75$  mm)-Round nose pier ( $l/b=3$ )- $Q=200$  l/s  
Floodplain



Photograph B.14: Run 7-Bed material 1 ( $d_{50} = 0.75$  mm)-Round nose pier ( $l/b=3$ )- $Q=200$  l/s  
Main channel

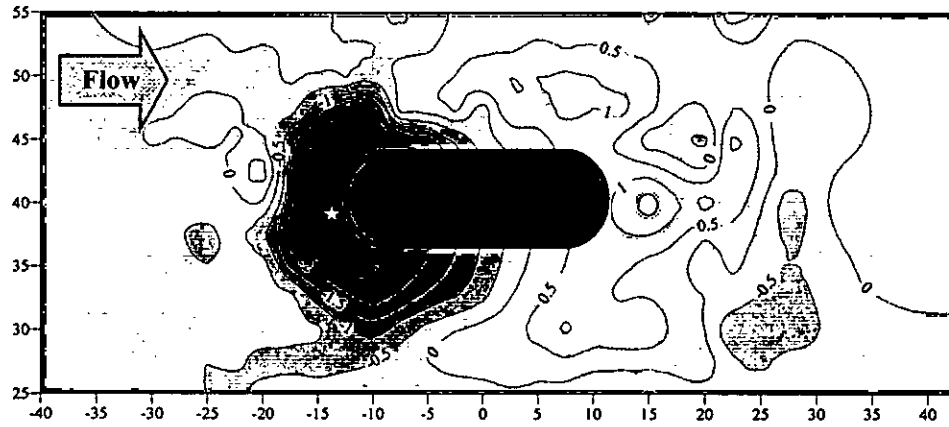


Figure B.15: Run 8-Bed material 1 ( $d_{50} = 0.75$  mm)-Round nose ( $l/b=3$ )- $Q=175$  l/s  
 ☆ Max.scour location  
 Floodplain

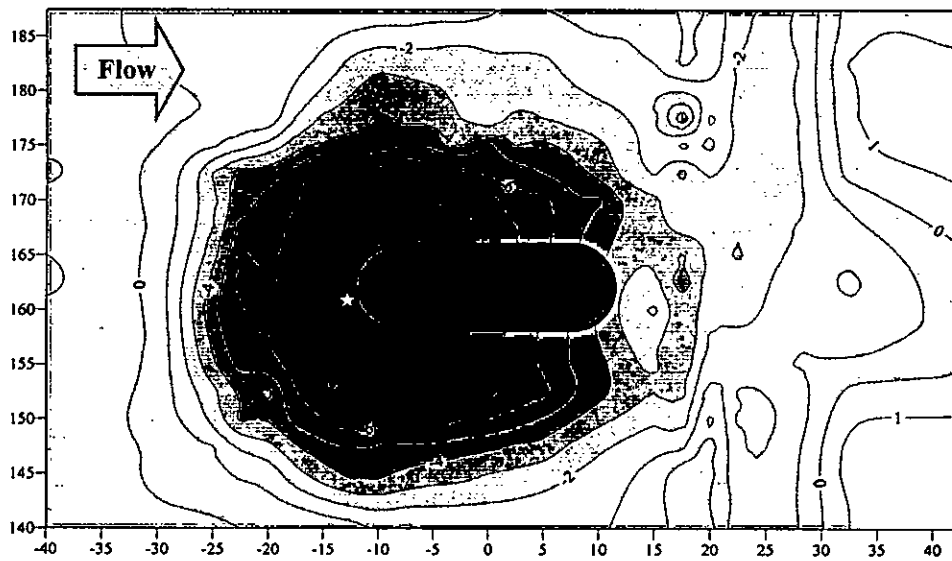
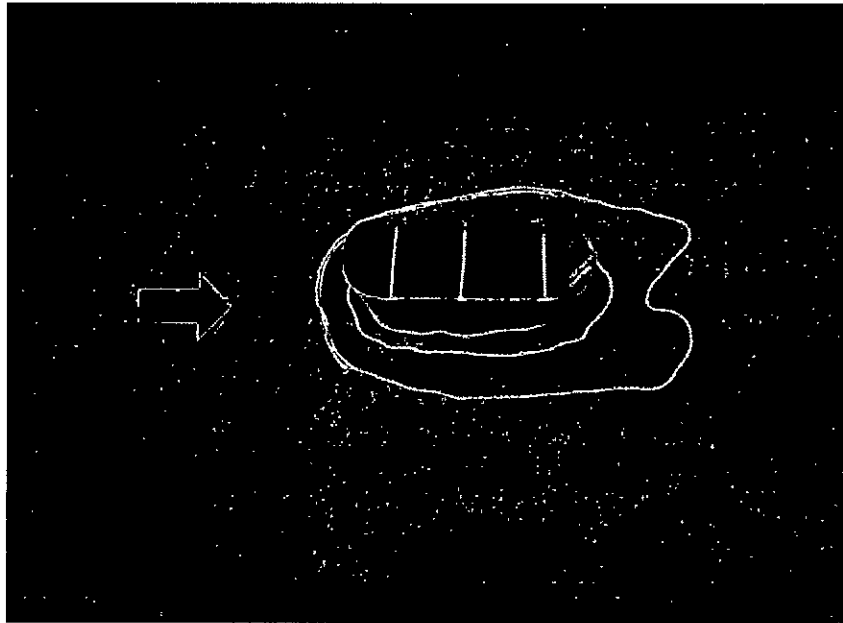
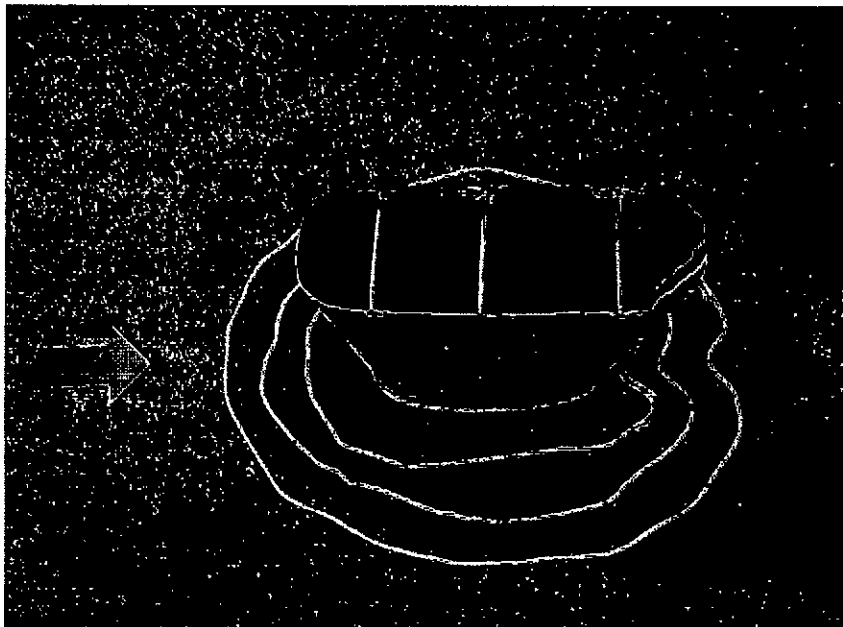


Figure B.16: Run 8-Bed material 1 ( $d_{50} = 0.75$  mm)-Round nose pier ( $l/b=3$ )- $Q=175$  l/s  
 ☆ Max.scour location  
 Main channel



Photograph B.15: Run 8-Bed material 1 ( $d_{50} = 0.75$  mm)-Round nose pier ( $l/b=3$ )- $Q=175$  l/s  
Floodplain



Photograph B.16: Run 8-Bed material 1 ( $d_{50} = 0.75$  mm)-Round nose pier ( $l/b=3$ )- $Q=175$  l/s  
Main channel

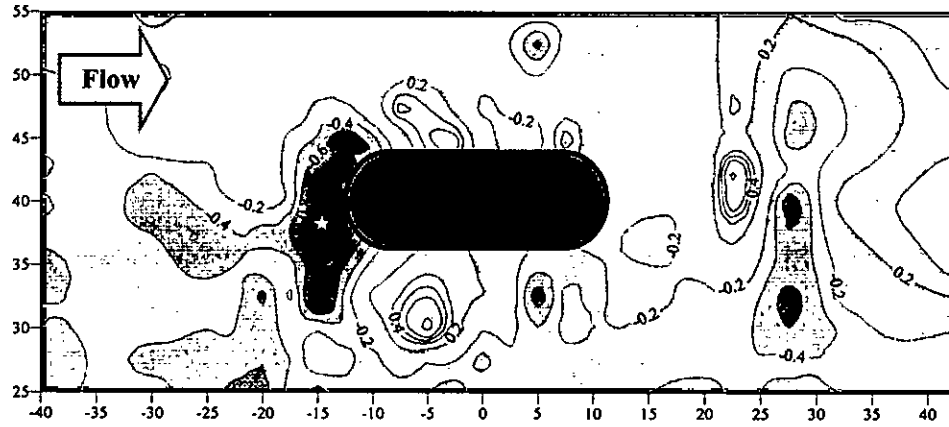


Figure B.17: Run 9-Bed material 1 ( $d_{50} = 0.75$  mm)-Round nose pier ( $l/b=3$ )- $Q=150$  l/s  
 ☆ Max.scour location  
 Floodplain

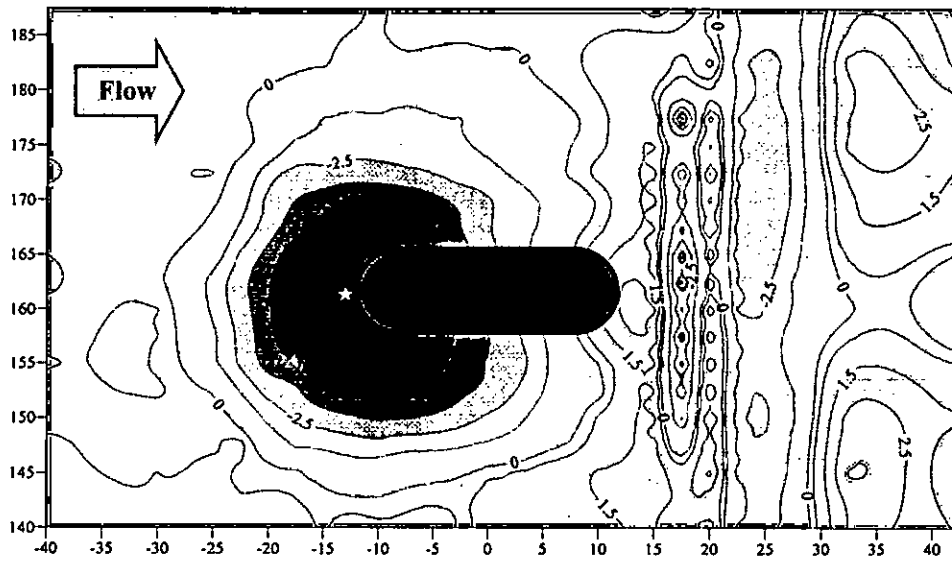
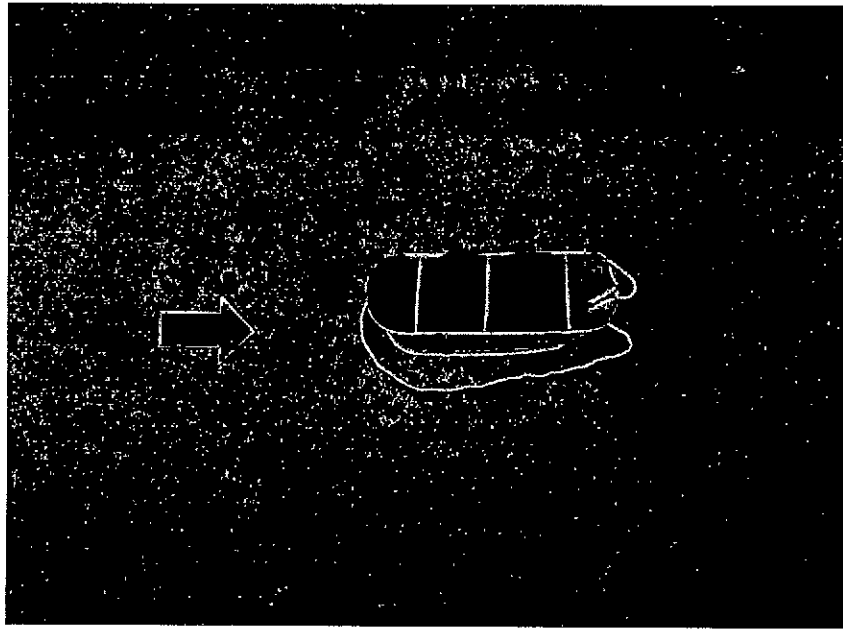
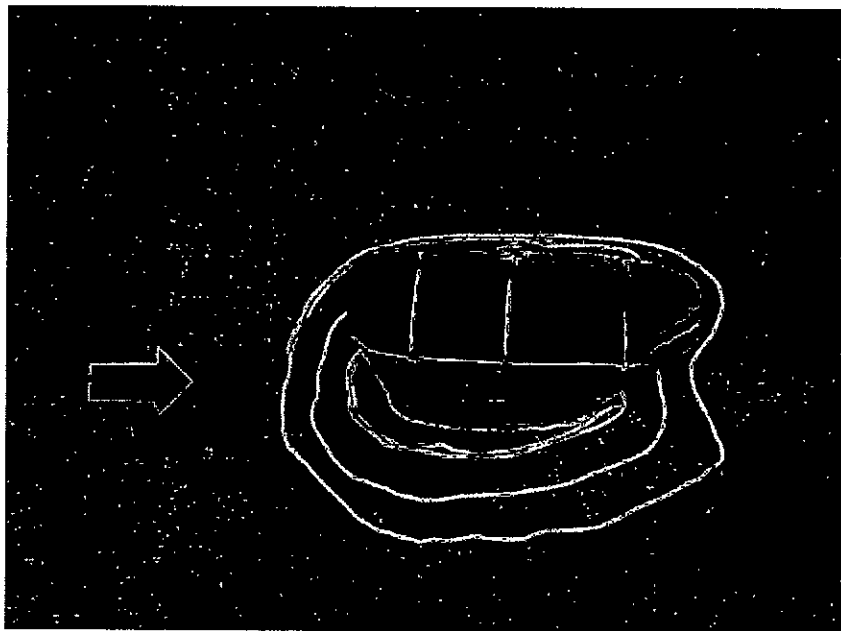


Figure B.18: Run 9-Bed material 1 ( $d_{50} = 0.75$  mm)-Round nose pier ( $l/b=3$ )- $Q=150$  l/s  
 ☆ Max.scour location  
 Main channel



Photograph B.17: Run 9-Bed material 1 ( $d_{50} = 0.75$  mm)-Round nose pier ( $l/b=3$ )- $Q=150$  l/s  
Floodplain



Photograph B.18: Run 9-Bed material 1 ( $d_{50} = 0.75$  mm)-Round nose pier ( $l/b=3$ )- $Q=150$  l/s  
Main channel

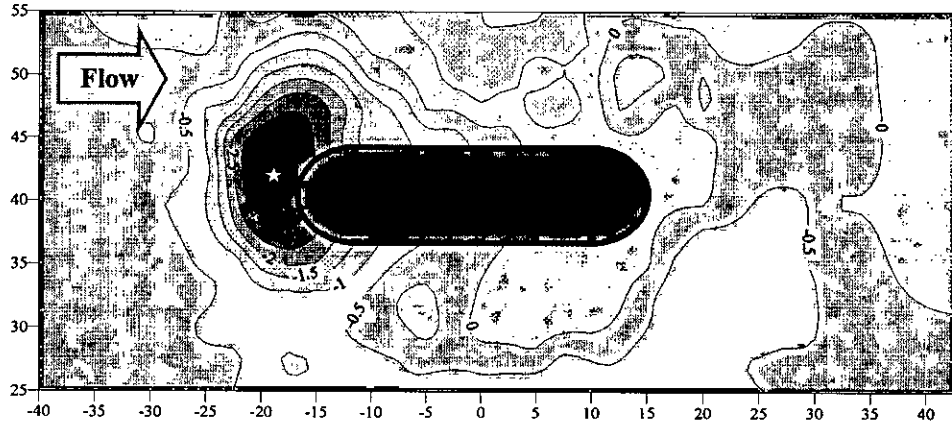


Figure B.19: Run 10-Bed material 1 ( $d_{50} = 0.75$  mm)-Round nose pier ( $l/b=4$ )- $Q=200$  l/s  
 ☆ Max.scour location  
 Floodplain

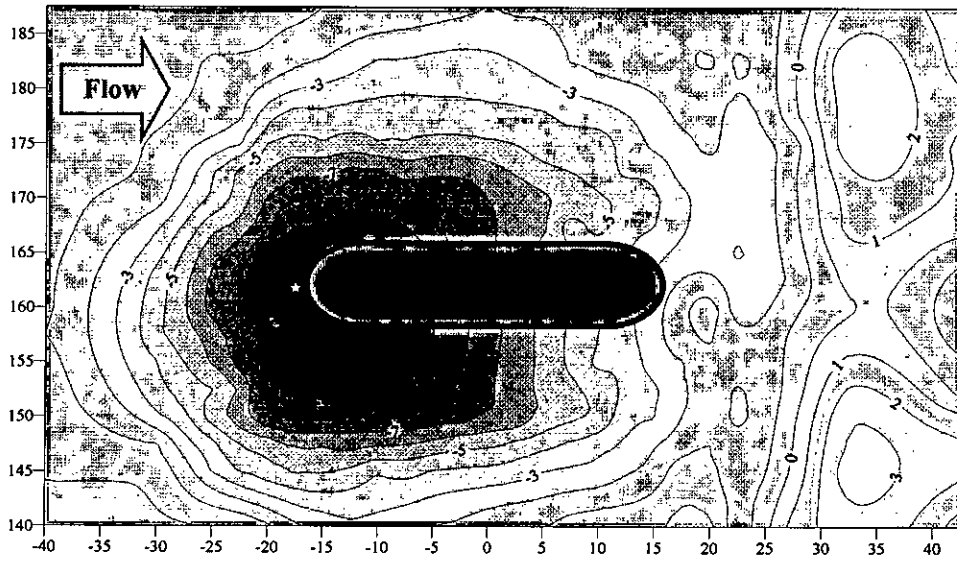
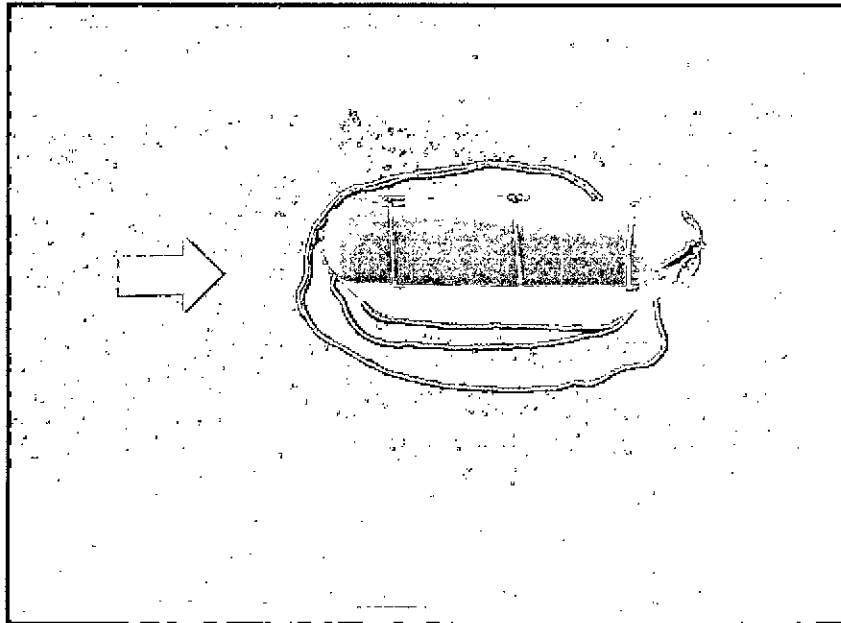
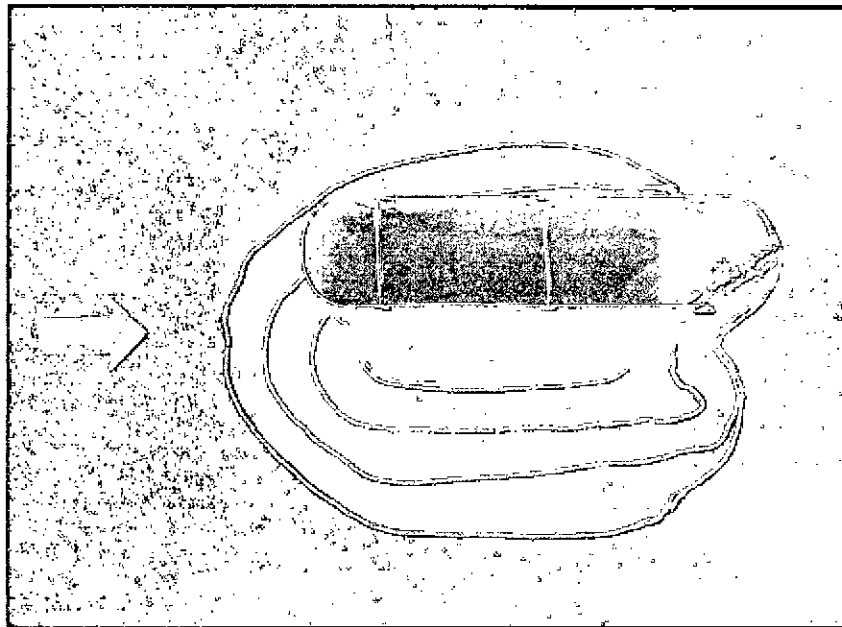


Figure B.20: Run 10-Bed material 1 ( $d_{50} = 0.75$  mm)-Round nose pier ( $l/b=4$ )- $Q=200$  l/s  
 ☆ Max.scour location  
 Main channel





Photograph B.19: Run 10-Bed material 1 ( $d_{50} = 0.75$  mm)-Round nose pier ( $l/b=4$ )- $Q=200$  l/s  
Floodplain



Photograph B.20: Run 10-Bed material 1 ( $d_{50} = 0.75$  mm)-Round nose pier ( $l/b=4$ )- $Q=200$  l/s  
Main channel

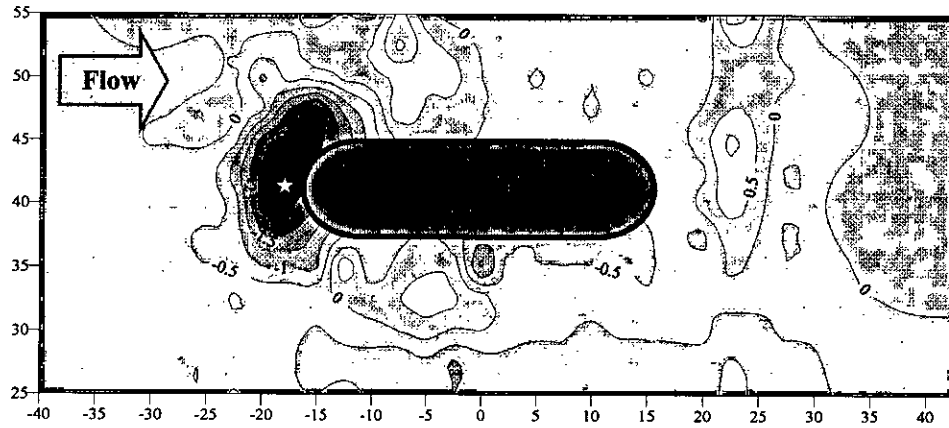


Figure B.21: Run 11-Bed material 1( $d_{50} = 0.75$  mm)-Round nose pier ( $l/b=4$ )- $Q=175$  l/s  
 ☆ Max.scour location  
 Floodplain

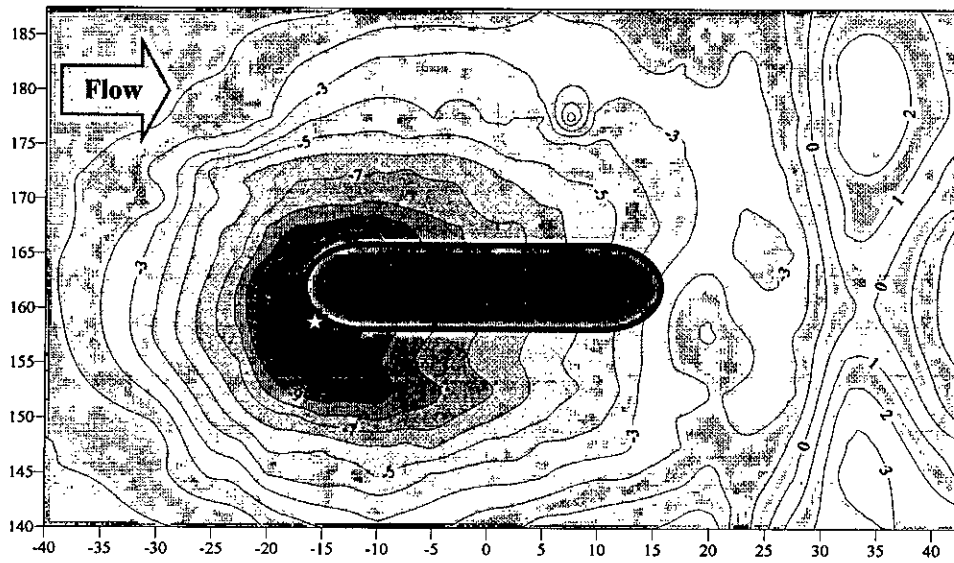
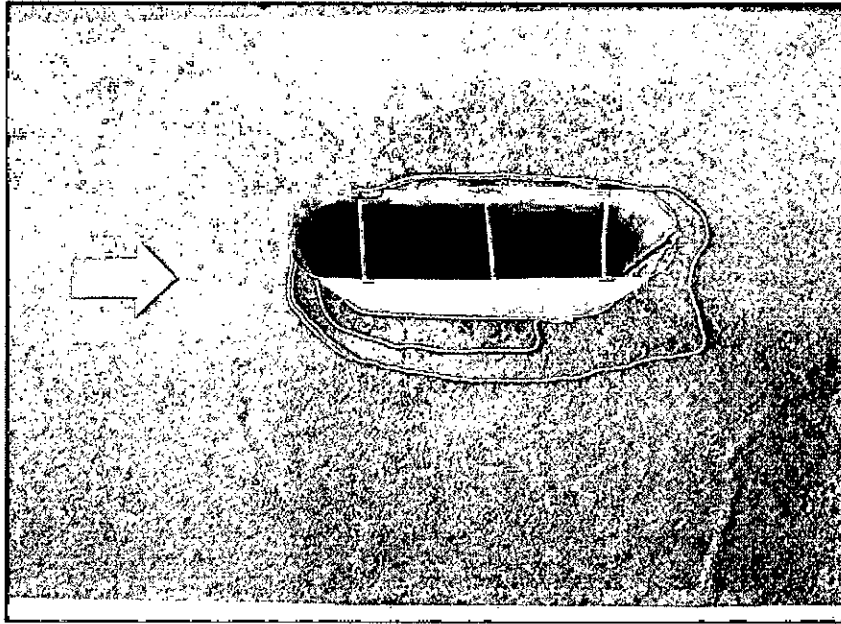
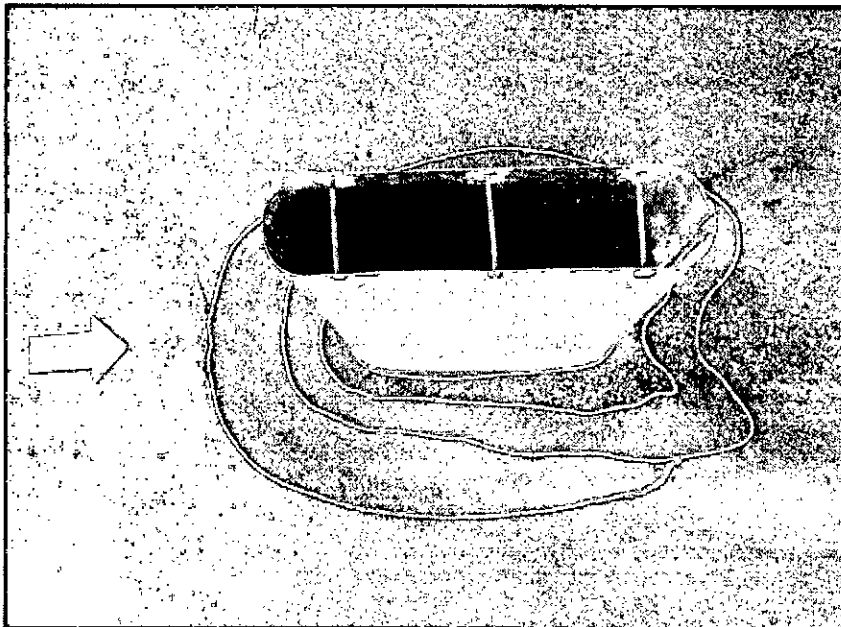


Figure B.22: Run 11-Bed material 1( $d_{50} = 0.75$  mm)-Round nose pier ( $l/b=4$ )- $Q=175$  l/s  
 ☆ Max.scour location  
 Main channel



Photograph B.21: Run 11-Bed material 1 ( $d_{50} = 0.75$  mm)-Round nose pier ( $l/b=4$ )- $Q=175$  l/s  
Floodplain



Photograph B.22: Run 11-Bed material 1 ( $d_{50} = 0.75$  mm)-Round nose pier ( $l/b=4$ )- $Q=175$  l/s  
Main channel

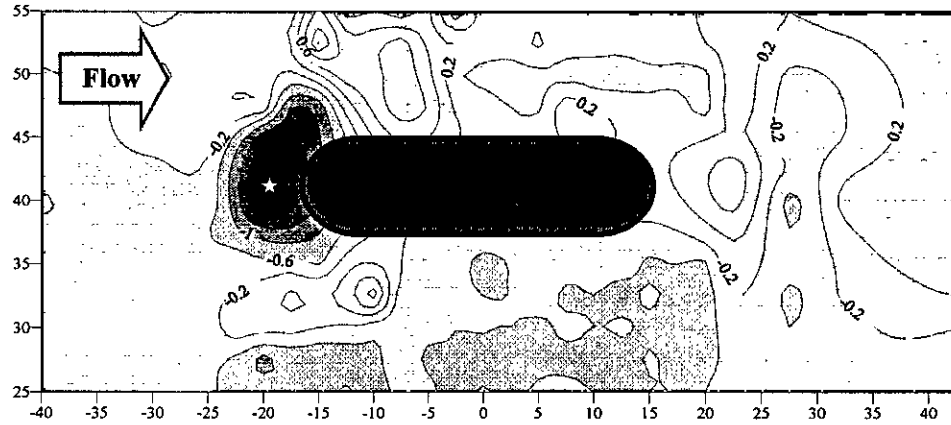


Figure B.23: Run 12-Bed material 1( $d_{50} = 0.75$  mm)-Round nose pier ( $l/b=4$ )- $Q=150$  l/s  
 ☆ Max.scour location  
 Floodplain

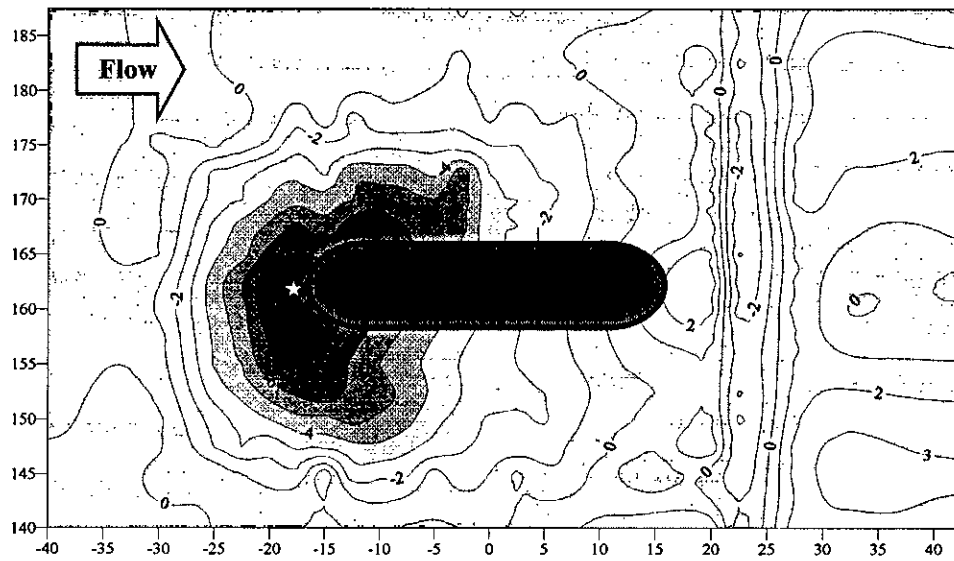
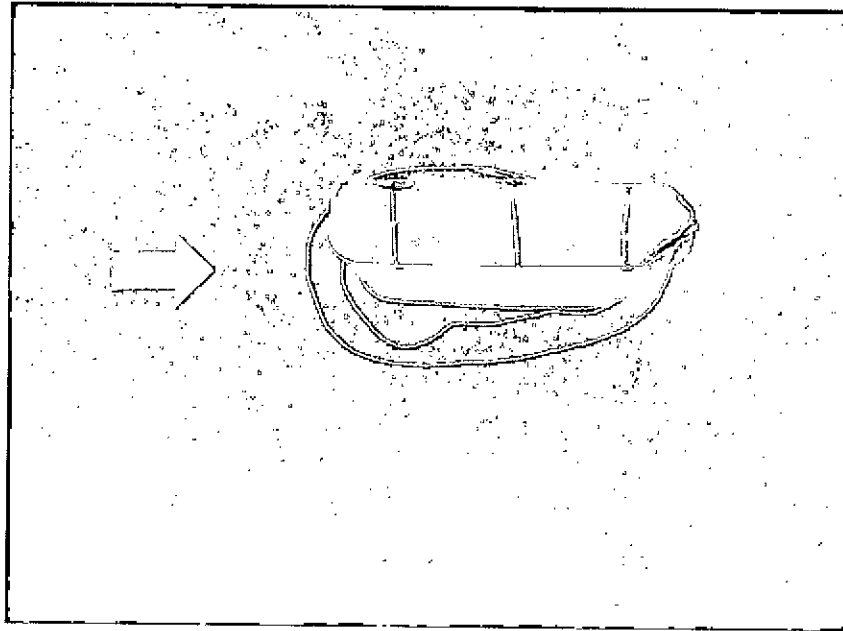
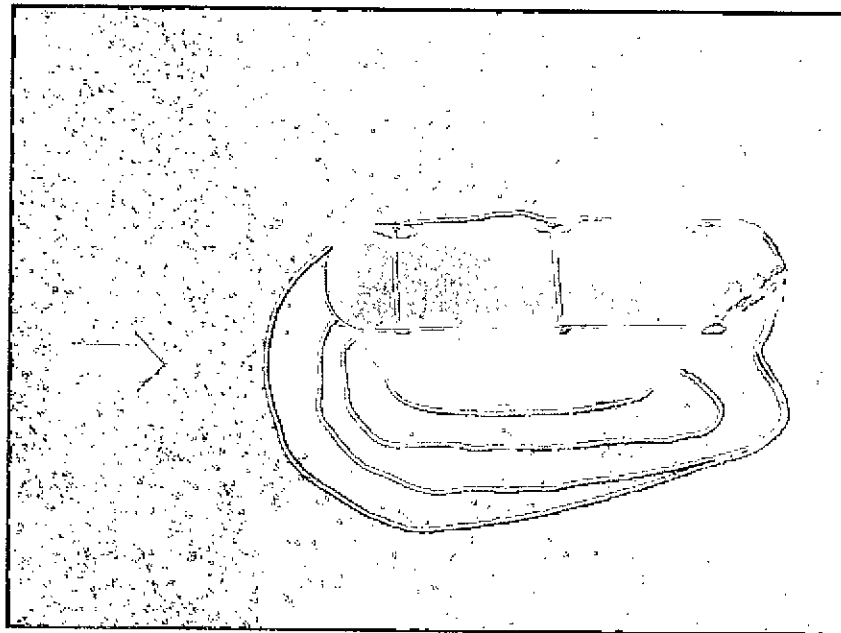


Figure B.24: Run 12-Bed material 1( $d_{50} = 0.75$  mm)-Round nose pier ( $l/b=4$ )- $Q=150$  l/s  
 ☆ Max.scour location  
 Main channel



Photograph B.23: Run 12-Bed material 1 ( $d_{50} = 0.75$  mm)-Round nose pier ( $l/b=4$ )- $Q=150$  l/s  
Floodplain



Photograph B.24: Run 12-Bed material 1 ( $d_{50} = 0.75$  mm)-Round nose pier ( $l/b=4$ )- $Q=150$  l/s  
Main channel

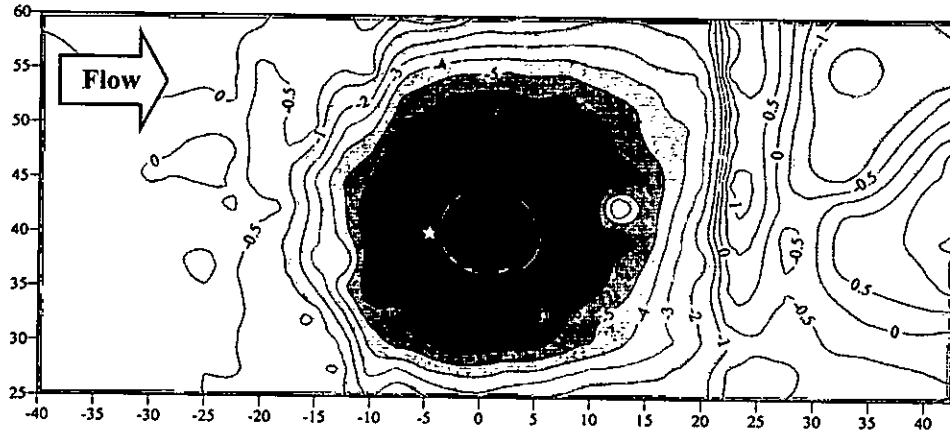


Figure B.25: Run 13-Bed material 2( $d_{50} = 0.18$  mm)-Circular pier ( $l/b=1$ )- $Q=200$  l/s  
 ☆ Max.scour location  
 Floodplain

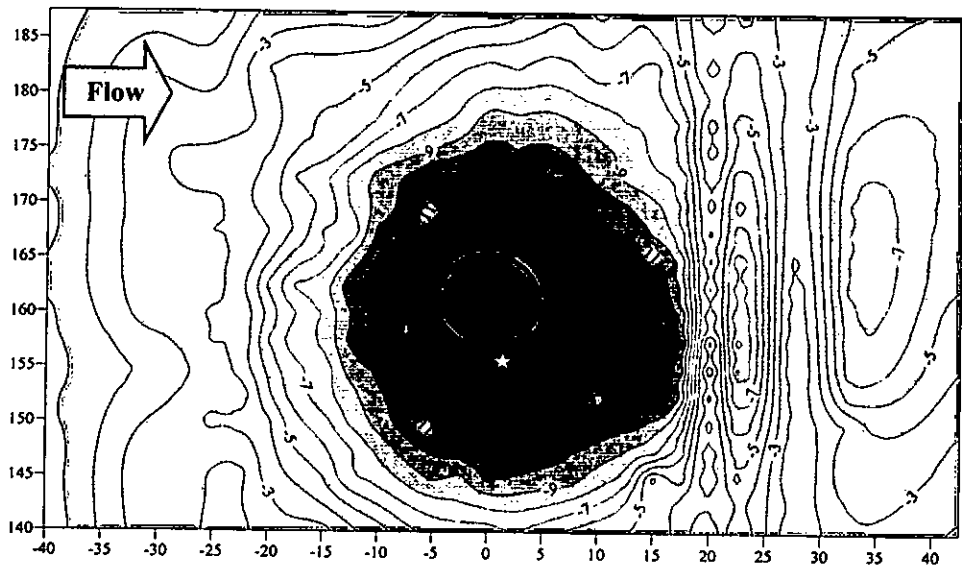
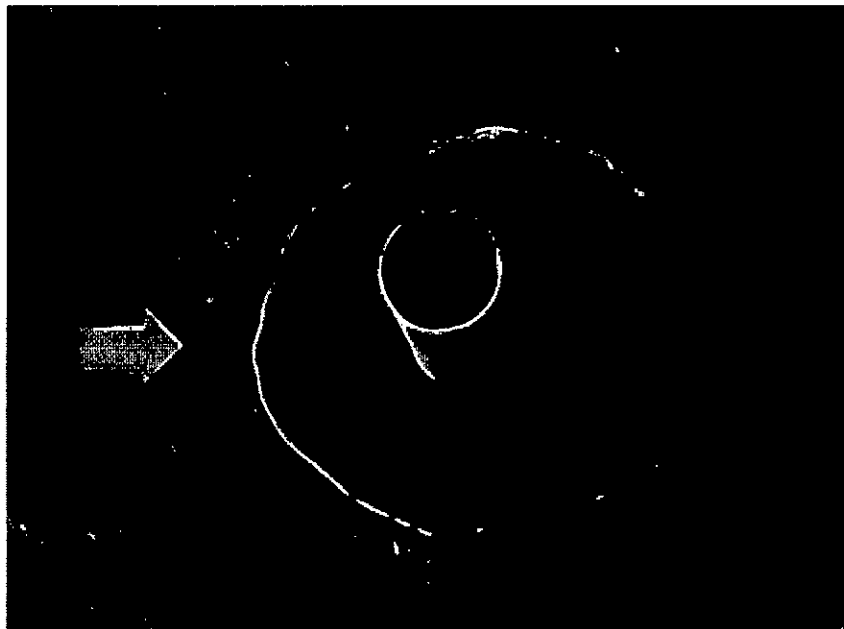


Figure B.26: Run 13-Bed material 2( $d_{50} = 0.18$  mm)-Circular pier ( $l/b=1$ )- $Q=200$  l/s  
 ☆ Max.scour location  
 Main channel



Photograph B.25: Run 13-Bed material 2 ( $d_{50} = 0.18$  mm)-Circular pier ( $l/b=1$ )- $Q=200$  l/s  
Floodplain



Photograph B.26: Run 13-Bed material 2 ( $d_{50} = 0.18$  mm)-Circular pier ( $l/b=1$ )- $Q=200$  l/s  
Main channel

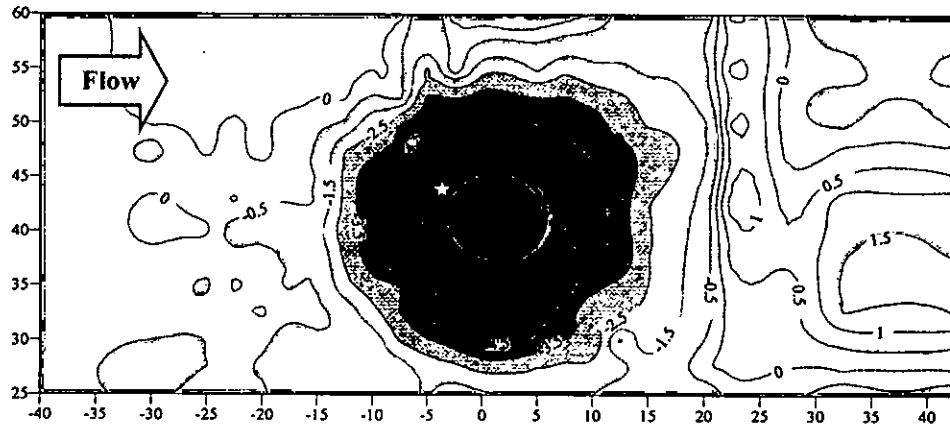


Figure B.27: Run 14-Bed material 2( $d_{50} = 0.18$  mm)-Circular pier ( $l/b=1$ )- $Q=175$  l/s  
 ☆ Max.scour location  
 Floodplain

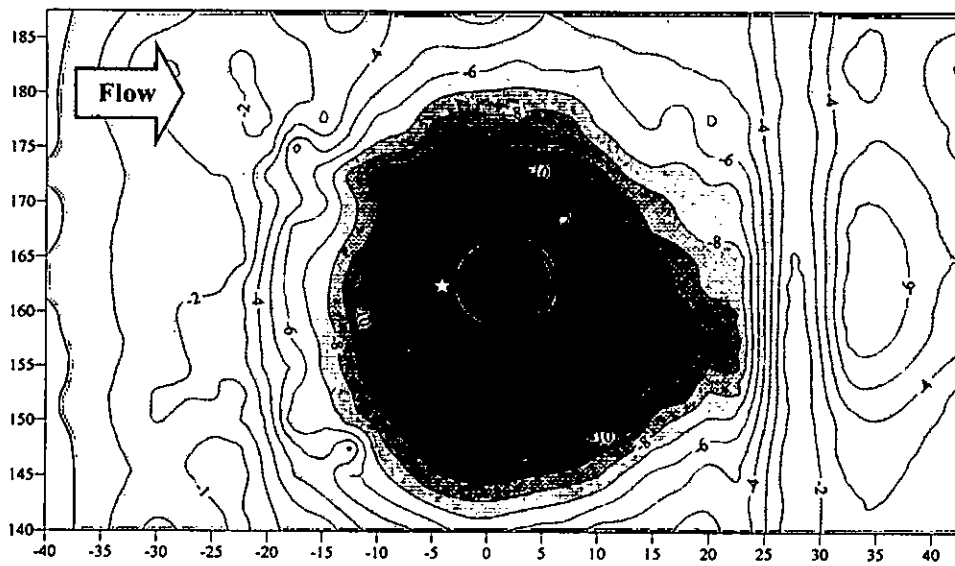
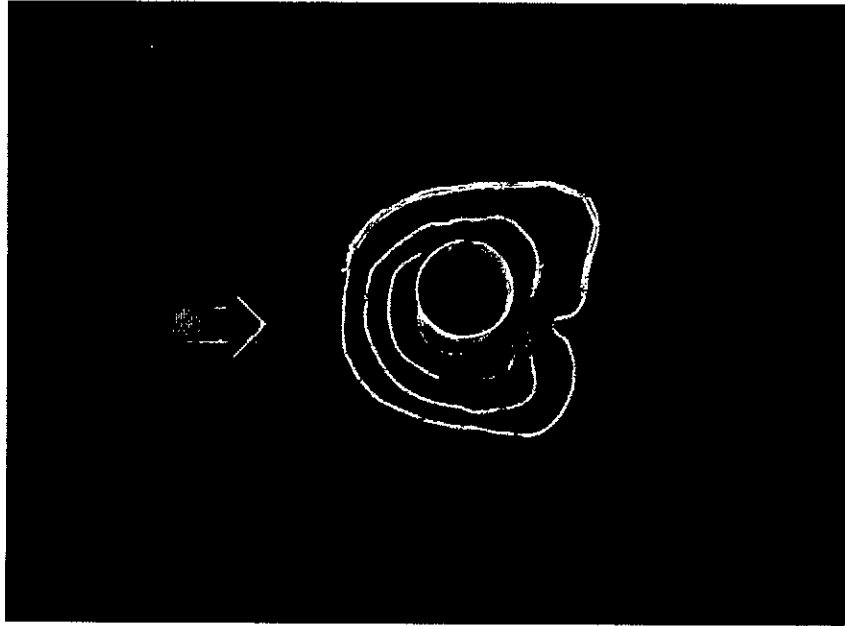
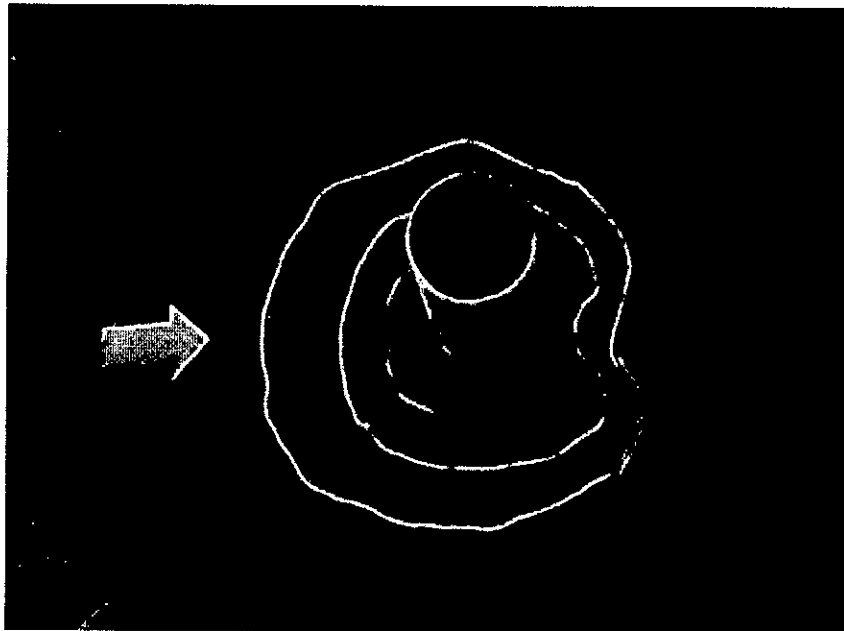


Figure B.28: Run 14-Bed material 2( $d_{50} = 0.18$  mm)-Circular pier ( $l/b=1$ )- $Q=175$  l/s  
 ☆ Max.scour location  
 Main channel





Photograph B.27: Run 14-Bed material 2( $d_{50} = 0.18$  mm)-Circular pier ( $l/b=1$ )- $Q=175$  l/s  
Floodplain



Photograph B.28: Run 14-Bed material 2( $d_{50} = 0.18$  mm)-Circular pier ( $l/b=1$ )- $Q=175$  l/s  
Main channel

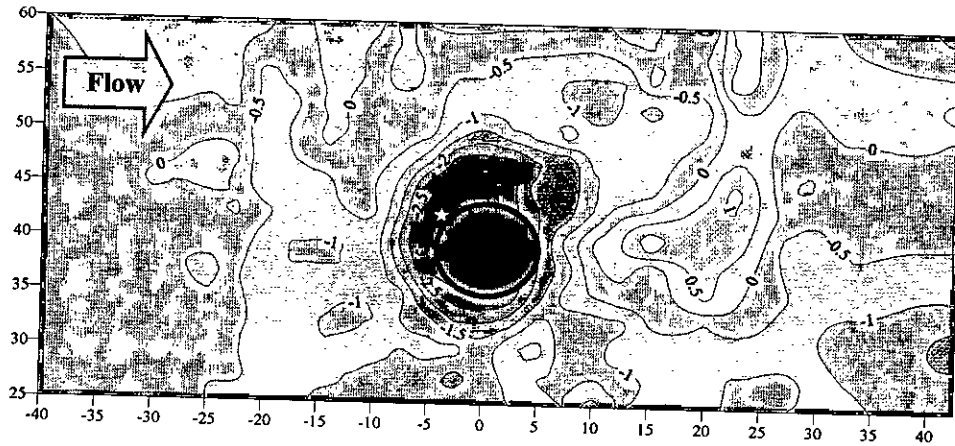


Figure B.29: Run 15-Bed material 2( $d_{50} = 0.18$  mm)-Circular pier ( $l/b=1$ )- $Q=175$  l/s  
 ☆ Max.scour location  
 Floodplain

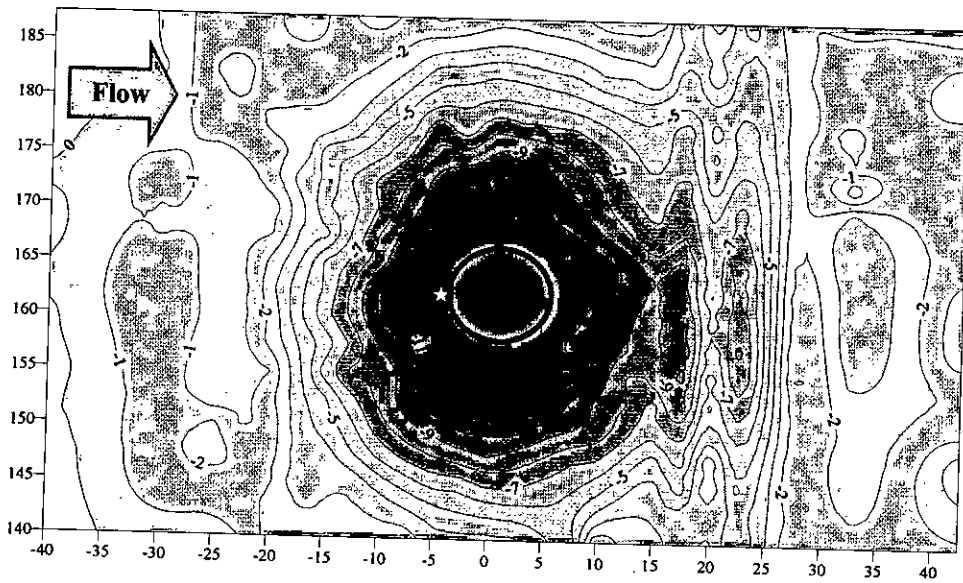
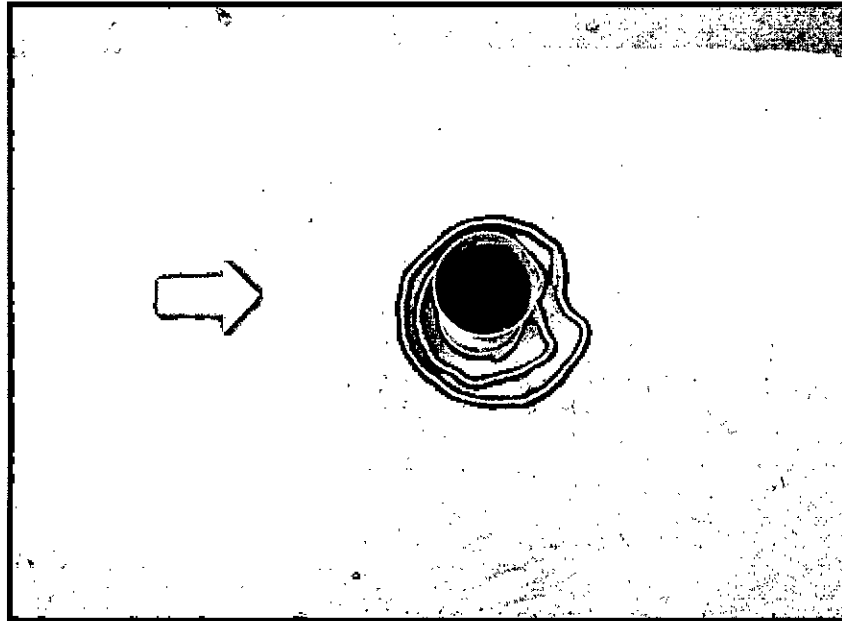
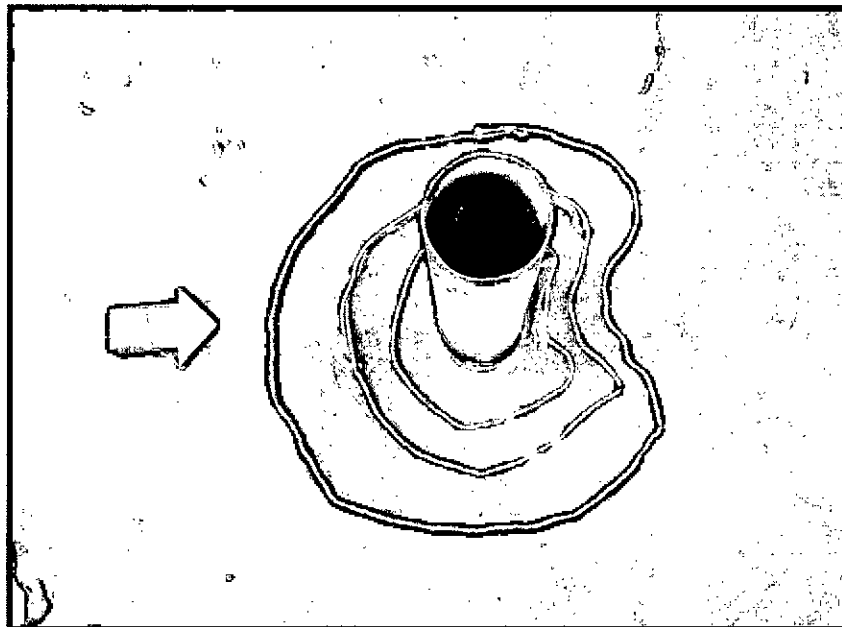


Figure B.30: Run 15-Bed material 2( $d_{50} = 0.18$  mm)-Circular pier ( $l/b=1$ )- $Q=150$  l/s  
 ☆ Max.scour location  
 Main channel



Photograph B.29: Run 15-Bed material 2( $d_{50} = 0.18$  mm)-Circular pier ( $l/b=1$ )- $Q=150$  l/s  
Floodplain



Photograph B.30: Run 15-Bed material 2( $d_{50} = 0.18$  mm)-Circular pier ( $l/b=1$ )- $Q=150$  l/s  
Main channel

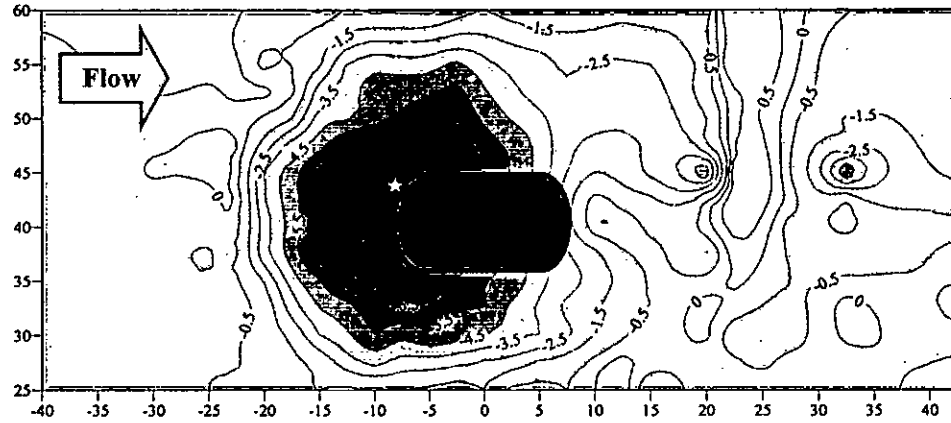


Figure B.31: Run 16-Bed material 2( $d_{50} = 0.18$  mm)-Round nose pier ( $l/b=2$ )- $Q=200$  l/s  
 ☆ Max.scour location  
 Floodplain

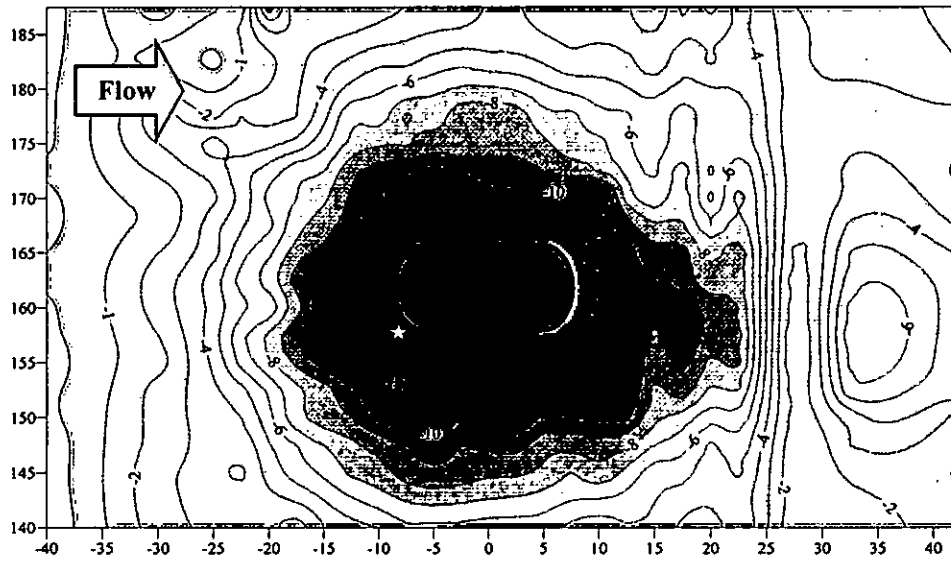
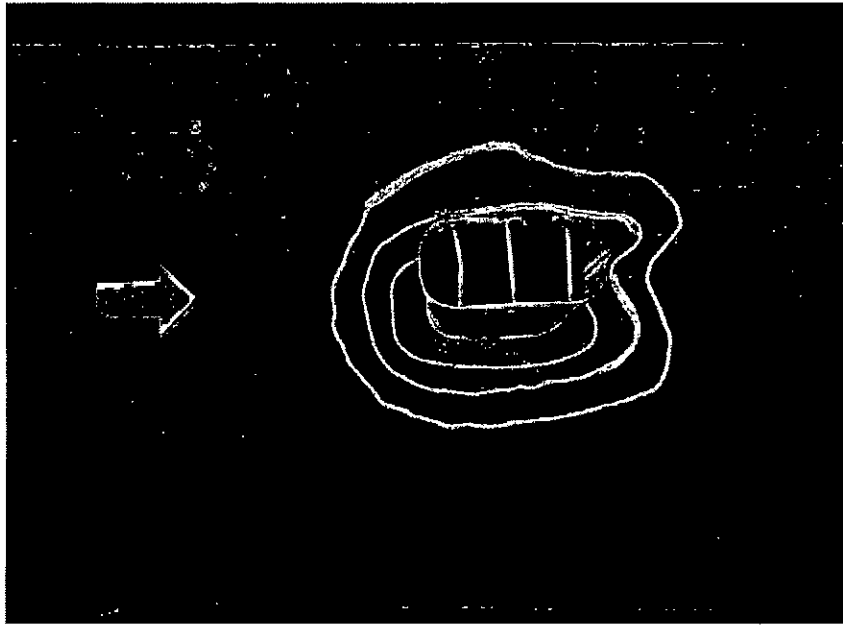
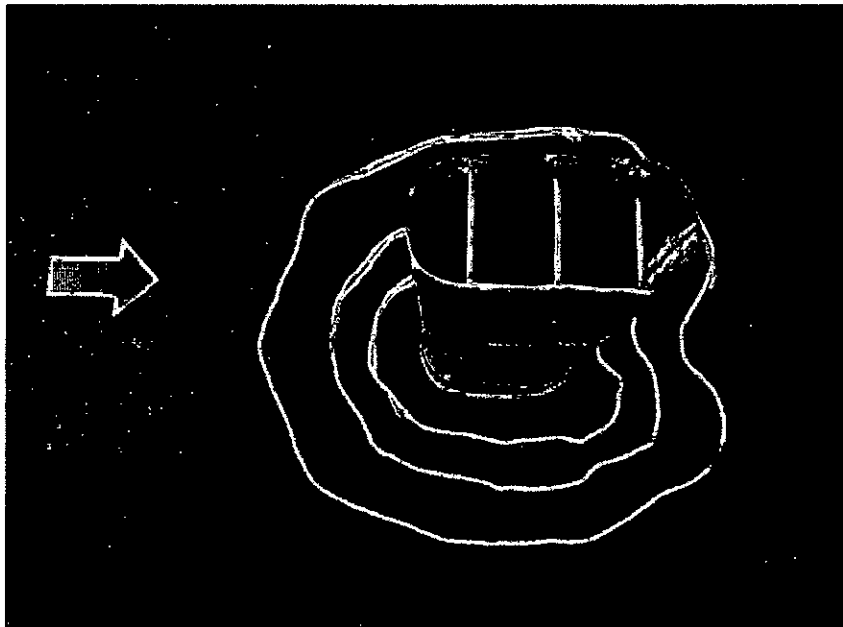


Figure B.32: Run 16-Bed material 2( $d_{50} = 0.18$  mm)-Round nose pier ( $l/b=2$ )- $Q=200$  l/s  
 ☆ Max.scour location  
 Main channel



Photograph B.31: Run 16-Bed material 2( $d_{50} = 0.18$  mm)-Round nose pier ( $l/b=2$ )- $Q=200$  l/s  
Floodplain



Photograph B.32: Run 16-Bed material 2( $d_{50} = 0.18$  mm)-Round nose pier ( $l/b=2$ )- $Q=200$  l/s  
Main channel

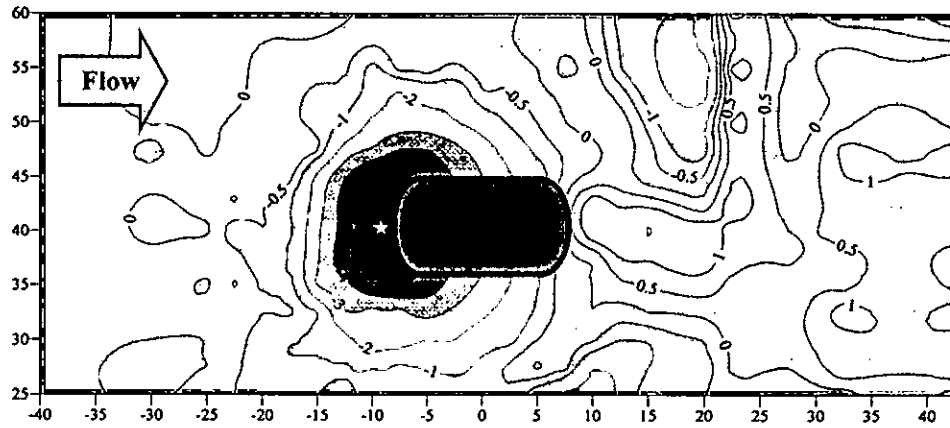


Figure B.33: Run 17-Bed material 2( $d_{50} = 0.18$  mm)-Round nose pier ( $l/b=2$ )- $Q=175$  l/s  
 ☆ Max.scour location  
 Floodplain

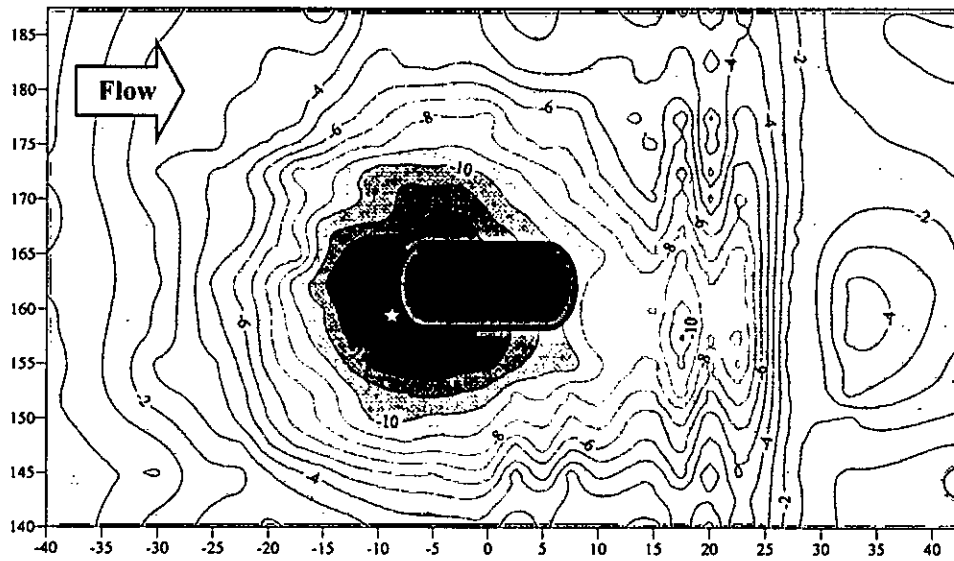
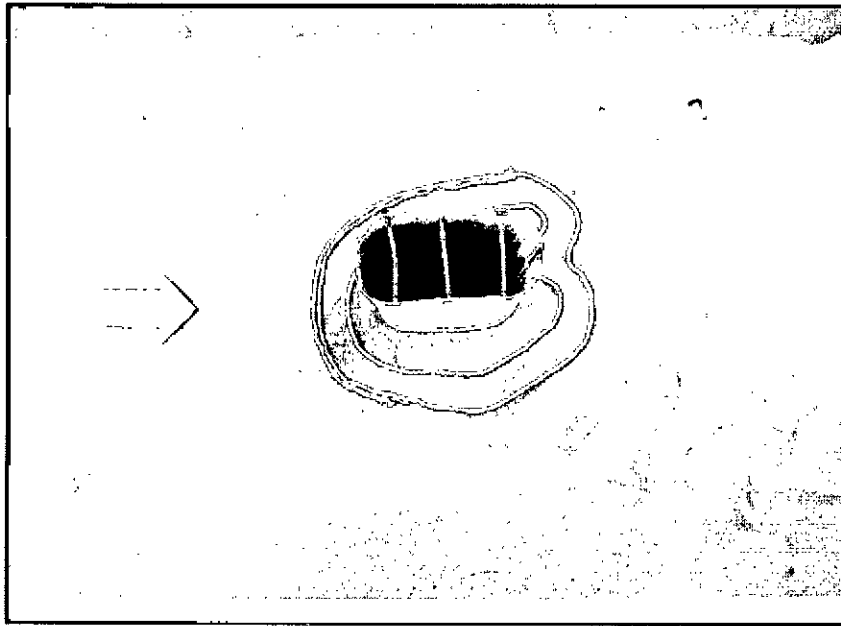
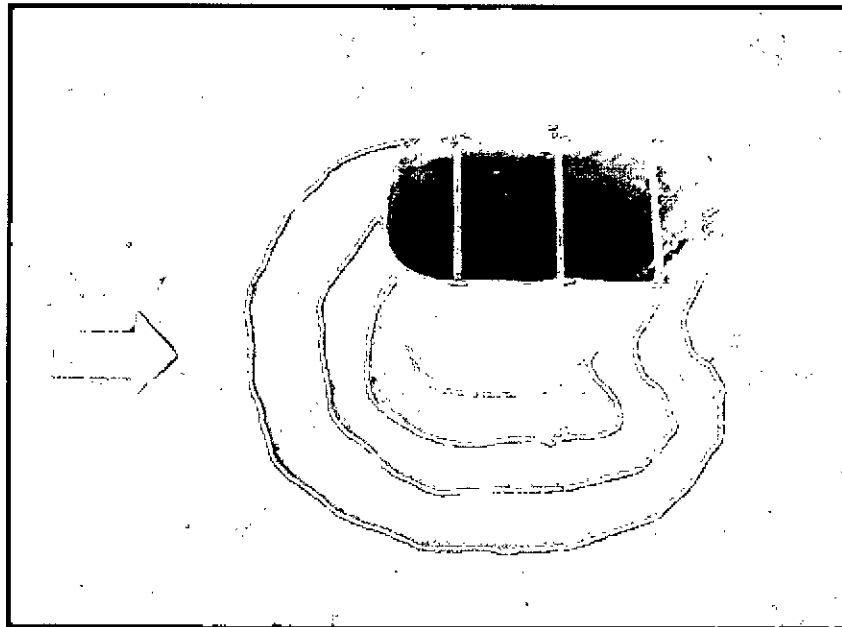


Figure B.34: Run 17-Bed material 2( $d_{50} = 0.18$  mm)-Round nose pier ( $l/b=2$ )- $Q=175$  l/s  
 ☆ Max.scour location  
 Main channel



Photograph B.33: Run 17-Bed material 2( $d_{50} = 0.18$  mm)-Round nose pier ( $l/b=2$ )- $Q=175$  l/s  
Floodplain



Photograph B.34: Run 17-Bed material 2( $d_{50} = 0.18$  mm)-Round nose pier ( $l/b=2$ )- $Q=175$  l/s  
Main channel

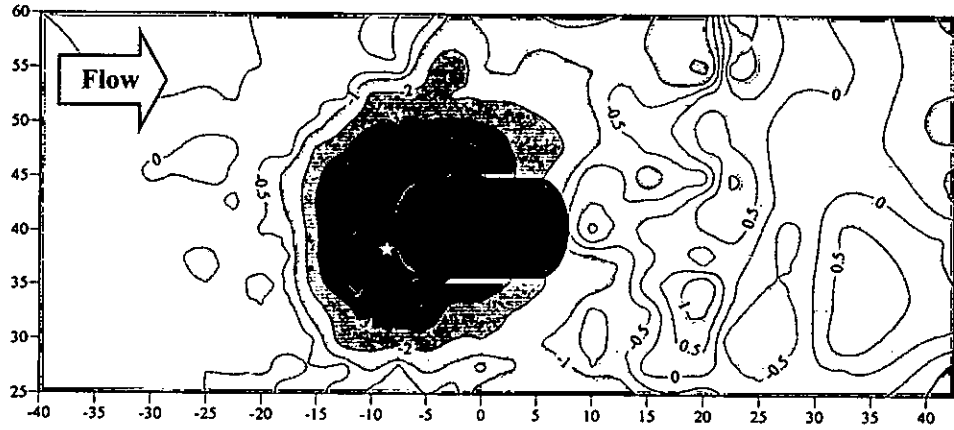


Figure B.35: Run 18-Bed material 2( $d_{50} = 0.18$  mm)-Round nose pier ( $l/b=2$ )- $Q=150$  l/s  
 ☆ Max.scour location  
 Floodplain

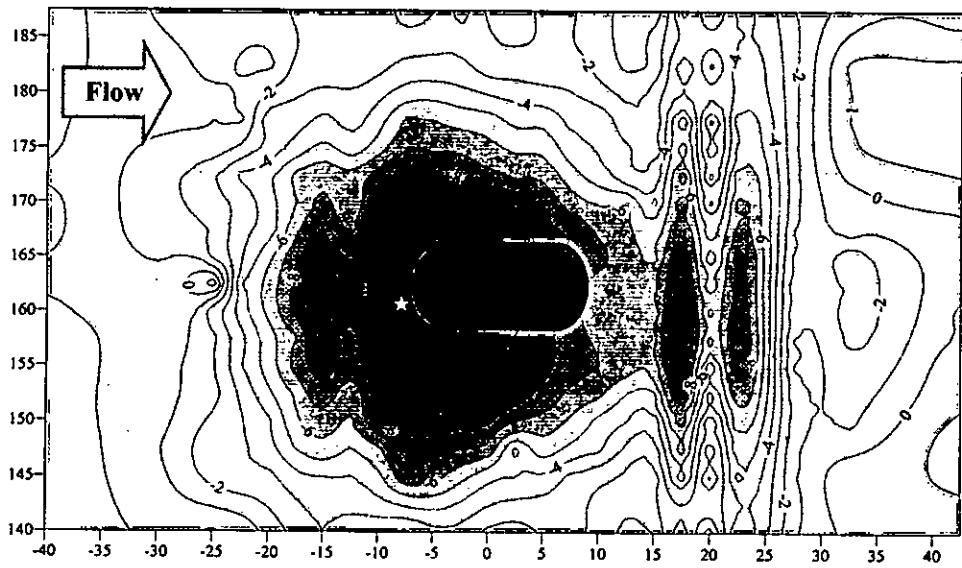
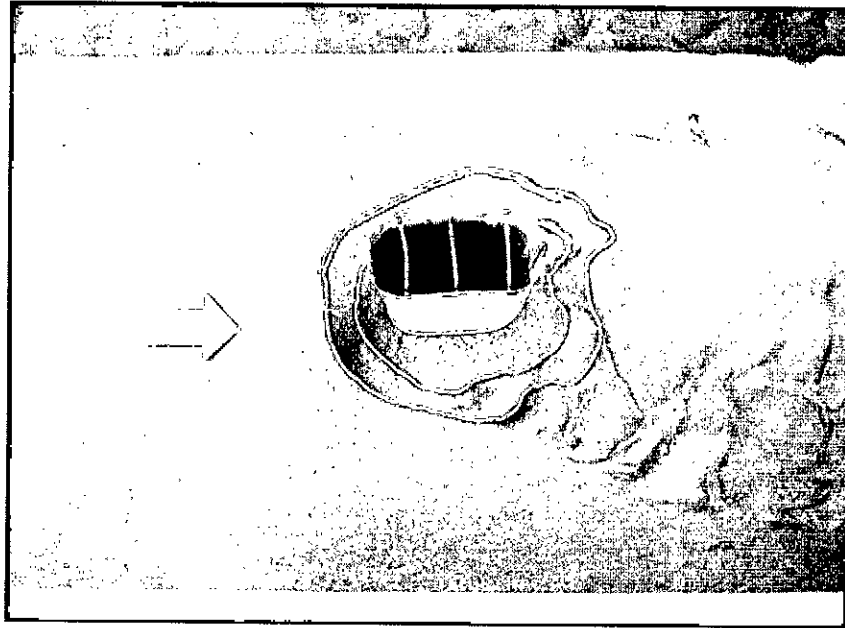
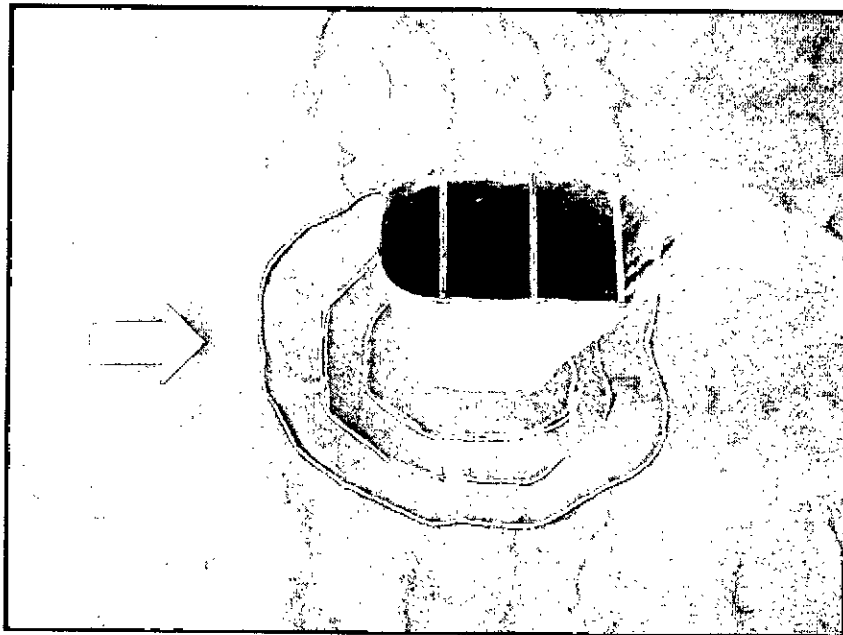


Figure B.36: Run 18-Bed material 2( $d_{50} = 0.18$  mm)-Round nose pier ( $l/b=2$ )- $Q=150$  l/s  
 ☆ Max.scour location  
 Main channel





Photograph B.35: Run 18-Bed material 2( $d_{50} = 0.18$  mm)-Round nose pier ( $l/b=2$ )- $Q=150$  l/s  
Floodplain



Photograph B.36: Run 18-Bed material 2( $d_{50} = 0.18$  mm)-Round nose pier ( $l/b=2$ )- $Q=150$  l/s  
Main channel

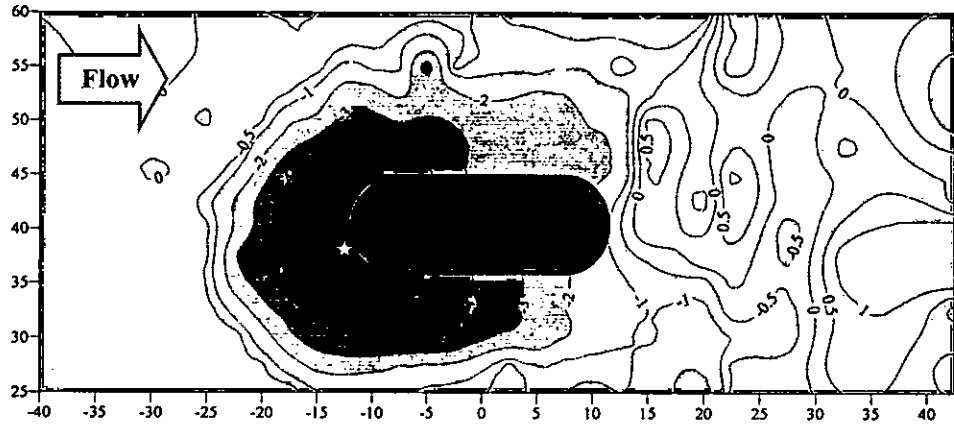


Figure B.37: Run 19-Bed material 2( $d_{50} = 0.18$  mm)-Round nose pier ( $l/b=3$ )- $Q=200$  l/s  
 ☆ Max.scour location  
 Floodplain

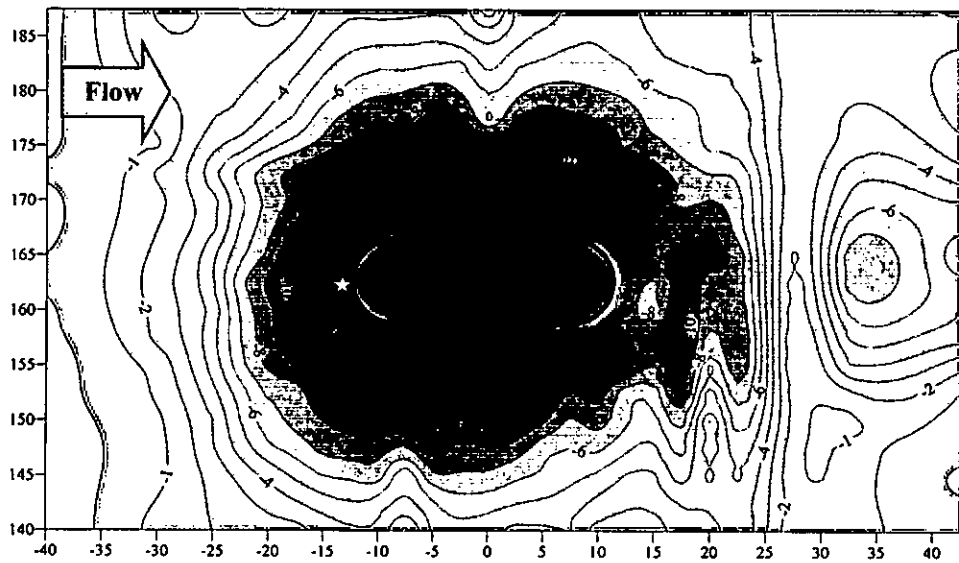
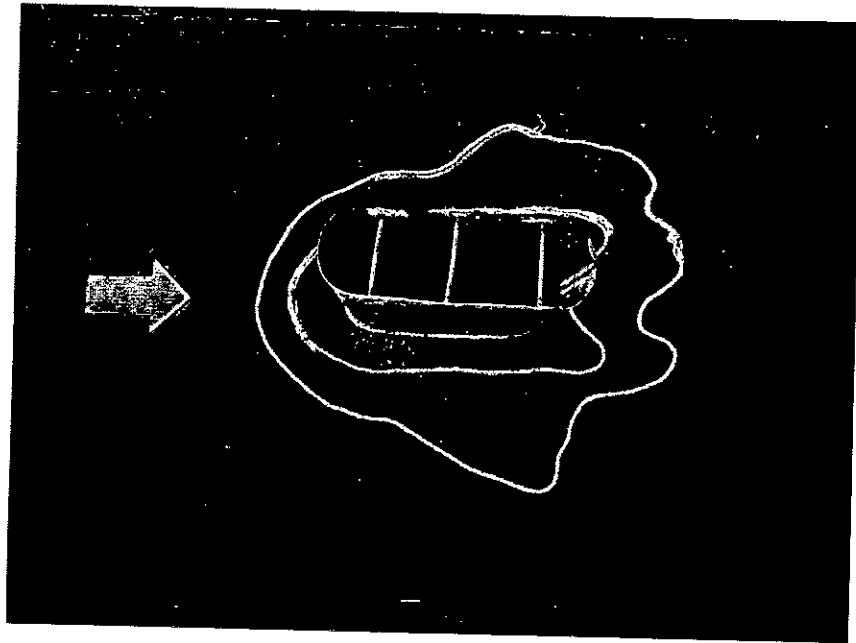
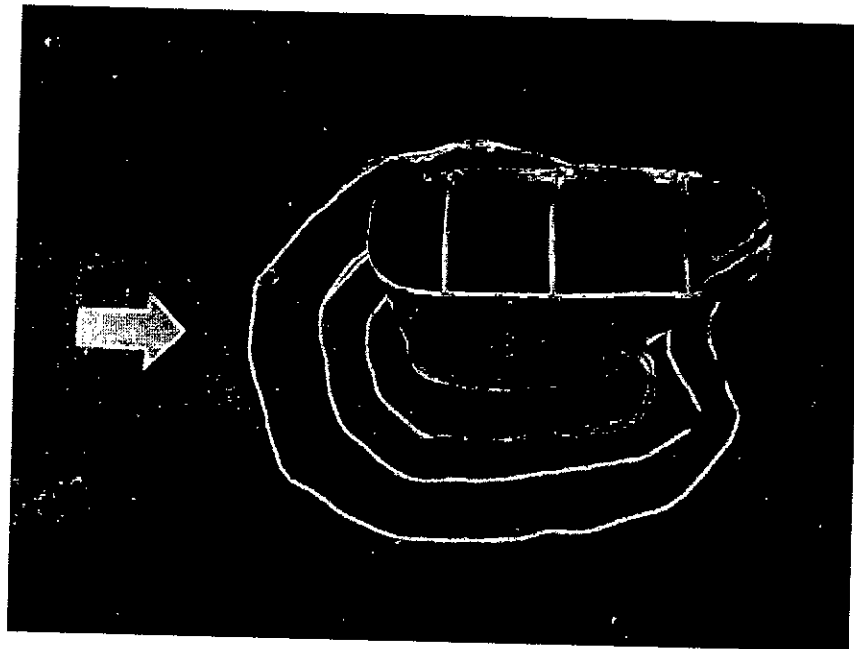


Figure B.38: Run 19-Bed material 2( $d_{50} = 0.18$  mm)-Round nose pier ( $l/b=3$ )- $Q=200$  l/s  
 ☆ Max.scour location  
 Main channel



Photograph B.37: Run 19-Bed material 2( $d_{50} = 0.18$  mm)-Round nose pier ( $l/b=3$ )- $Q=200$  l/s  
Floodplain



Photograph B.38: Run 19-Bed material 2( $d_{50} = 0.18$  mm)-Round nose pier ( $l/b=3$ )- $Q=200$  l/s  
Main channel

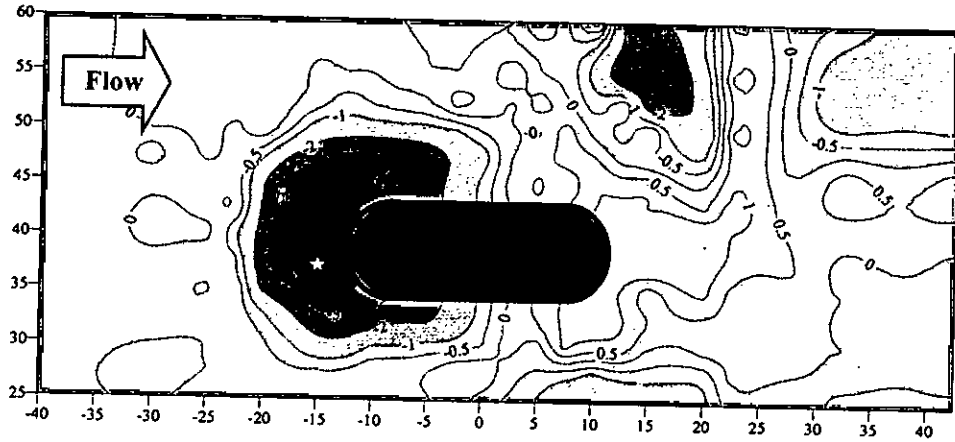


Figure B.39: Run 20-Bed material 2( $d_{50} = 0.18$  mm)-Round nose pier ( $l/b=3$ )- $Q=175$  l/s  
 ☆ Max.scour location  
 Floodplain

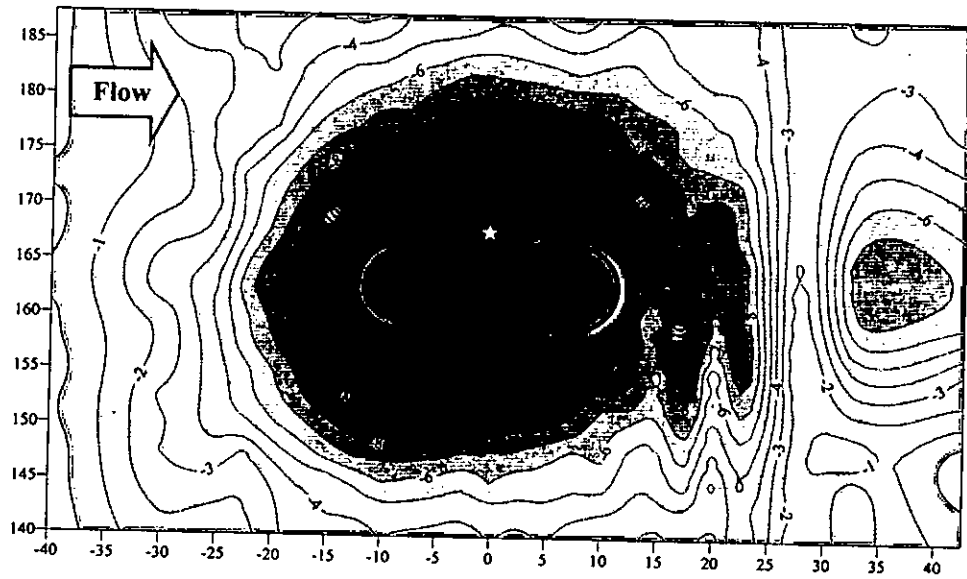
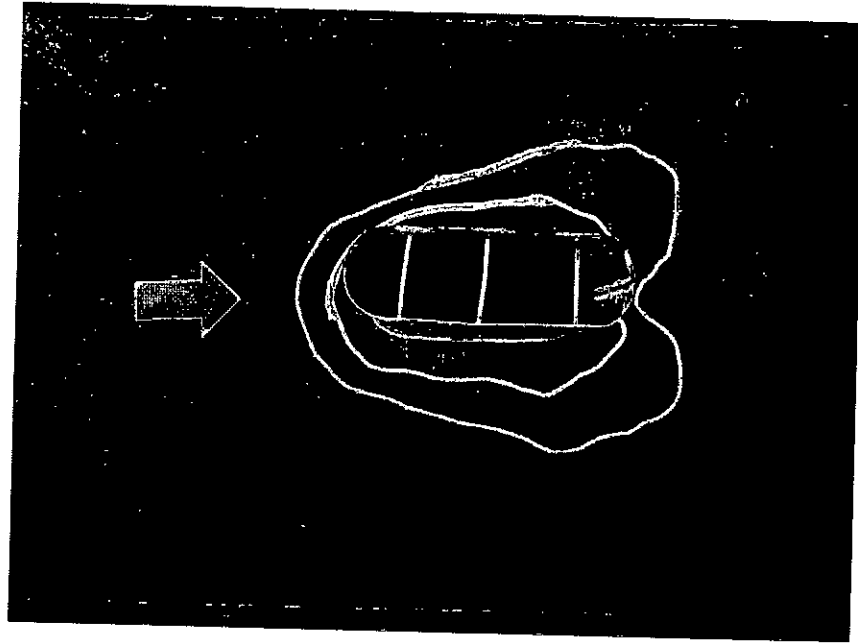
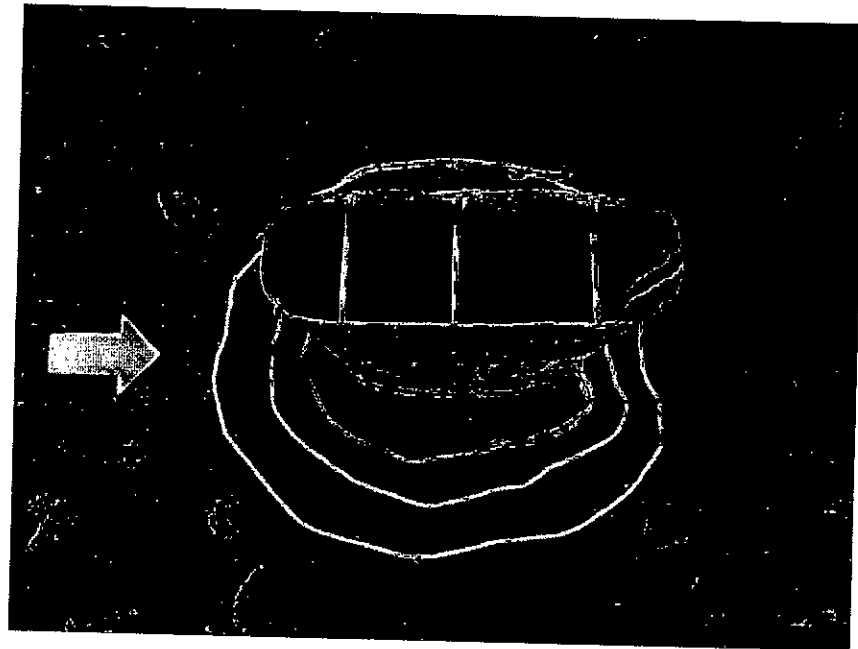


Figure B.40: Run 20-Bed material 2( $d_{50} = 0.18$  mm)-Round nose pier ( $l/b=3$ )- $Q=175$  l/s  
 ☆ Max.scour location  
 Main channel



Photograph B.39: Run 20-Bed material 2( $d_{50} = 0.18$  mm)-Round nose pier ( $l/b=3$ )- $Q=175$  l/s  
Floodplain



Photograph B.40: Run 20-Bed material 2( $d_{50} = 0.18$  mm)-Round nose pier ( $l/b=3$ )- $Q=175$  l/s  
Main channel

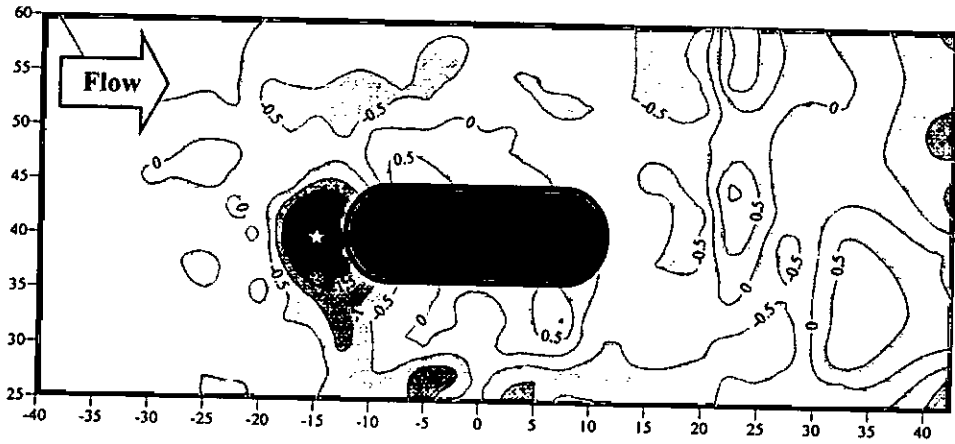


Figure B.41: Run 21-Bed material 2( $d_{50} = 0.18$  mm)-Round nose pier ( $l/b=3$ )- $Q=150$  l/s,  
 ☆ Max.scour location  
 Floodplain

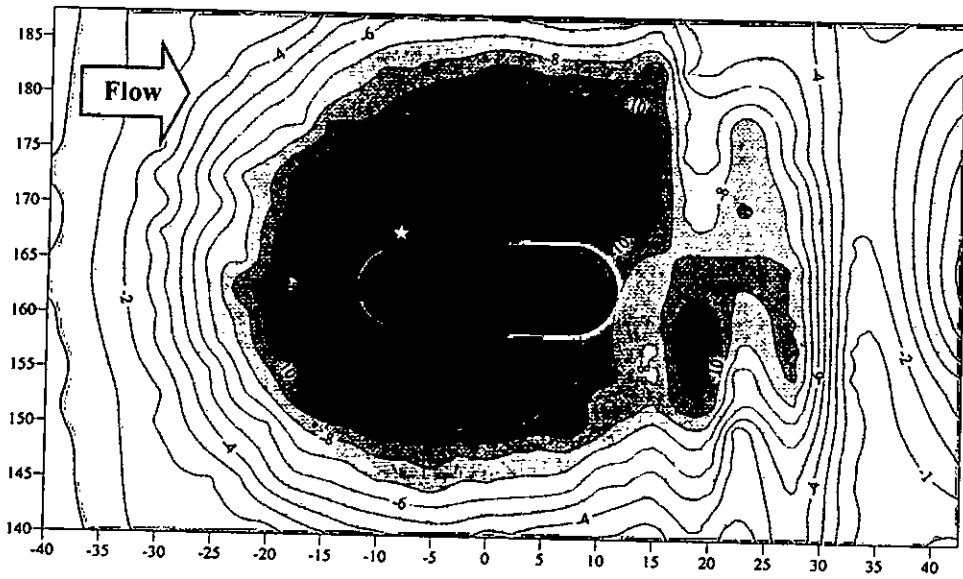
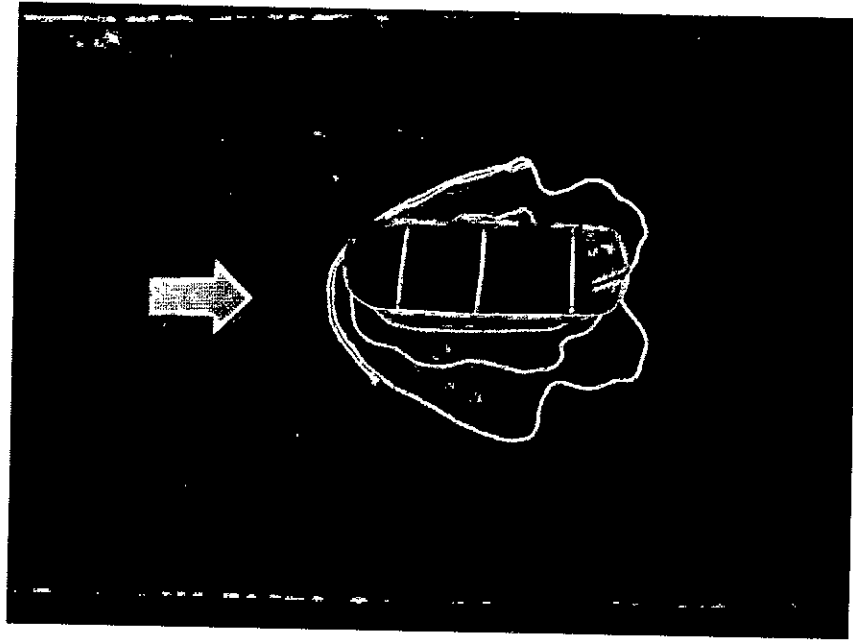
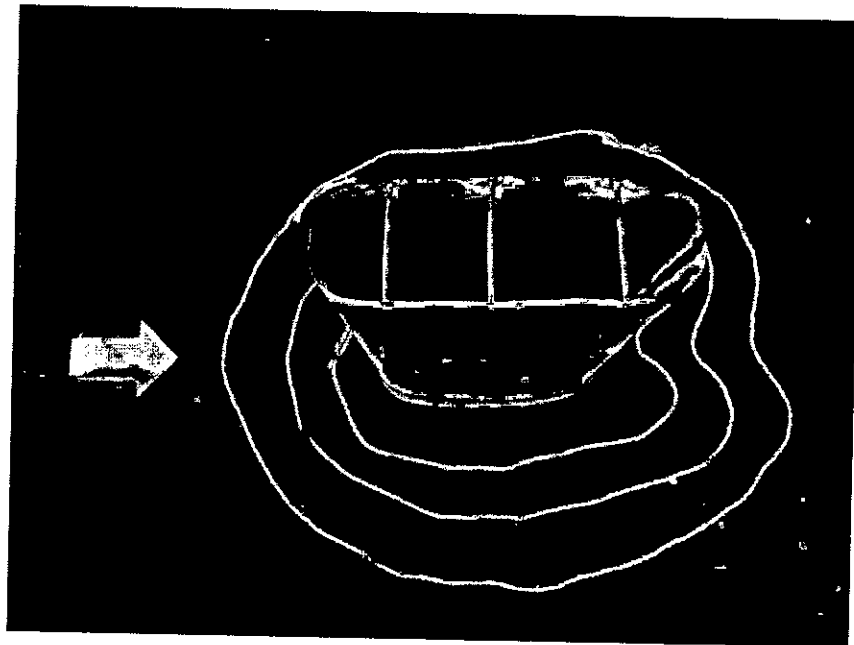


Figure B.42: Run 21-Bed material 2( $d_{50} = 0.18$  mm)-Round nose pier ( $l/b=3$ )- $Q=150$  l/s,  
 ☆ Max.scour location  
 Main channel



Photograph B.41: Run 21-Bed material 2( $d_{50} = 0.18$  mm)-Round nose pier ( $l/b=3$ )- $Q=150$  l/s  
Floodplain



Photograph B.42: Run 21-Bed material 2( $d_{50} = 0.18$  mm)-Round nose pier ( $l/b=3$ )- $Q=150$  l/s  
Main channel

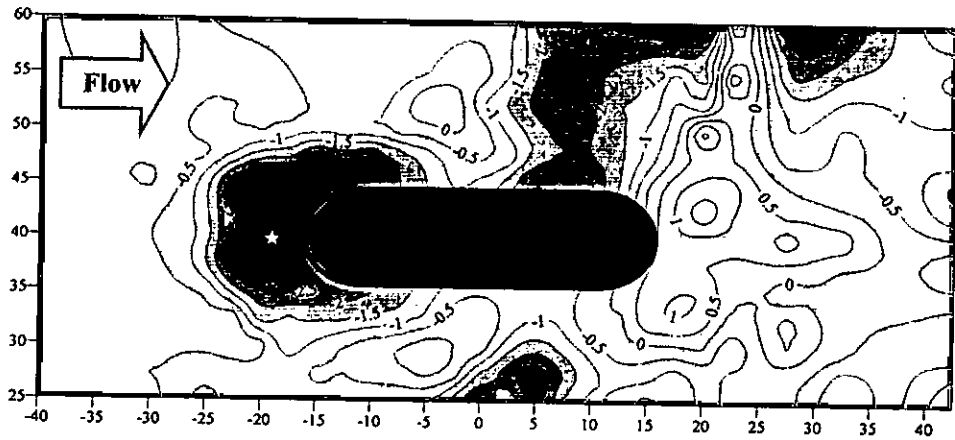


Figure B.43: Run 22-Bed material 2( $d_{50} = 0.18$  mm)-Round nose pier ( $l/b=4$ )- $Q=200$  l/s,  
 ☆ Max.scour location  
 Floodplain

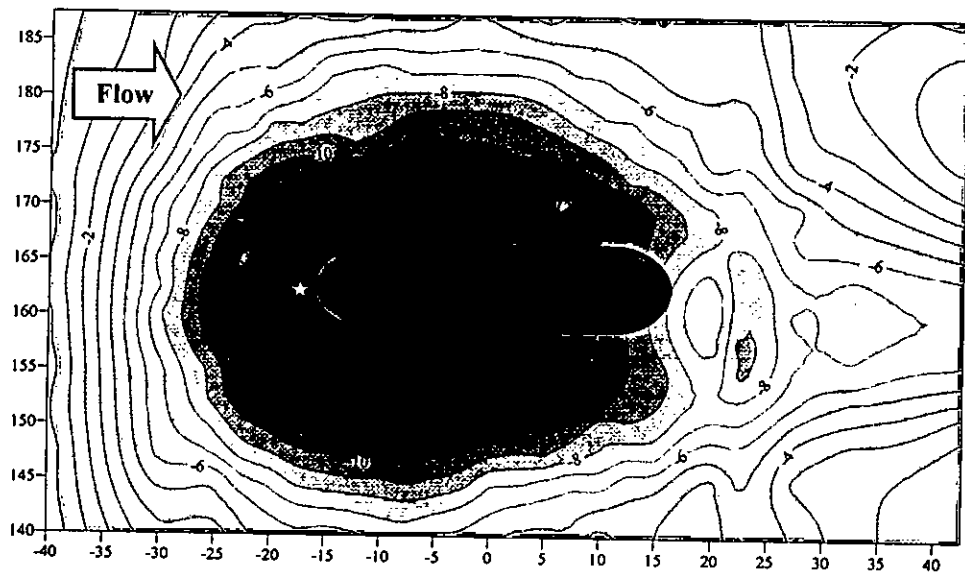
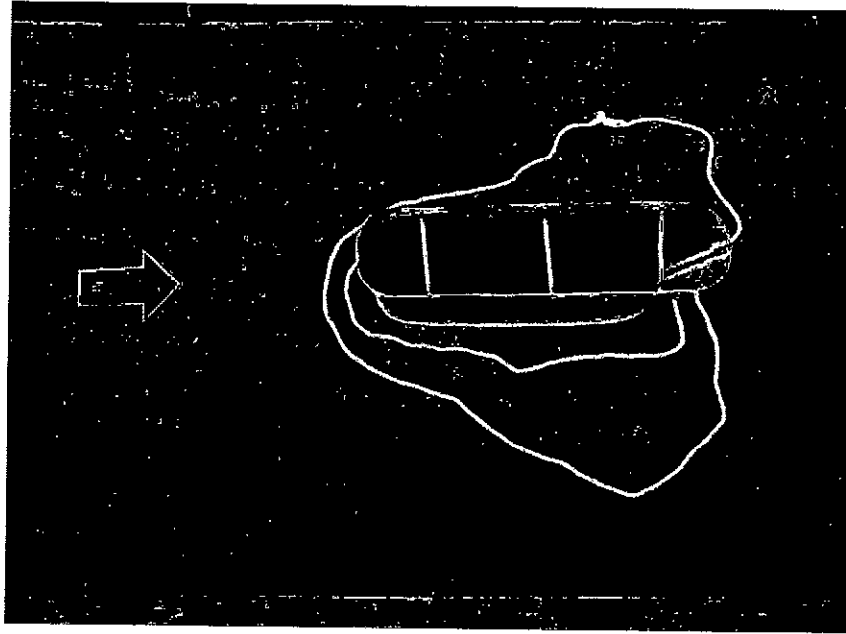
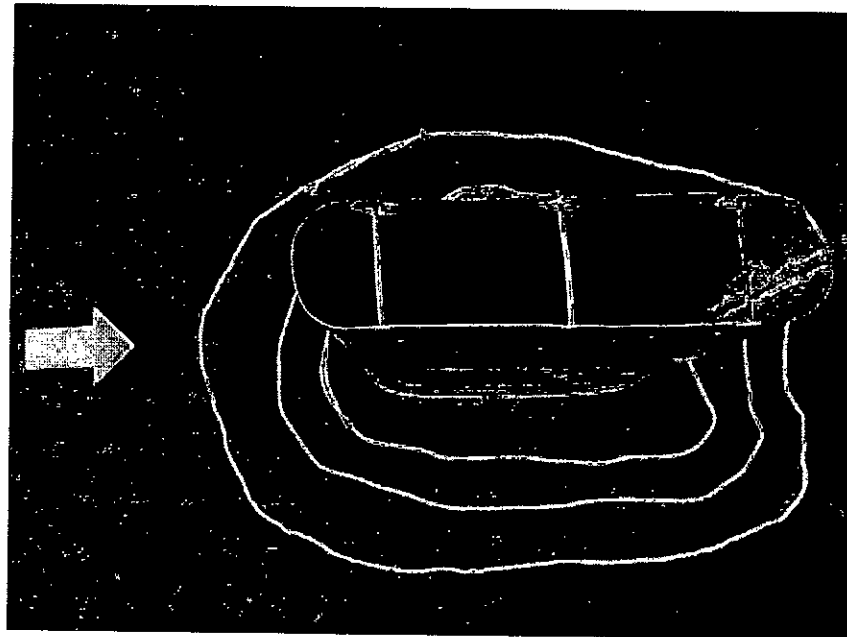


Figure B.44: Run 22-Bed material 2( $d_{50} = 0.18$  mm)-Round nose pier ( $l/b=4$ )- $Q=200$  l/s,  
 ☆ Max.scour location  
 Main channel





Photograph B.43: Run 22-Bed material 2( $d_{50} = 0.18$  mm)-Round nose pier ( $l/b=4$ )- $Q=200$  l/s  
Floodplain



Photograph B.44: Run 22-Bed material 2( $d_{50} = 0.18$  mm)-Round nose pier ( $l/b=4$ )- $Q=200$  l/s  
Main channel

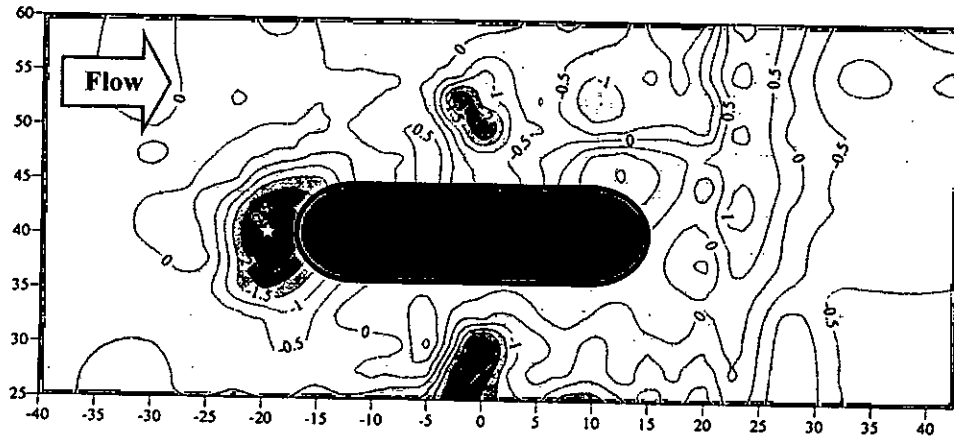


Figure B.45: Run 23-Bed material 2( $d_{50} = 0.18$  mm)-Round nose pier ( $l/b=4$ )- $Q=175$  l/s  
 ☆ Max.scour location  
 Floodplain

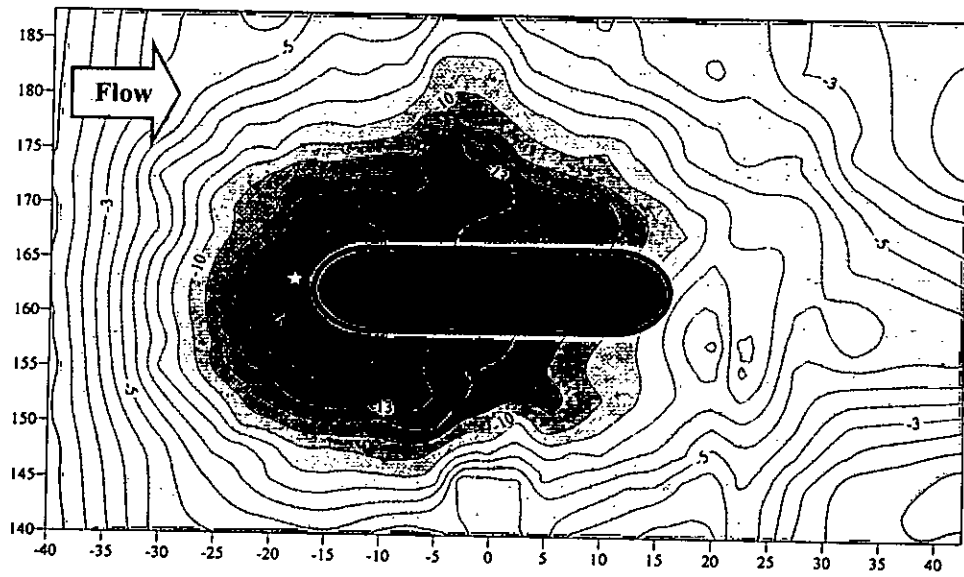
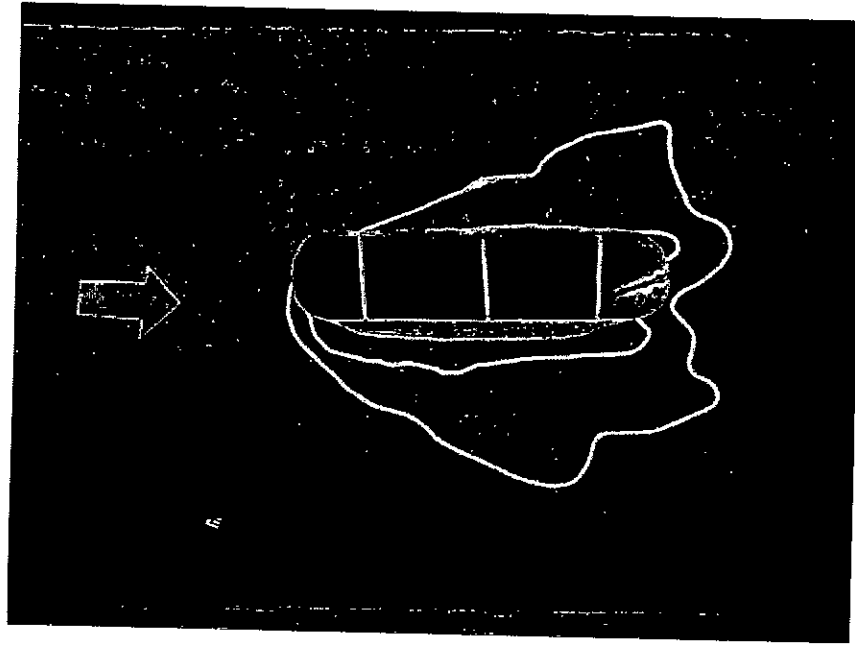
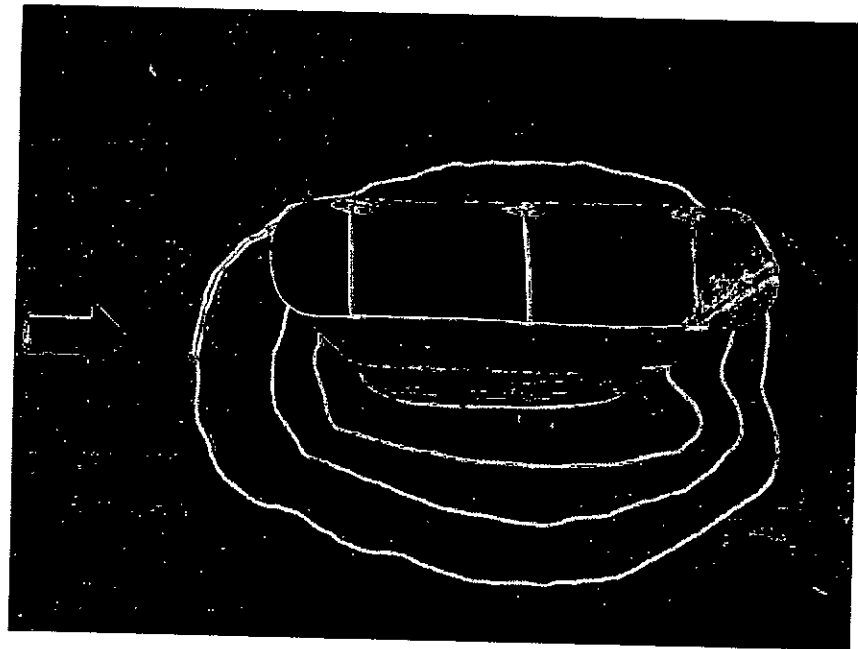


Figure B.46: Run 23-Bed material 2( $d_{50} = 0.18$  mm)-Round nose pier ( $l/b=4$ )- $Q=175$  l/s  
 ☆ Max.scour location  
 Main channel



Photograph B.45: Run 23-Bed material 2( $d_{50} = 0.18$  mm)-Round nose pier ( $l/b=4$ )- $Q=175$  l/s  
Floodplain



Photograph B.46: Run 23-Bed material 2( $d_{50} = 0.18$  mm)-Round nose pier ( $l/b=4$ )- $Q=175$  l/s  
Main channel

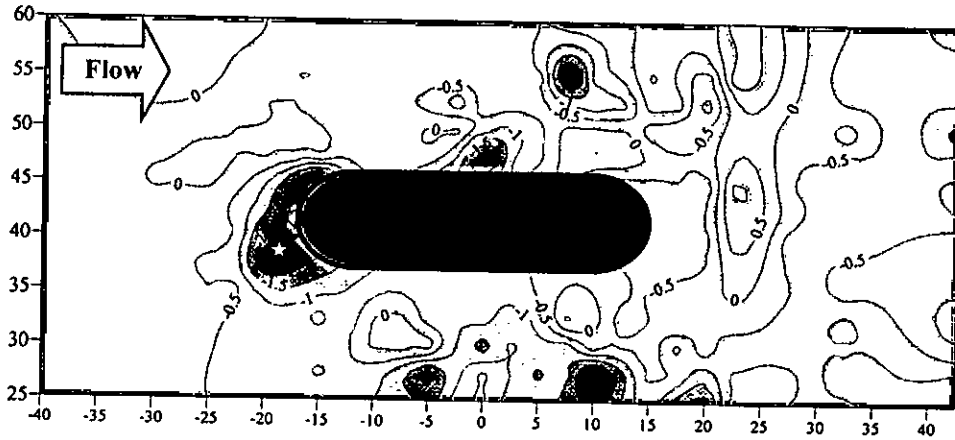


Figure B.47: Run 24-Bed material 2( $d_{50} = 0.18$  mm)-Round nose pier ( $l/b=4$ )- $Q=150$  l/s  
 ☆ Max.scour location  
 Floodplain

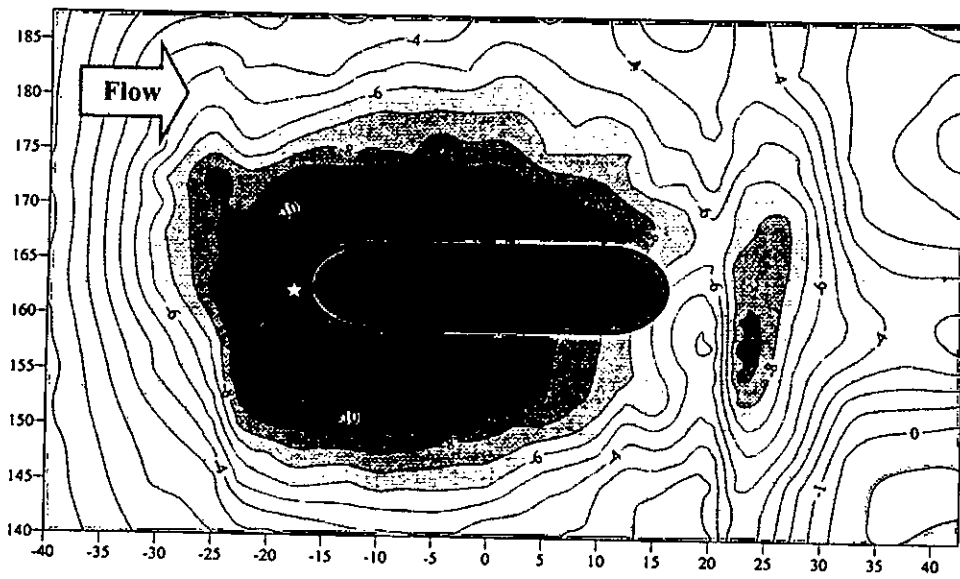
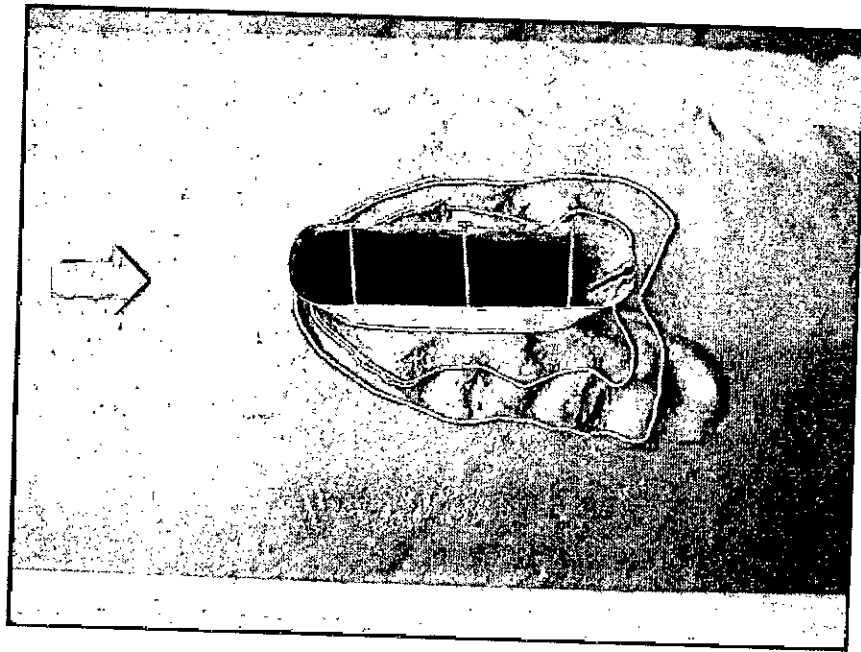
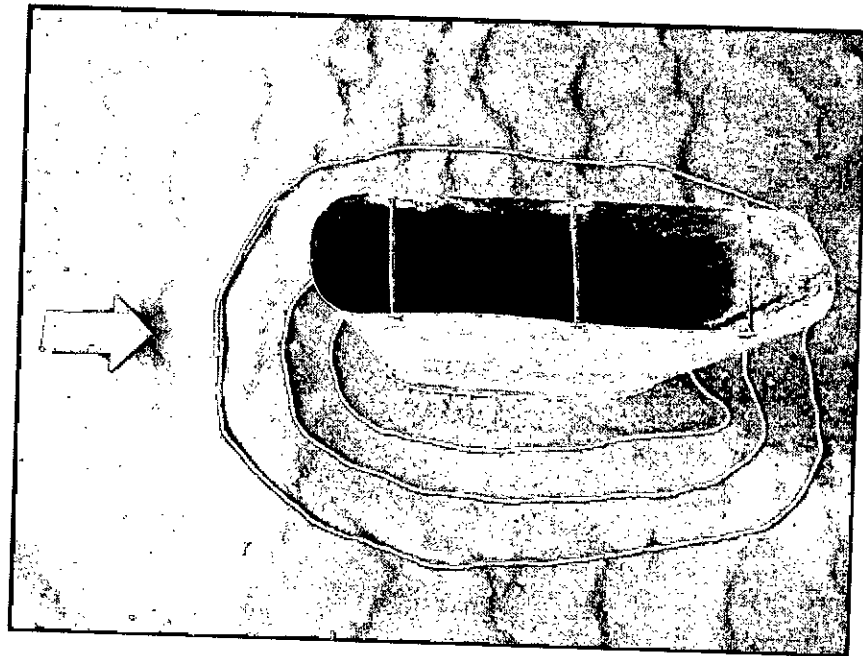


Figure B.48: Run 24-Bed material 2( $d_{50} = 0.18$  mm)-Round nose pier ( $l/b=4$ )- $Q=150$  l/s  
 ☆ Max.scour location  
 Floodplain



Photograph B.47: Run 24-Bed material 2( $d_{50} = 0.18$  mm)-Round nose pier ( $l/b=4$ )- $Q=150$  l/s  
Floodplain



Photograph B.48: Run 24-Bed material 2( $d_{50} = 0.18$  mm)-Round nose pier ( $l/b=4$ )- $Q=150$  l/s  
Main channel

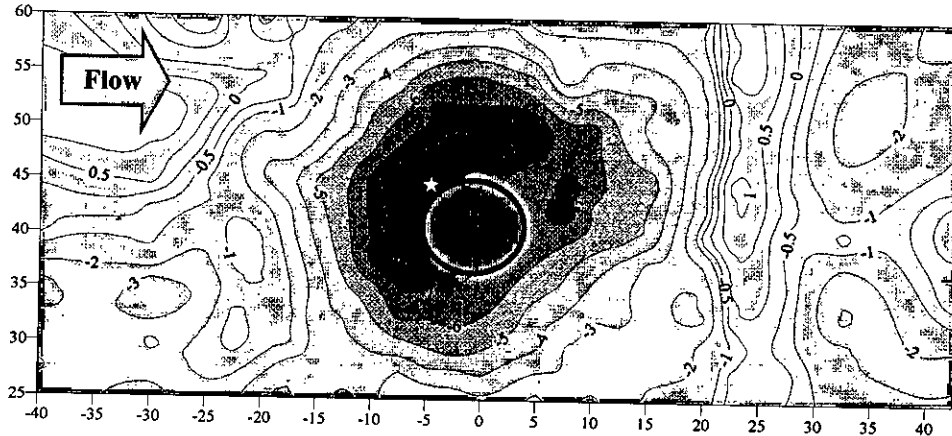


Figure B.49: Run 25-Bed material 3( $d_{50} = 0.12$  mm)-Circular pier ( $l/b=1$ )- $Q=200$  l/s  
 ☆ Max.scour location  
 Floodplain

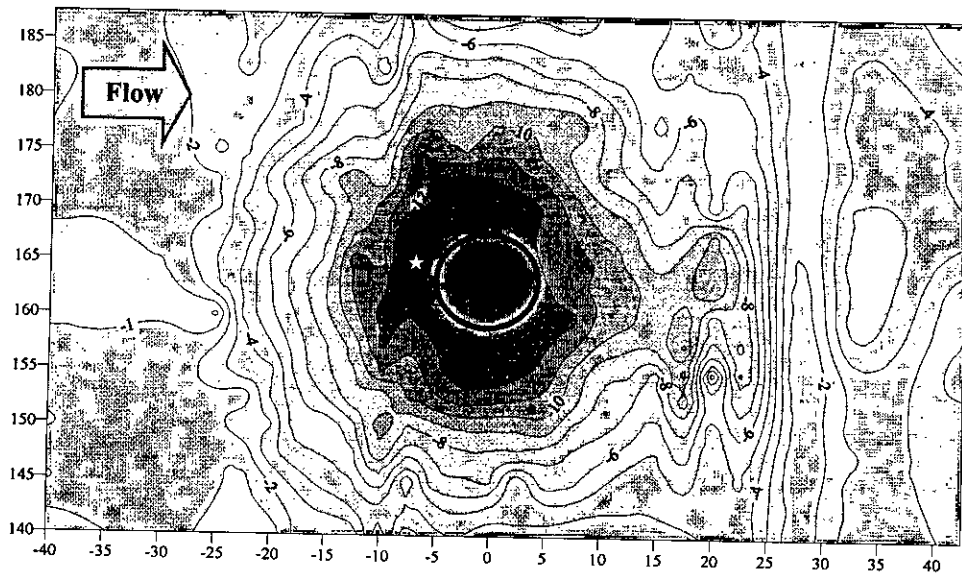
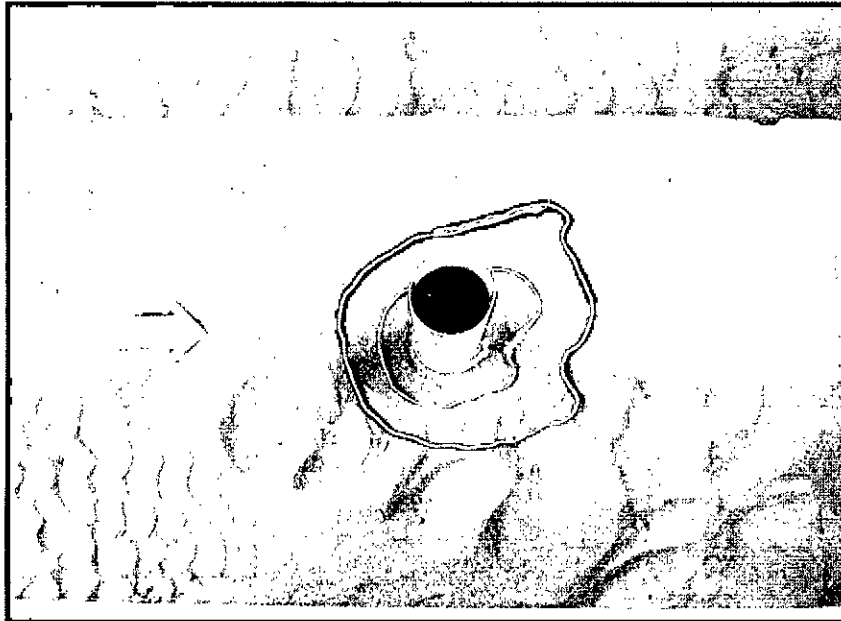
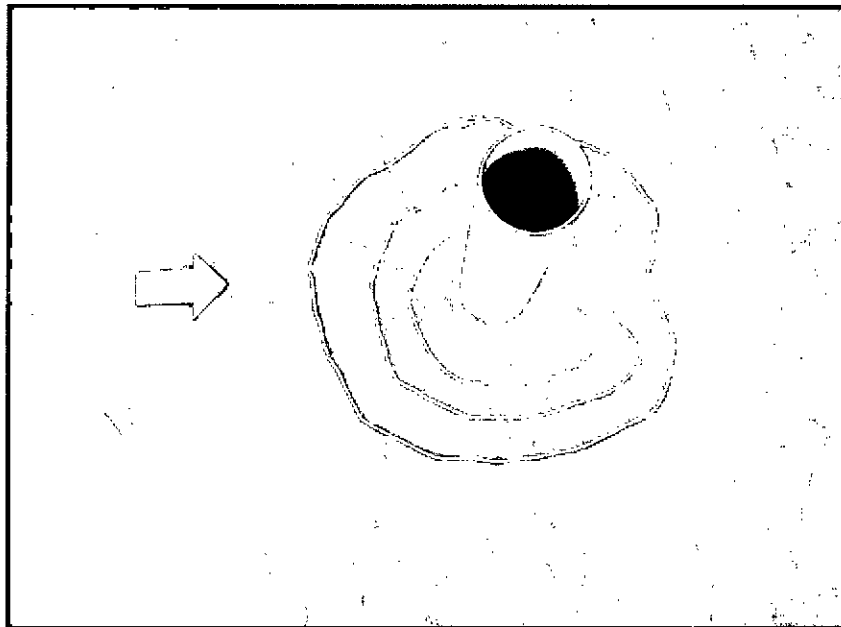


Figure B.50: Run 25-Bed material 3( $d_{50} = 0.12$  mm)-Circular pier ( $l/b=1$ )- $Q=200$  l/s  
 ☆ Max.scour location  
 Main channel



Photograph B.49: Run 25-Bed material 3( $d_{50} = 0.12$  mm)-Circular pier ( $l/b=1$ )- $Q=200$  l/s  
Floodplain



Photograph B.50: Run 25-Bed material 3( $d_{50} = 0.12$  mm)-Circular pier ( $l/b=1$ )- $Q=200$  l/s  
Main channel

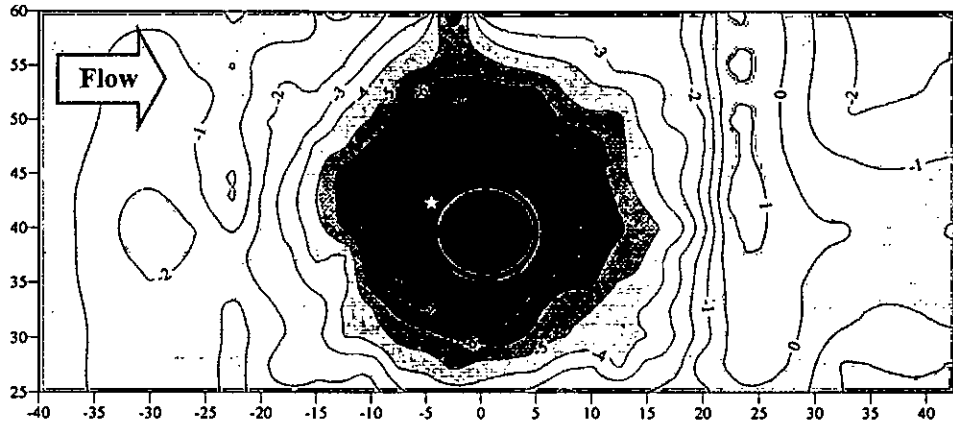


Figure B.51: Run 26-Bed material 3( $d_{50} = 0.12$  mm)-Circular pier ( $l/b=1$ )- $Q=175$  l/s  
 ☆ Max.scour location  
 Floodplain

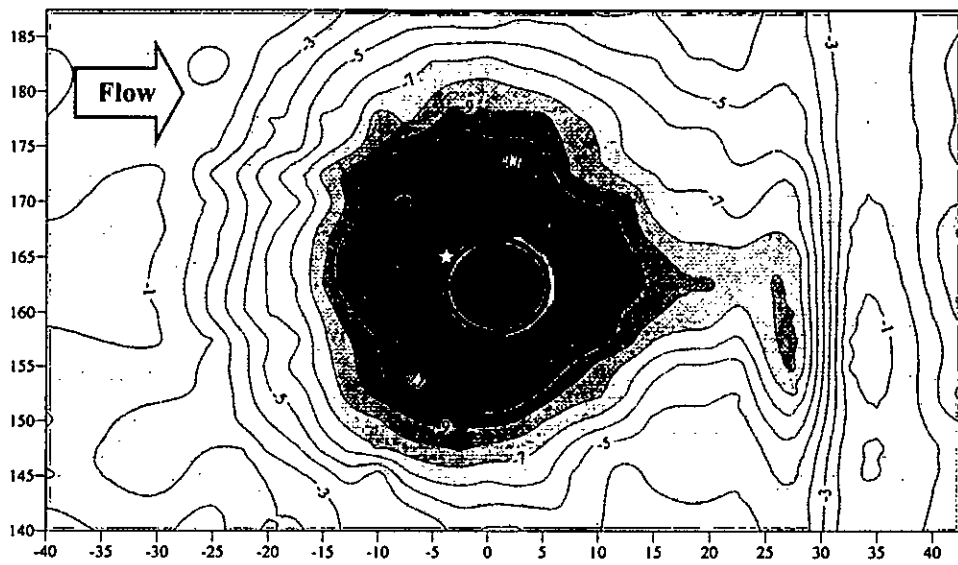
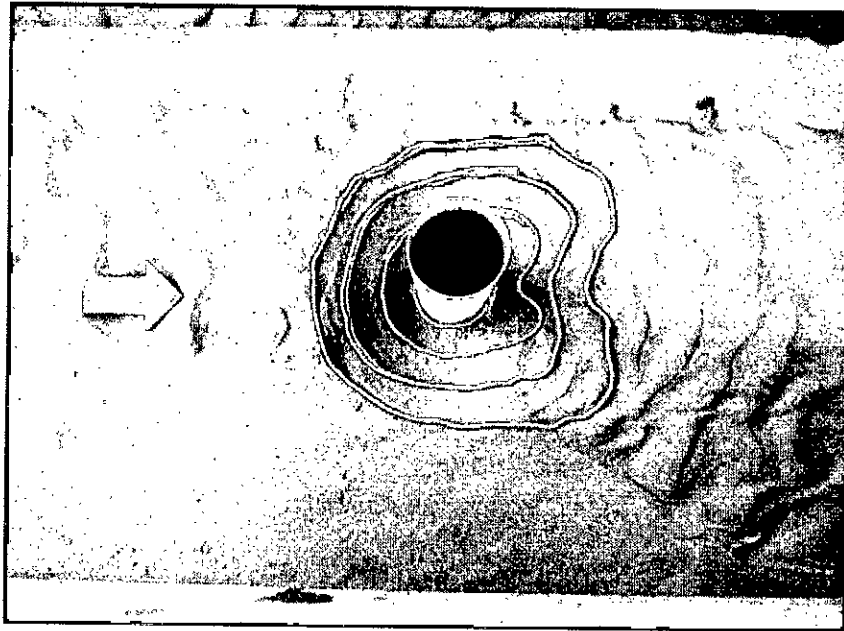
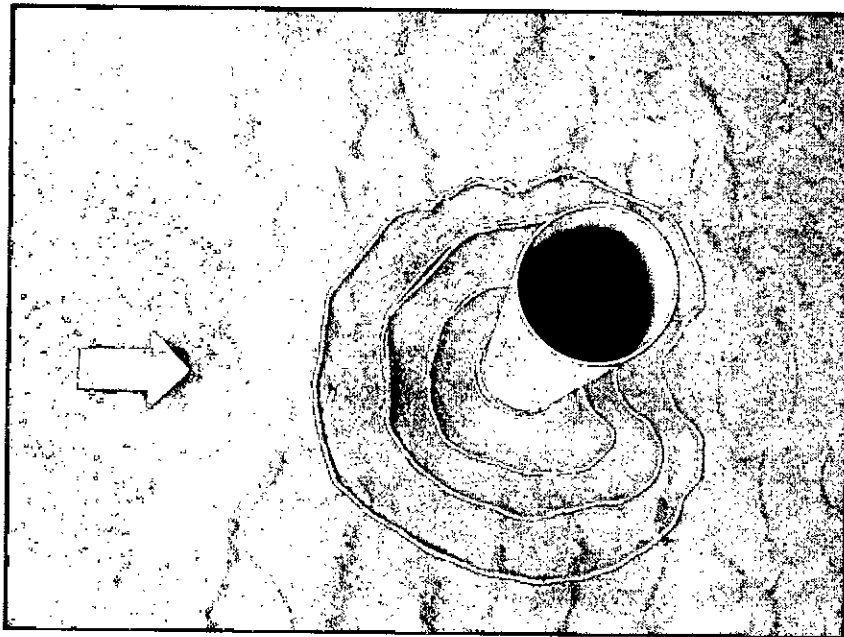


Figure B.52: Run 26-Bed material 3( $d_{50} = 0.12$  mm)-Circular pier ( $l/b=1$ )- $Q=175$  l/s  
 ☆ Max.scour location  
 Main channel





Photograph B.51: Run 26-Bed material 3 ( $d_{50} = 0.12$  mm)-Circular pier ( $l/b=1$ )- $Q=175$  l/s  
Floodplain



Photograph B.52: Run 26-Bed material 3 ( $d_{50} = 0.12$  mm)-Circular pier ( $l/b=1$ )- $Q=175$  l/s  
Main channel

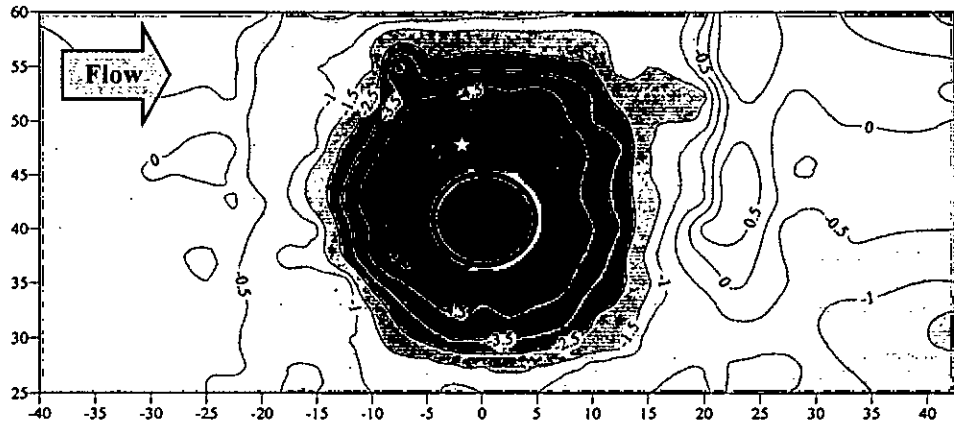


Figure B.53: Run 27-Bed material 3( $d_{50} = 0.12$  mm)-Circular pier ( $l/b=1$ )- $Q=150$  l/s  
 ☆ Max.scour location  
 Floodplain

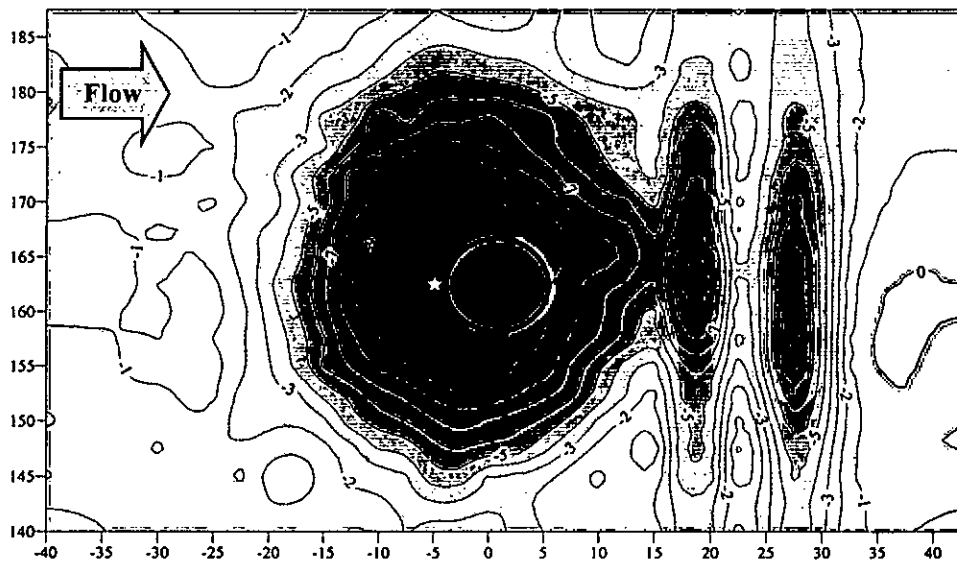
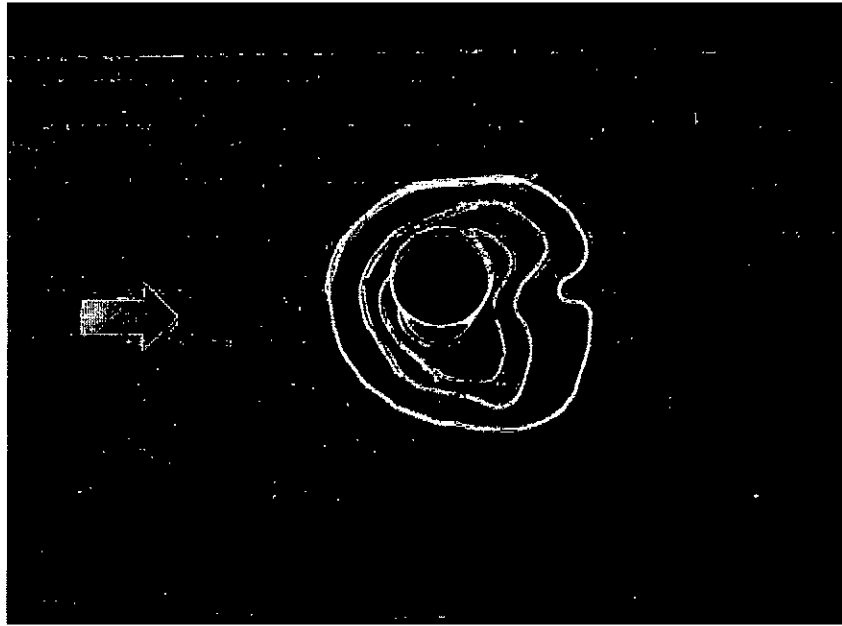
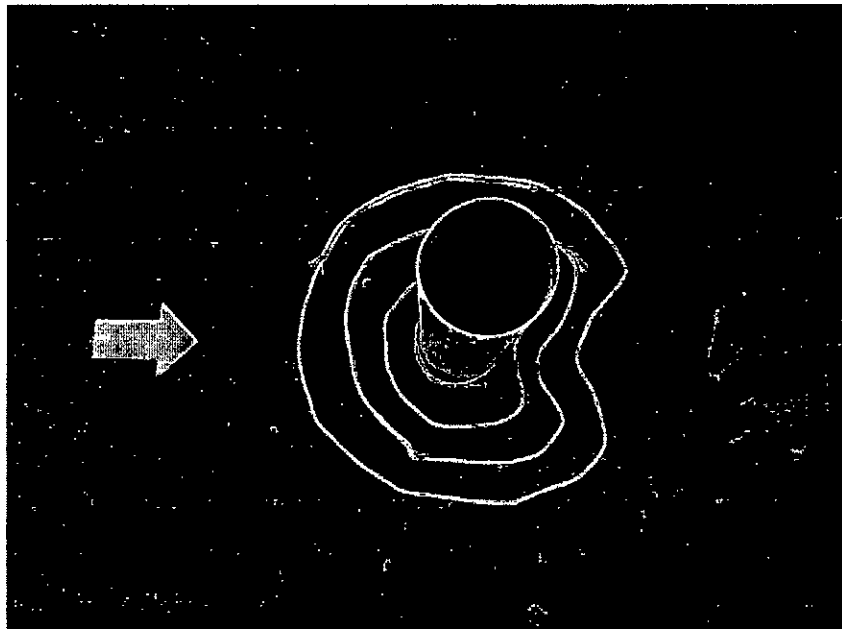


Figure B.54: Run 27-Bed material 3( $d_{50} = 0.12$  mm)-Circular pier ( $l/b=1$ )- $Q=150$  l/s  
 ☆ Max.scour location  
 Main channel



Photograph B.53: Run 27-Bed material 3( $d_{50} = 0.12$  mm)-Circular pier ( $l/b=1$ )- $Q=150$  l/s  
Floodplain



Photograph B.54: Run 27-Bed material 3( $d_{50} = 0.12$  mm)-Circular pier ( $l/b=1$ )- $Q=150$  l/s  
Main channel

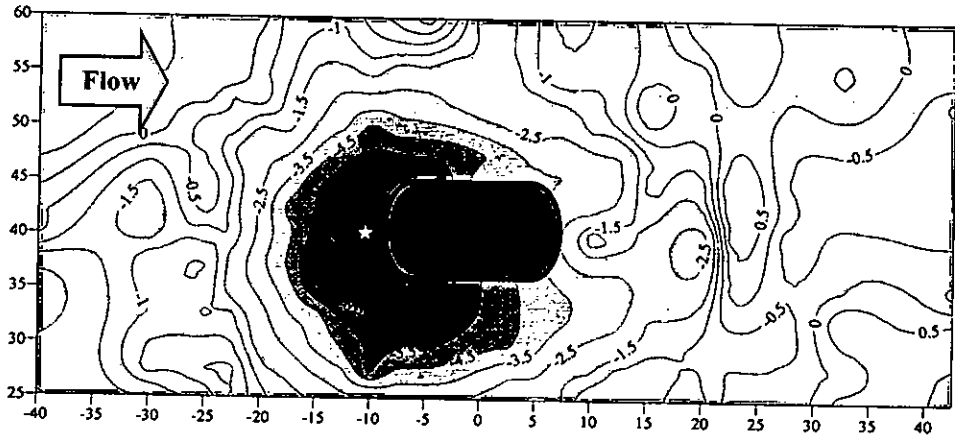


Figure B.55: Run 28-Bed material 3( $d_{50} = 0.12$  mm)-Round nose pier ( $l/b=2$ )- $Q=200$  l/s  
 ☆ Max.scour location  
 Floodplain

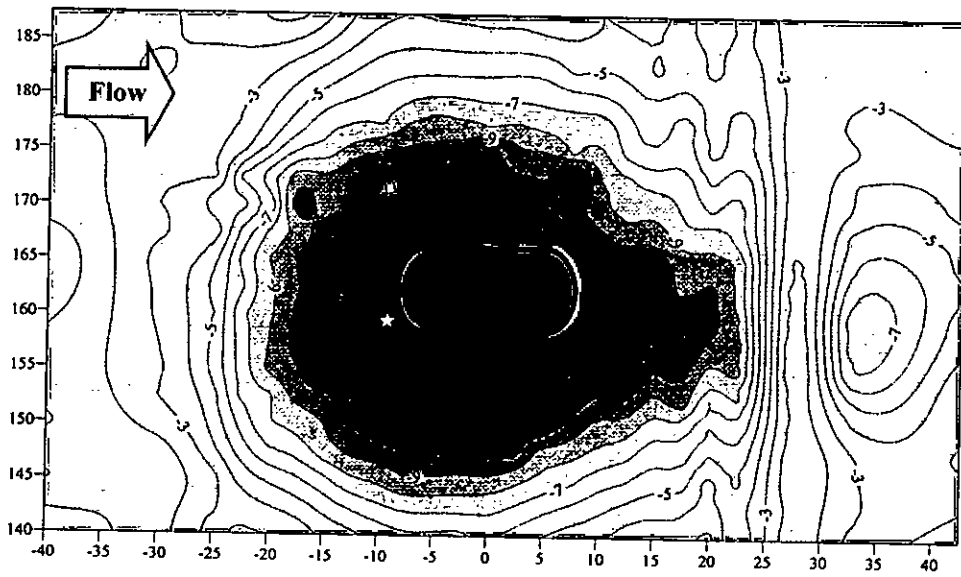
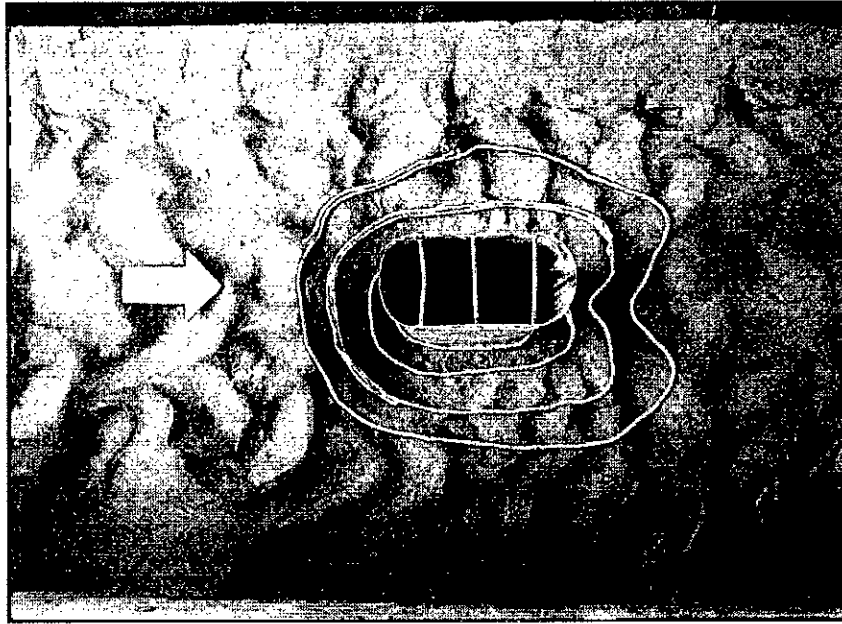
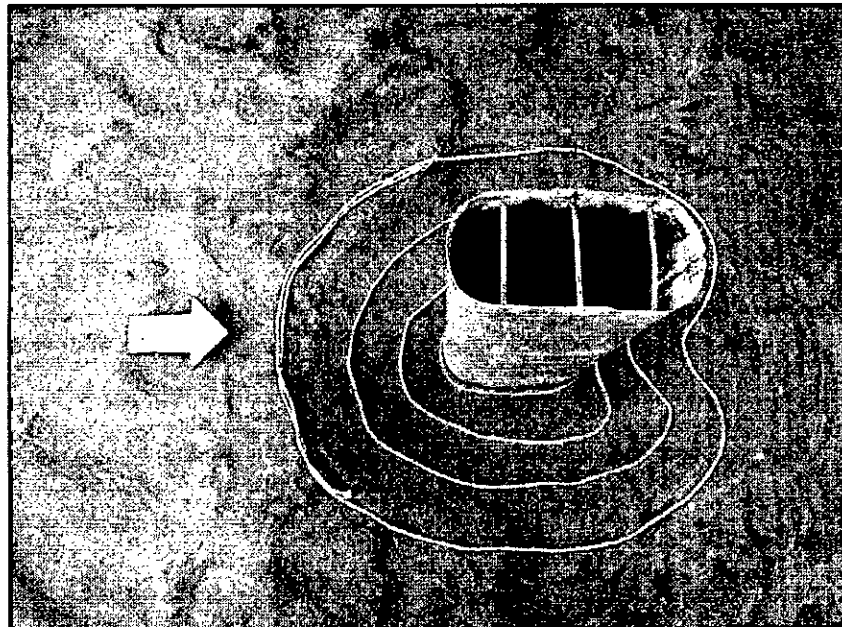


Figure B.56: Run 28-Bed material 3( $d_{50} = 0.12$  mm)-Round nose pier ( $l/b=2$ )- $Q=200$  l/s  
 ☆ Max.scour location  
 Main channel



Photograph B.55: Run 28-Bed material 3( $d_{50} = 0.12$  mm)-Round nose pier ( $l/b=2$ )- $Q=200$  l/s  
Floodplain



Photograph B.56: Run 28-Bed material 3( $d_{50} = 0.12$  mm)-Round nose pier ( $l/b=2$ )- $Q=200$  l/s  
Main channel

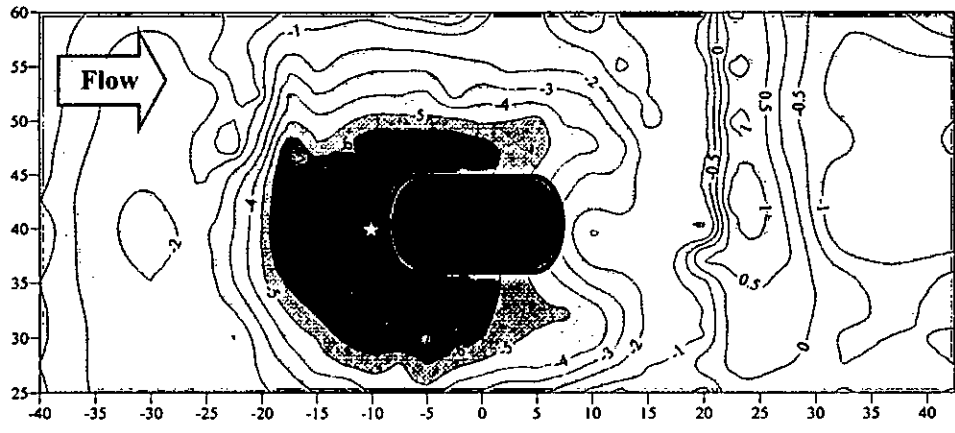


Figure B.57: Run 29-Bed material 3( $d_{50} = 0.12$  mm)-Round nose pier ( $l/b=2$ )- $Q=175$  l/s  
 ☆ Max.scour location  
 Floodplain

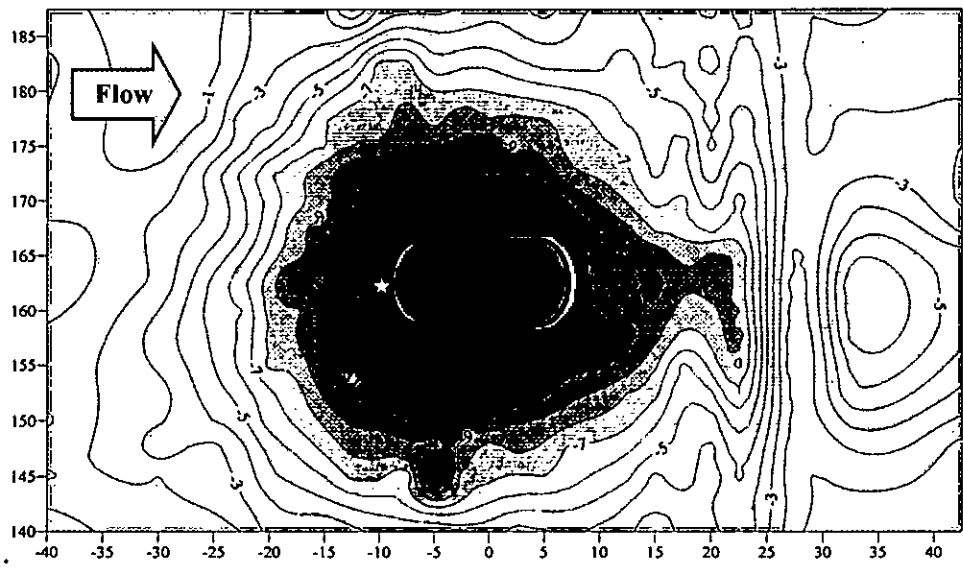
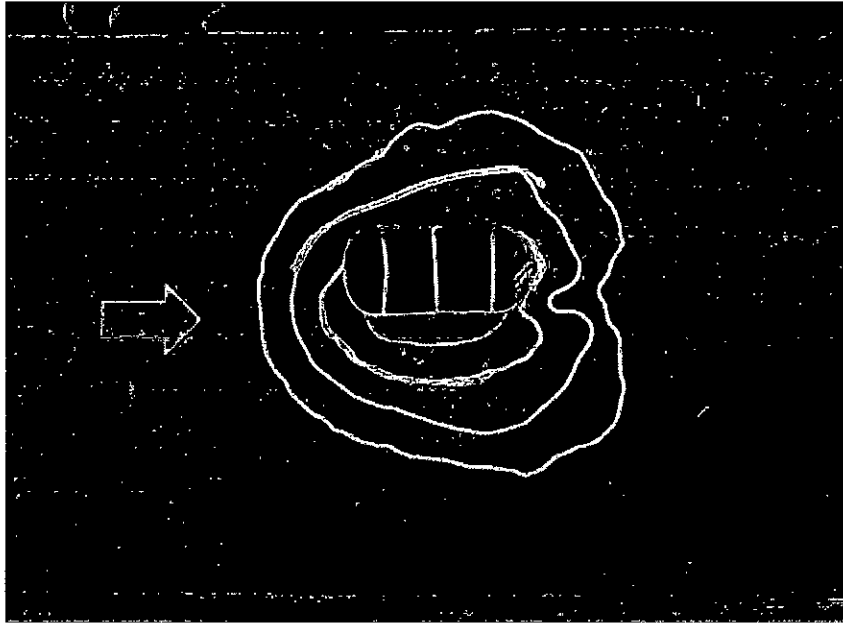
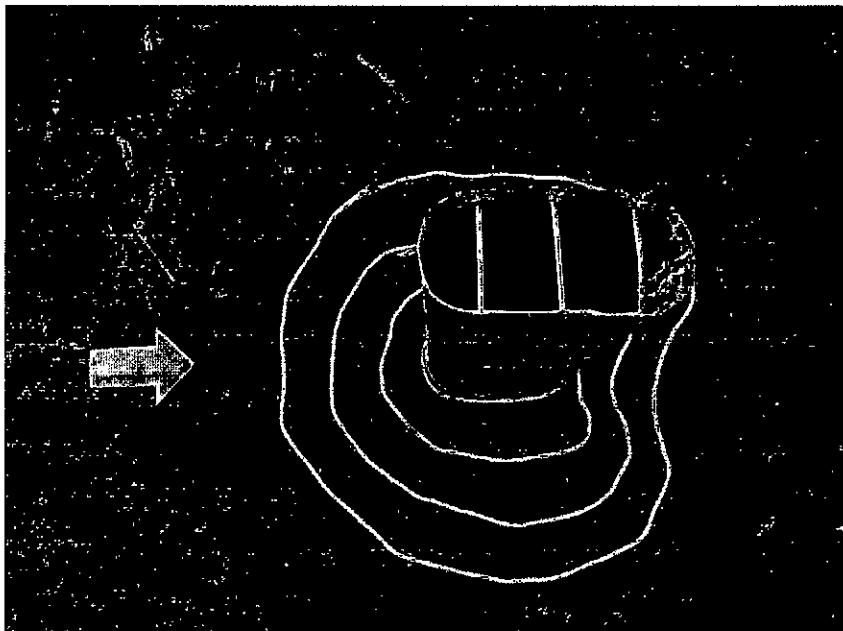


Figure B.58: Run 29-Bed material 3( $d_{50} = 0.12$  mm)-Round nose pier ( $l/b=2$ )- $Q=175$  l/s  
 ☆ Max.scour location  
 Main channel



Photograph B.57: Run 29-Bed material 3( $d_{50} = 0.12$  mm)-Round nose pier ( $l/b=2$ )- $Q=175$  l/s  
Floodplain



Photograph B.58: Run 29-Bed material 3( $d_{50} = 0.12$  mm)-Round nose pier ( $l/b=2$ )- $Q=175$  l/s  
Main channel

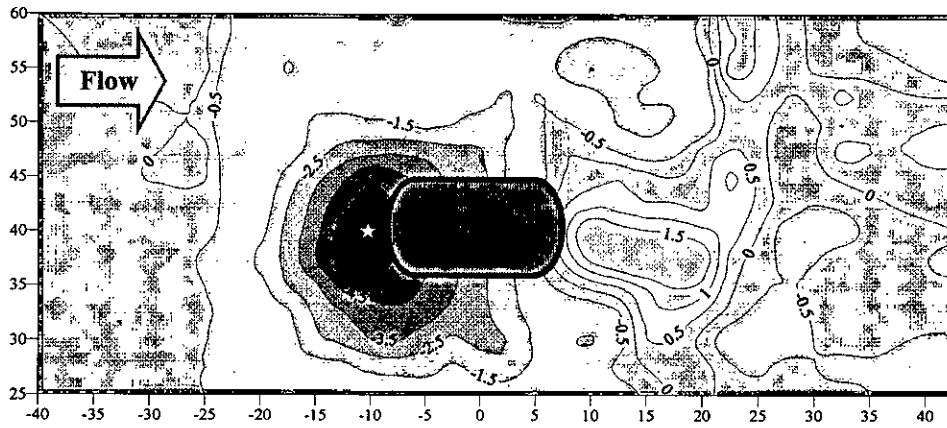


Figure B.59: Run 30-Bed material 3( $d_{50} = 0.12$  mm)-Round nose pier ( $l/b=2$ )- $Q=150$  l/s,  
 ☆ Max.scour location  
 Floodplain

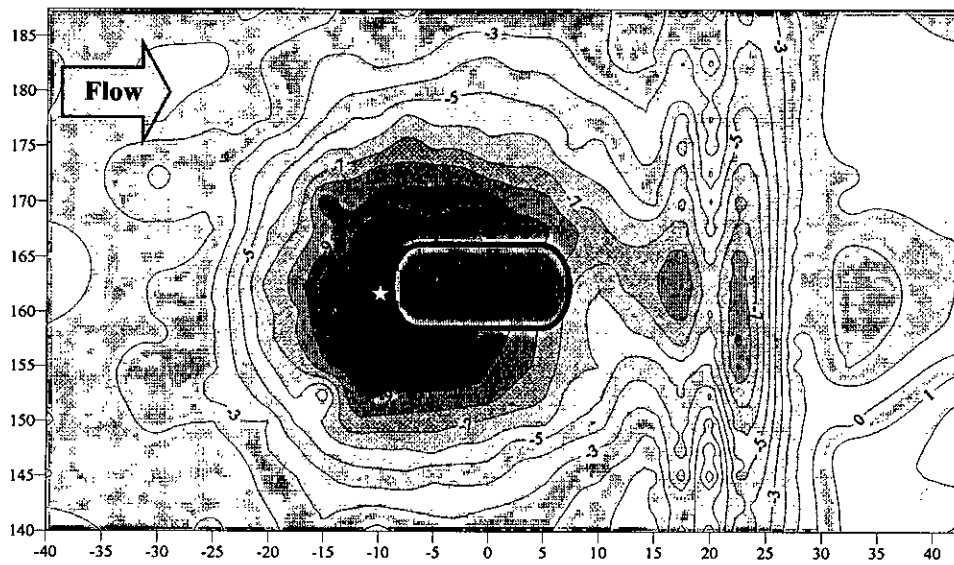
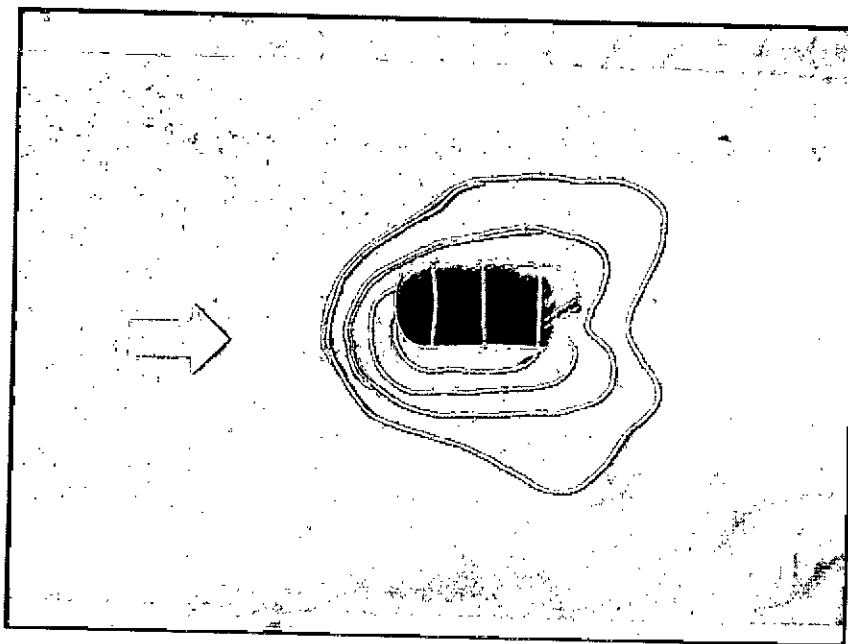
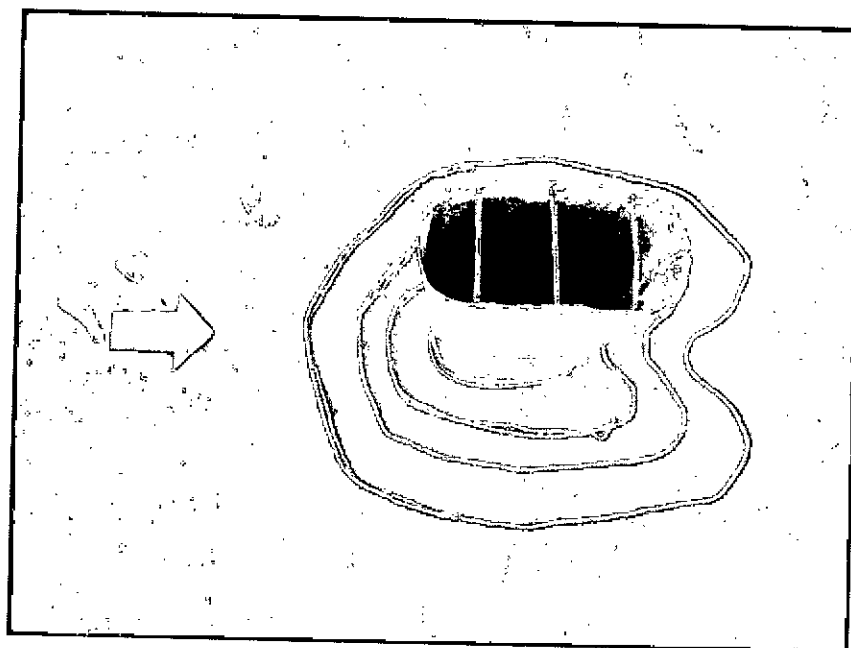


Figure B.60: Run 30-Bed material 3( $d_{50} = 0.12$  mm)-Round nose pier ( $l/b=2$ )- $Q=150$  l/s,  
 ☆ Max.scour location  
 Main channel





Photograph B.59: Run 30-Bed material 3 ( $d_{50} = 0.12$  mm)-Round nose pier ( $l/b=2$ )- $Q=150$  l/s  
Floodplain



Photograph B.60: Run 30-Bed material 3 ( $d_{50} = 0.12$  mm)-Round nose pier ( $l/b=2$ )- $Q=150$  l/s  
Main channel

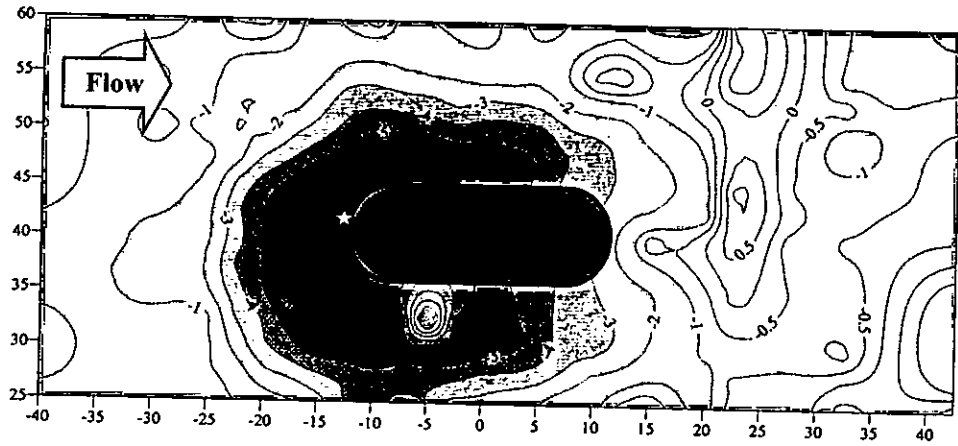


Figure B.61: Run 31-Bed material 3( $d_{50} = 0.12$  mm)-Round nose pier ( $l/b=3$ )- $Q=200$  l/s  
 ☆ Max.scour location  
 Floodplain

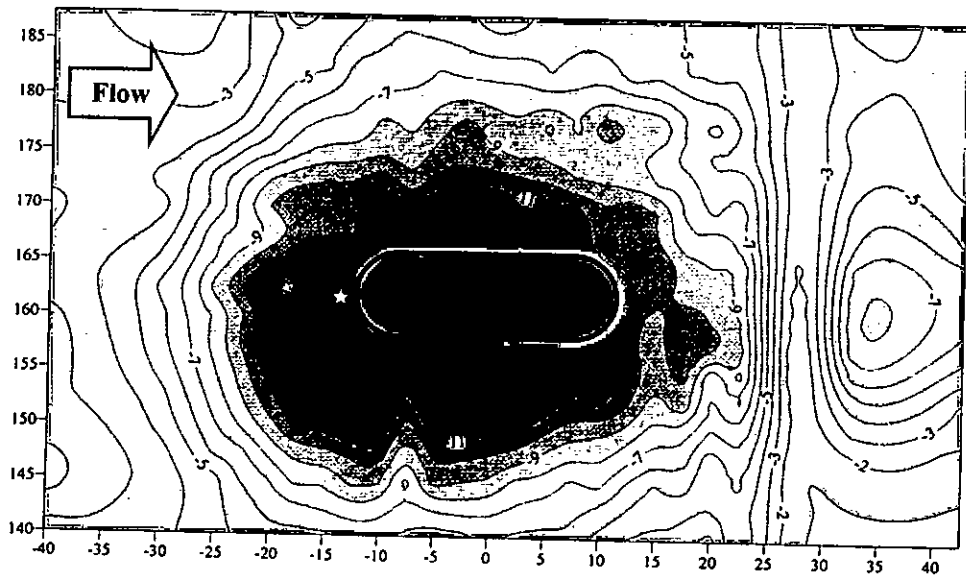
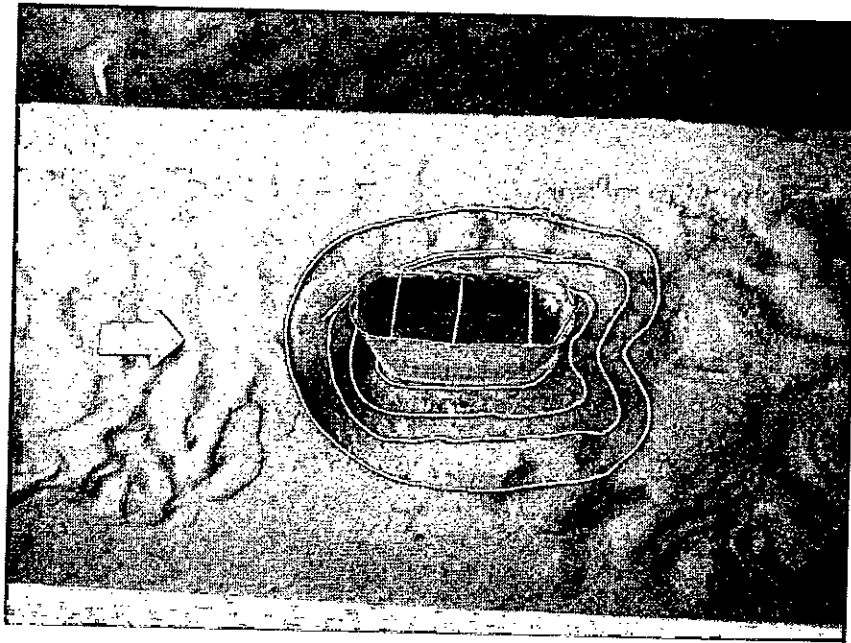
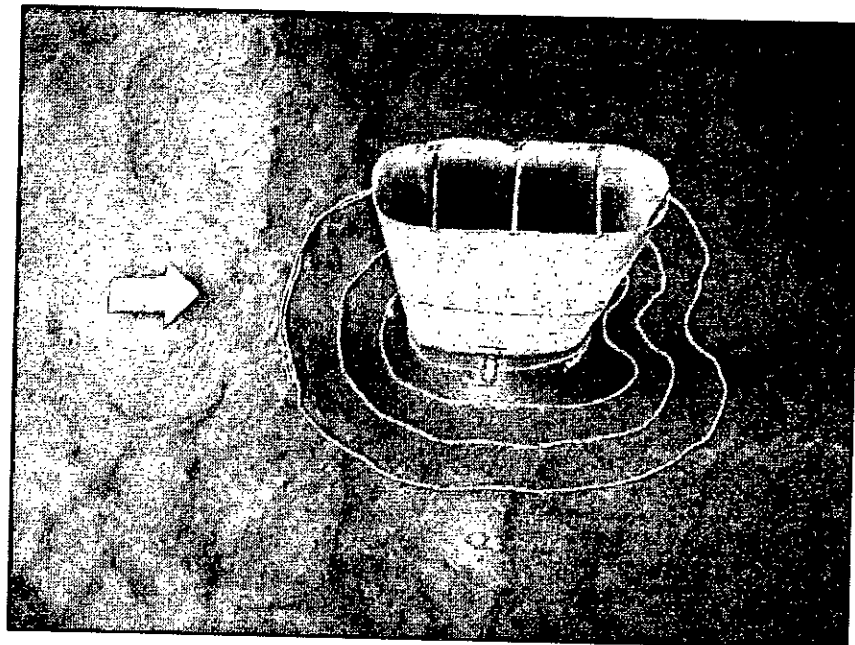


Figure B.62: Run 31-Bed material 3( $d_{50} = 0.12$  mm)-Round nose pier ( $l/b=3$ )- $Q=200$  l/s  
 ☆ Max.scour location  
 Main channel



Photograph B.61: Run 31-Bed material 3( $d_{50} = 0.12$  mm)-Round nose pier ( $l/b=3$ )- $Q=200$  l/s  
Floodplain



Photograph B.62: Run 31-Bed material 3( $d_{50} = 0.12$  mm)-Round nose pier ( $l/b=3$ )- $Q=200$  l/s  
Main channel

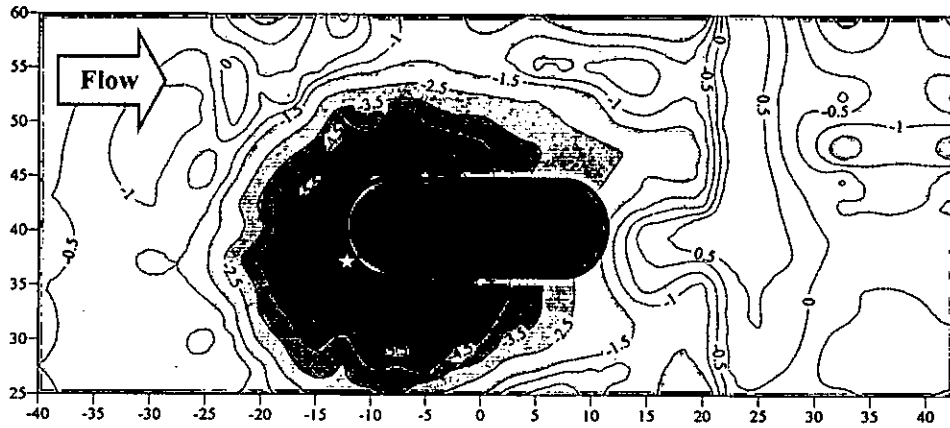


Figure B.63: Run 32-Bed material 3( $d_{50} = 0.12$  mm)-Round nose pier ( $l/b=3$ )- $Q=175$  l/s  
 ☆ Max.scour location  
 Floodplain

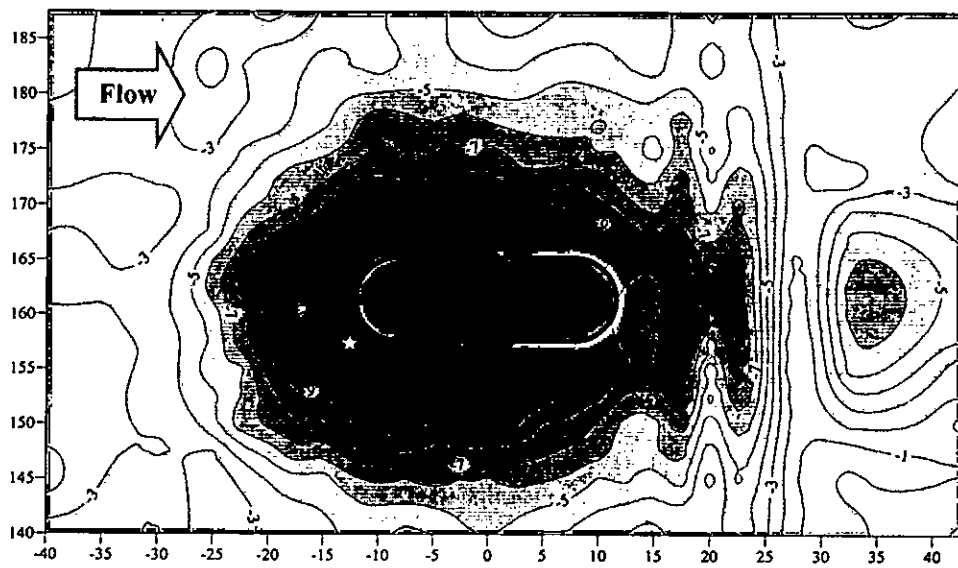
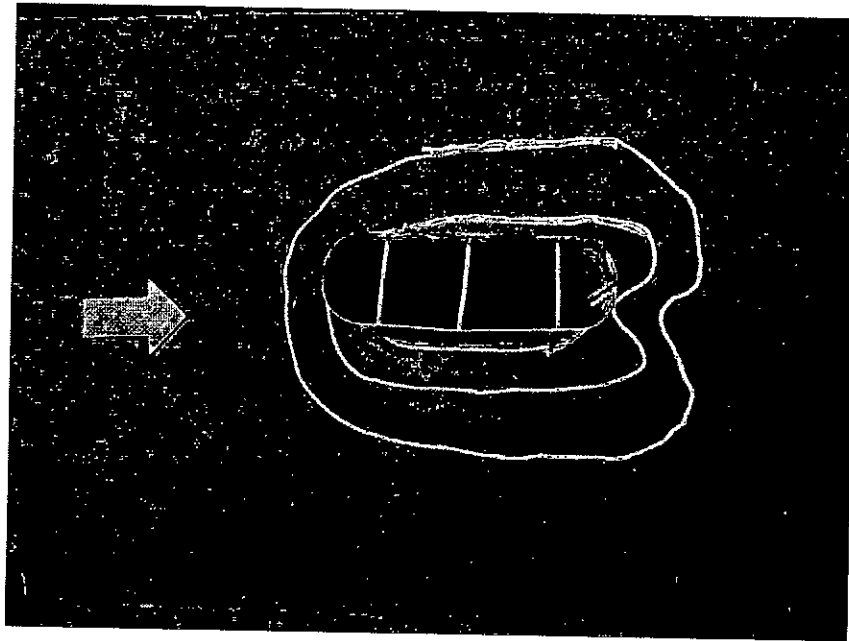
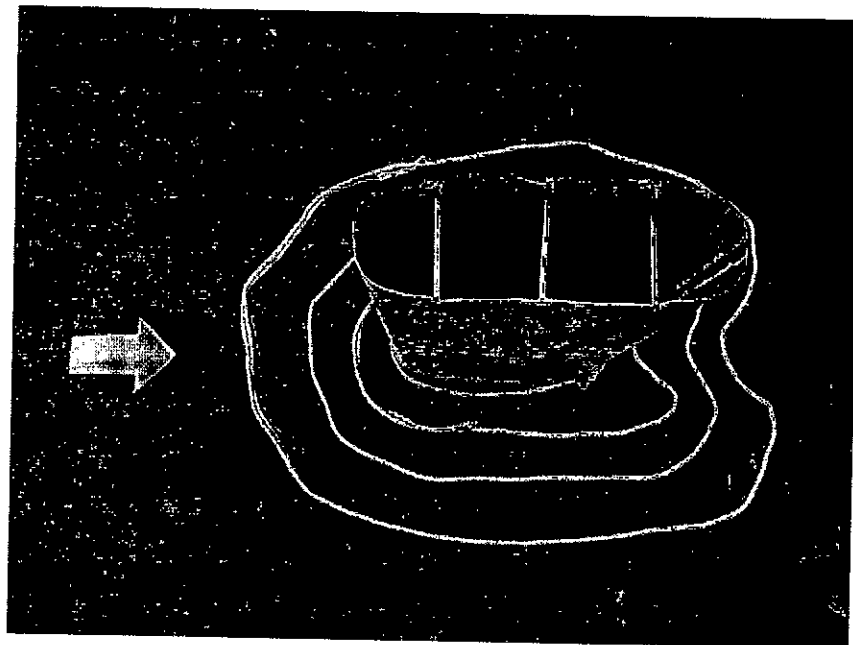


Figure B.64: Run 32-Bed material 3( $d_{50} = 0.12$  mm)-Round nose pier ( $l/b=3$ )- $Q=175$  l/s  
 ☆ Max.scour location  
 Main channel



Photograph B.63: Run 32-Bed material 3( $d_{50} = 0.12$  mm)-Round nose pier ( $l/b=3$ )- $Q=175$  l/s  
Floodplain



Photograph B.64: Run 32-Bed material 3( $d_{50} = 0.12$  mm)-Round nose pier ( $l/b=3$ )- $Q=175$  l/s  
Main channel

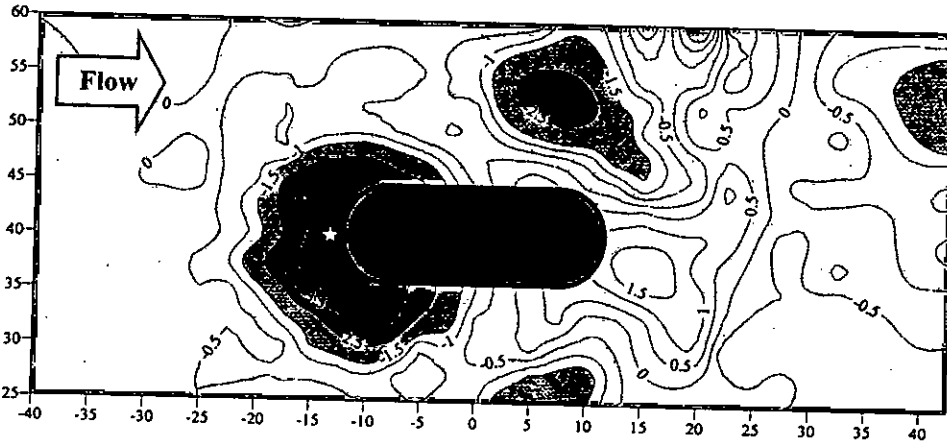


Figure B.65: Run 33-Bed material 3( $d_{50} = 0.12$  mm)-Round nose pier ( $l/b=3$ )- $Q=150$  l/s  
 ☆ Max.scour location  
 Floodplain

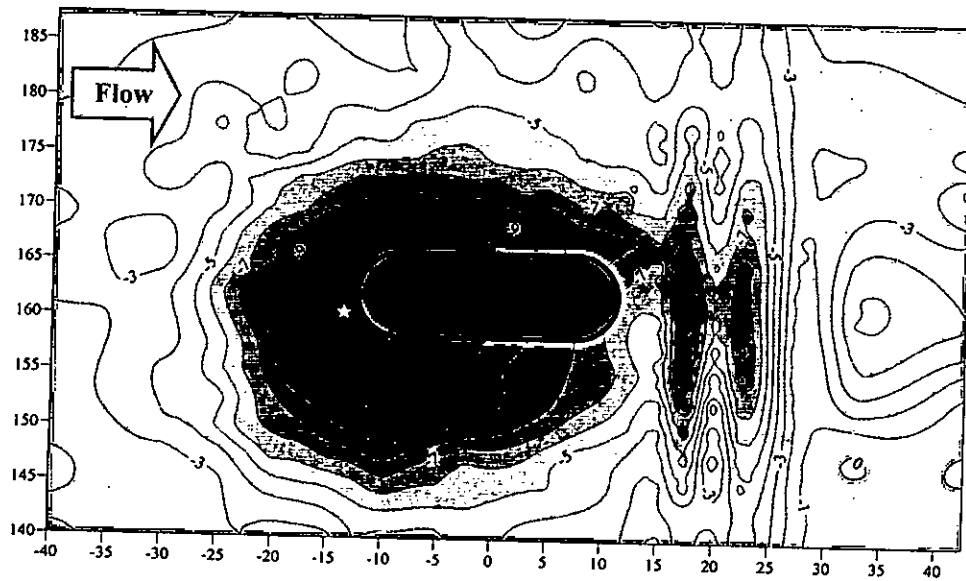
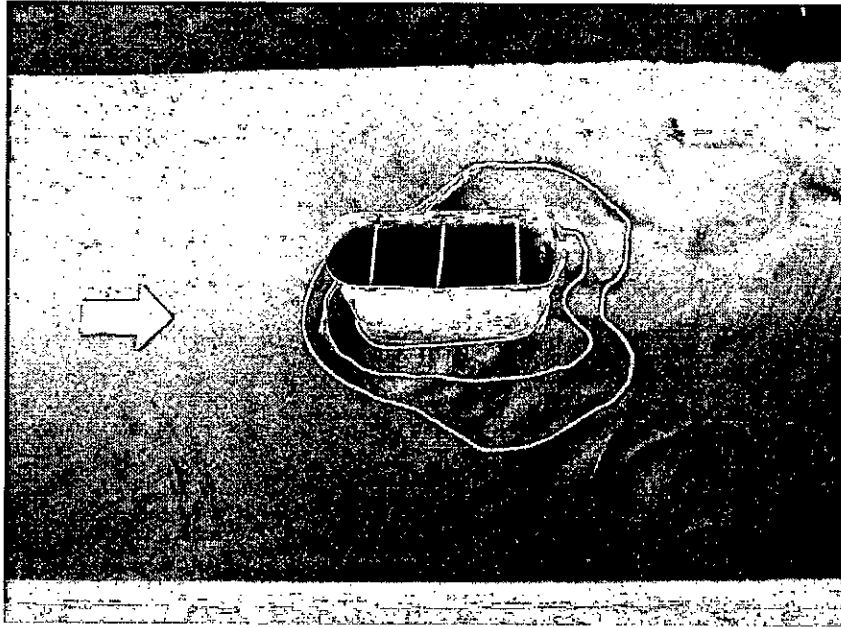
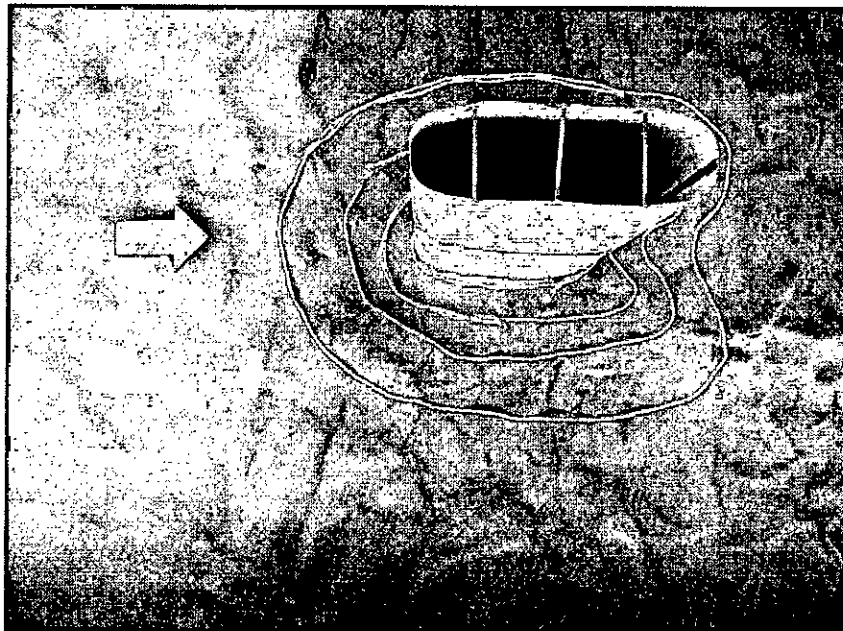


Figure B.66: Run 33-Bed material 3( $d_{50} = 0.12$  mm)-Round nose pier ( $l/b=3$ )- $Q=150$  l/s  
 ☆ Max.scour location  
 Main channel



Photograph B.65: Run 33-Bed material 3( $d_{50} = 0.12$  mm)-Round nose pier ( $l/b=3$ )- $Q=150$  l/s  
Floodplain



Photograph B.66: Run 33-Bed material 3( $d_{50} = 0.12$  mm)-Round nose pier ( $l/b=3$ )- $Q=150$  l/s  
Main channel

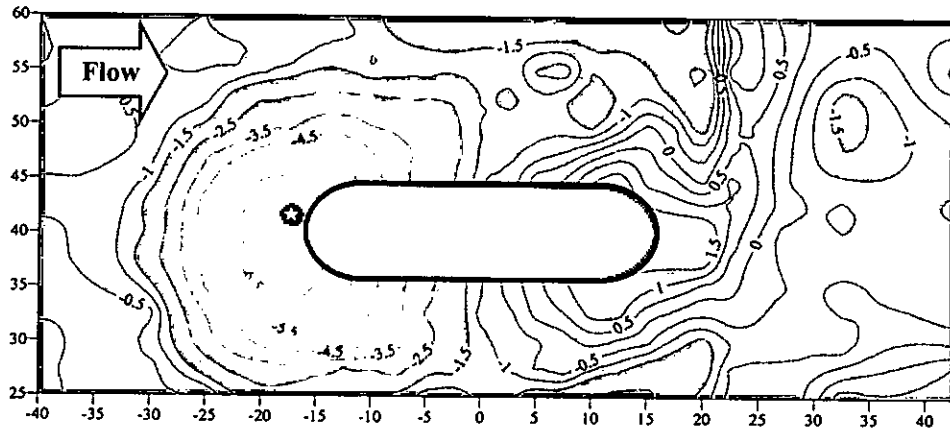


Figure B.67: Run 34-Bed material 3( $d_{50} = 0.12$  mm)-Round nose pier ( $l/b=4$ )- $Q=200$  l/s  
 ☆ Max.scour location  
 Floodplain

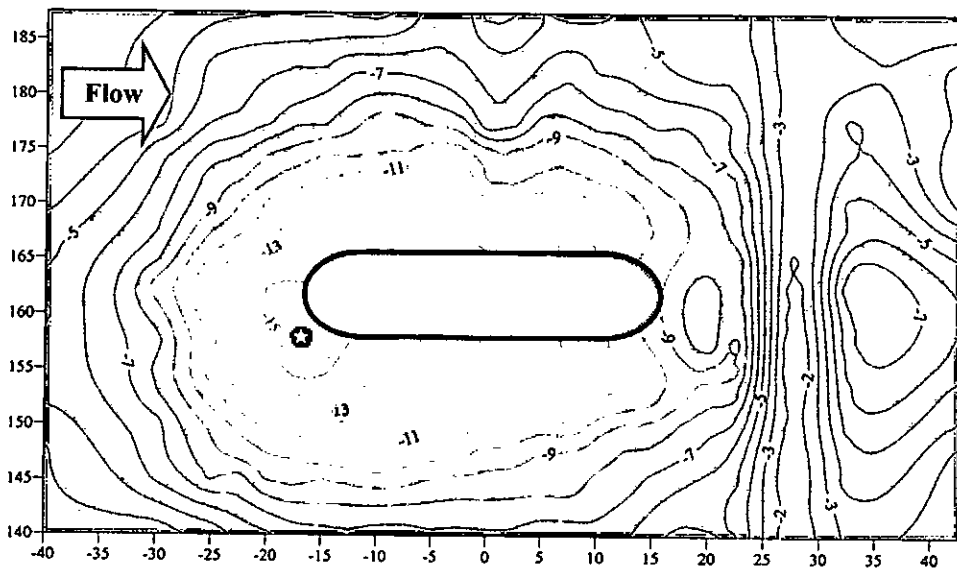
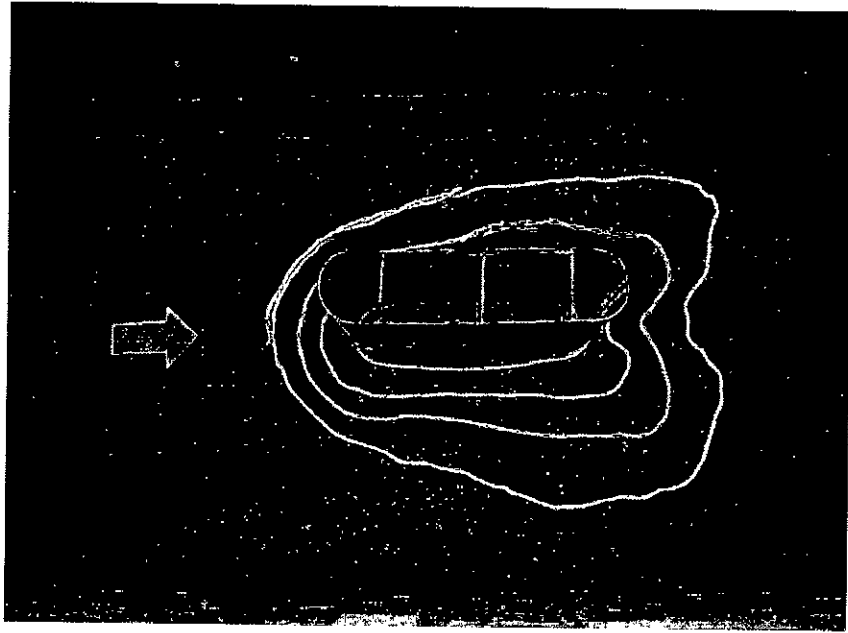
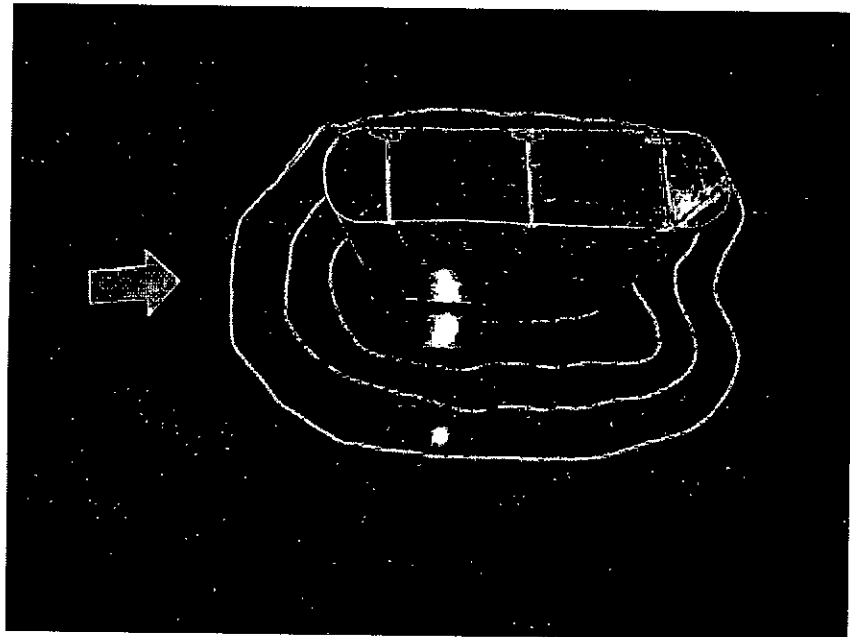


Figure B.68: Run 34-Bed material 3( $d_{50} = 0.12$  mm)-Round nose pier ( $l/b=4$ )- $Q=200$  l/s  
 ☆ Max.scour location  
 Main channel





Photograph B.67: Run 34-Bed material 3( $d_{50} = 0.12$  mm)-Round nose pier ( $l/b=4$ )- $Q=200$  l/s  
Floodplain



Photograph B.68: Run 34-Bed material 3( $d_{50} = 0.12$  mm)-Round nose pier ( $l/b=4$ )- $Q=200$  l/s  
Main channel

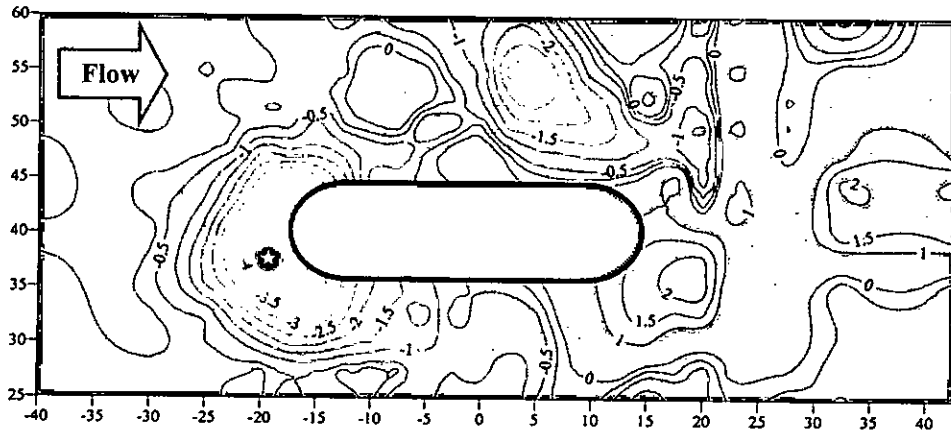


Figure B.69: Run 35-Bed material 3( $d_{50} = 0.12$  mm)-Round nose pier ( $l/b=4$ )- $Q=175$  l/s  
 ☆ Max.scour location  
 Floodplain

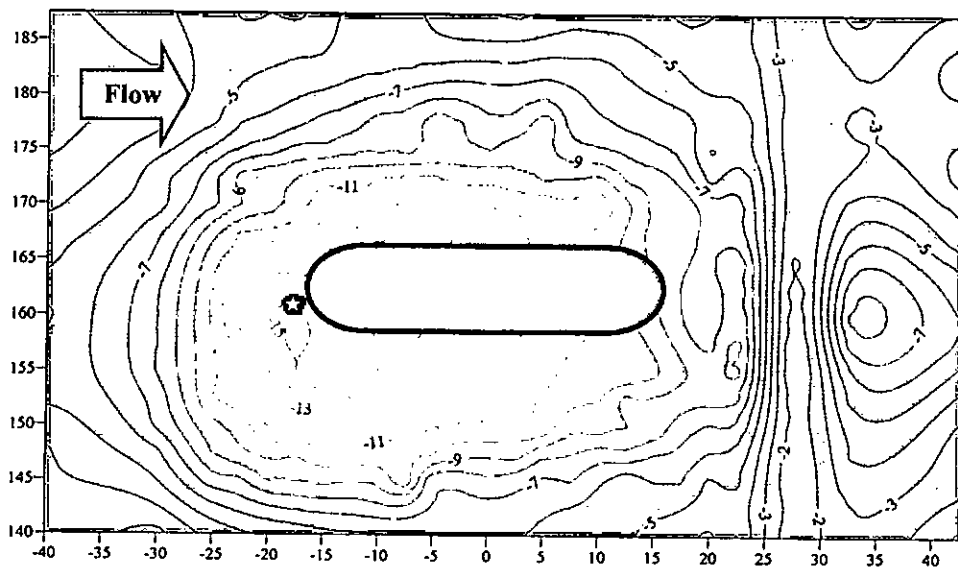
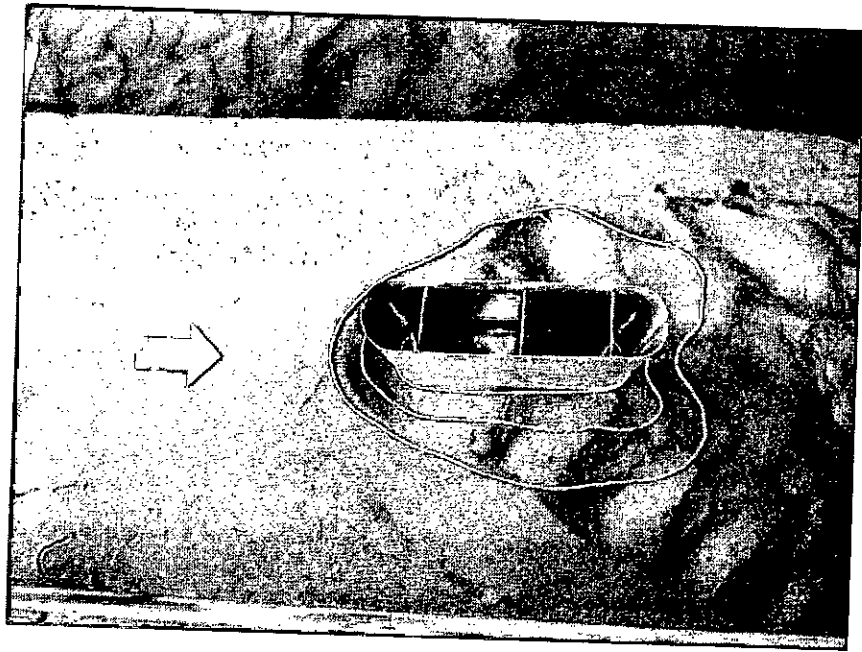
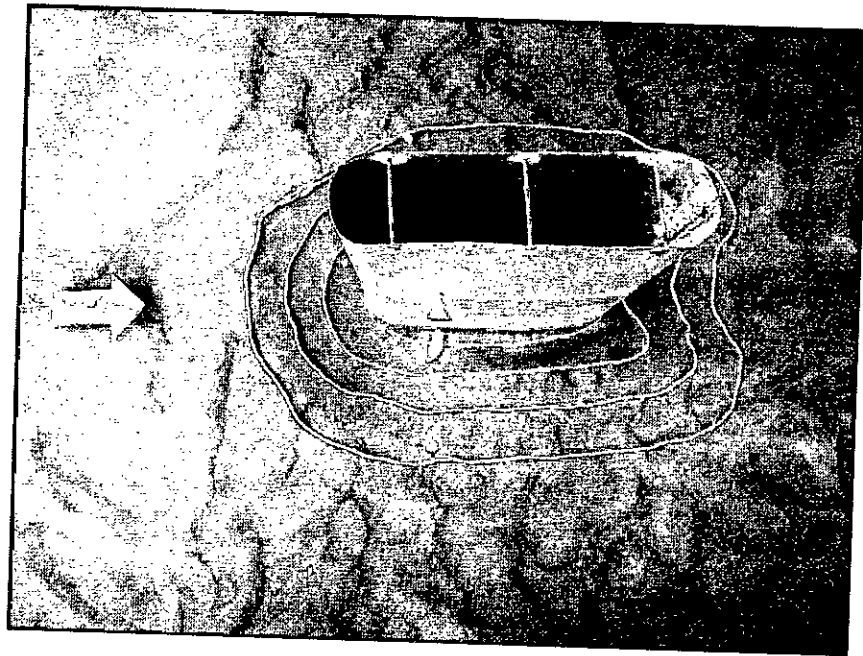


Figure B.70: Run 35-Bed material 3( $d_{50} = 0.12$  mm)-Round nose pier ( $l/b=4$ )- $Q=175$  l/s  
 ☆ Max.scour location  
 Main channel



Photograph B.69: Run 35-Bed material 3 ( $d_{50} = 0.12$  mm)-Round nose pier ( $l/b=4$ )- $Q=175$  l/s  
Floodplain



Photograph B.70: Run 35-Bed material 3 ( $d_{50} = 0.12$  mm)-Round nose pier ( $l/b=4$ )- $Q=175$  l/s  
Main channel

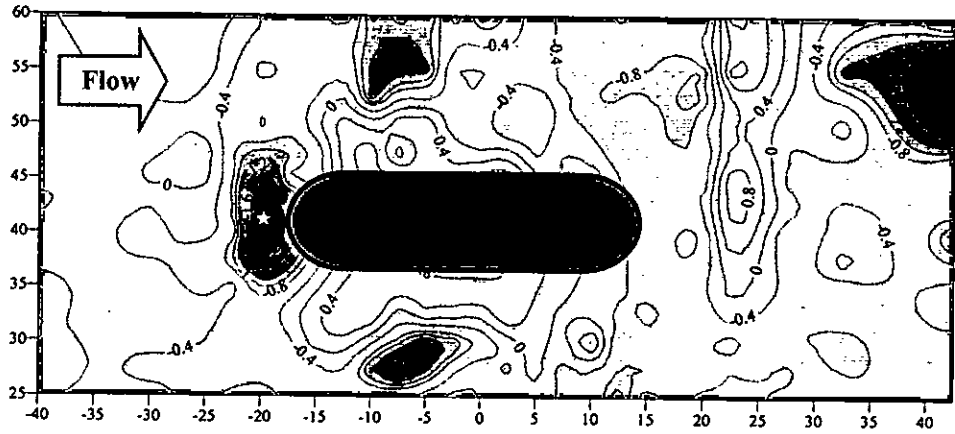


Figure B.71: Run 36-Bed material 3( $d_{50} = 0.12$  mm)-Round nose pier ( $l/b=4$ )- $Q=150$  l/s  
 ☆ Max.scour location  
 Floodplain

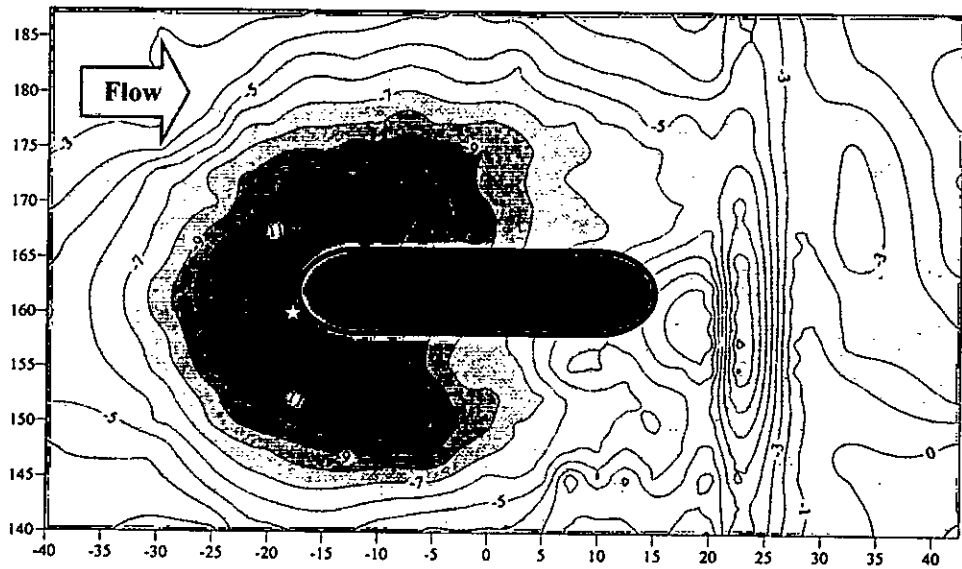
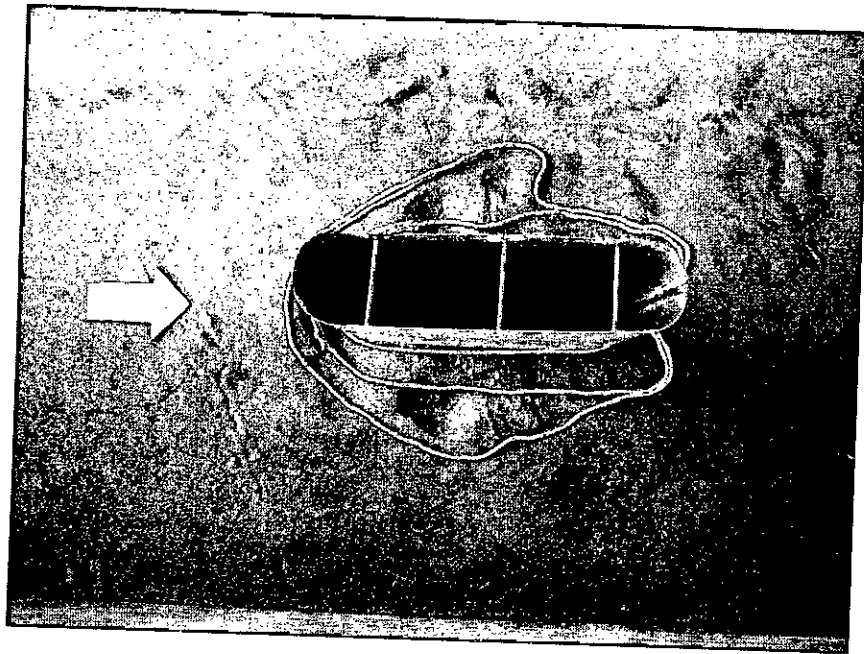
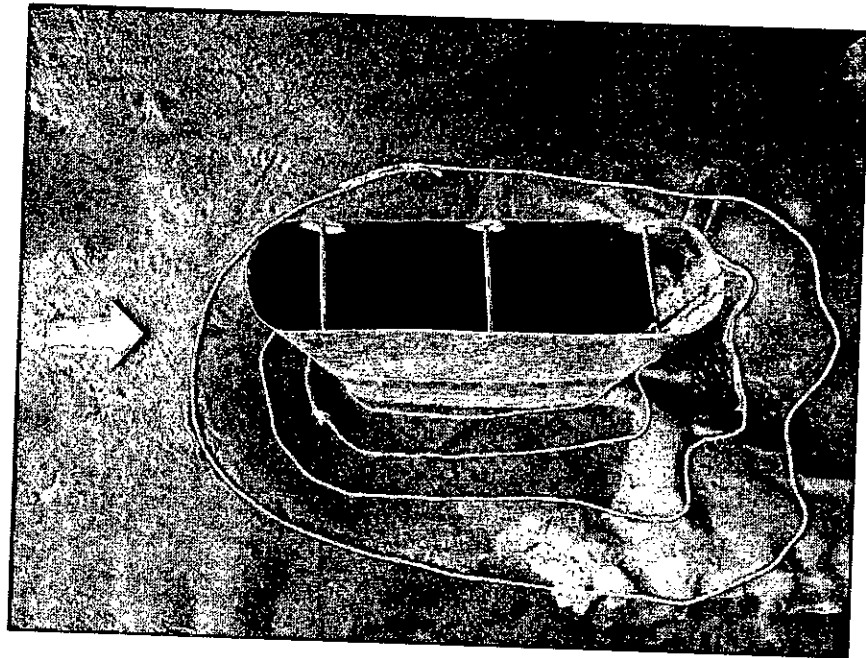


Figure B.72: Run 36-Bed material 3( $d_{50} = 0.12$  mm)-Round nose pier ( $l/b=4$ )- $Q=150$  l/s  
 ☆ Max.scour location  
 Main channel



Photograph B.71: Run 36-Bed material 3( $d_{50} = 0.12$  mm)-Round nose pier ( $l/b=4$ )- $Q=150$  l/s  
Floodplain



Photograph B.72: Run 36-Bed material 3( $d_{50} = 0.12$  mm)-Round nose pier ( $l/b=4$ )- $Q=150$  l/s  
Main channel

**Appendix C**  
**Velocity vector**

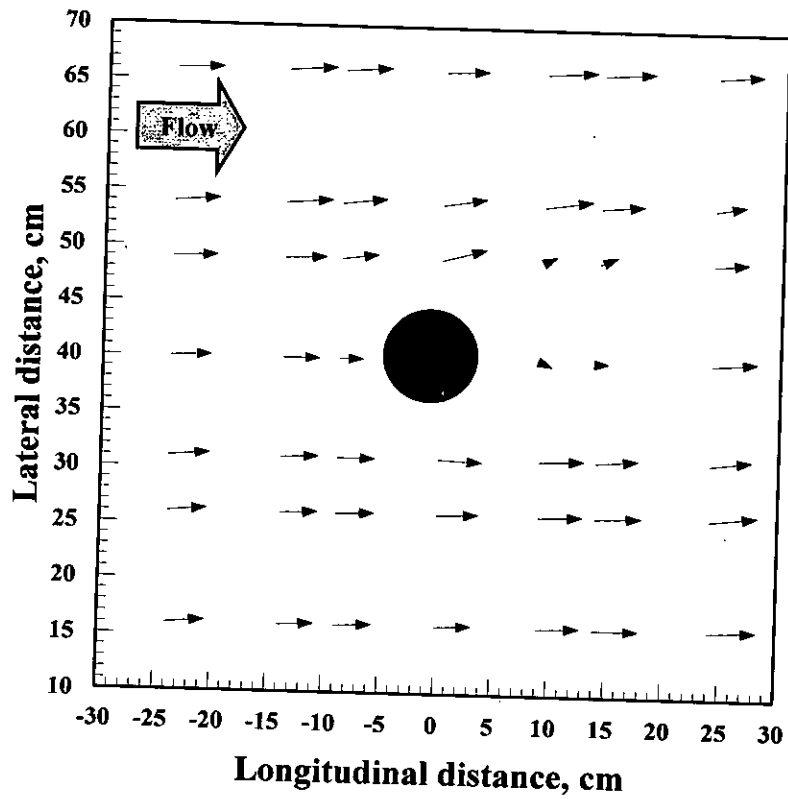


Figure C.1: Run 1-Bed material 1 ( $d_{50} = 0.75$  mm)-Circular pier ( $l/b=1$ )- $Q=200$  l/s  
Floodplain

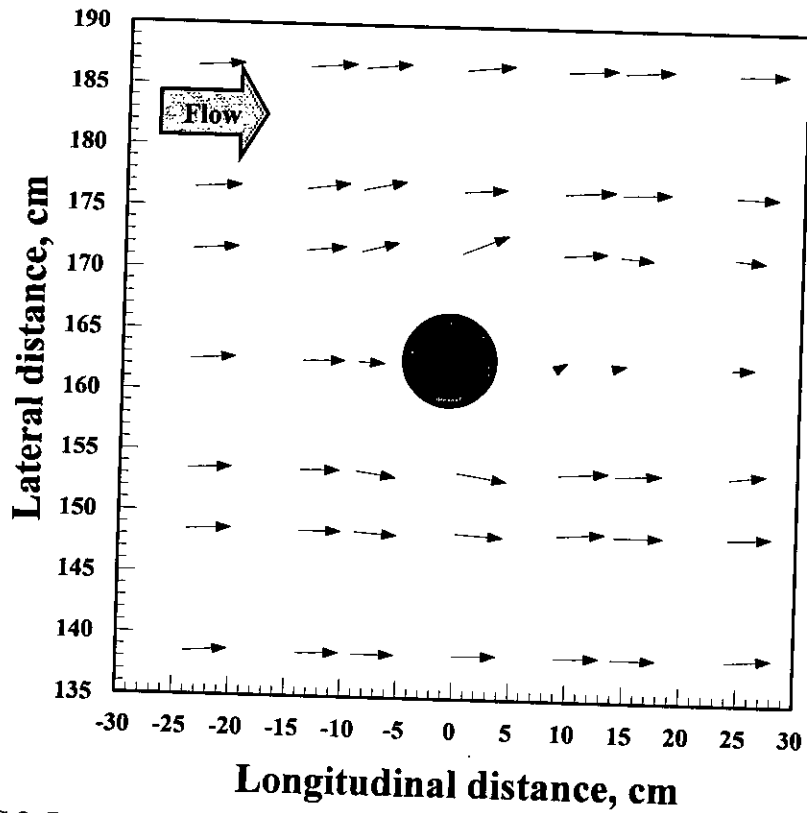


Figure C.2: Run 1-Bed material 1 ( $d_{50} = 0.75$  mm)-Circular pier ( $l/b=1$ )- $Q=200$  l/s  
Main channel

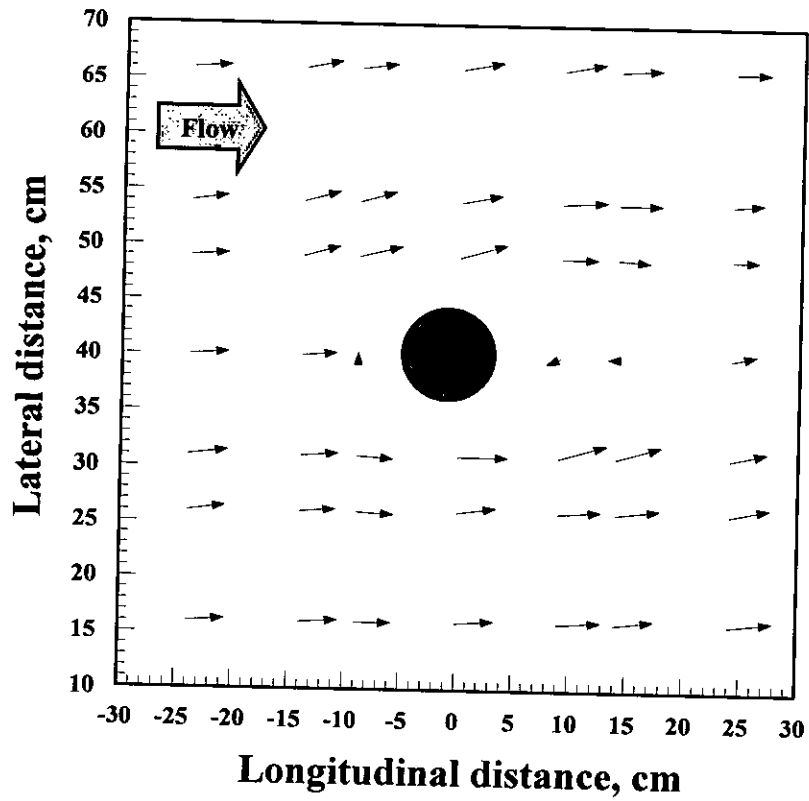


Figure C.3: Run 2-Bed material 1 ( $d_{50} = 0.75$  mm)-Circular pier ( $l/b=1$ )- $Q=175$  l/s  
Floodplain

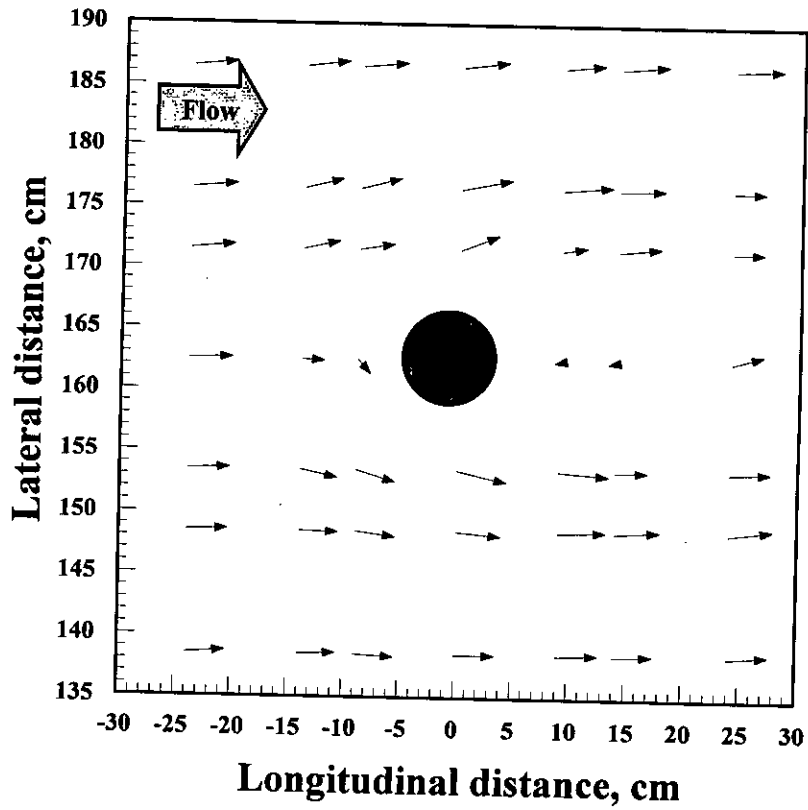


Figure C.4: Run 2-Bed material 1 ( $d_{50} = 0.75$  mm)-Circular pier ( $l/b=1$ )- $Q=175$  l/s  
Main channel



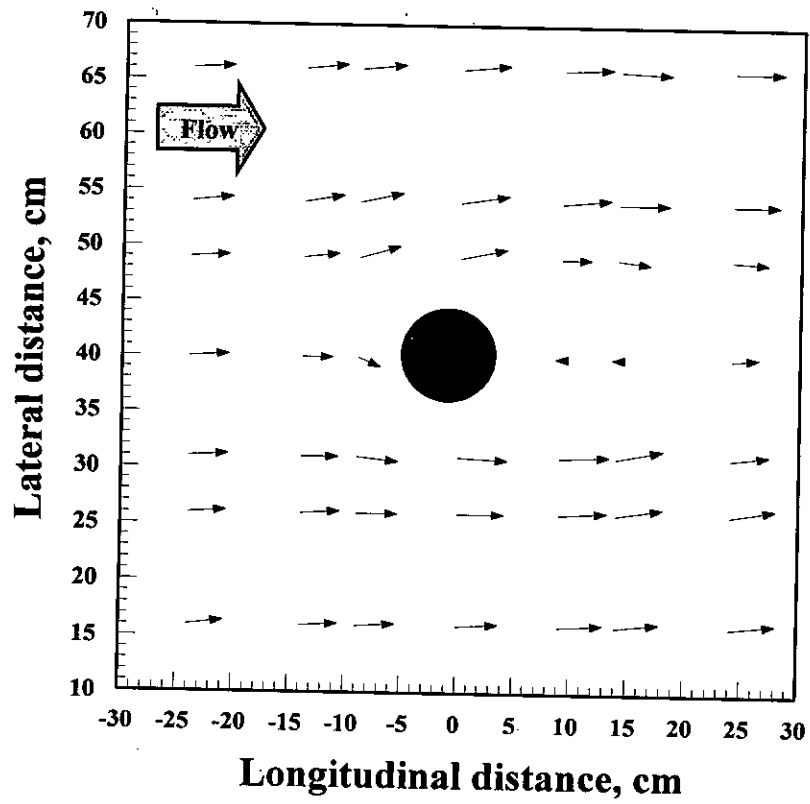


Figure C.5: Run 3-Bed material 1( $d_{50} = 0.75$  mm)-Circular pier ( $l/b=1$ )- $Q=150$  l/s  
Floodplain

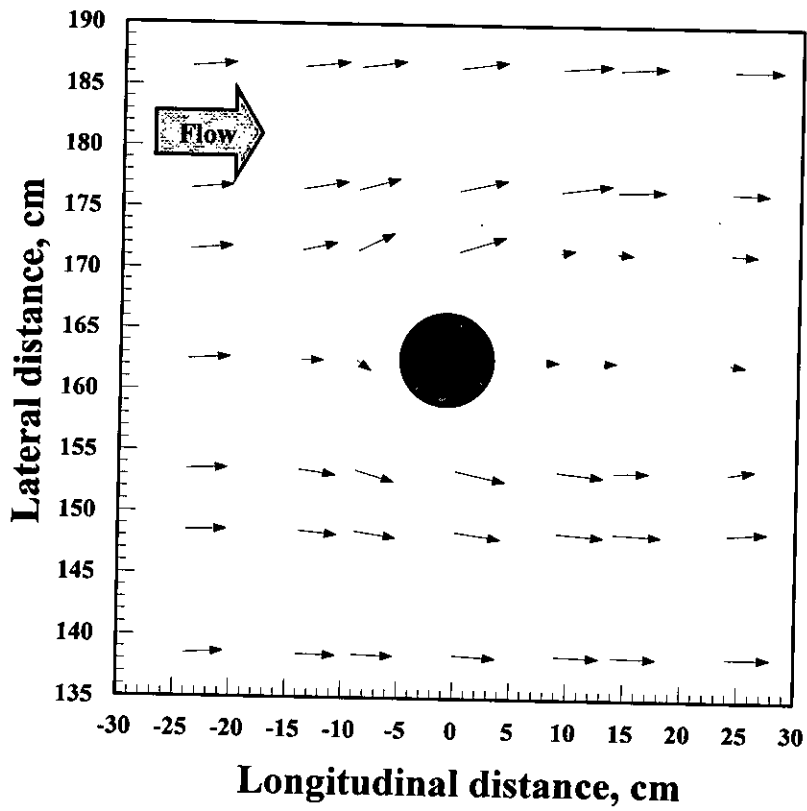


Figure C.6: Run 3-Bed material 1( $d_{50} = 0.75$  mm)-Circular pier ( $l/b=1$ )- $Q=150$  l/s  
Main channel

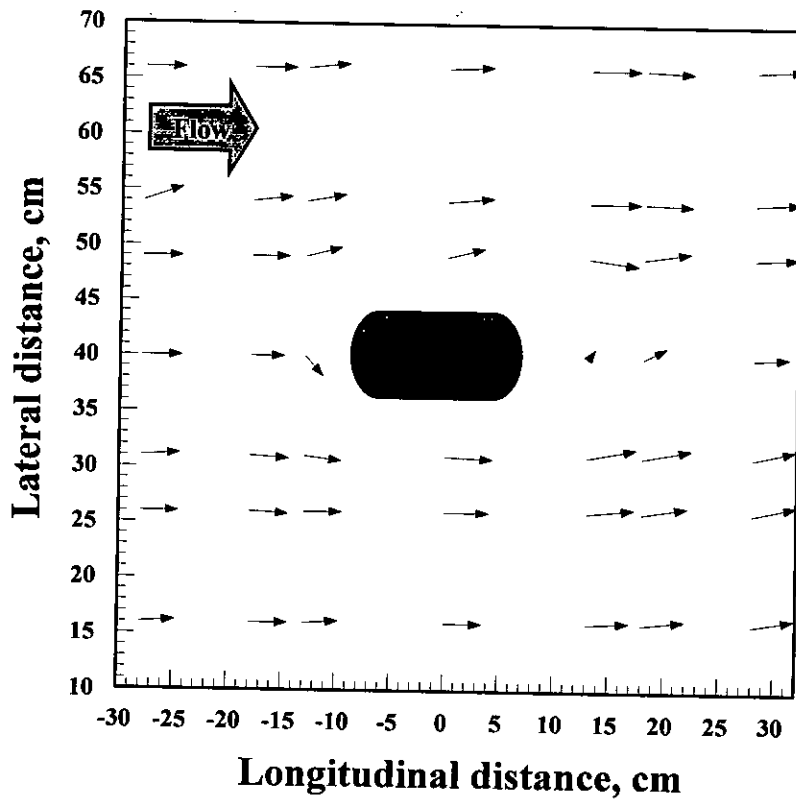


Figure C.7: Run 4-Bed material 1( $d_{50} = 0.75$  mm)-Round nose pier ( $l/b=2$ )- $Q=200$  l/s  
Floodplain

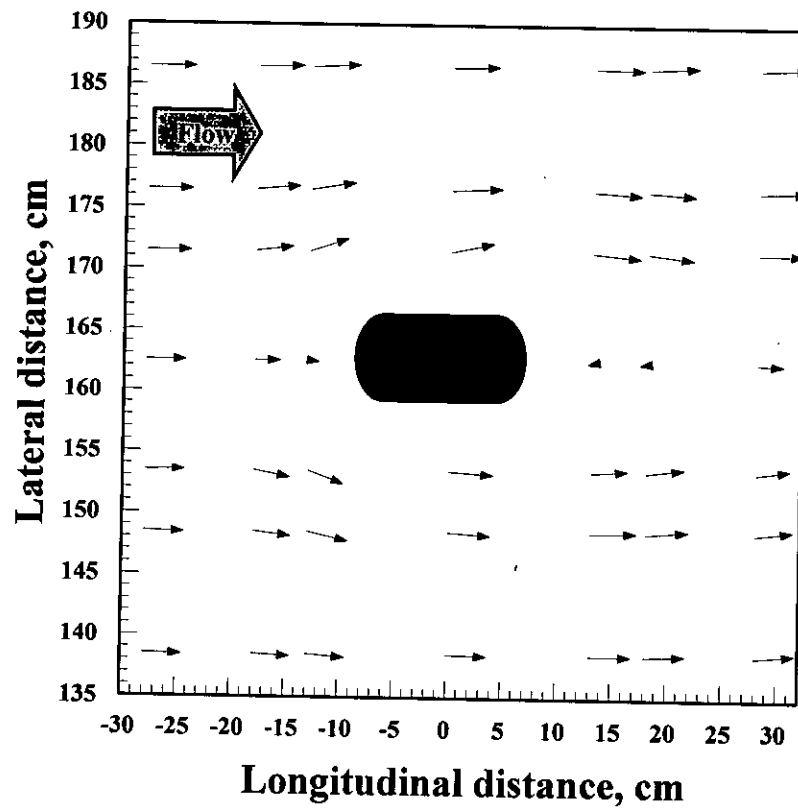


Figure C.8: Run 4-Bed material 1( $d_{50} = 0.75$  mm)-Round nose pier ( $l/b=2$ )- $Q=200$  l/s  
Main channel

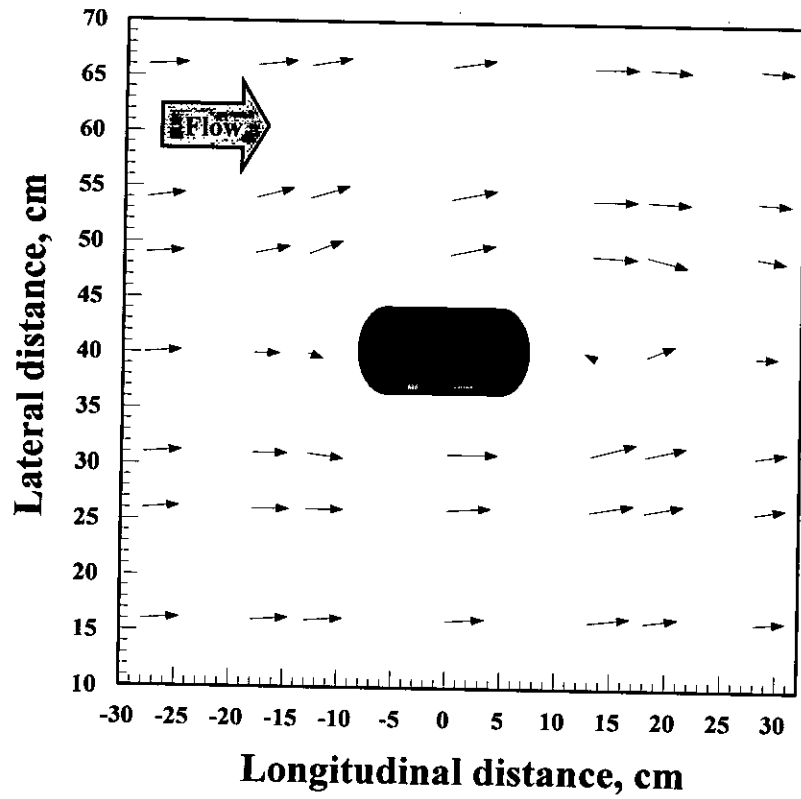


Figure C.9: Run 5-Bed material 1( $d_{50} = 0.75$  mm)-Round nose pier ( $l/b=2$ )- $Q=175$  l/s  
Floodplain

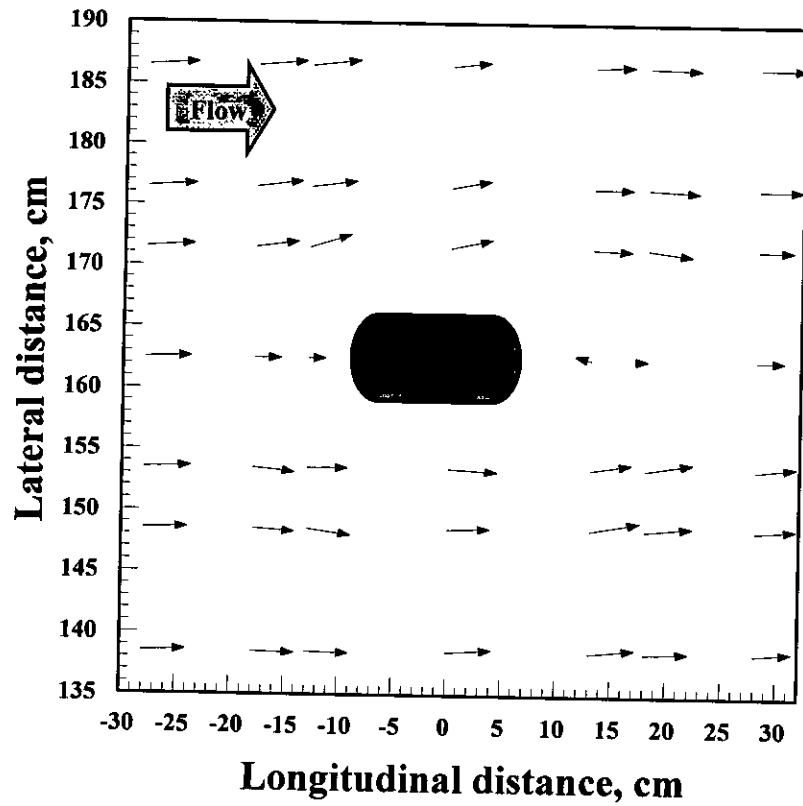


Figure C.10: Run 5-Bed material 1( $d_{50} = 0.75$  mm)-Round nose pier ( $l/b=2$ )- $Q=175$  l/s  
Main channel

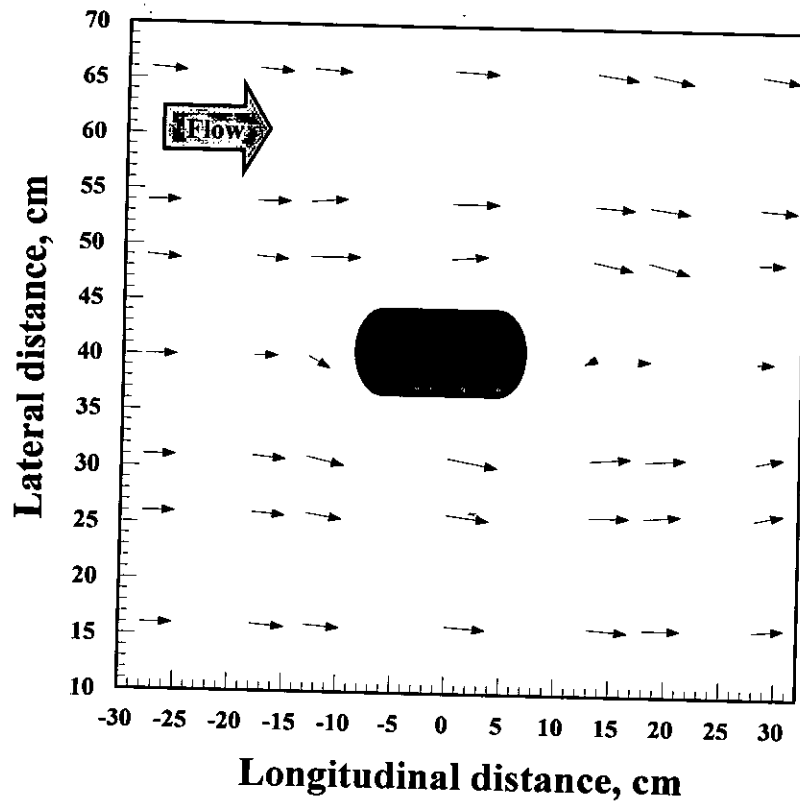


Figure C.11: Run 6-Bed material 1( $d_{50} = 0.75$  mm)-Round nose pier ( $l/b=2$ )- $Q=150$  l/s  
Floodplain

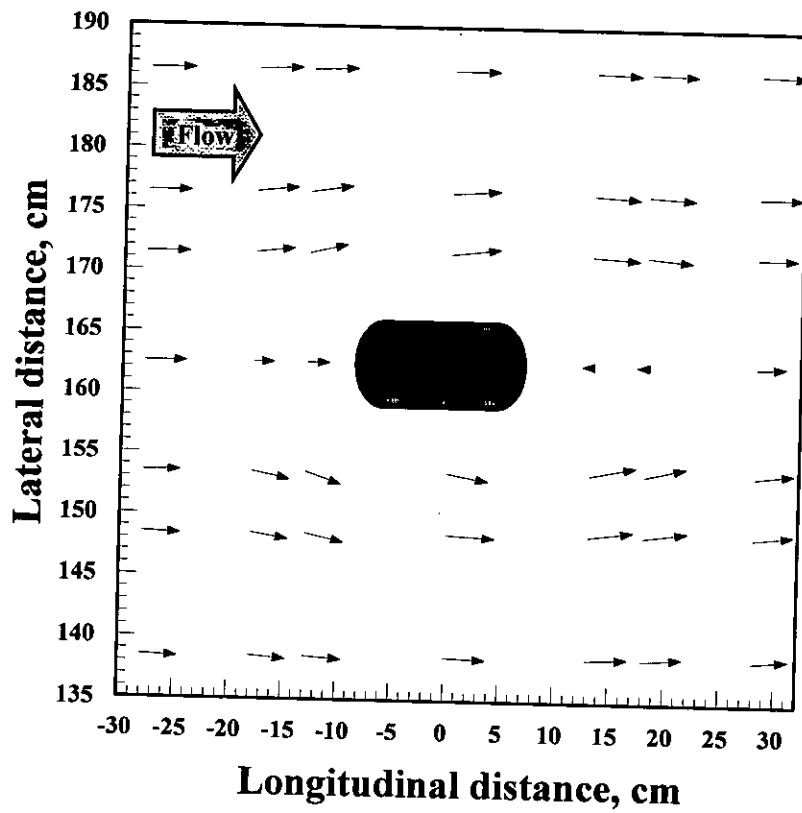


Figure C.12: Run 6-Bed material 1( $d_{50} = 0.75$  mm)-Round nose pier ( $l/b=2$ )- $Q=150$  l/s  
Main channel

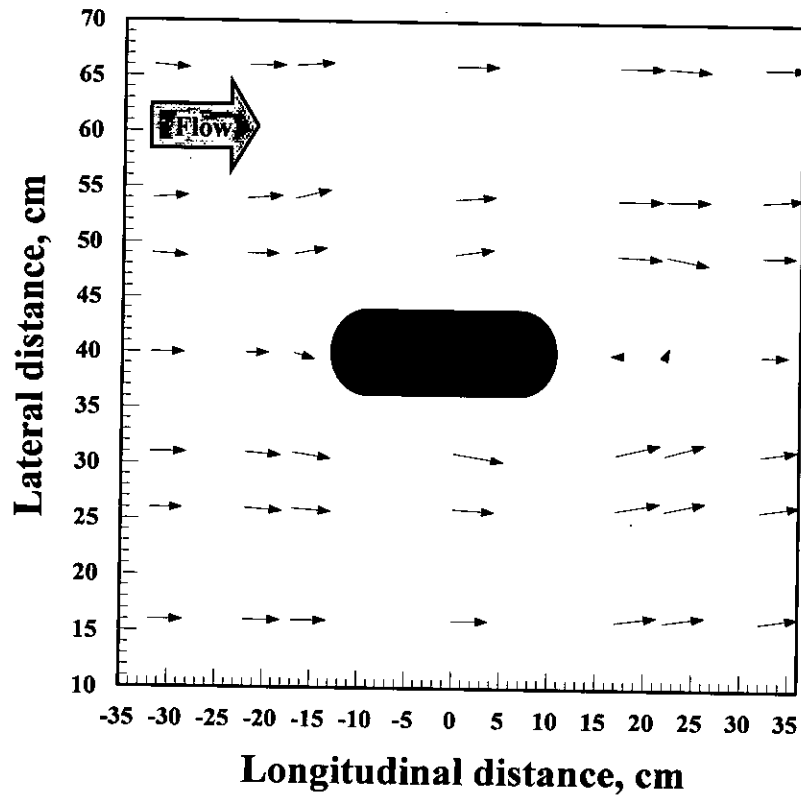


Figure C.13: Run 7-Bed material 1( $d_{50} = 0.75$  mm)-Round nose pier ( $l/b=3$ )- $Q=200$  l/s  
Floodplain

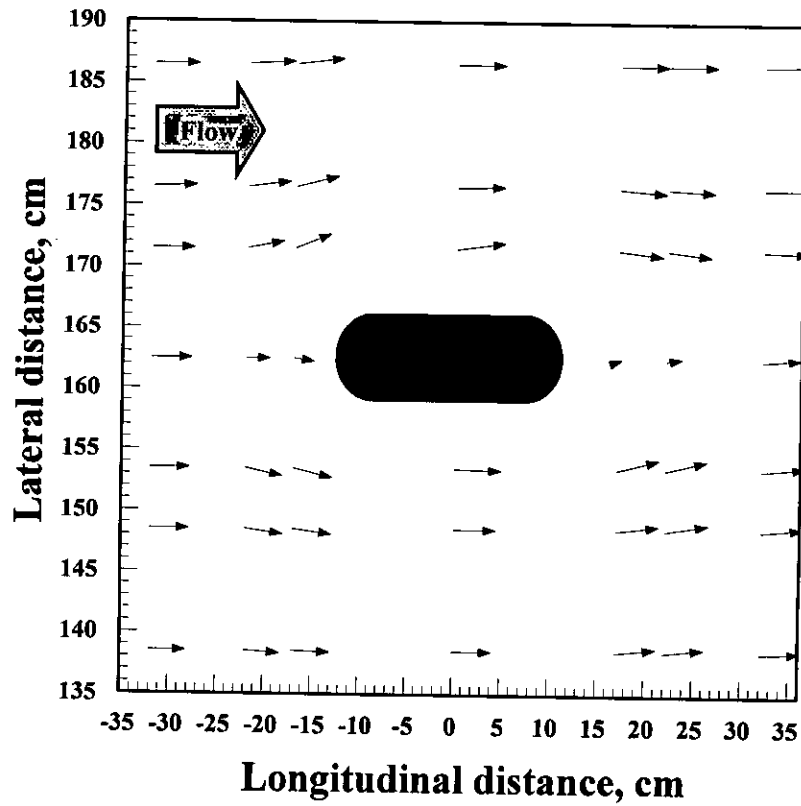


Figure C.14: Run 7-Bed material 1( $d_{50} = 0.75$  mm)-Round nose pier ( $l/b=3$ )- $Q=200$  l/s  
Main channel

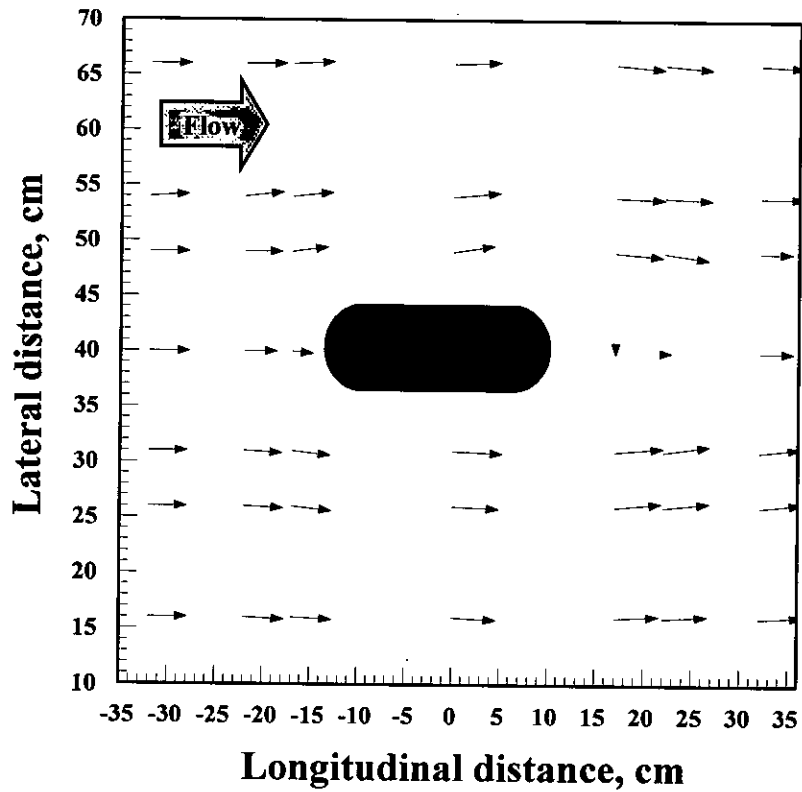


Figure C.15: Run 8-Bed material 1( $d_{50} = 0.75$  mm)-Round nose pier ( $l/b=3$ )- $Q=175$  l/s  
Floodplain

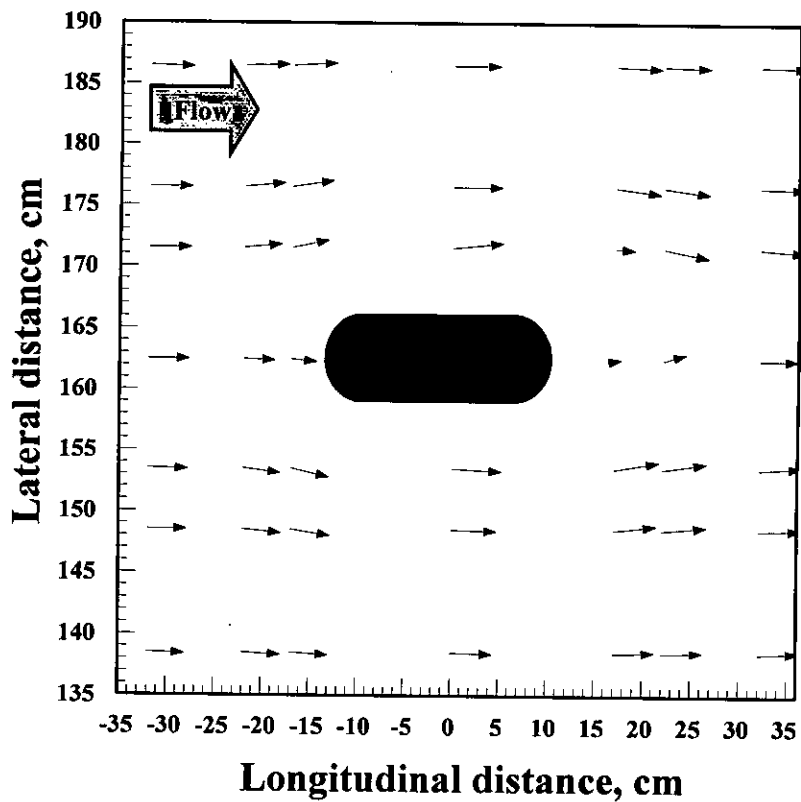


Figure C.16: Run 8-Bed material 1( $d_{50} = 0.75$  mm)-Round nose pier ( $l/b=3$ )- $Q=175$  l/s  
Main channel

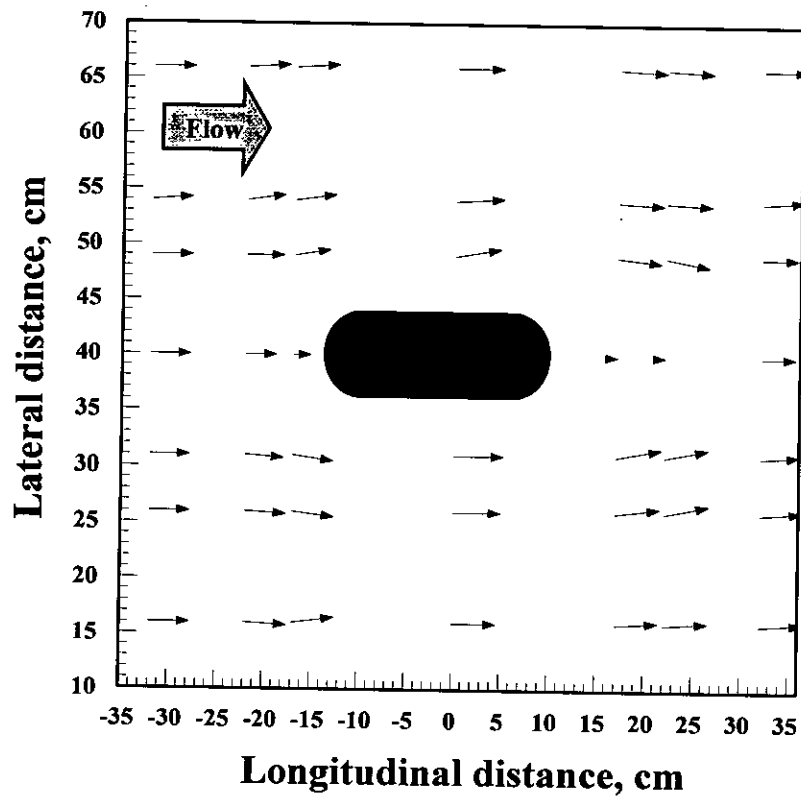


Figure C.17: Run 9-Bed material 1 ( $d_{50} = 0.75$  mm)-Round nose pier ( $l/b=3$ )- $Q=150$  l/s  
Floodplain

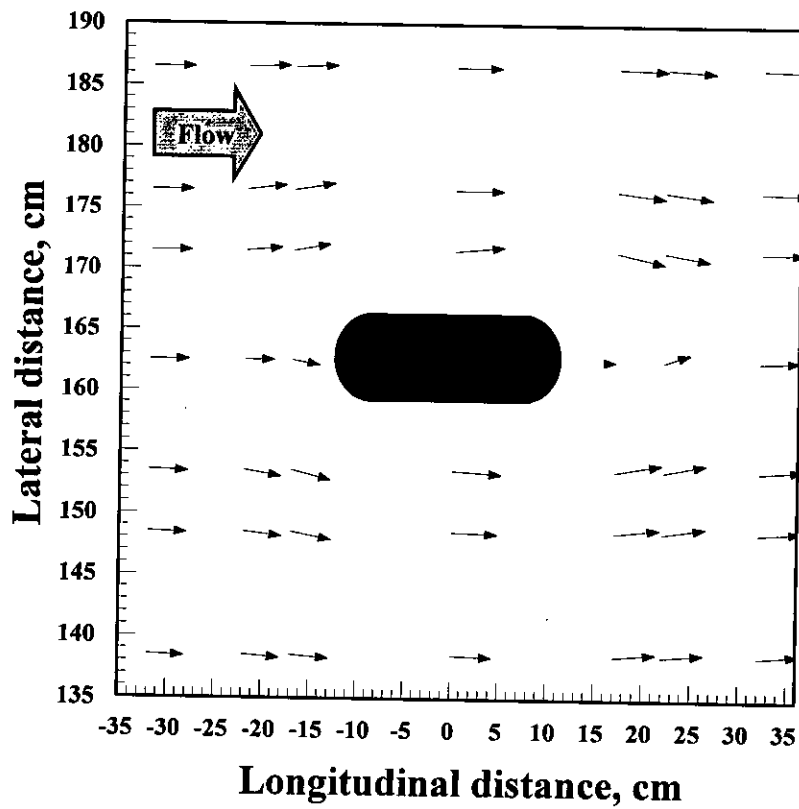


Figure C.18: Run 9-Bed material 1 ( $d_{50} = 0.75$  mm)-Round nose pier ( $l/b=3$ )- $Q=150$  l/s  
Main channel

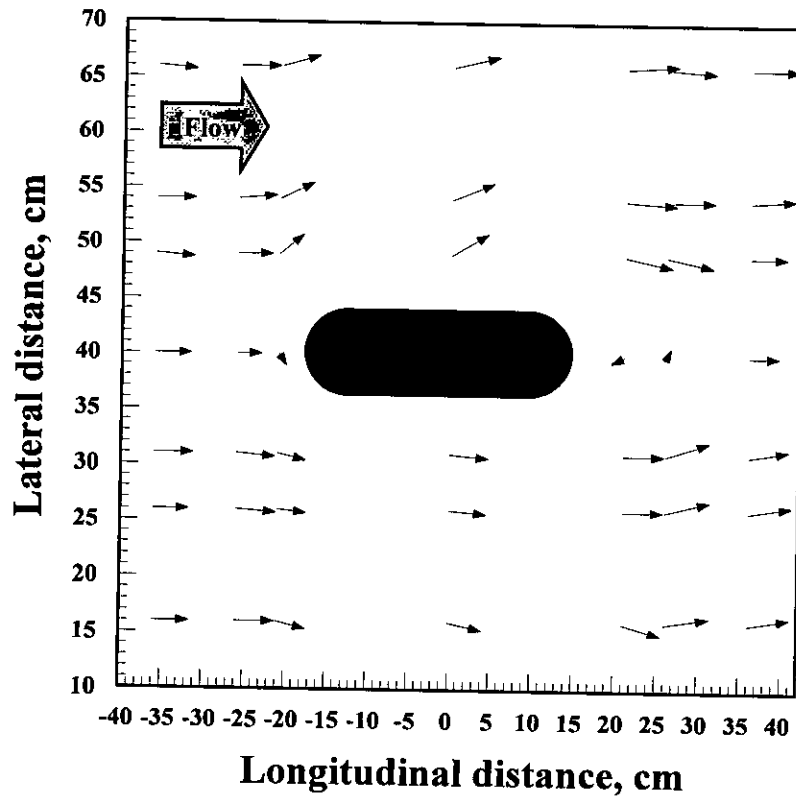


Figure C.19: Run 10-Bed material 1 ( $d_{50} = 0.75$  mm)-Round nose pier ( $l/b=4$ )- $Q=200$  l/s  
Floodplain

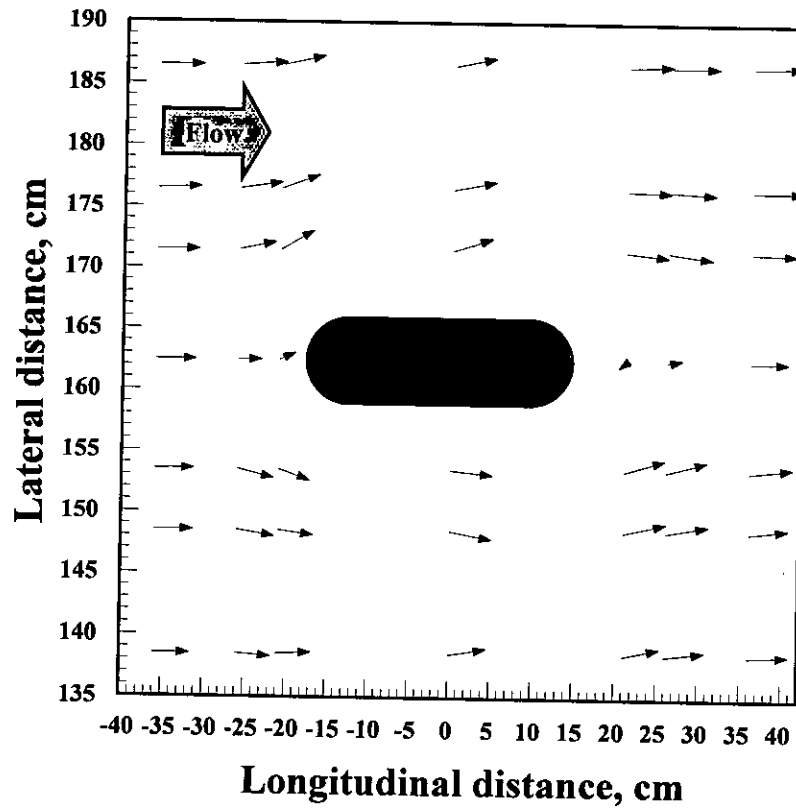


Figure C.20: Run 10-Bed material 1 ( $d_{50} = 0.75$  mm)-Round nose pier ( $l/b=4$ )- $Q=200$  l/s  
Main channel



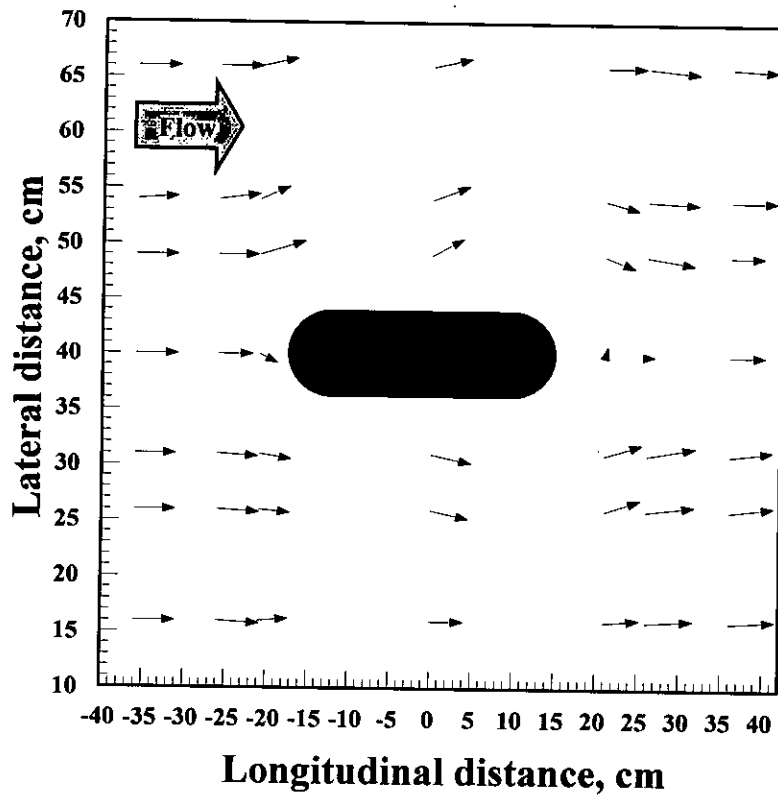


Figure C.21: Run 11-Bed material 1 ( $d_{50} = 0.75$  mm)-Round nose pier ( $l/b=4$ )- $Q=175$  l/s  
Floodplain

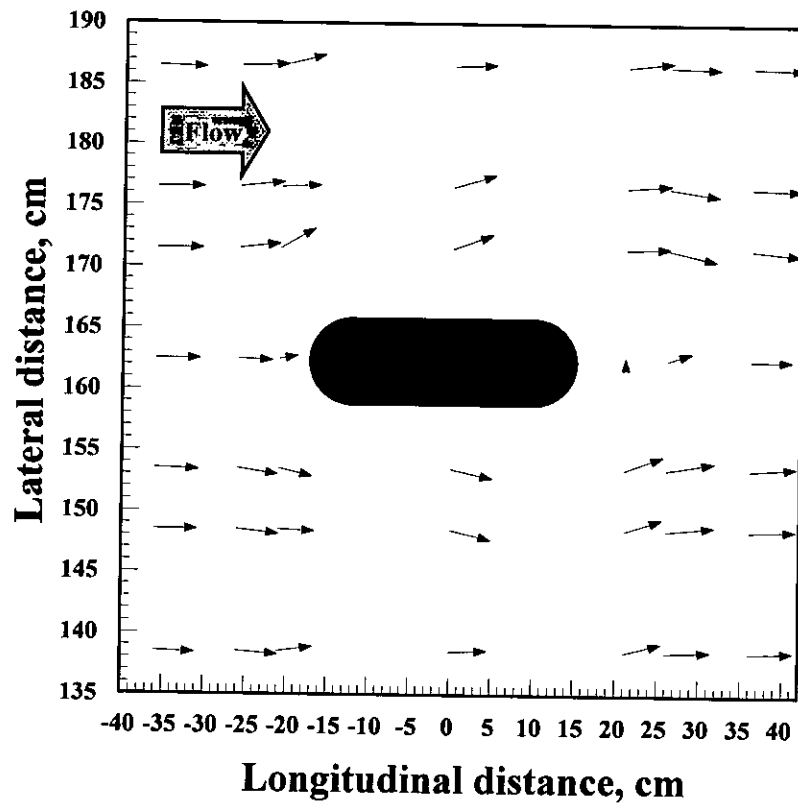


Figure C.22: Run 11-Bed material 1 ( $d_{50} = 0.75$  mm)-Round nose pier ( $l/b=4$ )- $Q=175$  l/s  
Main channel

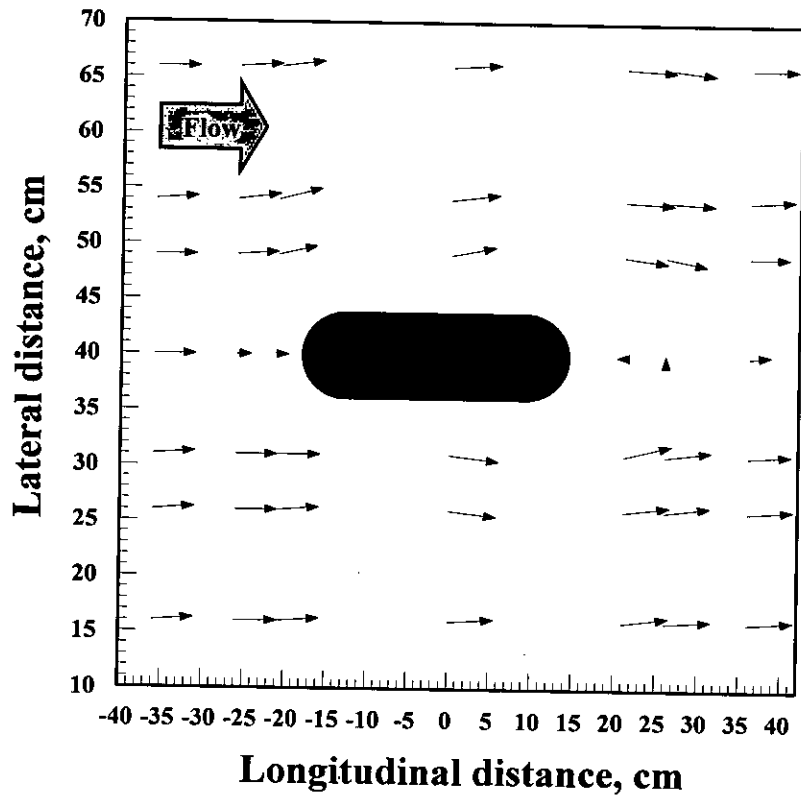


Figure C.23: Run 12-Bed material 1( $d_{50} = 0.75$  mm)-Round nose pier ( $l/b=4$ )- $Q=150$  l/s  
Floodplain

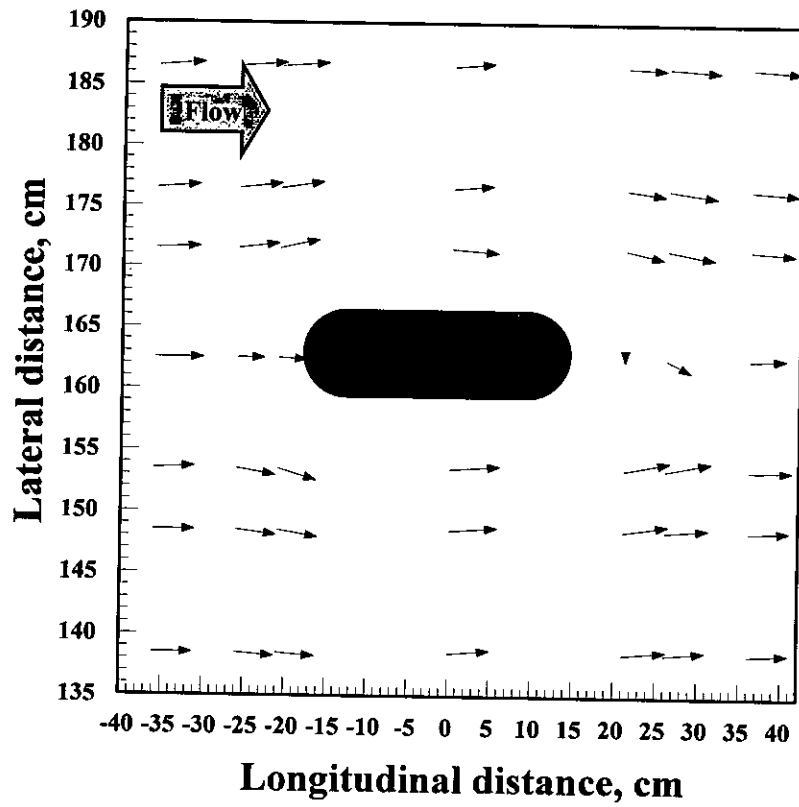


Figure C.24: Run 12-Bed material 1( $d_{50} = 0.75$  mm)-Round nose pier ( $l/b=4$ )- $Q=150$  l/s  
Main channel

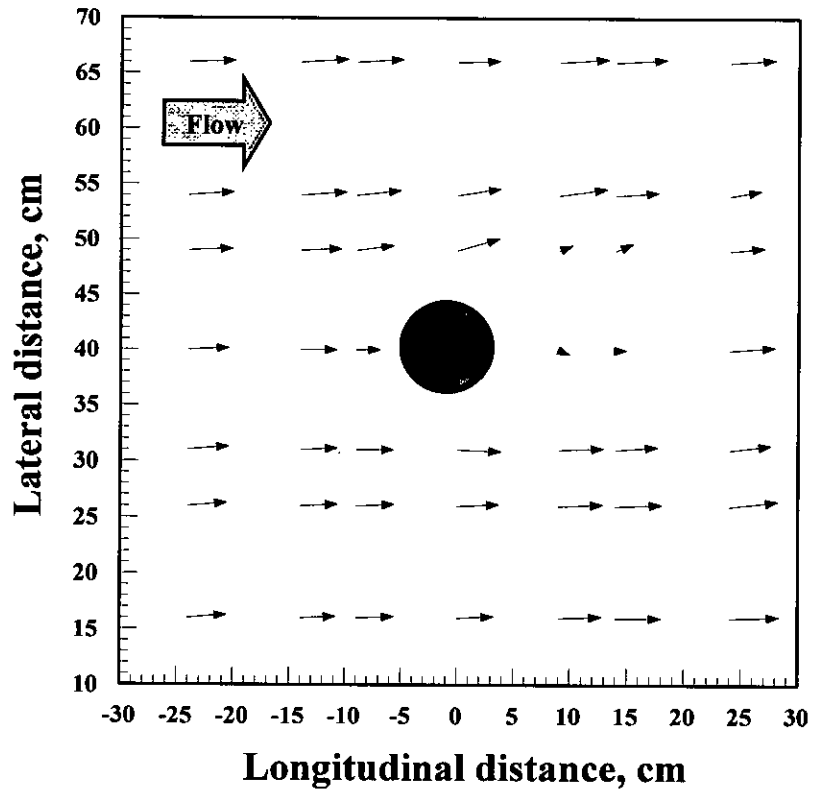


Figure C.25: Run 13-Bed material 2( $d_{50} = 0.18$  mm)-Circular pier ( $l/b=1$ )- $Q=200$  l/s  
Floodplain

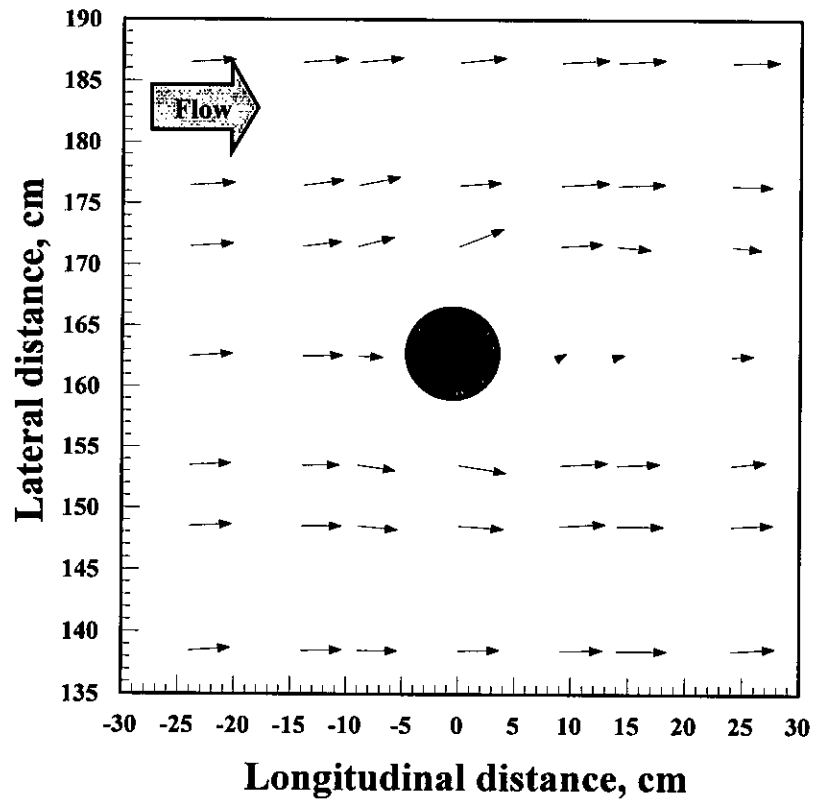


Figure C.26: Run 13-Bed material 2( $d_{50} = 0.18$  mm)-Circular pier ( $l/b=1$ )- $Q=200$  l/s  
Main channel

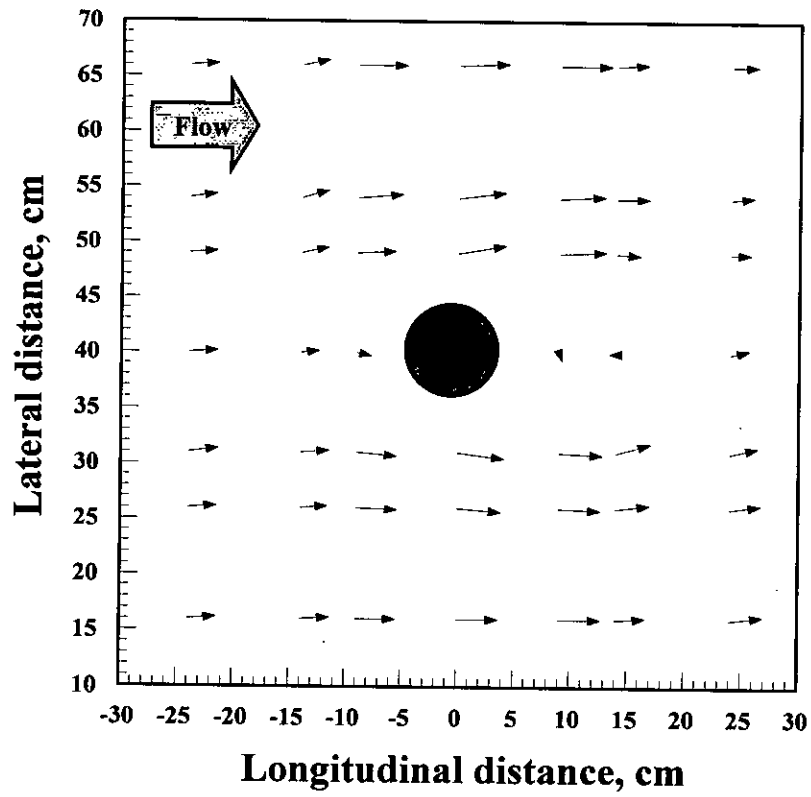


Figure C.27: Run 14-Bed material 2( $d_{50} = 0.18$  mm)-Circular pier ( $l/b=1$ )- $Q=175$  l/s  
Floodplain

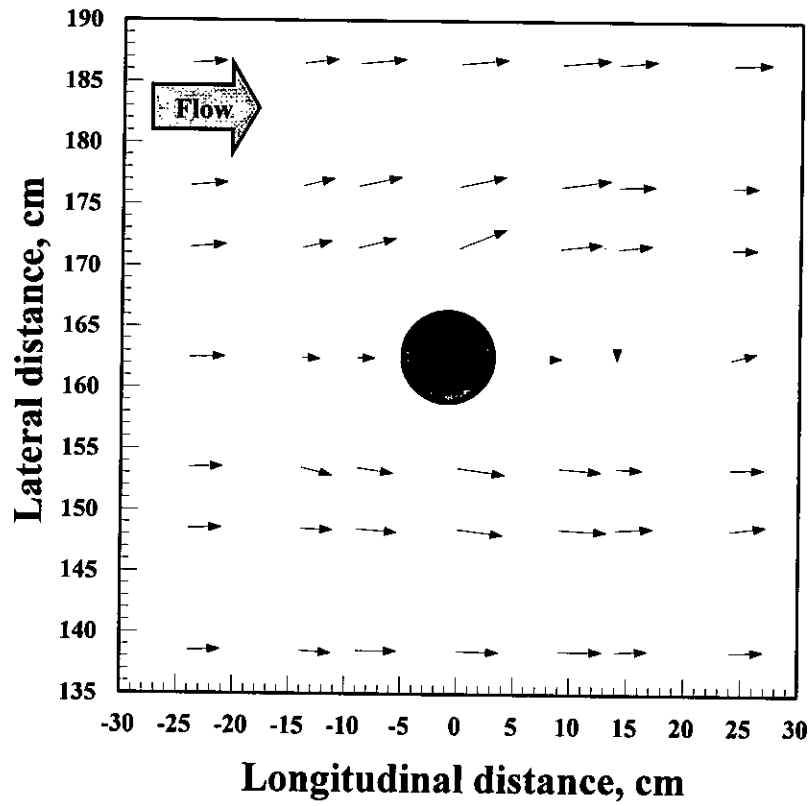


Figure C.28: Run 14-Bed material 2( $d_{50} = 0.18$  mm)-Circular pier ( $l/b=1$ )- $Q=175$  l/s  
Main channel

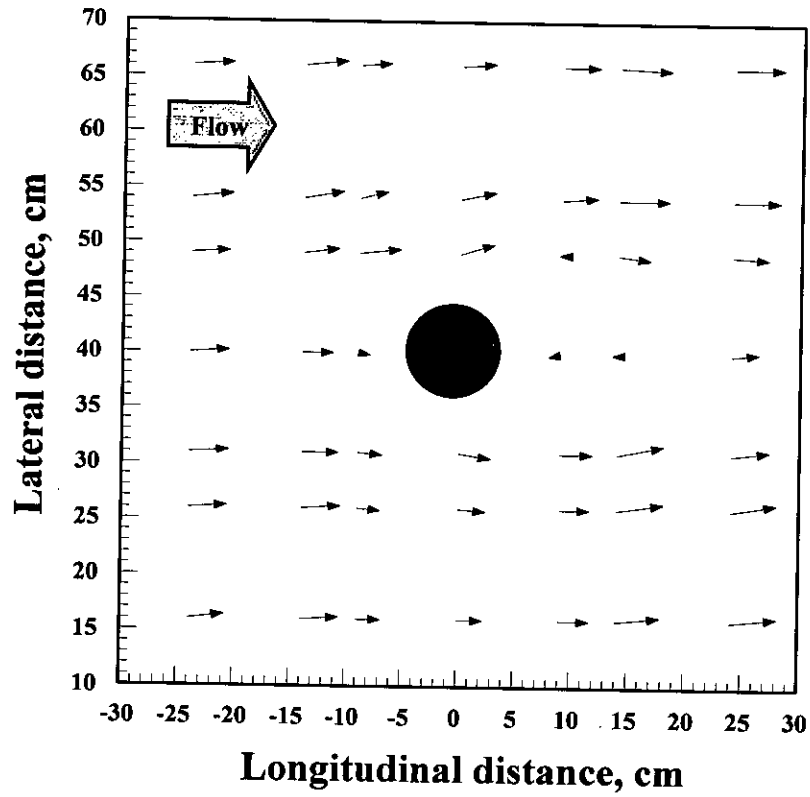


Figure C.29: Run 15-Bed material 2( $d_{50} = 0.18$  mm)-Circular pier ( $l/b=1$ )- $Q=150$  l/s Floodplain

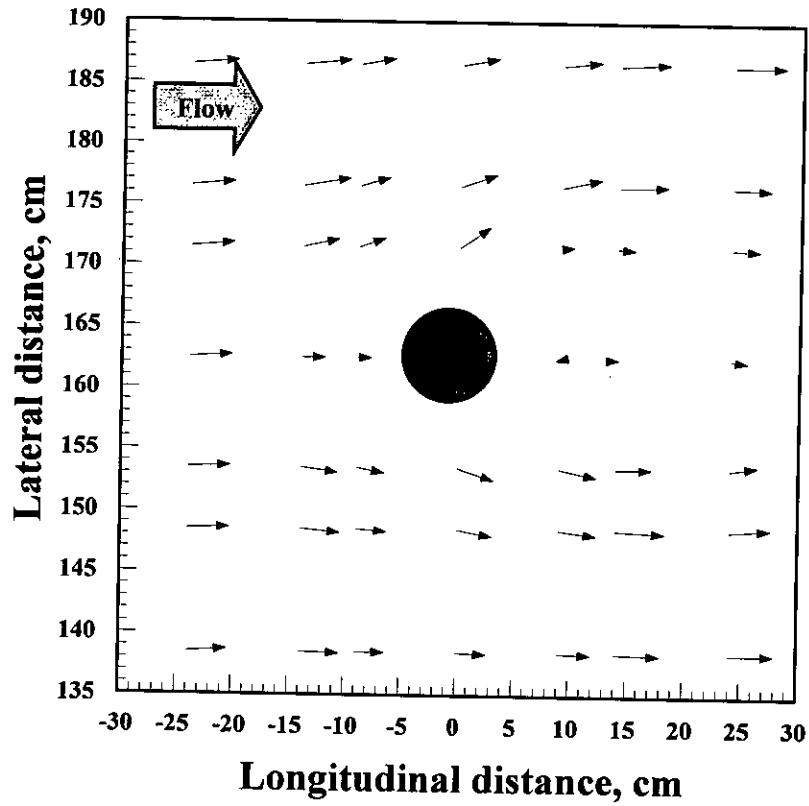


Figure C.30: Run 15-Bed material 2( $d_{50} = 0.18$  mm)-Circular pier ( $l/b=1$ )- $Q=150$  l/s Main channel

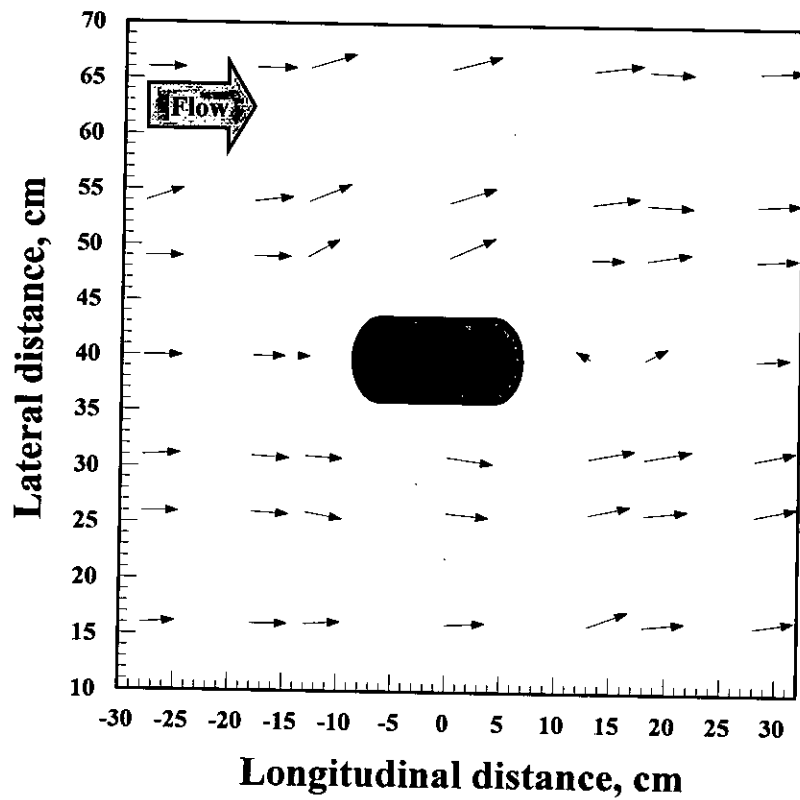


Figure C.31: Run 16-Bed material 2( $d_{50} = 0.18$  mm)-Round nose pier ( $l/b=2$ )- $Q=200$  l/s  
Floodplain

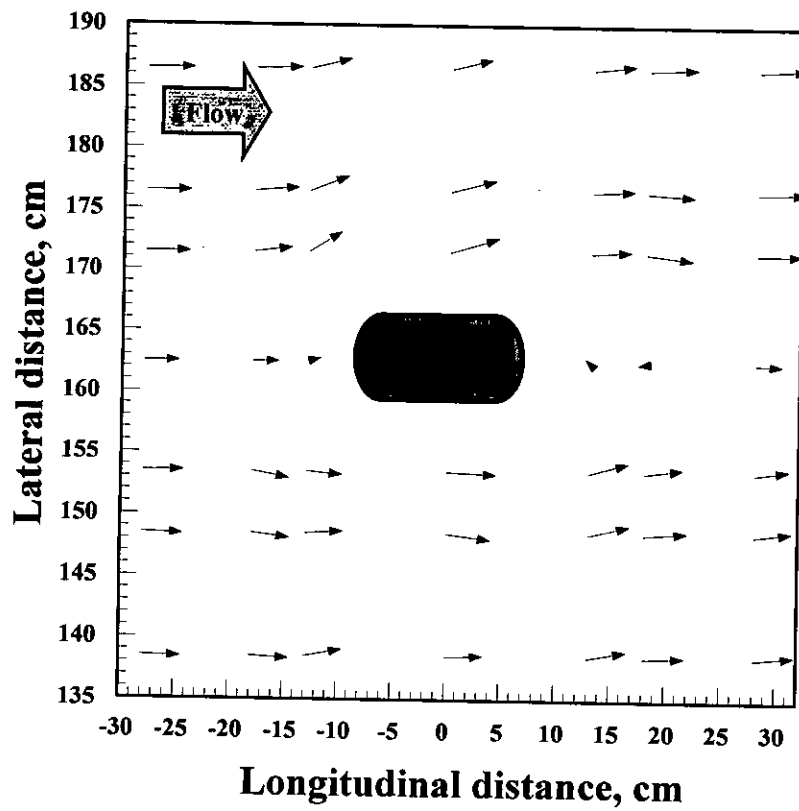


Figure C.32: Run 16-Bed material 2( $d_{50} = 0.18$  mm)-Round nose pier ( $l/b=2$ )- $Q=200$  l/s  
Main channel

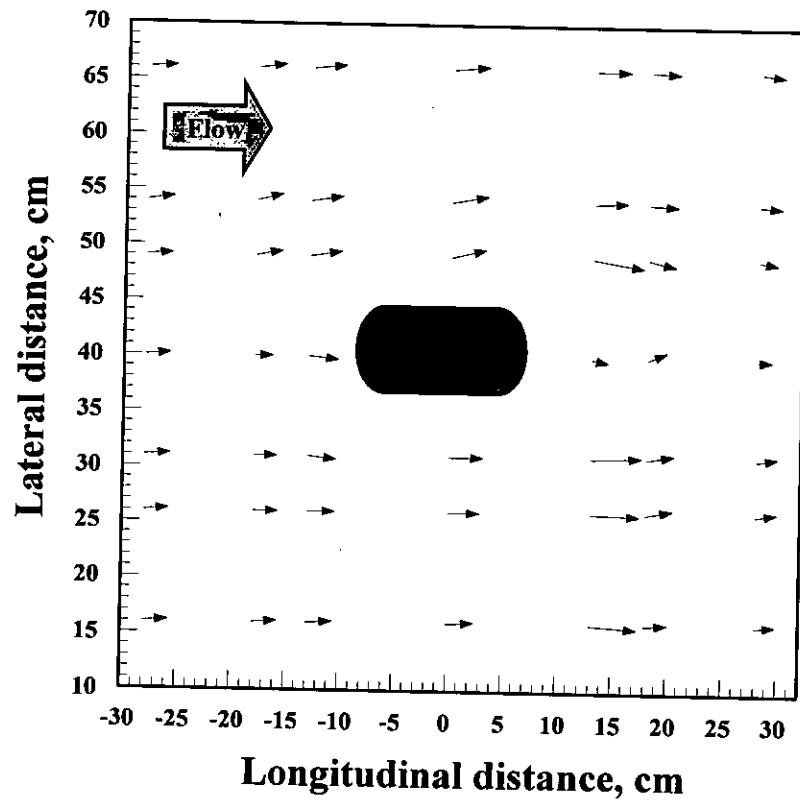


Figure C.33: Run 17-Bed material 2( $d_{50} = 0.18$  mm)-Round nose pier ( $l/b=2$ )- $Q=175$  l/s  
Floodplain

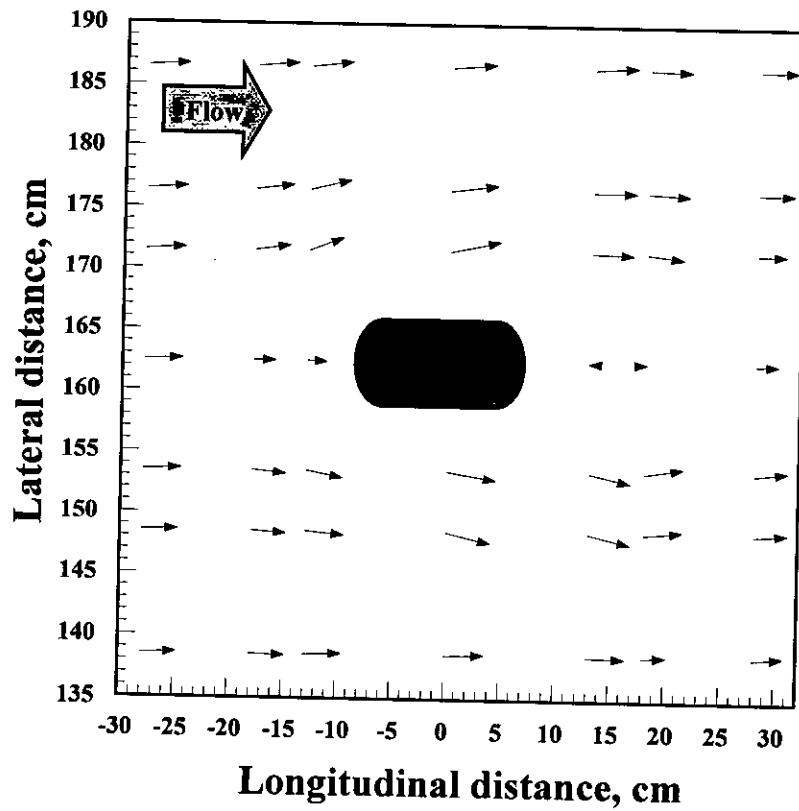


Figure C.34: Run 17-Bed material 2( $d_{50} = 0.18$  mm)-Round nose pier ( $l/b=2$ )- $Q=175$  l/s  
Main channel

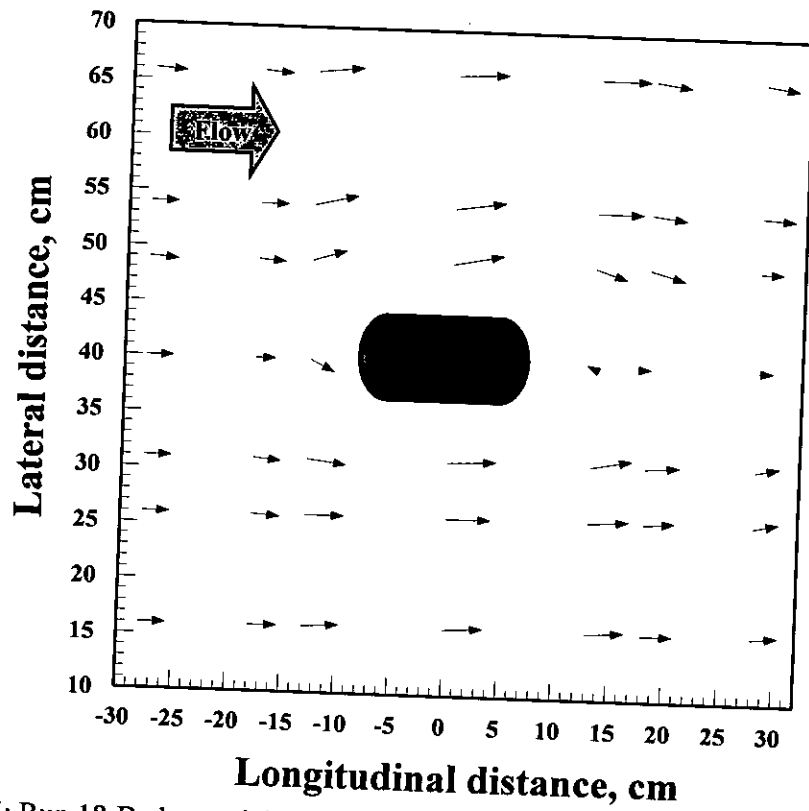


Figure C.35: Run 18-Bed material 2( $d_{50} = 0.18$  mm)-Round nose pier ( $l/b=2$ )- $Q=150$  l/s  
Floodplain

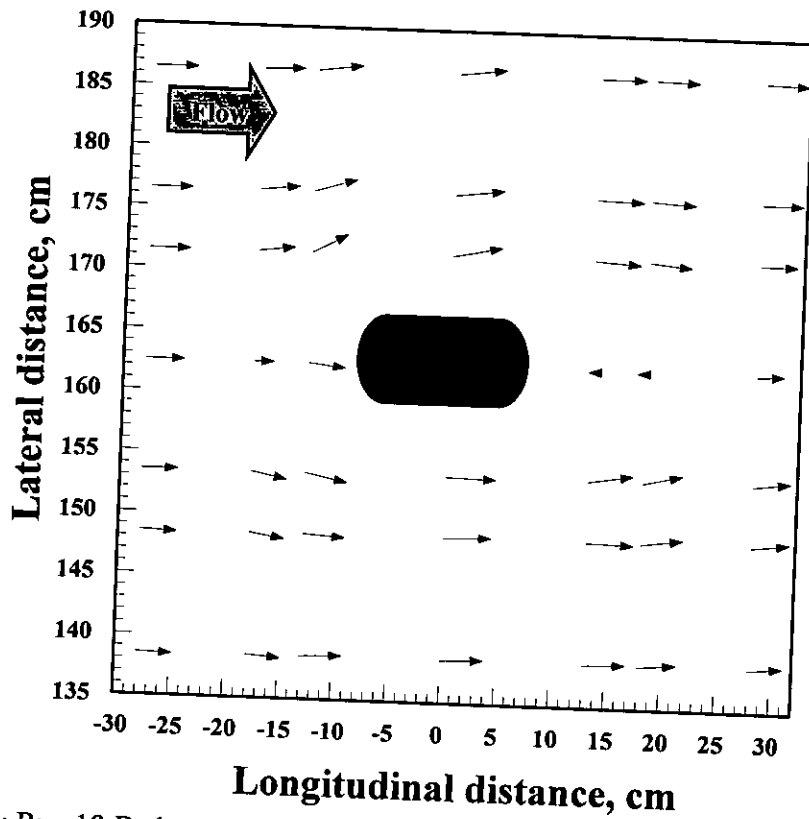


Figure C.36: Run 18-Bed material 2( $d_{50} = 0.18$  mm)-Round nose pier ( $l/b=2$ )- $Q=150$  l/s  
Main channel



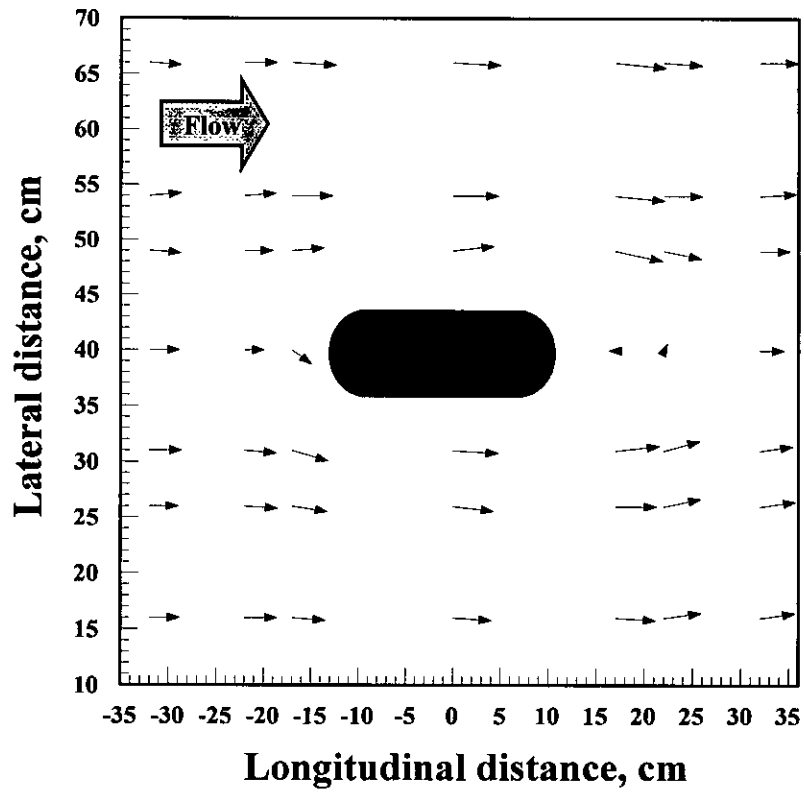


Figure C.37: Run 19-Bed material 2( $d_{50} = 0.18$  mm)-Round nose pier ( $l/b=3$ )- $Q=200$  l/s  
Floodplain

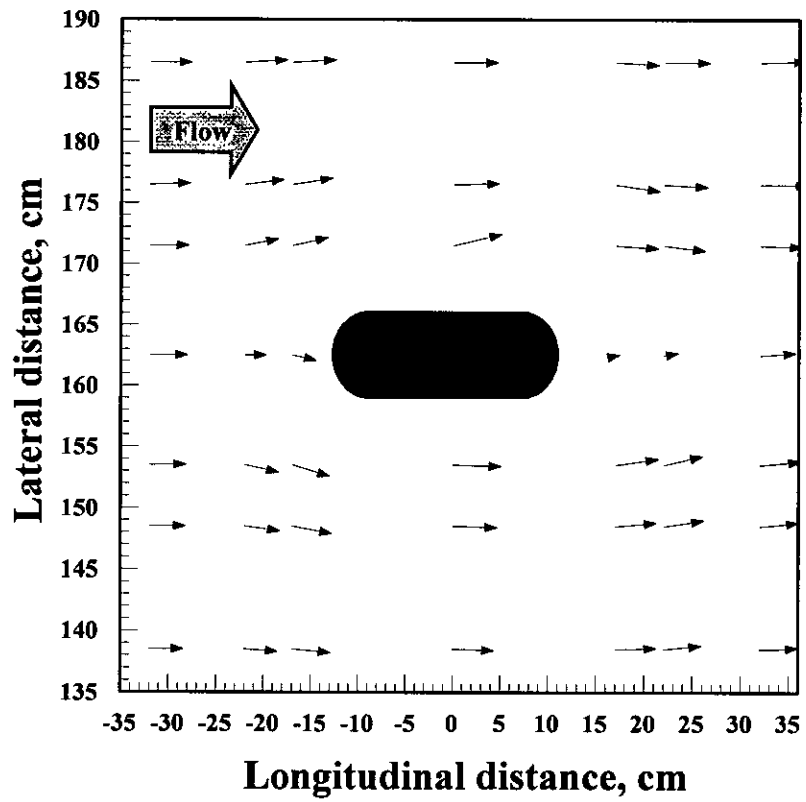


Figure C.38: Run 19-Bed material 2( $d_{50} = 0.18$  mm)-Round nose pier ( $l/b=3$ )- $Q=200$  l/s  
Main channel

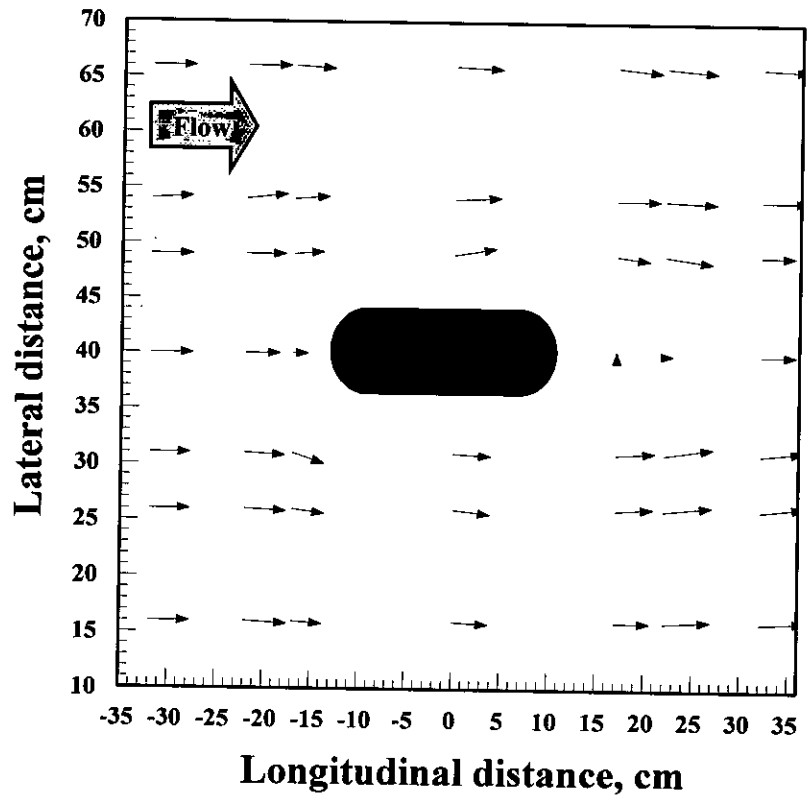


Figure C.39: Run 20-Bed material 2( $d_{50} = 0.18$  mm)-Round nose pier ( $l/b=3$ )- $Q=175$  l/s  
Floodplain

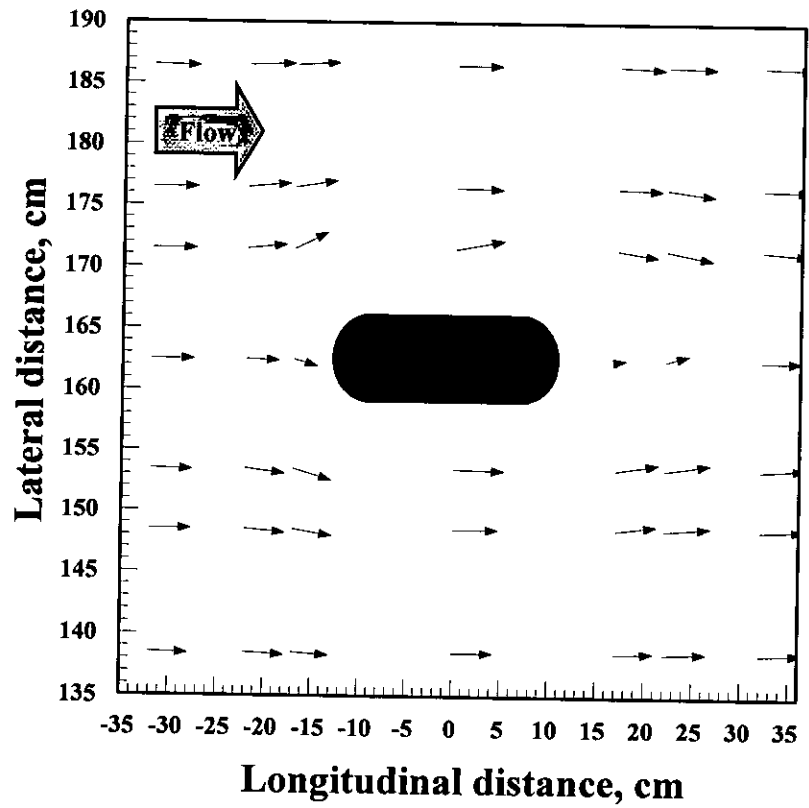


Figure C.40: Run 20-Bed material 2( $d_{50} = 0.18$  mm)-Round nose pier ( $l/b=3$ )- $Q=175$  l/s  
Main channel

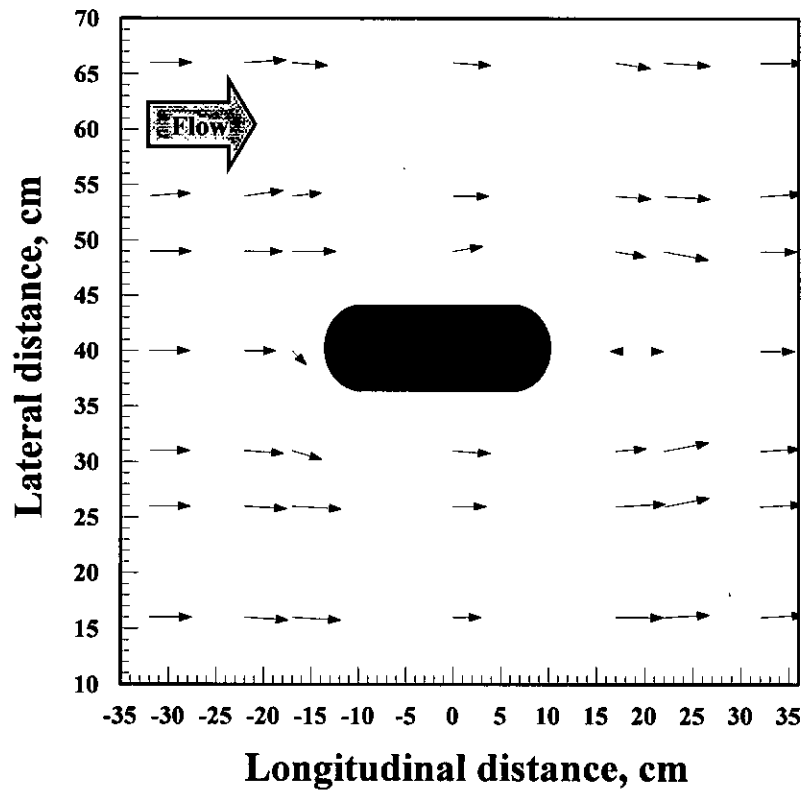


Figure C.41: Run 21-Bed material 2( $d_{50} = 0.18$  mm)-Round nose pier ( $l/b=3$ )- $Q=150$  l/s  
Floodplain

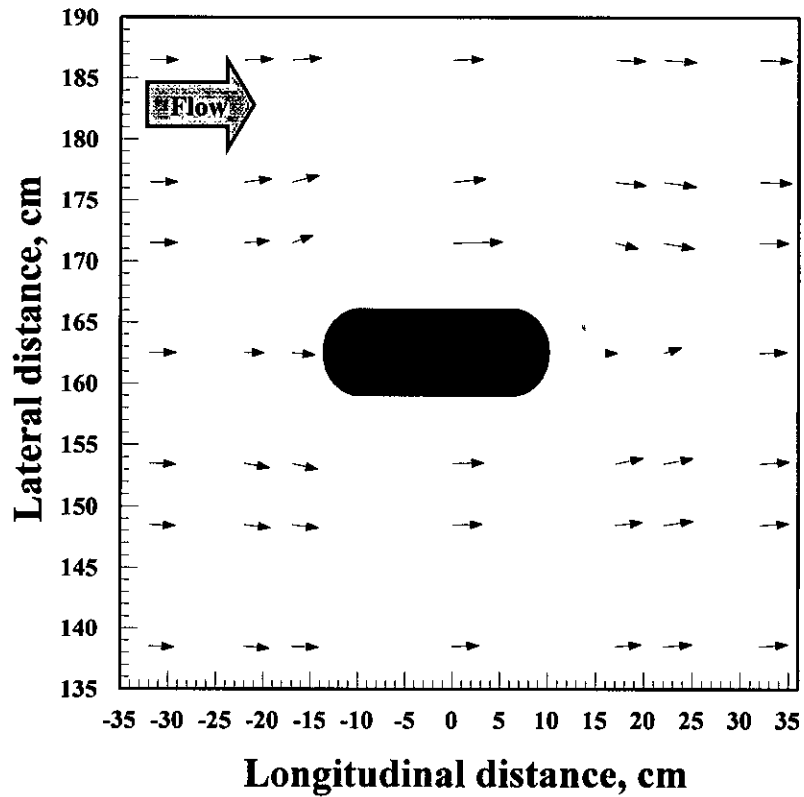


Figure C.42: Run 21-Bed material 2( $d_{50} = 0.18$  mm)-Round nose pier ( $l/b=3$ )- $Q=150$  l/s  
Main channel

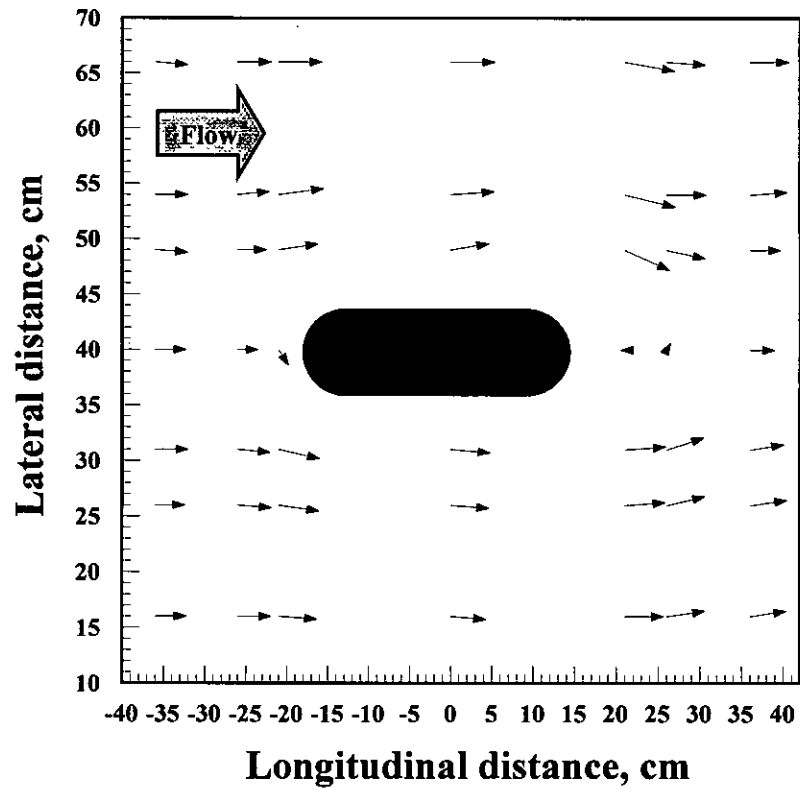


Figure C.43: Run 22-Bed material 2( $d_{50} = 0.18$  mm)-Round nose pier ( $l/b=4$ )- $Q=200$  l/s  
Floodplain

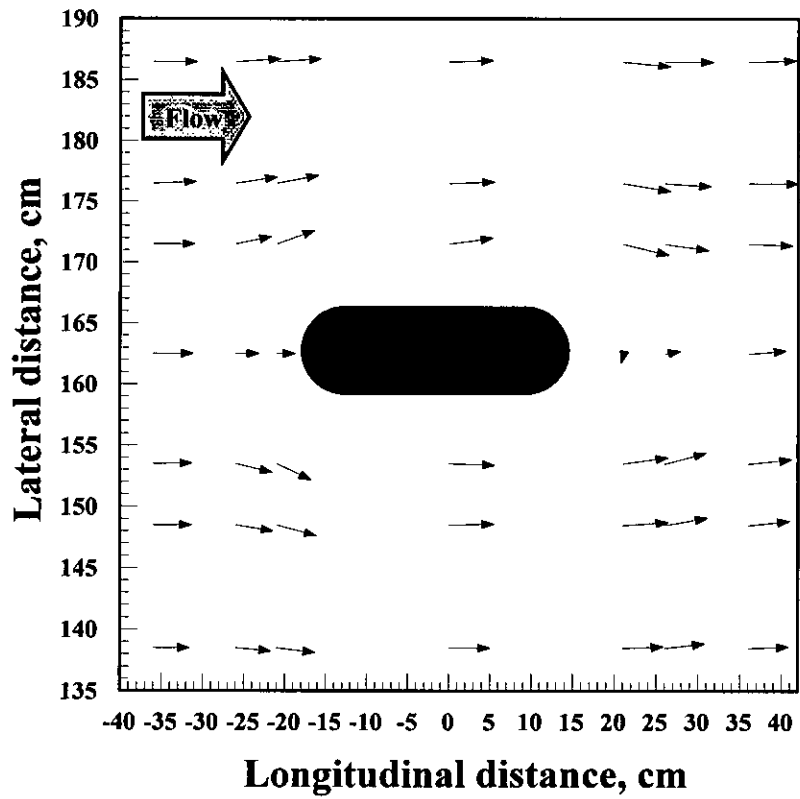


Figure C.44: Run 22-Bed material 2( $d_{50} = 0.18$  mm)-Round nose pier ( $l/b=4$ )- $Q=200$  l/s  
Main channel

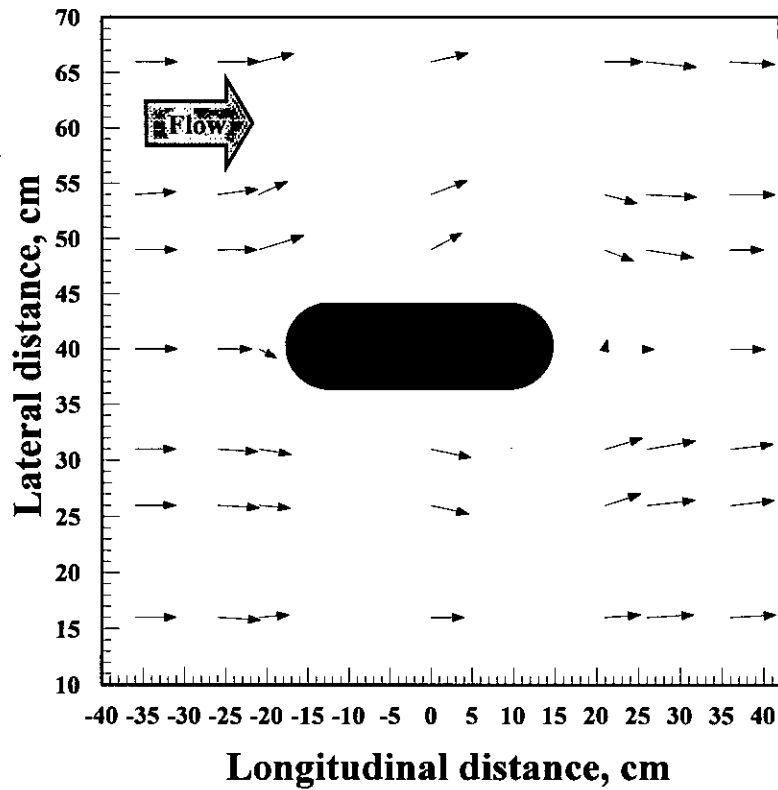


Figure C.45: Run 23-Bed material 2( $d_{50} = 0.18$  mm)-Round nose pier ( $l/b=4$ )- $Q=175$  l/s  
Floodplain

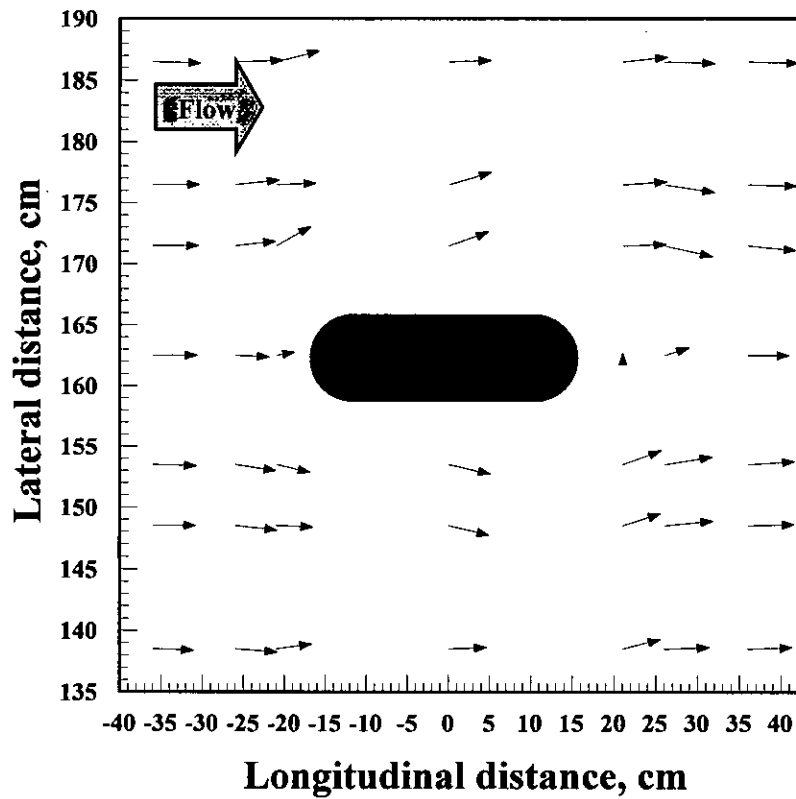


Figure C.46: Run 23-Bed material 2( $d_{50} = 0.18$  mm)-Round nose pier ( $l/b=4$ )- $Q=175$  l/s  
Main channel

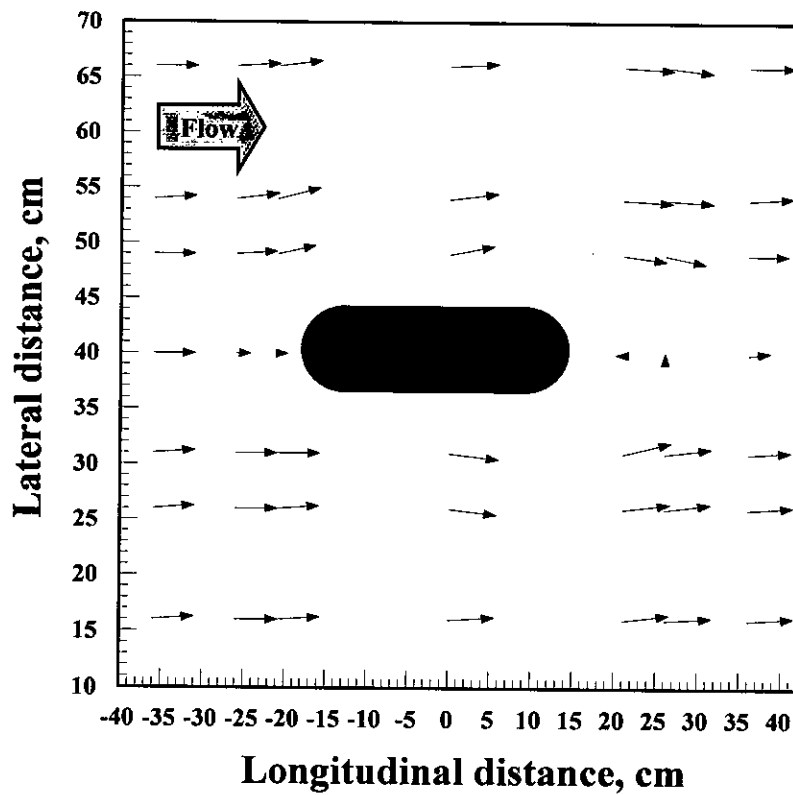


Figure C.47: Run 24-Bed material 2( $d_{50} = 0.18$  mm)-Round nose pier ( $l/b=4$ )- $Q=150$  l/s Floodplain

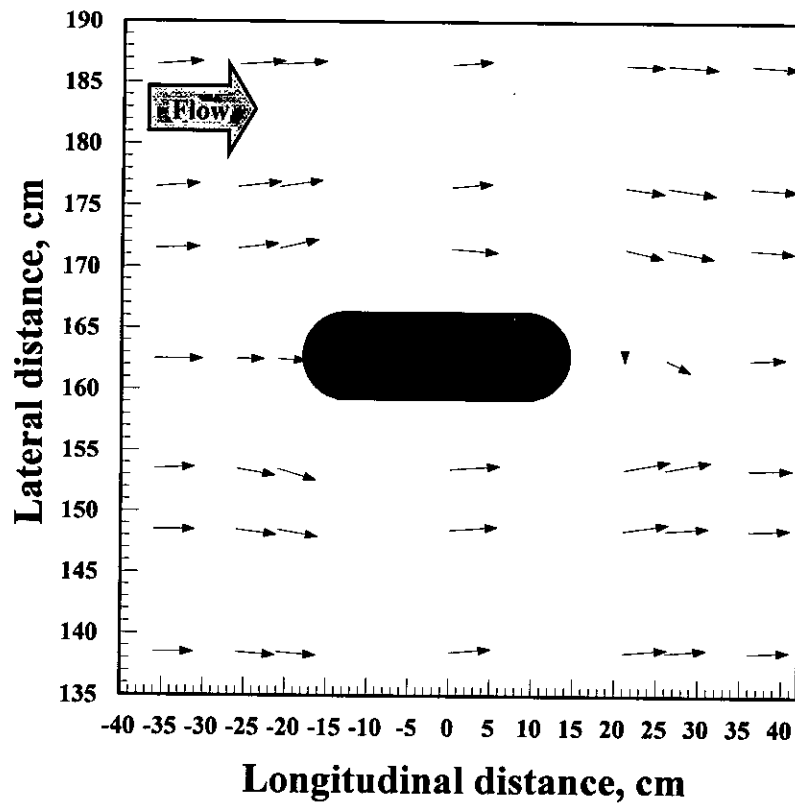


Figure C.48: Run 24-Bed material 2( $d_{50} = 0.18$  mm)-Round nose pier ( $l/b=4$ )- $Q=150$  l/s Main channel

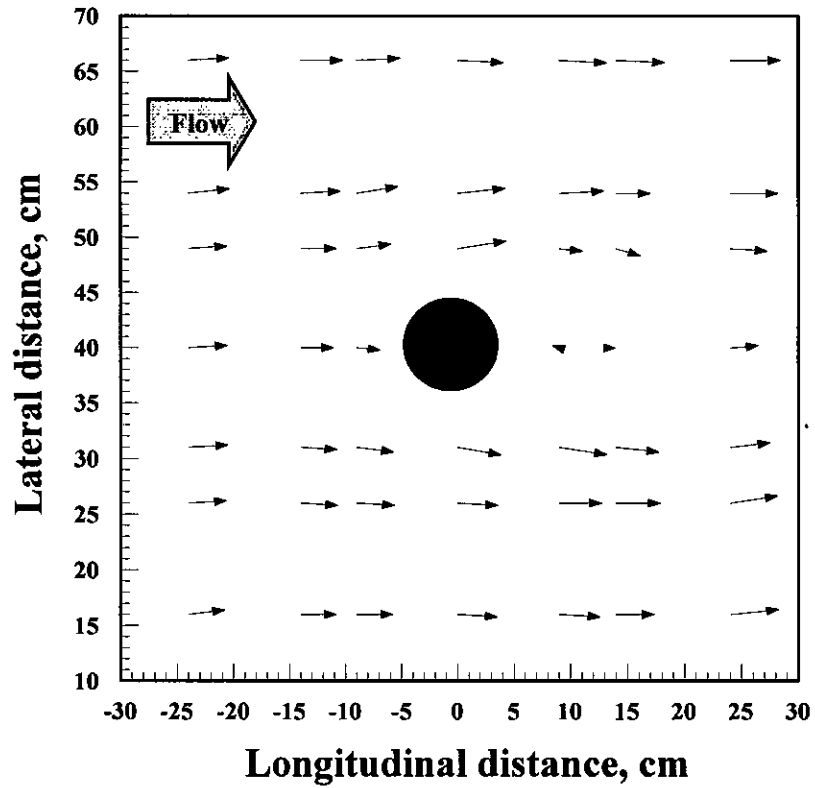


Figure C.49: Run 25-Bed material 3( $d_{50} = 0.12$  mm)-Circular pier ( $l/b=1$ )- $Q=200$  l/s  
Floodplain

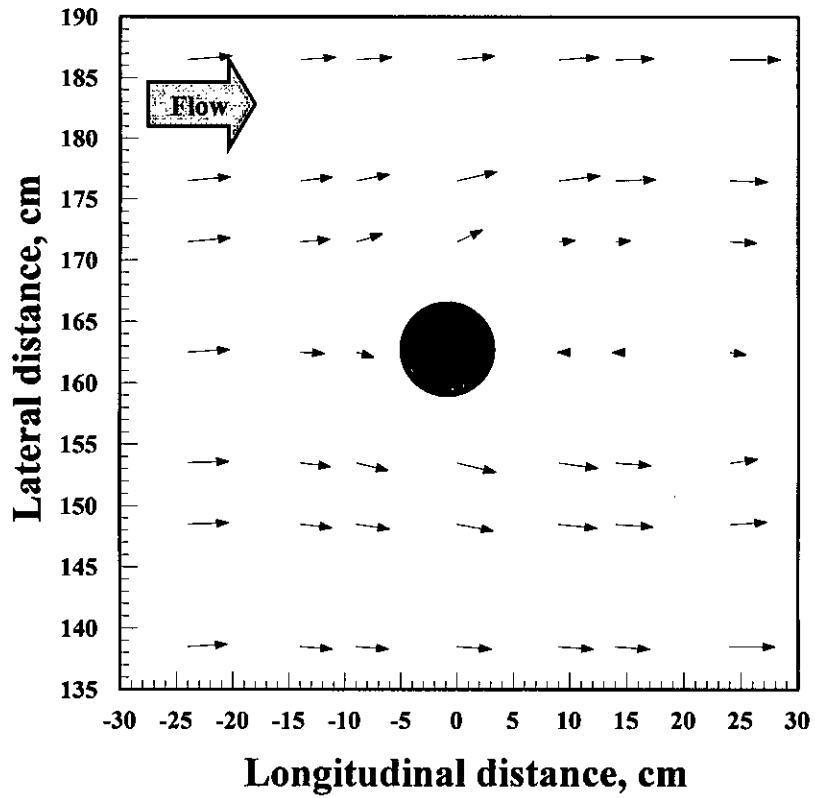


Figure C.50: Run 25-Bed material 3( $d_{50} = 0.12$  mm)-Circular pier ( $l/b=1$ )- $Q=200$  l/s  
Main channel

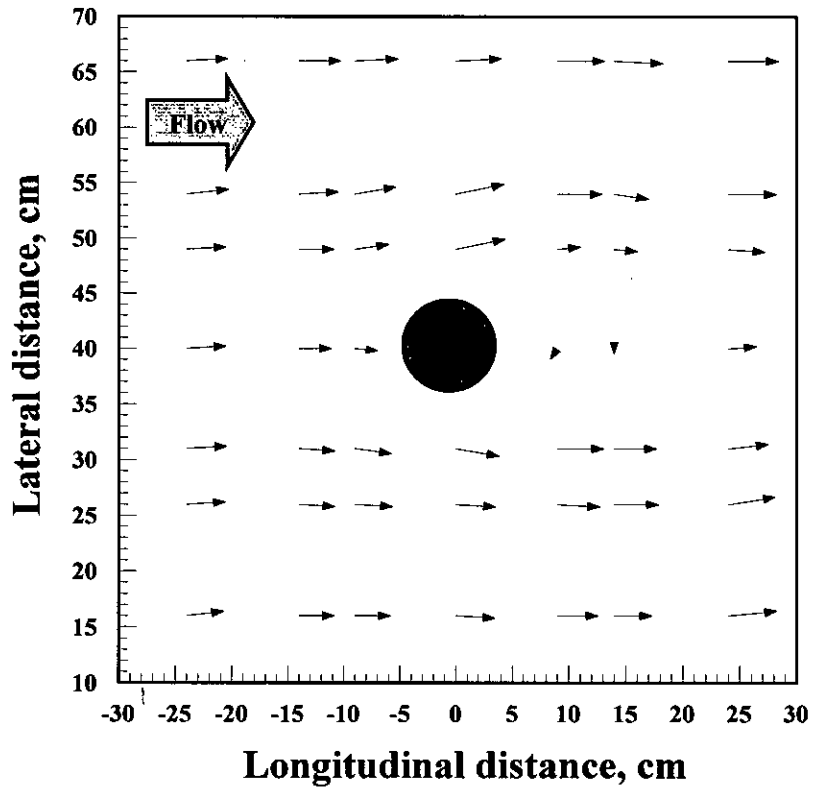


Figure C.51: Run 26-Bed material 3( $d_{50} = 0.12$  mm)-Circular pier ( $l/b=1$ )- $Q=175$  l/s  
Floodplain

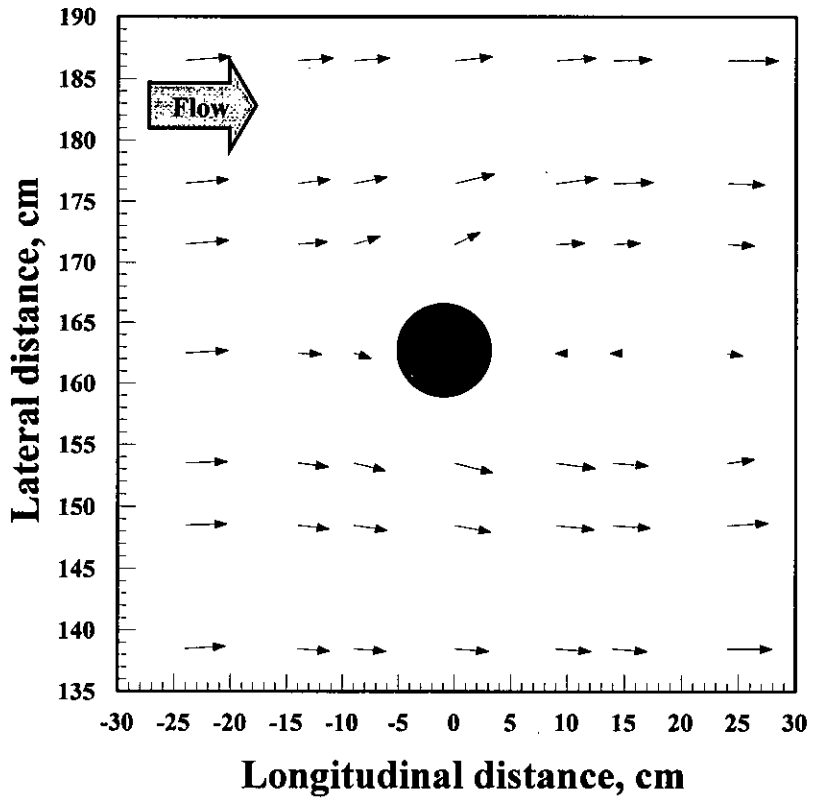


Figure C.52: Run 26-Bed material 3( $d_{50} = 0.12$  mm)-Circular pier ( $l/b=1$ )- $Q=175$  l/s  
Main channel



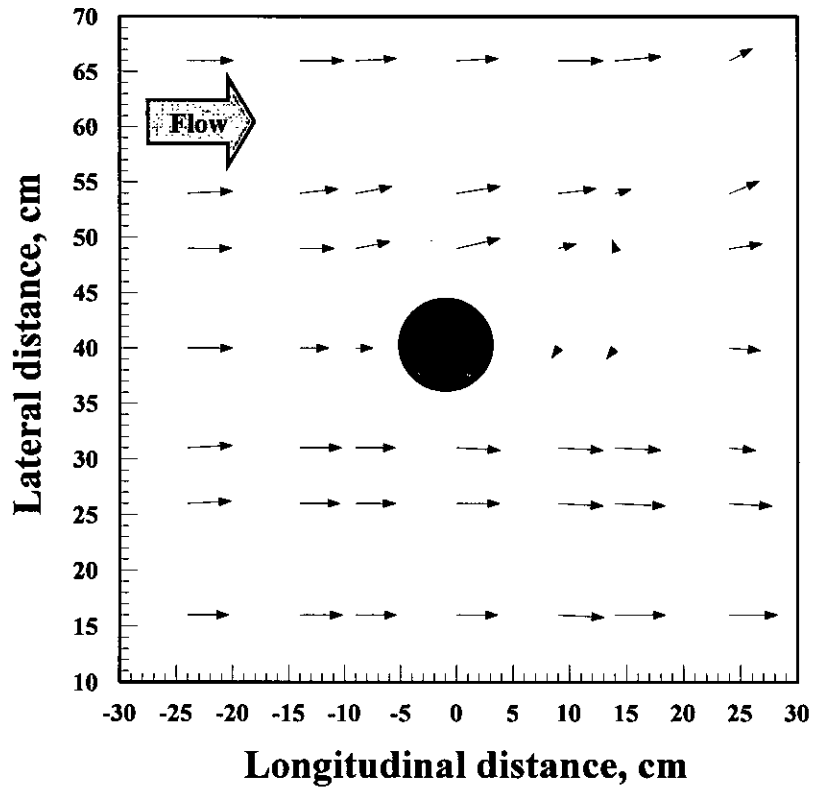


Figure C.53: Run 27-Bed material 3( $d_{50} = 0.12$  mm)-Circular pier ( $l/b=1$ )- $Q=150$  l/s  
Floodplain

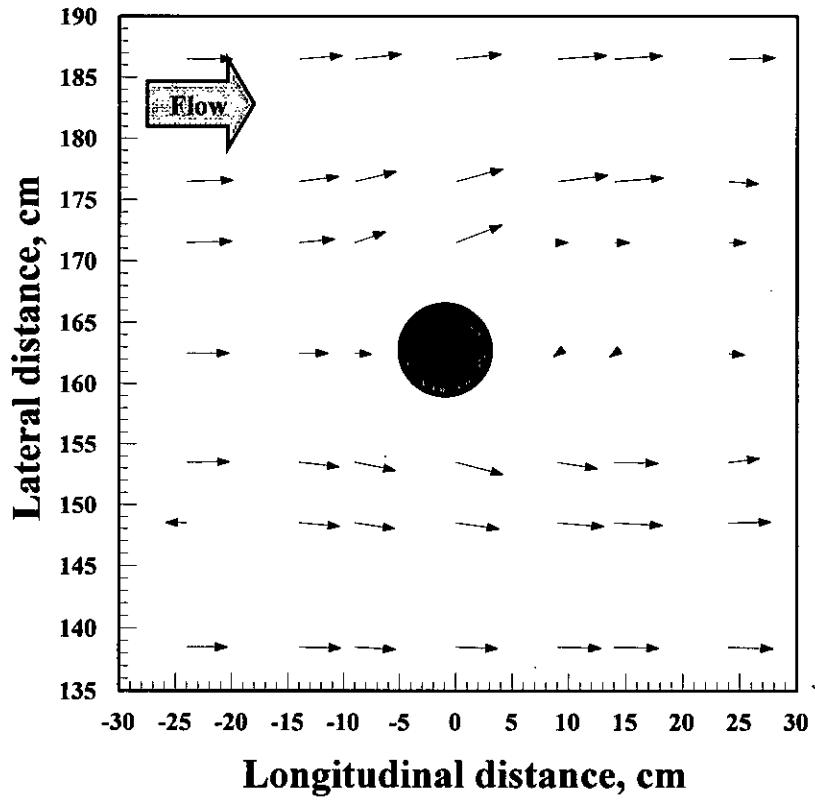


Figure C.54: Run 27-Bed material 3( $d_{50} = 0.12$  mm)-Circular pier ( $l/b=1$ )- $Q=150$  l/s  
Main channel

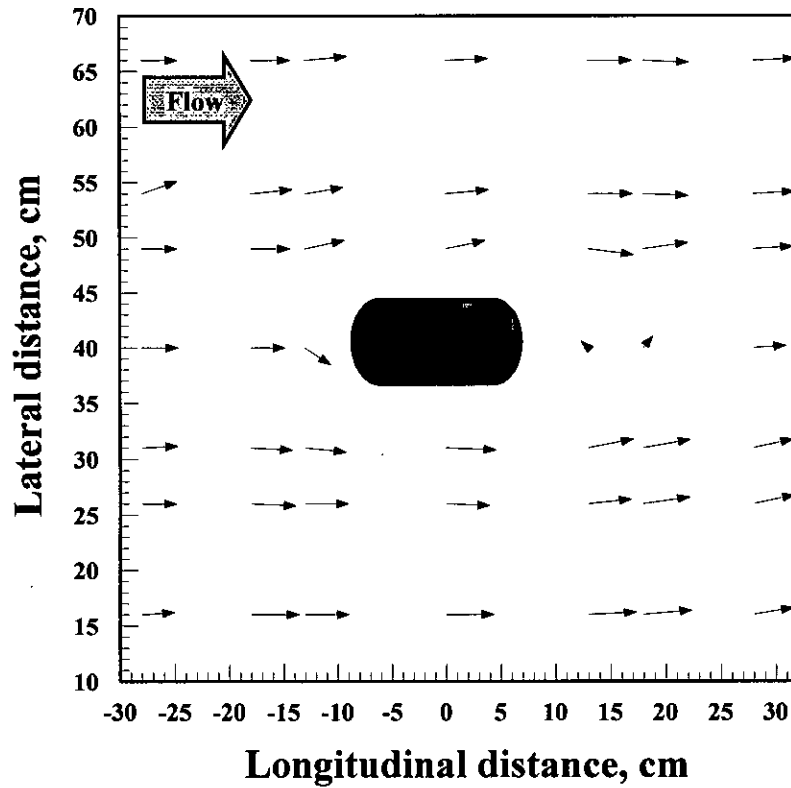


Figure C.55: Run 28-Bed material 3( $d_{50} = 0.12$  mm)-Round nose pier ( $l/b=2$ )- $Q=200$  l/s  
Floodplain

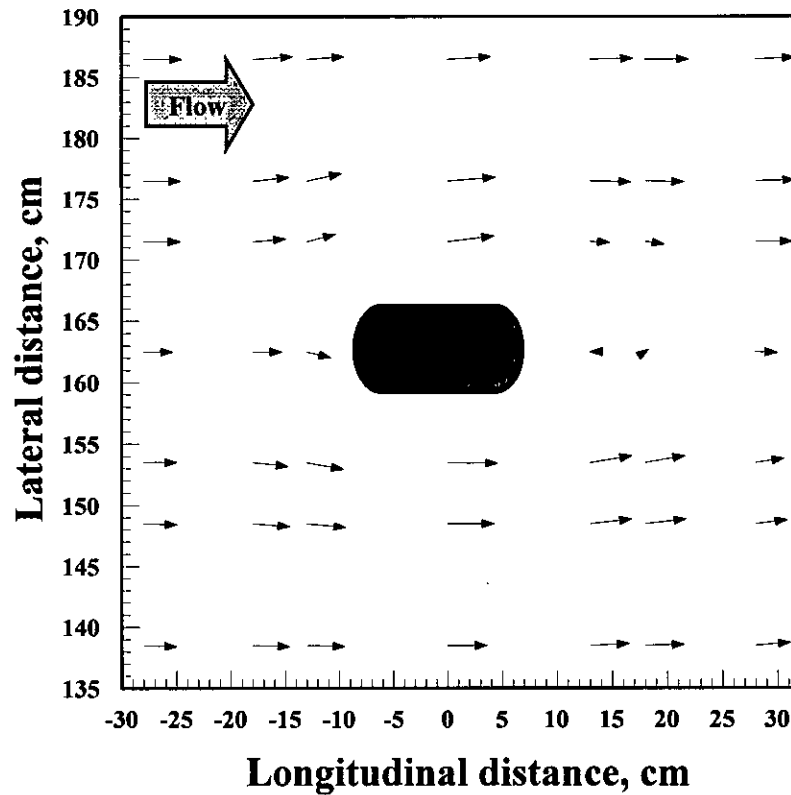


Figure C.56: Run 28-Bed material 3( $d_{50} = 0.12$  mm)-Round nose pier ( $l/b=2$ )- $Q=200$  l/s  
Main channel

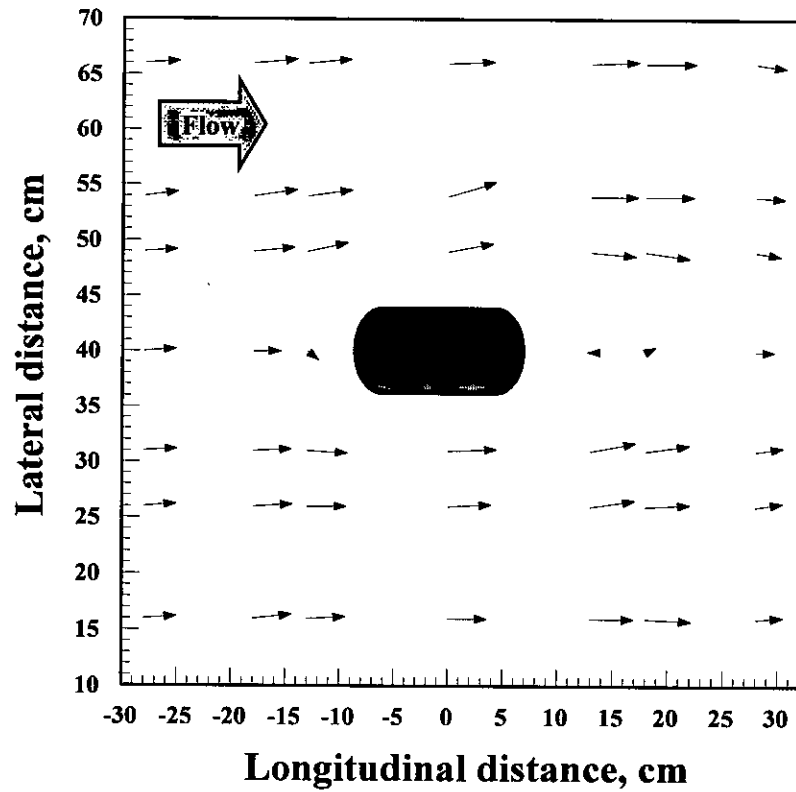


Figure C.57: Run 29-Bed material 3( $d_{50} = 0.12$  mm)-Round nose pier ( $l/b=2$ )- $Q=175$  l/s  
Floodplain

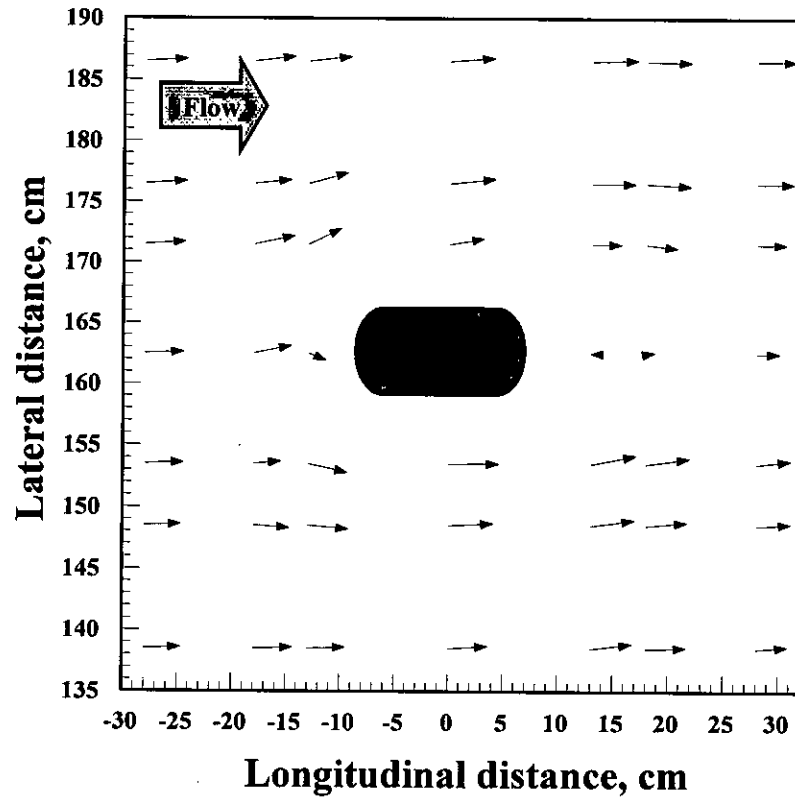


Figure C.58: Run 29-Bed material 3( $d_{50} = 0.12$  mm)-Round nose pier ( $l/b=2$ )- $Q=175$  l/s  
Main channel

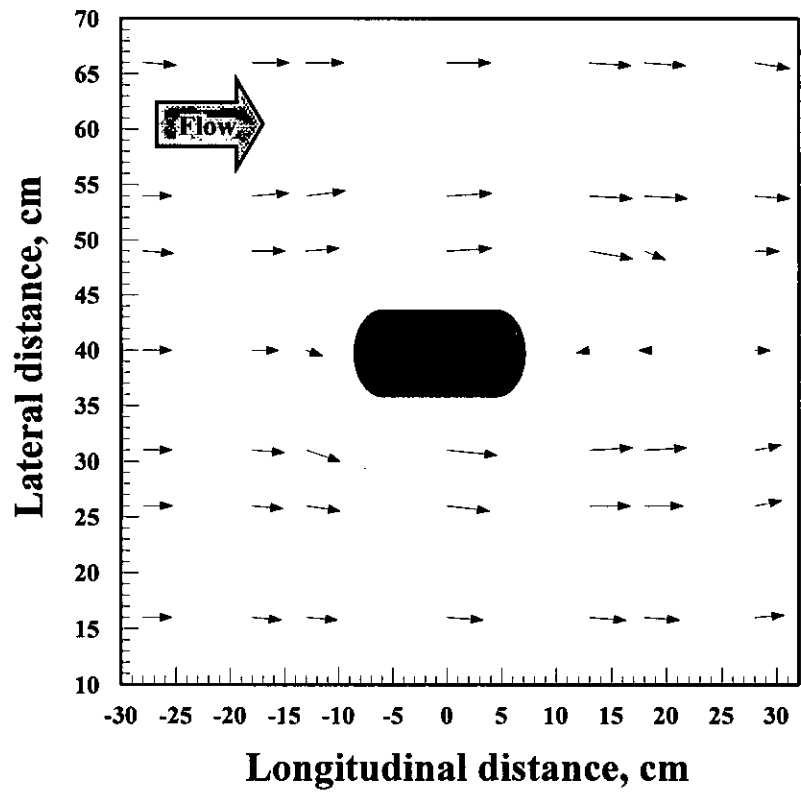


Figure C.59: Run 30-Bed material 3( $d_{50} = 0.12$  mm)-Round nose pier ( $l/b=2$ )- $Q=150$  l/s  
Floodplain

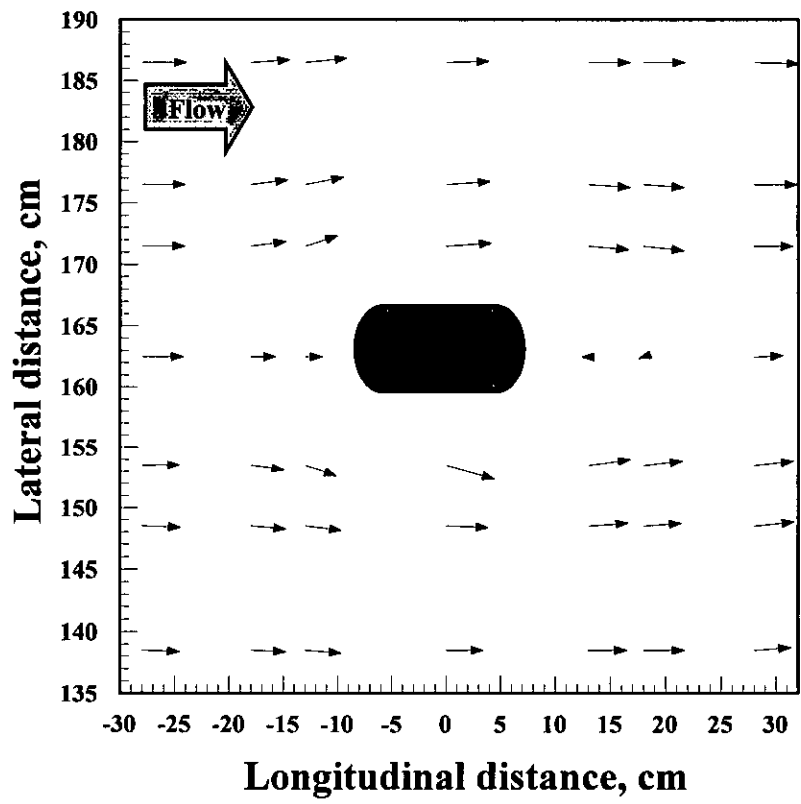


Figure C.60: Run 30-Bed material 3( $d_{50} = 0.12$  mm)-Round nose pier ( $l/b=2$ )- $Q=150$  l/s  
Main channel

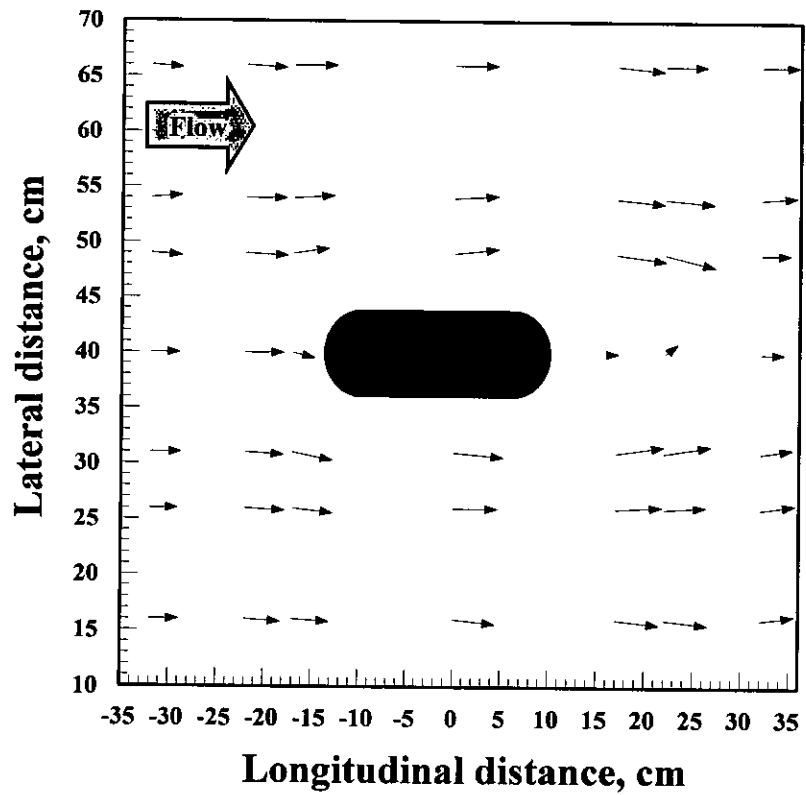


Figure C.61: Run 31-Bed material 3( $d_{50} = 0.12$  mm)-Round nose pier ( $l/b=3$ )- $Q=200$  l/s  
Floodplain

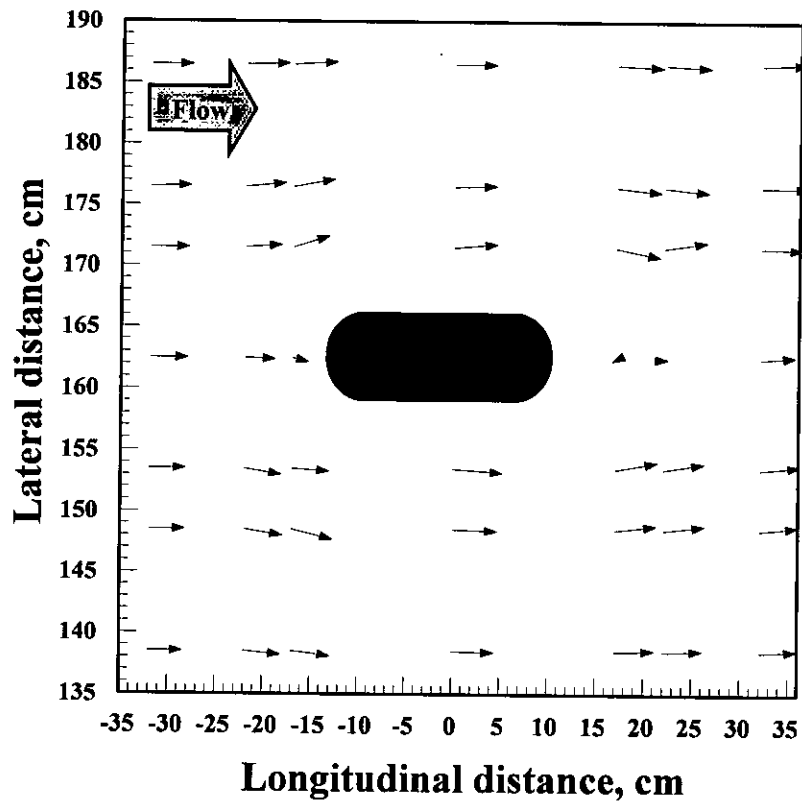


Figure C.62: Run 31-Bed material 3( $d_{50} = 0.12$  mm)-Round nose pier ( $l/b=3$ )- $Q=200$  l/s  
Main channel

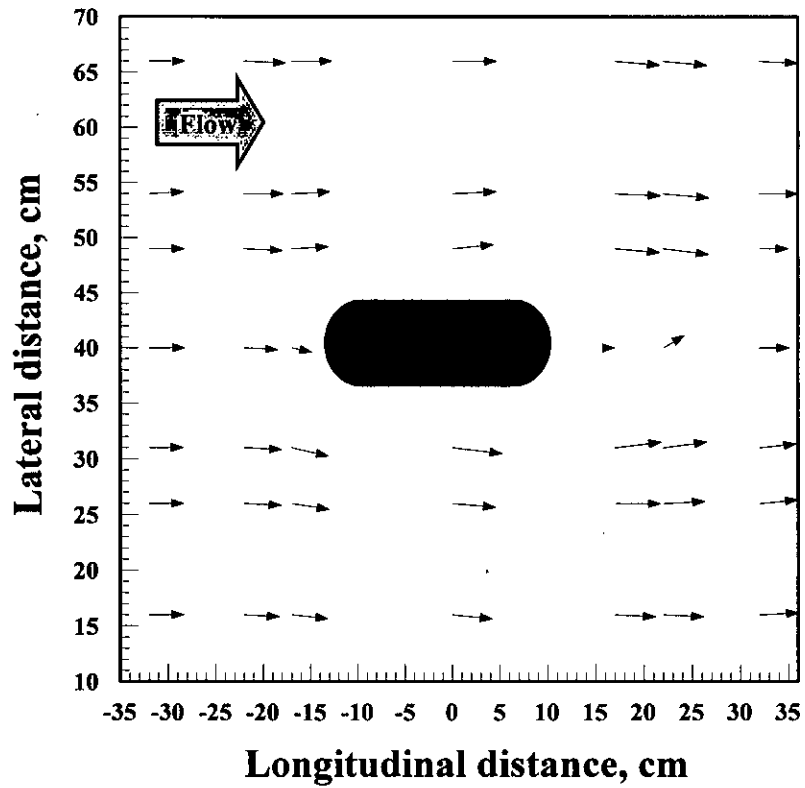


Figure C.63: Run 32-Bed material 3( $d_{50} = 0.12$  mm)-Round nose pier ( $l/b=3$ )- $Q=175$  l/s  
Floodplain

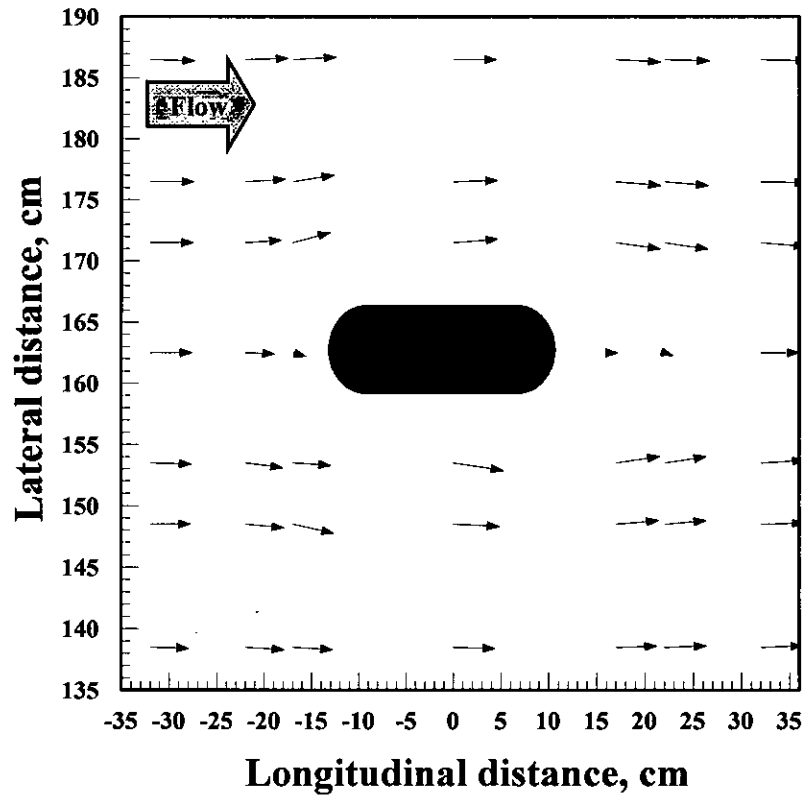


Figure C.64: Run 32-Bed material 3( $d_{50} = 0.12$  mm)-Round nose pier ( $l/b=3$ )- $Q=175$  l/s  
Main channel

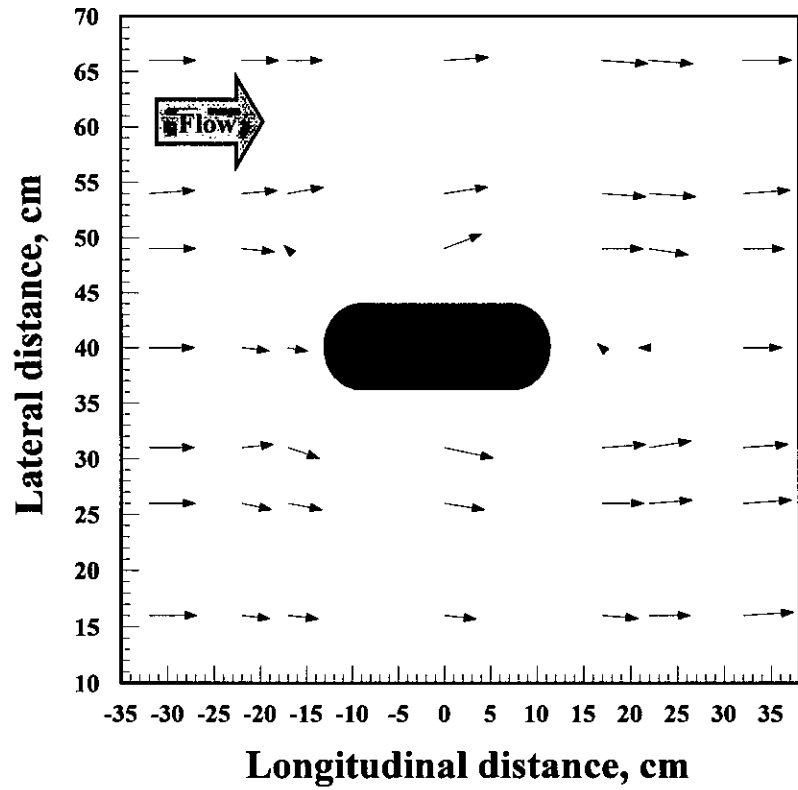


Figure C.65: Run 33-Bed material 3( $d_{50} = 0.12$  mm)-Round nose pier ( $l/b=3$ )- $Q=150$  l/s  
Floodplain

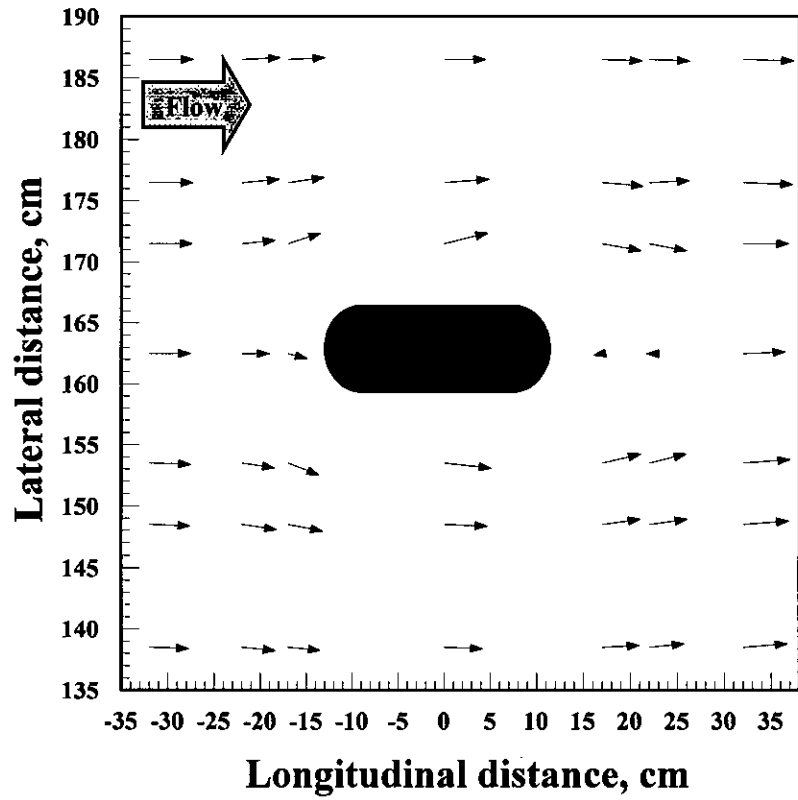


Figure C.66: Run 33-Bed material 3( $d_{50} = 0.12$  mm)-Round nose pier ( $l/b=3$ )- $Q=150$  l/s  
Main channel

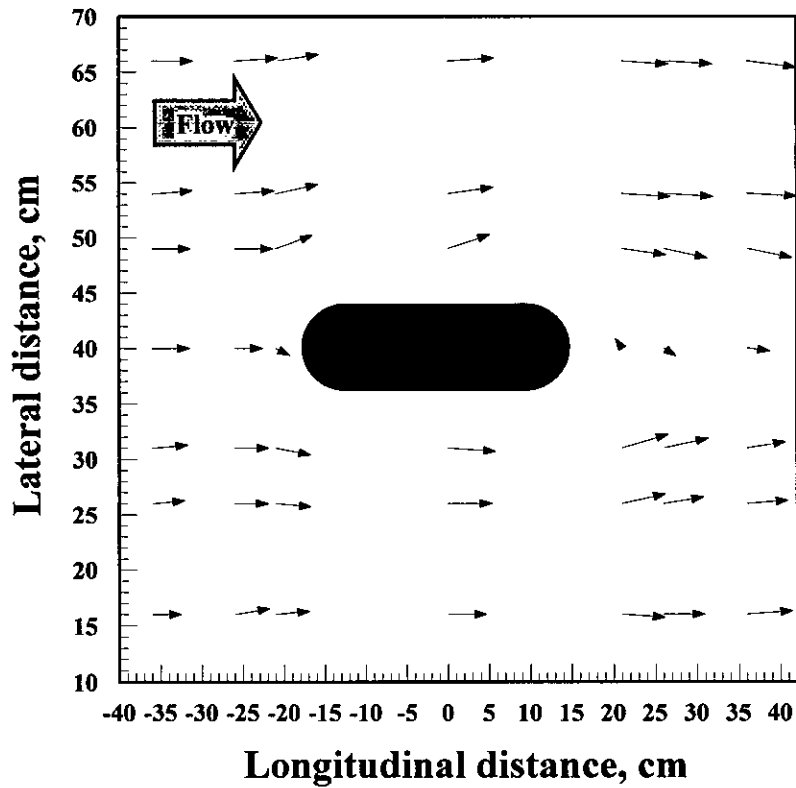


Figure C.67: Run 34-Bed material 3( $d_{50} = 0.12$  mm)-Round nose pier ( $l/b=4$ )- $Q=200$  l/s  
Floodplain

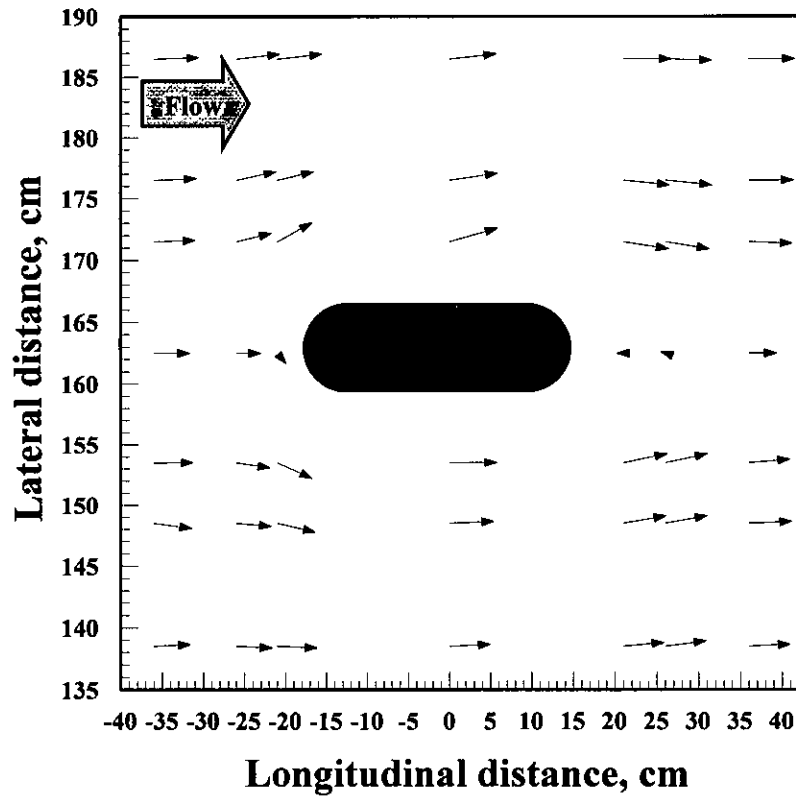


Figure C.68: Run 34-Bed material 3( $d_{50} = 0.12$  mm)-Round nose pier ( $l/b=4$ )- $Q=200$  l/s  
Main channel



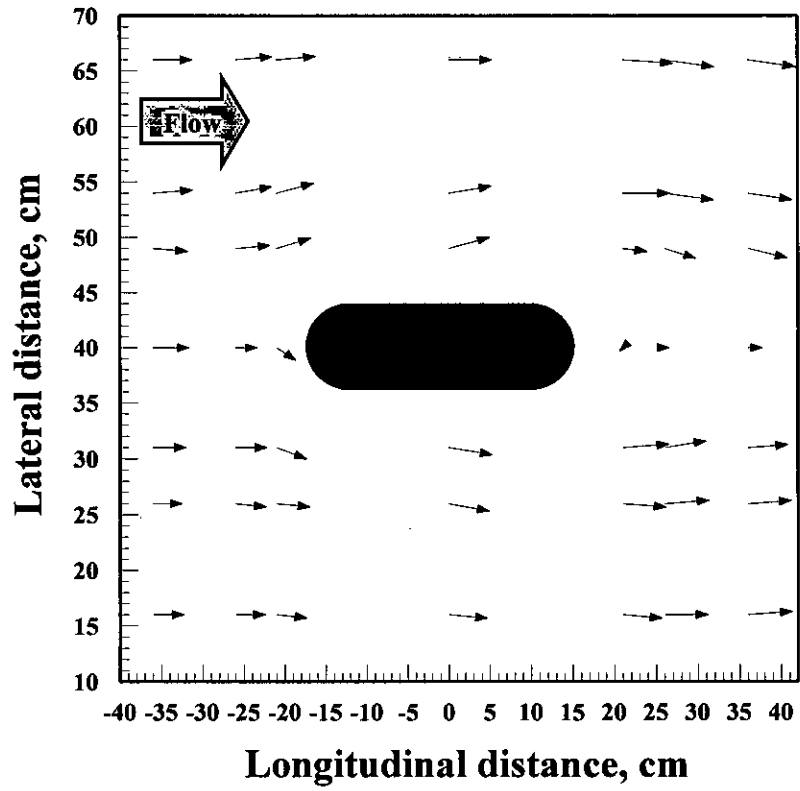


Figure C.69: Run 35-Bed material 3( $d_{50} = 0.12$  mm)-Round nose pier ( $l/b=4$ )- $Q=175$  l/s  
Floodplain

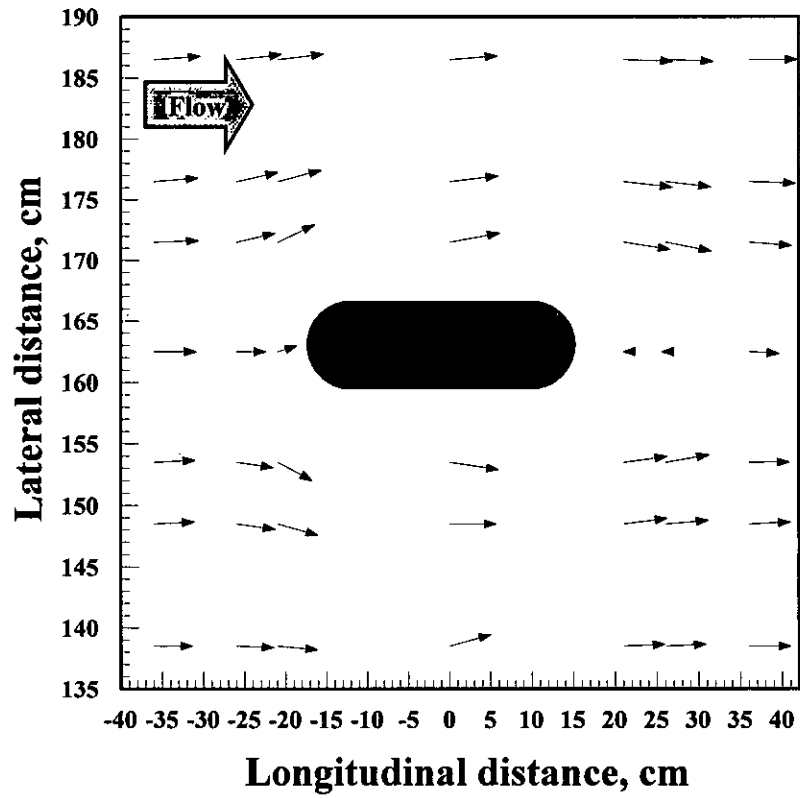


Figure C.70: Run 35-Bed material 3( $d_{50} = 0.12$  mm)-Round nose pier ( $l/b=4$ )- $Q=175$  l/s  
Main channel

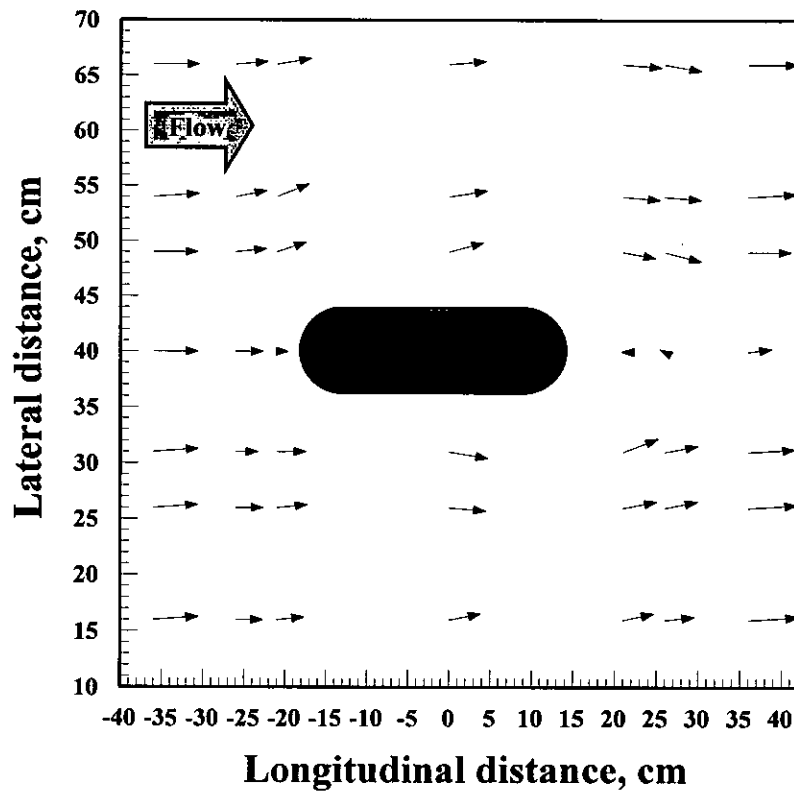


Figure C.71: Run 36-Bed material 3( $d_{50} = 0.12$  mm)-Round nose pier ( $l/b=4$ )- $Q=150$  l/s  
Floodplain

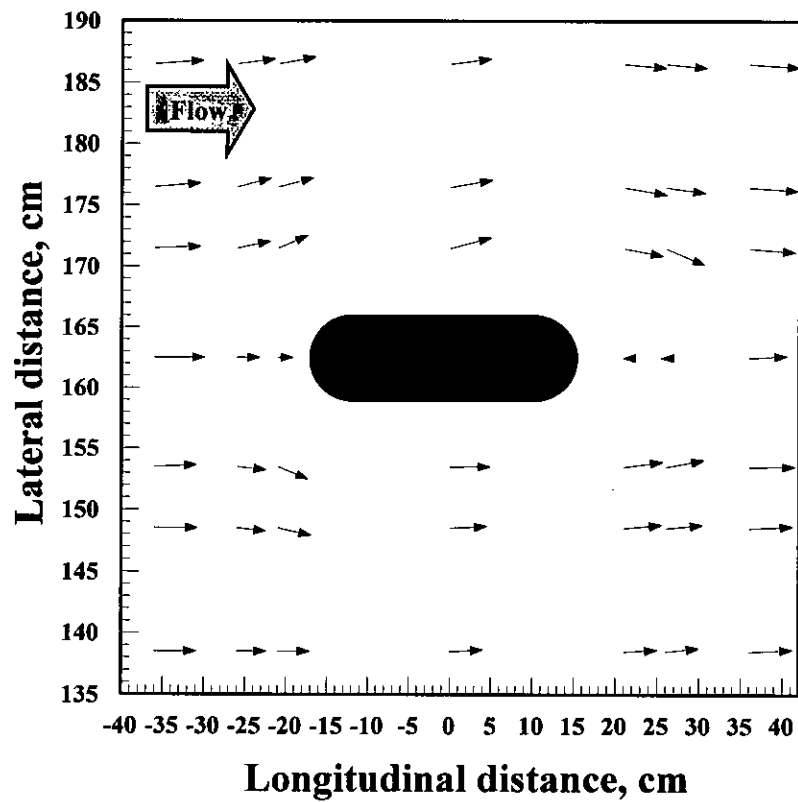


Figure C.72: Run 36-Bed material 3( $d_{50} = 0.12$  mm)-Round nose pier ( $l/b=4$ )- $Q=150$  l/s  
Main channel

**Appendix D**  
**V/V<sub>C</sub> contour map**

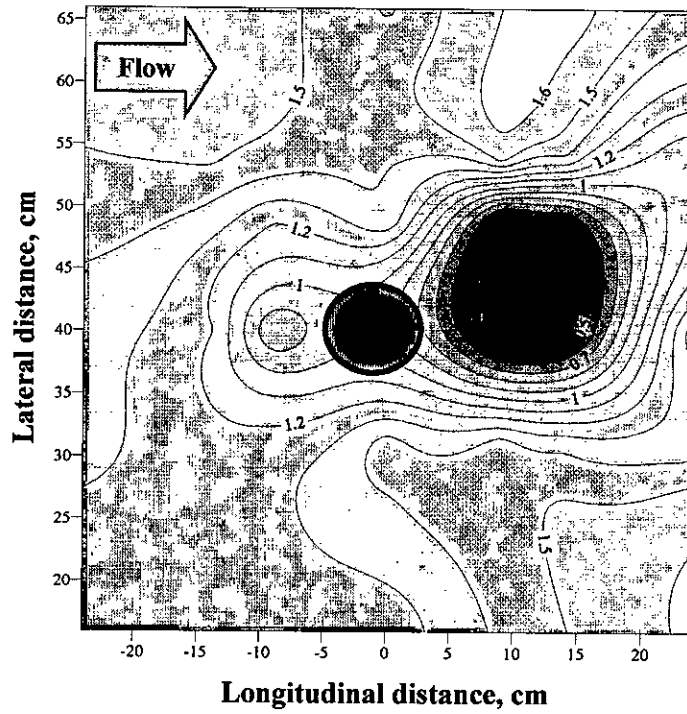


Figure D.1: Run 1-Bed material 1( $d_{50} = 0.75$  mm)-Circular pier ( $l/b=1$ )- $Q=200$  l/s  
Floodplain

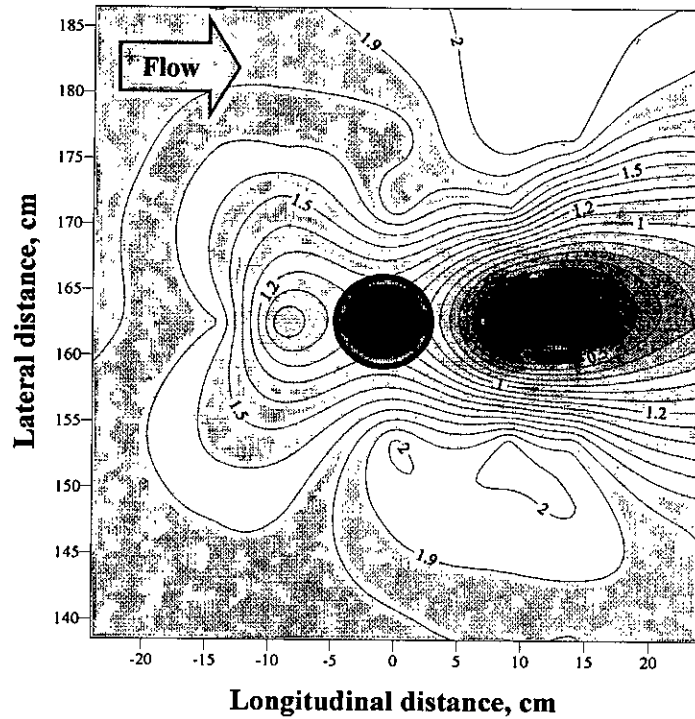


Figure D.2: Run 1-Bed material 1( $d_{50} = 0.75$  mm)-Circular pier ( $l/b=1$ )- $Q=200$  l/s  
Main channel

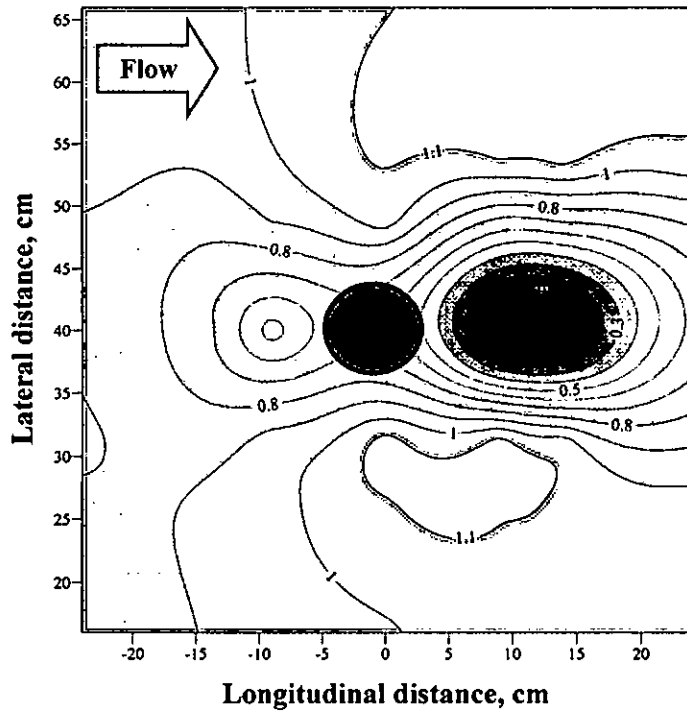


Figure D.3: Run 2-Bed material 1 ( $d_{50} = 0.75$  mm)-Circular pier ( $l/b=1$ )- $Q=175$  l/s  
Floodplain

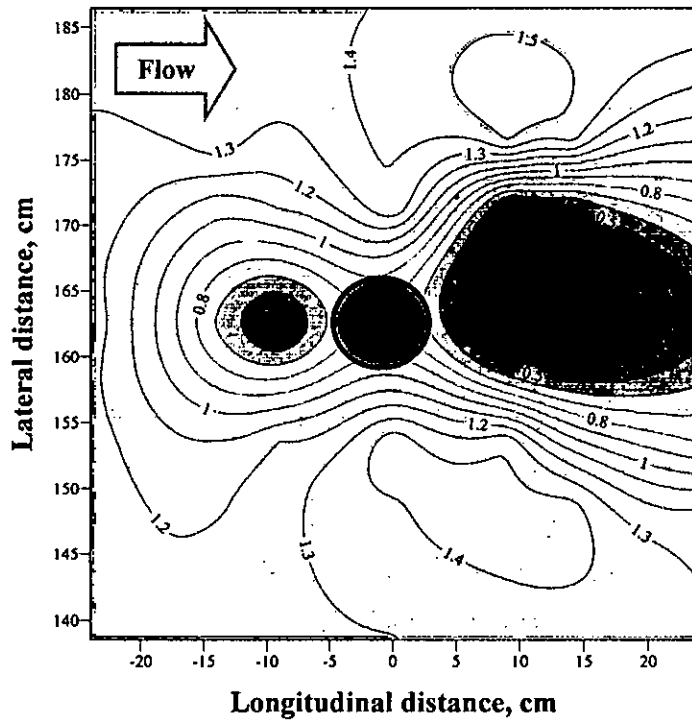


Figure D.4: Run 2-Bed material 1 ( $d_{50} = 0.75$  mm)-Circular pier ( $l/b=1$ )- $Q=175$  l/s  
Main channel

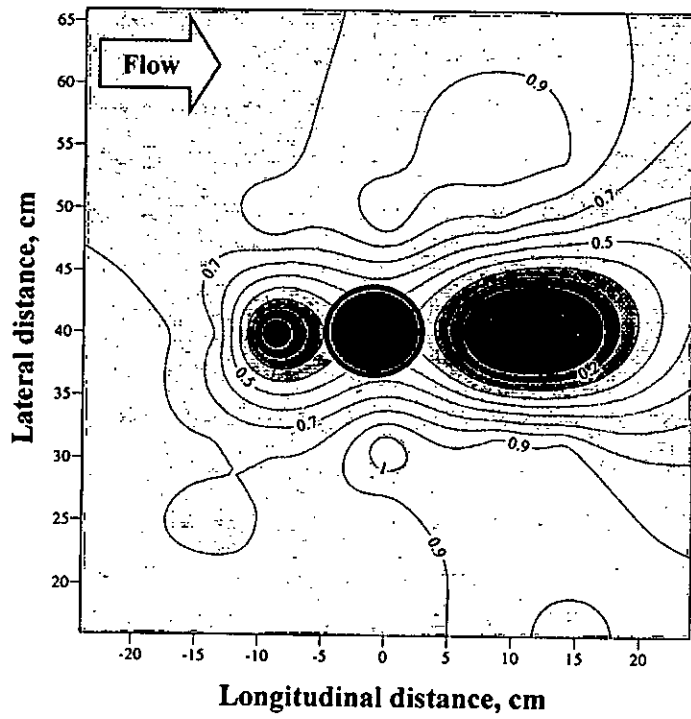


Figure D.5: Run 3-Bed material 1 ( $d_{50} = 0.75$  mm)-Circular pier ( $l/b=1$ )- $Q=150$  l/s  
Floodplain

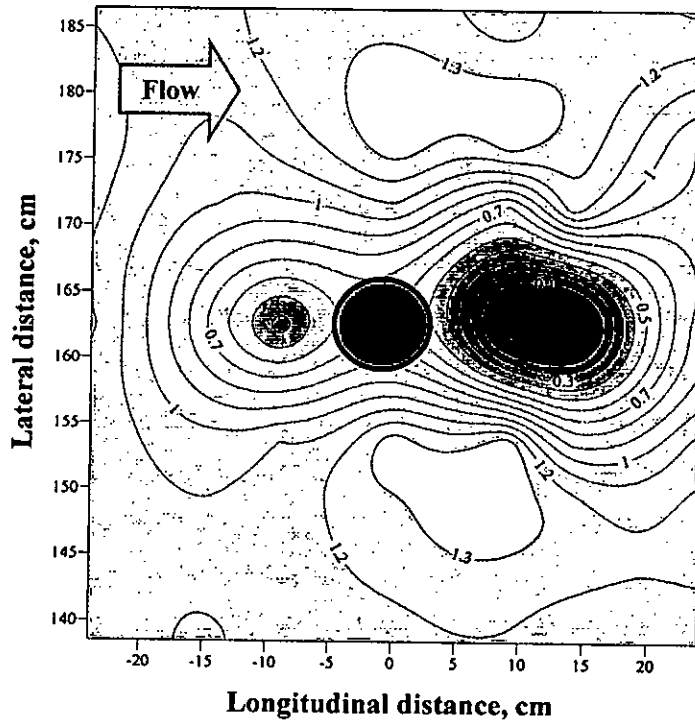


Figure D.6: Run 3-Bed material 1 ( $d_{50} = 0.75$  mm)-Circular pier ( $l/b=1$ )- $Q=150$  l/s  
Main channel

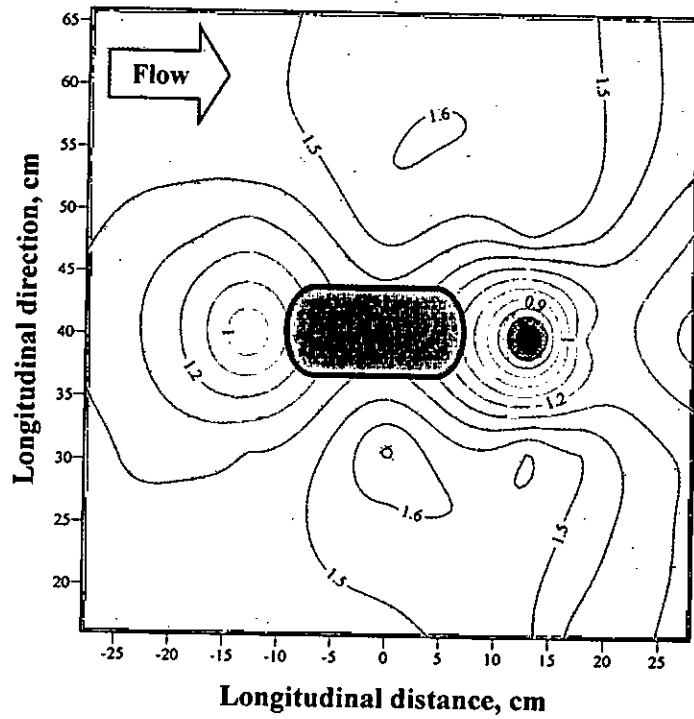


Figure D.7: Run 4-Bed material 1( $d_{50} = 0.75$  mm)-Round nose pier ( $l/b=2$ )- $Q=200$  l/s  
Floodplain

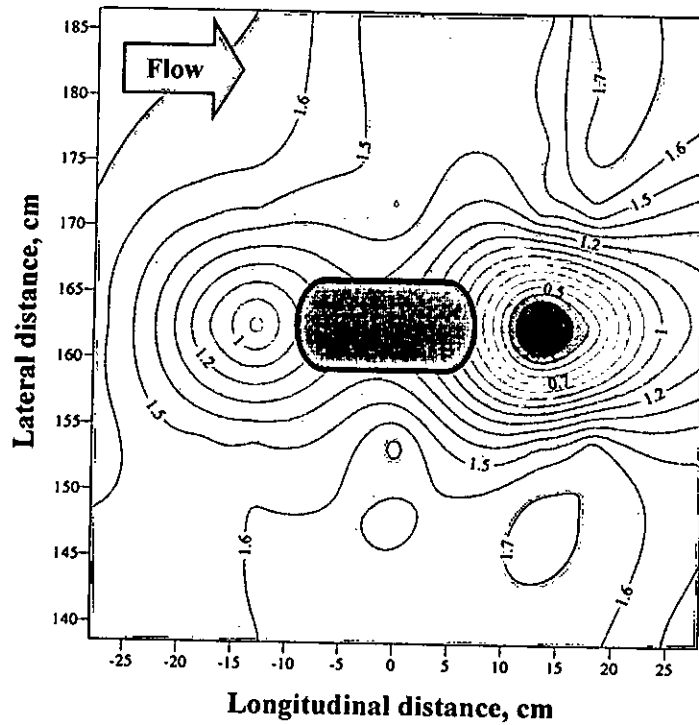


Figure D.8: Run 4-Bed material 1( $d_{50} = 0.75$  mm)-Round nose pier ( $l/b=2$ )- $Q=200$  l/s  
Main channel

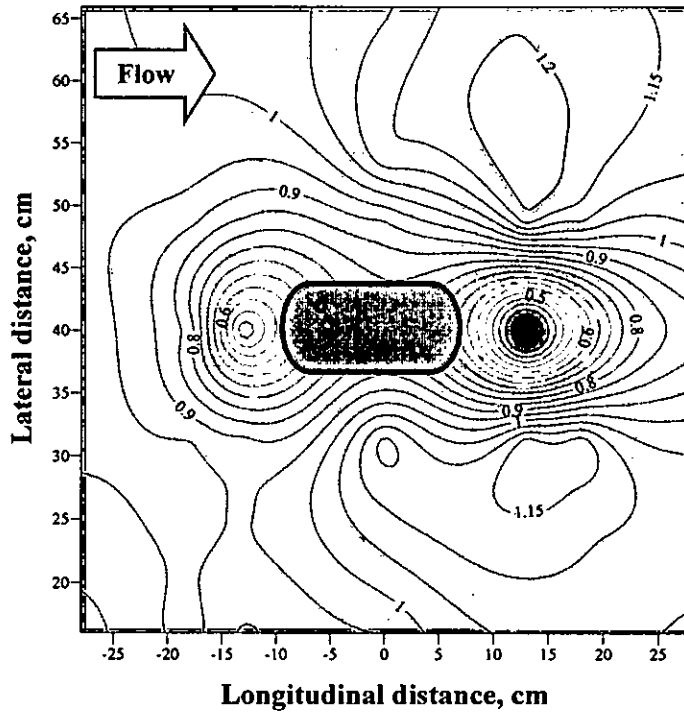


Figure D.9: Run 5-Bed material 1( $d_{50} = 0.75$  mm)-Round nose pier ( $l/b=2$ )- $Q=175$  l/s  
Floodplain

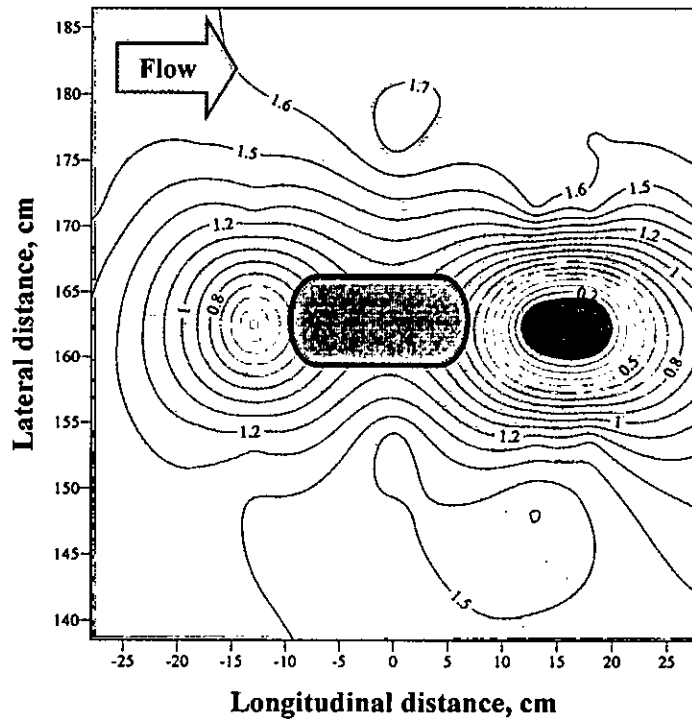


Figure D.10: Run 5-Bed material 1( $d_{50} = 0.75$  mm)-Round nose pier ( $l/b=2$ )- $Q=175$  l/s  
Main channel



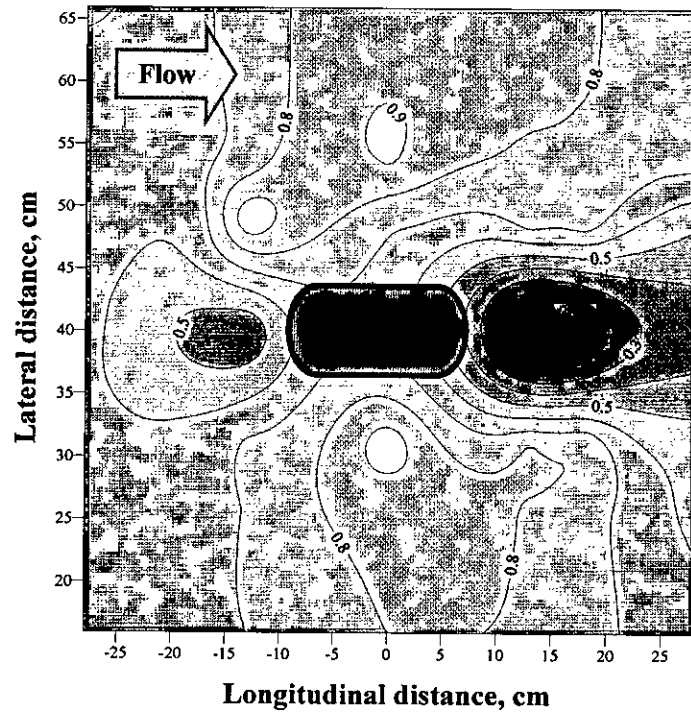


Figure D.11: Run 6-Bed material 1( $d_{50} = 0.75$  mm)-Round nose pier ( $l/b=2$ )- $Q=150$  l/s  
Floodplain

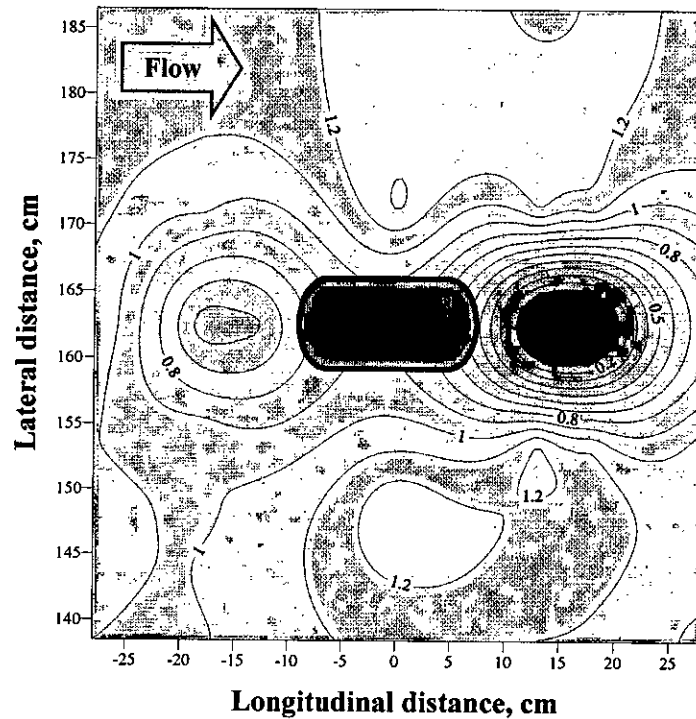


Figure D.12: Run 6-Bed material 1( $d_{50} = 0.75$  mm)-Round nose pier ( $l/b=2$ )- $Q=150$  l/s  
Main channel

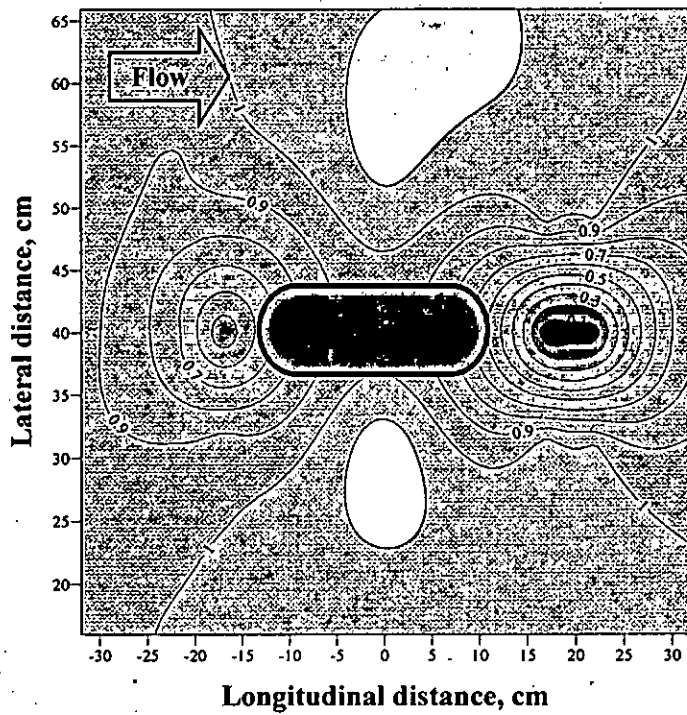


Figure D.13: Run 7-Bed material 1 ( $d_{50} = 0.75$  mm)-Round nose pier ( $l/b=3$ )- $Q=200$  l/s  
Floodplain

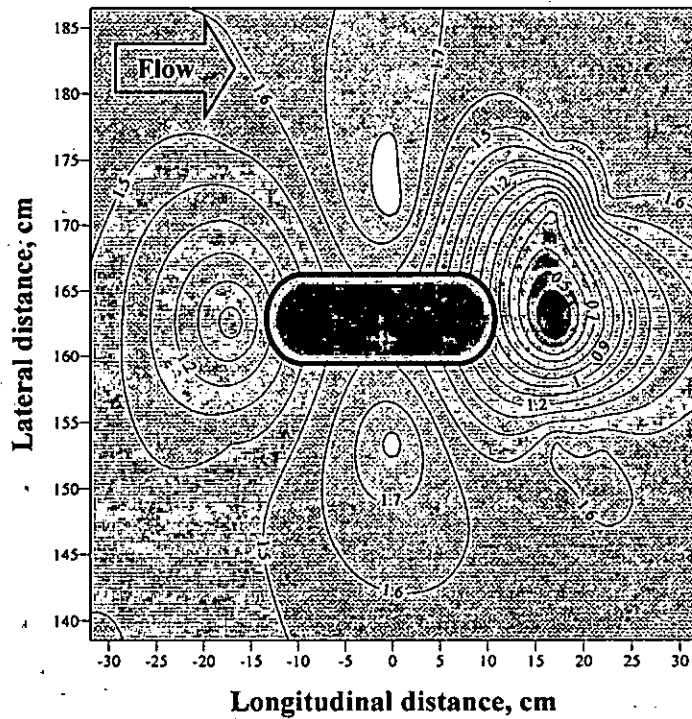


Figure D.14: Run 7-Bed material 1 ( $d_{50} = 0.75$  mm)-Round nose pier ( $l/b=3$ )- $Q=200$  l/s  
Main channel

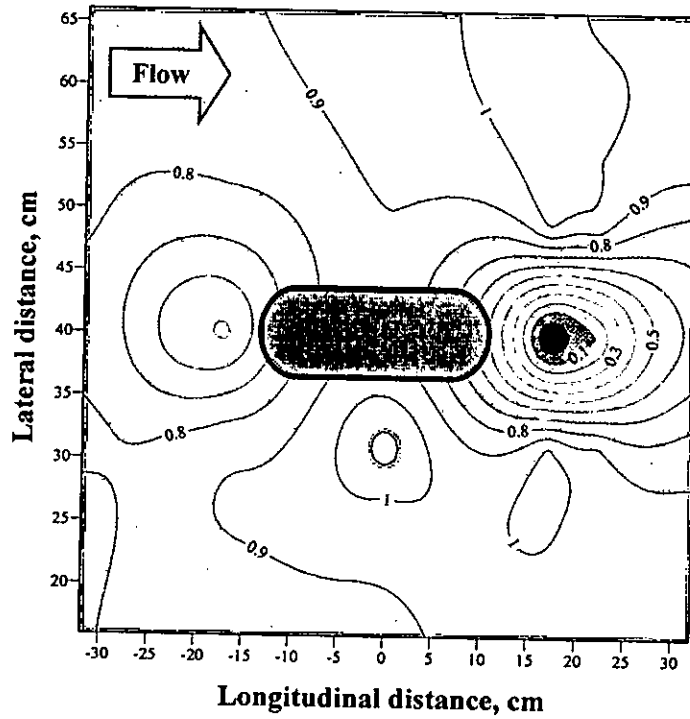


Figure D.15: Run 8-Bed material 1( $d_{50} = 0.75$  mm)-Round nose pier ( $l/b=3$ )- $Q=175$  l/s  
Floodplain

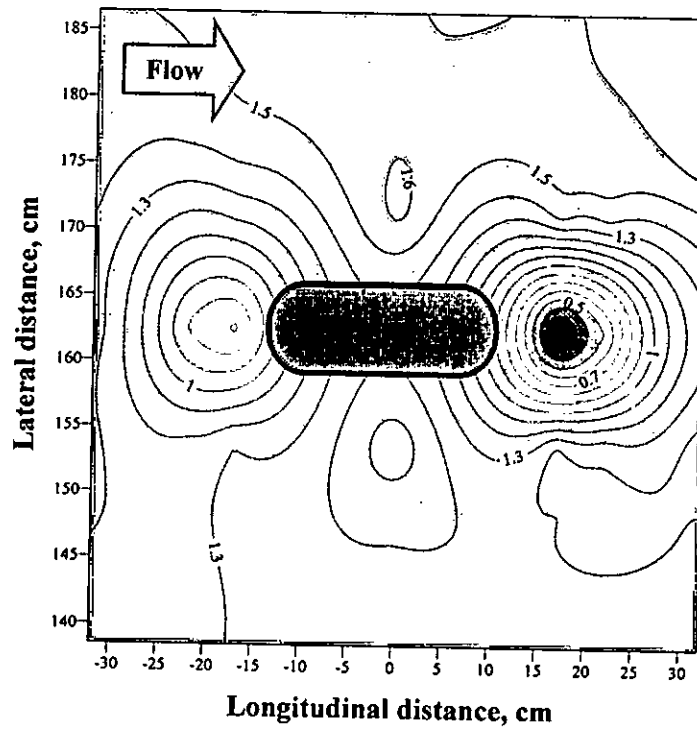


Figure D.16: Run 8-Bed material 1( $d_{50} = 0.75$  mm)-Round nose pier ( $l/b=3$ )- $Q=175$  l/s  
Main channel

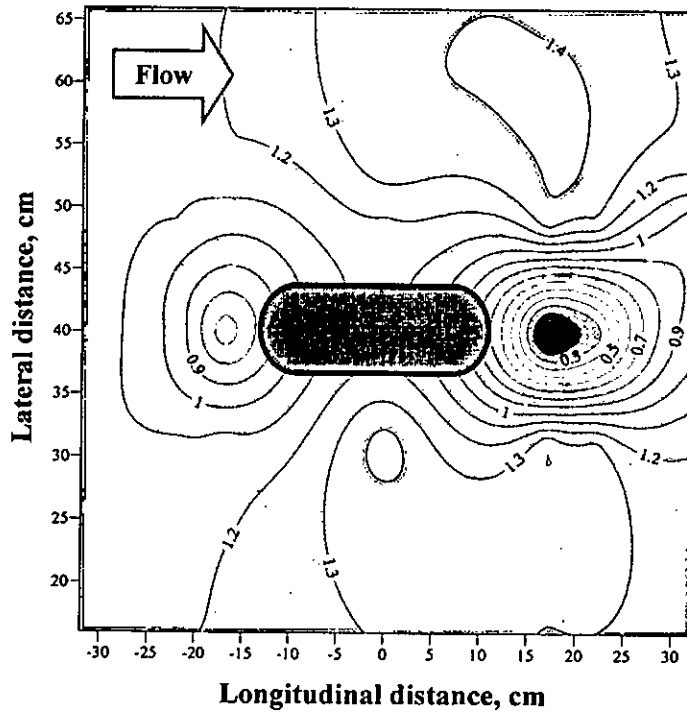


Figure D.17: Run 9-Bed material 1( $d_{50} = 0.75$  mm)-Round nose pier ( $l/b=3$ )- $Q=150$  l/s  
Floodplain

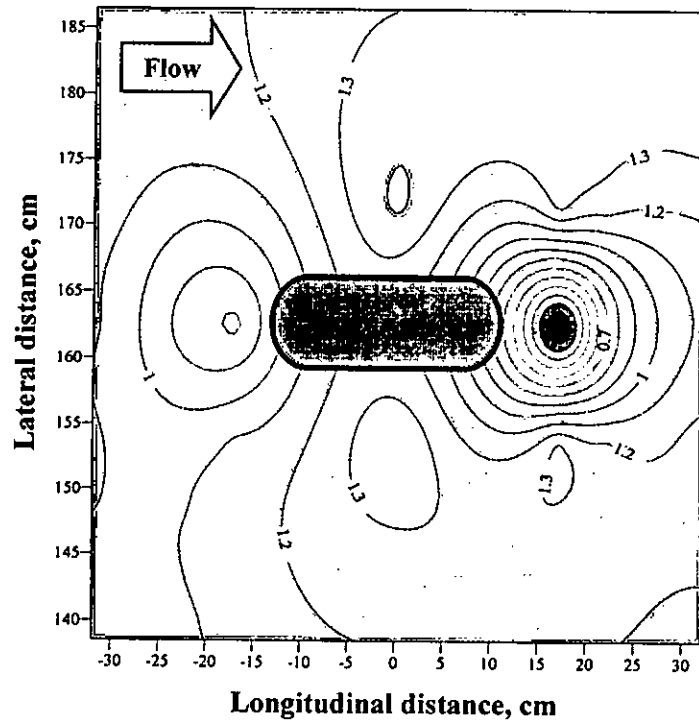


Figure D.18: Run 9-Bed material 1( $d_{50} = 0.75$  mm)-Round nose pier ( $l/b=3$ )- $Q=150$  l/s  
Main channel

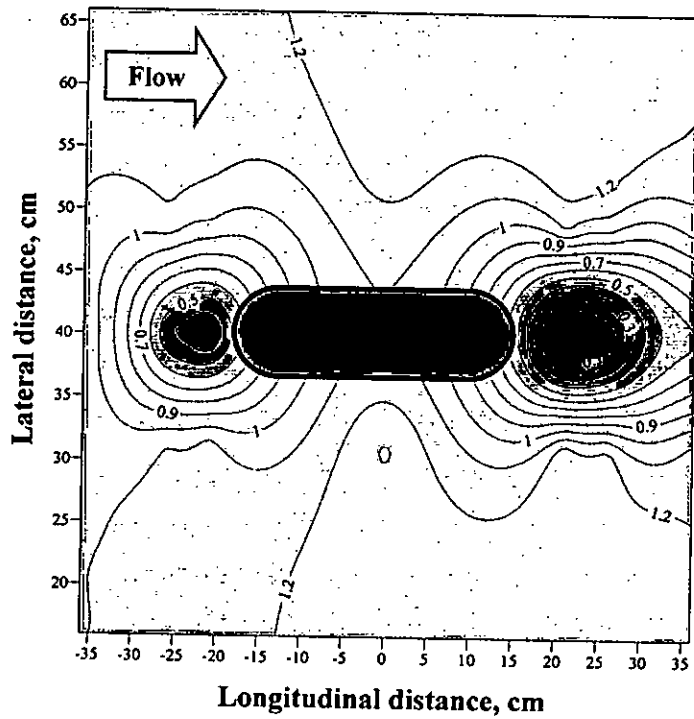


Figure D.19: Run 10-Bed material 1( $d_{50} = 0.75$  mm)-Round nose pier ( $l/b=4$ )- $Q=200$  l/s  
Floodplain

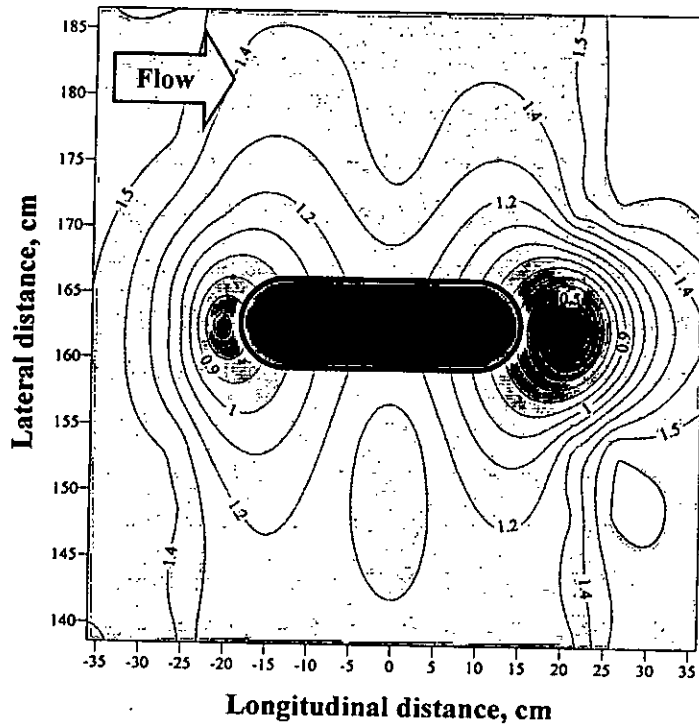


Figure D.20: Run 10-Bed material 1( $d_{50} = 0.75$  mm)-Round nose pier ( $l/b=4$ )- $Q=200$  l/s  
Main channel

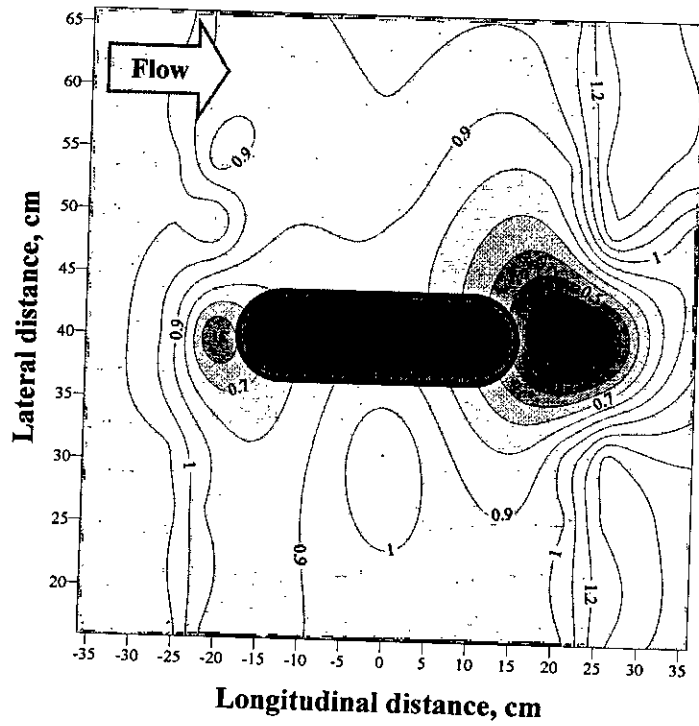


Figure D.21: Run 11-Bed material 1 ( $d_{50} = 0.75$  mm)-Round nose pier ( $l/b=4$ )- $Q=175$  l/s  
Floodplain

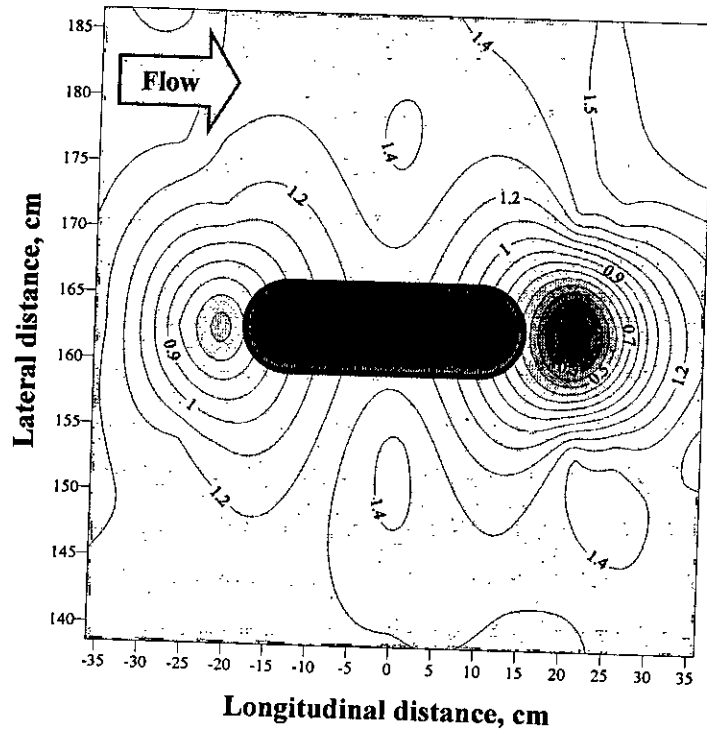


Figure D.22: Run 11-Bed material 1 ( $d_{50} = 0.75$  mm)-Round nose pier ( $l/b=4$ )- $Q=175$  l/s  
Main channel

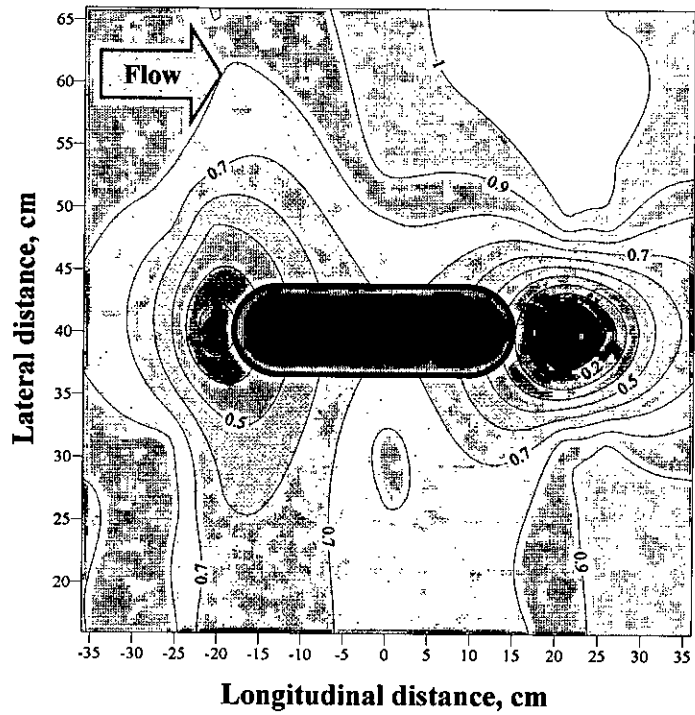


Figure D.23: Run 12-Bed material 1( $d_{50} = 0.75$  mm)-Round nose pier ( $l/b=4$ )- $Q=150$  l/s  
Floodplain

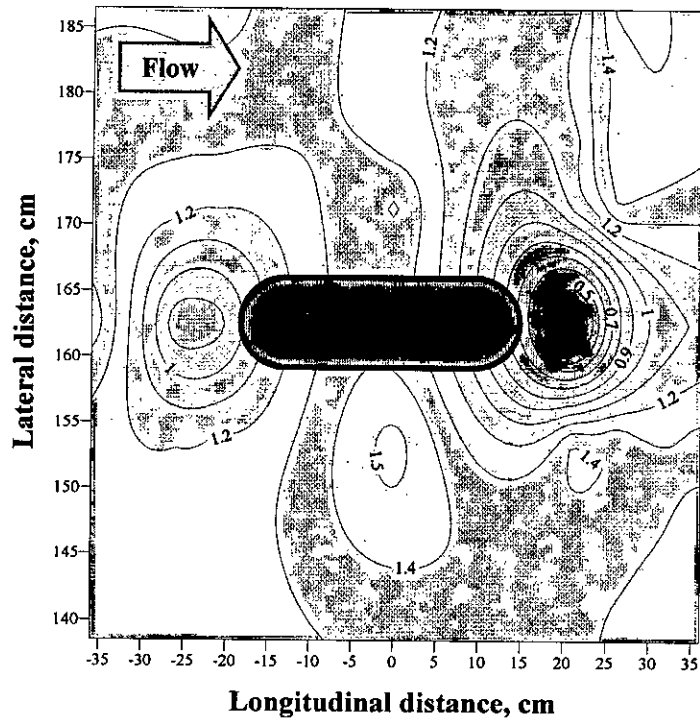


Figure D.24: Run 12-Bed material 1( $d_{50} = 0.75$  mm)-Round nose pier ( $l/b=4$ )- $Q=150$  l/s  
Main channel

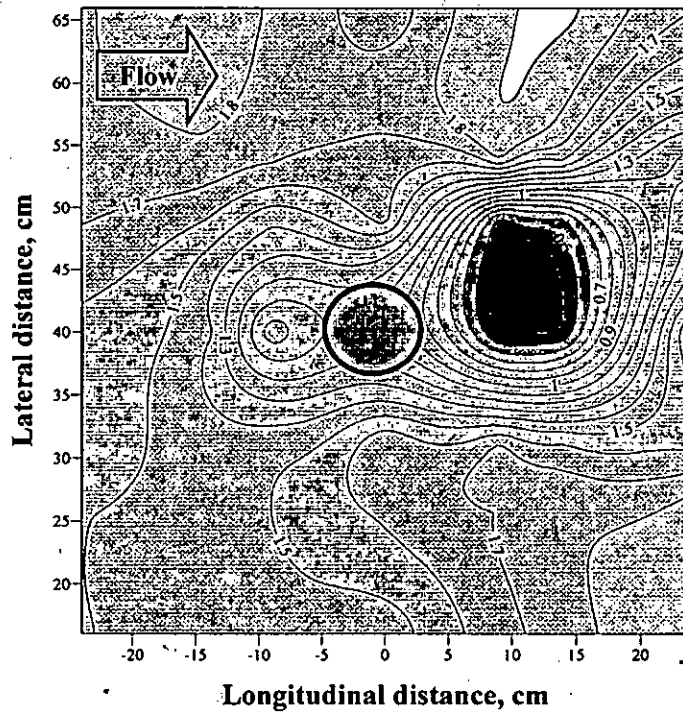


Figure D.25: Run 13-Bed material 2 ( $d_{50} = 0.18$  mm)-Circular pier ( $l/b=1$ )- $Q=200$  l/s  
Floodplain

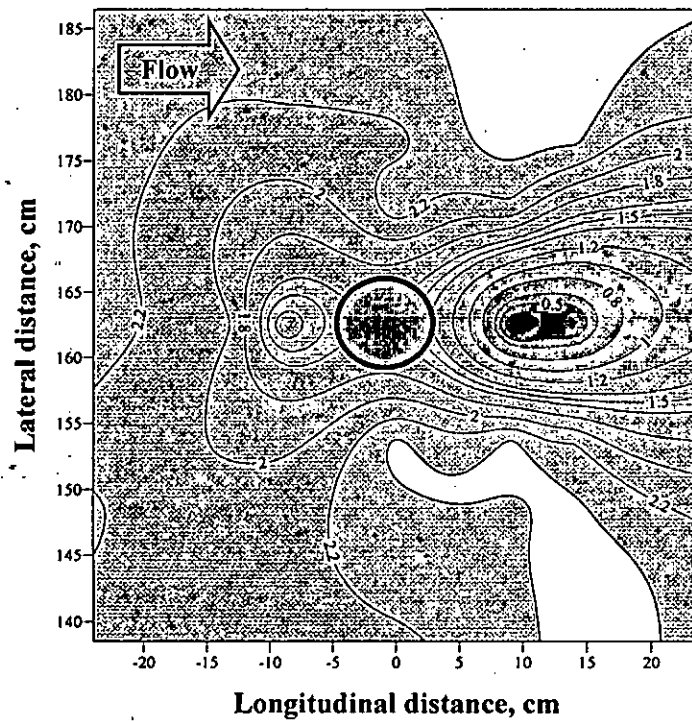


Figure D.26: Run 13-Bed material 2 ( $d_{50} = 0.18$  mm)-Circular pier ( $l/b=1$ )- $Q=200$  l/s  
Main channel



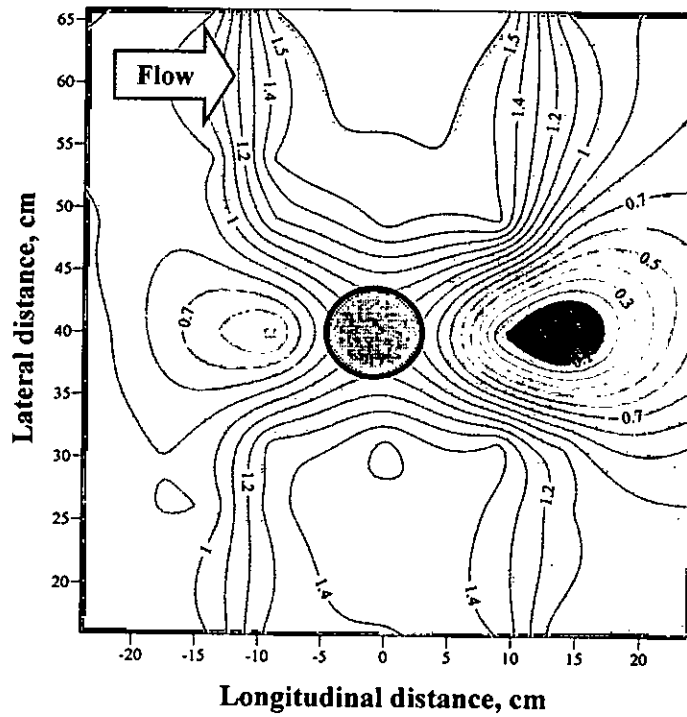


Figure D.27: Run 14-Bed material 2 ( $d_{50} = 0.18$  mm)-Circular pier ( $l/b=1$ )- $Q=175$  l/s  
Floodplain

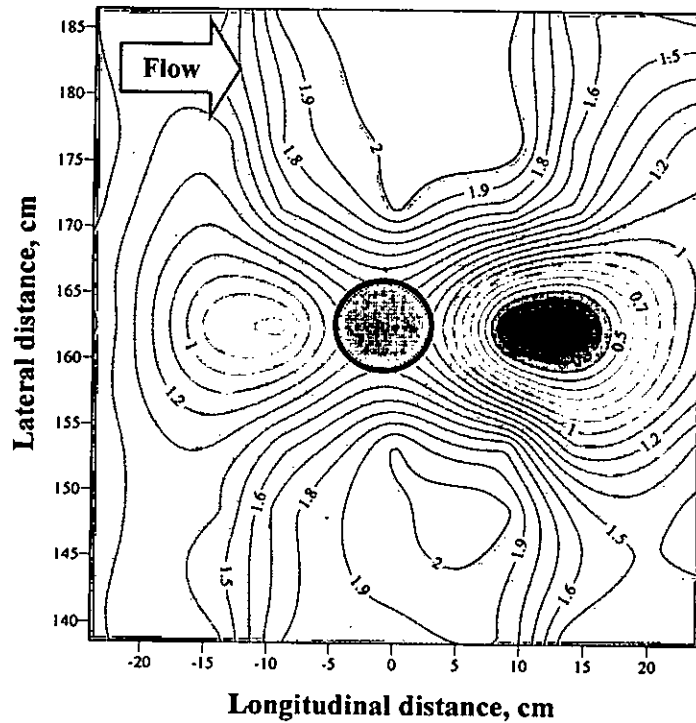


Figure D.28: Run 14-Bed material 2 ( $d_{50} = 0.18$  mm)-Circular pier ( $l/b=1$ )- $Q=175$  l/s  
Main channel



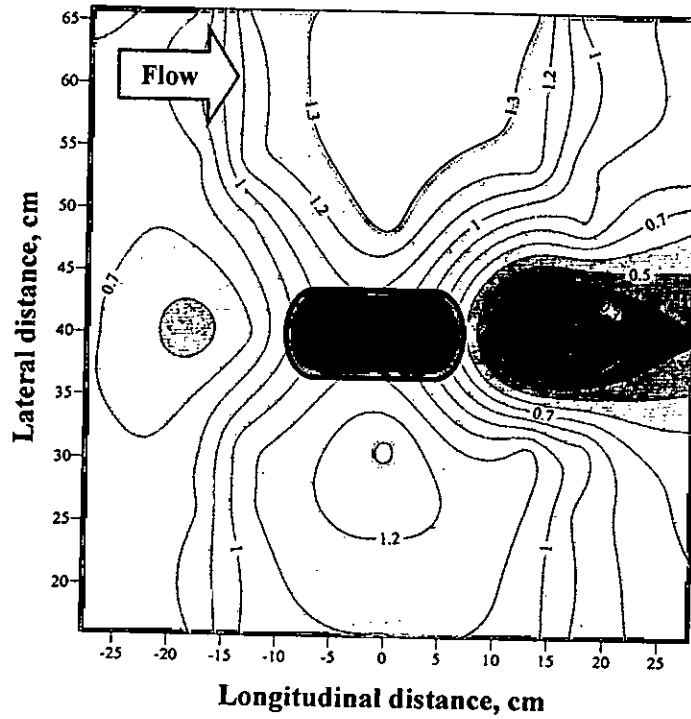


Figure D.31: Run 16-Bed material 2( $d_{50} = 0.18$  mm)-Round nose pier ( $l/b=2$ )- $Q=200$  l/s  
Floodplain

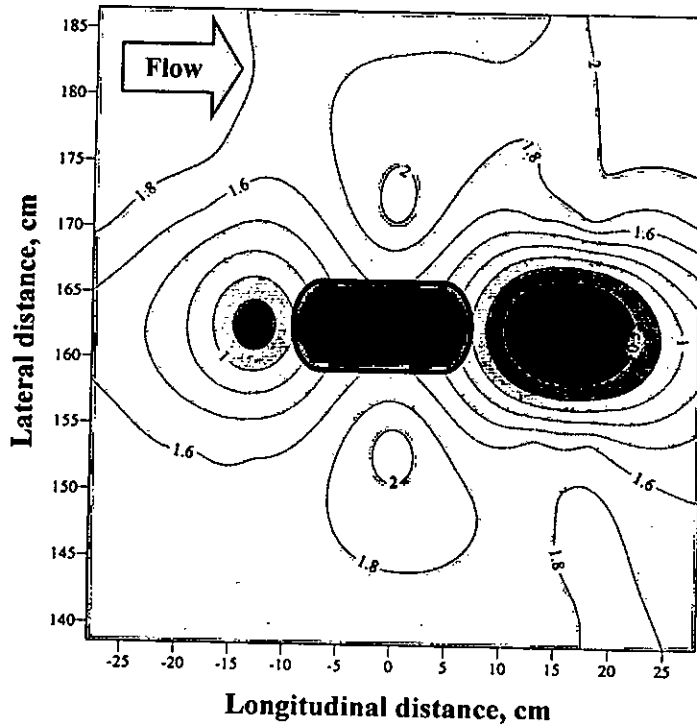


Figure D.32: Run 16-Bed material 2( $d_{50} = 0.18$  mm)-Round nose pier ( $l/b=2$ )- $Q=200$  l/s  
Main channel

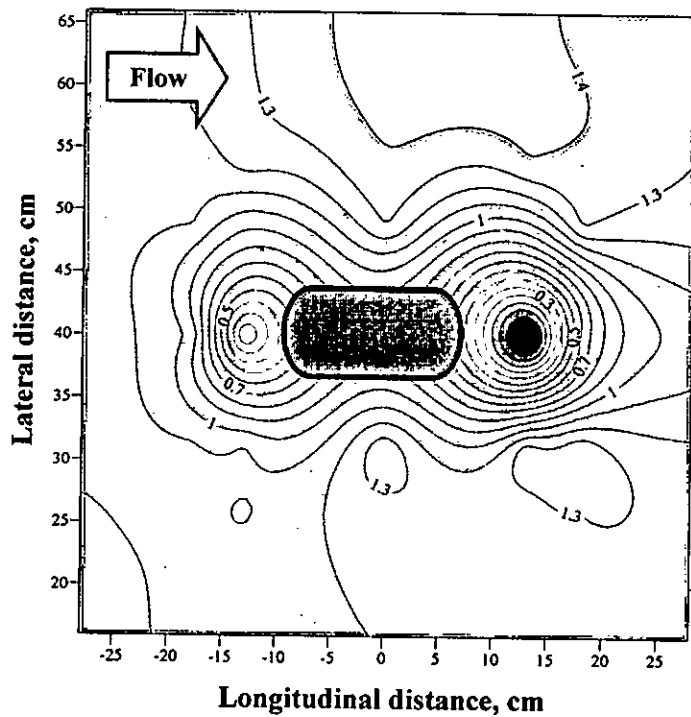


Figure D.33: Run 17-Bed material 2( $d_{50} = 0.18$  mm)-Round nose pier ( $l/b=2$ )- $Q=175$  l/s  
Floodplain

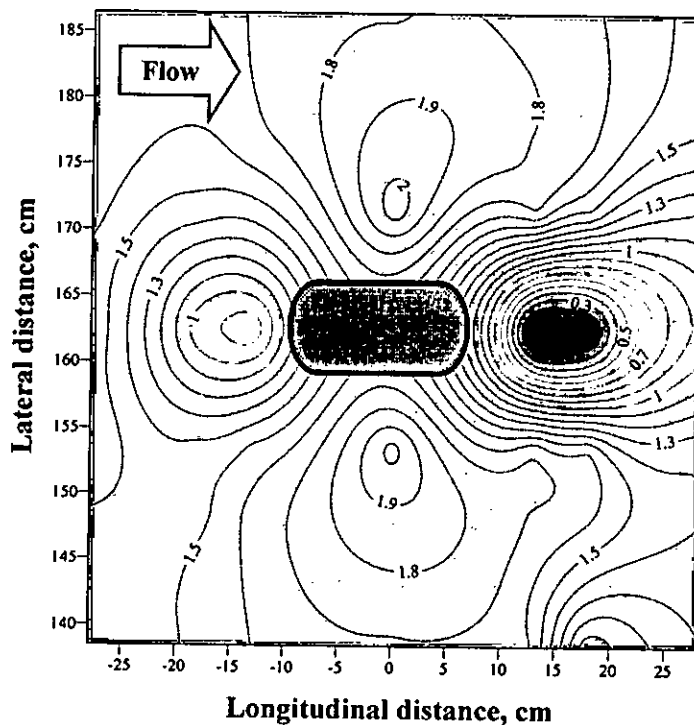


Figure D.34: Run 17-Bed material 2( $d_{50} = 0.18$  mm)-Round nose pier ( $l/b=2$ )- $Q=175$  l/s  
Main channel

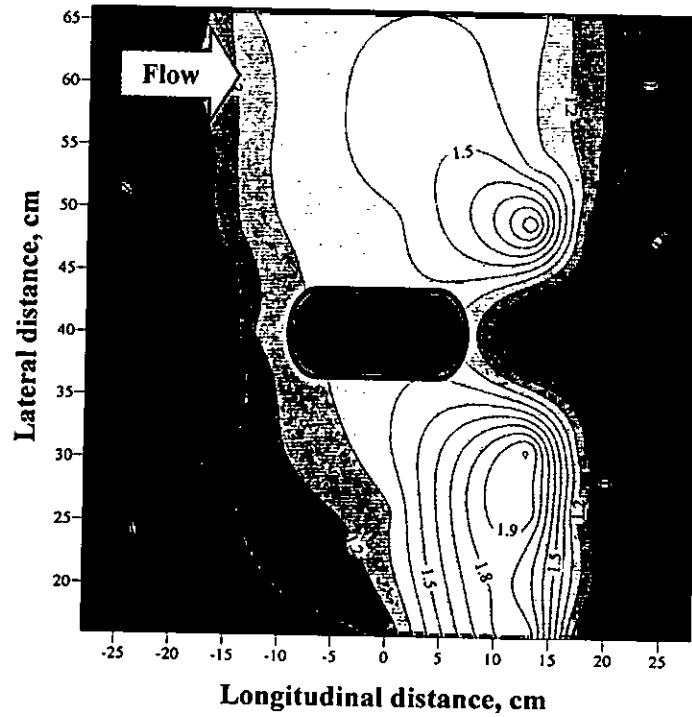


Figure D.35: Run 18-Bed material 2( $d_{50} = 0.18$  mm)-Round nose pier ( $l/b=2$ )- $Q=150$  l/s  
Floodplain

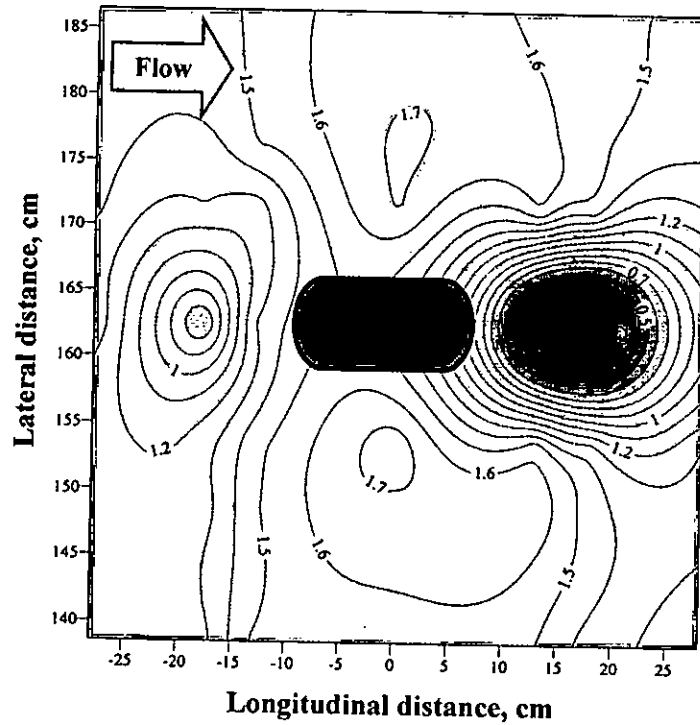


Figure D.36: Run 18-Bed material 2( $d_{50} = 0.18$  mm)-Round nose pier ( $l/b=2$ )- $Q=150$  l/s  
Main channel

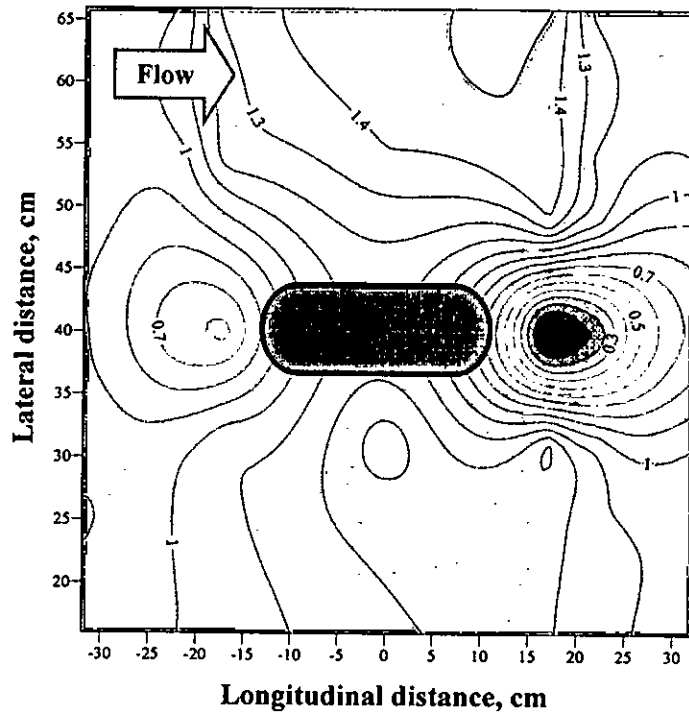


Figure D.37: Run 19-Bed material 2( $d_{50} = 0.18$  mm)-Round nose pier ( $l/b=3$ )- $Q=200$  l/s  
Floodplain

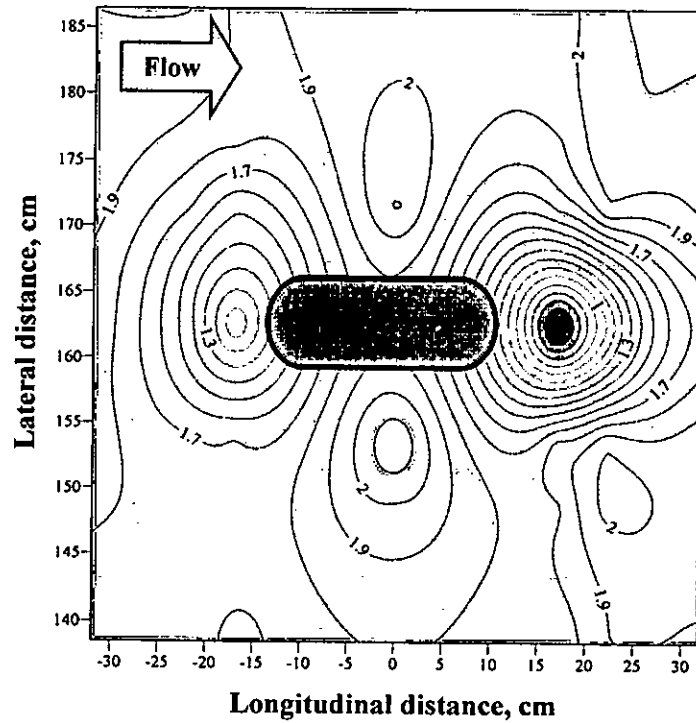


Figure D.38: Run 19-Bed material 2( $d_{50} = 0.18$  mm)-Round nose pier ( $l/b=3$ )- $Q=200$  l/s  
Main channel

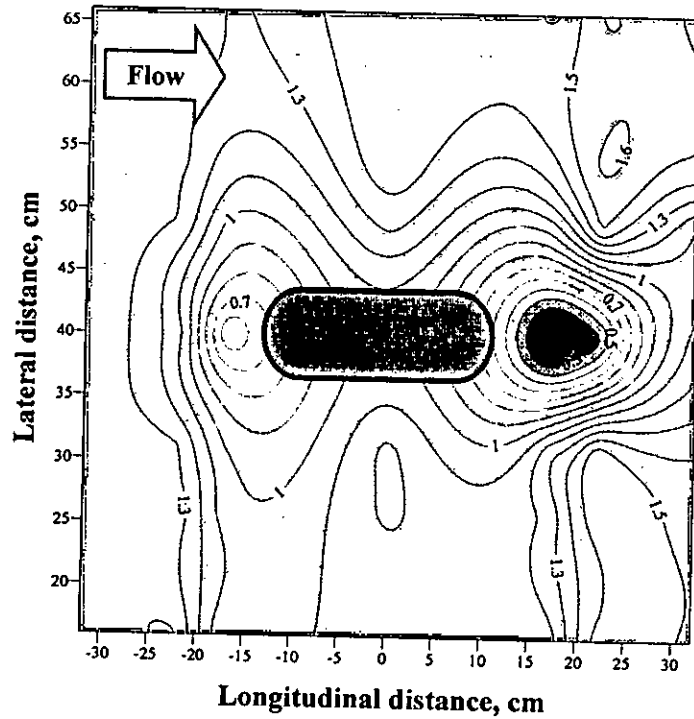


Figure D.39: Run 20-Bed material 2( $d_{50} = 0.18$  mm)-Round nose pier ( $l/b=3$ )- $Q=175$  l/s  
Floodplain

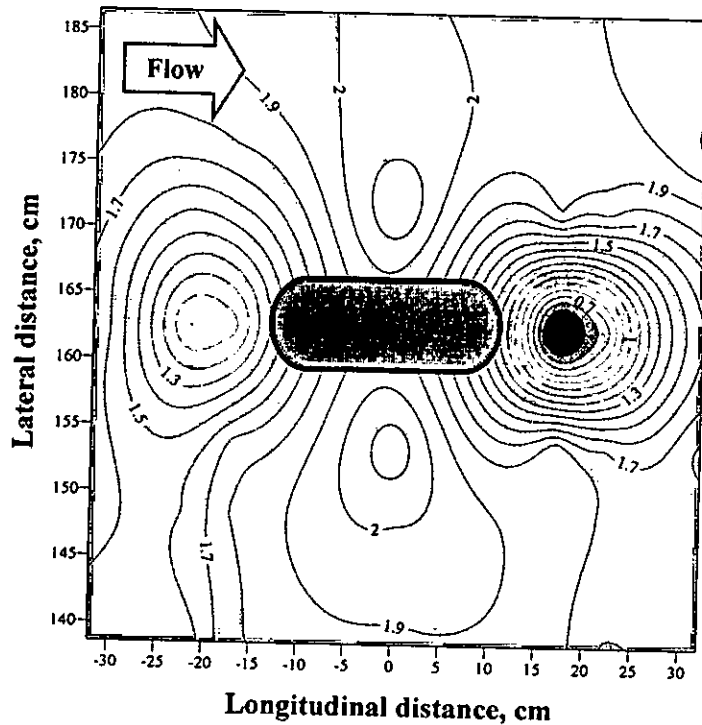


Figure D.40: Run 20-Bed material 2( $d_{50} = 0.18$  mm)-Round nose pier ( $l/b=3$ )- $Q=175$  l/s  
Main channel

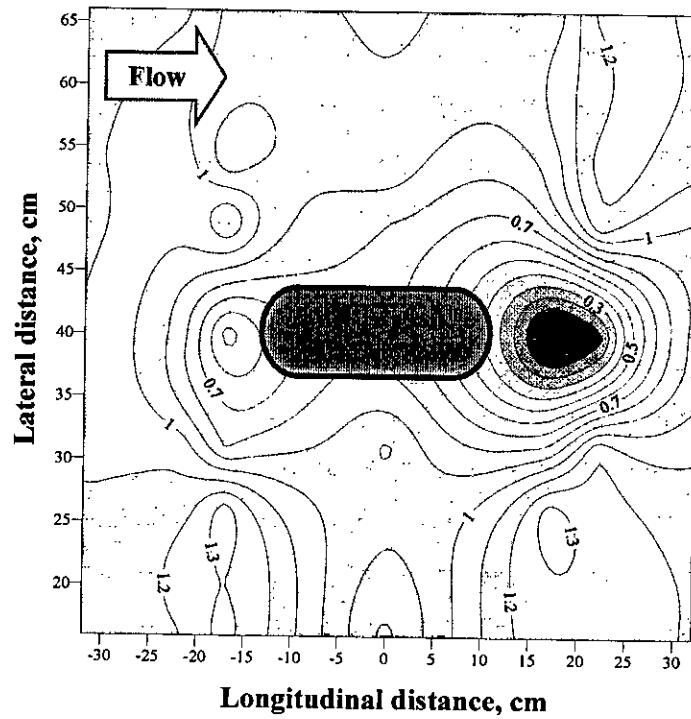


Figure D.41: Run 21-Bed material 2( $d_{50} = 0.18$  mm)-Round nose pier ( $l/b=3$ )- $Q=150$  l/s  
Floodplain

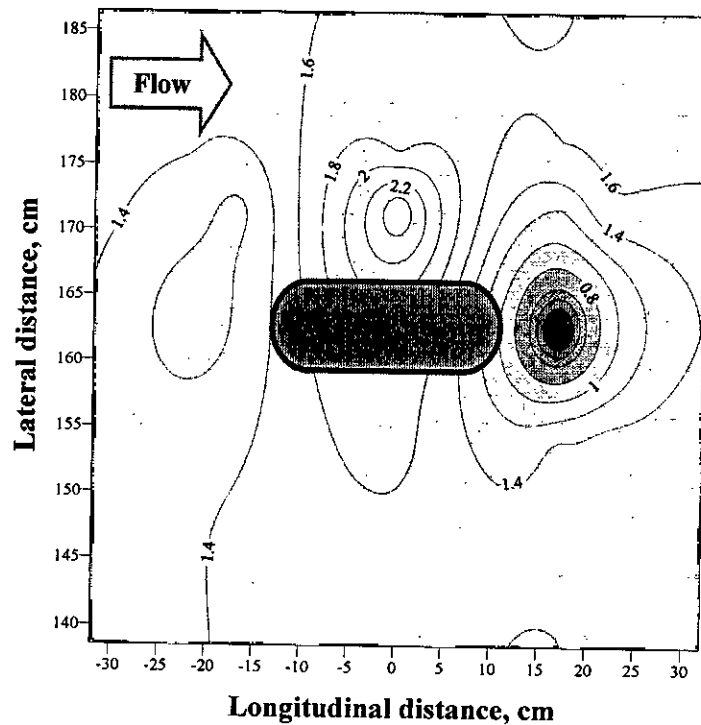


Figure D.42: Run 21-Bed material 2( $d_{50} = 0.18$  mm)-Round nose pier ( $l/b=3$ )- $Q=150$  l/s  
Main channel



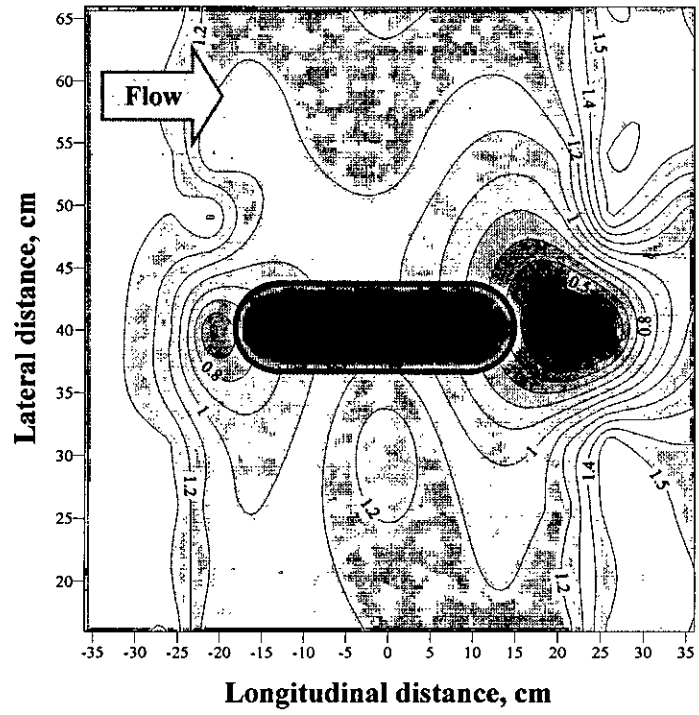


Figure D.43: Run 22-Bed material 2( $d_{50} = 0.18$  mm)-Round nose pier ( $l/b=4$ )- $Q=200$  l/s  
Floodplain

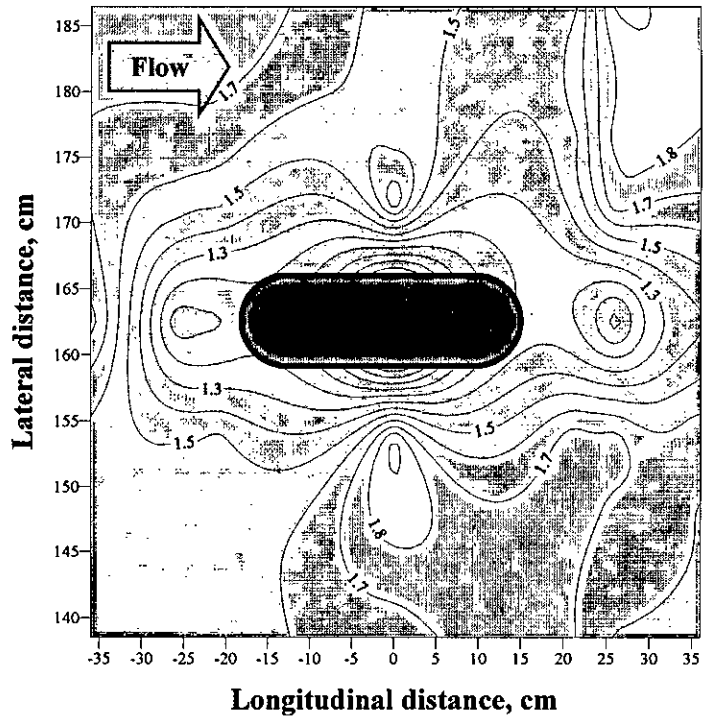


Figure D.44: Run 22-Bed material 2( $d_{50} = 0.18$  mm)-Round nose pier ( $l/b=4$ )- $Q=200$  l/s  
Main channel

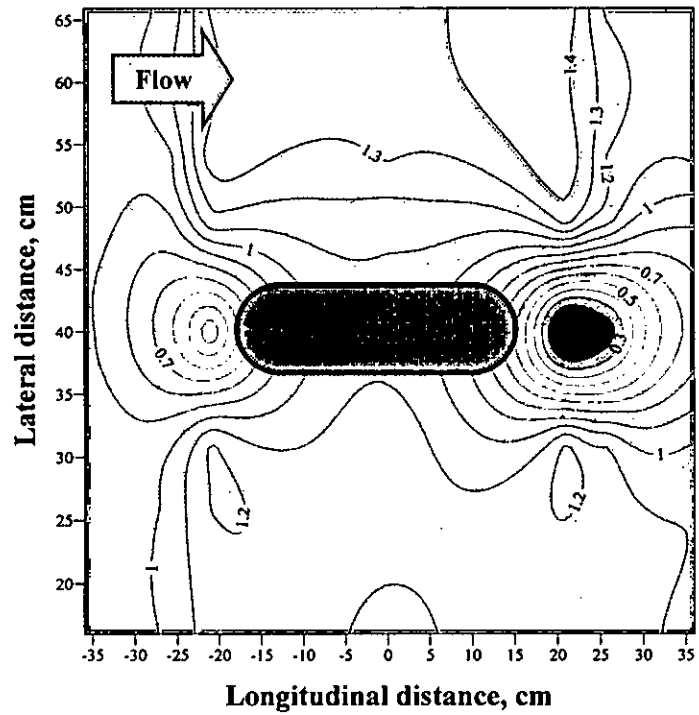


Figure D.45: Run 23-Bed material 2( $d_{50} = 0.18$  mm)-Round nose pier ( $l/b=4$ )- $Q=175$  l/s  
Floodplain

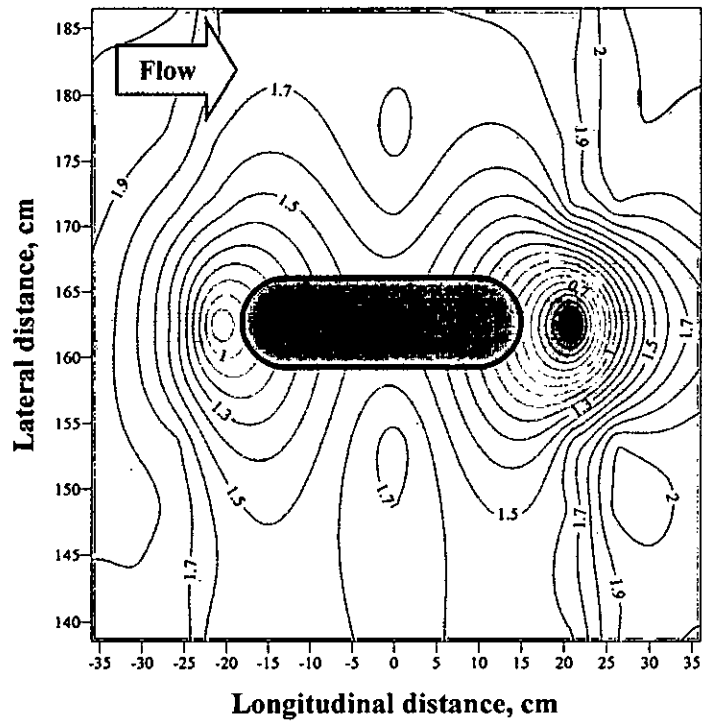


Figure D.46: Run 23-Bed material 2( $d_{50} = 0.18$  mm)-Round nose pier ( $l/b=4$ )- $Q=175$  l/s  
Main channel

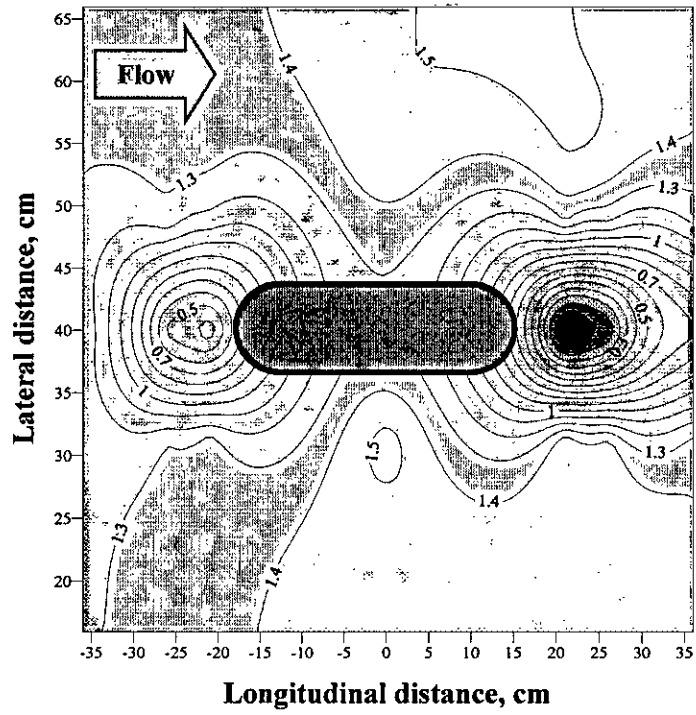


Figure D.47: Run 24-Bed material 2( $d_{50} = 0.18$  mm)-Round nose pier ( $l/b=4$ )- $Q=150$  l/s  
Floodplain

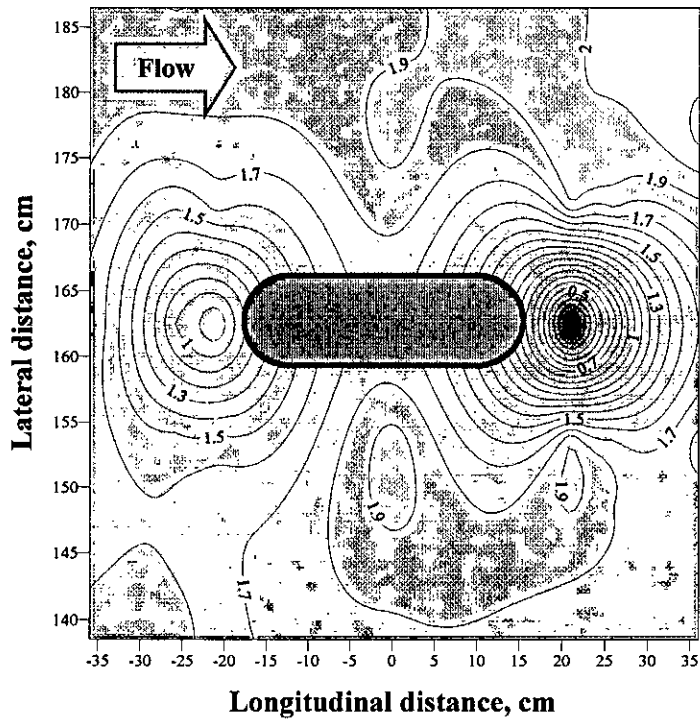


Figure D.48: Run 24-Bed material 2( $d_{50} = 0.18$  mm)-Round nose pier ( $l/b=4$ )- $Q=150$  l/s  
Main channel

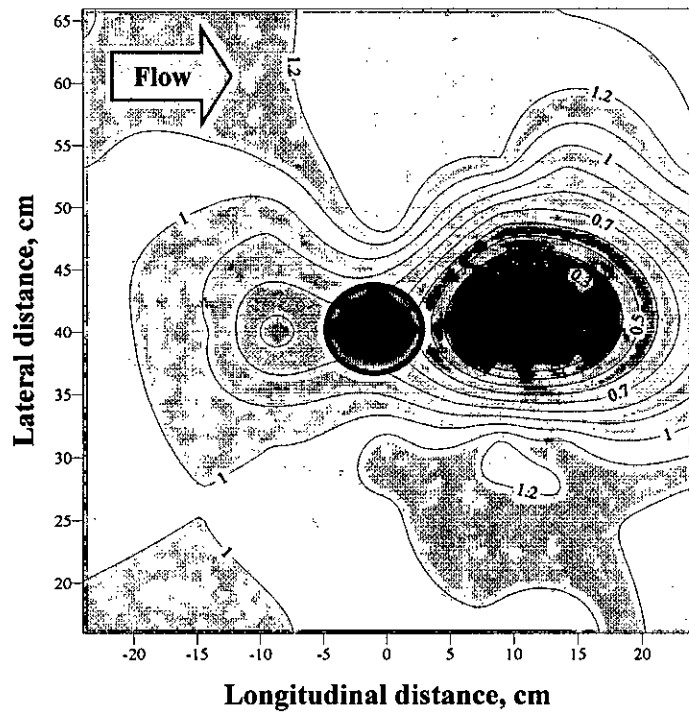


Figure D.49: Run 25-Bed material 3 ( $d_{50} = 0.12$  mm)-Circular pier ( $l/b=1$ )- $Q=200$  l/s  
Floodplain

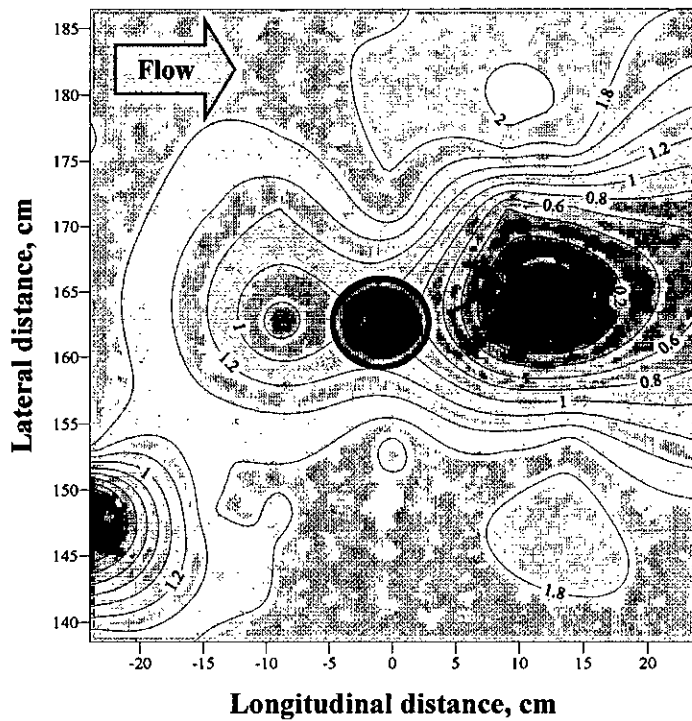


Figure D.50: Run 25-Bed material 3 ( $d_{50} = 0.12$  mm)-Circular pier ( $l/b=1$ )- $Q=200$  l/s  
Main channel

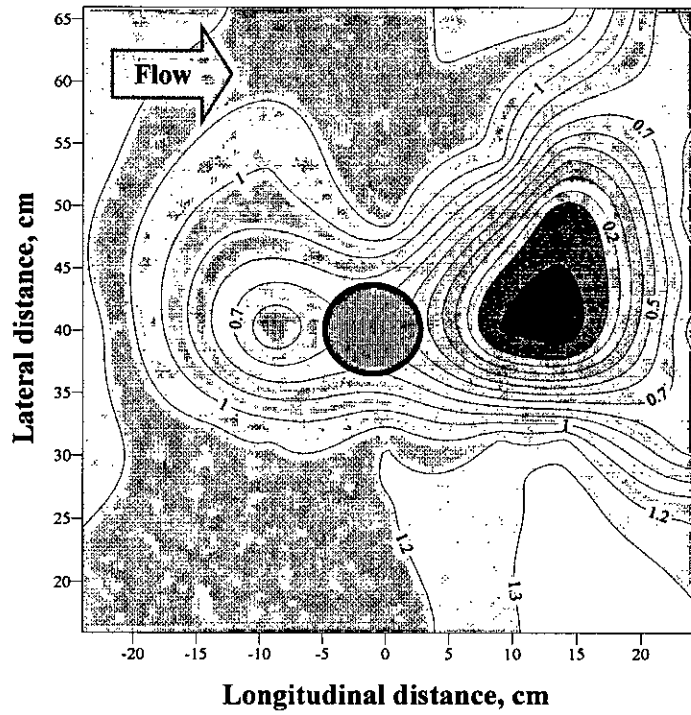


Figure D.51: Run 26-Bed material 3( $d_{50} = 0.12$  mm)-Circular pier ( $l/b=1$ )- $Q=175$  l/s  
Floodplain

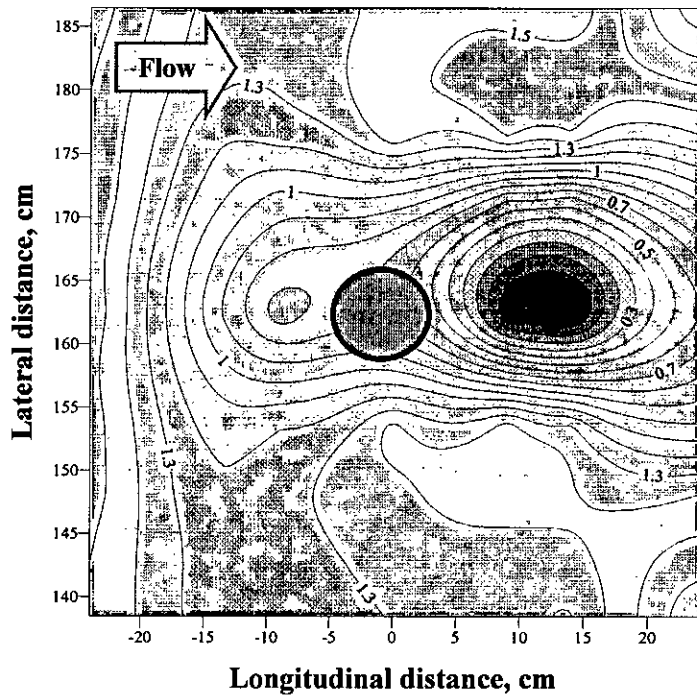


Figure D.52: Run 26-Bed material 3( $d_{50} = 0.12$  mm)-Circular pier ( $l/b=1$ )- $Q=175$  l/s  
Main channel

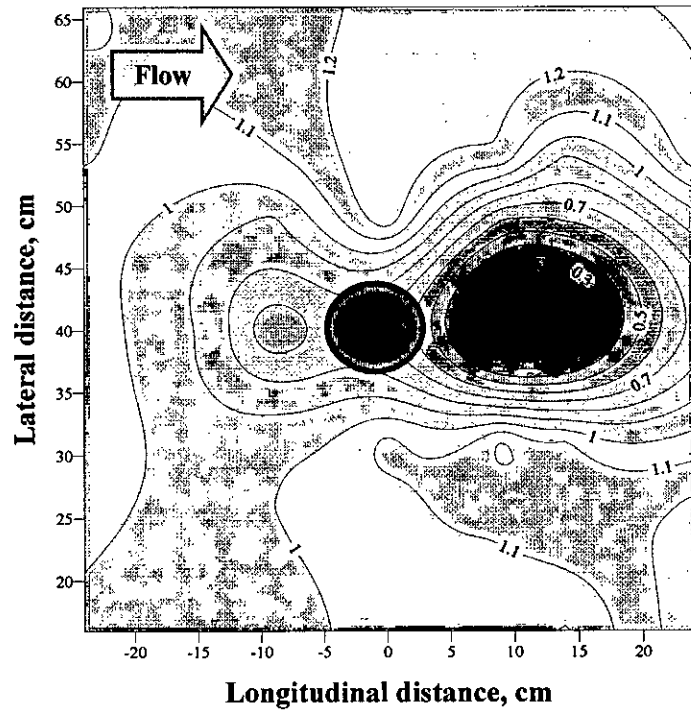


Figure D.53: Run 27-Bed material 3( $d_{50} = 0.12$  mm)-Circular pier ( $l/b=1$ )- $Q=150$  l/s  
Floodplain

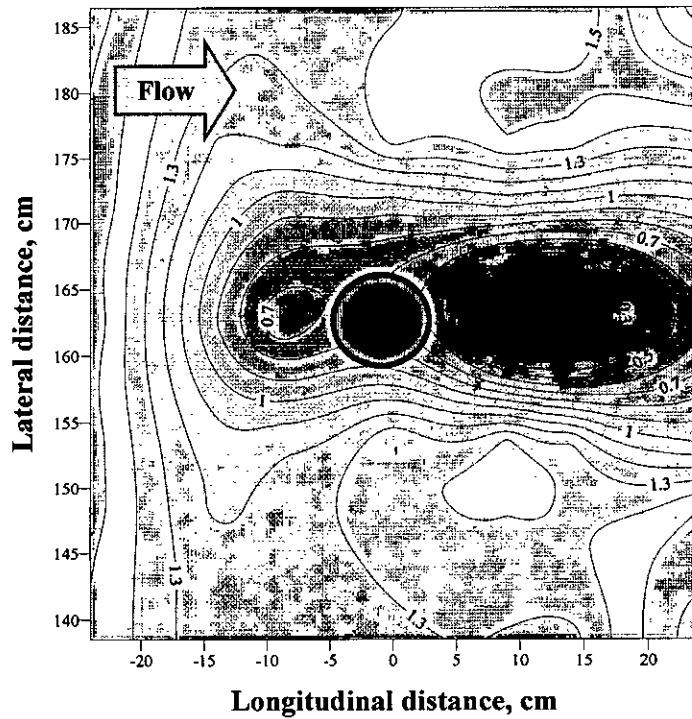


Figure D.54: Run 27-Bed material 3( $d_{50} = 0.12$  mm)-Circular pier ( $l/b=1$ )- $Q=150$  l/s  
Main channel

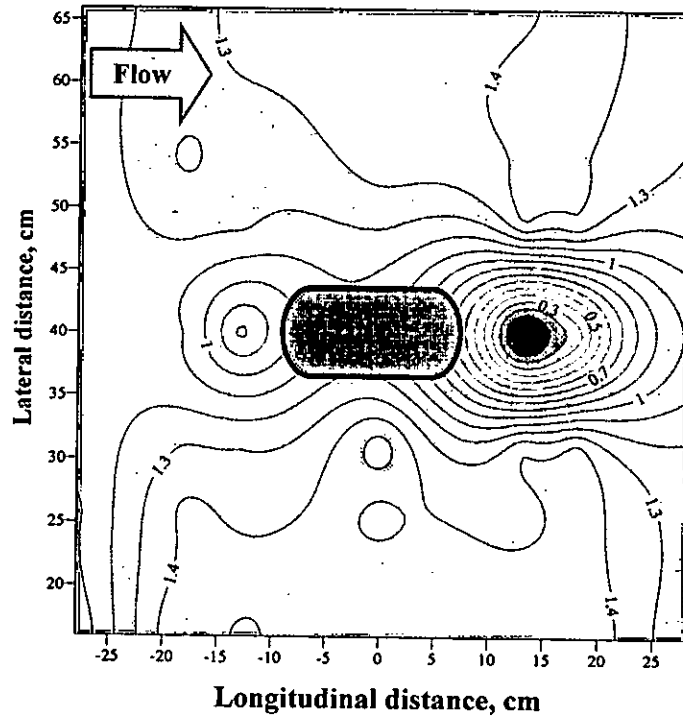


Figure D.55: Run 28-Bed material 3( $d_{50} = 0.12$  mm)-Round nose pier ( $l/b=2$ )- $Q=200$  l/s  
Floodplain

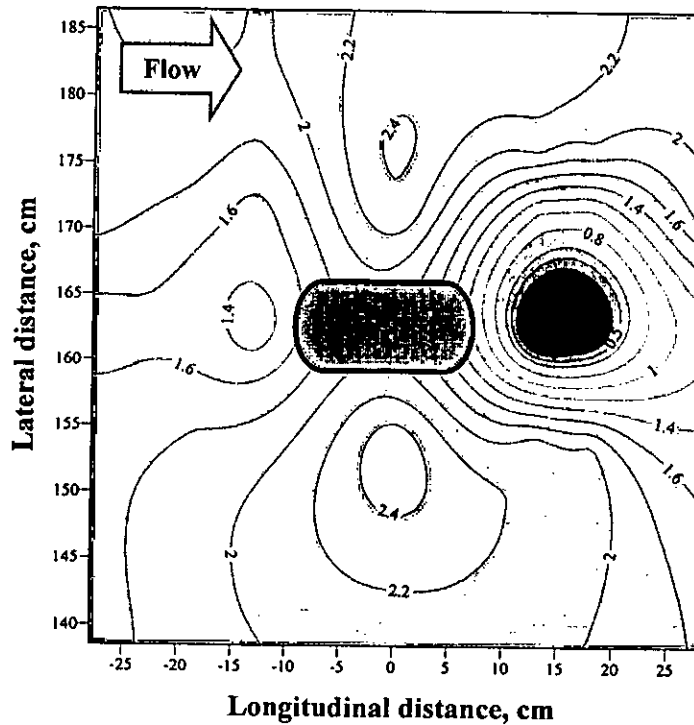


Figure D.56: Run 28-Bed material 3( $d_{50} = 0.12$  mm)-Round nose pier ( $l/b=2$ )- $Q=200$  l/s  
Main channel

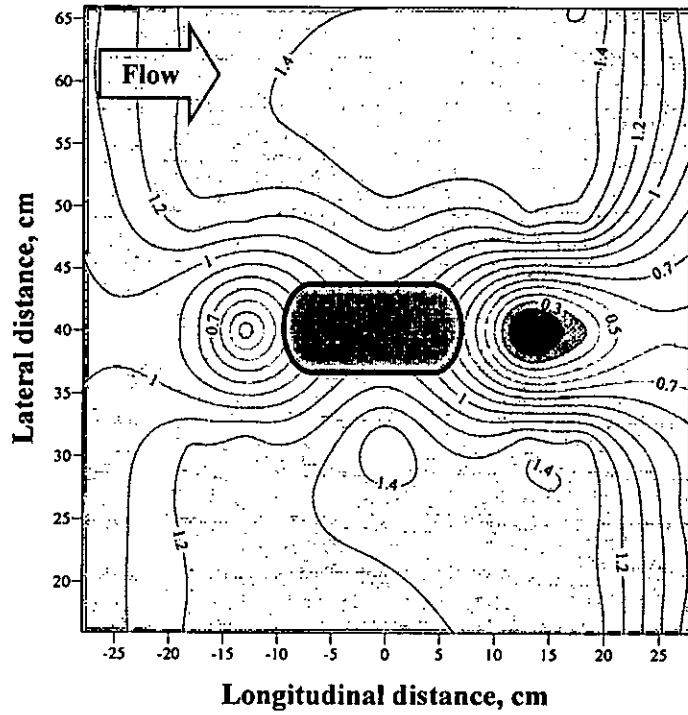


Figure D.57: Run 29-Bed material 3( $d_{50} = 0.12$  mm)-Round nose pier ( $l/b=2$ )- $Q=175$  l/s  
Floodplain

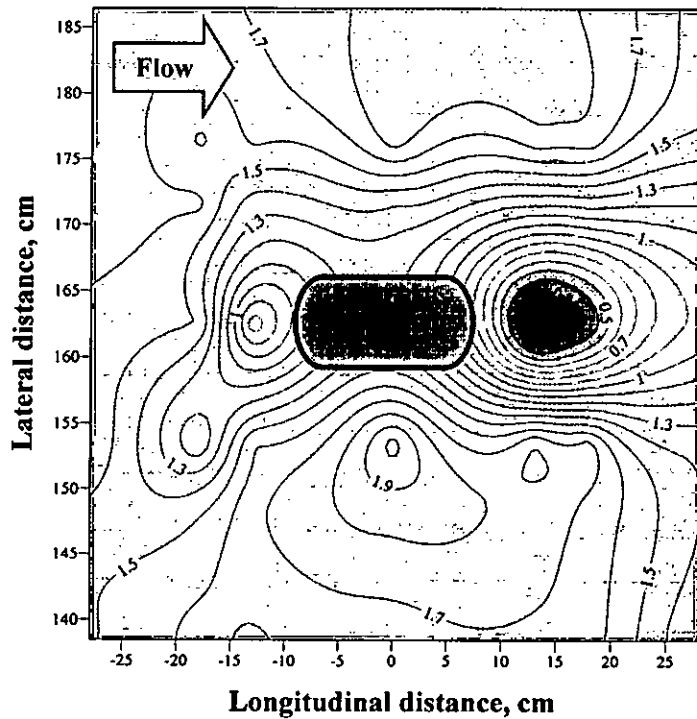


Figure D.58: Run 29-Bed material 3( $d_{50} = 0.12$  mm)-Round nose pier ( $l/b=2$ )- $Q=175$  l/s  
Main channel



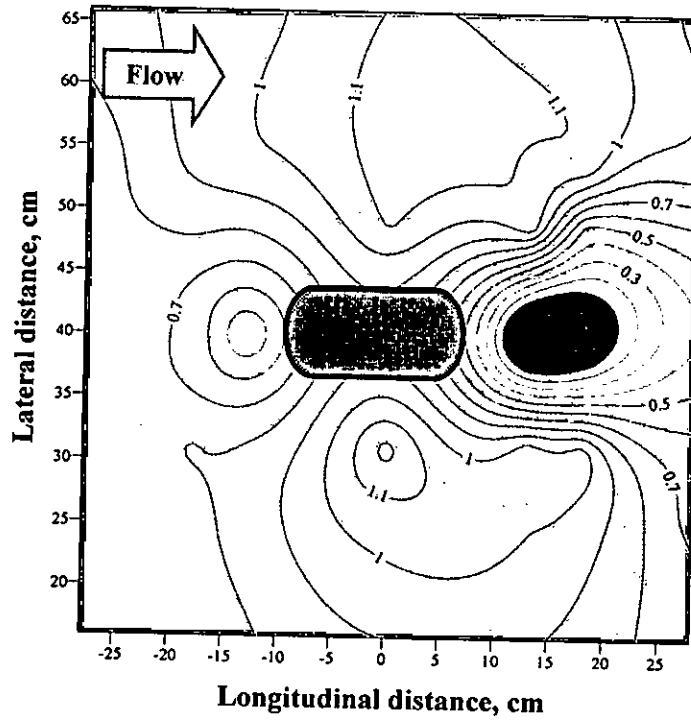


Figure D.59: Run 30-Bed material 3( $d_{50} = 0.12$  mm)-Round nose pier ( $l/b=2$ )- $Q=150$  l/s  
Floodplain

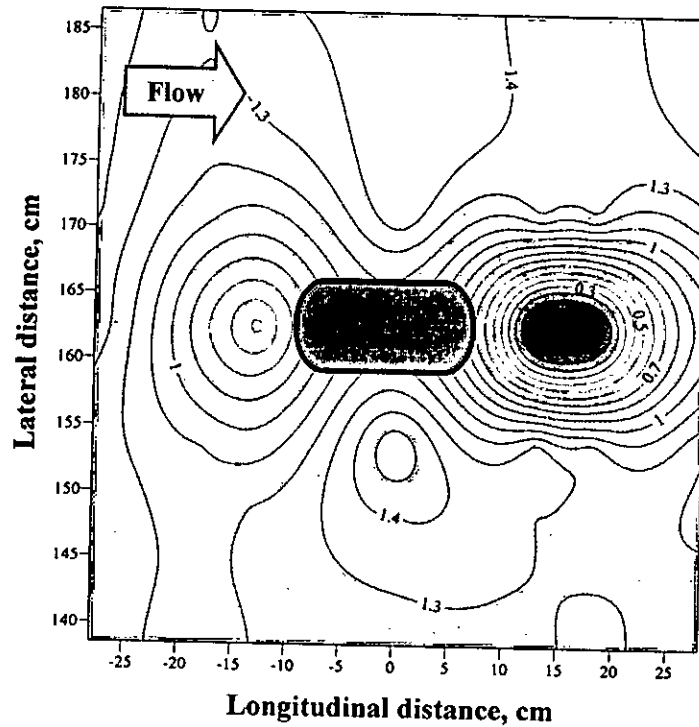


Figure D.60: Run 30-Bed material 3( $d_{50} = 0.12$  mm)-Round nose pier ( $l/b=2$ )- $Q=150$  l/s  
Main channel

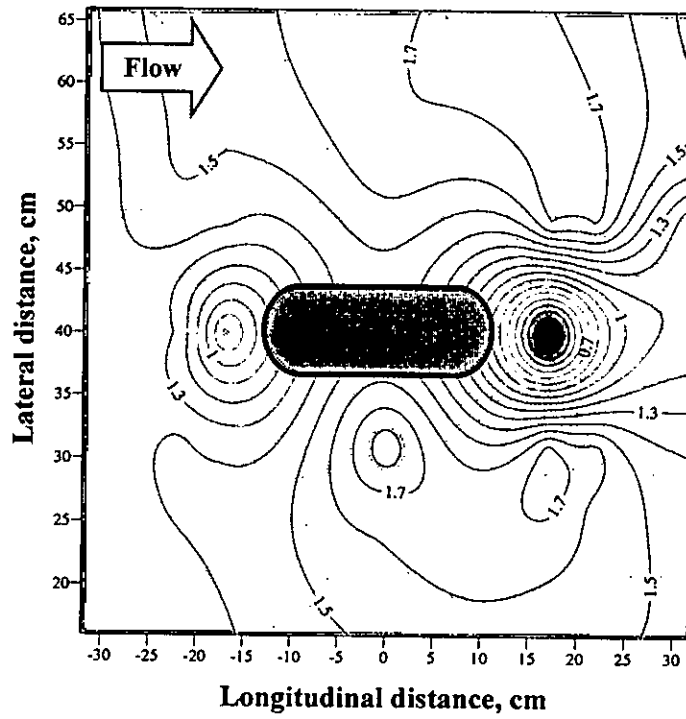


Figure D.61: Run 31-Bed material 3( $d_{50} = 0.12$  mm)-Round nose pier ( $l/b=3$ )- $Q=200$  l/s  
Floodplain

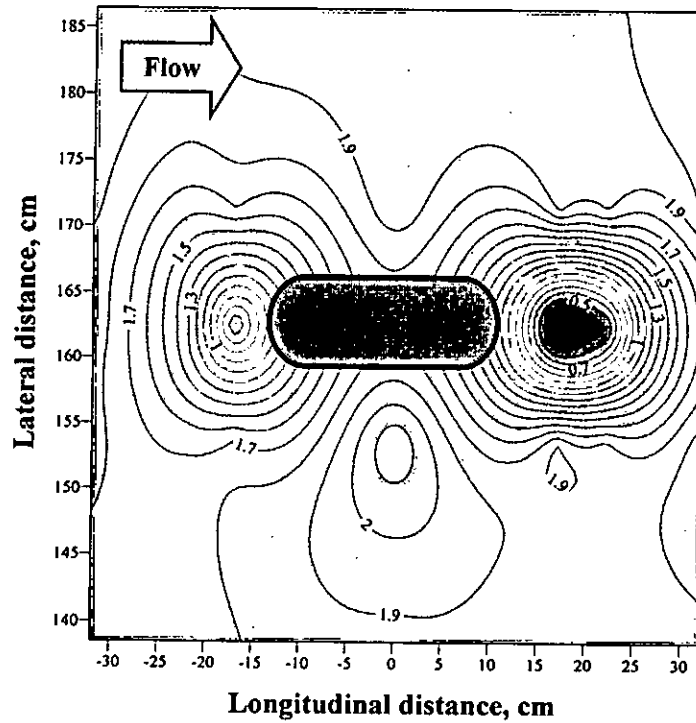


Figure D.62: Run 31-Bed material 3( $d_{50} = 0.12$  mm)-Round nose pier ( $l/b=3$ )- $Q=200$  l/s  
Main channel

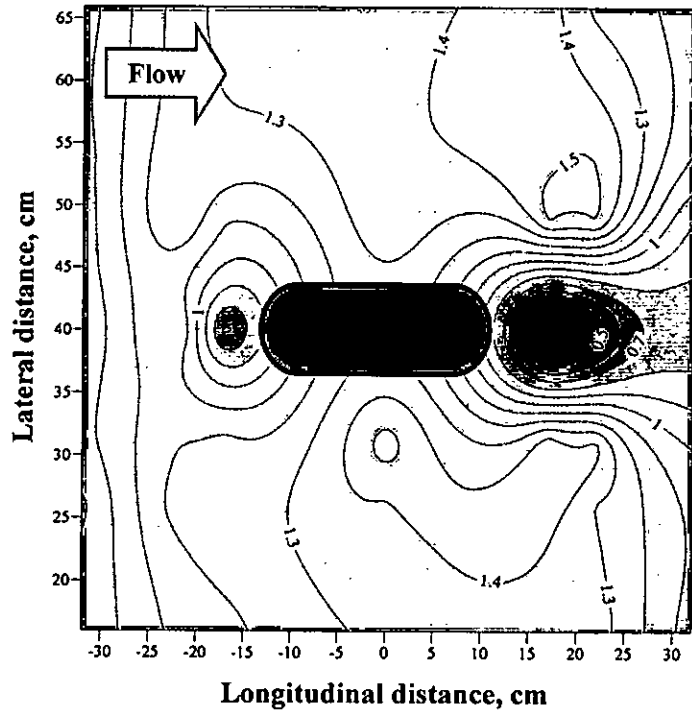


Figure D.63: Run 32-Bed material 3( $d_{50} = 0.12$  mm)-Round nose pier ( $l/b=3$ )- $Q=175$  l/s  
Floodplain

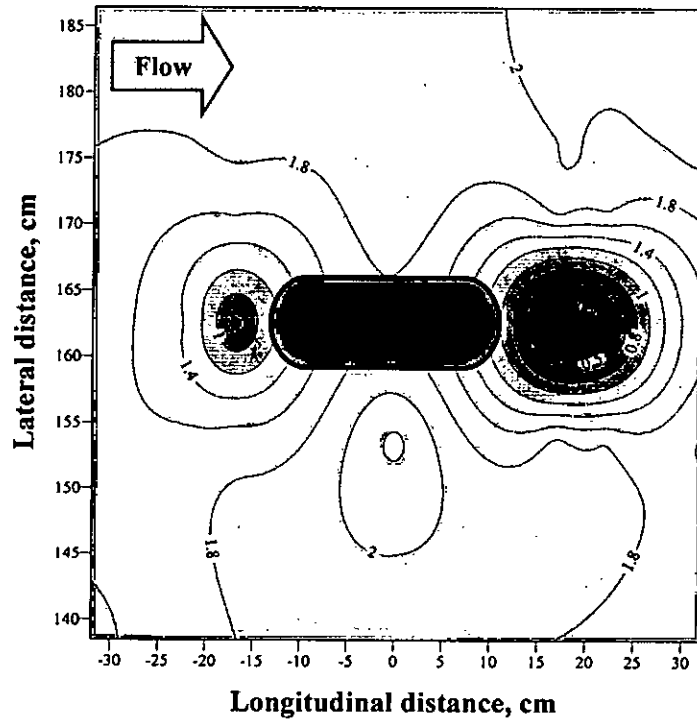


Figure D.64: Run 32-Bed material 3( $d_{50} = 0.12$  mm)-Round nose pier ( $l/b=3$ )- $Q=175$  l/s  
Main channel

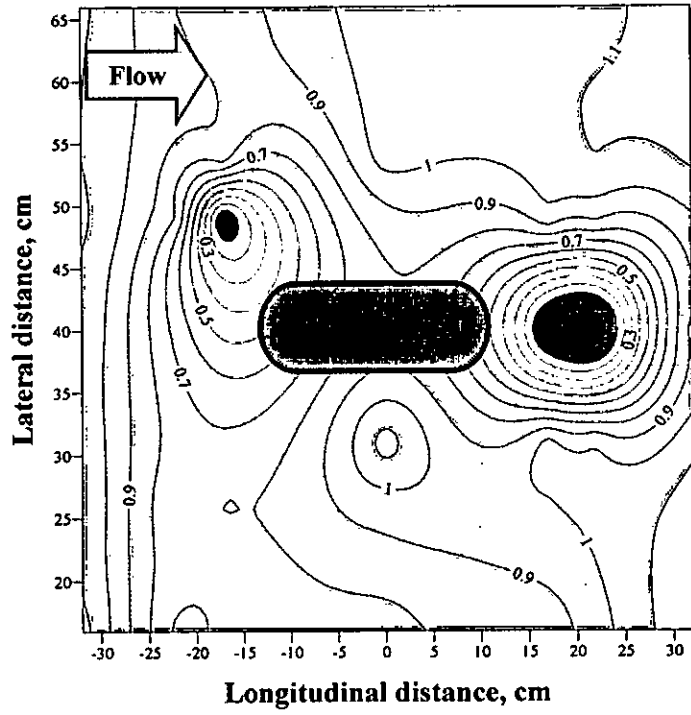


Figure D.65: Run 33-Bed material 3( $d_{50} = 0.12$  mm)-Round nose pier ( $l/b=3$ )- $Q=150$  l/s  
Floodplain

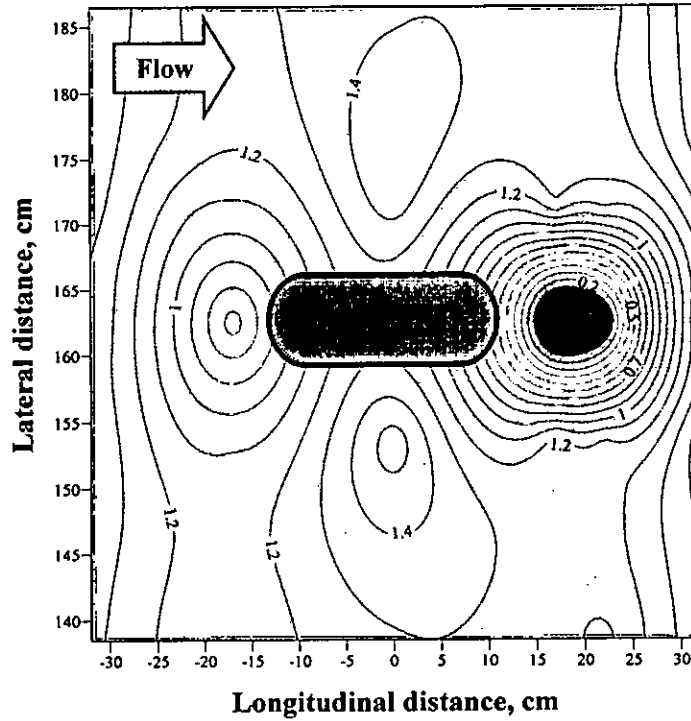


Figure D.66: Run 33-Bed material 3( $d_{50} = 0.12$  mm)-Round nose pier ( $l/b=3$ )- $Q=150$  l/s  
Main channel

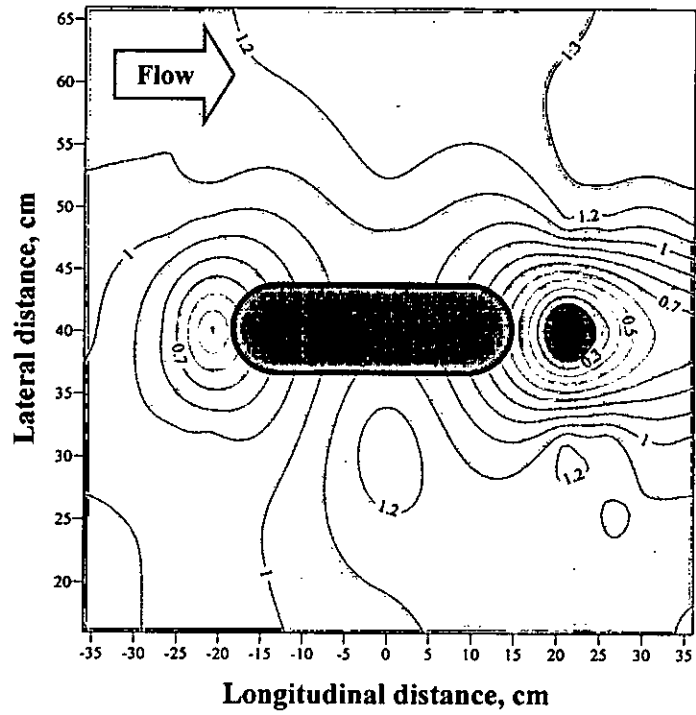


Figure D.67: Run 34-Bed material 3( $d_{50} = 0.12$  mm)-Round nose pier ( $l/b=4$ )- $Q=200$  l/s  
Floodplain

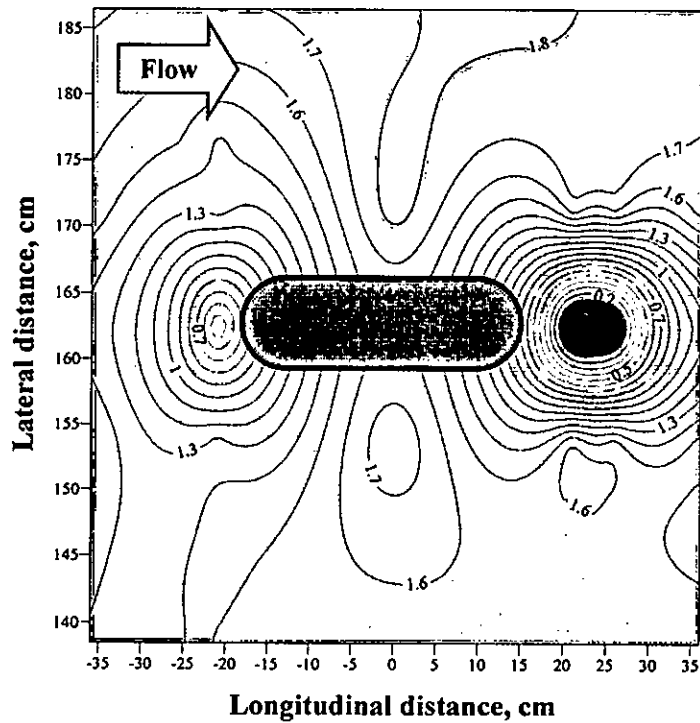


Figure D.68: Run 34-Bed material 3( $d_{50} = 0.12$  mm)-Round nose pier ( $l/b=4$ )- $Q=200$  l/s  
Main channel

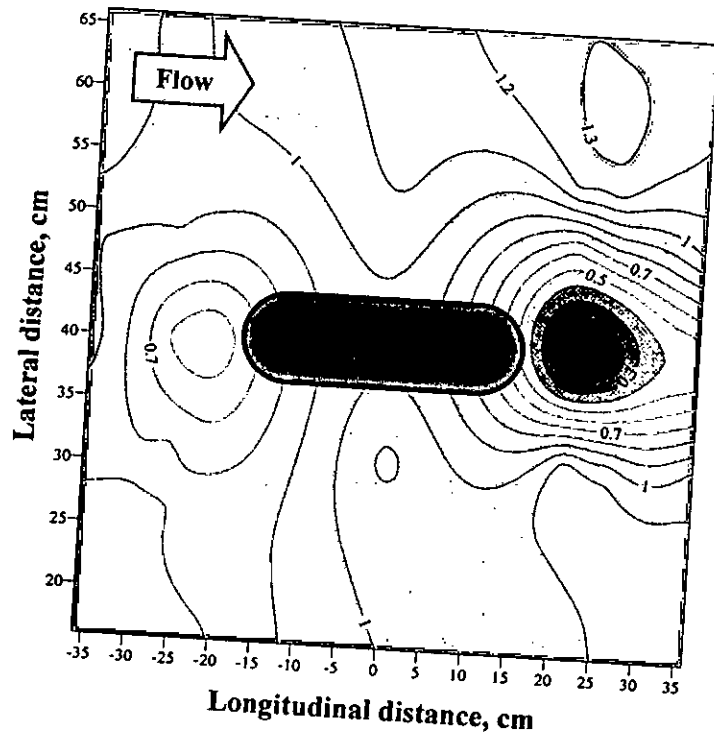


Figure D.69: Run 35-Bed material 3( $d_{50} = 0.12$  mm)-Round nose pier ( $l/b=4$ )- $Q=175$  l/s  
Floodplain

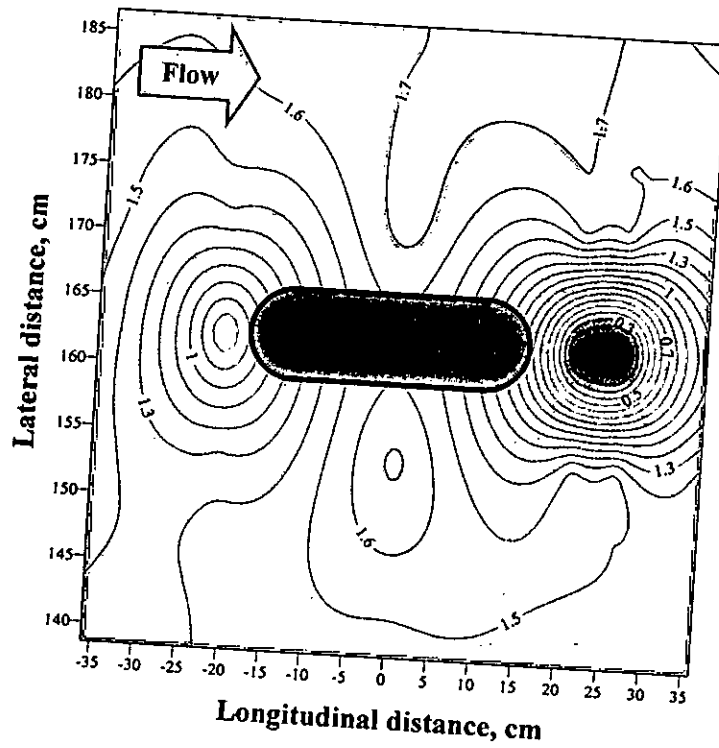


Figure D.70: Run 35-Bed material 3( $d_{50} = 0.12$  mm)-Round nose pier ( $l/b=4$ )- $Q=175$  l/s  
Main channel

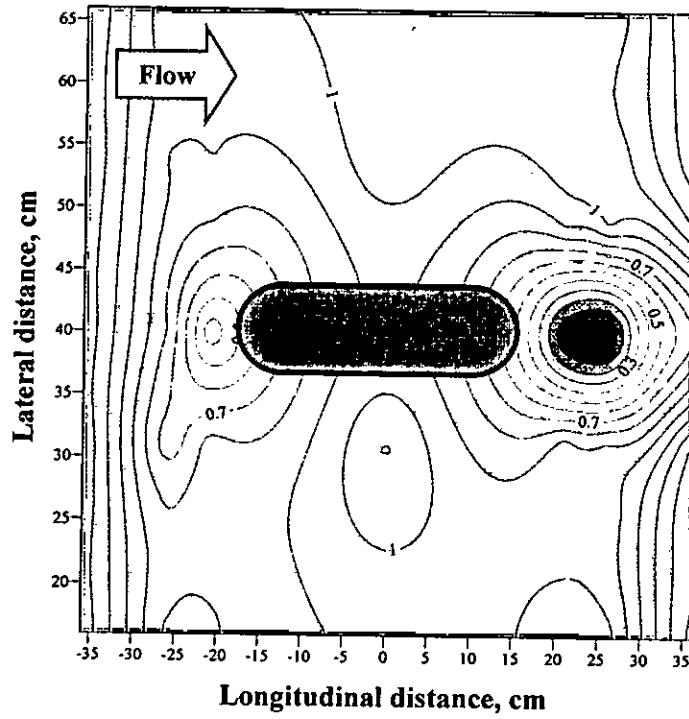


Figure D.71: Run 36-Bed material 3( $d_{50} = 0.12$  mm)-Round nose pier ( $l/b=4$ )- $Q=150$  l/s Floodplain

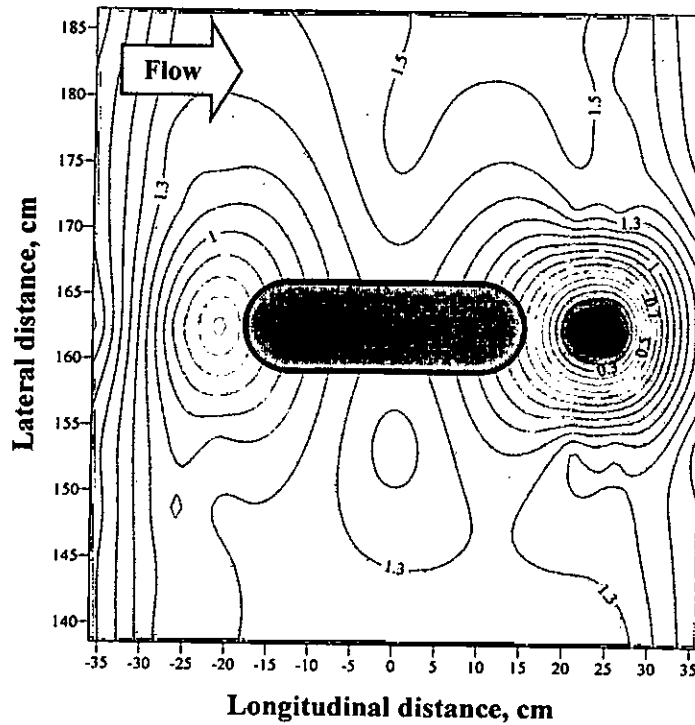


Figure D.72: Run 36-Bed material 3( $d_{50} = 0.12$  mm)-Round nose pier ( $l/b=4$ )- $Q=150$  l/s Main channel

**Appendix E**  
**Sample bed level and velocity data**



**Run:** 01  
**Bed material:** 1 ( $d_{50} = 0.75$  mm)  
**Pier:** Circular  
**l/b:** 1  
**Discharge:** 200 l/s  
**Date:** 15.07.2007

### FLOODPALIN BED LEVEL DATA

X	Y	Z
cm	cm	cm
-20	25	-0.7
-20	27.5	-0.6
-20	30	-0.5
-20	32.5	-0.7
-20	35	-0.3
-20	37.5	-0.5
-20	40	-0.1
-20	42.5	-0.1
-20	45	0.1
-20	47.5	-0.1
-20	50	-0.1
-20	52.5	0.2
-20	55	-0.1
-17.5	25	-0.6
-17.5	27.5	-0.5
-17.5	30	-0.7
-17.5	32.5	-0.3
-17.5	35	-0.3
-17.5	37.5	-0.5
-17.5	40	-0.1
-17.5	42.5	-0.2
-17.5	45	-0.1
-17.5	47.5	0.1
-17.5	50	-0.1
-17.5	52.5	0.1
-17.5	55	0.4
-15	25	-0.8
-15	27.5	-0.8
-15	30	-0.7
-15	32.5	-0.5
-15	35	-0.5
-15	37.5	-0.5
-15	40	-0.3
-15	42.5	-0.2
-15	45	-0.1
-15	47.5	-0.2
-15	50	-0.1
-15	52.5	0.2
-15	55	0

X	Y	Z
cm	cm	cm
-12.5	25	-0.6
-12.5	27.5	-0.7
-12.5	30	-0.7
-12.5	32.5	-0.6
-12.5	35	-1
-12.5	37.5	-1.7
-12.5	40	-2
-12.5	42.5	-1.9
-12.5	45	-1.6
-12.5	47.5	-0.8
-12.5	50	0.2
-12.5	52.5	0.2
-12.5	55	0.4
-10	25	-0.7
-10	27.5	-1
-10	30	-0.6
-10	32.5	-0.5
-10	35	-1.8
-10	37.5	-2.5
-10	40	-2.8
-10	42.5	-2.7
-10	45	-2.5
-10	47.5	-1.8
-10	50	-0.5
-10	52.5	0.3
-10	55	0.3
-7.5	25	-0.5
-7.5	27.5	-0.5
-7.5	30	-0.7
-7.5	32.5	-1.5
-7.5	35	-1.8
-7.5	37.5	-3.2
-7.5	40	-4.2
-7.5	42.5	-4
-7.5	45	-3.8
-7.5	47.5	-2.5
-7.5	50	-1.7
-7.5	52.5	0.3
-7.5	55	0.3

-5	25	-0.7
-5	27.5	-0.6
-5	30	-1
-5	32.5	-1.8
-5	35	-3.4
-5	47.5	-0.3
-5	50	-1.8
-5	52.5	-0.3
-5	55	0.5
-2.5	25	-0.7
-2.5	27.5	-0.3
-2.5	30	-1.2
-2.5	32.5	-2
-2.5	35	-3.3
-2.5	47.5	-3.5
-2.5	50	-1.9
-2.5	52.5	-0.3
-2.5	55	0.5
0	25	-0.7
0	27.5	-0.3
0	30	-1.6
0	32.5	-1.8
0	35	-3
0	47.5	-3
0	50	-1.7
0	52.5	0.2
0	55	0.4
2.5	25	-0.6
2.5	27.5	-0.3
2.5	30	0.2
2.5	32.5	-1.2
2.5	35	-1.5
2.5	47.5	-1.5
2.5	50	-0.6
2.5	52.5	0.6
2.5	55	0.8
5	25	-0.3
5	27.5	-0.3
5	30	0.2
5	32.5	-0.6
5	35	-0.7
5	37.5	-0.5
5	40	0.3
5	42.5	-0.1
5	45	0.3
5	47.5	-0.3
5	50	-0.3
5	52.5	1.2

5	55	0.7
7.5	25	-0.6
7.5	27.5	0
7.5	30	0.7
7.5	32.5	0
7.5	35	0.1
7.5	37.5	0.2
7.5	40	0.5
7.5	42.5	0.6
7.5	45	0.3
7.5	47.5	0.6
7.5	50	0.7
7.5	52.5	1.2
7.5	55	1.4
10	25	-0.2
10	27.5	0.2
10	30	0.7
10	32.5	0.4
10	35	0.2
10	37.5	0.2
10	40	0.7
10	42.5	1
10	45	1
10	47.5	1.2
10	50	1
10	52.5	1.3
10	55	1.6
12.5	25	-0.5
12.5	27.5	0.2
12.5	30	1
12.5	32.5	0.7
12.5	35	0.6
12.5	37.5	0.5
12.5	40	1.3
12.5	42.5	1.5
12.5	45	1.2
12.5	47.5	1.4
12.5	50	1.4
12.5	52.5	1.8
12.5	55	1.3
15	25	-0.5
15	27.5	0.5
15	30	1.2
15	32.5	1
15	35	0.7
15	37.5	0.7
15	40	1.2
15	42.5	1.7

15	45	1.5
15	47.5	1.5
15	50	1.7
15	52.5	2.1
15	55	1.4
20	25	-0.5
20	27.5	0.2
20	30	0.2
20	32.5	0.4
20	35	0.4
20	37.5	0.7
20	40	1.3
20	42.5	1.1
20	45	1.5
20	47.5	1.6
20	50	2.1
20	52.5	2
20	55	1.3
22.5	25	-0.3
22.5	27.5	-0.4
22.5	30	-1
22.5	32.5	-0.2
22.5	35	0.1
22.5	37.5	0.3
22.5	40	0.8
22.5	42.5	1
22.5	45	1.2
22.5	47.5	0.5
22.5	50	0.4
22.5	52.5	0.4
22.5	55	1.4
27.5	25	-0.5
27.5	27.5	-0.3
27.5	30	-0.8
27.5	32.5	-0.7
27.5	35	-0.5
27.5	37.5	-0.6
27.5	40	-0.8
27.5	42.5	-0.2
27.5	45	-0.5
27.5	47.5	-0.4
27.5	50	-0.3
27.5	52.5	0
27.5	55	0.2
32.5	25	-0.4
32.5	27.5	-0.3
32.5	30	-0.4
32.5	32.5	-0.1

32.5	35	-0.1
32.5	37.5	0.1
32.5	40	0.4
32.5	42.5	0.1
32.5	45	-0.2
32.5	47.5	-0.2
32.5	50	-0.1
32.5	52.5	0.1
32.5	55	0.5
42.5	25	-0.3
42.5	27.5	-0.4
42.5	30	-0.2
42.5	32.5	0.2
42.5	35	0.5
42.5	37.5	0.5
42.5	40	0.5
42.5	42.5	0.5
42.5	45	0.3
42.5	47.5	0.3
42.5	50	0.5
42.5	52.5	0.5
42.5	55	0.5

### MAIN CHANNEL BED LEVEL DATA

X	Y	Z
cm	cm	cm
-40	140	0.8
-40	145	0.5
-40	147.5	0.7
-40	150	0.2
-40	152.5	0.2
-40	155	0.6
-40	157.5	0.2
-40	160	0.2
-40	162.5	-0.2
-40	165	0
-40	167.5	0.3
-40	170	0.3
-40	172.5	-0.2
-40	175	0.2
-40	177.5	0.2
-40	182.5	0.3
-40	187.5	0.5
-30	140	0.9
-30	145	0.3
-30	147.5	0.2
-30	150	-0.3
-30	152.5	-0.5
-30	155	-0.4
-30	157.5	-0.4
-30	160	-0.6
-30	162.5	-0.8
-30	165	-0.6
-30	167.5	-0.2
-30	170	-0.3
-30	172.5	-0.6
-30	175	-0.6
-30	177.5	0.2
-30	182.5	-0.3
-30	187.5	0.3
-25	140	0.7
-25	145	0
-25	147.5	-0.3
-25	150	-0.8
-25	152.5	-1
-25	155	-1
-25	157.5	-1.1
-25	160	-1.7
-25	162.5	-2
-25	165	-1.4

X	Y	Z
cm	cm	cm
-25	167.5	-1
-25	170	-1
-25	172.5	-1.1
-25	175	-0.8
-25	177.5	-0.7
-25	182.5	-0.3
-25	187.5	0
-22.5	140	0.3
-22.5	145	-0.2
-22.5	147.5	-0.6
-22.5	150	-1
-22.5	152.5	-1.9
-22.5	155	-2.9
-22.5	157.5	-2.8
-22.5	160	-3.2
-22.5	162.5	-3.6
-22.5	165	-2.8
-22.5	167.5	-2.3
-22.5	170	-1.4
-22.5	172.5	-2.2
-22.5	175	-1.1
-22.5	177.5	-0.8
-22.5	182.5	-0.8
-22.5	187.5	0.3
-20	140	0
-20	145	-0.8
-20	147.5	-1.9
-20	150	-3.1
-20	152.5	-3.5
-20	155	-4.4
-20	157.5	-4.5
-20	160	-5.2
-20	162.5	-5.6
-20	165	-4.5
-20	167.5	-4
-20	170	-3.4
-20	172.5	0.7
-20	175	-1.8
-20	177.5	-1
-20	182.5	-0.7
-20	187.5	-0.2
-17.5	140	0.2
-17.5	145	-2.6
-17.5	147.5	-3.7

-17.5	150	-4.3
-17.5	152.5	-6.1
-17.5	155	-6.1
-17.5	157.5	-6.5
-17.5	160	-7
-17.5	162.5	-7.2
-17.5	165	-6.5
-17.5	167.5	-5.8
-17.5	170	-4.8
-17.5	172.5	-5.5
-17.5	175	-3.3
-17.5	177.5	-3
-17.5	182.5	-1.1
-17.5	187.5	-0.1
-15	140	-0.9
-15	145	-4.3
-15	147.5	-5.2
-15	150	-5.8
-15	152.5	-7.1
-15	155	-7.5
-15	157.5	-8
-15	160	-8.5
-15	162.5	-8.7
-15	165	-8
-15	167.5	-7.5
-15	170	-6.3
-15	172.5	-6.8
-15	175	-4.7
-15	177.5	-3.2
-15	182.5	-2.7
-15	187.5	-0.2
-12.5	140	-1.8
-12.5	145	-3.7
-12.5	147.5	-5.3
-12.5	150	-6.7
-12.5	152.5	-8.4
-12.5	155	-8.7
-12.5	157.5	-9.3
-12.5	160	-9.9
-12.5	162.5	-9.8
-12.5	165	-9.2
-12.5	167.5	-8.3
-12.5	170	-7.3
-12.5	172.5	-7.5
-12.5	175	-5.5
-12.5	177.5	-4.3
-12.5	182.5	-2.7
-12.5	187.5	-0.8

-10	140	-2.4
-10	145	-3.9
-10	147.5	-6
-10	150	-7.6
-10	152.5	-8.1
-10	155	-9.6
-10	157.5	-10.3
-10	160	-11.2
-10	162.5	-12
-10	165	-10.3
-10	167.5	-9.2
-10	170	-7.6
-10	172.5	-7.5
-10	175	-6
-10	177.5	-5.2
-10	182.5	-2.7
-10	187.5	-0.6
-7.5	140	-2.3
-7.5	145	-4.6
-7.5	147.5	-6.8
-7.5	150	-8.8
-7.5	152.5	-9.7
-7.5	155	-10.7
-7.5	157.5	-12.3
-7.5	160	-12.3
-7.5	162.5	-12.4
-7.5	165	-12.2
-7.5	167.5	-10.7
-7.5	170	-9
-7.5	172.5	-8.4
-7.5	175	-6.4
-7.5	177.5	-5.7
-7.5	182.5	-3.8
-7.5	187.5	-0.7
-5	140	-2.9
-5	145	-5.3
-5	147.5	-6.6
-5	150	-8.5
-5	152.5	-9.8
-5	155	-11.6
-5	167.5	-11.6
-5	170	-9.6
-5	172.5	-8.8
-5	175	-6.8
-5	177.5	-5.7
-5	182.5	-3.8
-5	187.5	-0.8
-2.5	140	-3.6

-2.5	145	-4.7
-2.5	147.5	-6.3
-2.5	150	-8.2
-2.5	152.5	-9.5
-2.5	155	-11.2
-2.5	167.5	-11
-2.5	170	-9.8
-2.5	172.5	-8.6
-2.5	175	-6.8
-2.5	177.5	-5.8
-2.5	182.5	-4.3
-2.5	187.5	-1.5
0	140	-3.3
0	145	-4.7
0	147.5	-6.3
0	150	-8
0	152.5	-9
0	155	-10.6
0	167.5	-10
0	170	-9.7
0	172.5	-8.6
0	175	-7.1
0	177.5	-6.5
0	182.5	-4.2
0	187.5	-2
2.5	140	-2.7
2.5	145	-4
2.5	147.5	-6
2.5	150	-7.2
2.5	152.5	-8.6
2.5	155	-8.8
2.5	167.5	-9.2
2.5	170	-8.7
2.5	172.5	-7.8
2.5	175	-6.5
2.5	177.5	-5.3
2.5	182.5	-4.1
2.5	187.5	-2.3
5	140	-3.3
5	145	-4.3
5	147.5	-5.4
5	150	-6.9
5	152.5	-7.8
5	155	-8
5	157.5	-8.6
5	160	-7.6
5	162.5	-7.6
5	165	-7.8

5	167.5	-8.2
5	170	-8
5	172.5	-7.3
5	175	-6.3
5	177.5	-5.3
5	182.5	-3.7
5	187.5	-2.5
7.5	140	-2.5
7.5	145	-2.8
7.5	147.5	-4.3
7.5	150	-3.3
7.5	152.5	-5.8
7.5	155	-6.5
7.5	157.5	-7
7.5	160	-7.2
7.5	162.5	-7.6
7.5	165	-7.8
7.5	167.5	-7.7
7.5	170	-7.2
7.5	172.5	-6.8
7.5	175	-5.6
7.5	177.5	-5
7.5	182.5	-3.5
7.5	187.5	-2.2
10	140	-2.6
10	145	-2.8
10	147.5	-3.8
10	150	-4.6
10	152.5	-4.8
10	155	-5.3
10	157.5	-5.8
10	160	-6.5
10	162.5	-7.3
10	165	-7.6
10	167.5	-7.3
10	170	-6.6
10	172.5	-5.7
10	175	-5.2
10	177.5	-4.7
10	182.5	-3.2
10	187.5	-2.2
12.5	140	-2.3
12.5	145	-2.5
12.5	147.5	-3.2
12.5	150	-4
12.5	152.5	-4.2
12.5	155	-4.2
12.5	157.5	-4.7

12.5	160	-5.2
12.5	162.5	-6.2
12.5	165	-6.3
12.5	167.5	-6
12.5	170	-6.3
12.5	172.5	-4.7
12.5	175	-4.5
12.5	177.5	-4.3
12.5	182.5	-2.8
12.5	187.5	-2.3
15	140	-2
15	145	-2.5
15	147.5	-2.8
15	150	-3.4
15	152.5	-3.5
15	155	-3.3
15	157.5	-3.8
15	160	-5.2
15	162.5	-5.7
15	165	-5.8
15	167.5	-5
15	170	-4.9
15	172.5	-4.3
15	175	-4.3
15	177.5	-3.6
15	182.5	-2.8
15	187.5	-2.6
17.5	140	-2.5
17.5	145	-2.7
17.5	147.5	-2.3
17.5	150	-2.7
17.5	152.5	-3.2
17.5	155	-3.8
17.5	157.5	-4.6
17.5	160	-4.7
17.5	162.5	-4.6
17.5	165	-3.9
17.5	167.5	-3.9
17.5	170	-3.8
17.5	172.5	-3.7
17.5	175	-3.1
17.5	177.5	-2.9
17.5	182.5	-2.6
17.5	187.5	-2.4
20	140	-1.8
20	145	-2.1
20	147.5	-2.2
20	150	-2.6

20	152.5	-2.7
20	155	-2.3
20	157.5	-2.7
20	160	-4.1
20	162.5	-3.9
20	165	-3.8
20	167.5	-3.8
20	170	-3.6
20	172.5	-3.1
20	175	-2.4
20	177.5	-2.5
20	182.5	-2.5
20	187.5	-1.9
22.5	140	-1.7
22.5	145	-1.8
22.5	147.5	-1.8
22.5	150	-2.2
22.5	152.5	-2.1
22.5	155	-1.6
22.5	157.5	-1.7
22.5	160	-2.6
22.5	162.5	-2.6
22.5	165	-3.1
22.5	167.5	-3.0
22.5	170	-3.0
22.5	172.5	-2.8
22.5	175	-2.4
22.5	177.5	-2.5
22.5	182.5	-2.3
22.5	187.5	-1.8
27.5	140	-1.2
27.5	145	-1.2
27.5	147.5	-1.3
27.5	150	-1.6
27.5	152.5	-1.5
27.5	155	-1.0
27.5	157.5	-1.0
27.5	160	-1.4
27.5	162.5	-1.4
27.5	165	-1.8
27.5	167.5	-2.0
27.5	170	-2.3
27.5	172.5	-2.3
27.5	175	-2.2
27.5	177.5	-2.2
27.5	182.5	-2.2
27.5	187.5	-2.0

32.5	140	-0.8
32.5	145	-0.7
32.5	147.5	-0.7
32.5	150	-0.7
32.5	152.5	-0.6
32.5	155	-0.4
32.5	157.5	0.2
32.5	160	-0.3
32.5	162.5	-0.5
32.5	165	-0.9
32.5	167.5	-1.4
32.5	170	-1.7
32.5	172.5	-1.7
32.5	175	-1.8
32.5	177.5	-1.8
32.5	182.5	-1.8
32.5	187.5	-1.3
42.5	140	-0.5
42.5	145	0.2
42.5	147.5	0.2
42.5	150	0.3
42.5	152.5	0.4
42.5	155	0.9
42.5	157.5	1.1
42.5	160	0.9
42.5	162.5	0.7
42.5	165	0.2
42.5	167.5	-0.3
42.5	170	-0.4
42.5	172.5	-0.8
42.5	175	-0.9
42.5	177.5	-1.2
42.2	182.5	-1.1
42.2	187.5	-1.2



Zero measurement	
V <sub>x</sub>	V <sub>y</sub>
-0.094	0.035

### FLOODPLAIN VELOCITY DATA

X	Y	Z	Mean V <sub>x</sub> Reading	Mean V <sub>y</sub> Reading	Mean V <sub>x</sub>	Mean V <sub>y</sub>
cm	cm	cm	m/s	m/s	m/s	m/s
-24	16	4.2	0.258	0.017	0.164	0.052
-24	26	4.2	0.257	0.017	0.163	0.052
-24	31	4.2	0.268	0.018	0.174	0.053
-24	40	4.2	0.266	0.017	0.172	0.052
-24	49	4.2	0.291	0.018	0.197	0.053
-24	54	4.2	0.299	0.021	0.205	0.056
-24	66	4.2	0.306	0.02	0.212	0.055
-14	16	4.2	0.239	0.009	0.145	0.044
-14	26	4.2	0.25	0.009	0.156	0.044
-14	31	4.2	0.248	0.007	0.154	0.042
-14	40	4.2	0.243	0.009	0.149	0.044
-14	49	4.2	0.272	0.02	0.178	0.055
-14	54	4.2	0.304	0.021	0.21	0.056
-14	66	4.2	0.312	0.025	0.218	0.06
-9	16	4.2	0.254	0.009	0.16	0.044
-9	26	4.2	0.256	0.004	0.162	0.039
-9	31	4.2	0.25	-0.006	0.156	0.029
-9	40	1.4	0.16	0.004	0.066	0.039
-9	40	2.8	0.151	0	0.057	0.035
-9	40	4.2	0.097	0.012	0.003	0.047
-9	40	5.6	0.137	0.013	0.043	0.048
-9	49	4.2	0.242	0.04	0.148	0.075
-9	54	4.2	0.293	0.028	0.199	0.063
-9	66	4.2	0.306	0.026	0.212	0.061
0	16	4.2	0.245	0.004	0.151	0.039
0	26	4.2	0.276	0.008	0.182	0.043
0	31	4.2	0.29	-0.019	0.196	0.016
0	40	4.2	0	0	0	0
0	49	4.2	0.278	0.081	0.184	0.116
0	54	4.2	0.282	0.042	0.188	0.077
0	66	4.2	0.277	0.019	0.183	0.054
9	16	4.2	0.283	0.005	0.189	0.04
9	26	4.2	0.29	0.009	0.196	0.044
9	31	4.2	0.293	0.008	0.199	0.043
9	40	4.2	0.063	-0.027	-0.031	0.008

9	49	4.2	0.077	0.038	-0.017	0.073
9	54	4.2	0.31	0.036	0.216	0.071
9	66	4.2	0.32	0.029	0.226	0.064
14	16	4.2	0.299	-0.001	0.205	0.034
14	26	4.2	0.302	0.004	0.208	0.039
14	31	4.2	0.275	0.013	0.181	0.048
14	40	4.2	0.07	-0.003	-0.024	0.032
14	49	4.2	0.099	0.053	0.005	0.088
14	54	4.2	0.278	0.021	0.184	0.056
14	66	4.2	0.329	0.025	0.235	0.06
24	16	4.2	0.323	0.006	0.229	0.041
24	26	4.2	0.315	0.032	0.221	0.067
24	31	4.2	0.27	0.032	0.176	0.067
24	40	4.2	0.293	0.032	0.199	0.067
24	49	4.2	0.221	0.033	0.127	0.068
24	54	4.2	0.199	0.03	0.105	0.065
24	66	4.2	0.291	0.033	0.197	0.068

Zero measurement	
V <sub>x</sub>	V <sub>y</sub>
-0.094	0.035

#### MAIN CHANNEL VELOCITY DATA

X	Y	Z	Mean V <sub>x</sub> Reading	Mean V <sub>y</sub> Reading	Mean V <sub>x</sub>	Mean V <sub>y</sub>
cm	cm	cm	m/s	m/s	m/s	m/s
-24	138.5	16.2	0.495	0.026	0.401	0.061
-24	148.5	16.2	0.504	0.024	0.41	0.059
-24	153.5	16.2	0.493	0.025	0.399	0.06
-24	162.5	16.2	0.511	0.033	0.417	0.068
-24	171.5	16.2	0.513	0.031	0.419	0.066
-24	176.5	16.2	0.525	0.034	0.431	0.069
-24	186.5	16.2	0.526	0.033	0.432	0.068
-14	138.5	16.2	0.487	0.011	0.393	0.046
-14	148.5	16.2	0.479	-0.001	0.385	0.034
-14	153.5	16.2	0.449	-0.002	0.355	0.033
-14	162.5	16.2	0.482	0.019	0.388	0.054
-14	171.5	16.2	0.459	0.053	0.365	0.088
-14	176.5	16.2	0.484	0.059	0.39	0.094
-14	186.5	16.2	0.528	0.044	0.434	0.079

-9	138.5	16.2	0.483	-0.002	0.389	0.033
-9	148.5	16.2	0.479	-0.035	0.385	0
-9	153.5	16.2	0.445	-0.062	0.351	-0.027
-9	162.5	5.4	0.351	-0.019	0.257	0.016
-9	162.5	10.8	0.322	-0.021	0.228	0.014
-9	162.5	16.2	0.379	-0.011	0.285	0.024
-9	162.5	21.6	0.337	0.001	0.243	0.036
-9	171.5	16.2	0.426	0.104	0.332	0.139
-9	176.5	16.2	0.488	0.09	0.394	0.125
-9	186.5	16.2	0.522	0.051	0.428	0.086
0	138.5	16.2	0.495	0.006	0.401	0.041
0	148.5	16.2	0.535	-0.03	0.441	0.005
0	153.5	16.2	0.556	-0.085	0.462	-0.05
0	162.5	16.2	0	0	0	0
0	171.5	16.2	0.525	0.192	0.431	0.227
0	176.5	16.2	0.488	0.028	0.394	0.063
0	186.5	16.2	0.542	0.051	0.448	0.086
9	138.5	16.2	0.504	0.011	0.41	0.046
9	148.5	16.2	0.535	0.032	0.441	0.067
9	153.5	16.2	0.558	0.032	0.464	0.067
9	162.5	16.2	0.063	0.032	-0.031	0.067
9	171.5	16.2	0.488	0.032	0.394	0.067
9	176.5	16.2	0.564	0.035	0.47	0.07
9	186.5	16.2	0.554	0.032	0.46	0.067
14	138.5	16.2	0.502	0.003	0.408	0.038
14	148.5	16.2	0.552	0.004	0.458	0.039
14	153.5	16.2	0.517	0.02	0.423	0.055
14	162.5	16.2	0.097	0.03	0.003	0.065
14	171.5	16.2	0.372	-0.037	0.278	-0.002
14	176.5	16.2	0.552	0.018	0.458	0.053
14	186.5	16.2	0.55	0.029	0.456	0.064
24	138.5	16.2	0.52	0.031	0.426	0.066
24	148.5	16.2	0.492	0.025	0.398	0.06
24	153.5	16.2	0.414	0.04	0.32	0.075
24	162.5	16.2	0.255	0.014	0.161	0.049
24	171.5	16.2	0.347	-0.033	0.253	0.002
24	176.5	16.2	0.478	-0.013	0.384	0.022
24	186.5	16.2	0.548	0.014	0.454	0.049

